NOVEL MOLECULAR TARGETS FOR THE TREATMENT OF PAIN

EDITED BY: Tally Largent-Milnes, John Michael Streicher and Meritxell Canals
PUBLISHED IN: Frontiers in Molecular Neuroscience

frontiers Research Topics

frontiers

ISSN 1664-8714
ISBN 978-2-88966-442-9
DOI 10.3389/978-2-88966-442-9

About Frontiers

Frontiers is more than just an open-access publisher of scholarly articles: it is a pioneering approach to the world of academia, radically improving the way scholarly research is managed. The grand vision of Frontiers is a world where all people have an equal opportunity to seek, share and generate knowledge. Frontiers provides immediate and permanent online open access to all its publications, but this alone is not enough to realize our grand goals.

Frontiers Journal Series

The Frontiers Journal Series is a multi-tier and interdisciplinary set of open-access, online journals, promising a paradigm shift from the current review, selection and dissemination processes in academic publishing. All Frontiers journals are driven by researchers for researchers; therefore, they constitute a service to the scholarly community. At the same time, the Frontiers Journal Series operates on a revolutionary invention, the tiered publishing system, initially addressing specific communities of scholars, and gradually climbing up to broader public understanding, thus serving the interests of the lay society, too.

Dedication to Quality

Each Frontiers article is a landmark of the highest quality, thanks to genuinely collaborative interactions between authors and review editors, who include some of the world's best academicians. Research must be certified by peers before entering a stream of knowledge that may eventually reach the public - and shape society; therefore, Frontiers only applies the most rigorous and unbiased reviews.
Frontiers revolutionizes research publishing by freely delivering the most outstanding research, evaluated with no bias from both the academic and social point of view. By applying the most advanced information technologies, Frontiers is catapulting scholarly publishing into a new generation.

What are Frontiers Research Topics?

Frontiers Research Topics are very popular trademarks of the Frontiers Journals Series: they are collections of at least ten articles, all centered on a particular subject. With their unique mix of varied contributions from Original Research to Review Articles, Frontiers Research Topics unify the most influential researchers, the latest key findings and historical advances in a hot research area! Find out more on how to host your own Frontiers Research Topic or contribute to one as an author by contacting the Frontiers Editorial Office: frontiersin.org/about/contact

NOVEL MOLECULAR TARGETS FOR THE TREATMENT OF PAIN

Topic Editors:
Tally Largent-Milnes, University of Arizona, United States
John Michael Streicher, University of Arizona, United States
Meritxell Canals, University of Nottingham, United Kingdom

Topic Editor John Streicher is a co-founder and equity partner of Teleport Pharmaceuticals, LLC. All other Topic Editors declare no competing interests with regards to the Research Topic subject.

Citation: Largent-Milnes, T., Streicher, J. M., Canals, M., eds. (2021). Novel Molecular Targets for the Treatment of Pain. Lausanne: Frontiers Media SA.
doi: 10.3389/978-2-88966-442-9

Table of Contents

frontiers in Molecular Neuroscience

EDITORIAL
published: 11 December 2020
doi: 10.3389/fnmol.2020.625714

Editorial: Novel Molecular Targets for the Treatment of Pain

Tally M. Largent-Milnes[1]*, *Meritxell Canals*[2,3]* and *John M. Streicher*[1]*

[1] Department of Pharmacology, College of Medicine, University of Arizona, Tucson, AZ, United States, [2] Division of Physiology, Pharmacology and Neuroscience, School of Life Sciences, Queen's Medical Centre, University of Nottingham, Nottingham, United Kingdom, [3] Centre of Membrane Proteins and Receptors, Universities of Birmingham and Nottingham, The Midlands, United Kingdom

Keywords: delta opioid receptor, mu opioid receptor, TIMP-1, heat shock protein 90, inflammation, cannabinoid, opioid, chronic pain

Editorial on the Research Topic

Novel Molecular Targets for the Treatment of Pain

The chronic pain and opioid epidemics are two interdependent public health crises that have challenged the United States, in particular, and the world in general for more than 20 years. Chronic pain affects more than 100 million people in the USA, is growing in incidence as the population ages, can severely impact patient quality of life, and has economic costs of more than $600 billion in the USA alone (Breivik et al., 2009; Gaskin and Richard, 2012). In response, opioid prescribing has risen rapidly for two decades, resulting in an opioid abuse and overdose crisis that claims more than 40,000 lives annually in the USA (Lozano et al., 2012; Warner et al., 2016). These twin crises highlight the vast medical and social need to develop new treatments for chronic pain that are non-opioid or mitigate the negative effects of opioid therapy. However, despite a rapid increase in our understanding of the basic science of the pain and opioid systems, this knowledge has not yet translated into new therapies (Woodcock et al., 2007; Olson et al., 2017).

By identifying new targets and new approaches to treat pain, we may be able to design new therapies to efficaciously treat chronic pain without the drawbacks of current opioid therapies. This collection of novel basic science research articles titled "Novel Molecular Targets for the Treatment of Pain" is intended to stimulate research into these novel targets by the scientific community, which could then lead to the clinical development of new drugs.

This collection naturally falls into several themes, the first of which is novel regulation of the mu opioid receptor (MOR), the primary target of clinical opioids like morphine (Matthes et al., 1996; Olson et al., 2019). Original research from the Briddon and Canals groups demonstrated novel molecular events for the MOR after stimulation by the high efficacy agonist DAMGO; understanding of exactly how the MOR desensitizes and internalizes could lead to new methods to manipulate this process to improve opioid therapy (Gondin et al.). Several review articles also highlighted new areas of research into MOR regulation. The Filizola group reviewed recent advances in modeling the MOR activation process using molecular dynamics simulation (Ribeiro and Filizola). The Traynor group reviewed the role of Regulator of G Protein Signaling (RGS) proteins in regulating MOR activation, including the use of novel inhibitors to produce opioid-sparing or enhancement of endogenous opioid activity (Senese et al.). Lastly, the Veldhuis group reviewed exciting recent advances in separating membrane from internalized receptor signaling, how internalized signaling contributes to pain states, and how these disparate signaling states can be targeted by location-biased drugs (Retamal et al.).

The next major theme consisted of targeting other anti-nociceptive receptor systems to achieve pain relief without the side effects of MOR stimulation, particularly addiction, and respiratory depression. The Massotte group used elegant peripherally-restricted knockout of the delta opioid receptor (DOR) to demonstrate that the β2-adrenergic agonist formoterol produced efficacious

Edited and reviewed by:
Jochen C. Meier, Technische Universitat Braunschweig, Germany

***Correspondence:**
Tally M. Largent-Milnes
tlargent@arizona.edu
Meritxell Canals
m.canals@nottingham.ac.uk
John M. Streicher
jstreicher@arizona.edu

Received: *03 November 2020*
Accepted: *23 November 2020*
Published: *11 December 2020*

Citation:
Largent-Milnes TM, Canals M and Streicher JM (2020) Editorial: Novel Molecular Targets for the Treatment of Pain. Front. Mol. Neurosci. 13:625714. doi: 10.3389/fnmol.2020.625714

anti-nociception in a neuropathic pain model via peripheral DOR (Ceredig et al.). This finding suggests that formoterol could be re-purposed from its current use as an adrenergic agonist as a novel non-opioid analgesic. The DOR has been a target of great interest for some time due to its ability to produce anti-nociception without addiction or respiratory depression, especially in inflammatory pain states. An overview of the DOR in pain and how it can be targeted in the future was written by the Gendron group, with a special emphasis on DOR intracellular trafficking, which strongly impacts receptor competency to relieve pain (Quirion et al.). The DOR has been implicated in other uses as well, such as the treatment of migraine pain (Charles and Pradhan, 2016).

Another alternate receptor system of interest is the cannabinoid receptor type-1 (CB_1R). The CB_1R can also produce anti-nociception, and while it can have unwanted psychoactive side effects, these side effects do not rise to the severity of addiction and respiratory depression caused by opioids (Rabgay et al., 2020). The CB_1R is also the main target of the phytocannabinoid Δ9-tetrahydrocannabinol from the plant *Cannabis sativa*, and is thus of great interest considering the growth in recreational and medicinal marijuana (Morales et al., 2017). A study in this collection from the Laprairie group found that the non-steroidal anti-inflammatory drug indomethacin acts as a positive allosteric modulator of the CB_1R (Laprairie et al.). This finding establishes a new CB_1R drug scaffold for the creation of novel therapeutics.

The third theme of our collection is inflammatory regulation, which can contribute to both pain and the side effects of opioid drugs (Okun et al., 2011; Pan et al., 2016). Original research from the Schmidt group showed that granulocyte-colony stimulating factor (G-CSF) induced the recruitment of Ly6G positive neutrophils to the site of oral cancer, which released endogenous opioids to prevent or block oral cancer pain (Scheff et al.). This suggests that G-CSF could be used as a novel therapeutic for oral cancers. Work from the Jang-Hern Lee group showed that interleukin-1β was released in the early stages of spinal cord neuropathic pain to repress P450c17 expression and slow the development of neuropathic pain (Choi et al.), suggesting that enhancing activity of this pathway could slow or prevent the development of neuropathy. Lastly, the Laumet group provided a comprehensive review of the role of T cells in pain, including in the transition to chronic pain and resolution of pain, suggesting new ways to manipulate these cells to improve different pain states (Laumet et al.).

The last theme of our collection is higher level organization of proteins that contribute to pain and anti-nociception. The Baumbauer group provided original research showing that Tissue Inhibitor of Metalloproteinases-1 (TIMP-1) attenuates the development of inflammatory pain, by preventing the tissue remodeling performed by metalloproteinases (Knight et al.). This work suggests that new approaches to block MMP activity could block the development of pain states. The Streicher group also provided original research showing that the Heat shock protein 90 (Hsp90) isoform Hsp90α and the co-chaperones p23 and Cdc37 promote opioid anti-nociception in the brain (Lei et al.), highlighting the potential of isoform-selective Hsp90 inhibitors to improve opioid therapy.

Together, this collection highlights exciting new advances in the pain field using molecular neuropharmacology. The work of decades has made it clear that no one "silver bullet" is the key to solving the problem of the chronic pain and opioid crises. Multiple novel approaches from multiple angles, including the novel targets highlighted here, will be needed to construct a comprehensive and multi-targeted solution for these challenges and assist the most patients possible. Any of the targets highlighted in this collection could be exploited to create new therapeutics. Our goal is for this collection to contribute to that conversation, progress, and clinical advance to the benefit of society.

AUTHOR CONTRIBUTIONS

All authors contributed equally to the writing and editing of the manuscript.

REFERENCES

Breivik, H., Cherny, N., Collett, B., De Conno, F., Filbet, M., Foubert, A. J., et al. (2009). Cancer-related pain: a pan-European survey of prevalence, treatment, and patient attitudes. *Ann. Oncol.* 20, 1420–1433. doi: 10.1093/annonc/mdp001

Charles, A., and Pradhan, A. A. (2016). Delta-opioid receptors as targets for migraine therapy. *Curr. Opin. Neurol.* 29, 314–319. doi: 10.1097/WCO.0000000000000311

Gaskin, D. J., and Richard, P. (2012). The economic costs of pain in the United States. *J. Pain* 13, 715–724. doi: 10.1016/j.jpain.2012.03.009

Lozano, R., Naghavi, M., Foreman, K., Lim, S., Shibuya, K., Aboyans, V., et al. (2012). Global and regional mortality from 235 causes of death for 20 age groups in 1990 and 2010: a systematic analysis for the Global Burden of Disease Study 2010. *Lancet* 380, 2095–2128. doi: 10.1016/S0140-6736(12)61728-0

Matthes, H. W., Maldonado, R., Simonin, F., Valverde, O., Slowe, S., Kitchen, I., et al. (1996). Loss of morphine-induced analgesia, reward effect and withdrawal symptoms in mice lacking the mu-opioid-receptor gene. *Nature* 383, 819–823. doi: 10.1038/383819a0

Morales, P., Hurst, D. P., and Reggio, P. H. (2017). Molecular targets of the phytocannabinoids: a complex picture. *Prog. Chem. Org. Nat. Prod.* 103, 103–131. doi: 10.1007/978-3-319-45541-9_4

Okun, A., Defelice, M., Eyde, N., Ren, J., Mercado, R., King, T., et al. (2011). Transient inflammation-induced ongoing pain is driven by TRPV1 sensitive afferents. *Mol. Pain* 7:4. doi: 10.1186/1744-8069-7-4

Olson, K. M., Duron, D. I., Womer, D., Fell, R., and Streicher, J. M. (2019). Comprehensive molecular pharmacology screening reveals potential new receptor interactions for clinically relevant opioids. *PLoS ONE* 14:e0217371. doi: 10.1371/journal.pone.0217371

Olson, K. M., Lei, W., Keresztes, A., Lavigne, J., and Streicher, J. M. (2017). Novel molecular strategies and targets for opioid drug discovery for the treatment of chronic pain. *Yale J. Biol. Med.* 90, 97–110.

Pan, Y., Sun, X., Jiang, L., Hu, L., Kong, H., Han, Y., et al. (2016). Metformin reduces morphine tolerance by inhibiting microglial-mediated neuroinflammation. *J. Neuroinflammation* 13:294. doi: 10.1186/s12974-016-0754-9

Rabgay, K., Waranuch, N., Chaiyakunapruk, N., Sawangjit, R., Ingkaninan, K., and Dilokthornsakul, P. (2020). The effects of cannabis, cannabinoids, and

their administration routes on pain control efficacy and safety: a systematic review and network meta-analysis. *J. Am. Pharm. Assoc. 60*, 225.e6–234.e6. doi: 10.1016/j.japh.2019.07.015

Warner, M., Trinidad, J. P., Bastian, B. A., Minino, A. M., and Hedegaard, H. (2016). Drugs most frequently involved in drug overdose deaths: United States, 2010-2014. *Natl. Vital. Stat. Rep.* 65, 1–15.

Woodcock, J., Witter, J., and Dionne, R. A. (2007). Stimulating the development of mechanism-based, individualized pain therapies. *Nat. Rev. Drug Discov.* 6, 703–710. doi: 10.1038/nrd 2335

Conflict of Interest: The authors declare that the research was conducted in the absence of any commercial or financial relationships that could be construed as a potential conflict of interest.

frontiers in Molecular Neuroscience

ORIGINAL RESEARCH
published: 01 May 2019
doi: 10.3389/fnmol.2019.00104

GRK Mediates μ-Opioid Receptor Plasma Membrane Reorganization

Arisbel B. Gondin[1,2,3], Michelle L. Halls[1], Meritxell Canals[1,2,3] and Stephen J. Briddon[2,3]**

[1] Drug Discovery Biology Theme, Monash Institute of Pharmaceutical Sciences, Monash University, Melbourne, VIC, Australia, [2] Division of Physiology, Pharmacology and Neuroscience, School of Life Sciences, Queen's Medical Centre, University of Nottingham, Nottingham, United Kingdom, [3] Centre of Membrane Proteins and Receptors, Universities of Birmingham and Nottingham, The Midlands, United Kingdom

Differential regulation of the μ-opioid receptor (MOP) has been linked to the development of opioid tolerance and dependence which both limit the clinical use of opioid analgesics. At a cellular level, MOP regulation occurs via receptor phosphorylation, desensitization, plasma membrane redistribution, and internalization. Here, we used fluorescence correlation spectroscopy (FCS) and fluorescence recovery after photobleaching (FRAP) to detect and quantify ligand-dependent changes in the plasma membrane organization of MOP expressed in human embryonic kidney (HEK293) cells. The low internalizing agonist morphine and the antagonist naloxone did not alter constitutive MOP plasma membrane organization. In contrast, the internalizing agonist DAMGO changed MOP plasma membrane organization in a pertussis toxin-insensitive manner and by two mechanisms. Firstly, it slowed MOP diffusion in a manner that was independent of internalization but dependent on GRK2/3. Secondly, DAMGO reduced the surface receptor number and the proportion of mobile receptors, and increased receptor clustering in a manner that was dependent on clathrin-mediated endocytosis. Overall, these results suggest the existence of distinct sequential MOP reorganization events at the plasma membrane and provide insights into the specific protein interactions that control MOP plasma membrane organization.

Keywords: G protein-coupled receptor, μ-opioid receptor, G protein-coupled receptor kinase, plasma membrane, fluorescence correlation spectroscopy, fluorescence recovery after photobleaching

OPEN ACCESS

Edited by:
Sung Jun Jung,
Hanyang University, South Korea

Reviewed by:
Seksiri Arttamangkul,
Oregon Health and Science University, United States
Michael M. Morgan,
Washington State University Vancouver, United States

****Correspondence:***
Meritxell Canals
Meritxell.canals@nottingham.ac.uk
Stephen J. Briddon
stephen.briddon@nottingham.ac.uk

Received: *14 February 2019*
Accepted: *08 April 2019*
Published: *01 May 2019*

Citation:
Gondin AB, Halls ML, Canals M and Briddon SJ (2019) GRK Mediates μ-Opioid Receptor Plasma Membrane Reorganization. Front. Mol. Neurosci. 12:104. doi: 10.3389/fnmol.2019.00104

Summary Statement

G protein-coupled receptor kinase modulates μ-opioid receptor micro-diffusion at the plasma membrane prior to internalization.

INTRODUCTION

The μ-opioid receptor (MOP) is the GPCR that mediates the analgesic effects of opioids such as morphine, fentanyl, and codeine. Despite being the mainstay analgesics for the treatment of acute pain, prolonged opioid use in inflammatory and chronic pain is severely limited by on-target adverse effects including tolerance and dependence. Furthermore, opioid prescription, abuse and overdose deaths have reached record levels globally (Rudd et al., 2016;

Abbreviations: AC, autocorrelation; ANOVA, analysis of variance; DAMGO, (D-Ala^2,N-Me-Phe^4,Gly^5-ol)-enkephalin; FCS, fluorescence correlation spectroscopy; FRAP, fluorescence recovery after photobleaching; GPCR, G protein-coupled receptor; GRK, GPCR kinase; HEK, human embryonic kidney; MOP, μ-opioid receptor; PCH, photon counting histogram; PTx, pertussis toxin.

Floyd and Warren, 2018), and the development of safer and more effective analgesics remains an unmet medical challenge. Differential regulation of MOP by morphine compared to other synthetic opioids or opioid peptides, has been linked to its increased propensity for tolerance and dependence (Duttaroy and Yoburn, 1995; Morgan and Christie, 2011; Williams et al., 2013); a better understanding of the molecular mechanisms governing MOP regulation is an important step in improving the therapeutic profiles of opioid analgesics.

As with other GPCRs, MOP-mediated signaling is initiated at the plasma membrane via protein–protein interactions between the receptor and its effectors. More recently, compartmentalization of GPCRs and their effectors within distinct subcellular locations or micro-domains of the plasma membrane has been shown to play a key role in their signaling (Sungkaworn et al., 2017; Eichel et al., 2018; Yanagawa et al., 2018). The concept that this may dictate specific cellular responses is particularly relevant in the context of MOP signaling, since MOP activation by different agonists results in distinct regulation and downstream signaling responses. For instance, the peptide agonist DAMGO causes multi-site phosphorylation of the receptor mediated by GRK2/3, inducing robust β-arrestin recruitment, and internalization. In contrast, the alkaloid agonist morphine causes limited receptor phosphorylation, and weak internalization (Doll et al., 2011; Lau et al., 2011; Just et al., 2013; Miess et al., 2018). MOP has been demonstrated to partition into lipid rafts and the dynamics of MOP diffusion at the plasma membrane contribute to the specific signaling responses elicited by different opioid ligands (Huang et al., 2007; Gaibelet et al., 2008; Zheng et al., 2008). For instance, the distribution of opioid receptors, including the MOP, into different nanoscale plasma membrane domains has been shown to be influenced by cholesterol (Rogacki et al., 2018), and MOP mobility, surface density, and the dynamics of plasma membrane lipids is affected by ethanol (Vukojevic et al., 2008b). Lateral mobility of MOP and MOP-G protein coupling is also changed differentially by the activating agonist (Sauliere-Nzeh Ndong et al., 2010) in a manner depending on the membrane cholesterol content (Melkes et al., 2016). Together, these studies suggest a link between distinct functional states of MOP and the dynamic organization of receptors within the plasma membrane. In addition, we have previously reported that DAMGO and morphine elicit different spatiotemporal signaling profiles, and that these are dictated by the lateral redistribution of MOP within the plasma membrane, rather than internalization (Halls et al., 2016). However, these previous studies lacked the temporal resolution required to investigate rapid diffusion changes of the receptor at the cell surface.

Live cell imaging techniques such as FCS and FRAP can provide greater temporal resolution to determine ligand-mediated changes in MOP dynamics and organization at the membrane. FCS is a highly sensitive confocal technique that can be used to quantify the diffusion and number of fluorescent species in small areas of living cells (Diekmann and Hoischen, 2014; Briddon et al., 2018). In FCS, fluorescent particles are excited as they pass through a small, defined confocal volume (∼0.2 fL) leading to time-dependent fluctuations in the detected fluorescence intensity; statistical analysis of these fluctuations using AC or PCH analysis allows the concentration and diffusion of fluorescent proteins to be determined in a small defined area (∼0.2 μm^2) of the plasma membrane. FRAP can be used in conjunction with FCS to measure diffusion properties over a larger membrane area and give an indication of the proportion of mobile and immobile proteins (Haustein and Schwille, 2004; Pucadyil et al., 2007).

Here, we investigate the effect of different ligands on the organization and dynamics of MOP at the plasma membrane. Using FCS we quantify changes in the movement (diffusion coefficient; D_{FCS}), number (particle number; N), and clustering (molecular brightness; ε) of a fluorescently labeled SNAP-tagged MOP within small micro-domains of the membrane. Additionally, we use FRAP to determine the diffusion coefficient (D_{FRAP}) and proportion of mobile (MF) receptors over a larger membrane area. We show that the internalizing agonist DAMGO slowed MOP diffusion in a time- and concentration-dependent manner, increased receptor clustering and the proportion of immobile MOP and reduced surface receptor number in a PTx -insensitive manner. These effects were not observed with the antagonist naloxone or the low internalizing agonist morphine. Notably, we were able to delineate the decrease in lateral mobility of MOP in response to DAMGO, which was dependent on GRK2/3 activity, from the clustering and decrease in MOP receptor number, which was dependent on clathrin-dependent endocytosis. These data provide insight into the role of GRKs as agonist-specific regulators of MOP micro-diffusion.

RESULTS

Basal Plasma Membrane Organization of SNAP-MOP Detected by FCS and FRAP

To study the organization of MOP within living cell membranes, we performed FCS measurements on HEK293 cells stably expressing N-terminally SNAP-tagged human MOP (SNAP-MOP). Addition of the SNAP-tag at the N-terminus of the MOP did not alter its function, as shown by the ability of both DAMGO and morphine to inhibit forskolin-induced cAMP production in a similar way to the FLAG-tagged MOP (pEC_{50}s: DAMGO = 7.67 ± 0.26 and 8.11 ± 0.08; morphine = 7.79 ± 0.31 and 7.92 ± 0.32 FLAG-MOP and SNAP-MOP, respectively, n = 4; **Supplementary Figures 1A,B**). Use of a SNAP-MOP fusion allowed specific labeling of cell surface MOP using a cell membrane impermeable SNAP-Surface® 488 (BG-488) dye that specifically and covalently binds to SNAP-tagged proteins present at the cell surface.

Fluorescence correlation spectroscopy measurements were performed on SNAP-MOP cells by positioning the confocal volume in *x-y* over the cell cytoplasm, and subsequently on the upper membrane at the peak intensity of a *z* scan (**Figure 1A**). FCS fluorescence fluctuation traces were recorded for 30s. The AC analysis yielded a two-component curve, consisting of a fast-diffusing component (τ_{D1}; 10–15% of amplitude) indicative of residual free SNAP label with the remainder a slow component (τ_{D2}) representing diffusion of the SNAP-MOP (see section "Materials and Methods"). The

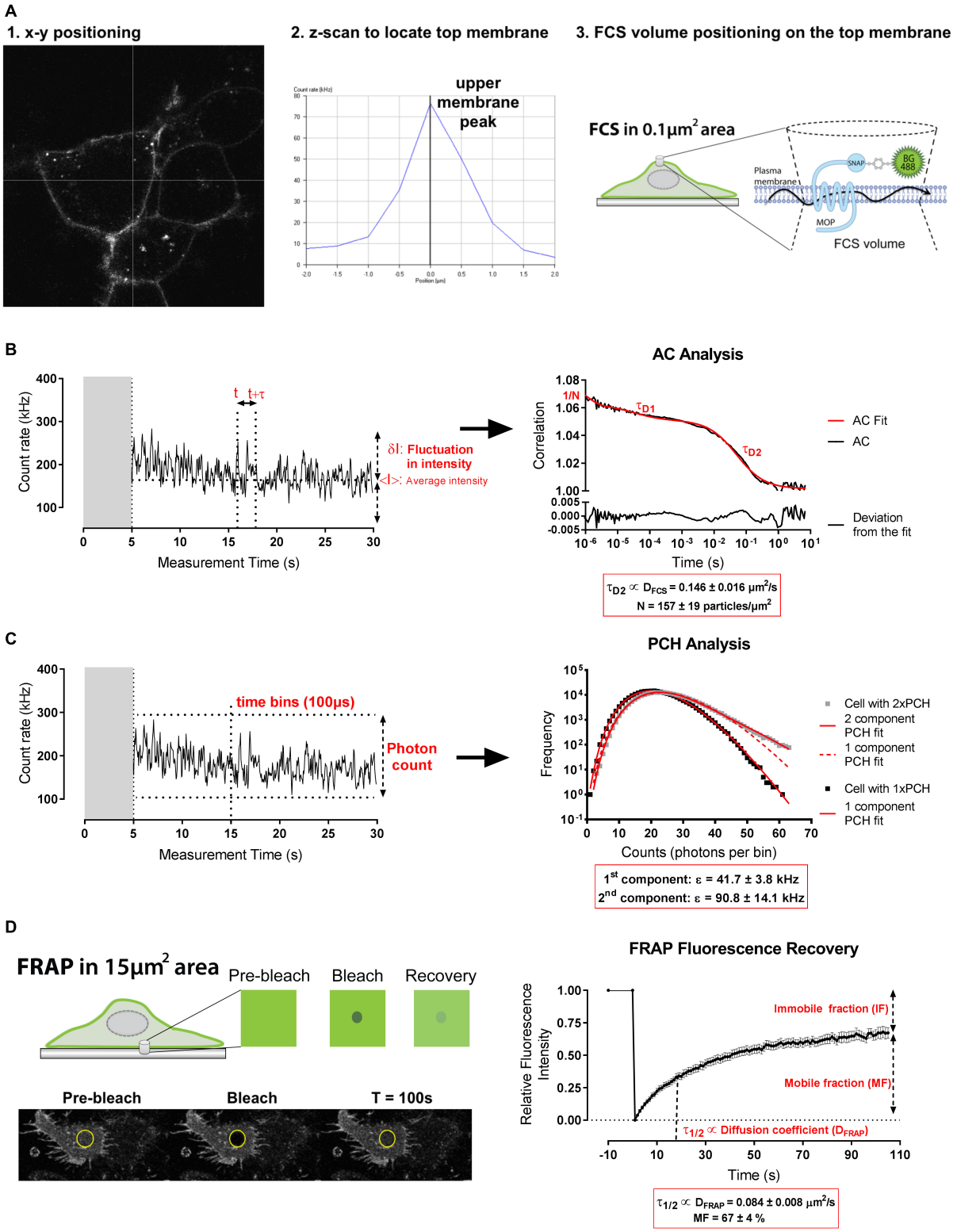

FIGURE 1 | Basal plasma membrane organization of MOP detected by FCS and FRAP. **(A)** FCS measurement volume was positioned on the upper membrane using a live confocal image (1) and an intensity scan in z (2). (3) Schematic representation of FCS measurements on the membrane of HEK293 SNAP-MOP cells labeled with SNAP-Surface 488 (BG-488) dye. **(B)** Representative fluctuation trace in basal conditions for autocorrelation (AC) analysis in which fluctuations in intensity (δI) from the intensity mean (<I>) are calculated at two time points (t and t+τ) for all t and a range of τ values to generate an AC function that provides the

(Continued)

FIGURE 1 | Continued
average dwell time (τ_D) and particle number (N). τ_{D1} represents the average dwell time of free BG-488 and was set to 32 μs; τ_{D2} represents the average dwell time of BG-488 bound to SNAP-MOP from which the receptor diffusion coefficient (D_{FCS}; $\mu m^2/s$) was calculated. N represents the number of particles and was used to calculate surface particle concentration ($N/\mu m^2$). **(C)** Representative fluctuation trace in basal conditions and subsequent PCH analysis in which the amplitude of the fluctuations can be analyzed by quantifying the photons in defined time bins (100 μs). Super-Poissonian statistical analysis of the resulting frequency histogram allows the molecular brightness (ε) of SNAP-MOP containing particles to be determined. Two representative cell measurements under basal conditions are shown with the fit (solid red line) to one component (black squares) or two components (gray squares) accordingly. The poor 1 component fit (dotted red line) for the cell trace represented in gray squares is also shown. **(D)** Schematic representation of FRAP method and representative image of a cell in basal conditions during the bleaching protocol. Fluorescence recovery average trace of SNAP-MOP in basal conditions that provides a half-time ($\tau_{1/2}$) from which the diffusion coefficient (D_{FRAP}; $\mu m^2/s$), and mobile and immobile fractions (MF and IF, respectively) are inferred.

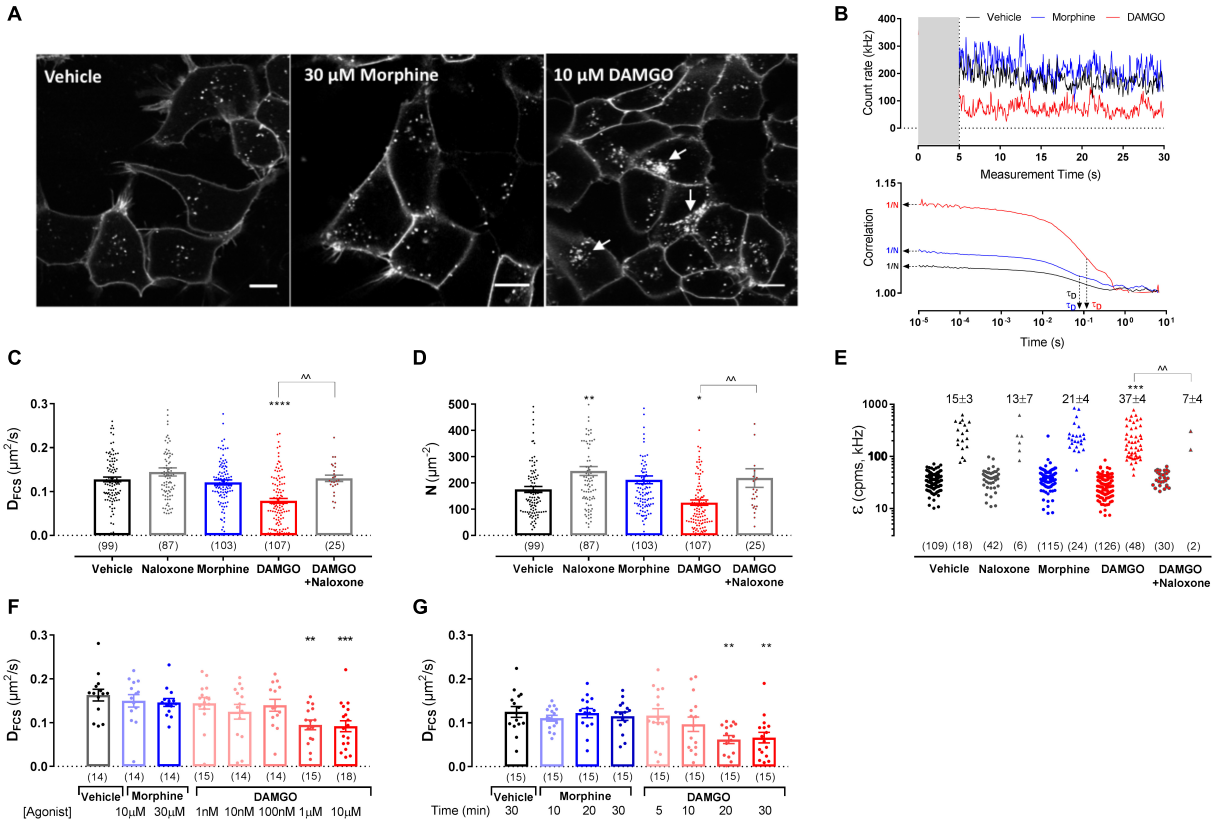

FIGURE 2 | Fluorescence correlation spectroscopy measurements in HEK293 SNAP-MOP cells following ligand stimulation. **(A)** Representative images from HEK293 SNAP-MOP cells labeled with SNAP-Surface 488 (BG-488) dye after stimulation with vehicle, 30 μM morphine or 10 μM DAMGO for 20 min. Scale bar 10 μm; arrows represent agonist-induced internalization. **(B)** Representative FCS traces from single HEK293 SNAP-MOP cells after stimulation with vehicle, 30 μM morphine, or 10 μM DAMGO for 20 min (gray area indicates the initial 5 s of data that were removed, see section "Materials and Methods"), and their corresponding AC fit indicating N and τ_D of SNAP-MOP. **(C)** Diffusion coefficient of SNAP-MOP upon stimulation with 30 μM naloxone, 30 μM morphine, 10 μM DAMGO (20 min, 37°C), or 10 μM DAMGO after pre-treatment with 30 μM naloxone (30 min, 37°C) (n = 25–107 cells from 5 to 23 independent experiments; one-way ANOVA, F(df1,df2): $F(4,416) = 15.04$, $P < 0.0001$). **(D)** Particle number of SNAP-MOP upon stimulation with 30 μM naloxone, 30 μM morphine, 10 μM DAMGO (20 min, 37°C), or 10 μM DAMGO after pre-treatment with 30 μM naloxone (30 min, 37°C) (n = 25–107 cells from a minimum of 5 independent experiments; $F(4,416) = 11.06$, $P < 0.0001$). **(E)** Molecular brightness of SNAP-MOP after stimulation with 30 μM naloxone, 30 μM morphine, 10 μM DAMGO, or 10 μM DAMGO after pre-treatment with 30 μM naloxone. For each condition, brightness values for the first (left) and second (right) component are shown [n = 30–126 cells from a minimum of 6 independent experiments; $F(4,82) = 5.74$, $P < 0.0001$], with the percentage of cells requiring a two-component fit annotated. **(F)** Diffusion coefficient of SNAP-MOP upon increasing concentration of morphine or DAMGO after 20 min incubation [n = 14–18 cells from 3 independent experiments; $F(7,110) = 4.14$, $P < 0.0001$]. **(G)** Diffusion coefficient of SNAP-MOP upon stimulation with 30 μM morphine or 10 μM DAMGO with increasing time incubation periods [n = 15 from 3 independent experiments; $F(7,113) = 4.36$, $P = 0.0003$]. Each data point on the scatter plots represents a measurement from an individual cell (number of cells in parenthesis) and column plots represent mean ± SEM of the indicated number of cells. * denotes significance vs. vehicle treatment and ^ denotes significance vs. DAMGO control in one-way ANOVA with Sidak's multiple comparisons test (*$P < 0.05$, **$P < 0.01$, ***$P < 0.001$, ****$P < 0.0001$, ^^$P < 0.01$).

average dwell time (τ_{D2}) and particle number (N) of the SNAP-MOP within the detection volume were obtained from the AC curve, from which the diffusion coefficient (D_{FCS}; $\mu m^2/s$), and receptor density ($N/\mu m^2$) were calculated (**Figure 1B** and see section "Materials and Methods"). These measurements showed that under basal conditions, D_{FCS} for the SNAP-MOP was

0.146 ± 0.016 μm^2/s with a receptor density (N) of 157 ± 19 particles/μm^2 (n = 14 cells) (**Figure 1B**). Analysis of the same fluorescence fluctuations using PCH analysis yielded the average molecular brightness (ε; counts per molecule per second, kHz) of the fluorescent species (**Figure 1C** and Materials and Methods), providing an indication of the extent of SNAP-MOP clustering. Under basal conditions PCH analysis of fluctuations from the majority (81%) of cells fitted to a single brightness component with an average ε of 41.7 ± 3.8 kHz (n = 21 cells) (**Figure 1C**). Interestingly, in 19% of the cells analyzed, a second brighter component (average ε = 90.8 ± 14.1 kHz) was detected (**Figure 1C**), indicating the presence of higher-order oligomeric forms of SNAP-MOP in basal conditions. Of note, the brighter component was always less abundant relative to the single component.

In order to ensure that accurate diffusion coefficients were obtained, excitation laser power was optimized to give a maximum signal to noise ratio (highest ε) with minimal spot photobleaching (indicated by no increase in D_{FCS} or decrease in N) (**Supplementary Figure 1C**). On the basis of these data, subsequent experiments used a laser power of ∼0.08 kW/cm^2. FCS measurements were also conducted on cells labeled with a range of BG-488 concentrations that ensured that all of the cell surface receptors had been labeled (saturated N) whilst minimizing the amount of free BG-488 label left after washing. At concentrations of BG-488 above 50 nM, the particle number (N) (**Supplementary Figure 1D**) and molecular brightness (ε) remained constant (**Supplementary Figure 1E**), indicating labeling of all cell surface receptors. On the basis of these data, subsequent experiments used 200 nM BG-488 label. It was also noted that as the concentration of BG-488 label increased, the number of cells that required a second component for the PCH fit also increased (**Supplementary Figure 1E**).

Since FCS only measures mobile receptor population, FRAP was performed over a larger area of the lower cell membrane of adherent cells to determine a macro diffusion coefficient (D_{FRAP}), as well as the proportions of mobile (MF) and immobile (IF) receptors (**Figure 1D**). Using a circular bleach area with radius of 2.2 μm (area ∼ 15 μm^2), FRAP measurements showed that under basal conditions 67 ± 4% of the receptor population is mobile over this area with a diffusion rate (D_{FRAP}) of 0.084 ± 0.008 μm^2/s which was slower than that measured for FCS (D_{FCS}).

Ligand-Induced Changes in the Plasma Membrane Organization of SNAP-MOP

The effect of ligand stimulation on SNAP-MOP membrane organization was then assessed using FCS and FRAP. Substantial fluorescence remained at the plasma membrane after stimulation with saturating concentrations of the poorly internalizing agonist morphine (30 μM) or the internalizing agonist DAMGO (10 μM) for 20 min (**Figure 2A**). This is not surprising since we have previously shown that DAMGO-induced internalization reached a maximum 1 h after agonist stimulation (Halls et al., 2016; Miess et al., 2018). We then recorded FCS fluctuation traces of SNAP-MOP following exposure to each ligand and performed AC and PCH analysis (**Figure 2B**). Stimulation with DAMGO (10 μM) caused a significant decrease in MOP diffusion co-efficient (D_{FCS}) (P < 0.0001, ANOVA and *post hoc* Sidak's test; n numbers

TABLE 1 | Diffusion coefficient (D_{FCS}), particle concentration (N) and clustering measured by FCS and diffusion coefficient (D_{FRAP}) and immobile fraction (IF) measured by FRAP of SNAP-MOP expressing cells under different treatment conditions.

Treatment conditions		FCS			FRAP	
		D_{FCS} (μm^2/s)	N (particles/μm^2)	Clustering (% cells)	D_{FRAP} (μm^2/s)	IF (%)
Control	Vehicle	0.128 ± 0.005	175 ± 11	15 ± 3	0.084 ± 0.008	34 ± 3
	Naloxone	0.145 ± 0.009	245 ± 17**	13 ± 7	0.089 ± 0.007	33 ± 2
	Morphine	0.121 ± 0.006	212 ± 15	21 ± 4	0.079 ± 0.005	33 ± 3
	DAMGO	0.079 ± 0.006§	125 ± 10*	37 ± 4***	0.080 ± 0.007	52 ± 4§
	DAMGO + Naloxone	0.130 ± 0.007^^	219 ± 35^^	7 ± 4^^	*ND*	*ND*
PTx	Vehicle	0.132 ± 0.012	155 ± 23	20 ± 0	*ND*	*ND*
	Naloxone	0.127 ± 0.013	241 ± 25	0 ± 0	*ND*	*ND*
	Morphine	0.122 ± 0.006	236 ± 20	0 ± 0	*ND*	*ND*
	DAMGO	0.093 ± 0.010#	170 ± 18	30 ± 13	*ND*	*ND*
Pitstop2	Vehicle	0.129 ± 0.012	112 ± 9	15 ± 6	0.105 ± 0.014	45 ± 4
	Morphine	0.126 ± 0.011	204 ± 19	21 ± 10	0.132 ± 0.027	24 ± 3#
	DAMGO	0.082 ± 0.010#	143 ± 16	21 ± 9	0.113 ± 0.031	48 ± 4
Cmpd101	Vehicle	0.126 ± 0.011	180 ± 19	13 ± 8	0.102 ± 0.013	40 ± 5
	Morphine	0.118 ± 0.010	217 ± 23	11 ± 4	0.085 ± 0.009	28 ± 3
	DAMGO	0.106 ± 0.008	243 ± 26	13 ± 5	0.084 ± 0.012	30 ± 4

**denotes significance vs. vehicle control (*P < 0.05, **P < 0.01, ***P < 0.001, § P < 0.0001) in one-way ANOVA with Sidak's multiple comparisons test. ^^denotes significance vs. DAMGO control (^^P < 0.01) in one-way ANOVA with Sidak's multiple comparisons test. #denotes significance vs. vehicle in the same inhibitor pre-treatment condition (#P < 0.05) in one-way ANOVA with Sidak's multiple comparisons test. ND, not determined. All data are shown as mean ± SEM. For clarity, n numbers (cells and independent experiments) are referred to in the appropriate figures and their legends but are from a minimum of 5 independent experiments.*

and ANOVA parameters given in figure legends for this and all subsequent *P* values) (**Figure 2C** and **Table 1**), a decrease in particle number (N) ($P = 0.032$) (**Figure 2D** and **Table 1**), and DAMGO stimulation increased the percentage of cells with a bright second component in PCH analysis (from 15% in vehicle to 37% in DAMGO-treated cells; $P = 0.0008$), suggesting that DAMGO stimulation induces clustering of SNAP-MOP (**Figure 2E** and **Table 1**). These changes were mediated by receptor activation, since they were not present in cells which were pre-treated with the MOP antagonist naloxone (10 μM) ($P = 0.001$, 0.008, and 0.004 for differences in D_{FCS}, N and clustering in presence and absence of naloxone, respectively). The slowing in diffusion caused by DAMGO was concentration- (**Figure 2F**) and time-dependent (**Figure 2G**), with a significant decrease in D_{FCS} seen at concentrations of 1 μM and above ($P = 0.003$), which is consistent with DAMGO's potency for recruitment of regulatory proteins (Miess et al., 2018), and after 20 min of stimulation, which is prior to internalization (Miess et al., 2018).

In contrast to DAMGO, stimulation with morphine (up to 30 μM) or naloxone alone (30 μM) did not cause any significant changes in D_{FCS} or clustering compared to vehicle treatment (P = 0.91 and 0.24, respectively; **Figures 2C–G**), indicating that changes in MOP plasma membrane organization are agonist-specific. Interestingly, incubation with naloxone alone significantly increased the particle number (N) compared to vehicle treatment ($P = 0.002$) (**Figure 2D**). This increase might indicate that naloxone prevents constitutive MOP internalization observed in vehicle (**Figure 2A**), resulting in an increase in surface receptor number.

Since FCS can only determine the properties of mobile receptors, we also used FRAP to assess whether ligand stimulation changes the proportion of mobile vs. immobile receptors (**Figure 3A**). Following exposure of cells to 10 μM DAMGO, the immobile fraction (IF) of MOP was significantly increased from 34 ± 3% in vehicle-treated cells to 52 ± 4% in DAMGO-treated conditions ($P < 0.0001$) (**Figure 3B**). In contrast, treatment with morphine or naloxone caused no change in mobile fraction compared to vehicle ($P = 0.99$ and 0.99, respectively). Contrary to the decrease in D_{FCS} induced by DAMGO, D_{FRAP} remained unchanged upon stimulation with any of the ligands (**Figure 3C**).

These data therefore suggest ligand-specific changes in MOP membrane organization, with DAMGO stimulation slowing MOP diffusion, reducing surface receptor number, increasing receptor clustering, and the proportion of immobile receptors. While these effects were reversed with naloxone, none of these changes were observed following stimulation with morphine.

MOP Membrane Reorganization Is Independent of $G_{i/o}$ Protein Activation

The dependence of MOP reorganization on G protein activation was then investigated using PTx as a $G\alpha_{i/o}$ inhibitor (100 ng/ml, overnight treatment). Consistent with previous data (Halls et al., 2016), inhibition of $G\alpha_{i/o}$ activation did not prevent DAMGO-induced MOP internalization (**Figure 4A**) at a PTx concentration that was effective at preventing agonist-induced adenylyl cyclase inhibition (**Figure 4B**). However, PTx treatment did not affect DAMGO-induced clustering (**Figure 4C** and **Table 1**) or slowing in diffusion (**Figure 4D** and **Table 1**). Altogether, these data suggest that G protein activation is not necessary for the changes in MOP membrane organization induced by DAMGO.

Effect of Internalization Inhibition on Ligand-Induced Changes in MOP Organization

To investigate whether the DAMGO-mediated changes in MOP organization were dependent on MOP internalization, we used an inhibitor of clathrin-dependent internalization, Pitstop2 (30 μM, 30 min pre-treatment), which has previously been shown to block DAMGO-induced MOP endocytosis (Halls et al., 2016). In FCS experiments, Pitstop2 prevented DAMGO-induced receptor clustering as shown by the reduction in the percentage of cells that showed the second brighter PCH component in the presence of the inhibitor ($P = 0.944$ DAMGO/Pitstop2 vs. Pitstop2 alone) (**Figure 5A**). There was also no DAMGO-mediated increase in immobile fraction detected using FRAP in the presence of Pitstop2 ($P = 0.95$) (**Table 1**). However, inhibiting internalization did not significantly affect the DAMGO-induced slowing in diffusion measured by FCS ($P = 0.028$ DAMGO/Pitstop2 vs. Pitstop2 alone) (**Figure 5B** and **Table 1**). Altogether, these data suggest that MOP diffuses laterally at the plasma membrane, clustering and immobilizing in clathrin-coated pits prior to internalization. Some MOP organization events such as clustering are dependent on clathrin-mediated endocytosis. However, Pitstop2 was not able to prevent the DAMGO-induced decrease in D_{FCS}, highlighting that a different molecular mechanism must be underlying this micro-diffusion event.

Effect of GRK Inhibition on Ligand-Induced Changes in MOP Organization

We then investigated a potential role for GRKs in MOP reorganization since interaction with and phosphorylation by these kinases occurs rapidly after receptor activation, prior to internalization and in an agonist-dependent manner (Miess et al., 2018). As expected from an event that precedes internalization, inhibition of GRK2/3 with Cmpd101 (30 μM, 30 min pre-treatment) prevented DAMGO-induced clustering measured with FCS ($P = 0.003$ DAMGO vs. DAMGO/Cmpd101; $P > 0.999$ DAMGO/Cmpd101 vs. Cmpd101 alone; **Figure 5C** and **Table 1**) and the increase in immobile fraction detected by FRAP ($P = 0.442$; **Table 1**). Remarkably, and unlike PitStop2, Cmpd101 also prevented the DAMGO-induced slowing as measured by decrease in D_{FCS} ($P = 0.550$ DAMGO/Cmpd101 vs. Cmpd101 alone; **Figure 5D** and **Table 1**). Cmpd101 treatment significantly reduced GRK2-Venus recruitment to FLAG-MOP-NLuc (**Figure 5E**) and phosphorylation at one of the key C-terminal phosphorylation residues

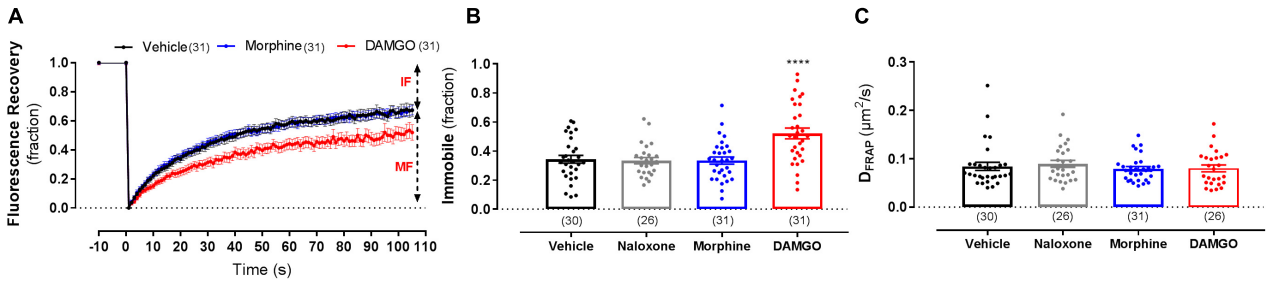

FIGURE 3 | Fluorescence recovery after photobleaching measurements on the lower membrane of HEK293 SNAP-MOP cells following ligand stimulation. **(A)** Fluorescence recovery curves of HEK293 SNAP-MOP cells during FRAP experiments under control conditions and following stimulation with 30 μM morphine or 10 μM DAMGO for 20 min at 37°C (n = 26–31 from 6 independent experiments). MF, mobile fraction and IF, immobile fraction. **(B)** Immobile fraction and **(C)** diffusion coefficient of SNAP-MOP as determined by FRAP (D_{FRAP}) analysis following stimulation with 30 μM naloxone, 30 μM morphine or 10 μM DAMGO (n = 26–31 from 6 independent experiments; one-way ANOVA, F(df1,df2): $F(3,114) = 10.48$, $P < 0.0001$). Each data point of the scatter plots represents an individual cell measurement (number of cells in parenthesis) and column plots represent mean ± SEM of the indicated number of cells. * denotes significance vs. vehicle treatment in one-way ANOVA with Sidak's multiple comparisons test (****$p < 0.0001$).

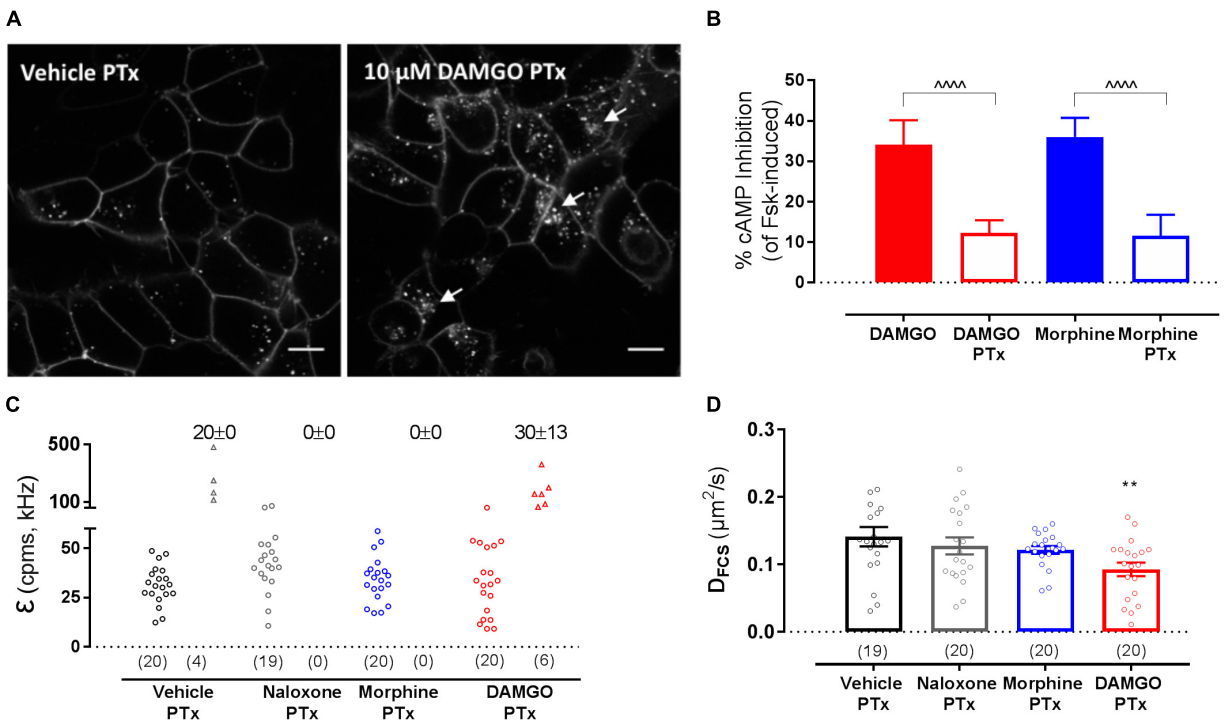

FIGURE 4 | Effect of pertussis toxin (PTx) pre-treatment on SNAP-MOP function and membrane organization. HEK293 SNAP-MOP cells were exposed to PTx (100 ng/ml overnight, 37°C). **(A)** Representative images of PTx pre-treated HEK293 SNAP-MOP cells after stimulation with vehicle or 10 μM DAMGO. Scale bar 10 μm, arrows represent agonist-induced internalization. **(B)** Agonist-mediated inhibition of forskolin-induced cAMP accumulation upon stimulation with 10 μM DAMGO or 10 μM morphine in control (closed bars) or PTx pre-treated cells (open bars) in a CAMYEL BRET assay. Data are shown as percentage of inhibition of cAMP induced by 10 μM forskolin and represent mean ± SEM of 3 independent experiments (one-way ANOVA, F(df1,df2): $F(3,12) = 30.17$, $P < 0.0001$). ^ denotes significance vs. DAMGO or morphine in the untreated condition (^^^^$P < 0.0001$) with Sidak's multiple comparisons test. **(C)** Molecular brightness [$F(3,12) = 5.4$, $P = 0.014$] and **(D)** diffusion coefficients from FCS measurements of SNAP-MOP after stimulation with 30 μM naloxone, 30 μM morphine or 10 μM DAMGO in PTx pre-treated cells (n = 19–20 cells from 4 independent experiments, $F(7,132) = 4.59$, $P = 0.0001$). For each condition, brightness values for the first (left) and second (right) component are shown, with the number of cells requiring a two-component fit indicated as percentage. Each data point on the scatter plots represents a measurement from an individual cell (number of cells in parenthesis) and column plots represent mean ± SEM of the indicated number of cells. * denotes significance vs. vehicle treatment in one-way ANOVA with Sidak's multiple comparisons test (**$P < 0.01$).

S375 (**Figure 5F**), indicating that Cmpd101 prevents both recruitment and subsequent activity of GRK2 at the MOP. These data suggest the existence of a GRK-dependent mechanism (scaffolding or phosphorylation), which results in the DAMGO-stimulated slowing in diffusion and precedes receptor clustering and internalization.

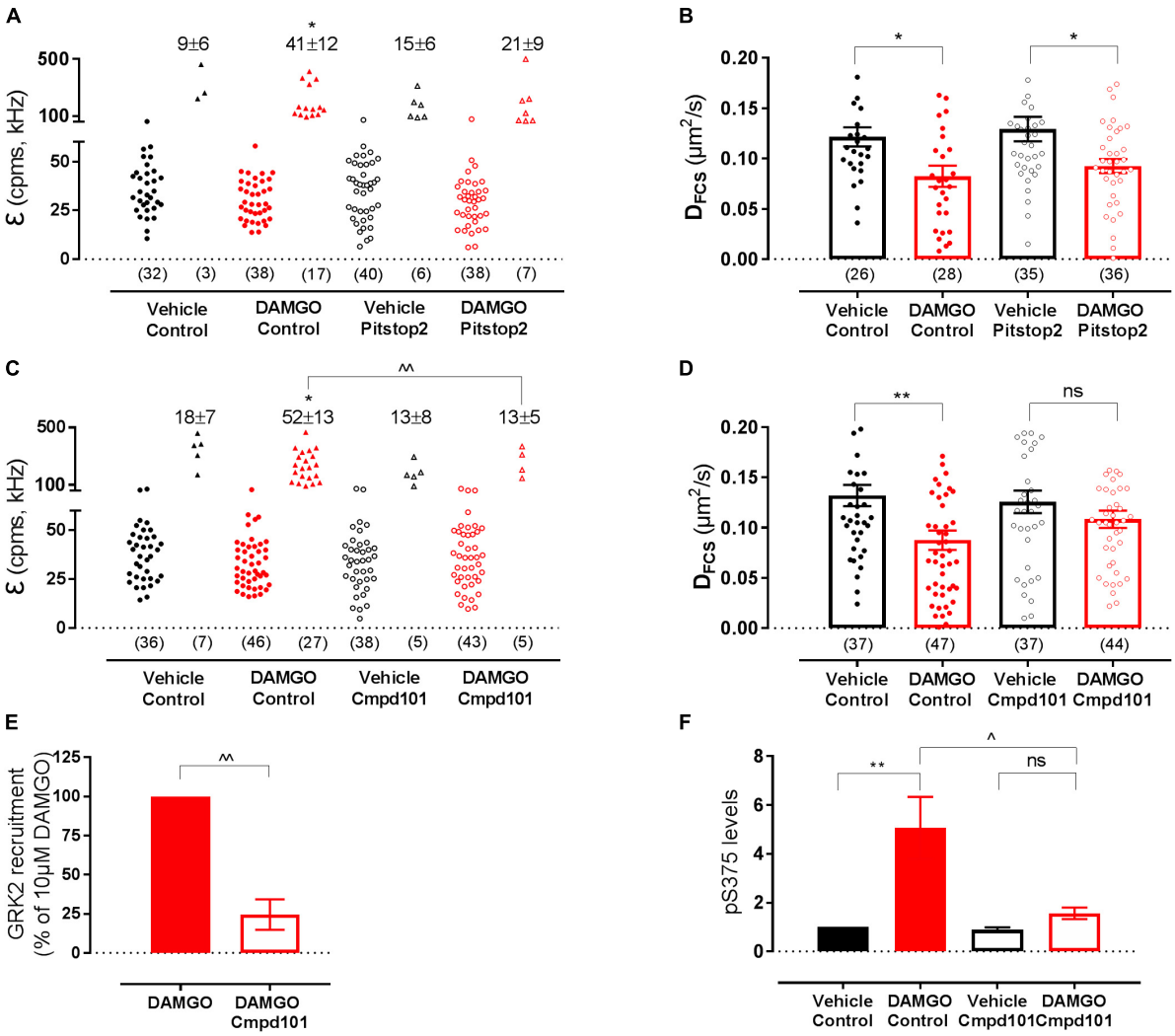

FIGURE 5 | Effect of internalization inhibitor Pitstop2 and GRK2/3 inhibitor Cmpd101 on SNAP-MOP membrane organization. HEK293 SNAP-MOP cells were exposed to the internalization inhibitor Pitstop2 (30 μM, 30 min, 37°C) or GRK2/3 inhibitor Cmpd101 (30 μM, 30 min, 37°C). **(A)** Molecular brightness of SNAP-MOP after stimulation with vehicle or 10 μM DAMGO in control or Pitstop2 pre-treated cells [n = 32–40 cells from 6 to 8 independent experiments, one-way ANOVA, F(df1,df2): F(3,26) 2.67, P = 0.060]. **(B)** Diffusion coefficient of SNAP-MOP upon stimulation with vehicle or 10 μM DAMGO in control or Pitstop2 pre-treated cells [n = 26–36 from 6 to 8 independent experiments, F(3,121) = 5.00, P = 0.003]. **(C)** Molecular brightness of SNAP-MOP after stimulation with vehicle or 10 μM DAMGO in control or Cmpd101 pre-treated cells [n = 36–46 cells from 6 to 8 independent experiments, F(3,28) = 4.86, P = 0.008]. **(D)** Diffusion coefficient of SNAP-MOP upon stimulation with vehicle or 10 μM DAMGO in control or Cmpd101 pre-treated cells [n = 37–47 cells from 6 to 8 independent experiments, F(3,161) = 4.15, P = 0.007]. For each condition of the molecular brightness data, brightness values for the first (left) and second (right) component are shown, with the number of cells requiring a two-component fit indicated as percentage. Each data point on the scatter plots represents a measurement from an individual cell (number of cells in parenthesis) and column plots represent mean ± SEM of the indicated number of cells or individual experiments. **(E)** HEK293 were transiently transfected with FLAG-MOP-NLuc and GRK2-Venus to measure GRK2 recruitment in a BRET assay after stimulation with 10 μM DAMGO in control or Cmpd101 pre-treated cells (n = 3 independent experiments). The BRET ratio of vehicle-treated cells was subtracted, data represent mean ± SEM normalized to control condition, ^^ denotes significance vs. DAMGO alone (P = 0.002, unpaired Student's t-test). **(F)** Quantification of pS375 FLAG-MOP upon stimulation with vehicle or 1 μM DAMGO in control or Cmpd101 pre-treated cells. Phosphorylation of S375 was quantified as the ratio of anti-phosphoS375 (pS375) MOP site antibody immunostaining divided by FLAG immunostaining and normalized to vehicle of the control condition [n = 3 independent experiments, F(3,8) = 9.348, P = 0.005]. * denotes significance vs. vehicle treatment and ^ denotes significance vs. DAMGO control in one-way ANOVA with Sidak's multiple comparisons test (ns, not significant, $P > 0.05$, *$P < 0.05$, **$P < 0.01$, ^$P < 0.05$, ^^$P < 0.01$).

DISCUSSION

The formation of highly dynamic signaling complexes at the plasma membrane of the cell is key for the generation of specific cellular responses to extracellular stimuli. Stimulation of transmembrane proteins such as GPCRs can alter the composition of these receptor-effector platforms to generate a tailored signaling profile. This is illustrated, for example, by the process of receptor internalization, where prolonged stimulation of a GPCR by an agonist leads to phosphorylation

of its intracellular domains which results in the recruitment of a myriad of regulatory proteins (including β-arrestins, AP-2, clathrin). These proteins facilitate receptor accumulation in clathrin-coated pits and trafficking of the receptor to intracellular compartments. While receptor endocytosis represents a macroscopic change in receptor reorganization, diffusion of adaptor proteins at the microscopic scale has been suggested to occur prior to internalization (Rappoport et al., 2006). Recent advances in quantitative live cell imaging techniques and receptor labeling have been instrumental in providing further information on these dynamic micro-changes in receptor organization that occur at the plasma membrane prior to receptor accumulation into intracellular compartments (Sungkaworn et al., 2017; Yanagawa et al., 2018). In addition, such studies have also demonstrated that effector proteins such as adenylyl cyclase redistribute and reorganize their micro-environment to generate highly specialized signaling hubs (Ayling et al., 2012).

Understanding such microdomain level diffusion events is of particular relevance for the MOP, since activation of MOP by different ligands results in distinct regulatory profiles. While endogenous opioid peptides and their analogs induce robust receptor internalization, other opioid ligands such as morphine are very weak at driving MOP internalization (Keith et al., 1996; Whistler and von Zastrow, 1998). Moreover, we have recently shown that differential activation of MOP also results in distinct spatiotemporal signaling profiles that are controlled by a change in distribution of the receptor within the plasma membrane (Halls et al., 2016). Here, we have used complementary imaging techniques (FCS and FRAP) to gain further understanding of the changes in plasma membrane MOP distribution that occur following receptor activation with DAMGO (an enkephalin derivative that causes robust MOP internalization) compared to morphine (a poor internalizing agonist).

Our data shows that only DAMGO, but not morphine, can change the lateral organization of the MOP from basal conditions in a concentration and time-dependent manner, prior to its movement to clathrin-coated pits and internalization. We detected significant DAMGO-induced slowing in diffusion at 1 μM after 20 min of stimulation, a time point at which internalization is minimal (Halls et al., 2016). For this reason, we anticipate that this slowing in diffusion alludes to an event prior to receptor endocytosis. DAMGO-induced reorganization occurs at two different levels; there is a micro-reorganization event (reflected in changes in the diffusion coefficient) and macro-reorganization event (which changes surface receptor number, clustering and immobile fraction). Differences between micro- and macro-level MOP organization were also illustrated by the slower MOP diffusion co-efficient determined by FRAP compared to FCS. This can be interpreted as a free local diffusion within a confined domain, but restricted movement across larger distances. Notably, DAMGO-induced changes were only seen in D_{FCS}, but not in D_{FRAP}, consisting with a local change in organization.

Additionally, we showed that the plasma membrane reorganization induced by DAMGO is independent of G protein activation and that the "macro" changes in MOP clustering are mediated by clathrin-dependent endocytosis. Interestingly, the initial slowing of the MOP was only prevented by Cmpd101, a GRK2/3 inhibitor, but was independent of (or occurs prior to) clathrin-mediated endocytosis. This suggests that the large-scale changes induced by internalization such as the decrease in particle number and the increase in molecular brightness represent clustering into coated pits where the receptor is immobilized within the clathrin lattice. We propose that a rapid reorganization event that involves a decrease of the diffusion of MOP occurs at the plasma membrane prior to internalization. Such lateral reorganization requires GRK2 and is likely to be responsible for the distinct agonist-specific signaling patterns that we have previously observed (as per Halls et al., 2016). This reorganization is followed by larger scale movements of the MOP into clathrin-coated pits resulting in clustering and endocytosis (**Figure 6**).

DAMGO-induced slowing in MOP diffusion could be caused by a change in the molecular composition of the receptor complex (i.e., direct interaction with GRKs, although interaction with other phosphorylation-dependent proteins cannot be dismissed) soon after receptor activation and prior to its accumulation in clathrin-coated pits. A change in the composition of the MOP complex on this timescale would be consistent with our previous observations of a DAMGO-induced receptor redistribution to control transient activation of cytosolic and nuclear ERK (Halls et al., 2016). Therefore, not only is the differential recruitment of GRK2/3 by DAMGO vs. morphine important for MOP regulation (Miess et al., 2018), it also plays an essential role in MOP diffusion events that facilitate activation of compartmentalized signaling, revealing a novel role of GRKs as agonist-specific regulators of MOP plasma membrane signaling. On that note, GRKs are typically recognized for their catalytic activity in mediating agonist-induced phosphorylation of GPCRs that eventually result in receptor internalization. Importantly, scaffolding roles for GRKs have also been described in which the kinase participates in the generation of a macromolecular signalosomes in a manner that can be independent of its kinase activity (Penela et al., 2010). The mechanism underlying this GRK-dependent micro-diffusion event of MOP remains to be elucidated and future studies should investigate whether it is the kinase or the scaffolding function of GRK2 that is required for the observed changes in plasma membrane reorganization of MOP.

Several studies have shown the complexity of MOP dynamics within the plasma membrane. Recent FCS and PALM studies have provided unprecedented details on the dynamic lateral organization of MOP and KOP. These studies have shown that in unstimulated cells, GFP tagged receptors are organized into nano-domains that partially overlap with cholesterol-rich domains and are excluded from GM1-ganglioside-enriched domains (Rogacki et al., 2018). However, this study did not report on the changes that may occur upon receptor stimulation. Previous FRAP studies using a GFP-MOP have investigated the lateral diffusion of MOP upon DAMGO and morphine stimulation (Sauliere-Nzeh Ndong et al., 2010). While morphine seemed to induce limited diffusion, with small domain size and diffusion coefficient, DAMGO displayed bigger changes in diffusion range in addition to the effects observed with morphine.

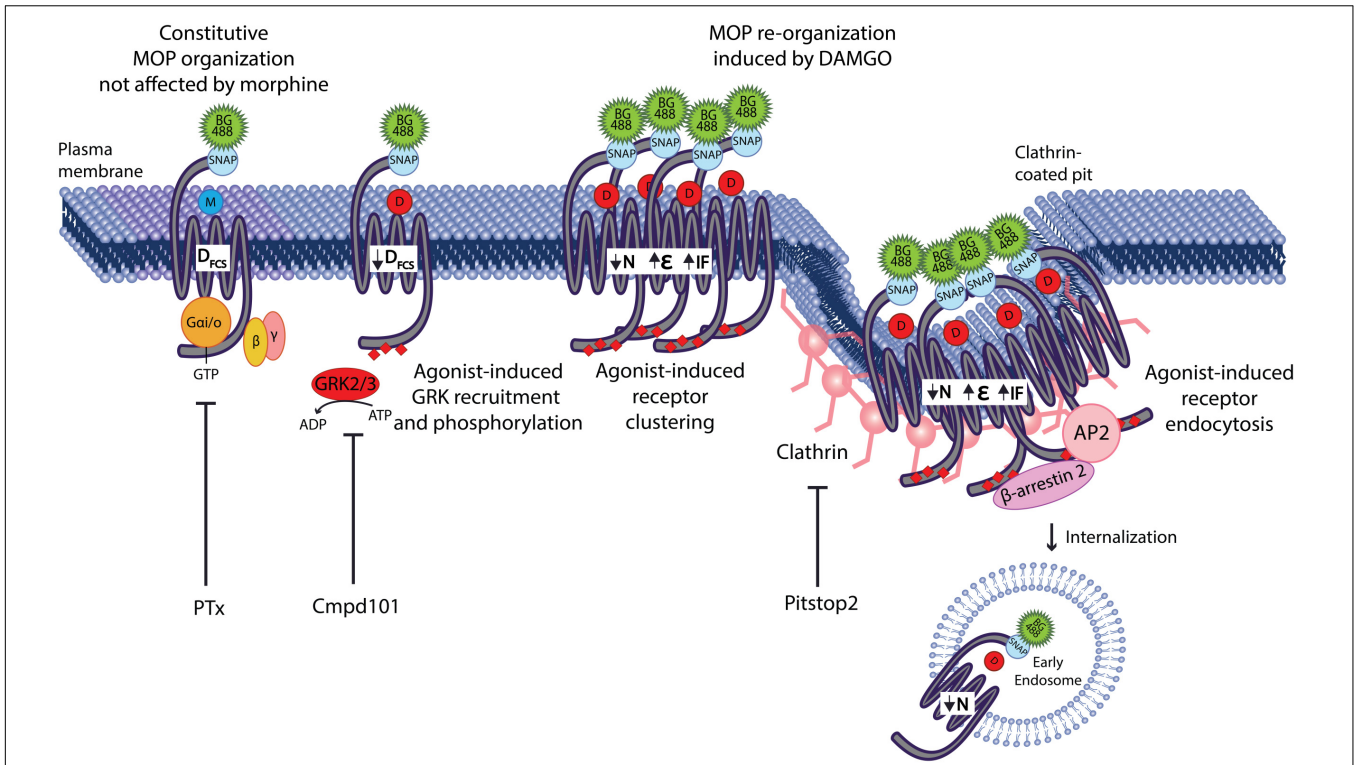

FIGURE 6 | GRK2 mediates MOP micro-diffusion events that precede internalization. Agonist stimulation of SNAP-MOP with morphine does not alter its constitutive plasma membrane organization. In contrast, agonist stimulation with DAMGO causes re-organization of SNAP-MOP indicated by the decrease in diffusion coefficient (D_{FCS}), the decrease in particle concentration (N), the increase in molecular brightness (ε), and the increase in immobile fraction (IF). G protein activation is not involved in SNAP-MOP plasma membrane organization, whereas GRK2/3 activity mediates DAMGO-induced slowing in D_{FCS} independent or prior to clustering and movement of SNAP-MOP into clathrin-coated pits to proceed toward internalization. The latter events are responsible for changes in macro-scale parameters such as the reduced N, increased ε and IF.

Interestingly, these latter long-range changes were absent when receptor endocytosis was inhibited, and the small-range changes seemed to be dependent on G protein activation. Although we did not observe changes in FRAP diffusion coefficients, our FRAP data, showing that upon treatment with Pitstop2 the immobile receptor fraction of DAMGO-activated MOP is not different than vehicle, is in line with these observations. A second FRAP study has shown ligand-dependent changes in the diffusion rate of MOP that are differentially affected by cholesterol depletion (Melkes et al., 2016). Such divergent results concerning the influence of agonists on the diffusion coefficients of MOP can, be attributed to different experimental conditions including the use of different fusion proteins. The attachment of a fluorescent protein tag to the receptor does not allow to distinguish between receptors that are already at the cell surface at the time of stimulation and newly synthesized receptors that are subsequently incorporated into the plasma membrane from the intracellular compartment, thus properties from different receptor pools might have been incorporated. Moreover, addition of the fluorescent protein within the C-terminus could interfere with complex formation and could affect the diffusion rates measured.

Experimental and computational evidence has also highlighted that the membrane organization of MOP can be influenced by changes in lipid content (Vukojevic et al., 2008a; Marino et al., 2016). Cholesterol has been shown to promote MOP homodimerization (Zheng et al., 2012), agonist binding (Gaibelet et al., 2008), coupling with G proteins (Gaibelet et al., 2008; Zheng et al., 2012), and translocation of β-arrestin (Qiu et al., 2011). Such movement between membrane domains with different lipid composition (e.g., cholesterol/non-cholesterol) could account for the slowing in MOP diffusion induced by DAMGO although further experiments should address the role of GRKs in this event. Nevertheless, this provides a potential mechanism by which the direct interaction of lipids with the receptor or the membrane micro-environment can facilitate interactions with specific signaling effectors and account for the agonist-specific spatiotemporal signaling elicited by the MOP (as per Halls et al., 2016).

In summary, we have described here that the plasma membrane reorganization of MOP at the micro scale level is dependent on GRK2/3 and at the macro scale level is dependent on clathrin-dependent internalization. This study therefore reveals an important and novel role of GRKs in modulating plasma membrane MOP organization; and provides evidence that the lateral diffusion of MOP represents a molecular event, distinct and prior to internalization, that is differentially regulated by opioids and controls its spatiotemporal signaling.

MATERIALS AND METHODS

Reagents

D-Ala^2,N-Me-Phe^4,Gly^5-ol-enkephalin was obtained from Mimotopes. Morphine, Rhodamine 6G and M2-anti-FLAG were from Sigma-Aldrich (Gillingham, Dorset, United Kingdom). Naloxone was from Tocris. SNAP-Surface 488 was from New England Biolabs (Ipswich, MA, United States). The antibody anti-pS375 was from Cell Signaling. Secondary antibodies (raised in donkey) conjugated to Alexa-Fluor 488 or 647 were from Jackson ImmunoResearch. Coelenterazine h was from NanoLight. Furimazine was from Promega. Compound 101 was from HelloBio. Pitstop2 was from Abcam. PTx was from Millipore.

Plasmids

To create the SNAP-MOP constructs, the full coding sequence for the human MOP (hMOP) was ligated into a pcDNA3.1(+) vector containing the 5-HT$_3$ receptor membrane localization signal sequence and the SNAP-tag (New England Biolabs, Ipswich, MA, United States) (Gherbi et al., 2015) and a neomycin resistance gene. Initial site-directed mutagenesis was required to remove the internal BamHI site in the MOP receptor while maintaining the amino acid sequence. Additional site-directed mutagenesis was performed to mutate the start codon (Met to Leu) on the MOP cDNAs. These were then ligated to the C-terminus of SNAP using BamHI and XhoI restriction enzymes. The resulting fusion protein contained a Gly-Ser linker between the SNAP open reading frame (ORF) and the MOP ORF.

To create the FLAG-MOP-NLuc, the NLuc sequence (Soave et al., 2016) was ligated immediately after the C-terminus of FLAG-mMOP cDNA without stop codon (Miess et al., 2018) with XhoI and XbaI restriction enzymes in a pcDNA3.1 vector. All sequences were confirmed by DNA sequencing.

GRK2-Venus was from D. Jensen (Columbia University, New York), CAMYEL sensor has been previously characterized (Jiang et al., 2007).

Generation of Cell Lines

Human embryonic kidney cells (ATCC, Middlesex, United Kingdom) were grown in Dulbecco's modified Eagle's medium (DMEM) supplemented with 10% (v/v) fetal calf serum and maintained at 37°C in a humidified incubator containing 5% CO_2. Cells were transfected with the pcDNA3.1+ vector containing SNAP-MOP constructs using Fugene HD (Promega) as transfection reagent according to the manufacturer's instructions. Twenty-four hours post transfection, the medium was supplemented with 1 mg/ml G418-selective pressure for 2 weeks for the generation of stable mixed population HEK293 SNAP-hMOP cell line.

Cell Plating and Treatments

Stable mixed population cell lines were plated onto poly-D-lysine–coated 8-well Labtek No.1 borosilicate chambered coverglasses (Nunc Nalgene International, Thermo Fisher Scientific). On the day of the experiment, SNAP tag labeling was performed by incubating cells with 200 nM (or as otherwise indicated) SNAP-Surface 488 (BG-488) dye in fresh cell culture media for 30 min at 37°C. Cells were washed in pre-warmed HEPES-buffered saline solution (HBSS; Briddon et al., 2004) containing 4.5 mM D-glucose and pretreated with inhibitors for 30 min at 37°C, except for pertussis toxin (PTx; 16 h pre-treatment). Inhibitors were used at the following concentrations: 30 μM Pitstop2, 30 μM Cmpd101, or 100 ng/ml PTx. Cells were then stimulated for 20 min (or as otherwise indicated) at 37°C with vehicle (0.3% v/v DMSO), 10 μM DAMGO, 30 μM morphine, 30 μM naloxone, or 10 μM DAMGO after pre-treatment for 30 min at 37°C with 30 μM naloxone.

Fluorescence Correlation Spectroscopy (FCS)

Cells were equilibrated to room temperature (22 ± 2°C) to minimize artifacts from temperature-induced plasma membrane fluctuations. FCS measurements were taken at room temperature on a Zeiss LSM510NLO Confocor 3 inverted confocal microscope using a 40× c-Apochromat 1.2 NA water-immersion objective (Carl Zeiss, Jena, Germany) as previously described (Ayling et al., 2012). The confocal volume was calibrated on the day of each experiment using 20 nM Rhodamine 6G (R6G; D = 2.8 × 10^{-10} m^2/s). The measurement volume was positioned in x and y over a flat portion of a healthy cell using a live confocal image, then approximately on the upper membrane in z. Precise z-positioning on the upper plasma membrane peak was performed using an intensity z-scan at 0.25 μm intervals for ±2 μm. Samples were excited using a 488 nm argon laser with power set to ∼0.08 kW/cm^2 as measured at the objective. Fluorescence fluctuations were then collected through a BP505-610IR emission filter for 1 × 30 s.

Autocorrelation and PCH analysis were performed using Zen2010 Black software (Carl Zeiss, Jena, Germany). The dimensions and volume of the detection volume as well as the structure parameter (ratio of volume height to diameter) were determined from a calibration FCS read using 20 nM Rhodamine 6G, fitted to a single 3D diffusion component with a triplet state pre-exponential, as previously described (Briddon et al., 2004). Prior to AC/PCH analysis, the initial 5–10 s of data were removed where bleaching was present (indicated by a rapid decrease in the average count rate) in order to ensure that AC functions reached an asymptote at G(0) = 1. Average MOP dwell times (τ_D) and particle number (N) were obtained from fitting of AC curves to a two-component diffusion model incorporating a pre-exponential component to account for fluorophore triple state (as per Ayling et al., 2012). This model consisted of a three-dimensional component (τ_{D1}) to account for the diffusion in solution of free SNAP BG-488 label, and a two-dimensional component (τ_{D2}) to account for the plasma membrane diffusion of the BG-488-labeled SNAP-MOP itself (**Figure 1B**). The average dwell time of free BG-488 (τ_{D1}) was fixed to 32 μs in the fitting process, having been measured directly using 20nM BG-488 in HBSS. The structure parameter was also fixed to the value determined in the calibration fit. All other parameters were allowed to vary in the fitting process. Free BG-488 concentration

(% τ_{D1} contribution to the AC amplitude was consistently between 10 and 15% of the total amplitude).

Average dwell time of the SNAP-MOP allowed calculation of the MOP diffusion coefficient (D_{FCS}) using the equation $D = \omega_0^2/4.\tau_D$, where ω_0 was the radius of the beam waist of the detection volume determined from the calibration data and τ_D was the average dwell time of SNAP-MOP in the volume as determined from the AC analysis. Particle number (N) was determined as the fractional contribution of the SNAP-MOP diffusing component (τ_{D2}) multiplied by the total particle number (N) as determined by the G(0) value of the fit of the AC curve. This was subsequently expressed in particles per μm^2 ($N/\mu m^2$), by normalizing to the area of the detection volume as projected onto a flat 2D membrane ($N/\pi\omega_0^2$).

Molecular brightness (ε) was determined using PCH analysis of the same fluctuation data. For PCH, the first-order correction was obtained from fitting of the R6G calibration data binned at 20 μs, and fixed to this value in subsequent fitting. Data from SNAP-MOP cells were fitted using a bin time of 100 μs. Data were fitted to either a one or two component PCH based on the goodness of fit at high photon counts per bin, visualized on a linear-log scale (**Figure 1C**).

Fluorescence Recovery After Photobleaching (FRAP)

Fluorescence recovery after photobleaching measurements were performed at room temperature on a Zeiss LSM510NLO Confocor 3 inverted confocal microscope using a 40× c-Apochromat 1.2 NA water-immersion objective using the Zeiss AIM3.5 software (Carl Zeiss, Jena, Germany). After manually focusing on the basal membrane of SNAP-MOP HEK293 cells, images were scanned using 488 nm excitation, with emission collected through a BP505-610IR filter, with pinhole set at 1 Airy unit and gain and offset adjusted to fit the linear response of the PMT detectors. Images (512 × 512 pixels) were acquired continually with no averaging on zoom 2 at a rate of ∼1 frame/second. Ten pre-bleach frames were acquired before bleaching (100 ms, 100% power during 30 iterations) a circular ROI of 2.14 μm radius (area = 14.8 μm^2) and fluorescence recovery was followed for a further 120 s.

Data were analyzed using the FRAP Wizard in Zen2010 Black software (Carl Zeiss, Germany). Fluorescence intensity within the bleached ROI of the bottom membrane was quantified over the time course of the experiment. This was background corrected using a similar sized ROI in an area of the image containing no cell and for bleaching during scanning using an ROI in a non-bleached cell. Pre-bleach frames were averaged and used as a baseline to normalize all post-bleach frames. Recovery curves were fitted to a simple exponential recovery curve to obtain a half time of recovery ($t_{1/2}$) and a recovery plateau (**Figure 1D**). The mobile fraction (MF) is defined as the intensity of this plateau as a percentage of the pre-bleach control, whilst the immobile fraction (IF) is the percentage difference between intensity of the recovery plateau and the pre-bleach intensity. Diffusion coefficient (D_{FRAP}) was calculated by using the equation $D = \omega^2/4.\tau_{1/2}$, where ω (μm) is the radius of the bleached area and $\tau_{1/2}$ (s) is the half-time recovery from the fitted curve in Zen2010.

Bioluminescence Resonance Energy Transfer (BRET)

Human embryonic kidney cells were transiently transfected in a 10 cm dish. For CAMYEL, cells were transfected with 2.5 μg of SNAP-MOP and 2.5 μg of CAMYEL biosensor. For GRK2 recruitment assay, cells were transfected with 1 μg FLAG-MOP-NLuc and 4 μg GRK2-Venus. After 24 h, cells were re-plated into poly-D-lysine-coated white opaque 96-well plates (CulturPlate, PerkinElmer) and allowed to adhere overnight. BRET experiments were performed 48 h post-transfection. Cells were washed with HBSS and equilibrated for 30 min at 37°C prior to the experiment. Coelenterazine or Furimazine was added to a final concentration of 5 μM before dual fluorescence/luminescence measurement in a LUMIstar Omega plate reader (BMG LabTech). The BRET signal was calculated as the ratio of light emitted at 530 nm by Venus over the light emitted at 430 nm by Renilla luciferase 8 (RLuc8) or Nano luciferase (NLuc).

For CAMYEL assays, vehicle or DAMGO (at the indicated concentration) was added to control or PTx-pretreated cells for 10 min and baseline was measured for 4 cycles, then 10 μM forskolin was added to induce cAMP production, and the BRET signal was measured for 30 min. CAMYEL concentration response curve was constructed with the data point at 10min after cAMP stimulation by forskolin. Data were normalized to 0% inhibition (forskolin-induced cAMP production) and 100% inhibition (vehicle only without forskolin-induced cAMP production).

For GRK2 recruitment kinetic experiments, the baseline BRET ratio was measured for 4 cycles, then either vehicle (0.01% v/v DMSO) or 10 μM DAMGO was added to control or Cmpd101-pretreated cells, and the BRET signal was measured for 30 min.

Anti-pS375 Immunocytochemistry

Human embryonic kidney cells transiently expressing FLAG-MOP were grown in a 96-well clear bottom plate (PerkinElmer). Cells were serum starved for at least 30 min and then incubated with vehicle or an EC_{50} concentration of DAMGO (1 μM) at 37°C for 5 min. Cells were then fixed in −30°C methanol for 10 min on ice. Antigen retrieval buffer was then applied, cells were heated in PBS supplemented with 10mM sodium citrate and 0.05% Tween-20 (pH 6.0) at 95°C for 20 min. Cells were then washed in PBS and incubated in blocking solution, 10% goat serum in PBS at room temperature for 30 min. Anti-FLAG mouse antibody and anti-phospho S375 rabbit antibody were diluted in blocking solution (1:1000 and 1:200, respectively) and added to cells for incubation overnight at room temperature. Cells were washed with PBS and incubated with AlexaFluor 488 (AF488) anti-mouse IgG and AlexaFluor 647 (AF647) anti-rabbit goat IgG secondary antibodies (1:1000 in blocking

solution) at room temperature for 1h. Cells were washed and imaged on the Operetta High Content Imaging System capturing AF488 and AF647 channels using a 20× objective. The mean fluorescence intensity of each channel was quantified from the raw 16-bit images using the Operetta analysis software and levels of phosphorylation were expressed as a ratio of pS375 (AF647)/FLAG (AF488) immunostaining and normalized to vehicle treatment in control conditions.

Statistical Analysis

Data representation and statistical analysis were performed using GraphPad Prism v7. FRAP and FCS data are presented as the mean ± SEM from '*n*' individual cells, with the number of independent experiments also stated. For statistical analysis of clustering from PCH data, the data are represented as the mean ± SEM of the % of cells requiring a two-component fit in each independent experiment. The BRET data was quantified as indicated and represent the mean ± SEM of at least three individual experiments. Statistical significance was determined by either unpaired Student's *t*-test or one-way ANOVA with *post hoc* Sidak's multiple comparison analysis. *P* values for the *post hoc* tests are given in the text, whilst details of one-way ANOVA parameters are given in the relevant figure and table legends.

DATA AVAILABILITY

The datasets generated for this study are available on request to the corresponding author.

AUTHOR CONTRIBUTIONS

AG performed and analyzed all the experiments and wrote the manuscript drafts and figures. SB, MC, and MH conceived the studies. SB supervised and designed FCS and FRAP experiments and data analysis. MH and MC supervised BRET experiments. All authors reviewed and edited the manuscript.

FUNDING

This work was supported by Medical Research Council grant number MR/N020081/1 to SB and the National Health and Medical Research Council (NHMRC) Project grant 1121029 to MC and MH.

ACKNOWLEDGMENTS

We thank Dr. Leigh Stoddart for technical assistance in molecular biology.We also thank the School of Life Sciences Imaging Facility (SLIM) at University of Nottingham for providing access to instrumentation and valuable guidance.

SUPPLEMENTARY MATERIAL

The Supplementary Material for this article can be found online at: https://www.frontiersin.org/articles/10.3389/fnmol.2019.00104/full#supplementary-material

REFERENCES

Ayling, L. J., Briddon, S. J., Halls, M. L., Hammond, G. R. V., Vaca, L., Pacheco, J., et al. (2012). Adenylyl cyclase AC8 directly controls its micro-environment by recruiting the actin cytoskeleton in a cholesterol-rich milieu. *J. Cell Sci.* 125, 869–886. doi: 10.1242/jcs.091090

Briddon, S. J., Kilpatrick, L. E., and Hill, S. J. (2018). Studying GPCR pharmacology in membrane microdomains: fluorescence correlation spectroscopy comes of age. *Trends Pharmacol. Sci.* 39, 158–174. doi: 10.1016/j.tips.2017.11.004

Briddon, S. J., Middleton, R. J., Cordeaux, Y., Flavin, F. M., Weinstein, J. A., George, M. W., et al. (2004). Quantitative analysis of the formation and diffusion of A1-adenosine receptor-antagonist complexes in single living cells. *Proc. Natl. Acad. Sci. U.S.A.* 101, 4673–4678. doi: 10.1073/pnas.0400420101

Diekmann, S., and Hoischen, C. (2014). Biomolecular dynamics and binding studies in the living cell. *Phys. Life Rev.* 11, 1–30. doi: 10.1016/j.plrev.2013.11.011

Doll, C., Konietzko, J., Poll, F., Koch, T., Hollt, V., and Schulz, S. (2011). Agonist-selective patterns of micro-opioid receptor phosphorylation revealed by phosphosite-specific antibodies. *Br. J. Pharmacol.* 164, 298–307. doi: 10.1111/j.1476-5381.2011.01382.x

Duttaroy, A., and Yoburn, B. C. (1995). The effect of intrinsic efficacy on opioid tolerance. *Anesthesiology* 82, 1226–1236. doi: 10.1097/00000542-199505000-00018

Eichel, K., Jullie, D., Barsi-Rhyne, B., Latorraca, N. R., Masureel, M., Sibarita, J. B., et al. (2018). Catalytic activation of beta-arrestin by GPCRs. *Nature* 557, 381–386. doi: 10.1038/s41586-018-0079-1

Floyd, C. N., and Warren, J. B. (2018). Opioids out of control. *Br. J. Clin. Pharmacol.* 84, 813–815. doi: 10.1111/bcp.13346

Gaibelet, G., Millot, C., Lebrun, C., Ravault, S., Saulière, A., André, A., et al. (2008). Cholesterol content drives distinct pharmacological behaviours of μ-opioid receptor in different microdomains of the CHO plasma membrane. *Mol. Membr. Biol.* 25, 423–435. doi: 10.1080/09687680802203380

Gherbi, K., May, L. T., Baker, J. G., Briddon, S. J., and Hill, S. J. (2015). Negative cooperativity across β(1)-adrenoceptor homodimers provides insights into the nature of the secondary low-affinity CGP 12177 β1-adrenoceptor binding conformation. *FASEB J.* 29, 2859–2871. doi: 10.1096/fj.14-265199

Halls, M. L., Yeatman, H. R., Nowell, C. J., Thompson, G. L., Gondin, A. B., Civciristov, S., et al. (2016). Plasma membrane localization of the mu-opioid receptor controls spatiotemporal signaling. *Sci. Signal.* 9, ra16. doi: 10.1126/scisignal.aac9177

Haustein, E., and Schwille, P. (2004). Single-molecule spectroscopic methods. *Curr. Opin. Struct. Biol.* 14, 531–540. doi: 10.1016/j.sbi.2004.09.004

Huang, P., Xu, W., Yoon, S. I., Chen, C., Chong, P. L., Unterwald, E. M., et al. (2007). Agonist treatment did not affect association of mu opioid receptors with lipid rafts and cholesterol reduction had opposite effects on the receptor-mediated signaling in rat brain and CHO cells. *Brain Res.* 1184, 46–56. doi: 10.1016/j.brainres.2007.09.096

Jiang, L. I., Collins, J., Davis, R., Lin, K. M., DeCamp, D., Roach, T., et al. (2007). Use of a cAMP BRET Sensor to Characterize a Novel Regulation of cAMP by the Sphingosine 1-Phosphate/G(13) Pathway. *J. Biol. Chem.* 282, 10576–10584. doi: 10.1074/jbc.m609695200

Just, S., Illing, S., Trester-Zedlitz, M., Lau, E. K., Kotowski, S. J., Miess, E., et al. (2013). Differentiation of opioid drug effects by hierarchical multi-site phosphorylation. *Mol. Pharmacol.* 83, 633–639. doi: 10.1124/mol.112.082875

Keith, D. E., Murray, S. R., Zaki, P. A., Chu, P. C., Lissin, D. V., Kang, L., et al. (1996). Morphine activates opioid receptors without causing their rapid internalization. *J. Biol. Chem.* 271, 19021–19024. doi: 10.1074/jbc.271.32.19021

Lau, E. K., Trester-Zedlitz, M., Trinidad, J. C., Kotowski, S. J., Krutchinsky, A. N., Burlingame, A. L., et al. (2011). Quantitative encoding of the effect of

a partial agonist on individual opioid receptors by multisite phosphorylation and threshold detection. *Sci. Signal.* 4, ra52. doi: 10.1126/scisignal.2001748

Marino, K. A., Prada-Gracia, D., Provasi, D., and Filizola, M. (2016). Impact of lipid composition and receptor conformation on the spatio-temporal organization of mu-Opioid receptors in a multi-component plasma membrane model. *PLoS Comput. Biol.* 12:e1005240. doi: 10.1371/journal.pcbi.1005240

Melkes, B., Hejnova, L., and Novotny, J. (2016). Biased mu-opioid receptor agonists diversely regulate lateral mobility and functional coupling of the receptor to its cognate G proteins. *Naunyn. Schmiedebergs Arch. Pharmacol.* 389, 1289–1300. doi: 10.1007/s00210-016-1293-8

Miess, E., Gondin, A. B., Yousuf, A., Steinborn, R., Mosslein, N., Yang, Y., et al. (2018). Multisite phosphorylation is required for sustained interaction with GRKs and arrestins during rapid mu-opioid receptor desensitization. *Sci. Signal.* 11:eaas9609. doi: 10.1126/scisignal.aas9609

Morgan, M. M., and Christie, M. D. J. (2011). Analysis of opioid efficacy, tolerance, addiction and dependence from cell culture to human. *Br. J. Pharmacol.* 164, 1322–1334. doi: 10.1111/j.1476-5381.2011.01335.x

Penela, P., Murga, C., Ribas, C., Lafarga, V., and Mayor, F. (2010). The complex G protein-coupled receptor kinase 2 (GRK2) interactome unveils new physiopathological targets. *Br. J. Pharmacol.* 160, 821–832. doi: 10.1111/j.1476-5381.2010.00727.x

Pucadyil, T. J., Mukherjee, S., and Chattopadhyay, A. (2007). Organization and dynamics of NBD-labeled lipids in membranes analyzed by fluorescence recovery after photobleaching. *J. Phys. Chem. B* 111, 1975–1983. doi: 10.1021/jp066092h

Qiu, Y., Wang, Y., Law, P. Y., Chen, H. Z., and Loh, H. H. (2011). Cholesterol regulates micro-opioid receptor-induced beta-arrestin 2 translocation to membrane lipid rafts. *Mol. Pharmacol.* 80, 210–218. doi: 10.1124/mol.110.070870

Rappoport, J. Z., Kemal, S., Benmerah, A., and Simon, S. M. (2006). Dynamics of clathrin and adaptor proteins during endocytosis. *Am. J. Physiol. Cell Physiol.* 291, C1072–C1081.

Rogacki, M. K., Golfetto, O., Tobin, S. J., Li, T., Biswas, S., Jorand, R., et al. (2018). Dynamic lateral organization of opioid receptors (kappa, muwt and muN40D) in the plasma membrane at the nanoscale level. *Traffic* doi: 10.1111/tra.12582 [Epub ahead of print].

Rudd, R. A., Seth, P., David, F., and Scholl, L. (2016). Increases in Drug and opioid-involved overdose deaths - United States, 2010-2015. *MMWR Morb Mortal Wkly Rep.* 65, 1445–1452. doi: 10.15585/mmwr.mm655051e1

Sauliere-Nzeh Ndong, A., Millot, C., Corbani, M., Mazeres, S., Lopez, A., and Salome, L. (2010). Agonist-selective dynamic compartmentalization of human Mu opioid receptor as revealed by resolutive FRAP analysis. *J. Biol. Chem.* 285, 14514–14520. doi: 10.1074/jbc.M109.076695

Soave, M., Stoddart, L. A., Brown, A., Woolard, J., and Hill, S. J. (2016). Use of a new proximity assay (NanoBRET) to investigate the ligand-binding characteristics of three fluorescent ligands to the human β. *Pharmacol. Res. Perspect.* 4:e00250. doi: 10.1002/prp2.250

Sungkaworn, T., Jobin, M. L., Burnecki, K., Weron, A., Lohse, M. J., and Calebiro, D. (2017). Single-molecule imaging reveals receptor-G protein interactions at cell surface hot spots. *Nature* 550, 543–547. doi: 10.1038/nature24264

Vukojevic, V., Ming, Y., D'Addario, C., Hansen, M., Langel, U., Schulz, R., et al. (2008a). Mu-opioid receptor activation in live cells. *FASEB J.* 22, 3537–3548. doi: 10.1096/fj.08-108894

Vukojevic, V., Ming, Y., D'Addario, C., Rigler, R., Johansson, B., and Terenius, L. (2008b). Ethanol/naltrexone interactions at the mu-opioid receptor. CLSM/FCS study in live cells. *PLoS One* 3:e4008. doi: 10.1371/journal.pone.0004008

Whistler, J. L., and von Zastrow, M. (1998). Morphine-activated opioid receptors elude desensitization by β-arrestin. *Proc. Natl. Acad. Sci. U.S.A.* 95, 9914–9919. doi: 10.1073/pnas.95.17.9914

Williams, J. T., Ingram, S. L., Henderson, G., Chavkin, C., von Zastrow, M., Schulz, S., et al. (2013). Regulation of mu-opioid receptors: desensitization, phosphorylation, internalization, and tolerance. *Pharmacol. Rev.* 65, 223–254. doi: 10.1124/pr.112.005942

Yanagawa, M., Hiroshima, M., Togashi, Y., Abe, M., Yamashita, T., Shichida, Y., et al. (2018). Single-molecule diffusion-based estimation of ligand effects on G protein-coupled receptors. *Sci. Signal.* 11:eaao1917. doi: 10.1126/scisignal.aao1917

Zheng, H., Chu, J., Qiu, Y., Loh, H. H., and Law, P. Y. (2008). Agonist-selective signaling is determined by the receptor location within the membrane domains. *Proc. Natl. Acad. Sci. U.S.A.* 105, 9421–9426. doi: 10.1073/pnas.0802253105

Zheng, H., Pearsall, E. A., Hurst, D. P., Zhang, Y., Chu, J., Zhou, Y., et al. (2012). Palmitoylation and membrane cholesterol stabilize mu-opioid receptor homodimerization and G protein coupling. *BMC Cell Biol.* 13:6. doi: 10.1186/1471-2121-13-6

Conflict of Interest Statement: The authors declare that the research was conducted in the absence of any commercial or financial relationships that could be construed as a potential conflict of interest.

frontiers in Molecular Neuroscience

ORIGINAL RESEARCH
published: 20 June 2019
doi: 10.3389/fnmol.2019.00153

Spinal Interleukin-1β Inhibits Astrocyte Cytochrome P450c17 Expression Which Controls the Development of Mechanical Allodynia in a Mouse Model of Neuropathic Pain

*Sheu-Ran Choi[1], Ho-Jae Han[1], Alvin J. Beitz[2] and Jang-Hern Lee[1]**

[1] Department of Veterinary Physiology, BK21 PLUS Program for Creative Veterinary Science Research, Research Institute for Veterinary Science, College of Veterinary Medicine, Seoul National University, Seoul, South Korea, [2] Department of Veterinary and Biomedical Sciences, College of Veterinary Medicine, University of Minnesota, Saint Paul, MN, United States

OPEN ACCESS

Edited by:
Meritxell Canals, University of Nottingham, United Kingdom

Reviewed by:
Vinicio Granados-Soto, Centro de Investigación y de Estudios Avanzados del Instituto Politécnico Nacional (CINVESTAV), Mexico
Lei Pei, Huazhong University of Science and Technology, China

***Correspondence:**
Jang-Hern Lee
jhl1101@snu.ac.kr

Received: *13 March 2019*
Accepted: *29 May 2019*
Published: *20 June 2019*

Citation:
Choi S-R, Han H-J, Beitz AJ and Lee J-H (2019) Spinal Interleukin-1β Inhibits Astrocyte Cytochrome P450c17 Expression Which Controls the Development of Mechanical Allodynia in a Mouse Model of Neuropathic Pain. Front. Mol. Neurosci. 12:153. doi: 10.3389/fnmol.2019.00153

We have recently demonstrated that sciatic nerve injury increases the expression of spinal cytochrome P450c17, a key neurosteroidogenic enzyme, which plays a critical role in the development of peripheral neuropathic pain. However, the modulatory mechanisms responsible for the expression of spinal P450c17 have yet to be examined. Here we investigated the possible involvement of interleukin-1β (IL-1β) in altering P450c17 expression during the induction phase of neuropathic pain. Neuropathic pain was produced by chronic constriction injury (CCI) of the right sciatic nerve in mice and mechanical allodynia was evaluated in the hind paws using a von-Frey filament (0.16 g). Western blotting and immunohistochemistry were performed to assess the expression of spinal IL-1β, interleukin-1 receptor type 1 (IL-1R1), P450c17, and GFAP. Spinal IL-1β was significantly increased on day 1 post-surgery and its receptor, IL-1R1 was expressed in GFAP-positive astrocytes. Intrathecal administration of the recombinant interleukin-1 receptor antagonist (IL-1ra, 20 ng) on days 0 and 1 post-surgery enhanced GFAP expression on day 1 post-surgery and induced an early increase in P450c17 expression in astrocytes, but not in neurons. Administration of IL-1β (10 ng) on days 0 and 1 post-surgery blocked the enhancement of both spinal P450c17 and GFAP expression induced by IL-1ra (20 ng) administration. Intrathecal administration of IL-1ra (20 ng) on days 0 to 3 post-surgery also facilitated the CCI-induced development of mechanical allodynia, and this early developed pain was dose-dependently attenuated by the administration of the P450c17 inhibitor, ketoconazole (1, 3, or 10 nmol) or the astrocyte metabolic inhibitor, fluorocitrate (0.01, 0.03, or 0.1 nmol). These results demonstrate that early increases in spinal IL-1β temporally inhibit astrocyte P450c17 expression and astrocyte activation ultimately controlling the development of mechanical

allodynia induced by peripheral nerve injury. These findings imply that spinal IL-1β plays an important role as an early, but transient, control mechanism in the development of peripheral neuropathic pain via the inhibition of astrocyte P450c17 expression and astrocyte activation.

Keywords: interleukin-1β, interleukin-1 receptor type 1, cytochrome P450c17, astrocytes, mechanical allodynia, neuropathic pain

INTRODUCTION

Neuropathic pain develops following injury to the nervous system and is often characterized by allodynia (the sensation of pain to non-noxious stimuli) and hyperalgesia (increased pain to a noxious stimuli) (Woolf and Mannion, 1999). The development of neuropathic pain involves a variety of pathophysiological changes in the nervous system, which are represented by peripheral sensitization (increased sensitivity of the nociceptor terminal) and central sensitization (increased synaptic efficacy of neurons in the spinal pain pathways) (Ji et al., 2003; Latremoliere and Woolf, 2009). Clinical recommended treatments include certain antidepressants, calcium channel α2-δ ligands, topical lidocaine, opioid analgesics, and antiepileptic medications depending on the patients' symptoms and the degree of pain severity (Dworkin et al., 2007). Once neuropathic pain has been established it is very difficult to control. Even with well-established medications, effectiveness is unpredictable, dosing can be complicated, analgesic onset is delayed, and side effects are common (Dworkin et al., 2007). As a result it is necessary to investigate and develop more effective therapeutic approaches based on the pathophysiological mechanisms underlying the development of neuropathic pain.

While neuronal dysfunction is thought to be a primary important cause of pain, recent evidence suggests that alterations in glial cells including astrocytes and microglial cells play a critical role in the initiation of persistent pain (Watkins et al., 2001; Tan et al., 2009). Under pathophysiological conditions, glial cells release various pro-inflammatory cytokines, which bind to the receptors located on other glia and neurons resulting in neuronal excitation in the spinal cord dorsal horn (Chen et al., 2014; Choi et al., 2018). It has been suggested that the pro-inflammatory cytokine,IL-1β is rapidly increased and released from activated microglial cells during the early phases of peripheral nerve damage or inflammation (Samad et al., 2001; Fu et al., 2006; Choi et al., 2015). Furthermore, IL-1β modulates the function of other adjacent cells including neurons and thus serves as a key mediator in the interaction between glia and neurons in a variety of pain states (Kim et al., 2004; Ren and Dubner, 2008). While previous studies have suggested a possible relationship between IL-1β and nociceptive signal transmission, the detailed mechanisms involved in this process remain unclear.

Diverse neurosteroidogenic enzymes are expressed in brain and spinal cord and catalyze the local synthesis of neurosteroids in the central nervous system (Baulieu, 1998; Patte-Mensah et al., 2006). Among neurosteroidogenic enzymes, P450c17 catalyzes the conversion of PREG into DHEA (Compagnone and Mellon, 2000). DHEA and its sulfate ester DHEA-S are known as pronociceptive mediators in the nervous system (Kibaly et al., 2008; Yoon et al., 2010). In a previous study, we demonstrated that CCI of sciatic nerve increases both the protein and mRNA levels of P450c17 in spinal astrocytes during the early phase of neuropathic pain (Choi et al., 2019). Furthermore, intrathecal administration of the P450c17 inhibitor, ketoconazole during the induction phase of neuropathic pain resulted in a significant analgesic effect on the development of neuropathic pain evoked by sciatic nerve injury in mice. Since spinal P450c17 plays a critical role in the development of neuropathic pain, it is important to investigate the regulatory mechanisms by which astrocyte P450c17 expression and activation are increased following peripheral nerve injury in order to better understand the pathophysiological mechanisms underlying the early phase of neuropathic pain. Our recent studies have demonstrated that microglial IL-1β suppresses both the astrocyte-specific gap junction protein, connexin-43 expression and astrocyte activation during the early phase of carrageenan-induced inflammation ultimately inhibiting the development of contralateral MA (Choi et al., 2015, 2017). Thus, we hypothesize that during the early phase of neuropathic pain development spinal IL-1β inhibits astrocyte activation through modulation of astrocyte P450c17 expression.

Thus, the present study was designed to determine whether IL-1β modulates astrocyte P450c17 expression and astrocyte activation in the spinal cord and to determine whether this modulation alters the development of neuropathic pain following peripheral nerve injury. To accomplish this we investigated whether: (i) sciatic nerve injury increases the expression of IL-1β in the lumbar spinal cord dorsal horn; (ii) IL-1R1, a functional receptor of IL-1β, is expressed in spinal astrocytes; (iii) the blockade of IL-1R1 using the recombinant IL-1 receptor antagonist (IL-1ra) modulates astrocyte P450c17 expression and pathological astrocyte activation; and (iv) this modulation is associated with the development of MA induced by peripheral nerve injury.

Abbreviations: CCI, chronic constriction injury; DHEA, dehydroepiandrosterone; FC, fluorocitrate; GFAP, glial fibrillary acidic protein; Iba-1, ionized calcium-binding adapter molecule 1; IL-1β, interleukin-1β; IL-1ra, interleukin-1 receptor antagonist; IL-1R1, interleukin-1 receptor type 1; i.t., intrathecal; ketoconazole, (±)-cis-1-Acetyl-4-(4-[(2-[2,4-dichlorophenyl]-2-[1H-imidazol-1-ylmethyl]-1,3-dioxolan-4-yl)-methoxy]phenyl)piperazine; MA, mechanical allodynia; NeuN, neuronal nuclei; NMDA, N-methyl-D-aspartate; NP, nucleus proprius; P450c17, cytochrome P450c17; PREG, pregnenolone; PWF, paw withdrawal frequency; SDH, superficial dorsal horn.

MATERIALS AND METHODS

Animals and Peripheral Nerve Injury Model

Four-week-old male Crl:CD1(ICR) mice (20–25 g) were purchased from the Laboratory Animal Center of Seoul National University (Seoul, South Korea). Animals had free access to food and water and were kept in temperature- and light-controlled rooms (23 ± 2°C, 12/12 h light/dark cycle) for at least 3 days prior to the beginning of the experiment. The experimental protocols for animal usage were reviewed and approved by the SNU Animal Care and Use Committee and were consistent with the Guide for the Care and Use of Laboratory Animals published by the United States National Institutes of Health (1985).

A CCI of the common sciatic nerve was performed according to the method described by Bennett and Xie with a minor modification (Bennett and Xie, 1988). Briefly, mice were anesthetized with 3% isoflurane in a mixture of N_2O/O_2 gas. The right sciatic nerve was exposed and three loose ligatures of 6-0 silk were placed around the nerve. Sham surgery was performed by exposing the sciatic nerve in the same manner, but without ligating the nerve. After surgery, animals recovered in clear plastic cages at 27°C with a thick layer of sawdust bedding.

Drugs and Intrathecal Administration

The following drugs were used: recombinant interleukin-1 receptor antagonist (IL-1ra; 6, 20, and 60 ng); recombinant IL-1β (10 ng); Keto (1, 3, and 10 nmol), a P450c17 inhibitor; and FC (0.01, 0.03, and 0.1 nmol), an astrocyte metabolic inhibitor. IL-1ra and IL-1β were purchased from R&D Systems (Minneapolis, MN, United States), and ketoconazole and FC from Sigma–Aldrich (St. Louis, MO, United States). The doses of all drugs were selected based on doses previously used in the literature including our previous studies showing that these doses produce maximal effects with no detectable side effects (Souter et al., 2000; Choi et al., 2015, 2019). All drugs used for the behavioral experiments were administered intrathecally twice a day on postoperative days 0–3, which represents the induction phase of pain development. For the Western blot and immunohistochemical experiments drugs were administered once on postoperative day 0 and once on postoperative day 1. IL-1ra and IL-1β were dissolved in physiological saline, ketoconazole was dissolved in 5% DMSO in corn oil, and FC was dissolved in 0.05% 1N HCl in physiological saline. IL-1β was co-administrated with IL-1ra on days 0 and 1. Thus, a mixture of IL-1β and IL-1ra was injected immediately after the operation and again on day 1 post-surgery, then, the spinal cord was sampled on day 1. The intrathecal injection volume was 5 μl.

Intrathecal drug administration was performed using a 50 μl Hamilton syringe connected to a 30-gauge needle as previously described (Hylden and Wilcox, 1980). Mice were briefly anesthetized with 3% isoflurane in a mixture of N_2O/O_2 gas to prevent any handling-induced stress and to allow for a more accurate injection of drugs. The mouse was held tightly between the thumb and middle finger at the level of the both iliac crests, and the fifth lumbar spinous process was palpated with the index finger. The needle was inserted through the vertebral column into the L_{5-6} intervertebral space and successful insertion of the needle into the intrathecal space was determined by a tail flick response. Each drug was slowly injected over a 10 s period. Then, the needle was carefully removed from the intervertebral space. The drug control groups received an identical injection of vehicle.

Assessment of Mechanical Allodynia

Pain behavioral testing was performed for ipsilateral (surgical-side) and contralateral hind paws of all animals 1 day before surgery in order to obtain normal baseline values of paw withdrawal responses to mechanical stimuli. Then, animals were randomly assigned to experimental and control groups. Animals were tested again at 1, 2, 3, 6, 9, and 14 days following CCI or sham surgery.

To assess nociceptive responses to innocuous mechanical stimuli (MA), we measured paw withdrawal response frequency (PWF) by using a von Frey filament with a force of 0.16 g (North Coast Medical, Morgan Hill, CA, United States) as described in a previous study from our laboratories (Moon et al., 2014). Mice were placed in acrylic cylinders on a wire mesh floor and allowed to habituate before testing. A von Frey filament was applied to the plantar surface of each hind paw for a 3 s period before being removed and we subsequently recorded whether there was a withdrawal of the hind limb to the filament. The filament was applied 10 times to the hind paw with a 10 s interval between each application. Then, the number of paw withdrawal responses was counted and the results of mechanical behavioral testing in the hind paw were expressed as a percent withdrawal response frequency (PWF, %), which represented the percentage of paw withdrawals out of the maximum of 10.

Western Blot Assay

Animals were deeply anesthetized with 3% isoflurane in a mixture of N_2O/O_2 gas. The Western blot assay was performed as described previously with minor modifications (Choi et al., 2013). Different groups of mice were euthanized at each of the five different time points used in this study (0, 1, 3, 7, and 14 days after CCI surgery) in order to examine the time-course changes in IL-1β- and IL-1R1-expression. Another set of animals were euthanized at day 1 post-CCI surgery in order to determine the effect of IL-1ra treatment on GFAP- and P450c17-expression. Animals were perfused transcardially with calcium-free Tyrode's solution and then the spinal cord was collected into an ice-cooled, saline-filled glass dish. The spinal cord dorsal horns of the lumbar enlargement segment were homogenized in lysis buffer (20 mM Tris–Hcl, 10 mM EGTA, 2 mM EDTA, pH 7.4 and proteinase inhibitors) containing 1% Triton X-100. Homogenates were subsequently centrifuged at 15,000 rpm for 40 min at 4°C and, then, the supernatant was used for Western blot analysis. The protein concentration was estimated by the Bradford dye assay (Bio-Rad Laboratories). Spinal cord homogenates (20–25 μg protein) were separated using 10% SDS-polyacrylamide

gel electrophoresis and transferred to nitrocellulose membrane. After the blots had been washed with TBST (10 mM Tris–Hcl, pH 7.6, 150 mM NaCl and 0.05% Tween-20), the membranes were blocked with 5% skimmed milk for 1 h at RT and incubated at 4°C overnight with a primary antibody specific for IL-1β (rabbit polyclonal anti-IL1 beta antibody, 1:2,000, cat# ab9787, Abcam plc.), IL-1R1 (goat polyclonal anti-IL-1R1 antibody, 1:2,000, cat# AF771, R&D Systems), GFAP (mouse monoclonal anti-GFAP antibody, 1:2,000, cat# MAB360, Millipore Co.), P450c17 (rabbit monoclonal anti-cytochrome P450 17A1 antibody, 1:1,000, cat# ab125022, Abcam plc.), or β-actin (mouse monoclonal anti-β-actin antibody, 1:5,000, cat# sc-47778, Santa Cruz Biotechnology Inc.). After washing with TBST, membranes were incubated for 4 h at 4°C with horseradish peroxidase (HRP)-conjugated anti-rabbit, anti-goat, or anti-mouse antibody (1:10,000, Santa Cruz Biotechnology Inc.). The bands were visualized with enhanced chemiluminescence (Amersham Biosciences). The positive pixel area of specific bands was measured with a computer-assisted image analysis system and normalized against the corresponding β-actin loading control bands. The mean value of control groups was set at 100% and, then, the % change relative to the mean value of control groups was calculated for each group.

Immunohistochemistry

Animals were deeply anesthetized with 3% isoflurane in a mixture of N_2O/O_2 gas and different groups of mice were euthanized at day 1 post-CCI surgery. The immunohistochemistry was performed as described previously with minor modifications (Roh et al., 2011). Mice were perfused transcardially with calcium-free Tyrode's solution and subsequently with fixative containing 4% paraformaldehyde in 0.1 M phosphate buffer (pH 7.4). The spinal cords were collected after perfusion, post-fixed in the identical fixative for 2 h at RT and then placed in 30% sucrose in PBS (pH 7.4) at 4°C. Serial transverse sections (40 μm) of the L_{4-5} spinal cord were cut using a cryostat (Leica CM1520, Leica Biosystems, Germany). Transverse spinal cord sections were incubated in blocking solution for 1 h at RT and then incubated for 2 days at 4°C with a primary antibody specific for IL-1β (rabbit polyclonal anti-IL1 beta antibody, 1:1,000, cat# ab9787, Abcam plc.), IL-1R1 (goat polyclonal anti-IL-1R1 antibody, 1:100, cat# AF771, R&D Systems), P450c17 (rabbit monoclonal anti-cytochrome P450 17A1 antibody, 1:1,000, cat# ab125022, Abcam plc.), GFAP (mouse monoclonal anti-GFAP antibody, 1:1,000, cat# MAB360, Millipore Co.), NeuN (mouse monoclonal anti-NeuN antibody, 1:1,000, cat# MAB377, Millipore Co.), or Iba-1 (rabbit anti-Iba1 antibody, 1:500, cat# 019-19741, Wako Pure Chemical Industries, Ltd.). The primary antibodies were detected by incubating the tissue in Alexa Fluor®488 goat anti-mouse antibody (1:400, Life Technologies), Alexa Fluor®488 donkey anti-goat antibody (1:400, Life Technologies), Alexa Fluor®568 donkey anti-rabbit antibody (1:400, Life Technologies), or Alexa Fluor®555 donkey anti-mouse antibody (1:400, Life Technologies) for 90 min at RT. Tissue sections were mounted on slides and visualized with a confocal laser scanning microscope (Fluoview 300, Olympus, Tokyo, Japan; Nikon Eclipse TE2000-E, Nikon, Japan).

Image Analysis

To analyze IL-1β- or GFAP-immunoreactive images, three to five spinal cord sections from the lumbar spinal cord segments were randomly selected from each animal, and were analyzed using a computer-assisted image analysis system (Metamorph version 7.7.2.0; Molecular Devices Corporation, PA, United States) as described in a previous study (Choi et al., 2016). To maintain a constant threshold for each image and to compensate for subtle variability of the immunostaining, we only measured areas that were 80% brightness in the range of intensity levels after background subtraction was performed. The positive pixel area of immunoreactive cells was quantified in the following three dorsal horn regions: (1) the SDH (laminae I and II); (2) the NP (laminae III and IV); and (3) the neck region (NECK, laminae V and VI). Then, the % threshold area [(positive pixel area/pixel area in each region) × 100] was counted. The average of % threshold area of immunoreactivity in each region per section from each animal was obtained and these values were averaged across each group and presented as group data. In addition, an average of 10 astrocytes from each animal with clear cell bodies and processes in lumbar spinal cord dorsal born were chosen for quantification of astrocyte morphology as described in a previous study (Lee et al., 2013). The astrocytes were analyzed with Metamorph software, generating data of cell body area (μm^2) and length of processes (μm) from the soma.

For analysis of P450c17 colocalization in specific cell types in the spinal cord dorsal horn, pairs of fluorescent images were acquired on the confocal microscope as red and green channels as described in previous studies (Moon et al., 2014; Choi et al., 2019). Overlap of a pair of images was visualized in merged images as yellow pixels, which were considered colocalized. To analyze the extent of colocalization of P450c17 with GFAP (astrocytes) or NeuN (neurons), we directly quantified the number of cells showing cell type-specific nuclei that contained P450c17 immunolabelling. We quantified immunostaining in the following three dorsal horn regions: (1) the SDH (laminae I and II); (2) the NP (laminae III and IV); and (3) the NECK (laminae V and VI). All analytical procedures described above were performed blindly without knowledge of the experimental conditions.

Data Presentation and Statistical Analysis

Data are expressed as the mean ± standard error of the mean (SEM). Statistical analyses were performed using Prism 5.0 (Graph Pad Software, San Diego, CA, United States). Repeated measures two-way (group and time) ANOVA was performed to determine differences in the behavioral data and One-way ANOVA was used to determine differences in the data obtained from Western blot assay and immunohistochemistry. *Post hoc* analysis was performed using a Bonferroni's multiple comparison test to determine the *P*-value among experimental groups.

Comparisons between 2 groups were analyzed by the two-tailed Student's *t*-test. The level of significance was set at $P < 0.05$.

RESULTS

Time Course Changes in IL-1β Expression in the Lumbar Spinal Cord Dorsal Horn of CCI Mice

To determine whether CCI of the sciatic nerve induces a significant change in spinal IL-1β expression, we examined changes in the protein expression of IL-1β over time after CCI using a Western blot analysis. Sciatic nerve injury significantly increased the amount of IL-1β protein in the ipsilateral lumbar spinal cord dorsal horn at day 1 post-surgery as compared with control mice. Subsequently IL-1β expression was dramatically decreased from 3 days to 14 post-surgery [**Figure 1A**; $F(4,25) = 5.728$, $P = 0.0021$]. By contrast, the amount of IL-1β in the contralateral lumbar spinal cord dorsal horn did not change following sciatic nerve injury as compared with the control group [**Figure 1B**; $F(4,25) = 1.175$, $P = 0.3611$]. We also examined changes in IL-1β-immunoreactivity in the lumbar spinal cord dorsal horn at day 1 post-surgery using an immunohistochemical approach. Sciatic nerve injury significantly increased IL-1β-immunoreactivity in the SDH (laminae I-II) region of the ipsilateral lumbar spinal cord dorsal horn as compared to that of the sham surgery animals [**Figure 1C**; SDH: $t(10) = 4.202$, $P = 0.0018$; NP: $t(10) = 1.936$, $P = 0.0816$;

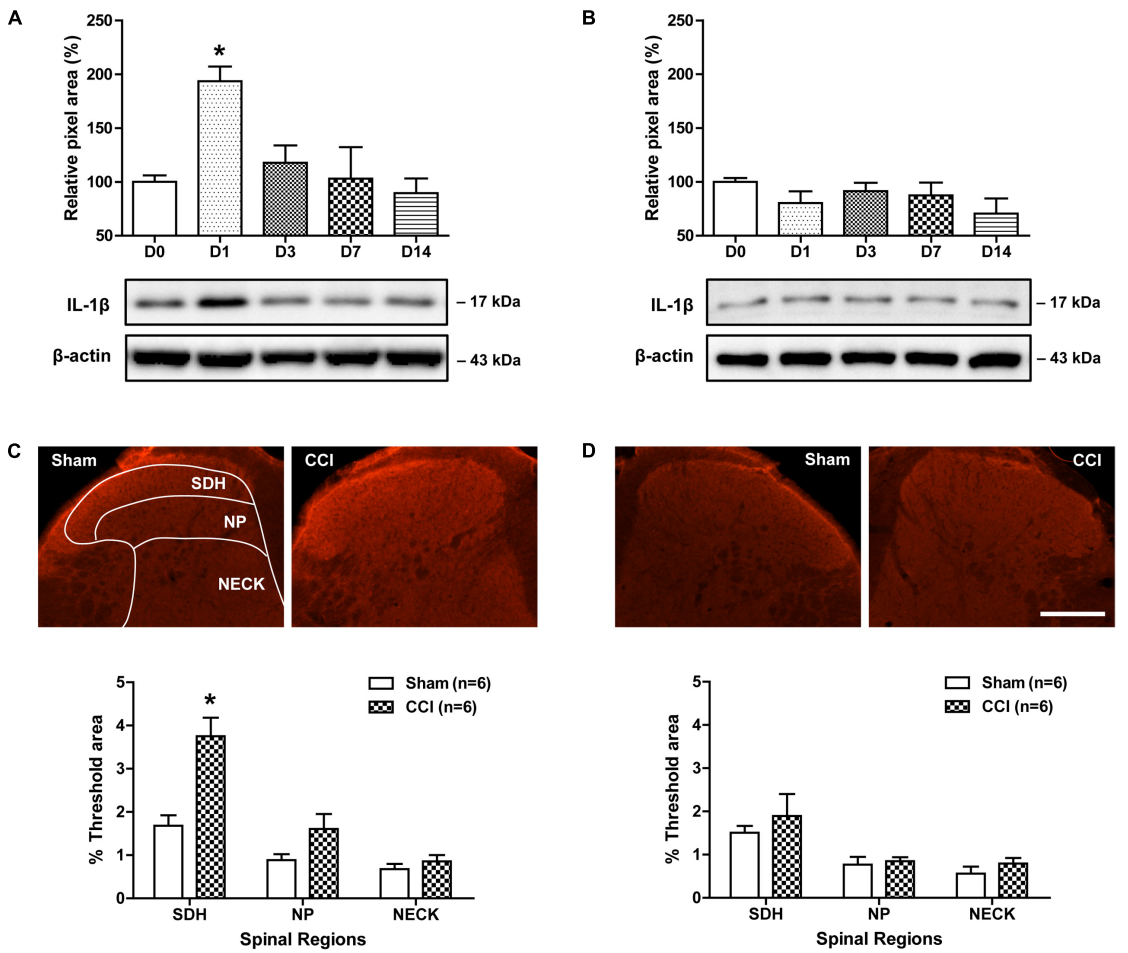

FIGURE 1 | Time course of changes in the expression of IL-1β in the lumbar spinal cord dorsal horn of CCI mice. **(A,B)** The graphs depicting the changes in the protein expression of IL-1β are shown in the upper portion, while representative immunoblots are presented in the lower portion. Results of Western blot analysis showed that the protein expression of IL-1β significantly increased at day 1 post-CCI surgery in the ipsilateral lumbar spinal cord dorsal horn **(A)**, while the expression of IL-1β in the contralateral dorsal horn **(B)** did not change following CCI. The spinal cord dorsal horn was sampled at 0, 1, 3, 7, and 14 days after surgery. $n = 6$ mice/group. $^*P < 0.05$ vs. D0. **(C,D)** Representative images showing the changes in IL-1β-immunoreactivity at postoperative day 1 in the lumbar spinal cord dorsal horn of CCI mice using immunohistochemistry. Fluorescent images of IL-1β in the superficial dorsal horn (SDH, lamina I-II), nucleus proprius (NP, lamina III-IV) and neck region (NECK, lamina V-VI) of sham and CCI mice. Fluorescence in the dorsal horn was quantitated using an image analysis system. Sciatic nerve injury significantly increased IL-1β-immunoreactivity in the SDH region of the ipsilateral lumbar spinal cord dorsal horn **(C)**, while IL-1β-immunoreactivity in the contralateral dorsal horn **(D)** did not change following CCI. $n = 6$ mice/group. $^*P < 0.05$ vs. Sham. Scale bar = 100 μm.

NECK: $t(10) = 0.9577$, $P = 0.3608$]. By contrast, IL-1β-immunoreactivity in the contralateral lumbar spinal cord dorsal horn did not change following sciatic nerve injury as compared with the control group [**Figure 1D**; SDH: $t(10) = 0.7205$, $P = 0.4877$; NP: $t(10) = 0.4023$, $P = 0.6959$; NECK: $t(10) = 1.112$, $P = 0.2921$]. These results show that sciatic nerve injury induces an early transient increase in IL-1β expression, especially in the SDH (laminae I-II) of the ipsilateral lumbar spinal cord.

Time Course Changes in Spinal IL-1R1 Expression and Effects of IL-1ra on the Development of Mechanical Allodynia in CCI Mice

Involvement of interleukin-1β exerts its effects by acting on the membrane bound IL-1R1, which activates signal transduction upon IL-1β stimulation (Sims et al., 1993). Thus in the next part of our study, we examined changes in the protein expression of IL-1R1 over time following CCI using a Western blot analysis. The protein amount of IL-1R1 in the ipsilateral [**Figure 2A**; $F(4,25) = 2.243$, $P = 0.0930$] and contralateral [**Figure 2B**; $F(4,25) = 1.484$, $P = 0.2369$] lumbar spinal cord dorsal horn did not change following sciatic nerve injury as compared with the control group.

In order to determine if the CCI-induced increase in the expression of IL-1β at day 1 post-surgery modulates the development of MA, we examined the effect of administration of the IL-1 receptor antagonist (IL-1ra; 6, 20, or 60 ng) on the development of MA. CCI of the sciatic nerve increased the PWF (%) to innocuous mechanical stimuli (MA) in the ipsilateral hind paw from 3 days post-CCI surgery as compared with sham group (**Figure 2C**). IL-1ra was administered intrathecally during the induction phase of neuropathic pain (from days 0 to 3 post-surgery) in order to neutralize spinal IL-1β signaling. Intrathecal administration of IL-1ra (20 or 60 ng) induced an early increase in the ipsilateral PWF beginning at day 1 post-surgery [**Figure 2C**; Group: $F(4,210) = 42.59$, $P < 0.0001$; Time: $F(6,210) = 25.98$, $P < 0.0001$; Interaction: $F(24,210) = 1.928$, $P = 0.0074$]. By contrast, i.t. administration of IL-1ra (6, 20, or 60 ng) during the induction phase of neuropathic pain (from days 0 to 3 post-surgery) had no effect on the PWF in the contralateral hind paw [**Figure 2D**; Group: $F(4,210) = 1.908$, $P = 0.1104$; Time: $F(6,210) = 2.987$, $P = 0.0081$; Interaction: $F(24,210) = 0.8927$, $P = 0.6120$].

Double immunostaining was performed with antibodies against the IL-1R1 and several cell specific markers to determine the cellular localization of IL-1R1 expression in the lumbar spinal cord dorsal horn at day 1 post-surgery (this day was selected because IL-1β expression was significantly increased at this timepoint). IL-1R1 expression was colocalized in GFAP-positive astrocytes in the SDHs, whereas there was no colocalization of IL-1R1 in NeuN-positive neurons or Iba-1-positive microglial cells in the SDHs of lumbar spinal cord (**Figure 2E**). These results demonstrate that the early activation of astrocyte IL-1R1 induced by increased IL-1β controls the development of MA following sciatic nerve injury.

Effects of IL-1ra on the Pathophysiological Changes in Astrocyte Activation in the Lumbar Spinal Cord Dorsal Horn of CCI Mice

To determine whether the CCI-induced early increase in spinal IL-1β expression modulates pathophysiological changes in astrocyte activation, we examined the effect of IL-1ra on the expression of GFAP, a major protein constituent of glial filaments in astrocytes of the central nervous system (Eng, 1985), in the lumbar spinal cord dorsal horn of CCI mice using Western blot analysis and immunohistochemistry. Results of Western blot analysis revealed that there was no change in GFAP expression in the ipsilateral lumbar spinal cord dorsal horn at day 1 post-CCI surgery as compared with sham group (**Figure 3A**). By contrast, intrathecal administration of IL-1ra (20 ng) on days 0 and 1 post-surgery significantly increased the expression of GFAP at day 1 post-surgery as compared with sham and vehicle-treated groups [**Figure 3A**; $F(2,15) = 8.306$, $P = 0.0037$]. However, there was no change in the expression of GFAP in the contralateral spinal cord dorsal horn after CCI and IL-1ra (20 ng) administration [**Figure 3B**; $F(2,15) = 0.05556$, $P = 0.9461$]. Immunohistochemical analysis showed that GFAP-immunoreactivity did not change in the ipsilateral lumbar spinal cord dorsal horn of CCI mice at day 1 post-surgery as compared with the sham group (**Figures 3C,D**). Intrathecal administration of IL-1ra significantly increased GFAP-immunoreactivity in the SDH (laminae I-II) and NP (laminae III-IV) regions at day 1 post-surgery as compared with sham group [**Figures 3C,D**; SDH: $F(2,15) = 9.280$, $P = 0.0024$; NP: $F(2,15) = 4.970$, $P = 0.0221$; NECK: $F(2,15) = 1.011$, $P = 0.3875$] further supporting what was observed in our Western blot analysis. When viewed under higher magnification astrocytes in the ipsilateral lumbar dorsal horn show hypertrophy with enlarged cell bodies [$F(2,15) = 9.639$, $P = 0.0020$] and elongated processes radiating from the soma [$F(2,15) = 10.91$, $P = 0.012$] in the IL-1ra-treated group at day 1 post-surgery as compared with sham and vehicle-treated groups (**Figures 3E,F**). These results suggest that the early activation of astrocyte IL-1R1 controls the induction of the pathophysiological changes in spinal astrocyte activation associated with CCI.

Effects of IL-1ra on the Expression of Astrocyte P450c17 in the Lumbar Spinal Cord Dorsal Horn of CCI Mice

To determine whether the CCI-induced early increase in spinal IL-1β expression modulates the protein expression of P450c17, we examined the effect of IL-1ra on the P450c17 expression in the lumbar spinal cord dorsal horn using Western blot analysis and immunohistochemistry. There was no change in the P450c17 expression in the ipsilateral lumbar spinal cord dorsal horn at day 1 post-CCI surgery

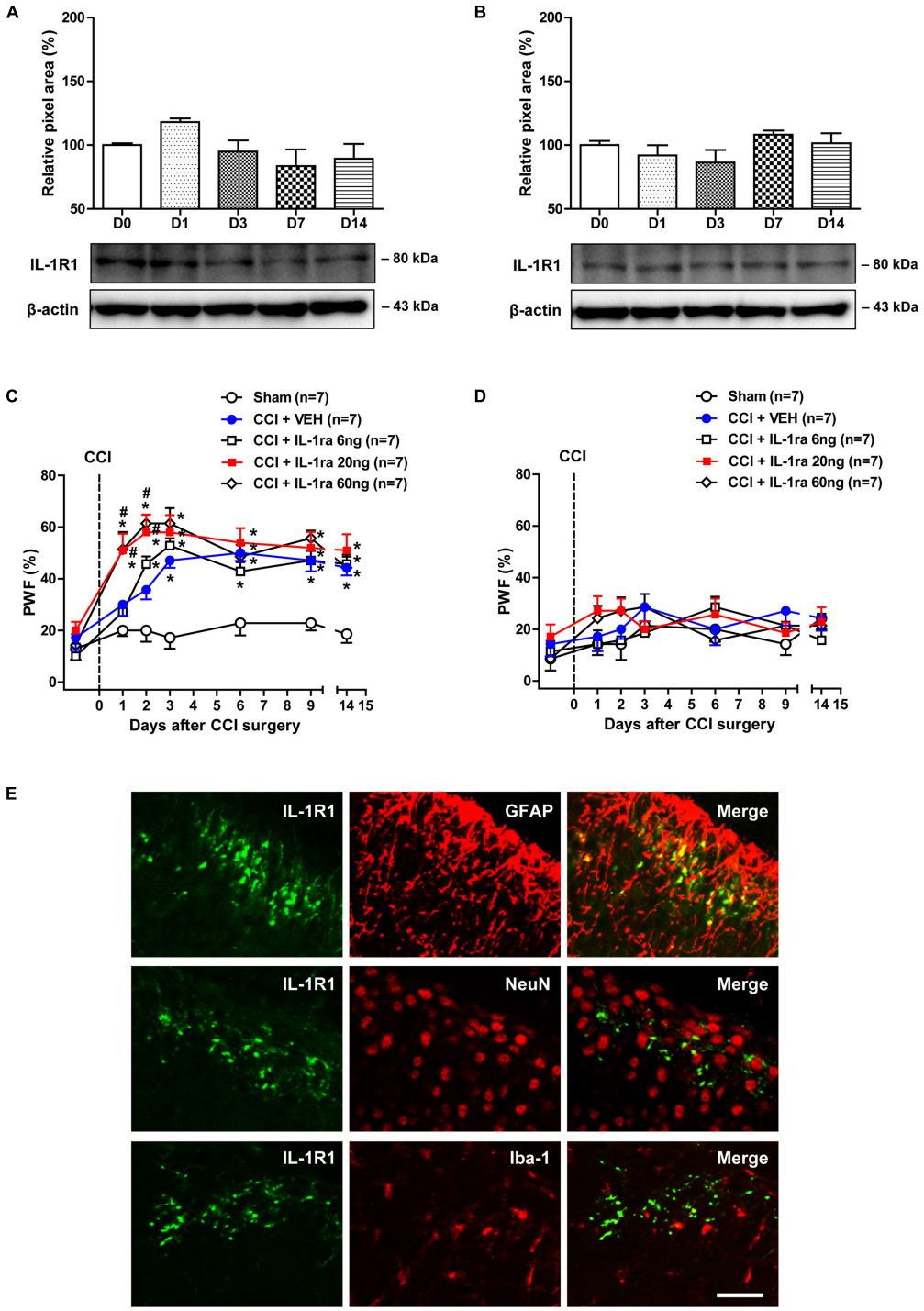

FIGURE 2 | Time course of changes in the expression of IL-1R1 and the effects of administration of an IL-1 receptor antagonist (IL-1ra; 6, 20, or 60 ng) on the CCI-induced development of MA. **(A,B)** The graphs depicting the changes in the protein expression of IL-1R1 are shown in the upper portion, while representative immunoblots are presented in the lower portion. Results of Western blot analysis showed that the protein expression of IL-1R1 did not change in the ipsilateral **(A)** and contralateral **(B)** lumbar spinal cord dorsal horn following CCI. The spinal cord dorsal horn was sampled at 0, 1, 3, 7, and 14 days after surgery. $n = 6$ mice/group. **(C,D)** Paw withdrawal frequency (PWF, %) was measured in hind paws using a von-Frey filament (0.16 g). Sciatic nerve injury increased the PWF to mechanical stimuli in the ipsilateral hind paw from day 3 post-surgery, while administration of IL-1ra (20 or 60 ng) induced a significant increase in the PWF beginning on day 1 post-surgery **(C)**. On the other hand, administration of IL-1ra had no effect on the PWF in the contralateral hind paw **(D)**. $n = 7$ mice/group. $^*P < 0.05$ vs. Sham; $\#P < 0.05$ vs. vehicle-treated group. **(E)** Using a double immunohistochemical approach these representative images depict colocalization (yellow) of IL-1R1 (green) with GFAP (red, a marker of astrocytes), but not with NeuN (red, a marker of neurons) or Iba-1 (red, a marker of microglial cells) at day 1 post-surgery in the superficial dorsal horn of lumbar spinal cord in CCI mice. Scale bar = 40 μm.

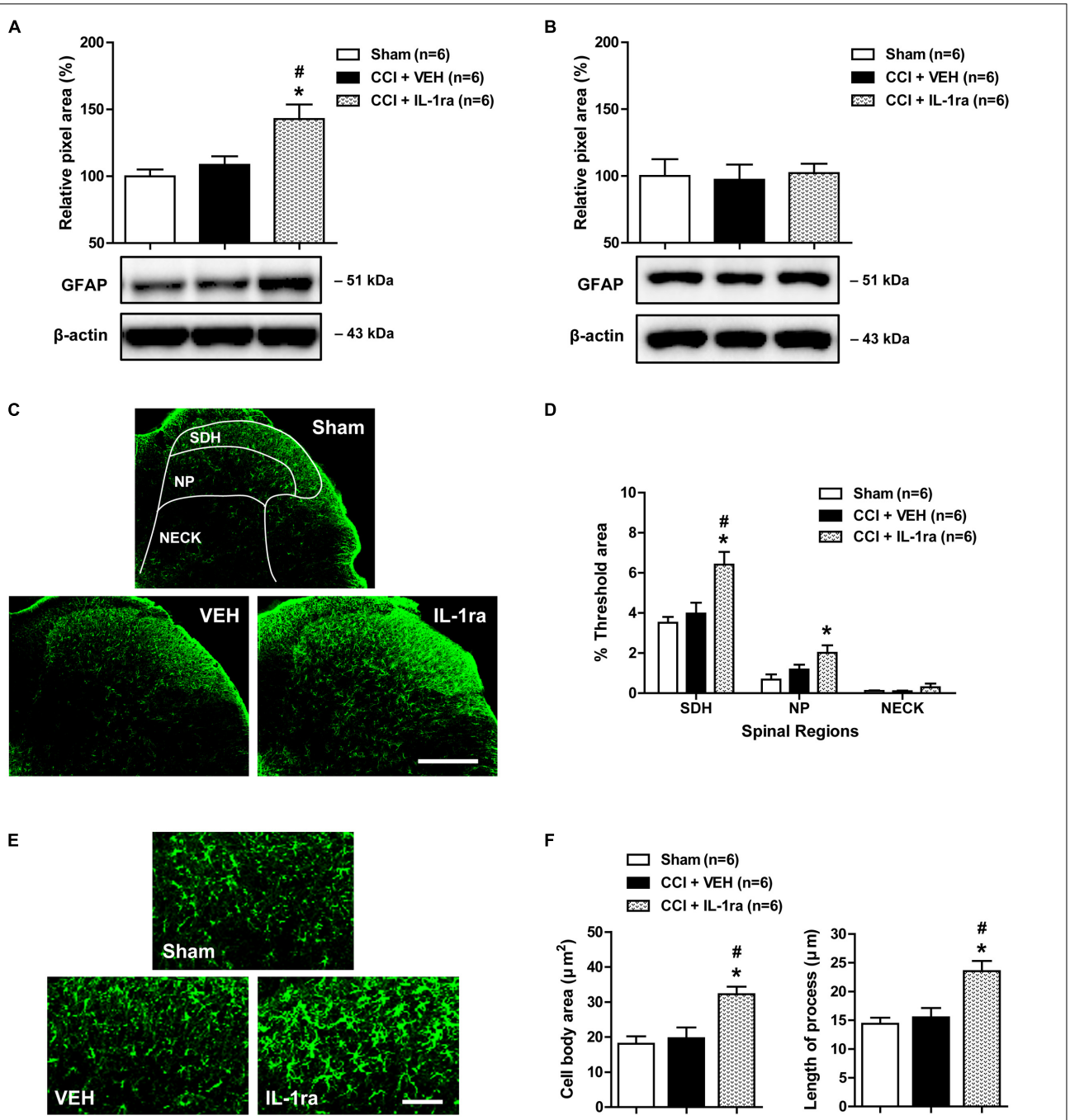

FIGURE 3 | Effects of IL-1 receptor antagonist (IL-1ra, 20 ng) administration on the expression of GFAP in the lumbar spinal cord dorsal horn of CCI mice. **(A)** Results of Western blot analysis showing that the protein expression of GFAP did not change following CCI at day 1 post-CCI surgery, while administration of IL-1ra increased the expression of GFAP in the ipsilateral lumbar spinal cord dorsal horn. **(B)** The expression of GFAP in the contralateral dorsal horn did not show any change after CCI and IL-1ra administration. $n = 6$ mice/group. **(C)** Representative images showing the changes in GFAP expression at day 1 post-surgery in the ipsilateral lumbar spinal cord dorsal horn of CCI mice using immunohistochemistry. Scale bar = 200 μm. **(D)** The immunofluorescence of GFAP in the superficial dorsal horn (SDH, lamina I-II), nucleus proprius (NP, lamina III-IV) and neck region (NECK, lamina V-VI) of mice was quantitated using an image analysis system. GFAP-immunoreactivity did not change following CCI at day 1 post-CCI surgery, while the administration of IL-1ra increased the expression of GFAP in the ipsilateral lumbar spinal cord dorsal horn. **(E)** Higher magnification images are shown in panel **(E)**. Scale bar = 40 μm. **(F)** The cell body area (μm^2) and the length of processes (μm) radiating from the soma of astrocytes did not change following CCI at day 1 post-surgery, while administration of IL-1ra increased the cell body area (μm^2) and the length of processes (μm). The spinal cord dorsal horn was sampled at day 1 post-surgery. $n = 6$ mice/group. $^*P < 0.05$ vs. Sham; $\#P < 0.05$ vs. vehicle-treated group.

as compared with the sham group. Conversely intrathecal administration of IL-1ra (20 ng) on days 0 and 1 post-surgery significantly increased the expression of P450c17 at day 1 post-surgery as compared with sham and vehicle-treated groups [**Figure 4A**; $F(2,21) = 6.507$, $P = 0.0063$]. However, there was no change in the expression of P450c17 in the contralateral spinal cord dorsal horn after CCI and IL-1ra (20 ng) administration [**Figure 4B**; $F(2,21) = 0.8167$, $P = 0.4554$]. In addition, the number of P450c17-immunostained astrocytes did not change in the ipsilateral lumbar spinal cord dorsal horn at day 1 post-surgery as compared with sham group (**Figures 4C,D**). Administration of IL-1ra significantly increased the number of P450c17-immunostained astrocytes in the SDH (laminae I-II) region at day 1 post-surgery as compared with the sham and vehicle-treated groups [**Figures 4C,D**; SDH: $F(2,15) = 8.416$, $P = 0.0035$; NP: $F(2,15) = 2.681$, $P = 0.1011$; NECK: $F(2,15) = 0.04425$, $P = 0.9568$]. On the other hand, there was no change in the number of P450c17-immunostained neurons in the ipsilateral lumbar spinal cord dorsal horn at day 1 post-surgery and no significant difference was observed between the vehicle-treated and IL-1ra-treated groups for P450c17 immunostaining in neurons [**Figures 4E,F**; SDH: $F(2,15) = 0.3540$, $P = 0.7076$; NP: $F(2,15) = 0.3894$, $P = 0.6841$; NECK: $F(2,15) = 0.04407$, $P = 0.9570$]. These results suggest that the early activation of astrocyte IL-1R1 controls the expression of P450c17, which is increased in spinal astrocytes following CCI.

Effects of IL-1β on the IL-1ra-Induced Early Increase in Spinal P450c17 Expression and Astrocyte Activation in CCI Mice

Next, we used Western blot analysis to examine whether blocking the direct effect of IL-1ra with spinal IL-1β would alter the increase in astrocyte P450c17 expression and astrocyte activation in the lumbar spinal cord dorsal horn. Intrathecal administration of IL-1ra (20 ng) on days 0 and 1 post-surgery significantly increased the expression of P450c17 in the ipsilateral spinal cord dorsal horn at day 1 post-surgery as compared with the vehicle-treated groups. This increase in P450c17 expression was significantly reduced by the intrathecal co-administration with IL-1β (10 ng in combination with IL-1ra) [**Figure 5A**; $F(2,15) = 5.556$, $P = 0.0156$]. In addition, intrathecal administration of IL-1ra (20 ng) on days 0 and 1 post-surgery significantly increased the expression of GFAP in the ipsilateral spinal cord dorsal horn at the 1 day post-surgery timepoint as compared with the vehicle-treated groups, and this increase was significantly reduced by the intrathecal administration of IL-1ra with IL-1β (10 ng in combination with IL-1ra) [**Figure 5B**; $F(2,15) = 7.399$, $P = 0.0058$]. However, there was no change in the expression of P450c17 [**Figure 5C**; $F(2,15) = 1.010$, $P = 0.3876$] and GFAP [**Figure 5D**; $F(2,15) = 0.07990$, $P = 0.9236$] in the contralateral spinal cord dorsal horn after drug administration. These results show that i.t. administration of IL-1β blocks the early increase in spinal P450c17 expression and astrocyte activation induced by blockade of spinal IL-1 receptors in CCI mice.

Effects of Ketoconazole or Fluorocitrate on the IL-1ra-Induced Early Development of Mechanical Allodynia in CCI Mice

We next examined whether intrathecal administration of the P450c17 inhibitor, ketoconazole or the astrocyte metabolic inhibitor, FC, would change the early development of MA induced by IL-1ra administration. Intrathecal administration of IL-1ra (20 ng) from days 0 to 3 post-surgery increased the PWF (%) to innocuous mechanical stimuli (MA) in the ipsilateral hind paw beginning at 1 day post-CCI surgery as compared with normal baseline values (**Figure 6A**). Treatment with the P450c17 inhibitor, ketoconazole (1, 3, or 10 nmol together with IL-1ra), significantly reduced this CCI/IL-1ra-induced development of MA in the ipsilateral hind paw [**Figure 6A**; Group: $F(3,196) = 37.58$, $P < 0.0001$; Time: $F(6,196) = 12.81$, $P < 0.0001$; Interaction: $F(18,196) = 2.189$, $P = 0.0047$]. By contrast, i.t. co-administration of ketoconazole with IL-1ra (20 ng) during the induction phase of neuropathic pain (from days 0 to 3 post-surgery) had no effect on the PWF in the contralateral hind paw [**Figure 6B**; Group: $F(3,196) = 0.8633$, $P = 0.4611$; Time: $F(6,196) = 0.5662$, $P = 0.7570$; Interaction: $F(18,196) = 1.483$, $P = 0.0990$]. In addition, intrathecal administration of the astrocyte metabolic inhibitor, FC (0.01, 0.03, or 0.1 nmol together with IL-1ra) significantly reduced the CCI-induced development of MA in the ipsilateral paw that developed beginning 1 day post-CCI surgery following IL-1ra administration [**Figure 6C**; Group: $F(3,140) = 26.39$, $P < 0.0001$; Time: $F(6,140) = 16.20$, $P < 0.0001$; Interaction: $F(18,140) = 1.391$, $P = 0.1447$]. By contrast, i.t. co-administration of FC with IL-1ra (20 ng) during the induction phase of neuropathic pain (from days 0 to 3 post-surgery) had no effect on the PWF in the contralateral hind paw [**Figure 6D**; Group: $F(3,140) = 1.445$, $P = 0.2325$; Time: $F(6,140) = 1.002$, $P = 0.4268$; Interaction: $F(18,140) = 0.9128$, $P = 0.5643$]. These results suggest that early increases in P450c17 expression and astrocyte activation contribute to the early development of ipsilateral MA induced by the inhibition of spinal IL-1 receptors in CCI mice.

DISCUSSION

This study demonstrates three important novel findings. First, CCI-induced sciatic nerve injury produces an early, but transient, increase in IL-1β expression in the SDH of the ipsilateral lumbar spinal cord. Moreover, we demonstrate that the IL-1 receptor type 1 (IL-1R1), a functional receptor of IL-1β, is expressed in GFAP-positive astrocytes, which are also exclusively located in the SDH region. Secondly, blockade of IL-1R1 with intrathecal administration of the IL-1 receptor antagonist (IL-1ra) during the early phase of peripheral neuropathy increased the expression of both astrocyte P450c17 and GFAP in the spinal cord dorsal horn, and this increase was blocked by IL-1β administration. Finally, intrathecal administration of IL-1ra significantly facilitated the development of MA, and this

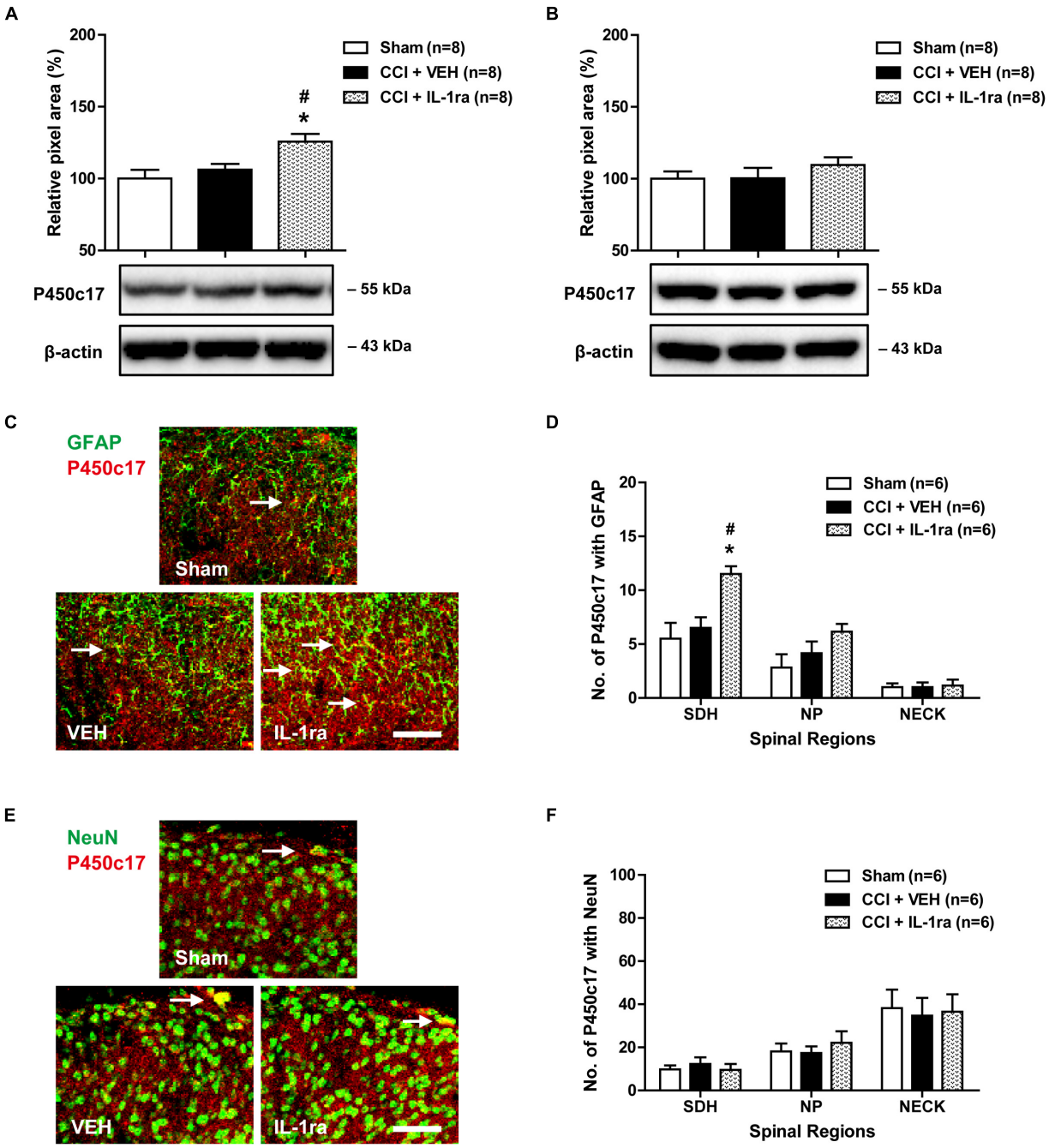

FIGURE 4 | Effects of IL-1 receptor antagonist (IL-1ra, 20 ng) administration on the expression of P450c17 in the lumbar spinal cord dorsal horn of CCI mice. **(A)** Results of Western blot analysis showed that the protein expression of P450c17 did not change at day 1 post-CCI surgery, while administration of IL-1ra increased the protein expression of P450c17 in the ipsilateral spinal cord dorsal horn. **(B)** The expression of P450c17 in the contralateral dorsal horn did not show any change after CCI and IL-1ra administration. $n = 8$ mice/group. **(C–F)** Using a double immunohistochemical approach these representative images depict colocalization (yellow) of P450c17 with GFAP (**C**; green, a marker of astrocytes) or NeuN (E; green, a marker of neurons) at day 1 post-surgery in the ipsilateral lumbar spinal cord dorsal horn of CCI mice. Scale bar = 50 μm. Colocalization was quantitated in the superficial dorsal horn (SDH, lamina I-II), nucleus proprius (NP, lamina III-IV) and neck region (NECK, lamina V-VI). The number of P450c17-immunostained astrocytes **(D)** did not change following CCI at day 1 post-CCI surgery, while administration of IL-1ra increased the number of P450c17-immunostained astrocytes in the SDH region of the ipsilateral lumbar spinal cord. The number of P450c17-immunostained neurons **(F)** did not change following CCI and treatment with IL-1ra. The spinal cord dorsal horn was sampled at day 1 post-surgery. $n = 6$ mice/group. $^*P < 0.05$ vs. Sham; $\#P < 0.05$ vs. vehicle-treated group.

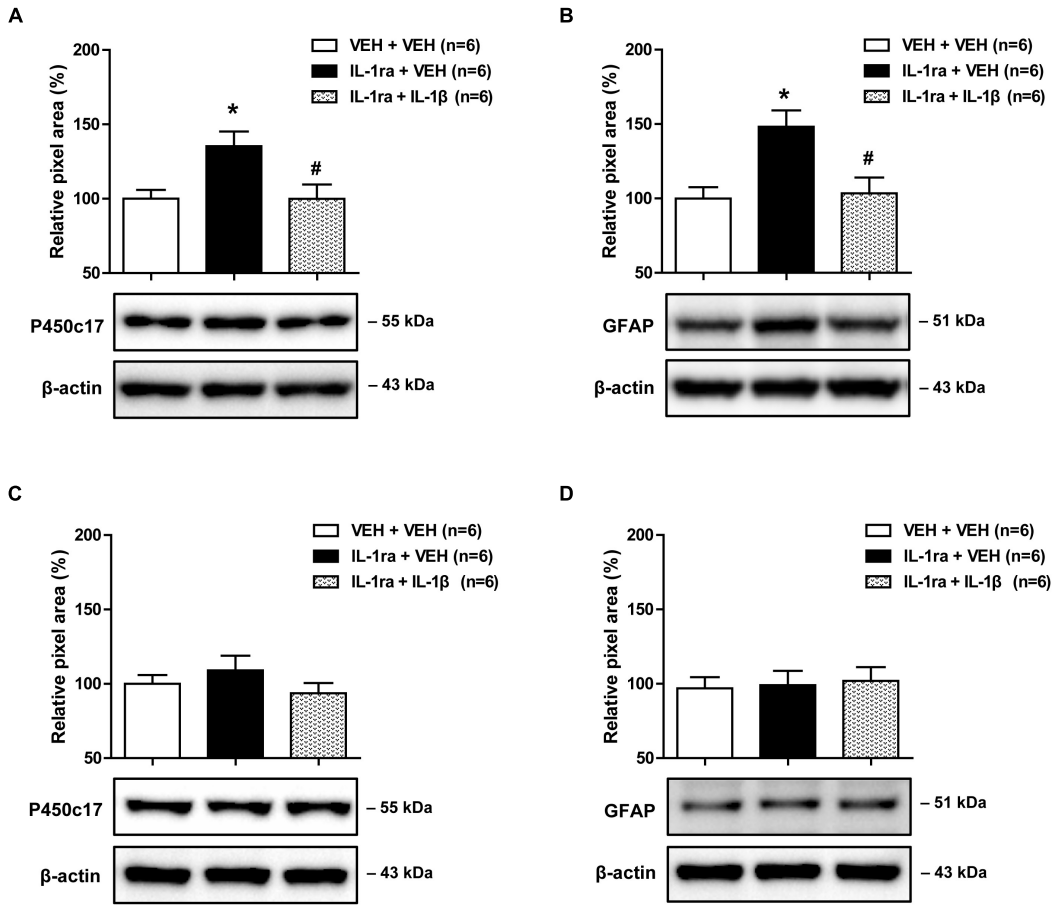

FIGURE 5 | Effects of IL-1β (10 ng) on the early increases in the expression of spinal P450c17 and astrocyte activation in IL-1 receptor antagonist (IL-1ra, 20 ng) treated CCI mice. **(A)** Results of Western blot analysis showed that the protein expression of P450c17 in the ipsilateral spinal cord dorsal horn was increased at day 1 post-CCI surgery by administration of IL-1ra, and this increase was blocked by the co-administration of IL-1β (10 ng) with IL-1ra. **(B)** Results of Western blot analysis showed that the protein expression of GFAP in the ipsilateral spinal cord dorsal horn was increased at day 1 post-CCI surgery by administration of IL-1ra, and this increase was blocked by co-administration of IL-1β (10 ng) with IL-1ra. **(C,D)** The expression of P450c17 **(C)** and GFAP **(D)** in the contralateral dorsal horn did not show any change after drug administration. The spinal cord dorsal horn was sampled at day 1 post-surgery. $n = 6$ mice/group. $^*P < 0.05$ vs. vehicle-treated group; $\#P < 0.05$ vs. IL-1ra-treated group.

facilitation was suppressed by intrathecal administration of either the P450c17 inhibitor, ketoconazole or the astrocyte metabolic inhibitor, FC. Collectively, we believe that this data significantly increases our understanding of one of the mechanisms underlying the development of neuropathic pain by demonstrating that the modulation of astrocyte P450c17 expression is closely associated with an early increased release of IL-1β in the lumbar spinal cord dorsal horn and this P450c17 modulation of IL-1β ultimately affects the development of MA induced by peripheral nerve injury. In the present study, we demonstrated that IL-1β expression was significantly increased in the SDH (laminae I-II) region of the ipsilateral spinal cord at 1 day following peripheral nerve injury. These results suggest that the expression of IL-1β is transiently upregulated during the early phase of neuropathic pain, which in turn can influence the activity of various adjacent cells in the SDH region of the spinal cord. There are two receptors for the interleukin-1 (IL-1) have been characterized; IL-1 type 1 receptor (IL-1R1) and IL-1 type 2 receptor (IL-1R2) (Ren and Torres, 2009). IL-1R2 lacks an intracellular domain and is incapable of signal transduction, while IL-1R1 is a transmembrane molecule that is responsible for IL-1β signal transducing (Sims et al., 1993). In the present study, double immunofluorescence staining of the IL-1 receptor type 1 and GFAP, a major protein constituent of glial filaments in astrocytes of the central nervous system (Eng, 1985), strongly supports a close interaction of IL-1β signaling with spinal astrocytes. Furthermore, blockade of IL-1R1 with an IL-1 receptor antagonist during the induction phase of neuropathic pain facilitated astrocyte hypertrophy with enlarged cell bodies and elongated processes radiating from the soma especially in the SDH, where primary afferent nociceptive C-fibers and myelinated A-fibers terminate and synapse with second order neurons (Todd, 2010). These results strongly suggest the possibility that the early transient increase in IL-1β plays an important role in the control of the pathological changes in adjacent astrocytes via binding to the IL-1 type 1 receptors on astrocytes located in SDH

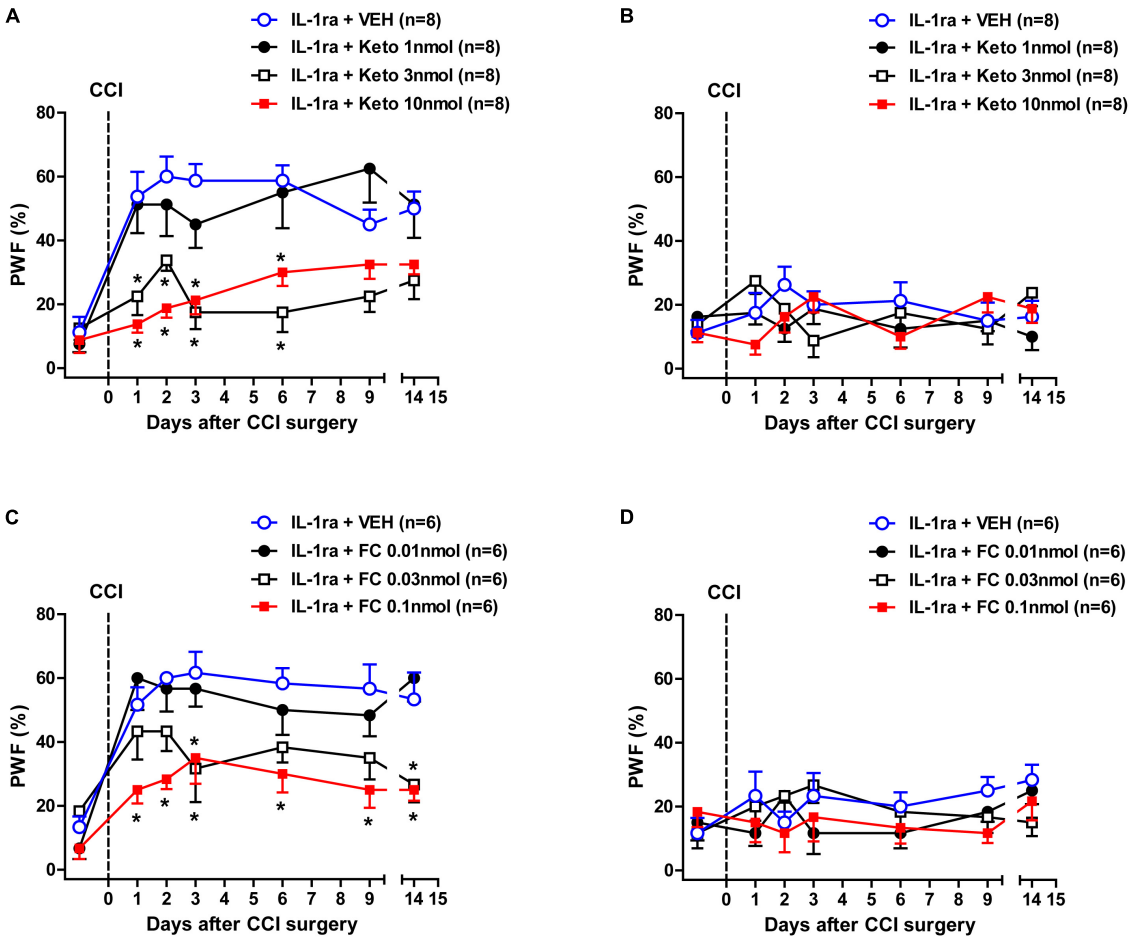

FIGURE 6 | Effects of the P450c17 inhibitor, ketoconazole (Keto, 1, 3, and 10 nmol) or the astrocyte metabolic inhibitor, fluorocitrate (FC, 0.01, 0.03, and 0.1 nmol) on the early development of mechanical allodynia in IL-1 receptor antagonist (IL-1ra, 20 ng) treated CCI mice. **(A–D)** Paw withdrawal frequency (PWF, %) was measured in hind paws using a von-Frey filament (0.16 g). IL-1ra administration induced an early increase in the PWF of the ipsilateral hind paw and this was significantly suppressed by the co-administration of ketoconazole with IL-1ra **(A)**. On the other hand, administration of ketoconazole in association with IL-1ra had no effect on the PWF in the contralateral hind paw **(B)**. $n = 8$ mice/group. $^*P < 0.05$ vs. IL-1ra-treated group. In addition, IL-1ra-induced an early increase in the PWF of the ipsilateral hind paw was significantly suppressed by the co-administration of fluorocitrate with IL-1ra **(C)**. Conversely, administration of fluorocitrate in association with IL-1ra had no effect on the PWF of the contralateral hind paw **(D)**. $n = 6$ mice/group. $^*P < 0.05$ vs. IL-1ra-treated group.

region, ultimately affecting nociceptive synaptic transmission following peripheral nerve injury.

It has become increasingly evident that IL-1β is released from activated microglial cells in response to a variety of inflammatory stimuli (Clark et al., 2010; Choi et al., 2015). Paclitaxel triggers the elevation of Ca^{2+} levels in microglial cells by activation of microglial toll like receptor 4, which leads to the rapid release of IL-1β from spinal microglial cells (Yan et al., 2019). In addition, the microglial P2X7 receptor is involved in the lipopolysaccharide (LPS)-induced release of IL-1β in the spinal cord dorsal horn (Clark et al., 2010). While astrocytes are also able to produce IL-1β, astrocytes are less likely to respond directly to LPS, but rather respond to cytokines that are released from microglial cells activated by LPS (Lee et al., 1993). Moreover, higher levels of cytokines are induced in microglial cells than in astrocytes (Lee et al., 1993). Thus, we propose that spinal microglial cells are a major source of IL-1β during the early phase of peripheral neuropathy. Furthermore, it has been reported that IL-4, -10, and -13 play a role in producing an analgesic effect in experimental inflammatory pain models suggesting that the endogenous release of these cytokines may limit the development of the nociceptive response during inflammatory pain reactions (Vale et al., 2003). This antinociceptive effect seems to be mediated through a peripheral mechanism involving the inhibition of the release of proinflammatory cytokines (Vale et al., 2003). Since microglial cells express the mRNAs for both the IL-4 and IL-10 cytokine receptors and since these cytokines function as negative regulators of microglial functions (Sawada et al., 1999), it is important to do future investigations on the role of diverse cytokines in the central mechanisms underlying the development of antinociception in inflammatory pain conditions.

In the present study, early blockade of the IL-1 receptor with an IL-1 receptor antagonist significantly enhances the expression of P450c17 in astrocytes. In addition, inhibition of

spinal P450c17 with the P450c17 inhibitor, ketoconazole blocks the early development of MA induced by administration of an IL-1 receptor antagonist, suggesting that the nerve injury-induced increase in IL-1β may produce an analgesic effect through inhibition of both the expression of astrocyte P450c17 and the concomitant production of neurosteroids in astrocytes as possible control mechanisms against the development of neuropathic pain. There are several studies supporting our concept that IL-1β has an analgesic effect on nociceptive signal transmission in the central nervous system. Souter et al. showed that intrathecal IL-1β dose-dependently suppressed carrageenan-induced inflammatory pain and this was not opioid-dependent (Souter et al., 2000). Kim et al. observed that IL-1β injected intracisternally produced antinociceptive effects in an NMDA-evoked pain model of the orofacial area, while the antinociceptive effect was mediated by an opioid pathway (Kim et al., 2004). Collectively these results suggest that IL-1β-induced analgesia occurs via different mechanisms in the spinal cord and at higher levels of the neuroaxis.

Interleukin-1 is a family of 11 cytokines that are the products of separate genes and play a central role in the regulation of immune and inflammatory responses (Rothwell and Luheshi, 2000). IL-1α and IL-1β are the agonists of IL-1 receptors, while IL-1ra binds to IL-1 receptors but does not induce any intracellular response (Arend et al., 1998). In the present study, IL-1ra induced an early increase in the expression of GFAP and P450c17, which was prevented by the co-administration of IL-1β with IL-1ra. Since not only IL-1β, but also endogenous IL-1α and IL-1ra are able to bind to IL-1 receptors, these results suggest that the effect of exogenous IL-1ra on both astrocyte activity and P450c17 expression is mediated in large part by blockade of IL-1β's action in this neuropathic pain model. It has been suggested that IL-1α and IL-1β act on the same receptor to differentially influence nociceptive transmission and the neuropathic pain response (Mika et al., 2008). In addition, Andre et al. suggested that IL-1α and IL-1β are identical in their ability to initiate downstream activation of mitogen-activated protein kinases and nuclear factor-kappa B, but IL-1β caused IL-6 release more potent than IL-1α, suggesting the possible existence of additional signaling pathway activated by IL-1β (Andre et al., 2005). The detail mechanisms underlying the effects of IL-1β in the central nervous system remain unclear, but the presence of endogenous IL-1α and IL-1ra suggests the possibility that this IL-1 family may influence the action of IL-1β by competing with that for binding sites of the receptor.

In a previous study from our laboratories, we showed that the protein expression of GFAP and P450c17 in the ipsilateral lumbar spinal cord dorsal horn was statistically increased at 3 days post-CCI surgery and that inhibition of astrocytes or P450c17 during this induction phase (from days 0 to 3 post-surgery) had significant analgesic effects on the CCI-induced development of neuropathic pain (Moon et al., 2014; Choi et al., 2019). By contrast, the protein expression of GFAP and P450c17 was gradually decreased and was not statistically different in the spinal cord dorsal horn of day 14 post-surgery mice compared with control mice and inhibition of P450c17 during this maintenance phase (from days 14 to 17 post-surgery) had no effect on the neuropathic pain that had already developed (data not shown). These results raise the possibility that during the maintenance phase, the stimulatory effect of P450c17 disappears and/or another inhibitory control factor appears. This should be further investigated in order to understand the different mechanisms associated with the induction versus the maintenance phases of neuropathic pain.

In the present study, we focused our investigation on whether IL-1β can have a negative modulatory effect on the development of neuropathic pain and thus serve as a transient negative control mechanism. By contrast, IL-1β has been reported to induce hyperalgesia by exerting robust cellular inflammatory actions as a pro-inflammatory cytokine *in vivo*. These actions are supported by several studies showing that peripheral IL-1β contributes to the development of inflammatory pain hypersensitivity by increasing cyclooxygenase-2 expression, leading to the release of prostanoids, which sensitize peripheral nociceptors (Samad et al., 2001). It has also been reported that spinal IL-1β increased the phosphorylation of the NMDA receptor GluN1 subunit and facilitated pain in a rat model of inflammatory pain (Zhang et al., 2008). While several studies using animal models have demonstrated that the inhibition of IL-1 significantly inhibits persistent pain, this did not occur in our study. In this regard, Gabay et al. (2011) showed that chronic pharmacological blockade of IL-1 signaling markedly reduced neuropathic pain symptoms, as reflected by attenuated MA. Conversely our results indicate that blockade of IL-1 signaling produces a robust but temporary antinociceptive effect. This discrepancy may be due to: (1) the early timepoint examined in this study; (2) differences in the animal models being examined; (3) the different time course of nociception in each model; (4) different routes of administration of IL-1ra or other drugs; and/or (5) the nervous system location being examined. These different experimental conditions can alter the micro-environment of the nervous system by changing the expression patterns of the IL-1 receptor, the activation of adjacent glial cells, and/or the release of other cytokines. Thus, the effect of IL-1β can be modified based on changes to any of these parameters. Since the evidence suggests that IL-1β can have contradictory roles, analgesia versus hyperalgesia, on nociception, it is important that the experimental design of future studies take this into account in order to exploit specific targeting of the IL-1β pathway. In this regard we plan to investigate the mechanisms underlying cytokine-induced modulation of pain transmission in more detail in future studies.

CONCLUSION

In conclusion, the present study demonstrates that the expression of IL-1β is significantly increased in the ipsilateral lumbar spinal cord dorsal horn of CCI mice and that blockade of central IL-1β signaling by intrathecal administration of IL-1 receptor antagonist during the induction phase of neuropathic pain not only facilitates the development of MA, but also increases both astrocyte P450c17 expression and pathological astrocyte activation in CCI mice. Collectively these results suggest that early increased spinal IL-1β plays an important

role as a transient analgesic mechanism that controls the development of neuropathic pain by inhibiting both the expression of astrocyte P450c17 and the activation of spinal astrocytes following peripheral nerve injury. This study offers new insights into a potential, but transient analgesic role of IL-1β in nociceptive processing at the level of the spinal cord and suggests that development of interleukin-1 receptor agonists may serve as novel and selective therapeutic agents for the prevention of the development of neuropathic pain following peripheral nerve injury.

DATA AVAILABILITY

The datasets for this manuscript are not publicly available because of a security issue. Requests to access the datasets should be directed to J-HL, jhl1101@snu.ac.kr.

ETHICS STATEMENT

The experimental protocols for animal usage were reviewed and approved by the SNU Animal Care and Use Committee and were consistent with the Guide for the Care and Use of Laboratory Animals published by the United States National Institutes of Health (1985).

AUTHOR CONTRIBUTIONS

S-RC contributed to the design of the study, acquisition and analysis of data, and drafting the manuscript. H-JH assisted molecular biological techniques and the data analysis of molecular biological experiments. AB was involved with data analysis and revised the manuscript for important intellectual content. J-HL contributed to the conception of the study, interpretation of data, and final approval of the version to be submitted.

FUNDING

This study was supported by the National Research Foundation of Korea (NRF) grant funded by the Government of South Korea (2017R1A2A2A05001402).

REFERENCES

Andre, R., Pinteaux, E., Kimber, I., and Rothwell, N. J. (2005). Differential actions of IL-1 alpha and IL-1 beta in glial cells share common IL-1 signalling pathways. *Neuroreport* 16, 153–157. doi: 10.1097/00001756-200502080-00017

Arend, W. P., Malyak, M., Guthridge, C. J., and Gabay, C. (1998). Interleukin-1 receptor antagonist: role in biology. *Annu. Rev. Immunol.* 16, 27–55. doi: 10.1146/annurev.immunol.16.1.27

Baulieu, E. E. (1998). Neurosteroids: a novel function of the brain. *Psychoneuroendocrinology* 23, 963–987. doi: 10.1016/s0306-4530(98)00071-7

Bennett, G. J., and Xie, Y. K. (1988). A peripheral mononeuropathy in rat that produces disorders of pain sensation like those seen in man. *Pain* 33, 87–107. doi: 10.1016/0304-3959(88)90209-6

Chen, G., Park, C. K., Xie, R. G., Berta, T., Nedergaard, M., and Ji, R. R. (2014). Connexin-43 induces chemokine release from spinal cord astrocytes to maintain late-phase neuropathic pain in mice. *Brain* 137, 2193–2209. doi: 10.1093/brain/awu140

Choi, H.-S., Roh, D.-H., Yoon, S.-Y., Choi, S.-R., Kwon, S.-G., Kang, S.-Y., et al. (2018). Differential involvement of ipsilateral and contralateral spinal cord astrocyte D-serine in carrageenan-induced mirror-image pain: role of σ1 receptors and astrocyte gap junctions. *Br. J. Pharmacol.* 175, 558–572. doi: 10.1111/bph.14109

Choi, H.-S., Roh, D.-H., Yoon, S.-Y., Kwon, S.-G., Choi, S.-R., Kang, S.-Y., et al. (2017). The role of spinal interleukin-1β and astrocyte connexin 43 in the development of mirror-image pain in an inflammatory pain model. *Exp. Neurol.* 287, 1–13. doi: 10.1016/j.expneurol.2016.10.012

Choi, H.-S., Roh, D.-H., Yoon, S.-Y., Moon, J.-Y., Choi, S.-R., Kwon, S.-G., et al. (2015). Microglial interleukin-1β in the ipsilateral dorsal horn inhibits the development of mirror-image contralateral mechanical allodynia through astrocyte activation in a rat model of inflammatory pain. *Pain* 156, 1046–1059. doi: 10.1097/j.pain.0000000000000148

Choi, S.-R., Roh, D.-H., Yoon, S.-Y., Choi, H.-S., Kang, S.-Y., Han, H.-J., et al. (2019). Spinal cytochrome P450c17 plays a key role in the development of neuropathic mechanical allodynia: involvement of astrocyte sigma-1 receptors. *Neuropharmacology* 149, 169–180. doi: 10.1016/j.neuropharm.2019.02.013

Choi, S.-R., Roh, D.-H., Yoon, S.-Y., Kang, S.-Y., Moon, J.-Y., Kwon, S.-G., et al. (2013). Spinal sigma-1 receptors activate NADPH oxidase 2 leading to the induction of pain hypersensitivity in mice and mechanical allodynia in neuropathic rats. *Pharmacol. Res.* 74, 56–67. doi: 10.1016/j.phrs.2013.05.004

Choi, S.-R., Roh, D.-H., Yoon, S.-Y., Kwon, S.-G., Choi, H.-S., Han, H.-J., et al. (2016). Astrocyte sigma-1 receptors modulate connexin 43 expression leading to the induction of below-level mechanical allodynia in spinal cord injured mice. *Neuropharmacology* 111, 34–46. doi: 10.1016/j.neuropharm.2016.08.027

Clark, A. K., Staniland, A. A., Marchand, F., Kaan, T. K., McMahon, S. B., and Malcangio, M. (2010). P2X7-dependent release of interleukin-1beta and nociception in the spinal cord following lipopolysaccharide. *J. Neurosci.* 30, 573–582. doi: 10.1523/JNEUROSCI.3295-09.2010

Compagnone, N. A., and Mellon, S. H. (2000). Neurosteroids: biosynthesis and function of these novel neuromodulators. *Front. Neuroendocrinol.* 21:56. doi: 10.1006/frne.1999.0188

Dworkin, R. H., O'Connor, A. B., Backonja, M., Farrar, J. T., Finnerup, N. B., and Jensen, T. S. (2007). Pharmacologic management of neuropathic pain: evidence-based recommendations. *Pain* 132, 237–251. doi: 10.1016/j.pain.2007.08.033

Eng, L. F. (1985). Glial fibrillary acidic protein (GFAP): the major protein of glial intermediate filaments in differentiated astrocytes. *J. Neuroimmunol.* 8, 203–214. doi: 10.1016/s0165-5728(85)80063-1

Fu, D., Guo, Q., Ai, Y., Cai, H., Yan, J., and Dai, R. (2006). Glial activation and segmental upregulation of interleukin-1beta (IL-1beta) in the rat spinal cord after surgical incision. *Neurochem. Res.* 31, 333–340. doi: 10.1007/s11064-005-9032-4

Gabay, E., Wolf, G., Shavit, Y., Yirmiya, R., and Tal, M. (2011). Chronic blockade of interleukin-1 (IL-1) prevents and attenuates neuropathic pain behavior and spontaneous ectopic neuronal activity following nerve injury. *Eur. J. Pain* 15, 242–248. doi: 10.1016/j.ejpain.2010.07.012

Hylden, J. L., and Wilcox, G. L. (1980). Intrathecal morphine in mice: a new technique. *Eur. J. Pharmacol.* 67, 313–316. doi: 10.1016/0014-2999(80)90515-4

Ji, R. R., Kohno, T., Moore, K. A., and Woolf, C. J. (2003). Central sensitization and LTP: do pain and memory share similar mechanisms? *Trends Neurosci.* 26, 696–705. doi: 10.1016/j.tins.2003.09.017

Kibaly, C., Meyer, L., Patte-Mensah, C., and Mensah-Nyagan, A. G. (2008). Biochemical and functional evidence for the control of pain mechanisms by dehydroepiandrosterone endogenously synthesized in the spinal cord. *FASEB J.* 22, 93–104. doi: 10.1096/fj.07-8930com

Kim, H. D., Lee, H. J., Choi, H. S., Ju, J. S., Jung, C. Y., Bae, Y. C., et al. (2004). Interleukin-1 beta injected intracisternally inhibited NMDA-evoked behavioral

response in the orofacial area of freely moving rats. *Neurosci. Lett.* 360, 37–40. doi: 10.1016/j.neulet.2004.01.059

Latremoliere, A., and Woolf, C. J. (2009). Central sensitization: a generator of pain hypersensitivity by central neural plasticity. *J. Pain* 10, 895–926. doi: 10.1016/j.jpain.2009.06.012

Lee, K. M., Chiu, K. B., Sansing, H. A., Didier, P. J., Ficht, T. A., Arenas-Gamboa, A. M., et al. (2013). Aerosol-induced brucellosis increases TLR-2 expression and increased complexity in the microanatomy of astroglia in rhesus macaques. *Front. Cell. Infect. Microbiol.* 3:86. doi: 10.3389/fcimb.2013.00086

Lee, S. C., Liu, W., Dickson, D. W., Brosnan, C. F., and Berman, J. W. (1993). Cytokine production by human fetal microglia and astrocytes. differential induction by lipopolysaccharide and IL-1 beta. *J. Immunol.* 150, 2659–2667.

Mika, J., Korostynski, M., Kaminska, D., Wawrzczak-Bargiela, A., Osikowicz, M., Makuch, W., et al. (2008). Interleukin-1 alpha has antiallodynic and antihyperalgesic activities in a rat neuropathic pain model. *Pain* 138, 587–597. doi: 10.1016/j.pain.2008.02.015

Moon, J.-Y., Roh, D.-H., Yoon, S.-Y., Choi, S.-R., Kwon, S.-G., Choi, H.-S., et al. (2014). sigma1 receptors activate astrocytes via p38 MAPK phosphorylation leading to the development of mechanical allodynia in a mouse model of neuropathic pain. *Br. J. Pharmacol.* 171, 5881–5897. doi: 10.1111/bph.12893

National Institutes of Health (1985). *Guide for the Care and Use of Laboratory Animals*, 2nd Edn. Washington, DC: National Institutes of Health.

Patte-Mensah, C., Kibaly, C., Boudard, D., Schaeffer, V., Béglé, A., Saredi, S., et al. (2006). Neurogenic pain and steroid synthesis in the spinal cord. *J. Mol. Neurosci.* 28, 17–31.

Ren, K., and Dubner, R. (2008). Neuron-glia crosstalk gets serious: role in pain hypersensitivity. *Curr. Opin. Anaesthesiol.* 21, 570–579. doi: 10.1097/ACO.0b013e32830edbdf

Ren, K., and Torres, R. (2009). Role of interleukin-1beta during pain and inflammation. *Brain Res. Rev.* 60, 57–64. doi: 10.1016/j.brainresrev.2008.12.020

Roh, D.-H., Choi, S.-R., Yoon, S.-Y., Kang, S.-Y., Moon, J.-Y., Kwon, S.-G., et al. (2011). Spinal neuronal NOS activation mediates sigma-1 receptor-induced mechanical and thermal hypersensitivity in mice: involvement of PKC-dependent GluN1 phosphorylation. *Br. J. Pharmacol.* 163, 1707–1720. doi: 10.1111/j.1476-5381.2011.01316.x

Rothwell, N. J., and Luheshi, G. N. (2000). Interleukin 1 in the brain: biology, pathology and therapeutic target. *Trends Neurosci.* 23, 618–625. doi: 10.1016/s0166-2236(00)01661-1

Samad, T. A., Moore, K. A., Sapirstein, A., Billet, S., Allchorne, A., Poole, S., et al. (2001). Interleukin-1beta-mediated induction of Cox-2 in the CNS contributes to inflammatory pain hypersensitivity. *Nature* 410, 471–475. doi: 10.1038/35068566

Sawada, M., Suzumura, A., Hosoya, H., Marunouchi, T., and Nagatsu, T. (1999). Interleukin-10 inhibits both production of cytokines and expression of cytokine receptors in microglia. *J. Neurochem.* 72, 1466–1471. doi: 10.1046/j.1471-4159.1999.721466.x

Sims, J. E., Gayle, M. A., Slack, J. L., Alderson, M. R., Bird, T. A., Giri, J. G., et al. (1993). Interleukin 1 signaling occurs exclusively via the type I receptor. *Proc. Natl. Acad Sci. U.S.A.* 90, 6155–6159. doi: 10.1073/pnas.90.13.6155

Souter, A. J., Garry, M. G., and Tanelian, D. L. (2000). Spinal interleukin-1beta reduces inflammatory pain. *Pain* 86, 63–68. doi: 10.1016/s0304-3959(99)00315-2

Tan, A. M., Zhao, P., Waxman, S. G., and Hains, B. C. (2009). Early microglial inhibition preemptively mitigates chronic pain development after experimental spinal cord injury. *J. Rehabil. Res. Dev.* 46, 123–133.

Todd, A. (2010). Neuronal circuitry for pain processing in the dorsal horn. *Nat. Rev. Neurosci.* 11, 823–836. doi: 10.1038/nrn2947

Vale, M. L., Marques, J. B., Moreira, C. A., Rocha, F. A., Ferreira, S. H., Poole, S., et al. (2003). Antinociceptive effects of interleukin-4, -10, and -13 on the writhing response in mice and zymosan-induced knee joint incapacitation in rats. *J. Pharmacol. Exp. Ther.* 304, 102–108. doi: 10.1124/jpet.102.038703

Watkins, L. R., Milligan, E. D., and Maier, S. F. (2001). Glial activation: a driving force for pathological pain. *Trends Neurosci.* 24, 450–455. doi: 10.1016/s0166-2236(00)01854-3

Woolf, C. J., and Mannion, R. J. (1999). Neuropathic pain: aetiology, symptoms, mechanisms, and management. *Lancet* 353, 1959–1964. doi: 10.1016/s0140-6736(99)01307-0

Yan, X., Li, F., Maixner, D. W., Yadav, R., Gao, M., Ali, M. W., et al. (2019). Interleukin-1beta released by microglia initiates the enhanced glutamatergic activity in the spinal dorsal horn during paclitaxel-associated acute pain syndrome. *Glia* 67, 482–497. doi: 10.1002/glia.23557

Yoon, S.-Y., Roh, D.-H., Seo, H.-S., Kang, S.-Y., Moon, J.-Y., Song, S., et al. (2010). An increase in spinal dehydroepiandrosterone sulfate (DHEAS) enhances NMDA-induced pain via phosphorylation of the NR1 subunit in mice: involvement of the sigma-1 receptor. *Neuropharmacology* 59, 460–467. doi: 10.1016/j.neuropharm.2010.06.007

Zhang, R. X., Li, A., Liu, B., Wang, L., Ren, K., Zhang, H., et al. (2008). IL-1ra alleviates inflammatory hyperalgesia through preventing phosphorylation of NMDA receptor NR-1 subunit in rats. *Pain* 135, 232–239. doi: 10.1016/j.pain.2007.05.023

Conflict of Interest Statement: The authors declare that the research was conducted in the absence of any commercial or financial relationships that could be construed as a potential conflict of interest.

frontiers in Molecular Neuroscience

REVIEW
published: 23 August 2019
doi: 10.3389/fnmol.2019.00207

Insights From Molecular Dynamics Simulations of a Number of G-Protein Coupled Receptor Targets for the Treatment of Pain and Opioid Use Disorders

*João Marcelo Lamim Ribeiro and Marta Filizola**

Department of Pharmacological Sciences, Icahn School of Medicine at Mount Sinai, New York, NY, United States

Effective treatments for pain management remain elusive due to the dangerous side-effects of current gold-standard opioid analgesics, including the respiratory depression that has led to skyrocketing death rates from opioid overdoses over the past decade. In an attempt to address the horrific opioid crisis worldwide, the National Institute on Drug Abuse has recently proposed boosting research on specific pharmacological mechanisms mediated by a number of G protein-coupled receptors (GPCRs). This research is expected to expedite the discovery of medications for opioid overdose and opioid use disorders, leading toward a safer and more effective treatment of pain. Here, we review mechanistic insights from recent all-atom molecular dynamics simulations of a specific subset of GPCRs for which high-resolution experimental structures are available, including opioid, cannabinoid, orexin, metabotropic glutamate, and dopamine receptor subtypes.

Keywords: GPCRs, opioid crisis, molecular dynamics, pain, opioid use disorder

OPEN ACCESS

Edited by:
Meritxell Canals, University of Nottingham, United Kingdom

Reviewed by:
Leonardo Pardo, Autonomous University of Barcelona, Spain
Hugo Gutiérrez De Teran, Uppsala University, Sweden

***Correspondence:**
Marta Filizola
marta.filizola@mssm.edu

Received: *31 May 2019*
Accepted: *07 August 2019*
Published: *23 August 2019*

Citation:
Ribeiro JML and Filizola M (2019) Insights From Molecular Dynamics Simulations of a Number of G-Protein Coupled Receptor Targets for the Treatment of Pain and Opioid Use Disorders. Front. Mol. Neurosci. 12:207. doi: 10.3389/fnmol.2019.00207

INTRODUCTION

Pain is a vital, albeit unpleasant, physiological response to tissue damage, but it can become a disease if it strikes in the absence of tissue injury, or continues long after appropriate tissue healing (Ringkamp et al., 2018). As a disease, pain poses an enormous socioeconomic burden on the people who suffer from it, as well as a huge financial strain worldwide. There are several different ways to categorize pain (e.g., chronic, nociceptive, neuropathic, etc.) and treatment decisions depend on the specific type of pain (Chang et al., 2015). For severe and chronic pain, the gold-standard painkillers remain opioid drugs, despite their dangerous side effects and abuse liability.

Overprescription of opioid analgesics in the nineties led to drug misuse, and the consequent "opioid epidemic" or "opioid crisis" in the United States, which has most recently expanded to heroin and other illicit synthetic opioids such as fentanyl and its analogs (Volkow et al., 2019). With an average of 130 Americans dying every day (Centers for Disease Control and Prevention [CDC], 2017), new scientific solutions are desperately needed to effectively manage pain while preventing or treating overdose and opioid use disorder (OUD) manifestations. This recognition recently led the leadership of the National Institutes of Health (NIH) and the National Institutes on Drug Abuse (NIDA) to launch initiatives aimed at accelerating the pace of scientific inquiry that is necessary to

address the opioid crisis. One of these initiatives enabled the prioritization of specific mechanisms and pharmacological targets whose study is expected to boost the development of novel drugs that have the highest probability of approval by the Food and Drug Administration (FDA) for the treatment of opioid overdose and OUD (Rasmussen et al., 2019). These "most wanted" mechanisms and targets (Rasmussen et al., 2019), which include several G protein-coupled receptors (GPCRs), were established based on published data and internal studies that the NIDA leadership deemed most promising for the development of improved therapeutics for OUDs.

In the classical view of GPCR-mediated downstream cellular signaling, the receptor transitions into active conformational states which are capable of recruiting and ultimately activating intracellular protein transducers such a G-proteins and β-arrestins. These active states are characterized by specific conformational changes at the intracellular end of the receptor, most notably exemplified by a different extent of outward movement of transmembrane helix 6 (TM6) away from TM3 (e.g., see experimentally determined inactive and active structures of a prototypic GPCR compared to intermediate states in **Figure 1**). Typically, GPCR activation is mediated by the binding of agonist ligands at the so-called orthosteric binding site, which is the same site where endogenous ligands bind. Antagonist and inverse agonist ligands, on the other hand, shift the conformational equilibrium toward inactive conformations of the receptor while partial agonists are expected to stabilize intermediate conformations between inactive and active states of the receptor. For years, drug design at GPCRs has mostly been focused on optimizing ligands for the receptor orthosteric site. However, by binding non-conserved regions of the receptor and directly affecting the binding and/or efficacy of orthosteric ligands, so-called positive and negative allosteric modulators (PAMs and NAMs, respectively) are receiving more and more attention for the development of improved therapeutics targeting GPCRs. Similarly, so-called biased agonists hold a great potential for drug discovery since they would stabilize receptor conformations that selectively recruit an intracellular protein instead of another, thereby triggering specific biological effects. **Figure 2** provides a cartoon depiction of the expected effect of the different types of ligands on the receptor.

Indeed, among the NIDA's ten most wanted medication development priorities in response to the opioid crisis (Rasmussen et al., 2019) are agonists, antagonists, partial agonists, PAMs, and/or NAMs at a number of GPCRs, including orexin-1 or 2, kappa opioid (KOP), $GABA_B$, muscarinic M5, nociceptin opioid peptide (NOP), metabotropic glutamate 2/3, ghrelin, dopamine D3, and cannabinoid CB-1 receptors. Additional NIDA-designated priority medications mediated by GPCRs (Rasmussen et al., 2019) included: (i) serotonin $5HT_{2C}$ agonists or PAMs, with or without $5HT_{2A}$ antagonist/NAM activity, (ii) biased μ-opioid (MOP) receptor agonists or PAMs, and (iii) NOP/MOP bifunctional agonists or PAMs.

One of the main obstacles to the development of new therapeutics for pain management or to treat or prevent opioid overdose or OUDs is the limited understanding of the relevant signal transduction mechanisms at the atomic level notwithstanding the recognized role of a number of GPCRs in the regulation of pain transmission and OUD manifestations, as well as the availability of high-resolution experimental structures for several of these GPCRs. Molecular dynamics (MD) simulations can provide a complementary perspective (Ribeiro and Filizola, 2019) on the molecular determinants underlying GPCR-mediated signaling mechanisms involved in pain transmission, respiratory depression, or clinical manifestations of OUD. Availability of more powerful hardware and software has made the use of MD simulations more affordable and available to a larger number of scientists. It is now straightforward for numerous groups to simulate timescales in the microsecond (μs) regime using high-performance computing resources accessible to a large number of academic institutions. Using either standard or enhanced MD simulations, the latter to access even longer timescales or a more extensive sampling, GPCRs are studied in terms of an ensemble of conformations between fully active and inactive states, with a number of factors, such as binding of ligands, lipids, ions, receptors, or intracellular proteins, shifting the equilibrium toward different states. While we refer the reader elsewhere for an overview of strengths and limitations of MD simulations in their application to GPCRs (e.g., Ribeiro and Filizola, 2019), we review here atomically detailed mechanistic insights from MD simulations of high-resolution experimental structures of a number of GPCR subtypes whose study might lead to faster development of medications for the treatment of pain or OUDs (see **Table 1** for a summary of all the MD studies reported herein). These GPCRs include opioid, cannabinoid, orexin, metabotropic glutamate, and dopamine receptor subtypes regulating distinctive pharmacological mechanisms. The position of the co-crystallized ligands in the respective high-resolution experimental structures used as a starting point for the MD simulations referenced herein is shown in **Figure 3**.

SYNOPSIS OF MD SIMULATION METHODS CITED HEREIN

The goal of this section is not to describe in detail the MD simulation methods and tools cited in this review, but rather provide a lay summary for the general audience. Interested readers are referred to the appropriate reviews, cited below, where the methods are described more thoroughly.

The aim of an MD simulation is to provide the time-evolution of a system by solving the appropriate equation(s) of motion. In these equations, the energy interactions between the particles of the system under study must be described. In principle, atomic-level interactions should be handled using quantum mechanics; however, due to the size of typical biological systems, it is often unfeasible to use the fully quantum description, and classical mechanics is used instead (Oren et al., 2001). The typical approach to modeling these interactions is to describe bonded and non-bonded atomic interactions by simple expressions, with different parameters in these expressions representing different atom types (Oren et al., 2001; Ponder and Case, 2003; Lopes et al., 2015; Nerenberg and Head-Gordon, 2018). The determination of an accurate set of parameters for use in these expressions

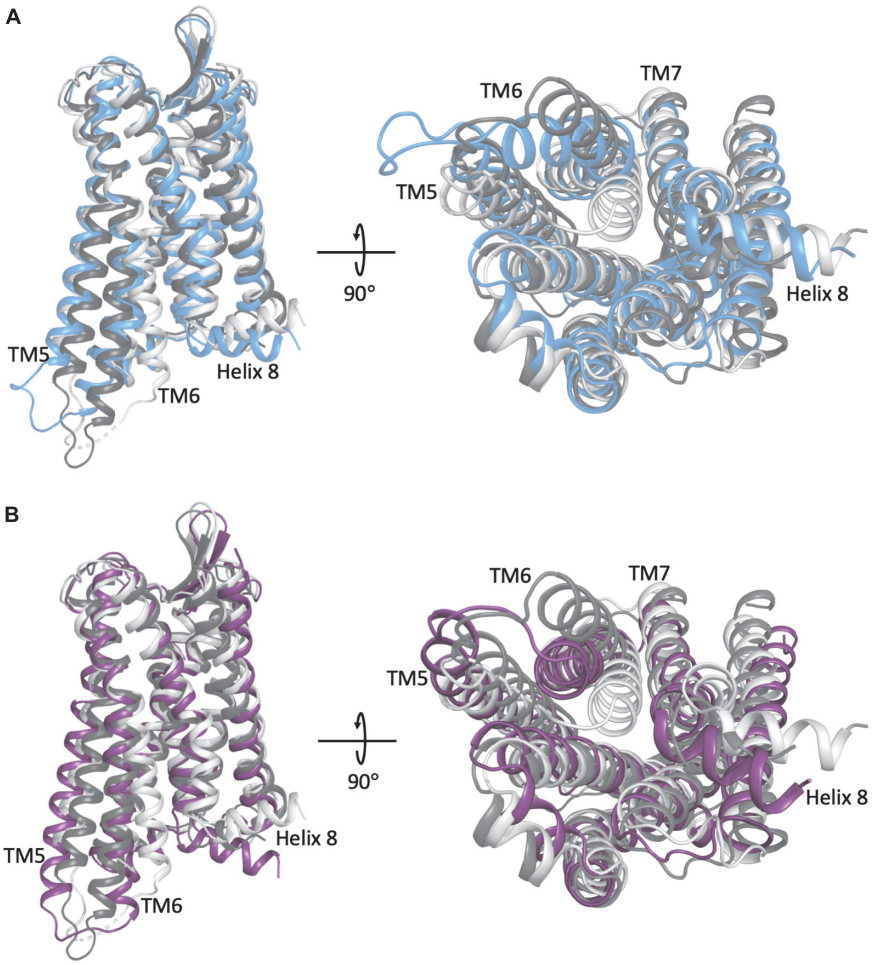

FIGURE 1 | A comparison of the representative conformation of the most probable metastable state within an intermediate region of **(A)** the morphine-bound MOP receptor, where the intermediate state is in light blue, and **(B)** the TRV-130-bound MOP receptor, where the intermediate state is in light purple, relative to the experimentally determined MOP receptor inactive and active states (light and dark gray, respectively). Note that the most dramatic differences between these conformations stem from the extent of outward movement of TM6 away from TM3, which is one of the most notable conformational changes that has been associated with receptor activation. Images on the right correspond to a 90° rotation of the receptor helical bundle, and represent the view from the intracellular domain.

(the so-called force field) is key to properly describe atomic interactions within biological systems, and it is therefore an intensive area of research. In the following sections, we will mention several different force fields that are currently available to the MD practitioner and have been used in the studies reported here, including those corresponding to the names of Assisted Model Building and Energy Refinement (AMBER) (Maier et al., 2015), Chemistry at Harvard Macromolecular Mechanics (CHARMM) (Best et al., 2012), General Amber force field (GAFF) (Wang et al., 2004), CHARMM General Force Field (CGenFF) (Vanommeslaeghe et al., 2010), etc. In addition, tools such as General Automated Atomic Model Parametrization (GAAMP) (Huang and Roux, 2013) have been developed to automatically generate force field parameters for small molecules not accurately described by the aforementioned force fields.

One of the major obstacles in using MD simulations for investigating biological problems is that the timescale for sampling the event of interest is often larger than the times that can be simulated (Bernardi et al., 2015). While the microsecond (μs) regime is nowadays accessible to a large number of MD practitioners, most biological events fall above that threshold (Valsson et al., 2016; Ribeiro et al., 2019). Enhanced sampling methods are designed to provide a faster exploration of the conformational space of the system under study. In this review, we report on studies carried out using two classes of enhanced sampling MD methods. One of these classes, exemplified by metadynamics and Gaussian accelerated molecular dynamics (GaMD) simulations, uses an artificial biasing force to speed up the rate at which the process of interest is sampled, and so long as this is done in a careful manner, the effect of the "bias" can be "reweighed" to recover "unbiased" information. The other class of enhanced sampling MD simulations is exemplified by adaptive sampling protocols, in which successive batches of simulations are started from regions of conformational space

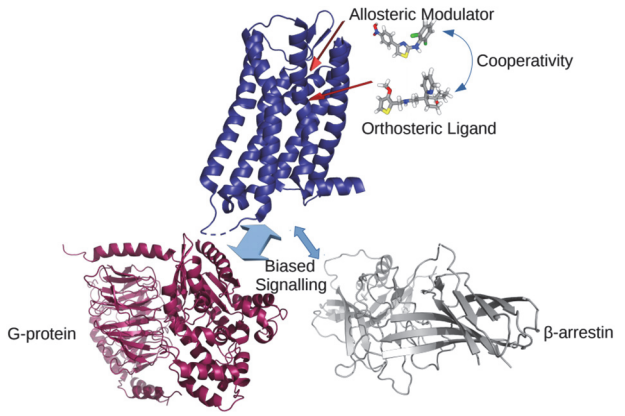

FIGURE 2 | A cartoon representation of the effects of different ligands on a GPCR. The cooperativity between allosteric and orthosteric ligands can shift their affinities for the receptor, and/or bias the GPCR coupling to a particular intracellular partner.

that have been undersampled, thus accelerating the sampling of important, but slow, events (Husic and Pande, 2018; Ribeiro et al., 2019). Throughout the remainder of this review we refer to unbiased MD as simulations in which trajectories are propagated without the help of enhanced sampling techniques, although adaptive sampling techniques are, in principle, not biased (Husic and Pande, 2018).

OPIOID RECEPTORS

Overdose deaths by prescription, illegal, or synthetic opioids have mostly been attributed to the activation of the MOP receptor, a rhodopsin-like (class A) GPCR located, in part, on brainstem neurons that control respiration. In an attempt to develop improved opioid therapeutics with limited respiratory depression and other unwanted side effects (Janecka et al., 2019), attention has recently shifted to G protein-biased agonists of the MOP receptor. These MOP receptor ligands are believed to produce anti-nociceptive action by stabilizing a receptor conformation that preferentially activates G-protein over β-arrestin, the latter shown to be linked to unwanted side effects (Bohn et al., 1999; Raehal et al., 2005).

Recent MD simulations have been leveraged to reveal the molecular details behind G-protein biased agonism at the MOP receptor (Schneider et al., 2016; Kapoor et al., 2017; Cheng et al., 2018). In particular, oliceridine, also known as TRV-130, a G protein-biased MOP receptor ligand that reached phase III clinical trials for management of moderate to severe pain (Viscusi et al., 2019), has been the subject of a number of MD simulations (Schneider et al., 2016; Kapoor et al., 2017; Cheng et al., 2018). Our group, for instance, investigated the binding of TRV-130 from the bulk solvent to the MOP receptor, as well as its preferred mode of interaction at the crystallographically identified orthosteric binding site, using ∼44 μs of unbiased all-atom MD simulations (Schneider et al., 2016). These MD simulations had the MOP receptor placed in a 1-palmitoyl-2-oleoyl-sn-glycero-3-phosphocholine (POPC)/cholesterol lipid membrane environment and used the CHARMM36 force-field to represent the protein and lipid molecules, and CGenFF for the TRV-130 ligand. The results of these simulations suggested that intermediate binding states of TRV-130 at the so-called vestibule region of the MOP receptor directed ligand access to the orthosteric site, and that two energetically indistinguishable conformations could be adopted in the orthosteric binding pocket. Additional microsecond-scale, unbiased simulations of the MOP receptor bound to TRV-130 or the classical orthosteric opioid drug morphine (Schneider et al., 2016) suggested differences in the allosteric coupling between the MOP receptor orthosteric site and the receptor intracellular region induced by the two different ligands. Notably, we found that residues in direct or water-mediated contact with either ligand did not exhibit a main role in the communication between the orthosteric binding site and the intracellular region of the MOP receptor, notwithstanding their contribution to stable ligand binding at the orthosteric pocket. In addition, unlike the morphine-bound receptor, in which the most contributing residues to the allosteric coupling between the orthosteric binding site and the intracellular region of the MOP receptor resided in both transmembrane (TM) helices TM3 and TM6, the TRV-130 complex did not have strong contributors to the co-information in TM6 (Schneider et al., 2016).

To obtain a more thorough investigation of the molecular details of ligand-induced MOP receptor activation, we recently built a Markov state model (MSM) using over 400 μs of MD simulations of the MOP receptor embedded in a POPC/cholesterol membrane mimetic environment with either morphine or TRV-130 bound at the orthosteric binding site (Kapoor et al., 2017). Here, the CHARMM36 and CGenFF force-fields were also used. The MSM revealed that the conformational landscape of the MOP receptor in complex with either ligand contained several kinetic macrostates (i.e., metastable states) in addition to those corresponding to crystal-like active or inactive conformations of the receptor, defining two different intermediate regions of the conformational space for each ligand-MOP complex. These regions contained different conformational states stabilized by morphine or TRV-130, which may or may not get ever resolved experimentally and yet be useful for the rational design of improved opioids with reduced side effects. Shown as an example in **Figure 1** are representative conformations of the most probable metastable states within the intermediate regions available to the simulated morphine-bound and TRV130-bound MOP complexes compared to active or inactive crystallographic states of MOP, which are characterized by a different extent of TM6 outward movement. Another important observation of this MSM analysis was the existence of different activation/deactivation pathways induced by the classical or G protein-biased opioid ligand, which confirmed the substantial difference in the receptor dynamics induced by the two different ligands.

In a recent investigation, unbiased MD simulations were used to study the MOP receptor in a ligand-free form, as well as in complex with TRV-130, the agonist BU72, the antagonist

TABLE 1 | A compilation of the MD-based studies that have been reported in this review article.

Receptor(s)	Ligand(s)	Force field	Simulation technique	Aggregate simulation length	References
MOP	TRV-130, Morphine, Ligand-free	CHARMM36, CGenFF	Unbiased MD	53.25 μs	Schneider et al., 2016
MOP	TRV-130, Morphine	CHARMM36, CGenFF	Adaptive sampling MD	460 μs	Kapoor et al., 2017
MOP	TRV-130, BU72, Naltrexone, β-FNA, Ligand-free	CHARMM36, CGenFF	Unbiased MD	1.5 μs	Cheng et al., 2018
MOP	BMS-986122, (R)-Methadone, Buprenorphine, Ligand-free	AMBER03, Stockholm, GAFF	Unbiased MD	5.2 μs	Bartuzi et al., 2019
MOP, KOP	Morphine, Levallorphan, JDTic, Ligand-free	CHARMM36, CGenFF	Unbiased MD	12.5 μs	Yuan et al., 2015
KOP	5′-GNTI, 6′-GNTI, Ligand-free	CHARMM36, CGenFF	Unbiased MD	1.9 μs	Cheng et al., 2016
KOP	MP1104, JDTic, Ligand-free	AMBER ff14SB, LIPID11, GAFF	Gaussian accelerated MD	12 μs	An et al., 2018
NOP	Cebranopadol, C24, Ligand-free	AMBER ff99SB	Unbiased MD	3 μs	Della Longa and Arcovito, 2019
DOP	BMS-986187, SNC-80	CHARMM36, CGenFF	Metadynamics	3.6 μs	Shang et al., 2016
CB1	THC, THCV, Taranabant, Ligand-free	CHARMM36, CGenFF	Unbiased MD	8 μs	Jung et al., 2018
CB1	CP 55,940, GAT228	CHARMM36, CGenFF	MetaDynamics	–	Saleh et al., 2018
OX2	Suvorexant	AMBER ff98SB, GAFF, Lipid 14	Unbiased MD	400 ns	Bai et al., 2018
OX2	Suvorexant, Nag26, Orexin-A, Ligand-free	AMBER 99sb-ildn, Slipids, GAFF, OPSL-AA	Unbiased MD	36 μs	Karhu et al., 2019
D3R	PF-4363467	CHARMM36, GAAMP	Adaptive sampling MD	680 μs	Ferruz et al., 2018
D2R, D3R	SB269652	CHARMM36, GAAMP	Adaptive sampling MD	76.5 μs	Verma et al., 2018
D3R	LS-3-134, 4 derivatives	AMBER ff14SB, GAFF	Unbiased MD	4.5 μs	Hayatshahi et al., 2018
mGluR1	FITM	CHARMM27, CGenFF	Unbiased MD, Adaptive biasing force	150 ns, 360 ns	Bai and Yao, 2016
mGluR5	Mavoglurant, Dipraglurant, Basimglurant, STX107, MPEP, Fenobam, 51D, 51E	AMBER ff14SB, Lipid14, GAFF	Unbiased MD	800 ns	Fu et al., 2018

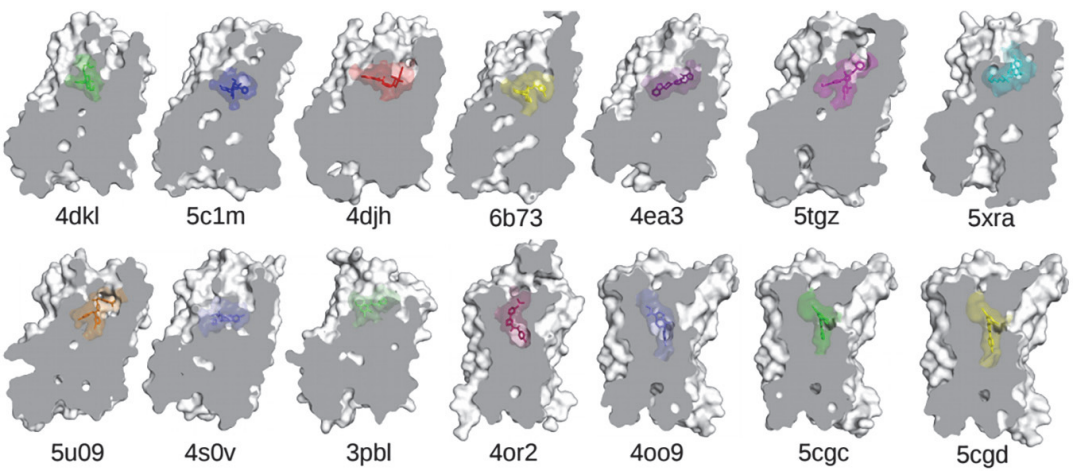

FIGURE 3 | The experimentally determined high-resolution GPCR structures, together with their bound ligands, used in the MD-based studies discussed in this review. Nanobodies and other interacting proteins were removed. PDB 4dkl, The antagonist β-FNA bound to the MOP receptor; PDB 5c1m, The agonist BU72 bound to the MOP receptor; PDB 4djh, The antagonist JDTic bound to the KOP receptor; PDB 6b73, The agonist MP1104 bound to the KOP receptor; PDB 4ea3, The peptide mimetic antagonist compound 24 bound to the NOP receptor; PDB 5tgz, The antagonist AM6538 bound to the CB1 receptor; PDB 5xra, The agonist AM11542 bound to the CB1 receptor; PDB 5u09, The inverse agonist taranabant bound to the CB1 receptor; PDB 4s0v, The antagonist suvorexant bound to the OX2 receptor; PDB 3pbl, The antagonist eticlopride bound to the D3 receptor; PDB 4or2, The negative allosteric modulator FITM bound to the transmembrane domain of mGluR1; PDB 4oo9, The negative allosteric modulator mavoglurant bound to the transmembrane domain of mGluR5; PDB 5cgc, The negative allosteric modulator 3-chloro-4-fluoro-5-[6-(1H-pyrazol-1-yl)pyrimidin-4-yl]benzonitrile bound to the transmembrane domain of mGluR5; PDB 5cgd, The negative allosteric modulator 3-chloro-5-[6-(5-fluoropyridin-2-yl)pyrimidin-4-yl]benzonitrile bound to the transmembrane domain of mGluR5.

naltrexone (NTX), or the antagonist β-FNA. These simulations were each run for 300 ns with the MOP receptor embedded in a POPC membrane environment, the ligands parameters derived from CGenFF, and both the lipid and receptor molecules described by CHARMM36 force field parameters. Notably, simulations of the TRV-130-MOP receptor complex drew attention to two residues in TM6 and TM7, specifically, $Y326^{7.43}$ and $W293^{6.48}$, which had been shown to be important for MOP receptor biased signaling by mutagenesis studies. Superscript residue numbers here and throughout the text refer to the Ballesteros–Weinstein generic numbering scheme (Ballesteros and Weinstein, 1995) wherein the first digit corresponds to the transmembrane helix number and the second digit is a sequence number relative to the most conserved residue in a helix, which is assigned a value of 50. However, corrections to this numbering scheme incorporating structural information have been proposed (Isberg et al., 2015) and will be reported in parenthesis for those residues whose numbering may diverge from Ballesteros-Weinstein's, such as $Y326^{7.43}$ (renumbered $Y326^{7.42}$ by Isberg et al., 2015).

Similar to MOP receptor agonists, centrally acting KOP receptor agonists can be effective in the treatment of pain, but their dysphoric and hallucinogenic side effects have limited their clinical usefulness (Land et al., 2008), shifting focus to the development of peripherally restricted KOP agonists as analgesics with reduced abuse liability (Hasebe et al., 2004) or KOP antagonists for the treatment of substance use disorders (Carlezon and Krystal, 2016). The structural basis of agonism or antagonism at the MOP and KOP receptors has recently been studied using unbiased all-atom MD simulations (Yuan et al., 2015). A total of four ligand-opioid receptor complexes embedded in a POPC membrane environment were simulated, including the KOP receptor in complex with the JDTic antagonist, the MOP receptor complexed with the agonist morphine, and either the MOP or KOP receptor in complex with levallorphan, a morphinan ligand acting as an antagonist at the MOP receptor and an agonist at the KOP receptor (Yuan et al., 2015). The simulations – each 3 μs in length – made use of CGenFF in their description of the ligands, and the CHARMM36 force field for all remaining molecules. In these simulations, the authors found that the amount of water penetration into the interior of the receptors, which is a known characteristic of GPCR activation, was higher when the receptor was complexed with an agonist as opposed to an antagonist (Yuan et al., 2015). In particular, the levallorphan-MOP and JDTic-KOP complexes formed a σ – π stacking interaction with the $Y320^{7.43}$ ($Y320^{7.42}$ as per Isberg et al., 2015) residue, which tended to block water penetration into the interior. Solvent accessible surface area calculations on subsequent short MD simulations of several other agonists or antagonists in complex with either the KOP or MOP receptors showed these values were higher for receptors in complex with agonists as opposed to antagonists (Yuan et al., 2015).

The conformational changes induced by 6′-Guanidinonaltrindole (6′-GNTI), a G-protein biased agonist that is selective for the KOP receptor, or the antagonist 5′-Guanidinonaltrindole (5′-GNTI) have recently been studied using unbiased all-atom MD simulations (Cheng et al., 2016). In this work, ∼600 ns MD simulations were performed on the ligand-free KOP receptor, as well as the receptor in complex with either 5′-GNTI or 6′-GNTI, with each system embedded in an explicit POPC membrane environment (Cheng et al., 2016). The MD simulations of the KOP receptor bound to the antagonist 5′-GNTI drew attention to the hydrogen bond between $S324^{7.47}$ and $V69^{1.42}$ as the basis for the stabilization of the kink angle on TM7 at about 150°, and possibly deriving antagonistic activity. In contrast, the MD simulation of the G-protein biased agonist 6′-GNTI bound to the KOP receptor showed a different value for this kink angle, and highlighted an interaction of the ligand guanidinium group with the $E297^{6.58}$ residue, together with the steric effect from $I294^{6.55}$, as key contributors to the rotation of TM6, a known hallmark of GPCR activation (Cheng et al., 2016). The possible absence of guanidinium-$E297^{6.58}$ interaction in the MOP or the δ-opioid receptor (DOP) receptor due to this residue replacement by a lysine or tryptophan, respectively, was interpreted as the basis for the lack of 6′-GNTI agonism in those opioid receptor subtypes.

More recently, the KOP receptor conformational changes induced by the agonist MP1104 or the antagonist JDTic were investigated using enhanced sampling MD simulations (An et al., 2018). Specifically, using the generalized AMBER force field for the ligands and the AMBER ff14SB force field for the protein, the GaMD method was used to enhance the sampling of long-time, large-scale conformational rearrangements associated with KOP receptor activation by introducing a biasing harmonic potential on certain dihedral angles. The following systems were all simulated in an explicit POPC membrane environment: the ligand-free KOP receptor in an inactive or active conformation, the latter with or without an intracellular protein, the JDTic-inactive KOP receptor complex, and the MP1104-active KOP receptor complex with or without a stabilizing intracellular partner (An et al., 2018). Taken together, the results of these simulations showed that while the agonist stabilized specific functional domains in an active-like conformation, the antagonist shifted the conformational equilibrium toward an inactive conformation. Notably, the inactive ligand-free state of the KOP receptor was the most stable one, in contrast to the ligand-free active form of the receptor, which readily transitioned to an intermediate state characterized by a reduced TM6 outward movement (An et al., 2018). Finally, the results revealed a hydrophobic interaction between $Y246^{5.58}$ and TM6 in the intermediate metastable state that hindered the transition between the inactive and active conformations of the KOP receptor (An et al., 2018).

The NOP receptor is another opioid target of interest for powerful pain relief with reduced side effects. MD simulations using the AMBER ff99sb force field were recently used to investigate the molecular effect of the novel analgesic cebranopadol (CBP) – which acts as an agonist at both NOP and MOP receptors – on the NOP receptor (Della Longa and Arcovito, 2019). These simulations, run in an explicit POPC membrane environment, used the high-resolution structure of the NOP receptor in complex with the antagonist C24 as a starting point for 1 μs-long simulations of the ligand-free NOP

receptor, the C24-NOP receptor complex, and the CBP-NOP receptor complex (Della Longa and Arcovito, 2019). In all cases, the simulations did not sample the large amplitude motions of the transmembrane helices associated with receptor activation even in the presence of the agonist CBP (Della Longa and Arcovito, 2019). The CBP ligand did, however, destabilize the inactive NOP receptor conformation relative to both the ligand-free NOP receptor and the C24-NOP receptor complex such that the NOP receptor bound to CBP could sample a much wider region of the local conformational space (Della Longa and Arcovito, 2019). The authors used these MD simulations to determine some of the earliest microswitches that lead to destabilizing the initial inactive conformation. A histogram of the conformational space of the M134$^{3.36}$ and W276$^{6.48}$ residues located in the orthosteric site revealed that a conformational switch to their active-like positions was accessible to the agonist-receptor complex (Della Longa and Arcovito, 2019). In addition, the time evolution of the conformation of these residues showed that in the agonist-receptor complex these active-like states were "locked" in place for the remainder of the simulation (Della Longa and Arcovito, 2019).

Allosteric modulators of opioid receptors (Remesic et al., 2017) constitute another priority area of research with expected higher probability of success in the development of medications in response to the opioid crisis (Rasmussen et al., 2019). NIDA's "most wanted" allosteric modulators of opioid receptors include MOP PAMs (Rasmussen et al., 2019). One of the reasons why MOP PAMs are of potential interest is that by increasing the potency and/or efficacy of classical opioid drugs, they are expected to produce the same analgesic response achieved by higher doses of opioid drug while simultaneously presenting fewer on-target overdosing risks. Most importantly, these compounds may not be subject to the compensatory mechanisms deriving from chronic MOP activation (e.g., tolerance, dependence, and increased toxicity) because they preserve the temporal and spatial fidelity of signaling *in vivo* by acting only in the presence of endogenous or other orthosteric ligands (Remesic et al., 2017).

Since experimental high-resolution structures of opioid receptors in complex with allosteric modulators are yet to be published, and automated docking protocols do not yield single binding poses that can be clearly distinguished from the rest, MD simulations can make valuable contributions toward locating allosteric binding sites in opioid receptors, as well as revealing the molecular basis for their binding modes, as we recently demonstrated in an application to the DOP receptor. Specifically, we used metadynamics to simulate the binding of a recently discovered allosteric modulator BMS-986187 of opioid receptors (Burford et al., 2015; Livingston et al., 2018) to the DOP receptor in complex with the orthosteric ligand SNC-80 (Shang et al., 2016). The simulations identified the two most stable binding modes with near-degenerate energies that were discriminated experimentally based on functional studies of normal and mutant receptors (Shang et al., 2016). **Figure 4** summarizes the essence of this integrated computational-experimental work, which gave support to the BMS-986187 binding pose in cyan color as the most likely to occur based on the impact of specific mutations (e.g., L/W300$^{7.35}$) on either the intrinsic binding affinity of the PAM or the affinity/efficacy of the orthosteric ligand.

The structural basis for the effect that another allosteric modulator, BMS-986122, has on MOP in complex with either the partial agonist buprenorphine or the agonist methadone, was recently investigated using μs-scale unbiased MD simulations in an explicit membrane mimetic environment (Bartuzi et al., 2019). The results suggested that specific dynamic movements that are characteristic of full receptor activation, such as for instance the bending and rotation of TM7, can be induced by the allosteric modulator even in the presence of a partial agonist at the orthosteric binding site (Bartuzi et al., 2019).

CANNABINOID RECEPTORS

The cannabinoid receptor 1 (CB1) is another important class A GPCR drug target for the development of new analgesics with reduced side effects. For instance, PAMs of this receptor have been shown to suppress pathological pain without producing tolerance or dependence (Slivicki et al., 2018). These properties, alongside their potentially reduced psychoactive side effects due to their lack of intrinsic activity and inherent ceiling efficacy, make CB1 PAMs potentially better therapeutics for inflammation and chronic pain compared to CB1 orthosteric agonists (Wootten et al., 2013). CB1 antagonists have also been reported to exert analgesia in animal models of inflammatory arthritis and hyperalgesia with reduced side effects (Croci and Zarini, 2007; Ueda et al., 2014). Based on these insights, the CB1 receptor is a target of interest for the development of improved therapeutics to combat the opioid crisis (Rasmussen et al., 2019). Luckily, a number of high-resolution experimental structures for either inactive or active CB1 receptors have been made available (Hua et al., 2016, 2017; Shao et al., 2016; Krishna Kumar et al., 2019) and can be used to study CB1-mediated functional mechanisms at a molecular level for the purpose of guiding rational drug discovery.

A recent unbiased MD simulation-based investigation used these structures in order to gain insight into the features that could explain the different efficacy profiles of partial agonists, antagonists, and inverse agonists bound to the CB1 receptor, and could eventually be used for the design of novel therapeutics targeting the CB1 (Jung et al., 2018). Specifically, analysis of these MD simulations made it possible to discriminate the dynamic tendencies of inactive and active CB1 structures in the presence of ligands with different efficacies while the molecular mechanics Poisson–Boltzmann surface area (MM-PBSA) method was used to assess the contribution of individual ligand-receptor interactions to the binding of the partial agonist Δ^9-tetrahydrocannabinol (THC), the antagonist Δ^9-tetrahydrocannabivarin (THCV), and the inverse agonist taranabant from ligand binding free energy decompositions of the CB1-ligand complexes. These MD simulations revealed that binding of the inverse agonist to the active CB1 receptor structure made TM1 less rigid, leading to larger root-mean-square deviations of the possible contacts between TM1 and 2,

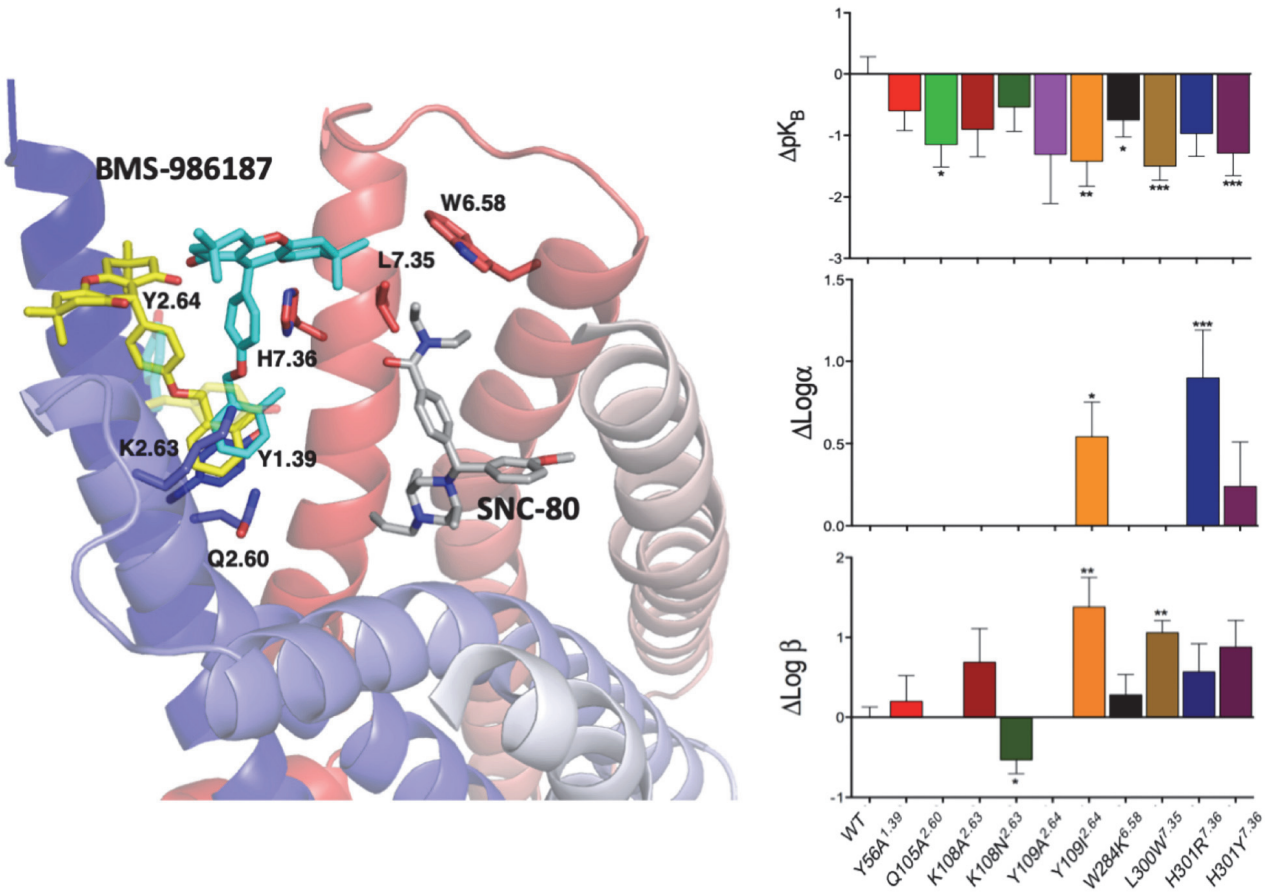

FIGURE 4 | The two energetically most favorable binding modes of the allosteric modulator BMS-986187 – colored yellow and cyan – at the DOP receptor in complex with the orthosteric ligand SNC-80, which is colored in gray. In sticks are the DOP receptor residues in the putative DOP allosteric site used in mutagenesis experiments to help validate the most likely binding mode. The plots to the right show the effect of mutations on the affinity of the allosteric ligand (top right), the induced changes in affinity of the orthosteric ligand (middle plot), and the changes in orthosteric ligand efficacy when the allosteric ligand is bound (bottom right). The experimental data support the predicted BMS-986187 binding mode in cyan color as the most favorable one. Astars indicate the statistical significance levels as given by Dunnet's test p values (*$p < 0.05$, **$p < 0.01$, and ***$p < 0.001$).

as well as TM1 and TM7, compared to either the partial agonist-bound or the antagonist-bound active CB1 receptor complex. In addition, the simulations drew attention to large conformational changes involving residues Phe200$^{3.36}$ and Trp356$^{6.48}$ in the orthosteric binding site. In the inactive CB1 receptor, the inverse agonist taranabant – through a direct interaction with Trp356$^{6.48}$ – stabilized the conformation of Trp356$^{6.48}$ and Phe200$^{3.36}$ with respect to one another while the partial agonist THC and antagonist THCV did not. In contrast, in the CB1 active conformation, taranabant induced a different dynamic behavior for the interaction of Trp356$^{6.48}$ and Phe200$^{3.36}$ compared to the partial agonist THC. Furthermore, changes in the binding free energies showed that the partial agonist THC preferred the CB1 active conformation, whereas the simulated inverse agonist taranabant remained more favorably bound to the CB1 inactive conformation via a stable interaction with residue Trp356$^{6.48}$ (Jung et al., 2018) during the afforded simulation timescale.

In another recent investigation, biased MD simulations were used to probe the binding sites and modes of the CP 55,940 agonist and the GAT228 mixed agonist/PAM (so-called Ago-PAM) to the CB1 receptor (Saleh et al., 2018). Ligand binding events to the CB1 receptor were enhanced using the multiple-walker metadynamics biasing protocol (Saleh et al., 2017) and a funnel-shaped restraint applied to the ligand in the bulk, both for the purpose of aiding convergence (Saleh et al., 2018). The simulation of CP 55,940 binding to the ligand-free CB1 receptor – run for 2 μs to achieve convergence – showed a single, deep minimum along the binding potential of mean force (PMF) (Saleh et al., 2018). The location of this deep minimum corresponded to the orthosteric binding site in the high-resolution structure of the CB1 receptor (Saleh et al., 2018). The binding mode of CP 55,940 was found to reproduce all of the interactions observed in the high-resolution structure of the THC agonist AM11542 bound to the CB1 receptor, except for the interaction with F174$^{2.61}$, which was replaced by an interaction with residue F102 in the N-terminal region of the receptor (Saleh et al., 2018). In contrast, the binding simulations of the GAT228 Ago-PAM to the ligand-free CB1 receptor, showed

two PMF minima corresponding to binding at different sites of the receptor. These two minima had similar affinities (Saleh et al., 2018), which suggests an equilibrium between binding at the two different receptor sites, thus providing structural context to the experimentally observed partial agonistic effect of GAT228 (Saleh et al., 2018). While the PMF global minimum corresponded to GAT228 bound to the orthosteric site via a cluster of hydrophobic interactions with Val196$^{3.32}$, Leu193$^{3.29}$, and seven additional Phe residues (Saleh et al., 2018), the other PMF minimum defined a putative CB1 receptor allosteric site (Saleh et al., 2018). Notably, simulations of the binding of GAT228 to the CP 55,940-CB1 receptor complex revealed a 3 Å RMSD displacement of the CP 55,940 binding mode induced by GAT228 binding preferentially at an allosteric site defined by residues W279$^{5.43}$, Y275$^{5.39}$, W356$^{6.48}$, and the N-terminus F268 (Saleh et al., 2018), through a hydrogen bond between the indole hydrogen atom of GAT228 and T197$^{3.33}$ (Saleh et al., 2018).

OREXIN RECEPTORS

The orexin (OX) 1 and 2 receptors, expressed throughout the CNS, are neuropeptide receptors that belong to the β-branch of the rhodopsin-like GPCRs (Yin et al., 2016). Although these receptors are known to be important in regulating mammalian sleep patterns (Yin et al., 2015, 2016; Wacker and Roth, 2016), they have recently received attention in the development of therapeutics to address the opioid crisis (Rasmussen et al., 2019). Although high-resolution experimental structures exist for both the OX1 and OX2 receptors bound to antagonists (Yin et al., 2015, 2016; Suno et al., 2018), recent MD-based studies have focused on the OX2 receptor (Bai et al., 2018; Karhu et al., 2019). The earliest of these studies used 200 ns of unbiased MD simulations of the antagonist suvorexant bound to the OX2 wild-type and N324$^{6.55}$A mutant receptors embedded in a POPC lipid environment to understand the dynamic interplay between the horseshoe shape pocket of the receptor revealed by crystallography (Yin et al., 2015) and the boat conformation of the ligand at an atomic level of detail (Bai et al., 2018). In line with the notion of a loss of antagonist binding ability and signaling response in the N324$^{6.55}$A mutant, the results of these simulations showed a distorted horseshoe shape pocket of the N324$^{6.55}$A mutant of the OX2 receptor compared to wild-type receptor, suggesting that an intact horseshoe shape pocket is required for optimal suvorexant binding and antagonistic activity (Bai et al., 2018).

Molecular determinants of OX2 receptor binding and activation were further investigated in a recent MD-based work (Karhu et al., 2019) focused on comparing the receptor dynamic behavior induced by the agonist Nag26 or the antagonist suvorexant, in addition to predicting the mode of binding of the endogenous ligand orexin-A at the OX2 receptor (Karhu et al., 2019). The microsecond-long unbiased MD simulations of Nag26 or suvorexant bound to the OX2 receptor revealed very different dynamic behaviors between the agonist and antagonist, with the agonist exhibiting much increased flexibility and completely different interaction patterns (Karhu et al., 2019). In particular, while suvorexant induced stabilization of the Q134$^{3.32}$–Y354$^{7.43}$ (renumbered Y354$^{7.42}$ according to Isberg et al., 2015) hydrogen bond, Nag26 promoted counterclockwise rotation of the TM5 extracellular end, influencing the interactions among TM4, 5, and 6 (Karhu et al., 2019).

DOPAMINE RECEPTORS

The dopamine D3 receptor has also received attention as a drug target for mitigating the opioid crisis (Rasmussen et al., 2019) in large part because of its potential for opioid dependence treatment (Kumar et al., 2016). Recent work on this receptor highlighted the importance of using MD simulations to predict ligand binding at the D3 receptor in agreement with inferences from site-directed mutagenesis (Ferruz et al., 2018). In particular, binding of the antagonist PF-4363467 from the bulk to the dopamine D3 receptor was simulated with ACEMD (Harvey et al., 2009) directed sampling and MSMs generated using High-Throughput Molecular Dynamics (HTMD), using the CHARMM36 force field for the protein and POPC lipid, and ligand force field parameters generated with the GAAMP tool within HTMD. An adaptive sampling protocol was used for these simulations, according to which MSMs were built from successive batches of simulations to identify starting conformations for the next batch, thus affording thorough exploration of the conformational landscape without biasing the potential. A total of over 680 μs of simulation was carried out, resulting in the sampling of two binding paths, which differed in the presence of a second intermediate state in the minor binding path. This intermediate state corresponded to PF-4363467 bound to the D3 receptor at a position between the extracellular vestibule and the orthosteric site. The main structural difference between the predicted PF-4363467-D3 receptor complex and the crystallographically determined eticlopride-D3 receptor complex (Chien et al., 2010) was the formation of an aromatic cryptic pocket between TM5 and TM6 involving residues F338$^{6.44}$, W342$^{6.48}$, L343$^{6.49}$, F345$^{6.51}$, and F346$^{6.52}$ deriving from the displacement of residues F197$^{5.47}$ and F346$^{6.52}$ (Ferruz et al., 2018).

The SB269652 ligand is a bitopic D2 and D3 receptor ligand with negative allosteric modulation activity (Silvano et al., 2010) that has received research attention for the treatment of drug abuse (Verma et al., 2018). By nature of being bitopic, SB269652 binds to both the orthosteric binding site and an allosteric binding site in the receptor. Previous molecular modeling studies suggested that the tetrahydroisoquinoline (THIQ) moiety of SB269652 binds to the orthosteric binding site via an ionic interaction with D$^{3.32}$ whereas the indole-2-carboxamide moiety of SB269652 protruded into a putative allosteric site between TM2 and TM7, forming a hydrogen bond with the E$^{2.65}$ (renumbered E$^{2.64}$ according to Isberg et al., 2015) residue (Guo et al., 2008; Lane et al., 2014). However, mutagenesis and structure activity relationship studies of SB269652 questioned that this hydrogen bond alone could determine the compound allosteric properties (Lane et al., 2014; Mistry et al., 2015;

Shonberg et al., 2015), calling for an in depth dynamics study. Thus, adaptive sampling MD simulations using MSMs were recently used to obtain mechanistic insights into the role of the $E^{2.65}$ residue in the binding and allosteric properties of SB269652 at both the D2 and D3 receptors (Verma et al., 2018). Specifically, simulations were carried out for the ligand bound to the wild-type D2 receptor, the $E^{2.65}$A D2 receptor mutant, the wild-type D3 receptor, or the $E^{2.65}$A D3 receptor – all of which were embedded in a POPC lipid environment – for a total of 76.5 μs, with the simulation time of each complex ranging between 15.9 and 21.3 μs (Verma et al., 2018). The THIQ moiety of SB269652 bound at the orthosteric site was shown to be quite stable in both the D2 and D3 receptors, although subtle differences in its binding poses were observed, due in large part to different interactions between the ligand and the extracellular loop 2 (Verma et al., 2018). This is in agreement with previous chimera mutagenesis results that showed the affinities for the D2 and D3 receptors were different in large part due to the extracellular loop 2 (ECL2) (Silvano et al., 2010). In contrast, the indole-2-carboxamide moiety of SB269652 bound at the allosteric site was shown to undergo significant fluctuations, with the MSM analysis revealing two equiprobable metastable states in the wild-type D2 and D3 receptors, but three different metastable states in both the $E^{2.65}$A D2 and D3 receptor mutants (Verma et al., 2018). Furthermore, the results suggested that the $E^{2.65}$ residue mediated the allosteric properties of SB269652 by not only forming a direct hydrogen bond with SB269652, but also by impacting the overall shape and size of the allosteric binding site.

Another recent joint experimental-computational publication also made use of MD simulations to help explain the molecular basis for the binding of bitopic arylamide phenylpiperazine ligands selective for the D3 receptor over D2 (Hayatshahi et al., 2018). Specifically, studies were focused on the prototypic arylamide phenylpiperazine LS-3-134 ligand, which has been found to act as a D3 receptor partial agonist and has also been shown to be 150-fold more selective for the D3 receptor relative to the D2 receptor (Tu et al., 2011). Radioligand binding studies showed that the greatest contribution to the binding energy of the LS-3-134 ligand to the D3 receptor was the phenylpiperazine moiety, but that the arylamide moiety heavily influenced ligand selectivity for the D3 receptor (Hayatshahi et al., 2018). The MD simulations were used to explain the effect that analogs of the piperazine moiety had on the binding affinity. In particular, three different 300 ns unbiased MD simulations were run for LS-3-134 as well as four of its analogs bound to the D3 receptor, revealing that the number of contacts between the protonated nitrogen of piperazine and the $D^{3.32}$ residue tended to decrease as the size of the piperazine increased, with the exception of only one compound. Calculation of their respective binding energies using MM-PBSA showed that the strength of the electrostatic interaction with the $D^{3.32}$ residue generally decreased as the size of the piperazine substituent increased. Umbrella sampling simulations were used to generate a PMF aimed at mimicking the unbinding of the ligand protonated nitrogen from the $D^{3.32}$ residue, and the depth of the bound state in the PMF also agreed with the experimental trend except for one of the analogs (Hayatshahi et al., 2018).

METABOTROPIC GLUTAMATE RECEPTORS

Metabotropic glutamate receptors (mGluRs) belong to the glutamate (Class C) subfamily of GPCRs given that their endogenous ligand is the neurotransmitter glutamate. Owing to the demonstrated important role of glutamate in pain sensation and transmission, these receptors have been suggested to be promising potential targets for novel pain relieving medications (Pereira and Goudet, 2018). There are eight different subtypes of mGluRs, which are divided into group I (mGluR1 and 5), group II (mGluR2 and 3), and group III (mGluR4, 6, 7, and 8) receptors. While group I mGluRs signal via $G_{\alpha q}$, groups II and III signal via $G_{\alpha i}$. Several articles suggest opposing effects of the group I vs. group II and III receptors in reference to antinociception, with group I antagonists or group II/III agonists in the spotlight from a drug discovery perspective. In particular, mGluR2/3 agonists or PAMs have been listed among NIDA's "most wanted" medications in response to the opioid epidemics (Rasmussen et al., 2019).

Like other class C GPCRs, mGluRs are structurally different from rhodopsin-like (class A) GPCRs in that they have a large extracellular domain, also known as Venus Flytrap Domain (VFD), in addition to the 7 transmembrane helical domain (7TMD). Unlike class A GPCRs, the endogenous ligand binding site of mGluRs is located in the extracellular VFD, whereas the transmembrane helical bundle is the primary site for allosteric modulators. Another significant uniqueness is that these receptors are obligate dimers by virtue of a disulfide bond between their VFDs.

Experimental high-resolution structures exist for the 7TMD of $mGluR_1$ (Wu et al., 2014) and the 7TMD and VFT of $mGluR_5$ (Doré et al., 2014; Christopher et al., 2015, 2018; Koehl et al., 2019). There are not, however, published high-resolution structures of the 7TMD of $mGluR_2$ and $mGluR_3$, although their VFT domain has been determined by X-ray crystallography (Muto et al., 2007). Thus, we report here two recent MD-based studies, one for $mGluR_1$ and another for $mGluR_5$, both using their high-resolution experimental structures as starting conformations. To investigate $mGluR_1$ allosteric modulation mechanism at an atomic level of detail appropriate for designing potent NAMs of this receptor, Bai and Yao carried out both biased and unbiased MD simulations on wild-type $mGluR_1$ dimer, as well as its T815M and Y805A mutants, in complex with a NAM known as FITM (4-fluoro-*N*-(4-(6-(isopropylamino)pyrimidin-4-yl)thiazol-2-yl)-*N*-methylbenzamide), and embedded in a POPC lipid membrane environment (Bai and Yao, 2016). The simulations used the CHARMM27 force field for the protein and lipid, and the CGenFF force field for FITM. The unbinding PMF, calculated using an adaptive biasing force, revealed an intermediate ligand-binding state along the NAM-mGluR1 dissociation path, stabilized by interactions with residues S735, $T748^{ECL2}$, $C746^{ECL2}$, $K811^{7.28}$ (renumbered $K811^{7.29}$ according

to Isberg et al., 2015) (Bai and Yao, 2016). While hydrogen bonding between FITM and Y805 was identified as a major contributor to stable ligand binding at the crystallographically determined allosteric site, ligand hydrogen bonding to T748 was found to be a crucial factor in stabilizing FITM in an intermediate binding site (Bai and Yao, 2016). Finally, weak interaction analysis of the stabilizing and destabilizing non-covalent interactions using unbiased MD simulations corroborated the importance of van der Waals and hydrogen bond interactions between Y805 and T815 residues in stabilizing the ligand at the binding site.

In another recent unbiased MD investigation, the structural basis for the binding of several NAMs in preclinical or clinical development (mavoglurant, dipraglurant, basimglurant, STX107, and fenobam), as well as three additional NAMs (MPEP, 51D, and 51E) at mGluR5, was elucidated (Fu et al., 2018). The simulations used an explicit POPC membrane in which to embed the ligand-mGluR5 complexes. The force field parameters of the protein atoms were based on the AMBER ff14SB force field, while the force field parameters of the lipid atoms used the Lipid14 force field and ligands were parametrized with the GAFF force field using the Antechamber program. To begin, five NAMs (dipraglurant, basimglurant, STX107, fenobam, and MPEP) were docked to the mGluR5 receptor allosteric site and short 100 ns MD simulations were used to assess the stabilities of the predicted docked poses. Using the final 50 ns of these trajectories, MM/GBSA calculations were carried out to rank the ligands according to their binding free energies. Using the per-residue free energies, eleven residues – $I625^{2.46}$, $I651^{3.36}$, $S654^{3.39}$, $P655^{3.40}$, $L744^{5.44}$, $W785^{6.50}$, $F788^{6.53}$, $M802^{7.32}$ (renumbered $M802^{7.33}$ according to Isberg et al., 2015), $V806^{7.36}$ ($V806^{7.37}$ as per Isberg et al., 2015), $S809^{7.39}$ ($S809^{7.40}$ as per Isberg et al., 2015), and $A810^{7.40}$ ($A810^{7.41}$ as per Isberg et al., 2015) – were identified as the main contributors to the stable binding of all studied NAMs to $mGluR_5$. The apolar nature of most of these eleven residues further suggested that ligands with hydrophobic scaffolds might be better mGluR5 binders.

CONCLUDING REMARKS

In this work, we have reviewed recent MD-based investigations of a number of GPCRs that are currently in the spotlight for pain management or to treat or prevent OUD clinical manifestations. With the continued advancements in both computer hardware and MD simulation software, as well as sophisticated tools for analysis of increasingly larger datasets generated by MD simulations, atomic-level insights into the dynamical behavior of GPCRs involved in important pharmacological mechanisms are expected to contribute more and more to the rapid development of therapeutics in response to the opioid crisis.

AUTHOR CONTRIBUTIONS

JR and MF wrote the manuscript.

FUNDING

The MF's lab is funded by National Institutes of Health grants DA045473 and DA038882 for work on opioid receptors. Computations are run on resources available through the Scientific Computing Facility at Mount Sinai and the Extreme Science and Engineering Discovery Environment under MCB080077, which is supported by the National Science Foundation grant number ACI-1053575.

REFERENCES

An, X., Bai, Q., Bing, Z., Zhou, S., Shi, D., Liu, H., et al. (2018). How does agonist and antagonist binding lead to different conformational ensemble equilibria of the κ-Opioid receptor: insight from long-time gaussian accelerated molecular dynamics simulation. *ACS Chem. Neurosci.* 10, 1575–1584. doi: 10.1021/acschemneuro.8b00535

Bai, Q., Pérez-Sánchez, H., Shi, Z., Li, L., Shi, D., Liu, H., et al. (2018). Computational studies on horseshoe shape pocket of human orexin receptor type 2 and boat conformation of suvorexant by molecular dynamics simulations. *Chem. Biol. Drug Des.* 92, 1221–1231. doi: 10.1111/cbdd.13181

Bai, Q., and Yao, X. (2016). Investigation of allosteric modulation mechanism of metabotropic glutamate receptor 1 by molecular dynamics simulations, free energy and weak interaction analysis. *Sci. Rep.* 6:21763. doi: 10.1038/srep21763

Ballesteros, J. A., and Weinstein, H. (1995). "Integrated methods for the construction of three-dimensional models and computational probing of structure-function relations in G protein-coupled receptors," in *Methods in Neurosciences*, eds S. C. Sealfon, and P. M. Conn, (San Diego, CA: Academic Press), 366–428. doi: 10.1016/s1043-9471(05)80049-7

Bartuzi, D., Kaczor, A. A., and Matosiuk, D. (2019). Molecular mechanisms of allosteric probe dependence in μ opioid receptor. *J. Biomol. Struct. Dyn.* 37, 36–47. doi: 10.1080/07391102.2017.1417914

Bernardi, R. C., Melo, M. C. R., and Schulten, K. (2015). Enhanced sampling techniques in molecular dynamics simulations of biological systems. *Biochim. Biophys. Acta* 1850, 872–877. doi: 10.1016/j.bbagen.2014.10.019

Best, R. B., Zhu, X., Shim, J., Lopes, P. E., Mittal, J., Feig, M., et al. (2012). Optimization of the additive CHARMM all-atom protein force field targeting improved sampling of the backbone ϕ, ψ and side-chain χ1 and χ2 dihedral angles. *J. Chem. Theory Comput.* 8, 3257–3273. doi: 10.1021/ct300400x

Bohn, L. M., Lefkowitz, R. J., Gainetdinov, R. R., Peppel, K., Caron, M. G., and Lin, F. T. (1999). Enhanced morphine analgesia in mice lacking beta-arrestin 2. *Science* 286, 2495–2498. doi: 10.1126/science.286.5449.2495

Burford, N. T., Livingston, K. E., Canals, M., Ryan, M. R., Budenholzer, L. M., Han, Y., et al. (2015). Discovery, synthesis, and molecular pharmacology of selective positive allosteric modulators of the delta-opioid receptor. *J. Med. Chem.* 58, 4220–4229. doi: 10.1021/acs.jmedchem.5b00007

Carlezon, W. A. Jr., and Krystal, A. D. (2016). Kappa-Opioid antagonists for psychiatric disorders: from bench to clinical trials. *Depress. Anxiety* 33, 895–906. doi: 10.1002/da.22500

Centers for Disease Control and Prevention [CDC], (2017). *Wide-Ranging Online Data for Epidemiologic Research (WONDER)*. Atlanta, GA: CDC.

Chang, D. S., Raghavan, R., Christiansen, S., and Cohen, S. P. (2015). Emerging targets in treating pain. *Curr. Opin. Anaesthesiol.* 28, 379–397. doi: 10.1097/ACO.0000000000000216

Cheng, J., Sun, X., Li, W., Liu, G., Tu, Y., and Tang, Y. (2016). Molecular switches of the κ opioid receptor triggered by 6′-GNTI and 5′-GNTI. *Sci. Rep.* 6:18913. doi: 10.1038/srep18913

Cheng, J.-X., Cheng, T., Li, W.-H., Liu, G.-X., Zhu, W.-L., and Tang, Y. (2018). Computational insights into the G-protein-biased activation and inactivation

mechanisms of the μ opioid receptor. *Acta Pharmacol. Sin.* 39:154. doi: 10.1038/aps.2017.158

Chien, E. Y., Liu, W., Zhao, Q., Katritch, V., Han, G. W., Hanson, M. A., et al. (2010). Structure of the human dopamine D3 receptor in complex with a D2/D3 selective antagonist. *Science* 330, 1091–1095. doi: 10.1126/science.1197410

Christopher, J. A., Aves, S. J., Bennett, K. A., Doreì, A. S., Errey, J. C., Jazayeri, A., et al. (2015). Fragment and structure-based drug discovery for a class C GPCR: discovery of the mGlu5 negative allosteric modulator HTL14242 (3-chloro-5-[6-(5-fluoropyridin-2-yl) pyrimidin-4-yl] benzonitrile). *J. Med. Chem.* 58, 6653–6664. doi: 10.1021/acs.jmedchem.5b00892

Christopher, J. A., Orgovaìn, Z. N., Congreve, M., Doreì, A. S., Errey, J. C., Marshall, F. H., et al. (2018). Structure-based optimization strategies for G protein-coupled receptor (GPCR) allosteric modulators: a case study from analyses of new metabotropic glutamate receptor 5 (mGlu5) X-ray structures. *J. Med. Chem.* 62, 207–222. doi: 10.1021/acs.jmedchem.7b01722

Croci, T., and Zarini, E. (2007). Effect of the cannabinoid CB1 receptor antagonist rimonabant on nociceptive responses and adjuvant-induced arthritis in obese and lean rats. *Br. J. Pharmacol.* 150, 559–566. doi: 10.1038/sj.bjp.0707138

Della Longa, S., and Arcovito, A. (2019). Microswitches for the activation of the nociceptin receptor induced by cebranopadol: hints from microsecond molecular dynamics. *J. Chem. Inform Model.* 59, 818–831. doi: 10.1021/acs.jcim.8b00759

Doré, A. S., Okrasa, K., Patel, J. C., Serrano-Vega, M., Bennett, K., Cooke, R. M., et al. (2014). Structure of class C GPCR metabotropic glutamate receptor 5 transmembrane domain. *Nature* 511, 557–562. doi: 10.1038/nature13396

Ferruz, N., Doerr, S., Vanase-Frawley, M. A., Zou, Y., Chen, X., Marr, E. S., et al. (2018). Dopamine D3 receptor antagonist reveals a cryptic pocket in aminergic GPCRs. *Sci. Rep.* 8:897. doi: 10.1038/s41598-018-19345-7

Fu, T., Zheng, G., Tu, G., Yang, F., Chen, Y., Yao, X., et al. (2018). Exploring the binding mechanism of metabotropic glutamate receptor 5 negative allosteric modulators in clinical trials by molecular dynamics simulations. *ACS Chem. Neurosci.* 9, 1492–1502. doi: 10.1021/acschemneuro.8b00059

Guo, W., Urizar, E., Kralikova, M., Mobarec, J. C., Shi, L., Filizola, M., et al. (2008). Dopamine D2 receptors form higher order oligomers at physiological expression levels. *EMBO J.* 27, 2293–2304. doi: 10.1038/emboj.2008.153

Harvey, M. J., Giupponi, G., and Fabritiis, G. D. (2009). ACEMD: accelerating biomolecular dynamics in the microsecond time scale. *J. Chem. Theory Comput.* 5, 1632–1639. doi: 10.1021/ct9000685

Hasebe, K., Kawai, K., Suzuki, T., Kawamura, K., Tanaka, T., Narita, M., et al. (2004). Possible pharmacotherapy of the opioid kappa receptor agonist for drug dependence. *Ann. N. Y. Acad. Sci.* 1025, 404–413. doi: 10.1196/annals.1316.050

Hayatshahi, H. S., Xu, K., Griffin, S. A., Taylor, M., Mach, R. H., Liu, J., et al. (2018). Analogues of arylamide phenylpiperazine ligands to investigate the factors influencing D3 dopamine receptor bitropic binding and receptor subtype selectivity. *ACS Chem Neurosci.* 9, 2972–2983. doi: 10.1021/acschemneuro.8b00142

Hua, T., Vemuri, K., Nikas, S. P., Laprairie, R. B., Wu, Y., Qu, L., et al. (2017). Crystal structures of agonist-bound human cannabinoid receptor CB 1. *Nature* 547, 468–471. doi: 10.1038/nature23272

Hua, T., Vemuri, K., Pu, M., Qu, L., Han, G. W., Wu, Y., et al. (2016). Crystal structure of the human cannabinoid receptor CB1. *Cell* 167, 750–762.e14. doi: 10.1016/j.cell.2016.10.004

Huang, L., and Roux, B. (2013). Automated force field parameterization for nonpolarizable and polarizable atomic models based on ab initio target data. *J. Chem. Theory Comput.* 9, 3543–3556. doi: 10.1021/ct4003477

Husic, B. E., and Pande, V. S. (2018). Markov state models: from an art to a science. *J. Am. Chem. Soc.* 140, 2386–2396. doi: 10.1021/jacs.7b12191

Isberg, V., de Graaf, C., Bortolato, A., Cherezov, V., Katritch, V., Marshall, F. H., et al. (2015). Generic GPCR residue numbers - aligning topology maps while minding the gaps. *Trends Pharmacol. Sci.* 36, 22–31. doi: 10.1016/j.tips.2014.11.001

Janecka, A., Piekielna-Ciesielska, J., and Wtorek, K. (2019). Biased agonism as an emerging strategy in the search for better opioid analgesics. *Curr. Med. Chem.* doi: 10.2174/0929867326666190506103124 [Epub ahead of print].

Jung, S. W., Cho, A. E., and Yu, W. (2018). Exploring the ligand efficacy of cannabinoid receptor 1 (CB1) using molecular dynamics simulations. *Sci. Rep.* 8:13787. doi: 10.1038/s41598-018-31749-z

Kapoor, A., Martinez-Rosell, G., Provasi, D., De Fabritiis, G., and Filizola, M. (2017). Dynamic and kinetic elements of μ-Opioid receptor functional selectivity. *Sci. Rep.* 7:11255. doi: 10.1038/s41598-017-11483-8

Karhu, L. V., Magarkar, A., Bunker, A., and Xhaard, H. G. (2019). Determinants of orexin receptor binding and activation–a molecular dynamics study. *J. Phys. Chem. B* 123, 2609–2622. doi: 10.1021/acs.jpcb.8b10220

Koehl, A., Hu, H., Feng, D., Sun, B., Zhang, Y., Robertson, M. J., et al. (2019). Structural insights into the activation of metabotropic glutamate receptors. *Nature* 566, 79–84. doi: 10.1038/s41586-019-0881-4

Krishna Kumar, K., Shalev-Benami, M., Robertson, M. J., Hu, H., Banister, S. D., Hollingsworth, S. A., et al. (2019). Structure of a signaling cannabinoid receptor 1-G protein complex. *Cell* 176, 448–458.e12. doi: 10.1016/j.cell.2018.11.040

Kumar, V., Bonifazi, A., Ellenberger, M. P., Keck, T. M., Pommier, E., Rais, R., et al. (2016). Highly selective dopamine D3 receptor (D3R) antagonists and partial agonists based on eticlopride and the D3R crystal structure: new leads for opioid dependence treatment. *J. Med. Chem.* 59, 7634–7650. doi: 10.1021/acs.jmedchem.6b00860

Land, B. B., Bruchas, M. R., Lemos, J. C., Xu, M., Melief, E. J., and Chavkin, C. (2008). The dysphoric component of stress is encoded by activation of the dynorphin kappa-opioid system. *J. Neurosci.* 28, 407–414. doi: 10.1523/JNEUROSCI.4458-07.2008

Lane, J. R., Donthamsetti, P., Shonberg, J., Draper-Joyce, C. J., Dentry, S., Michino, M., et al. (2014). A new mechanism of allostery in a G protein–coupled receptor dimer. *Nat. Chem. Biol.* 10, 745–752. doi: 10.1038/nchembio.1593

Livingston, K. E., Stanczyk, M. A., Burford, N. T., Alt, A., Canals, M., and Traynor, J. R. (2018). Pharmacologic evidence for a putative conserved allosteric site on opioid receptors. *Mol. Pharmacol.* 93, 157–167. doi: 10.1124/mol.117.109561

Lopes, P. E., Guvench, O., and MacKerell, A. D. Jr. (2015). Current status of protein force fields for molecular dynamics simulations. *Methods Mol. Biol.* 1215, 47–71. doi: 10.1007/978-1-4939-1465-4_3

Maier, J. A., Martinez, C., Kasavajhala, K., Wickstrom, L., Hauser, K. E., and Simmerling, C. (2015). ff14SB: improving the accuracy of protein side chain and backbone parameters from ff99SB. *J. Chem. Theory Comput.* 11, 3696–3713. doi: 10.1021/acs.jctc.5b00255

Mistry, S. N., Shonberg, J., Draper-Joyce, C. J., Klein Herenbrink, C., Michino, M., Shi, L., et al. (2015). Discovery of a novel class of negative allosteric modulator of the dopamine D2 receptor through fragmentation of a bitopic ligand. *J. Med. Chem.* 58, 6819–6843. doi: 10.1021/acs.jmedchem.5b00585

Muto, T., Tsuchiya, D., Morikawa, K., and Jingami, H. (2007). Structures of the extracellular regions of the group II/III metabotropic glutamate receptors. *Proc. Natl. Acad. Sci. U.S.A.* 104, 3759–3764. doi: 10.1073/pnas.0611577104

Nerenberg, P. S., and Head-Gordon, T. (2018). New developments in force fields for biomolecular simulations. *Curr. Opin. Struct. Biol.* 49, 129–138. doi: 10.1016/j.sbi.2018.02.002

Oren, M. B., Alexander, D. M. Jr., Benoit, R., and Masakatsu, W. (2001). *Computational Biochemistry and Biophysics*. Boca Raton, FL: CRC Press.

Pereira, V., and Goudet, C. (2018). Emerging trends in pain modulation by metabotropic glutamate receptors. *Front. Mol. Neurosci.* 11:464. doi: 10.3389/fnmol.2018.00464

Ponder, J. W., and Case, D. A. (2003). Force fields for protein simulations. *Adv. Protein Chem.* 66, 27–85. doi: 10.1016/s0065-3233(03)66002-x

Raehal, K. M., Walker, J. K., and Bohn, L. M. (2005). Morphine side effects in beta-arrestin 2 knockout mice. *J. Pharmacol. Exp. Ther.* 314, 1195–1201. doi: 10.1124/jpet.105.087254

Rasmussen, K., White, D. A., and Acri, J. B. (2019). NIDA's medication development priorities in response to the Opioid Crisis: ten most wanted. *Neuropsychopharmacology* 44, 657–659. doi: 10.1038/s41386-018-0292-5

Remesic, M., Hruby, V. J., Porreca, F., and Lee, Y. S. (2017). Recent advances in the realm of allosteric modulators for opioid receptors for future therapeutics. *ACS Chem. Neurosci.* 8, 1147–1158. doi: 10.1021/acschemneuro.7b00090

Ribeiro, J. M. L., and Filizola, M. (2019). Allostery in G protein-coupled receptors investigated by molecular dynamics simulations. *Curr. Opin. Struct. Biol.* 55, 121–128. doi: 10.1016/j.sbi.2019.03.016

Ribeiro, J. M. L., Tsai, S. T., Pramanik, D., Wang, Y., and Tiwary, P. (2019). Kinetics of Ligand-Protein dissociation from all-atom simulations: are we there yet? *Biochemistry* 58, 156–165. doi: 10.1021/acs.biochem.8b00977

Ringkamp, M., Dougherty, P. M., and Raja, S. N. (2018). "Anatomy and physiology of the pain signaling process," in *Essentials of Pain Medicine*, eds H. T. Benzon, S. N. Raja, S. M. Fishman, and S. S. Liu, (Amsterdam: Elsevier), 3.–10.

Saleh, N., Hucke, O., Kramer, G., Schmidt, E., Montel, F., Lipinski, R., et al. (2018). Multiple binding sites contribute to the mechanism of mixed agonistic and positive allosteric modulators of the cannabinoid CB1 receptor. *Angewandte Chem.* 130, 2610–2615. doi: 10.1002/anie.201708764

Saleh, N., Ibrahim, P., Saladino, G., Gervasio, F. L., and Clark, T. (2017). An efficient metadynamics-based protocol to model the binding affinity and the transition state ensemble of G-protein-coupled receptor ligands. *J. Chem. Inform. Model.* 57, 1210–1217. doi: 10.1021/acs.jcim.6b00772

Schneider, S., Provasi, D., and Filizola, M. (2016). How oliceridine (TRV-130) binds and stabilizes a μ-opioid receptor conformational state that selectively triggers G protein signaling pathways. *Biochemistry* 55, 6456–6466. doi: 10.1021/acs.biochem.6b00948

Shang, Y., Yeatman, H. R., Provasi, D., Alt, A., Christopoulos, A., Canals, M., et al. (2016). Proposed mode of binding and action of positive allosteric modulators at opioid receptors. *ACS Chem. Biol.* 11, 1220–1229. doi: 10.1021/acschembio.5b00712

Shao, Z., Yin, J., Chapman, K., Grzemska, M., Clark, L., Wang, J., et al. (2016). High-resolution crystal structure of the human CB1 cannabinoid receptor. *Nature* 540, 602–606. doi: 10.1038/nature20613

Shonberg, J., Draper-Joyce, C., Mistry, S. N., Christopoulos, A., Scammells, P. J., Lane, J. R., et al. (2015). Structure-activity study of N-((trans)-4-(2-(7-cyano-3,4-dihydroisoquinolin-2(1H)-yl)ethyl)cyclohexyl)-1H-ind ole-2-carboxamide (SB269652), a bitopic ligand that acts as a negative allosteric modulator of the dopamine D2 receptor. *J. Med. Chem.* 58, 5287–5307. doi: 10.1021/acs.jmedchem.5b00581

Silvano, E., Millan, M. J., la Cour, C. M., Han, Y., Duan, L., Griffin, S. A., et al. (2010). The tetrahydroisoquinoline derivative SB269, 652 is an allosteric antagonist at dopamine D3 and D2 receptors. *Mol. Pharmacol.* 78, 925–934. doi: 10.1124/mol.110.065755

Slivicki, R. A., Xu, Z., Kulkarni, P. M., Pertwee, R. G., Mackie, K., Thakur, G. A., et al. (2018). Positive allosteric modulation of cannabinoid receptor Type 1 suppresses pathological pain without producing tolerance or dependence. *Biol. Psychiatry* 84, 722–733. doi: 10.1016/j.biopsych.2017.06.032

Suno, R., Kimura, K. T., Nakane, T., Yamashita, K., Wang, J., Fujiwara, T., et al. (2018). Crystal structures of human orexin 2 receptor bound to the subtype-selective antagonist EMPA. *Structure* 26, 7–19.e5. doi: 10.1016/j.str.2017.11.005

Tu, Z., Li, S., Cui, J., Xu, J., Taylor, M., Ho, D., et al. (2011). Synthesis and pharmacological evaluation of fluorine-containing D3 dopamine receptor ligands. *J. Med. Chem.* 54, 1555–1564. doi: 10.1021/jm101323b

Ueda, M., Iwasaki, H., Wang, S., Murata, E., Poon, K. Y., Mao, J., et al. (2014). Cannabinoid receptor type 1 antagonist, AM251, attenuates mechanical allodynia and thermal hyperalgesia after burn injury. *Anesthesiology* 121, 1311–1319. doi: 10.1097/ALN.0000000000000422

Valsson, O., Tiwary, P., and Parrinello, M. (2016). Enhancing important fluctuations: rare events and metadynamics from a conceptual viewpoint. *Annu. Rev. Phys. Chem.* 67, 159–184. doi: 10.1146/annurev-physchem-040215-112229

Vanommeslaeghe, K., Hatcher, E., Acharya, C., Kundu, S., Zhong, S., Shim, J., et al. (2010). CHARMM general force field: a force field for drug-like molecules compatible with the CHARMM all-atom additive biological force fields. *J. Comput. Chem.* 31, 671–690. doi: 10.1002/jcc.21367

Verma, R. K., Abramyan, A. M., Michino, M., Free, R. B., Sibley, D. R., Javitch, J. A., et al. (2018). The E2. 65A mutation disrupts dynamic binding poses of SB269652 at the dopamine D2 and D3 receptors. *PLoS Comput. Biol.* 14:e1005948. doi: 10.1371/journal.pcbi.1005948

Viscusi, E. R., Skobieranda, F., Soergel, D. G., Cook, E., Burt, D. A., and Singla, N. (2019). APOLLO-1: a randomized placebo and active-controlled phase III study investigating oliceridine (TRV130), a G protein-biased ligand at the micro-opioid receptor, for management of moderate-to-severe acute pain following bunionectomy. *J. Pain Res.* 12, 927–943. doi: 10.2147/JPR.S171013

Volkow, N. D., Jones, E. B., Einstein, E. B., and Wargo, E. M. (2019). Prevention and treatment of opioid misuse and addiction: a review. *JAMA Psychiatry* 76, 208–216. doi: 10.1001/jamapsychiatry.2018.3126

Wacker, D., and Roth, B. L. (2016). An alerting structure: human orexin receptor 1. *Nat. Struct. Mol. Biol.* 23, 265–266. doi: 10.1038/nsmb.3198

Wang, J., Wolf, R. M., Caldwell, J. W., Kollman, P. A., and Case, D. A. (2004). Development and testing of a general amber force field. *J. Comput. Chem.* 25, 1157–1174. doi: 10.1002/jcc.20035

Wootten, D., Christopoulos, A., and Sexton, P. M. (2013). Emerging paradigms in GPCR allostery: implications for drug discovery. *Nat. Rev. Drug Discov.* 12, 630–644. doi: 10.1038/nrd4052

Wu, H., Wang, C., Gregory, K. J., Han, G. W., Cho, H. P., Xia, Y., et al. (2014). Structure of a class C GPCR metabotropic glutamate receptor 1 bound to an allosteric modulator. *Science* 344, 58–64. doi: 10.1126/science.1249489

Yin, J., Babaoglu, K., Brautigam, C. A., Clark, L., Shao, Z., Scheuermann, T. H., et al. (2016). Structure and ligand-binding mechanism of the human OX 1 and OX 2 orexin receptors. *Nat. Struct. Mol. Biol.* 23, 293–299. doi: 10.1038/nsmb.3183

Yin, J., Mobarec, J. C., Kolb, P., and Rosenbaum, D. M. (2015). Crystal structure of the human OX 2 orexin receptor bound to the insomnia drug suvorexant. *Nature* 519, 247–250. doi: 10.1038/nature14035

Yuan, S., Palczewski, K., Peng, Q., Kolinski, M., Vogel, H., and Filipek, S. (2015). The mechanism of ligand-induced activation or inhibition of μ-and κ-Opioid receptors. *Angewandte Chem. Int. Ed.* 54, 7560–7563. doi: 10.1002/anie.201501742

Conflict of Interest Statement: The authors declare that the research was conducted in the absence of any commercial or financial relationships that could be construed as a potential conflict of interest.

frontiers in Molecular Neuroscience

REVIEW
published: 11 September 2019
doi: 10.3389/fnmol.2019.00216

T Cells as an Emerging Target for Chronic Pain Therapy

Geoffroy Laumet[1,2]*, *Jiacheng Ma*[2], *Alfred J. Robison*[1], *Susmita Kumari*[2], *Cobi J. Heijnen*[2] *and Annemieke Kavelaars*[2]

[1]*Department of Physiology, Michigan State University, East Lansing, MI, United States,* [2]*Laboratories of Neuroimmunology, Department of Symptom Research, The University of Texas MD Anderson Cancer Center, Houston, TX, United States*

The immune system is critically involved in the development and maintenance of chronic pain. However, T cells, one of the main regulators of the immune response, have only recently become a focus of investigations on chronic pain pathophysiology. Emerging clinical data suggest that patients with chronic pain have a different phenotypic profile of circulating T cells compared to controls. At the preclinical level, findings on the function of T cells are mixed and differ between nerve injury, chemotherapy, and inflammatory models of persistent pain. Depending on the type of injury, the subset of T cells and the sex of the animal, T cells may contribute to the onset and/or the resolution of pain, underlining T cells as a major player in the transition from acute to chronic pain. Specific T cell subsets release mediators such as cytokines and endogenous opioid peptides that can promote, suppress, or even resolve pain. Inhibiting the pain-promoting functions of T cells and/or enhancing the beneficial effects of pro-resolution T cells may offer new disease-modifying strategies for the treatment of chronic pain, a critical need in view of the current opioid crisis.

Keywords: chronic pain, T cells, cytokines, neuroimmune, opioids

OPEN ACCESS

Edited by:
Tally Largent-Milnes, University of Arizona, United States

Reviewed by:
Temugin Berta, University of Cincinnati, United States
Ritobrata Goswami, Indian Institute of Technology Kharagpur, India

***Correspondence:**
Geoffroy Laumet
laumetge@msu.edu

Received: *29 June 2019*
Accepted: *26 August 2019*
Published: *11 September 2019*

Citation:
Laumet G, Ma J, Robison AJ, Kumari S, Heijnen CJ and Kavelaars A (2019) T Cells as an Emerging Target for Chronic Pain Therapy. Front. Mol. Neurosci. 12:216. doi: 10.3389/fnmol.2019.00216

PAIN MODULATION BY CYTOKINES AND IMMUNE CELLS

Pain is one of the cardinal signs of inflammation, and anti-inflammatory drugs are the first-line therapy in many acute and chronic pain conditions. In patients, chronic pain is often associated with signs of activation of the immune system as characterized by increased circulating levels of pro-inflammatory cytokines (Davies et al., 2007; Koch et al., 2007; Uçeyler et al., 2007a,b, 2011; Cameron and Cotter, 2008; Kraychete et al., 2010; Held et al., 2019). The circulating level of the anti-inflammatory cytokines interleukin (IL)-10 and IL-4 were higher in patients with painless neuropathy than in patients with painful neuropathy and controls (Uçeyler et al., 2007b; Held et al., 2019).

The immune system can be divided into two functional arms: the innate and adaptive immune systems. The contribution of the innate immune system (macrophages, neutrophils, microglia. . .) and proinflammatory cytokines to the transition from acute to chronic pain has been well established and reviewed elsewhere (Scholz and Woolf, 2007; Grace et al., 2014; McMahon et al., 2015; Ji et al., 2016; Chen et al., 2018; Baral et al., 2019). Innate immune cells and released cytokines modulate both peripheral and central sensitization, leading to pain hypersensitivity. Peripheral sensitization is defined as a reduction in the threshold of excitability of sensory neurons,

which thus become hyperexcitable. One interesting property of some pro-inflammatory cytokines (e.g., IL-1β) is their ability to interact directly with pain-sensing neurons (nociceptors among sensory neurons) to sensitize them and render them hyperexcitable, increasing the afferent input into the spinal cord (Binshtok et al., 2008; Baral et al., 2019). Moreover, in the dorsal horn of the spinal cord, cytokines facilitate the development of central sensitization (enhanced responses of pain spinal circuits). For example, Tumor Necrosis Factor α (TNFα) enhances the frequency of spontaneous excitatory post-synaptic current in lamina II neurons of the spinal cord (Kawasaki et al., 2008). Central sensitization in the spinal cord is thought to contributes to the transition to chronic pain and the spreading of pain beyond the site of primary insult (Woolf and Salter, 2000; Ji et al., 2016).

The role of the adaptive immune cells is less clear. The adaptive immune system is comprised of B and T cells (lymphocytes), and a few recent findings point out a potential role for B cells in pain, mainly through the production of autoantibodies (Andoh and Kuraishi, 2004; Klein et al., 2012; Hunt et al., 2018). However, the present review focuses on the emerging role of T cells in pain.

OVERVIEW OF THE T CELL SUBSETS

T cells express a unique antigen receptor complex on their surface: T cell receptor (TCR). In most T cells, the TCR is composed of two highly variable protein chains, α and β. The uniqueness of the TCR results from genetic rearrangements in the thymus driven by the proteins encoded by the recombination activating genes RAG1 and RAG2. The resulting unique TCRs have a very high degree of antigen specificity. TCR forms a complex with the co-receptor Cluster of Differentiation 3 (CD3) which is used as a marker to identify T cells. This TCR complex recognizes antigenic epitopes in the context of the Major Histocompatibility Complex (MHC). CD8+ T cells recognize antigen in the context of MHC-I that is expressed by virtually every nucleated cell, including neurons. In contrast, CD4+ T cells recognize MHC-II antigen which is presented specifically by antigen presenting cells (APC) such as macrophages, microglia, B cells and dendritic cells.

The CD4+ T cells are so-called T helper (Th) cells because they help cells from both the innate and adaptive immune system to optimize their response. CD4+ T cells can differentiate into functionally different subsets including Th1, Th2, Th17 or regulatory T cells (Treg; Zhu and Paul, 2008). These subsets differ from each other in their pattern of cytokine production and specific expression of characteristic transcription factors. Briefly, Th1 cells express T-bet and signal transducer and activator of transcription (STAT) 4 and release gamma-Interferon (IFNγ) and IL-2; Th2 cells express GATA3 and STAT5 and release IL-4, IL-10 and IL-13; Th17 cells express RORγT and release IL-17; and Treg express forkhead box P3 (FOXP3) and release Tumor Growth Factor (TGF)β and IL-10. Treg are a very interesting subset of T cells as their main role is to suppress the activity of other immune cells including the other subsets of T cells. The cytokines in the environment (Mousset et al., 2019), signaling through the antigen receptor, and level of engagement of specific co-stimulatory and co-inhibitory molecules on the cell surface of T cells orientate the fate of activated CD4+ T cells to specific helper subset. For example, high concentrations of IL-12 + IFNγ instruct the naïve T cells to differentiate into a Th1 profile, while IL-4 + IL-2 promote Th2 and IL-6 + IL-21 + TGFβ instruct toward Th17 subset differentiation. The anti-inflammatory cytokine TGFβ turns the cells toward the Treg fate (**Figure 1**). Other subsets of CD4+ T cells have been identified such as Th9, Th22, follicular T cell and

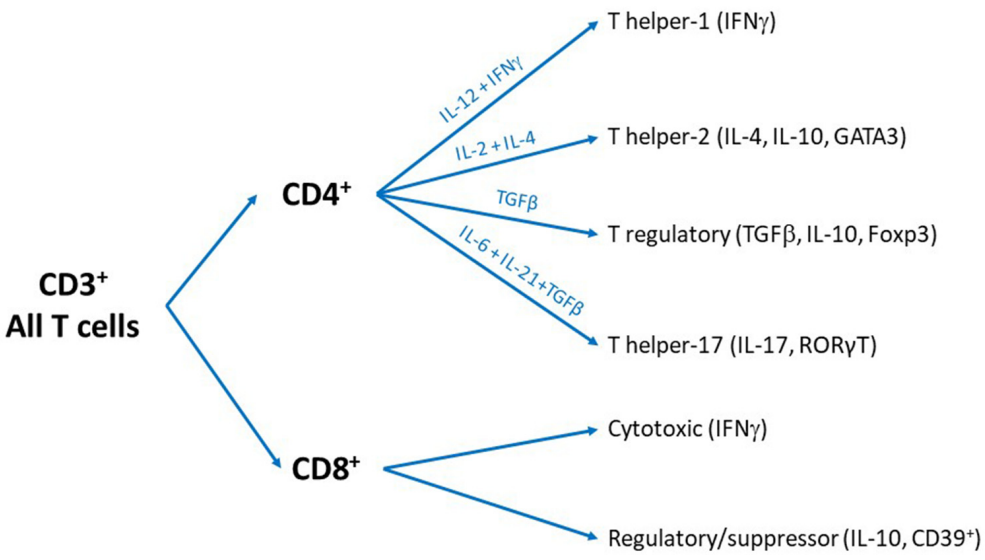

FIGURE 1 | Overview of the different subsets of T cells. All T cells are cluster of differentiation 3 (CD3)+ and can be divided into two subsets: CD4+ and CD8+ T cells. We recognize that some T cells are CD3- or CD4- CD8- cells and other subsets exist but these particular phenotypes are beyond the scope of the present review.

Natural killer T cell (NKT; Zhu and Paul, 2008; Hirahara and Nakayama, 2016; Mousset et al., 2019), but will not be discussed in this review because their contribution to pain is completely unknown.

The CD8+ T cells can be differentiated into cytotoxic T cells (CTL) and suppressor/regulatory T cells. The best characterized role of the CD8+ T cells is to kill virus-infected and tumor cells. The CTLs carry out all the attention of research on the CD8+ T cells, but the suppressor/regulatory CD8+ T cells have often been neglected. The role of the different phenotypes of CD8+ T cells (Tc1, Tc2, Tc9, Tc17) and memory status (effector, central memory, effector memory. . .; Mousset et al., 2019) has not been investigated in chronic pain and thus will not be discussed in the present review.

Another type of T cell is the γδ T cells, which have a distinct TCR. In contrast to the αβ-TCR, γδ-TCR are invariant and less abundant (Itohara et al., 1993). In the circulation, only 5% of T cells are γδ T cells (Glusman et al., 2001), but they represent a high proportion of gut- and skin-resident immune cells, where they are localized near the sensory neurons (Marshall et al., 2019).

PHENOTYPE OF CIRCULATING T CELLS IN PATIENTS WITH CHRONIC PAIN

Few studies have analyzed circulating T cell counts and subsets in patients with chronic pain. Those studies are often small, and the parameters analyzed vary. Studies in patients with chronic pain do not report changes in the total number of circulating T cells compared to pain-free matched controls (Mangiacavalli et al., 2010; Luchting et al., 2015). Likewise, the number of circulating CD4+ and CD8+ T cells seems unchanged in various chronic pain conditions (Brennan et al., 1994). However, in patients with chronic headache, a lower number of CD8+ T cells, and consequently higher CD4+/CD8+ ratio was found compared to control individuals (Gilman-Sachs et al., 1989).

In general, assessment of the total number of circulating T cell subsets in patients with chronic pain is not very informative. To gain more insight into the role of T cells in chronic pain, some studies investigated the functional subsets of CD4+ T cells. These studies found an imbalance in the ratio of Th1/Th2 (Liu et al., 2006; Mangiacavalli et al., 2010) and Th17/Treg ratio (Tang et al., 2013; Luchting et al., 2014, 2015). To avoid bias, the absence of infection was controlled in these patients. Contrary to the expected pro-inflammatory profile, these studies actually found indication of an anti-inflammatory shift in T cell profile toward Th2 and Treg. Consistently, the expression of the specific Th17 transcription factor RORγT and cytokine IL-17 were decreased as well in complex regional pain syndrome (CRPS) patients (Haas et al., 2011; Heyn et al., 2019). In another study in CRPS patients, the number of Tregs did not change, but the specific sub-subset of CD39+ Treg was decreased (Heyn et al., 2019). In contrast, a stronger Th1 response was observed in T cells from patients with neuropathic pain as compared to controls when the cells were stimulated *in vitro* with myelin-derived antigen (Diederich et al., 2018). Further analysis reported changes in specific markers for sub-subsets of T cells. Furthermore, smoking affects both the development of chronic pain and T cell phenotypes (Scott et al., 1999; Power et al., 2001; Vargas-Rojas et al., 2011), strengthening the argument for a connection. In patients with chronic pain, smoking increased the Th17/Treg ratio measured by flow cytometry and mRNA expression of RORγT and FOXP3, and this increased Th17/Treg ratio was associated with higher pain sensitivity (Heyn et al., 2018).

Given that T cells are easy to access peripherally, they represent an attractive pool for identification of potential biomarkers to survey the development of chronic pain. However, the clinical relevance of measuring circulating T cells is not yet clear, and additional studies are necessary to identify potential biomarkers. It is also important to note that the phenotype of T cells can be affected by pain-killers (e.g., morphine; Ranganathan et al., 2009; Wiese et al., 2016; Plein and Rittner, 2018), potentially complicating any findings in patients after they begin treatment.

T CELLS IN NEUROIMMUNE INTERACTIONS

T cells play an important role in the communication between the nervous and immune systems, and one of the most studied interactions between T cells and the nervous system is the anti-inflammatory reflex (Tracey, 2009). During systemic inflammation, proinflammatory cytokines activate the afferent vagus nerve which initiates a reflex response. β2-adrenergic receptor-expressing T cells react to noradrenaline released by the sympathetic splenic nerve, triggering the production of acetylcholine by T cells. Acetylcholine signals to macrophages to switch from the production of pro-inflammatory to anti-inflammatory cytokines such as IL-10, thus dampening the immune response (Pavlov and Tracey, 2017). The anti-inflammatory reflex is absent in nude mice lacking T cells, and adoptive transfer of T cells restores the anti-inflammatory reflex, confirming the crucial role of T cells in this neuroimmune communication (Rosas-Ballina et al., 2011).

T cell function is also directly influenced by nociceptors. Upon activation, nociceptors release glutamate, calcitonin gene-related peptide (CGRP), and Substance P (SP). The canonical role of theses neurotransmitters and neuropeptides is to activate second order neurons in the dorsal horn of the spinal cord to signal pain into the central nervous system (CNS). In addition to this neuronal transmission role, activated nociceptors release these neurotransmitters and neuropeptides at their peripheral endings, regulating activity of local immune cells including T cells. T cells express inotropic and metabotropic glutamate receptors, SP and CGRP receptors (Rameshwar et al., 1992; Ganor et al., 2003; Mikami et al., 2011; Ohtake et al., 2015; Szklany et al., 2016). Activation of these receptors regulates various T cell functions such as adhesion, chemotactic migration, proliferation and immunological phenotypes (Hosoi et al., 1993; Levite et al., 1998; Hood et al., 2000; Levite, 2000; Talme et al., 2008; Mikami et al., 2011). Not surprisingly, nociceptor–T cell interaction has a critical role in chronic inflammatory diseases and in immune defense against infection (Basbaum and Levine, 1991; Razavi et al., 2006; Chiu et al., 2013; Cohen et al., 2019).

Genetic ablation of nociceptors alters the immune response to sterile injury or infection and pathogen control (Chiu et al., 2013; Talbot et al., 2015; Baral et al., 2019).

Critically, the interaction between T cells and the nervous system is bidirectional, and T cells regulate neuronal function in the central and peripheral nervous systems. For instance, meningeal T cells secrete IL-4 to trigger brain derived neurotrophic factor (BDNF) production to enhance neurogenesis in the brain (Ziv et al., 2006). In an inflammatory skin disease model, Th2 cells trigger itch by secretion of IL-31, which binds to its receptor on sensory neurons, triggering calcium release, phosphorylation of ERK1/2 and activation of TRPA1 channel, driving neuronal activation and itch (Cevikbas et al., 2014).

Given the role of T cells in neuroimmune interactions, they likely have an important impact on the transition from acute to chronic pain. To identify the role of T cells in chronic pain, multiple pain models have been used, including models of nerve injury-induced neuropathic pain, inflammatory pain, and chemotherapy-induced peripheral neuropathy (CIPN). In this review, we will not discuss data collected from models of autoimmune disorders, such as multiple sclerosis, because the key role of T cells in autoimmunity itself makes it difficult to disentangle the specific role of T cells in pain in these models (Dendrou et al., 2015).

CONTRIBUTION OF T CELLS TO PAIN SENSITIVITY IN NAïVE ANIMALS

The contribution of T cells to pain can be evaluated by comparing pain-related behaviors in WT and T cell-deficient rodents. These animals often carry a genetic mutation in one of the genes involved in the rearrangement of the antigen receptor such as *Rag1*, *Rag2*, or Protein Kinase, DNA-Activated, Catalytic Subunit (*Prkdc* for severe combined immunodeficiency—SCID mice). Therefore, they lack the entire adaptive immune system (B and T cells). This lack of adaptive immune cells from birth may induce compensatory mechanisms and alter the innate immune cells and may even influence the neuronal circuitry (Filiano et al., 2016). On the other hand, the use of these transgenic animals is the cleanest way to deplete T cells preclinically. To critically evaluate the contribution of T cells, WT mice are compared to mice deficient for the whole adaptive immune system (simplified and referred to T-cell-deficient mice in this review) including the *Rag1*$^{-/-}$, *Rag2*$^{-/-}$, nude and SCID mice, as well as to mice reconstituted with specific populations of T cells (**Figure 2**).

At baseline, T-cell-deficient rodents are indistinguishable from control counterparts in response to mechanical stimuli in at least 3 different mouse genetic backgrounds (CD1, BALB and C57) and athymic rats (Moalem et al., 2004; Cao and DeLeo, 2008; Costigan et al., 2009; Vicuña et al., 2015; Krukowski et al., 2016; Rosen et al., 2017; Laumet et al., 2019). Reconstitution of T cell-deficient rodents with any type of T cells also does not alter the baseline pain sensitivity in male and female mice. Only one publication reported increased pain sensitivity in male and female mice that lack the adaptive immune system (Rosen et al., 2019), and an important difference is that this study included up to 40 animals per group while previous studies that did not observe differences investigated 5–10 mice per group. These findings suggest that there may be a small but statistically significant difference in baseline pain sensitivity between WT and T-cell-deficient mice.

CONTRIBUTION OF T CELLS TO THE TRANSITION FROM ACUTE TO CHRONIC PAIN

The next paragraphs cover studies with male rodents unless otherwise indicated, and these data are summarized in **Table 1** while the contribution to each CD4+ T cell subset is listed in **Table 2**. The potential role of sex differences is discussed at the end of this section. Advancing age is an important risk factor for chronic pain, and it is important to note that most of the studies discussed below were conducted in relatively young adult rodents.

Nerve Injury-Induced Neuropathic Pain

In preclinical studies, neuropathic pain is usually induced by peripheral nerve injury through a surgical intervention (CCI, chronic constriction injury; SNI, spared nerve injury; SNL, spinal nerve injury; PSNL, partial sciatic nerve injury; SNT, spinal nerve transection).

Infiltration of T Cells Into the Nervous System Following Nerve Injury

Nerve injury generates an organized cascade of events to stimulate the inflammatory responses (Gadani et al., 2015). Immediately after injury, alarmins are released and glial cells surrounding the nerve are activated. In the following minutes, cytokines and chemokines are secreted, and neutrophils are recruited. Neutrophils are almost always the first peripheral immune cells to invade sites of injury. In hours to days, monocyte-derived macrophages will infiltrate the damaged nerve while T cells usually arrive days to weeks post-injury, first infiltrating the site of injury and distal part of the nerve, then the dorsal root ganglia (DRG, a cluster of the cell bodies of sensory neurons), and finally the dorsal horn of the spinal cord. Moalem et al. (2004) examined the kinetics of T cell infiltration of the sciatic nerve in response to CCI in rats. T cells were not observed in uninjured sciatic nerve (sham and contralateral nerve), and few T cells were detected at 3 days after injury. Significant T cell infiltration was observed at 7 days and peaked at 21 days at proximal (125 T cells/0.5 mm^2 detected by anti-αβ TCR antibody) and distal sites of the injury (Moalem et al., 2004). Infiltrated T cells were still present at 40 days after injury (the last time point checked). This pattern is consistent with studies using different nerve injury models in rats and in mice, wherein few T cells were found at the site of injury at 3 days post-surgery and the number of T cells significantly increased from 7 to 28 days post-surgery (Cui et al., 2000; Kleinschnitz et al., 2006; Labuz et al., 2009; Austin et al., 2012; Kobayashi et al., 2015). T cells represented almost 10% of the infiltrating immune cells at 15 days after the injury (Labuz et al., 2009).

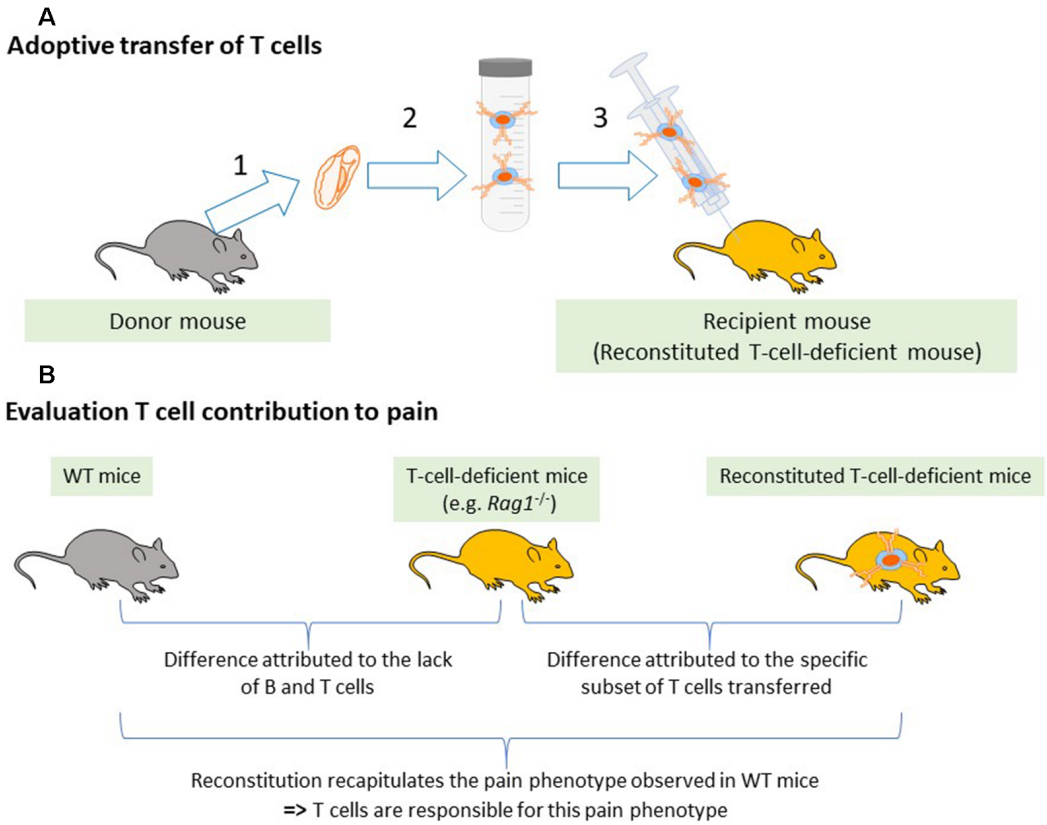

FIGURE 2 | Reconstitution of T-cell-deficient mice. **(A)** Adaptive transfer of T cells from WT mice to T cell-deficient mice. (1) Lymphoid tissues such as the spleen, lymph nodes, or blood are collected from donor mice. (2) T cells or specific subsets of T cells are isolated using magnetic beads. (3) Selected T cells are injected into T-cell-deficient mice. **(B)** Evaluation of T cell contribution to pain. To attribute a pain phenotype to a function of T cells, the pain behavior in the immunodeficient mice must be different from the WT mice and reconstitution of the immunodeficient mice with T cells must normalize the pain response.

Austin et al. (2012) reported 150–200 TCR+ cells/0.5 mm^2 at the injury site at 28 days post-CCI.

Invading T cells may come from the circulation and are thought to penetrate the nerve from the endoneurial vasculature rather than migration across the nerve sheath (Eliav et al., 1999; Kobayashi et al., 2015). The infiltration of T cells appears to depend on phagocytic cells, as depletion of these cells using clodronate-liposome treatment prevented the infiltration of CD4+ T cells, suggesting that previous infiltration of innate immune cells is necessary for T cells to infiltrate the injured nerve.

Naïve DRGs lack a tight blood-nerve barrier and contain a low number of both CD4+ and CD8+ T cells (Austin et al., 2012; Liu et al., 2014; Vicuña et al., 2015; Krukowski et al., 2016). In contrast to the circulation, where 65%–70% of T cells are CD4+, in DRG 60%–70% are CD8+ T cells, indicating a regulated infiltration (McLachlan and Hu, 2014; Krukowski et al., 2016). The number of T cells increases in the DRG in response to both spinal and sciatic nerve injury (Hu and McLachlan, 2002; Austin et al., 2012; Du et al., 2018). Similar to the nerve, the number of T cells at 3 days post-surgery was not different between sham and injured DRGs but starts to increase after 7 days. The number of T cells increased 4–6 times at 28 days after nerve injury and persisted for at least 12 weeks (Hu and McLachlan, 2002). Interestingly, in this model, the T cells invading the DRG were mostly CD4+, inducing a switch in the CD4+/CD8+ ratio (McLachlan and Hu, 2014). The route taken by T cells to infiltrate into the DRG is still unknown. They possibly come from blood vessels or from the DRG and spinal meninges, specifically at the subarachnoid angle (Hu and McLachlan, 2002). Using IHC and lymphadenectomy approaches, a recent study demonstrated that after SNI, CD4+ T cells from lumbar lymph nodes begin migrating into the dorsal root leptomeninges to invade the DRG of the injured axons (Du et al., 2018). The lumbar sympathetic chain may be required for this migration (Hu and McLachlan, 2002; McLachlan and Hu, 2014), and lumbar DRG-invading T cells, mostly CD4+, are drained by the sciatic lymph node (McLachlan and Hu, 2014).

T cells are hardly detectable, if at all, in the spinal cords of naïve animals. However, as has been proposed for the brain, it is possible that T cells penetrate the CNS parenchyma but only in very small number and for a very short time, making them virtually undetectable (Kipnis et al., 2012). In response to injury, T cells may migrate into the spinal cord through the leptomeninges to reach the cerebral spinal fluid (CSF) as

TABLE 1 | Pain hypersensitivity phenotypes in T-cell-deficient or T-cell-depleted rodents compared to WT or IgG-treated controls.

Chronic pain model	T cell depletion model	Sex	Pain sensitivity vs. controls	References
CCI	Nude (rats)	M	Reduced	Moalem et al. (2004)
CCI	*Rag1*$^{-/-}$	M	Reduced	Kleinschnitz et al. (2006)
SNT	Nude and *Cd4*$^{-/-}$	M	Reduced	Cao and DeLeo (2008)
SNI	*Rag1*$^{-/-}$	M	Reduced	Costigan et al. (2009)
CCI	SCID	M	Identical	Labuz et al. (2010)
PSNL	Anti-CD4	M	Reduced	Kobayashi et al. (2015)
SNI	*Rag2*$^{-/-}$	No info	Reduced	Vicuña et al. (2015)
SNI	*Rag1*$^{-/-}$and Nude	F	Identical	Rosen et al. (2017)
mSNI	Anti-αβTCR (rats)	M	Reduced	Du et al. (2018)
Paclitaxel	*Rag1*$^{-/-}$	M	Prolonged	Krukowski et al. (2016)
Cisplatin	*Rag1*$^{-/-}$ and *Rag2*$^{-/-}$	M + F	Prolonged	Laumet et al. (2019)
CFA + OVA	Nude	No info	Prolonged	Boué et al. (2012)
CFA	TCRβ$^{-/-}$	M	Identical	Ghasemlou et al. (2015)
CFA	*Rag1*$^{-/-}$		Identical	Sorge et al. (2015)
CFA	*Rag2*$^{-/-}$	M	Prolonged	Basso et al. (2016)
CFA	*Rag1*$^{-/-}$and Nude	F	Identical	Rosen et al. (2017)
CFA	TCRδ$^{-/-}$	M + F	Identical	Petrović et al. (2019)
CFA	*Rag2*$^{-/-}$	M	Prolonged	Laumet et al. (2016)
DSS visceral pain	SCID	No info	increased	Boué et al. (2014)
Formalin	*Tcrd*$^{-/-}$	M + F	Identical	Petrović et al. (2019)
Formalin	Nude	M + F	increased	Rosen et al. (2019)
Morphine analgesia	*Rag1*$^{-/-}$, *Cd4*$^{-/-}$ and Nude	M + F	Reduced	Rosen et al. (2019)
Plantar incision	*Tcrb*$^{-/-}$	M	Identical	Ghasemlou et al. (2015)
Plantar incision	*Tcrd*$^{-/-}$	M + F	Identical	Petrović et al. (2019)

CCI, chronic constriction injury; CFA, complete Freund's adjuvant; DSS, dextran sulfate sodium; mSNI, modified SNI; OVA, ovalbumin immunization; PSNL, partial sciatic nerve ligation; SNI, spared nerve injury; SNT, spinal nerve transection; M, male; F, female.

TABLE 2 | Contribution of each CD4+ T cell subsets to pain sensitivity.

T helper subset	Pain sensitivity	Potential mechanisms	References
Th1	↑	Production of proinflammatory cytokines	Moalem et al. (2004) and Draleau et al. (2014)
Th2	↓	Production of anti-inflammatory cytokines (IL-10) and endogenous opioids	Moalem et al. (2004), Leger et al. (2011), Boué et al. (2014) and Basso et al. (2018)
Th17	↑	Production of proinflammatory cytokines and activation of microglia and macrophages	Kleinschnitz et al. (2006) and Huo et al. (2019)
Treg	↓	Production of anti-inflammatory cytokines (IL-10)	Austin et al. (2012), Liu et al. (2014), Lees et al. (2015) and Duffy et al. (2019)

they infiltrate the dorsal root leptomeninges following nerve injury or in autoimmune disease (Schläger et al., 2016; Du et al., 2018). With immunostaining approaches, several studies observed the presence of CD4+ T cells in the dorsal horn of the spinal cord after PSNL, SNI and SNT (Cao and DeLeo, 2008; Costigan et al., 2009; Leger et al., 2011). However, even in these models, the number of T cells in the spinal cord stays very low. Flow cytometry experiments confirmed the presence of CD4+ T cells in the spinal cord at 7 days after nerve injury (Cao and DeLeo, 2008). In the SNT model, the phenotypes of infiltrated CD4+ cells are T-Bet+, IFNγ+, TNF-α+, and GM-CSF+, GATA3- or IL-4-, suggesting a Th1 phenotype (Draleau et al., 2014). The specific combination of adhesion molecules expressed in the spinal cord facilitates the infiltration of α4β1 integrin-expressing immune cells. Among T cells, Th1 cells have higher expression of α4β1, rendering them more likely to infiltrate the spinal cord than other T cell subsets (Rothhammer et al., 2011). In contrast, another study using staining with anti-CD2 to label all T cells and anti-CD8 to identify this specific subset did not observe T cell infiltration in the dorsal horn spinal cord from day 2 to 42 post-SNI (Gattlen et al., 2016). Thus, there are conflicting reports as to whether and how subsets of T cells enter the spinal cord in response to pain or injury, and further studies in this area will be critical.

In healthy conditions, T cells are virtually absent of the brain parenchyma but are present in the surrounding meninges (Kipnis et al., 2012). To our knowledge, the potential infiltration of T cells into brain areas associated with pain has not been investigated.

Contribution of T Cells to Nerve-Injury Induced Pain Hypersensitivity

The contribution of T cells to chronic pain can be investigated in WT mice by depletion or neutralization of T cells with antibodies. Administration of anti-CD4 antibody to deplete mice of functional CD4+ T cells, starting 4 days before surgery, reduced pain sensitivity following PSNL (Kobayashi et al., 2015). Repetitive intrathecal injections of anti-αβ-TCR antibody to deplete mice of all functional αβ T cells starting at 3 days post-SNI alleviated mechanical pain hypersensitivity as well. Interestingly, mechanical allodynia returned once the treatment

was terminated and T cells may have repopulated the mouse (Du et al., 2018). One of the pioneer studies to use T cell-deficient animals (athymic rats) investigated the contribution of T cells to neuropathic pain induced by CCI. Nude rats developed reduced thermal and mechanical pain hypersensitivity compared to WT following CCI (Moalem et al., 2004). Reconstitution of athymic nude rats with IFNγ and IL-2 producing Th1 cells restored the pain behavior, while reconstitution with Th2 cells producing the anti-inflammatory cytokines IL-10, IL-4 and IL-13 further reduced thermal pain sensitivity after CCI (Moalem et al., 2004). In mice, a first investigation found that Rag1$^{-/-}$ mice developed similar mechanical pain but reduced thermal pain hypersensitivity after CCI compared to WT mice (Kleinschnitz et al., 2006). Another study reported that mechanical allodynia was completely prevented in *Rag1*$^{-/-}$ mice following SNI (Costigan et al., 2009). Reconstitution of T-cell-deficient mice with T cells (as done with athymic rats previously) is a necessary experiment to attribute the observed effects to the lack of T cells, as *Rag1*$^{-/-}$ mice also lack B cells. This issue has been addressed by Cao and Deleo, as they observed that nude mice have reduced pain sensitivity after SNT and reconstitution of nude mice with CD4+ T cells restored pain hypersensitivity (Cao and DeLeo, 2008). Further, the aggravating effect of T cells on neuropathic pain was confirmed in *Cd4*$^{-/-}$ mice (Cao and DeLeo, 2008). Similar findings were obtained using *Rag2*$^{-/-}$ mice, which did not develop mechanical pain hypersensitivity after SNI surgery. The authors confirmed that *Rag2*$^{-/-}$ mice reconstituted with T cells behave like WT mice in response to SNI (Vicuña et al., 2015). Taken together, these studies indicate a detrimental role for T cells in chronic pain induced by nerve injury. However, there are a few publications showing that SCID and *Rag1*$^{-/-}$ mice developed mechanical allodynia like WT mice in both sexes in response to nerve injury (Sorge et al., 2015; Rosen et al., 2017). A comparison of the infiltration of T cells and the development of pain hypersensitivity after CCI, PSNL, or complete axotomy, found that while all axotomized rats developed pain hypersensitivity, only one third of rats with CCI and PSNL showed allodynia. However, T cells infiltration was observed in the three models and there was no relation between numbers of infiltrating T cells in peripheral nerves and development of allodynia (Cui et al., 2000). In addition, in most publications, the pain hypersensitivity does not correlate with T cell infiltration, as maximal intensity of pain is observed before infiltration and recruitment of T cells. It remains unclear how T-cell-deficient mice are fully protected from SNI (Costigan et al., 2009; Vicuña et al., 2015) while T cells start infiltrating the damaged somatosensory system only several days after injury. These data may suggest an alteration of the early immune response to nerve injury in *Rag1*$^{-/-}$ and *Rag2*$^{-/-}$ mice owing to the impact of T cells on the homeostasis of the innate immune cells.

Treg cells are a particularly interesting subset because they inhibit T cell proliferation and cytokine production. In PSNL-treated mice, injection of anti-CD25 antibody depleted Treg cells in the spleen and lymph nodes and prolonged mechanical pain hypersensitivity (Austin et al., 2012). Targeting CD25 is not specific to the elimination of Treg cells since other immune cells (e.g., monocytes and activated T cells) express CD25 as well. In order to achieve a more effective and specific depletion of Tregs, the same group took advantage of the DEREG mice. DEREG stands for DEpletion of T-REG cells, and in this mouse model, the human diphtheria toxin receptor is expressed under the control of the Foxp3 promoter. When these mice are treated with diphtheria toxin, the Foxp3+ (Treg) cells are specifically depleted. Flow cytometry confirmed Treg depletion, and an increase in CD4+ effector T cells was also observed. Following diphtheria toxin treatment, the DEREG mice showed enhanced mechanical allodynia in response to CCI, with neither the contralateral paw nor the WT mice affected by diphtheria toxin administration (Lees et al., 2015). Thus, Tregs appear to play a protective role in pain after nerve injury.

Infiltration of T Cells in Diabetic Painful Neuropathy Model

In a model of diabetes type I peripheral neuropathy induced by injection of streptozotocin, T cells infiltrated the DRG at a very late stage. Significant presence of T cells in the DRG was not detected before 19 weeks post-injection, although mechanical pain and spontaneous pain were evidenced earlier (from 8 weeks post-injection; Agarwal et al., 2018). Interestingly, peripheral nerves from patients with diabetic neuropathy showed massive T cell infiltration of the endoneurial and epineurial compartments. In diabetic patients (type I and II) with peripheral neuropathy, approximatively 25 times more CD3+ T cells were counted per section in sural nerve biopsies compared to control patients. The infiltrated T cells were mostly CD8+ T cells and CD25+ cells, an indication of CD4+ or CD8+ Treg (Younger et al., 1996). However, the contribution of T cells to diabetic painful neuropathy has not been investigated yet.

Contribution of T Cells to Chemotherapy-Induced Peripheral Neuropathy (CIPN)

CIPN is a common side effect of cancer treatment and is often associated with pain. The role of T cells in CIPN has been studied in models of systemic injection of chemotherapeutic agents such as paclitaxel, cisplatin, or oxaliplatin. In a model of paclitaxel-induced neuropathic pain, Liu reported that intrathecal anti-CD8 reduced mechanical allodynia on day 5 and 6 after paclitaxel. This study also showed that intrathecal injection of CD8+ T cells worsened pain hypersensitivity, while injection of Treg cells briefly reduced mechanical allodynia (Liu et al., 2014). These effect might result from the specific route of injection used here, as T cells are not present (or are at a very low level) in the spinal cords of control and CIPN animals (Janes et al., 2015; Denk et al., 2016; Gattlen et al., 2016; Krukowski et al., 2016), in contrast to the experimental autoimmune encephalomyelitis (EAE) model in which a substantial infiltration of T cells is observed in the spinal cord (Rothhammer et al., 2011; Duffy et al., 2019). These beneficial and detrimental effects of Treg and CD8+ T cells, respectively, were not reproduced in transgenic mice. Treg depletion, using the DEREG mice, did not affect pain hypersensitivity after oxaliplatin (Makker et al., 2017). In

CIPN induced by either paclitaxel or cisplatin, *Rag1*$^{-/-}$ or *Rag2*$^{-/-}$ female and male mice develop mechanical allodynia with similar intensity to WT mice. Strikingly, the resolution of chemotherapy-induced mechanical allodynia was significantly delayed in the absence of T cells (Krukowski et al., 2016; Laumet et al., 2019). Reconstitution with CD8+, but not CD4+, T cells restored the resolution of mechanical allodynia (Krukowski et al., 2016). While most studies cited above focus only on evoked-pain behaviors, our studies showed that the absence of T cells also impairs the resolution of spontaneous pain assessed by conditioned place preference, and reconstitution with CD8+ T cells normalized the resolution of spontaneous pain (Laumet et al., 2019).

Interestingly, the adoptive transfer of CD8+ T cells into T-cell-deficient mice after CIPN had fully developed failed to promote resolution of pain (Laumet et al., 2019). These findings indicate that the CD8+ T cells have to be exposed to cisplatin in order to be capable of promoting resolution of CIPN. In other words, the CD8+ T cells need to be "*educated*" to acquire the capacity to promote resolution of CIPN by exposure to cisplatin. In support of this idea, adoptive transfer of CD8+ T cells from cisplatin-treated WT mice did indeed promote resolution of established CIPN in *Rag2*$^{-/-}$ mice. This T cell education appears to be independent of antigen recognition by the TCR because reconstitution of *Rag2*$^{-/-}$ mice with CD8+ T cells with mutated TCRs that recognize and respond only to one irrelevant antigen (chicken ovalbumin) retained the capacity to induce CIPN resolution (Laumet et al., 2019). Interestingly, the neuroprotective effects of T cells after brain trauma was also independent of antigen recognition by the TCR (Walsh et al., 2015).

Contribution of T Cells to Inflammatory Pain

Inflammatory pain is modeled by injection of Complete Freund's adjuvant (CFA), formalin, or other inflammatory agents into the paw. In response to intraplantar CFA injection, immune cells (CD45+) infiltrate the paw. T cells represented 2%–4% of infiltrated immune cells, and their percentage remain unchanged over in the first 96 h (Rittner et al., 2001) but showed significant increases after 7 days that are maintained for at least 14 days (Ghasemlou et al., 2015). After CFA, the severity of mechanical allodynia was identical in WT and in five different strains of T-cell-deficient mice (nude, *Tcrb*$^{-/-}$, *Tcrd*$^{-/-}$, *Rag1*$^{-/-}$ and *Rag2*$^{-/-}$; Ghasemlou et al., 2015; Sorge et al., 2015; Laumet et al., 2016, 2019; Petrović et al., 2019). These data indicate that inflammatory pain hypersensitivity in the CFA model develops independently of T cells. While the onset and severity of inflammatory allodynia are similar between WT and T-cell-deficient mice, several independent studies reported that the resolution of mechanical allodynia was significantly delayed in T-cell-deficient mice (Boué et al., 2011, 2012; Basso et al., 2016; Laumet et al., 2016). Reconstitution of *Rag1*$^{-/-}$ or *Rag2*$^{-/-}$ mice with WT T cells normalized resolution of CFA-induced mechanical allodynia. Similar findings were obtained after intraplantar injection of IL-1β (Kavelaars lab, unpublished data). The pain behavior in response to formalin was worsened in nude mice compared to WT, and reconstitution of nude mice with CD4+ T cells normalized their response to formalin in both sexes (Rosen et al., 2019). In the antigen- and collagen-induced models of arthritis, CD8+ T cell depletion worsened the pain hypersensitivity (Baddack-Werncke et al., 2017), while in a postsurgical pain model, no alteration in thermal and mechanical hypersensitivity was reported in *Tcrb*$^{-/-}$and *Tcrd*$^{-/-}$ mice compared to WT mice (Ghasemlou et al., 2015; Petrović et al., 2019). The lack of contribution of γδ T cells to inflammatory pain induced by plantar incision was reported in both sexes (Petrović et al., 2019), and these mice deficient in γδ T cells have a normal pattern of αβ T cells. In conclusion, the existing literature indicates that, in inflammatory pain models, T cells are beneficial or neutral to the pain phenotype.

Contribution of T Cells to Sex Differences in Pain Signaling

Like most of the preclinical research in pain (Mogil, 2012), the role of T cells has been almost exclusively studied in male rodents, but recent evidence suggests that T cells may contribute to sex differences in pain signaling. Key studies in this area showed that inhibition of microglia relieved nerve injury-induced pain only in male mice (Sorge et al., 2015; Taves et al., 2016; Luo et al., 2018). Critically, this sex difference disappeared in T-cell-deficient mice (*Rag1*$^{-/-}$ and nude mice; Sorge et al., 2015; Mapplebeck et al., 2018). Moreover, a beneficial role of T cells became apparent when comparing pregnant WT and T-cell-deficient mice. In late pregnant WT mice, CFA- and SNI-induced allodynia are suppressed, but this does not happen in T-cell-deficient mice (*Rag1*$^{-/-}$ and nude mice). Adoptive transfer of CD4+ T cells restored pregnancy analgesia (Rosen et al., 2017). T cells are also responsible for the reduced morphine analgesia observed in female mice, and this sex difference in morphine analgesic sensitivity was restored by adoptive transfer of male CD4+ T cells to female nude mice (Rosen et al., 2019). Notably, however, no sex difference was observed in the contribution of CD8+ T cells to CIPN resolution (Laumet et al., 2019). In summary, these data indicate complex interactions between T cells and sex in pain signaling, although the physiology of these interactions remains to be uncovered.

TARGETING T CELLS FOR THE TREATMENT OF CHRONIC PAIN

Accumulating literature indicates that T cells contribute to the transition from acute to chronic pain. While in nerve injury models T cells are mostly detrimental, they are mostly beneficial in models of inflammatory pain and CIPN. A potential explanation for this apparent discrepancy may be in the T cell subsets engaged. As mentioned above, Th1 cells are more likely to increase pain, while Th2, Treg, and CD8+ T cells are protective. This would mean that two potential therapeutic strategies can be developed: (i) blocking the pain promoting functions and/or subsets of T cells; and (ii) enhancing the beneficial effects and/or subsets of T cells.

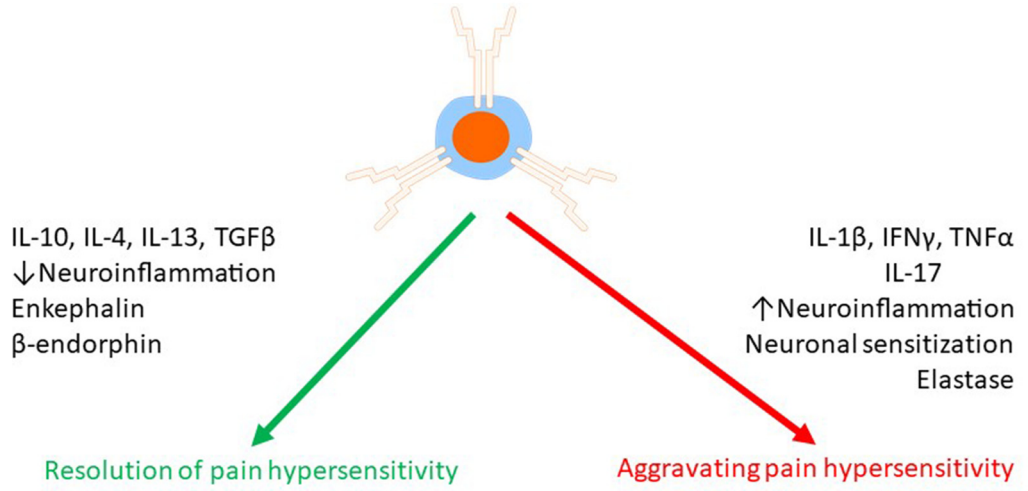

FIGURE 3 | Effects of T cells on chronic pain. T cells can both suppress and promote chronic pain. T cells release a variety of mediators such as pro- and anti-inflammatory cytokines, endogenous opioids, and proteases to regulate pain either *via* a direct effect on pain sensing neurons or indirectly *via* modulation of neuroinflammation.

Potential Mechanisms Underlying the Pain Increasing Effects of T Cells

The pain promoting effect of T cells may result from amplification of neuroinflammation (**Figure 3**). For example, it has been proposed that Th1 and Th17 cells facilitate macrophage infiltration in the damaged nerve and DRG (Kleinschnitz et al., 2006; Kobayashi et al., 2015). In the spinal cord, $Cd4^{-/-}$ mice showed less astrocyte activation at 14 days after SNT (Draleau et al., 2014). In the injured nerve, the infiltrated T cells (Th17 cells) produce IL-17, and this may contribute to microgliosis *via* stimulation of the IL-17 receptors expressed on microglia (Kleinschnitz et al., 2006). Consistent with this model, inhibition of IL-17 signaling reduced microgliosis, mechanical allodynia, and paw flinches associated with bone cancer pain (Huo et al., 2019).

In addition to cytokines, T cells produce the serine protease leukocyte elastase (LE, encoded by the gene *Elane*). LE is released by infiltrated T cells in the DRG after SNI, and it activates matrix metalloprotease 9 (MMP9) which facilitates neuropathic pain (Ferry et al., 1997; Ji et al., 2009). To assess the critical role of LE-producing T cells in neuropathic pain, Vicuña et al. (2015) reconstituted $Rag2^{-/-}$ mice with T cells from WT or $Elane^{-/-}$ mice and monitored their pain sensitivity following SNI. The lack of LE in the T cells prevented the development of neuropathic pain.

Following nerve injury, infiltrated CD4+ T cells in the dorsal horn of the spinal cord are often associated with increased pain (Cao and DeLeo, 2008; Costigan et al., 2009; Leger et al., 2011). Therefore, a potential therapeutic strategy may be to target the infiltration of the CD4+ T cells into the spinal cord. Repurposing drugs that have been developed to block the infiltration of T cells in the central nervous system in multiple sclerosis may be an attractive strategy to treat neuropathic pain induced by nerve injury. FTY720, a drug used to treat multiple sclerosis, sequesters T cells in the lymph nodes and prevents the infiltration of the nervous system. After PSNL, FTY720-treated mice showed less mechanical and thermal pain sensitivity compared to vehicle-treated mice (Kobayashi et al., 2015). An important caveat is that FTY720 may also reduce pain by mechanisms independent of T cell sequestration (Doyle et al., 2019). Approaches based on blocking α4 integrin to prevent the infiltration of CD4+ T cells into the dorsal horn of the spinal cord are attractive as well (Yednock et al., 1992; Rothhammer et al., 2011), though such antibodies have not yet been tested in chronic pain models. An alternative way to prevent the infiltration of pathogenic CD4+ T cells into the DRG and spinal cord is through surgical sympathectomy (McLachlan and Hu, 2014; Du et al., 2018). Surgical sympathectomy is effective at alleviating neuropathic and inflammatory pain (Agarwal-Kozlowski et al., 2011; Iwase et al., 2012; Xie et al., 2016), but whether this pain relief resulted from blocking T cell infiltration is unknown.

Mechanisms Underlying the Beneficial Effect of T Cells

Recent studies indicate that T cells also promote the resolution of pain and prevent the transition from acute to chronic pain (**Figure 3**). The pathways triggered by T cells to resolve pain are not fully understood, but some mechanisms have been elucidated. The subsets of Treg cells, Th2 cells, and suppressor CD8+ T cells have been shown to reduce or resolve pain, and this is likely through their capacity to switch the milieu to an anti-inflammatory environment (Moalem et al., 2004; Austin et al., 2012; Lees et al., 2015; Baddack-Werncke et al., 2017). Importantly, promoting the anti-inflammatory activity of T cells can be achieved by activation of the anti-inflammatory reflex *via* electrical vagus nerve stimulation (Chakravarthy et al., 2015), suggesting a possible translational treatment.

Many neuroprotective and pain resolving effects of CD8+, Th2 and Treg cells could be recapitulated by IL-10 administration and are absent in mice lacking IL-10, pointing to IL-10 as a major player in the beneficial effects of T cells (Frenkel et al., 2005; Liesz et al., 2009; Xie et al., 2015; Krukowski et al., 2016; Laumet et al., 2018; Duffy et al., 2019). IL-10 alleviates inflammation and pain in various chronic pain models (Wagner et al., 1998; Plunkett et al., 2001; Eijkelkamp et al., 2016; Krukowski et al., 2016), and it is possible that T cells act through IL-10 production. However, it is also possible that T cells do not produce IL-10 themselves but induce other cells to synthesize and release IL-10 (Xin et al., 2011; Krukowski et al., 2016). Resolution of mechanical allodynia was similar in *Rag1*$^{-/-}$ reconstituted with WT or *Il10*$^{-/-}$ CD8+ T cells, indicating that CD8+ T cells were not the source of the IL-10 required for resolution of pain (Krukowski et al., 2016). Likewise, in models of nerve injury and inflammation-induced depression-like behavior, CD4+ and CD3+ T cells conferred neuroprotection and facilitated resolution by inducing IL-10 production from CNS-resident cells (Xin et al., 2011; Laumet et al., 2018). After spinal cord injury, Th1 cells secrete IFNγ to trigger IL-10 production by macrophages and microglia which will promote resolution of motor deficits (Ishii et al., 2013). Alternatively, in models of acute systemic inflammation, Treg secrete IL-13 to induce IL-10 production by IL-13R+ macrophages (Proto et al., 2018). Thus, how T cells induce the production of IL-10 to resolve pain is not yet understood.

In addition to cytokines, T cells release endogenous opioids to induce analgesia (Kavelaars et al., 1991; Kavelaars and Heijnen, 2000; Sitte et al., 2007; Labuz et al., 2010; Celik et al., 2016; Basso et al., 2018). Endogenous opioids can bind opioid receptors on sensory neurons to dampen pain signaling (Stein et al., 1990, 2003; Labuz et al., 2010). The mRNAs of proenkephalin (encoding the enkephalins) and proopiomelanocortin (encoding the endorphins) can be induced in T cells (Kavelaars et al., 1991; Kavelaars and Heijnen, 2000; Labuz et al., 2010; Boué et al., 2014; Basso et al., 2016). *Ex vivo*, T cells from mice immunized with ovalbumin in CFA produce up to seven time more proenkephalin *Penk* mRNA in response to antigen stimulation than naïve CD4+ T cells (Boué et al., 2011, 2012). *In vivo*, T cells have a critical role in stress-induced analgesia, which is known to be mediated by endogenous opioids. Restraint stress-induced analgesia was absent in athymic nude mice and reduced in WT mice after T cell depletion (Labuz et al., 2006; Rosen et al., 2019). The release of endogenous opioids by T cells during stress-induced analgesia was partly dependent on the receptor for corticotropin-releasing factor (CRF; Labuz et al., 2010). The analgesic effects of T cell-producing endogenous opioids have been investigated in models of chronic pain as well. Infiltrated T cells and other leukocytes in the damaged nerve produce and release opioid peptides (Labuz et al., 2009). Interestingly, while T cells may represent only 11% of infiltrated leukocytes in injured nerves, they constituted approximately 50% of opioid peptide-containing immune cells (Labuz et al., 2010). As mentioned above, pregnancy analgesia (reduced pain sensitivity in the SNI and CFA models in late pregnant mice) was absent in T-cell-deficient mice (*Rag1*$^{-/-}$ and nude) and was restored after adoptive transfer of T cells (Rosen et al., 2017). Rosen et al proposed that T cells promote pregnancy analgesia because they induce upregulation of the *oprd1* expression (δ Opioid Receptor, δOR) in the spinal cord. Indeed, the lack of *oprd1* impaired pregnancy analgesia (Rosen et al., 2017). Similarly, in the CFA model, δOR (but not μOR or κOR) antagonist blocked the endogenous analgesic effect of T cells (Boué et al., 2012). In chronic inflammatory pain models, both CD4+ and CD8+ T cells contribute to endogenous opioid-dependent analgesia and pain resolution (Boué et al., 2011, 2012, 2014; Baddack-Werncke et al., 2017). In contrast to WT T cells, adoptive transfer of T cells from *Penk*$^{-/-}$ mice did not induce resolution of CFA-induced allodynia, suggesting that T cells promote resolution of inflammatory pain by enkephalin release (Basso et al., 2016). Notably, T-cell-derived enkephalins increase the number of Th2 cells and reduced the numbers of Th1 and Th17 cells (Boué et al., 2014; Basso et al., 2018). These findings indicate that in addition to their direct analgesic effects, endogenous opioids released by T cells may also suppress pain *via* their anti-inflammatory effects.

Beside the role of T cells in endogenous analgesia, T cells play a role in pain relief induced by exogenous opioids. T-cell-deficient mice (*Rag1*$^{-/-}$, nude and *Cd4*$^{-/-}$ mice) showed reduced morphine analgesia in the formalin and tail-withdrawal tests. Reconstitution with CD4+ but not CD8+ T cells restored morphine analgesia (Rosen et al., 2019). T cell-mediated endogenous analgesia is stimulated by administration of exogenous opioids, as T cells increase the production and release of endogenous opioids in response to exogenous opioid (Labuz et al., 2006; Boué et al., 2012; Celik et al., 2016; **Figure 4**). Finally, administration of synthetic opioid agonists in the damaged nerve produces analgesia which is dependent of infiltrated leukocytes [as mentioned above, 50% of opioid-producing leukocytes are T cells (Labuz et al., 2010)].

Reprogramming T Cells Toward a Pro-resolution Phenotype

There are a variety of potential pathways to promote a pro-resolution phenotype in T cells, many of which are sensitive to existing compounds. T cell subsets are not stable and can be "re-fated" upon appropriate stimulation. For example, Th17 cells naturally acquire an anti-inflammatory phenotype to then become IL-10-producing Tregs to resolve inflammation in various models of chronic inflammation (Gagliani et al., 2015). This plasticity presents an attractive therapeutic opportunity to switch pain promoting Th1 and Th17 cells to a phenotype that promotes resolution of pain and inflammation such as Treg or Th2 cells.

Glatiramer acetate (GA), a drug with good safety profiles and tolerability used to reduce the frequency of multiple sclerosis relapse, has immunomodulatory properties (Dhib-Jalbut, 2003; Arnon and Aharoni, 2004; Blanchette and Neuhaus, 2008). GA increased the number of IL-10-producing CD4+ T cells in the dorsal horn of spinal cord, reduced the activation of

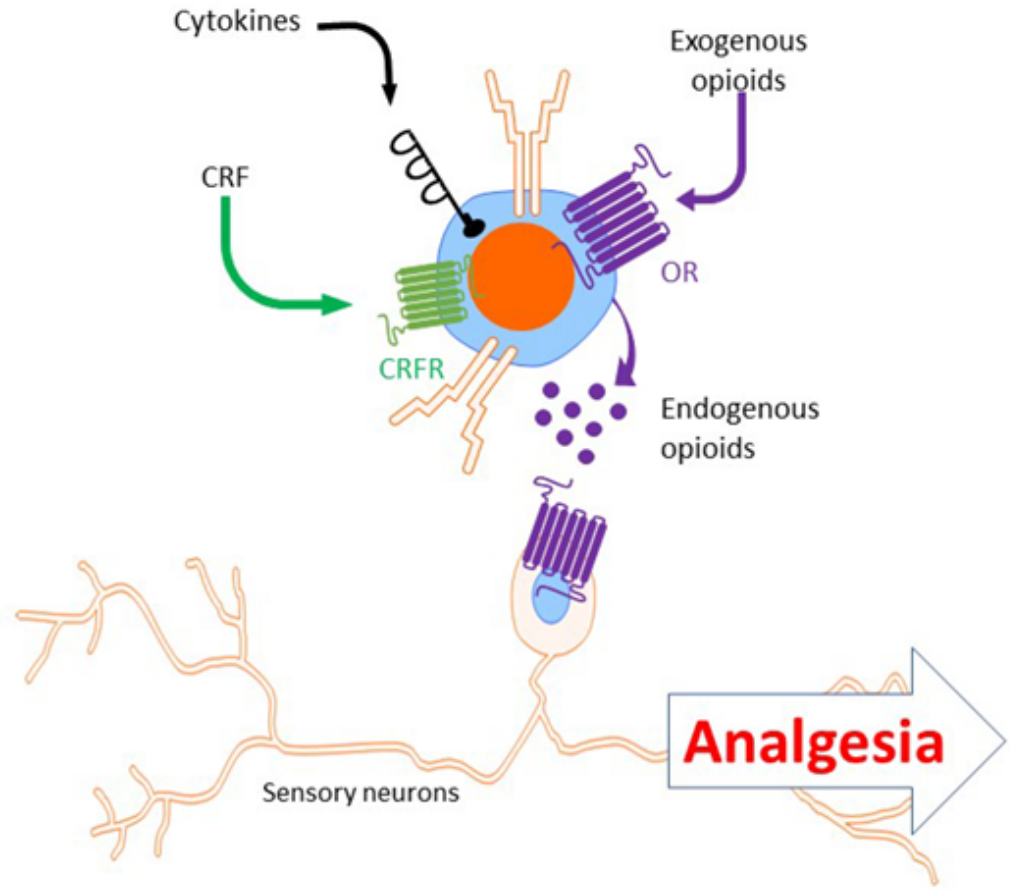

FIGURE 4 | Analgesia induced by T cells secreting endogenous opioids. Upon stimulation with CRF, cytokines or exogenous opioids, T cells release endogenous opioids (e.g.: enkephalins, β-endorphin). Endogenous opioids released by T cells bind opioid receptors (e.g.: μ- and δ-opioid receptors) on sensory neurons to induce analgesia. CRF, corticotropin releasing factor; OR, opioid receptors.

microglia, and alleviated allodynia in models of inflammatory and neuropathic pain (Sharma et al., 2008; Leger et al., 2011).

Experimentally, Treg response can be amplified by treatment with the superagonist of the B7 receptor for co-stimulation: CD28 (supCD28). In the CCI model, supCD28 administration expanded the number of Treg cells in the injured sciatic nerve and spinal cord. SupCD28-stimulated Tregs reduced the number of macrophages in the sciatic nerve and the DRG and decreased astrocyte and microglia activation in the spinal cord as well. SupCD28 did not affect the onset of CCI-induced mechanical allodynia but accelerated its resolution (Austin et al., 2012).

Another way to stimulate the pro-resolution T cell pathway could be *via* vaccination with CNS-restricted self-antigens (Schwartz and Moalem, 2001). After axotomy, immunization with myelin-derived peptide (myelin oligodendrocyte glycoprotein: MOG) stimulated neuron survival by recruiting autoreactive T cells to the site of injury (Moalem et al., 1999; Hauben et al., 2000a,b). The beneficial effects MOG immunization may rely on IL-10 producing CD4+ T cells (Frenkel et al., 2005). However, despite the high incidence of chronic neuropathic pain after nerve injury, the immunization strategy has not yet been tested in chronic pain models.

CD8+ T cells are mostly beneficial in animal models of inflammatory pain and CIPN (Krukowski et al., 2016; Baddack-Werncke et al., 2017). As described above, in order to resolve CIPN, CD8+ T cells need to be educated. Interestingly, adoptive transfer of educated CD8+ T cells before chemotherapy prevented the development of pain in response to cisplatin or paclitaxel treatment (Laumet et al., 2019). If we can develop ways to educate CD8+ T cells *in vitro* to promote resolution of pain, one could envision that CD8+ T cells from a patient with CIPN can be educated *ex vivo* to acquire a pro-resolution phenotype and be re-injected as an autograft to the same patient to treat CIPN (**Figure 5**).

FUTURE DIRECTIONS

The significant growth of our knowledge of the involvement of T cells in the transition from acute to chronic pain in the last few years highlights the complexity of its disparate beneficial and pain aggravating effects. In order to make further progress

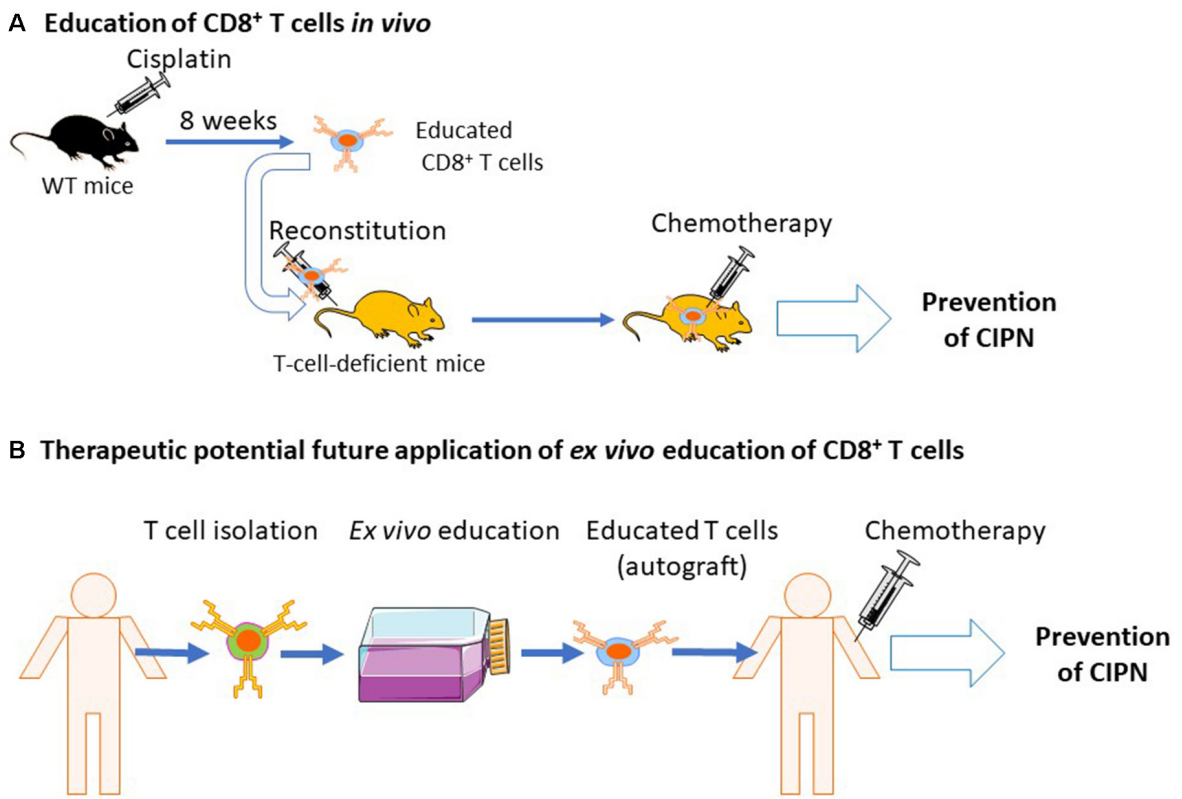

FIGURE 5 | Education of CD8+ T cells by cisplatin and potential clinical translation. **(A)** Naïve mice are treated with cisplatin and allowed to recover from chemotherapy-induced peripheral neuropathy (CIPN). Now educated, CD8+ T cells are isolated and injected into T-cell-deficient mice. The recipient mice, reconstituted with educated CD8+ T cells, are now protected from CIPN (Laumet et al., 2019). **(B)** Potential future clinical applications of educated CD8+ T cells. T cells are collected from cancer patients before chemotherapy. It may be possible to educate T cells in *ex vivo* cultures to acquire a pro-resolution phenotype. Educated CD8+ T cells could then be re-injected to the same patient as an autograft which may protect the patient from CIPN.

in our comprehension of the role of T cells in chronic pain, it is necessary to investigate other Th subsets (e.g., Th9 and Th22) and identify phenotypic profiles of T cells in patients suffering from chronic pain and CIPN as well as in animal models. These T cell profiles may be diverse, with specific features for different chronic pain conditions. Thus, identifying a T cell signature of chronic pain could inform the search for treatment targets for specific groups of patients. Alternatively, a recent study measured DNA methylation in circulating T cells at 9 months after peripheral nerve injury. The authors showed genome-wide changes in DNA methylation in circulating T cells. Intriguingly, these changes in the T cells methylome remarkably overlapped (72%) with the DNA methylation modifications in the prefrontal cortex (Massart et al., 2016). Nerve injury reprograms DNA methylation in the peripheral and central nervous systems, and these changes in DNA methylation are linked with pain hypersensitivity and comorbid depression-like behavior (Tajerian et al., 2013; Garriga et al., 2018). Thus, assessing epigenetic changes in circulating T cells may provide a non-invasive window to uncover epigenetic modifications in the peripheral and central nervous systems associated with chronic pain.

In addition to identifying potential biomarkers, targeting T cells offers the potential to develop disease-modifying therapy. The development of T cell-based therapy would have the potential to not only dampen neuroinflammation but also promote repair and permanent recovery from chronic pain. An important issue for the development of T cell-based therapy for chronic pain is the recognition of antigens by the TCR. Whether T cells need to recognize an antigen for their beneficial or detrimental effects on pain is an open question. We demonstrated that CD8+ T cells do not need to recognize a specific antigen to induce resolution of CIPN (Laumet et al., 2019). In contrast, T cells do need to recognize an antigen to facilitate the release endogenous opioid to alleviate inflammatory pain (Boué et al., 2011, 2012). The potential requirement of antigen recognition for resolution of pain would influence how we could engineer T cells to treat chronic pain. Additionally, signaling molecules (e.g., chemokines) that recruit T cells and their cellular source are of great interest as well, as they represent another attractive therapeutic target. Pharmacological modulation of chemokine signaling may allow us to selectively attract pro-resolution T cells to the site of injury and block the infiltration of pathological pain promoting T cells.

It is interesting to point out that T cells also contribute to the resolution of depression-like and anxiety-like behaviors (Cohen et al., 2006; Lewitus et al., 2009; Brachman et al., 2015; Clark et al., 2016; Laumet et al., 2018), two disorders that are frequently co-morbid with chronic pain. Thus, a dysfunctional T cell-mediated endogenous resolution system may be the link between chronic pain and its psychiatric comorbidities, and a thorough understanding of the role of T cells may help resolve not only chronic pain, but also comorbid mental disorders.

AUTHOR CONTRIBUTIONS

GL drafted the manuscript. GL and AK designed the review. JM, AR, SK, CH and AK provided critical inputs.

FUNDING

This work was supported by the American Pain Society (GL) and the National Institute of Health R01 NS073939 and R01 CA227064 (AK and CH).

REFERENCES

Agarwal, N., Helmstädter, J., Rojas, D. R., Bali, K. K., Gangadharan, V., and Kuner, R. (2018). Evoked hypoalgesia is accompanied by tonic pain and immune cell infiltration in the dorsal root ganglia at late stages of diabetic neuropathy in mice. *Mol. Pain* 14:1744806918817975. doi: 10.1177/1744806918817975

Agarwal-Kozlowski, K., Lorke, D. E., Habermann, C. R., Schulte am Esch, J., and Beck, H. (2011). Interventional management of intractable sympathetically mediated pain by computed tomography-guided catheter implantation for block and neuroablation of the thoracic sympathetic chain: technical approach and review of 322 procedures. *Anaesthesia* 66, 699–708. doi: 10.1111/j.1365-2044.2011.06765.x

Andoh, T., and Kuraishi, Y. (2004). Direct action of immunoglobulin G on primary sensory neurons through Fc γ receptor I. *FASEB J.* 18, 182–184. doi: 10.1096/fj.02-1169fje

Arnon, R., and Aharoni, R. (2004). Mechanism of action of glatiramer acetate in multiple sclerosis and its potential for the development of new applications. *Proc. Natl. Acad. Sci. U S A* 101, 14593–14598. doi: 10.1073/pnas.0404887101

Austin, P. J., Kim, C. F., Perera, C. J., and Moalem-Taylor, G. (2012). Regulatory T cells attenuate neuropathic pain following peripheral nerve injury and experimental autoimmune neuritis. *Pain* 153, 1916–1931. doi: 10.1016/j.pain.2012.06.005

Baddack-Werncke, U., Busch-Dienstfertig, M., González-Rodríguez, S., Maddila, S. C., Grobe, J., Lipp, M., et al. (2017). Cytotoxic T cells modulate inflammation and endogenous opioid analgesia in chronic arthritis. *J. Neuroinflammation* 14:30. doi: 10.1186/s12974-017-0804-y

Baral, P., Udit, S., and Chiu, I. M. (2019). Pain and immunity: implications for host defence. *Nat. Rev. Immunol.* 19, 433–447. doi: 10.1038/s41577-019-0147-2

Basbaum, A. I., and Levine, J. D. (1991). The contribution of the nervous system to inflammation and inflammatory disease. *Can. J. Physiol. Pharmacol.* 69, 647–651. doi: 10.1139/y91-096

Basso, L., Boué, J., Mahiddine, K., Blanpied, C., Robiou-du-Pont, S., Vergnolle, N., et al. (2016). Endogenous analgesia mediated by $CD4^+$ T lymphocytes is dependent on enkephalins in mice. *J. Neuroinflammation* 13:132. doi: 10.1186/s12974-016-0591-x

Basso, L., Garnier, L., Bessac, A., Boué, J., Blanpied, C., Cenac, N., et al. (2018). T-lymphocyte-derived enkephalins reduce T_h1/T_h17 colitis and associated pain in mice. *J. Gastroenterol.* 53, 215–226. doi: 10.1007/s00535-017-1341-2

Binshtok, A. M., Wang, H., Zimmermann, K., Amaya, F., Vardeh, D., Shi, L., et al. (2008). Nociceptors are interleukin-1β sensors. *J. Neurosci.* 28, 14062–14073. doi: 10.1523/JNEUROSCI.3795-08.2008

Blanchette, F., and Neuhaus, O. (2008). Glatiramer acetate: evidence for a dual mechanism of action. *J. Neurol.* 255, 26–36. doi: 10.1007/s00415-008-1005-5

Boué, J., Basso, L., Cenac, N., Blanpied, C., Rolli-Derkinderen, M., Neunlist, M., et al. (2014). Endogenous regulation of visceral pain *via* production of opioids by colitogenic $CD4^+$ T cells in mice. *Gastroenterology* 146, 166–175. doi: 10.1053/j.gastro.2013.09.020

Boué, J., Blanpied, C., Brousset, P., Vergnolle, N., and Dietrich, G. (2011). Endogenous opioid-mediated analgesia is dependent on adaptive T cell response in mice. *J. Immunol.* 186, 5078–5084. doi: 10.4049/jimmunol.1003335

Boué, J., Blanpied, C., Djata-Cabral, M., Pelletier, L., Vergnolle, N., and Dietrich, G. (2012). Immune conditions associated with CD4+ T effector-induced opioid release and analgesia. *Pain* 153, 485–493. doi: 10.1016/j.pain.2011.11.013

Brachman, R. A., Lehmann, M. L., Maric, D., and Herkenham, M. (2015). Lymphocytes from chronically stressed mice confer antidepressant-like effects to naive mice. *J. Neurosci.* 35, 1530–1538. doi: 10.1523/JNEUROSCI.2278-14.2015

Brennan, P. C., Graham, M. A., Triano, J. J., Hondras, M. A., and Anderson, R. J. (1994). Lymphocyte profiles in patients with chronic low back pain enrolled in a clinical trial. *J. Manipulative Physiol. Ther.* 17, 219–227.

Cameron, N. E., and Cotter, M. A. (2008). Pro-inflammatory mechanisms in diabetic neuropathy: focus on the nuclear factor kappa B pathway. *Curr. Drug Targets* 9, 60–67. doi: 10.2174/138945008783431718

Cao, L., and DeLeo, J. A. (2008). CNS-infiltrating $CD4^+$ T lymphocytes contribute to murine spinal nerve transection-induced neuropathic pain. *Eur. J. Immunol.* 38, 448–458. doi: 10.1002/eji.200737485

Celik, M. Ö., Labuz, D., Henning, K., Busch-Dienstfertig, M., Gaveriaux-Ruff, C., Kieffer, B. L., et al. (2016). Leukocyte opioid receptors mediate analgesia *via* Ca^{2+}-regulated release of opioid peptides. *Brain Behav. Immun.* 57, 227–242. doi: 10.1016/j.bbi.2016.04.018

Cevikbas, F., Wang, X., Akiyama, T., Kempkes, C., Savinko, T., Antal, A., et al. (2014). A sensory neuron-expressed IL-31 receptor mediates T helper cell-dependent itch: involvement of TRPV1 and TRPA1. *J. Allergy Clin. Immunol.* 133, 448–460. doi: 10.1016/j.jaci.2013.10.048

Chakravarthy, K., Chaudhry, H., Williams, K., and Christo, P. J. (2015). Review of the uses of vagal nerve stimulation in chronic pain management. *Curr. Pain Headache Rep.* 19:54. doi: 10.1007/s11916-015-0528-6

Chen, G., Zhang, Y.-Q., Qadri, Y. J., Serhan, C. N., and Ji, R.-R. (2018). Microglia in pain: detrimental and protective roles in pathogenesis and resolution of pain. *Neuron* 100, 1292–1311. doi: 10.1016/j.neuron.2018.11.009

Chiu, I. M., Heesters, B. A., Ghasemlou, N., Von Hehn, C. A., Zhao, F., Tran, J., et al. (2013). Bacteria activate sensory neurons that modulate pain and inflammation. *Nature* 501, 52–57. doi: 10.1038/nature12479

Clark, S. M., Soroka, J. A., Song, C., Li, X., and Tonelli, L. H. (2016). $CD4^+$ T cells confer anxiolytic and antidepressant-like effects, but enhance fear memory processes in *Rag2*$^{-/-}$ *mice*. *Stress* 19, 303–311. doi: 10.1080/10253890.2016.1191466

Cohen, J. A., Edwards, T. N., Liu, A. W., Hirai, T., Jones, M. R., Wu, J., et al. (2019). Cutaneous $TRPV1^+$ neurons trigger protective innate type 17 anticipatory immunity. *Cell* 178, 919.e14–932.e14. doi: 10.1016/j.cell.2019.06.022

Cohen, H., Ziv, Y., Cardon, M., Kaplan, Z., Matar, M. A., Gidron, Y., et al. (2006). Maladaptation to mental stress mitigated by the adaptive immune system *via* depletion of naturally occurring regulatory CD4+CD25+ cells. *J. Neurobiol.* 66, 552–563. doi: 10.1002/neu.20249

Costigan, M., Moss, A., Latremoliere, A., Johnston, C., Verma-Gandhu, M., Herbert, T. A., et al. (2009). T-cell infiltration and signaling in the adult dorsal spinal cord is a major contributor to neuropathic pain-like hypersensitivity. *J. Neurosci.* 29, 14415–14422. doi: 10.1523/JNEUROSCI.4569-09.2009

Cui, J. G., Holmin, S., Mathiesen, T., Meyerson, B. A., and Linderoth, B. (2000). Possible role of inflammatory mediators in tactile hypersensitivity in rat models of mononeuropathy. *Pain* 88, 239–248. doi: 10.1016/s0304-3959(00)00331-6

Davies, A. L., Hayes, K. C., and Dekaban, G. A. (2007). Clinical correlates of elevated serum concentrations of cytokines and autoantibodies in patients with

spinal cord injury. *Arch. Phys. Med. Rehabil.* 88, 1384–1393. doi: 10.1016/j.apmr.2007.08.004

Dendrou, C. A., Fugger, L., and Friese, M. A. (2015). Immunopathology of multiple sclerosis. *Nat. Rev. Immunol.* 15, 545–558. doi: 10.1038/nri3871

Denk, F., Crow, M., Didangelos, A., Lopes, D. M., and McMahon, S. B. (2016). Persistent alterations in microglial enhancers in a model of chronic pain. *Cell Rep.* 15, 1771–1781. doi: 10.1016/j.celrep.2016.04.063

Dhib-Jalbut, S. (2003). Glatiramer acetate (Copaxone) therapy for multiple sclerosis. *Pharmacol. Ther.* 98, 245–255. doi: 10.1016/s0163-7258(03)00036-6

Diederich, J.-M., Staudt, M., Meisel, C., Hahn, K., Meinl, E., Meisel, A., et al. (2018). Neurofascin and compact myelin antigen-specific T cell response pattern in chronic inflammatory demyelinating polyneuropathy subtypes. *Front. Neurol.* 9:171. doi: 10.3389/fneur.2018.00171

Doyle, T. M., Chen, Z., Durante, M., and Salvemini, D. (2019). Activation of sphingosine-1-phosphate receptor 1 in the spinal cord produces mechanohypersensitivity through the activation of inflammasome and IL-1β pathway. *J. Pain* 20, 956–964. doi: 10.1016/j.jpain.2019.02.007

Draleau, K., Maddula, S., Slaiby, A., Nutile-McMenemy, N., De Leo, J., and Cao, L. (2014). Phenotypic identification of spinal cord-infiltrating CD4+ T lymphocytes in a murine model of neuropathic pain. *J. Pain Relief* 3:003. doi: 10.4172/2167-0846.s3-003

Du, B., Ding, Y.-Q., Xiao, X., Ren, H.-Y., Su, B.-Y., and Qi, J.-G. (2018). CD4+ αβ T cell infiltration into the leptomeninges of lumbar dorsal roots contributes to the transition from acute to chronic mechanical allodynia after adult rat tibial nerve injuries. *J. Neuroinflammation* 15:81. doi: 10.1186/s12974-018-1115-7

Duffy, S. S., Keating, B. A., Perera, C. J., Lees, J. G., Tonkin, R. S., Makker, P. G. S., et al. (2019). Regulatory T cells and their derived cytokine, interleukin-35, reduce pain in experimental autoimmune encephalomyelitis. *J. Neurosci.* 39, 2326–2346. doi: 10.1523/JNEUROSCI.1815-18.2019

Eijkelkamp, N., Steen-Louws, C., Hartgring, S. A. Y., Willemen, H. L. D. M., Prado, J., Lafeber, F. P. J. G., et al. (2016). IL4–10 fusion protein is a novel drug to treat persistent inflammatory pain. *J. Neurosci.* 36, 7353–7363. doi: 10.1523/JNEUROSCI.0092-16.2016

Eliav, E., Herzberg, U., Ruda, M. A., and Bennett, G. J. (1999). Neuropathic pain from an experimental neuritis of the rat sciatic nerve. *Pain* 83, 169–182. doi: 10.1016/s0304-3959(99)00102-5

Ferry, G., Lonchampt, M., Pennel, L., de Nanteuil, G., Canet, E., and Tucker, G. C. (1997). Activation of MMP-9 by neutrophil elastase in an *in vivo* model of acute lung injury. *FEBS Lett.* 402, 111–115. doi: 10.1016/s0014-5793(96)01508-6

Filiano, A. J., Xu, Y., Tustison, N. J., Marsh, R. L., Baker, W., Smirnov, I., et al. (2016). Unexpected role of interferon-γ in regulating neuronal connectivity and social behaviour. *Nature* 535, 425–429. doi: 10.1038/nature18626

Frenkel, D., Huang, Z., Maron, R., Koldzic, D. N., Moskowitz, M. A., and Weiner, H. L. (2005). Neuroprotection by IL-10-producing MOG CD4+ T cells following ischemic stroke. *J. Neurol. Sci.* 233, 125–132. doi: 10.1016/j.jns.2005.03.022

Gadani, S. P., Walsh, J. T., Lukens, J. R., and Kipnis, J. (2015). Dealing with danger in the CNS: the response of the immune system to injury. *Neuron* 87, 47–62. doi: 10.1016/j.neuron.2015.05.019

Gagliani, N., Amezcua Vesely, M. C., Iseppon, A., Brockmann, L., Xu, H., Palm, N. W., et al. (2015). Th17 cells transdifferentiate into regulatory T cells during resolution of inflammation. *Nature* 523, 221–225. doi: 10.1038/nature14452

Ganor, Y., Besser, M., Ben-Zakay, N., Unger, T., and Levite, M. (2003). Human T cells express a functional ionotropic glutamate receptor GluR3 and glutamate by itself triggers integrin-mediated adhesion to laminin and fibronectin and chemotactic migration. *J. Immunol.* 170, 4362–4372. doi: 10.4049/jimmunol.170.8.4362

Garriga, J., Laumet, G., Chen, S.-R., Zhang, Y., Madzo, J., Issa, J.-P. J., et al. (2018). Nerve injury-induced chronic pain is associated with persistent DNA methylation reprogramming in dorsal root ganglion. *J. Neurosci.* 38, 6090–6101. doi: 10.1523/JNEUROSCI.2616-17.2018

Gattlen, C., Clarke, C. B., Piller, N., Kirschmann, G., Pertin, M., Decosterd, I., et al. (2016). Spinal cord T-cell infiltration in the rat spared nerve injury model: a time course study. *Int. J. Mol. Sci.* 17:352. doi: 10.3390/ijms17030352

Ghasemlou, N., Chiu, I. M., Julien, J.-P., and Woolf, C. J. (2015). CD11b+Ly6G- myeloid cells mediate mechanical inflammatory pain hypersensitivity. *Proc. Natl. Acad. Sci. U S A* 112, E6808–E6817. doi: 10.1073/pnas.1501372112

Gilman-Sachs, A., Robbins, L., and Baum, L. (1989). Flow cytometric analysis of lymphocyte subsets in peripheral blood of chronic headache patients. *Headache* 29, 290–294. doi: 10.1111/j.1526-4610.1989.hed2905290.x

Glusman, G., Rowen, L., Lee, I., Boysen, C., Roach, J. C., Smit, A. F., et al. (2001). Comparative genomics of the human and mouse T cell receptor loci. *Immunity* 15, 337–349. doi: 10.1016/s1074-7613(01)00200-x

Grace, P. M., Hutchinson, M. R., Maier, S. F., and Watkins, L. R. (2014). Pathological pain and the neuroimmune interface. *Nat. Rev. Immunol.* 14, 217–231. doi: 10.1038/nri3621

Haas, J. D., Nistala, K., Petermann, F., Saran, N., Chennupati, V., Schmitz, S., et al. (2011). Expression of miRNAs miR-133b and miR-206 in the Il17a/f locus is co-regulated with IL-17 production in αβ and γδ T cells. *PLoS One* 6:e20171. doi: 10.1371/journal.pone.0020171

Hauben, E., Butovsky, O., Nevo, U., Yoles, E., Moalem, G., Agranov, E., et al. (2000a). Passive or active immunization with myelin basic protein promotes recovery from spinal cord contusion. *J. Neurosci.* 20, 6421–6430. doi: 10.1523/JNEUROSCI.20-17-06421.2000

Hauben, E., Nevo, U., Yoles, E., Moalem, G., Agranov, E., Mor, F., et al. (2000b). Autoimmune T cells as potential neuroprotective therapy for spinal cord injury. *Lancet* 355, 286–287. doi: 10.1016/s0140-6736(99)05140-5

Held, M., Karl, F., Vlckova, E., Rajdova, A., Escolano-Lozano, F., Stetter, C., et al. (2019). Sensory profiles and immune related expression patterns of patients with and without neuropathic pain after peripheral nerve lesion. *Pain* doi: 10.1097/j.pain.0000000000001623 [Epub ahead of print].

Heyn, J., Azad, S. C., and Luchting, B. (2019). Altered regulation of the T-cell system in patients with CRPS. *Inflamm. Res.* 68, 1–6. doi: 10.1007/s00011-018-1182-3

Heyn, J., Luchting, B., and Azad, S. C. (2018). Smoking associated T-Cell imbalance in patients with chronic pain. *Nicotine Tob. Res.* doi: 10.1093/ntr/nty199 [Epub ahead of print].

Hirahara, K., and Nakayama, T. (2016). $CD4^+$ T-cell subsets in inflammatory diseases: beyond the Th1/Th2 paradigm. *Int. Immunol.* 28, 163–171. doi: 10.1093/intimm/dxw006

Hood, V. C., Cruwys, S. C., Urban, L., and Kidd, B. L. (2000). Differential role of neurokinin receptors in human lymphocyte and monocyte chemotaxis. *Regul. Pept.* 96, 17–21. doi: 10.1016/s0167-0115(00)00195-6

Hosoi, J., Murphy, G. F., Egan, C. L., Lerner, E. A., Grabbe, S., Asahina, A., et al. (1993). Regulation of Langerhans cell function by nerves containing calcitonin gene-related peptide. *Nature* 363, 159–163. doi: 10.1038/363159a0

Hu, P., and McLachlan, E. M. (2002). Macrophage and lymphocyte invasion of dorsal root ganglia after peripheral nerve lesions in the rat. *Neuroscience* 112, 23–38. doi: 10.1016/s0306-4522(02)00065-9

Hunt, M. A., Nascimento, D. S. M., Bersellini Farinotti, A., and Svensson, C. I. (2018). Autoantibodies hurt: transfer of patient-derived CASPR2 antibodies induces neuropathic pain in mice. *Neuron* 97, 729–731. doi: 10.1016/j.neuron.2018.02.008

Huo, W., Liu, Y., Lei, Y., Zhang, Y., Huang, Y., Mao, Y., et al. (2019). Imbalanced spinal infiltration of Th17/Treg cells contributes to bone cancer pain *via* promoting microglial activation. *Brain Behav. Immun.* 79, 139–151. doi: 10.1016/j.bbi.2019.01.024

Ishii, H., Tanabe, S., Ueno, M., Kubo, T., Kayama, H., Serada, S., et al. (2013). *ifn*-γ-dependent secretion of IL-10 from Th1 cells and microglia/macrophages contributes to functional recovery after spinal cord injury. *Cell Death Dis.* 4:e710. doi: 10.1038/cddis.2013.234

Itohara, S., Mombaerts, P., Lafaille, J., Iacomini, J., Nelson, A., Clarke, A. R., et al. (1993). T cell receptor δ gene mutant mice: independent generation of αβ T cells and programmed rearrangements of γδ TCR genes. *Cell* 72, 337–348. doi: 10.1016/0092-8674(93)90112-4

Iwase, T., Takebayashi, T., Tanimoto, K., Terashima, Y., Miyakawa, T., Kobayashi, T., et al. (2012). Sympathectomy attenuates excitability of dorsal root ganglion neurons and pain behaviour in a lumbar radiculopathy model. *Bone Joint Res.* 1, 198–204. doi: 10.1302/2046-3758.19.2000073

Janes, K., Wahlman, C., Little, J. W., Doyle, T., Tosh, D. K., Jacobson, K. A., et al. (2015). Spinal neuroimmune activation is independent of T-cell infiltration and attenuated by A3 adenosine receptor agonists in a model of oxaliplatin-

induced peripheral neuropathy. *Brain Behav. Immun.* 44, 91–99. doi: 10.1016/j.bbi.2014.08.010

Ji, R.-R., Chamessian, A., and Zhang, Y.-Q. (2016). Pain regulation by non-neuronal cells and inflammation. *Science* 354, 572–577. doi: 10.1126/science.aaf8924

Ji, R.-R., Xu, Z.-Z., Wang, X., and Lo, E. H. (2009). Matrix metalloprotease regulation of neuropathic pain. *Trends Pharmacol. Sci.* 30, 336–340. doi: 10.1016/j.tips.2009.04.002

Kavelaars, A., Ballieux, R. E., and Heijnen, C. J. (1991). Two different signalling pathways for the induction of immunoreactive β-endorphin secretion by human peripheral blood mononuclear cells. *Endocrinology* 128, 765–770. doi: 10.1210/endo-128-2-765

Kavelaars, A., and Heijnen, C. J. (2000). Expression of preproenkephalin mRNA and production and secretion of enkephalins by human thymocytes. *Ann. N Y Acad. Sci.* 917, 778–783. doi: 10.1111/j.1749-6632.2000.tb05443.x

Kawasaki, Y., Zhang, L., Cheng, J.-K., and Ji, R.-R. (2008). Cytokine mechanisms of central sensitization: distinct and overlapping role of interleukin-1β, interleukin-6, and tumor necrosis factor-α in regulating synaptic and neuronal activity in the superficial spinal cord. *J. Neurosci.* 28, 5189–5194. doi: 10.1523/JNEUROSCI.3338-07.2008

Kipnis, J., Gadani, S., and Derecki, N. C. (2012). Pro-cognitive properties of T cells. *Nat. Rev. Immunol.* 12, 663–669. doi: 10.1038/nri3280

Klein, C. J., Lennon, V. A., Aston, P. A., McKeon, A., and Pittock, S. J. (2012). Chronic pain as a manifestation of potassium channel-complex autoimmunity. *Neurology* 79, 1136–1144. doi: 10.1212/WNL.0b013e3182698cab

Kleinschnitz, C., Hofstetter, H. H., Meuth, S. G., Braeuninger, S., Sommer, C., and Stoll, G. (2006). T cell infiltration after chronic constriction injury of mouse sciatic nerve is associated with interleukin-17 expression. *Exp. Neurol.* 200, 480–485. doi: 10.1016/j.expneurol.2006.03.014

Kobayashi, Y., Kiguchi, N., Fukazawa, Y., Saika, F., Maeda, T., and Kishioka, S. (2015). Macrophage-T cell interactions mediate neuropathic pain through the glucocorticoid-induced tumor necrosis factor ligand system. *J. Biol. Chem.* 290, 12603–12613. doi: 10.1074/jbc.m115.636506

Koch, A., Zacharowski, K., Boehm, O., Stevens, M., Lipfert, P., von Giesen, H.-J., et al. (2007). Nitric oxide and pro-inflammatory cytokines correlate with pain intensity in chronic pain patients. *Inflamm. Res.* 56, 32–37. doi: 10.1007/s00011-007-6088-4

Kraychete, D. C., Sakata, R. K., Issy, A. M., Bacellar, O., Santos-Jesus, R., and Carvalho, E. M. (2010). Serum cytokine levels in patients with chronic low back pain due to herniated disc: analytical cross-sectional study. *Sao Paulo Med. J.* 128, 259–262. doi: 10.1590/s1516-31802010000500003

Krukowski, K., Eijkelkamp, N., Laumet, G., Hack, C. E., Li, Y., Dougherty, P. M., et al. (2016). $CD8^+$ T cells and endogenous IL-10 are required for resolution of chemotherapy-induced neuropathic pain. *J. Neurosci.* 36, 11074–11083. doi: 10.1523/JNEUROSCI.3708-15.2016

Labuz, D., Berger, S., Mousa, S. A., Zöllner, C., Rittner, H. L., Shaqura, M. A., et al. (2006). Peripheral antinociceptive effects of exogenous and immune cell-derived endomorphins in prolonged inflammatory pain. *J. Neurosci.* 26, 4350–4358. doi: 10.1523/JNEUROSCI.4349-05.2006

Labuz, D., Schmidt, Y., Schreiter, A., Rittner, H. L., Mousa, S. A., and Machelska, H. (2009). Immune cell-derived opioids protect against neuropathic pain in mice. *J. Clin. Invest.* 119, 278–286. doi: 10.1172/JCI36246

Labuz, D., Schreiter, A., Schmidt, Y., Brack, A., and Machelska, H. (2010). T lymphocytes containing β-endorphin ameliorate mechanical hypersensitivity following nerve injury. *Brain Behav. Immun.* 24, 1045–1053. doi: 10.1016/j.bbi.2010.04.001

Laumet, G., Dantzer, R., Krukowski, K. N., Heijnen, C. J., and Kavelaars, A. (2016). Abstract # 1720 T lymphocytes are required for resolution of inflammatory pain and depression-like behavior. *Brain Behav. Immun.* 57, e5–e6. doi: 10.1016/j.bbi.2016.07.022

Laumet, G., Edralin, J. D., Chiang, A. C.-A., Dantzer, R., Heijnen, C. J., and Kavelaars, A. (2018). Resolution of inflammation-induced depression requires T lymphocytes and endogenous brain interleukin-10 signaling. *Neuropsychopharmacology* 43, 2597–2605. doi: 10.1038/s41386-018-0154-1

Laumet, G., Edralin, J. D., Dantzer, R., Heijnen, C. J., and Kavelaars, A. (2019). Cisplatin educates CD8+ T cells to prevent and resolve chemotherapy-induced peripheral neuropathy in mice. *Pain* 160, 1459–1468. doi: 10.1097/j.pain.0000000000001512

Lees, J. G., Duffy, S. S., Perera, C. J., and Moalem-Taylor, G. (2015). Depletion of Foxp3+ regulatory T cells increases severity of mechanical allodynia and significantly alters systemic cytokine levels following peripheral nerve injury. *Cytokine* 71, 207–214. doi: 10.1016/j.cyto.2014.10.028

Leger, T., Grist, J., D'Acquisto, F., Clark, A. K., and Malcangio, M. (2011). Glatiramer acetate attenuates neuropathic allodynia through modulation of adaptive immune cells. *J. Neuroimmunol.* 234, 19–26. doi: 10.1016/j.jneuroim.2011.01.005

Levite, M. (2000). Nerve-driven immunity. The direct effects of neurotransmitters on T-cell function. *Ann. N Y Acad. Sci.* 917, 307–321. doi: 10.1111/j.1749-6632.2000.tb05397.x

Levite, M., Cahalon, L., Hershkoviz, R., Steinman, L., and Lider, O. (1998). Neuropeptides, *via* specific receptors, regulate T cell adhesion to fibronectin. *J. Immunol.* 160, 993–1000.

Lewitus, G. M., Wilf-Yarkoni, A., Ziv, Y., Shabat-Simon, M., Gersner, R., Zangen, A., et al. (2009). Vaccination as a novel approach for treating depressive behavior. *Biol. Psychiatry* 65, 283–288. doi: 10.1016/j.biopsych.2008.07.014

Liesz, A., Suri-Payer, E., Veltkamp, C., Doerr, H., Sommer, C., Rivest, S., et al. (2009). Regulatory T cells are key cerebroprotective immunomodulators in acute experimental stroke. *Nat. Med.* 15, 192–199. doi: 10.1038/nm.1927

Liu, H., Xia, X., Wu, Y., Pan, L., Jin, B., Shang, X., et al. (2006). Detection of peripheral blood Th1/Th2 cell ratio in patients with chronic abacterial prostatitis/chronic pelvic pain syndrome. *Zhonghua Nan Ke Xue* 12, 330–332, 336.

Liu, X.-J., Zhang, Y., Liu, T., Xu, Z.-Z., Park, C.-K., Berta, T., et al. (2014). Nociceptive neurons regulate innate and adaptive immunity and neuropathic pain through MyD88 adapter. *Cell Res.* 24, 1374–1377. doi: 10.1038/cr.2014.106

Luchting, B., Rachinger-Adam, B., Heyn, J., Hinske, L. C., Kreth, S., and Azad, S. C. (2015). Anti-inflammatory T-cell shift in neuropathic pain. *J. Neuroinflammation* 12:12. doi: 10.1186/s12974-014-0225-0

Luchting, B., Rachinger-Adam, B., Zeitler, J., Egenberger, L., Möhnle, P., Kreth, S., et al. (2014). Disrupted TH17/Treg balance in patients with chronic low back pain. *PLoS One* 9:e104883. doi: 10.1371/journal.pone.0104883

Luo, X., Fitzsimmons, B., Mohan, A., Zhang, L., Terrando, N., Kordasiewicz, H., et al. (2018). Intrathecal administration of antisense oligonucleotide against p38α but not p38β MAP kinase isoform reduces neuropathic and postoperative pain and TLR4-induced pain in male mice. *Brain Behav. Immun.* 72, 34–44. doi: 10.1016/j.bbi.2017.11.007

Makker, P. G. S., Duffy, S. S., Lees, J. G., Perera, C. J., Tonkin, R. S., Butovsky, O., et al. (2017). Characterisation of immune and neuroinflammatory changes associated with chemotherapy-induced peripheral neuropathy. *PLoS One* 12:e0170814. doi: 10.1371/journal.pone.0170814

Mangiacavalli, S., Corso, A., De Amici, M., Varettoni, M., Alfonsi, E., Lozza, A., et al. (2010). Emergent T-helper 2 profile with high interleukin-6 levels correlates with the appearance of bortezomib-induced neuropathic pain. *Br. J. Haematol.* 149, 916–918. doi: 10.1111/j.1365-2141.2010.08138.x

Mapplebeck, J. C. S., Dalgarno, R., Tu, Y., Moriarty, O., Beggs, S., Kwok, C. H. T., et al. (2018). Microglial P2X4R-evoked pain hypersensitivity is sexually dimorphic in rats. *Pain* 159, 1752–1763. doi: 10.1097/j.pain.0000000000001265

Marshall, A. S., Silva, J. R., Bannerman, C. A., Gilron, I., and Ghasemlou, N. (2019). Skin-resident γδ T cells exhibit site-specific morphology and activation states. *J. Immunol. Res.* 2019:9020234. doi: 10.1155/2019/9020234

Massart, R., Dymov, S., Millecamps, M., Suderman, M., Gregoire, S., Koenigs, K., et al. (2016). Overlapping signatures of chronic pain in the DNA methylation landscape of prefrontal cortex and peripheral T cells. *Sci. Rep.* 6:19615. doi: 10.1038/srep19615

McLachlan, E. M., and Hu, P. (2014). Inflammation in dorsal root ganglia after peripheral nerve injury: effects of the sympathetic innervation. *Auton. Neurosci.* 182, 108–117. doi: 10.1016/j.autneu.2013.12.009

McMahon, S. B., La Russa, F., and Bennett, D. L. H. (2015). Crosstalk between the nociceptive and immune systems in host defence and disease. *Nat. Rev. Neurosci.* 16, 389–402. doi: 10.1038/nrn3946

Mikami, N., Matsushita, H., Kato, T., Kawasaki, R., Sawazaki, T., Kishimoto, T., et al. (2011). Calcitonin gene-related peptide is an important regulator of

cutaneous immunity: effect on dendritic cell and T cell functions. *J. Immunol.* 186, 6886–6893. doi: 10.4049/jimmunol.1100028

Moalem, G., Leibowitz-Amit, R., Yoles, E., Mor, F., Cohen, I. R., and Schwartz, M. (1999). Autoimmune T cells protect neurons from secondary degeneration after central nervous system axotomy. *Nat. Med.* 5, 49–55. doi: 10.1038/4734

Moalem, G., Xu, K., and Yu, L. (2004). T lymphocytes play a role in neuropathic pain following peripheral nerve injury in rats. *Neuroscience* 129, 767–777. doi: 10.1016/j.neuroscience.2004.08.035

Mogil, J. S. (2012). Sex differences in pain and pain inhibition: multiple explanations of a controversial phenomenon. *Nat. Rev. Neurosci.* 13, 859–866. doi: 10.1038/nrn3360

Mousset, C. M., Hobo, W., Woestenenk, R., Preijers, F., Dolstra, H., and van der Waart, A. B. (2019). Comprehensive phenotyping of T cells using flow cytometry. *Cytometry A* 95, 647–654. doi: 10.1002/cyto.a.23724

Ohtake, J., Kaneumi, S., Tanino, M., Kishikawa, T., Terada, S., Sumida, K., et al. (2015). Neuropeptide signaling through neurokinin-1 and neurokinin-2 receptors augments antigen presentation by human dendritic cells. *J. Allergy Clin. Immunol.* 136, 1690–1694. doi: 10.1016/j.jaci.2015.06.050

Pavlov, V. A., and Tracey, K. J. (2017). Neural regulation of immunity: molecular mechanisms and clinical translation. *Nat. Neurosci.* 20, 156–166. doi: 10.1038/nn.4477

Petrović, J., Silva, J. R., Bannerman, C. A., Segal, J. P., Marshall, A. S., Haird, C. M., et al. (2019). γδ T cells modulate myeloid cell recruitment but not pain during peripheral inflammation. *Front. Immunol.* 10:473. doi: 10.3389/fimmu.2019.00473

Plein, L. M., and Rittner, H. L. (2018). Opioids and the immune system—friend or foe. *Br. J. Pharmacol.* 175, 2717–2725. doi: 10.1111/bph.13750

Plunkett, J. A., Yu, C. G., Easton, J. M., Bethea, J. R., and Yezierski, R. P. (2001). Effects of interleukin-10 (IL-10) on pain behavior and gene expression following excitotoxic spinal cord injury in the rat. *Exp. Neurol.* 168, 144–154. doi: 10.1006/exnr.2000.7604

Power, C., Frank, J., Hertzman, C., Schierhout, G., and Li, L. (2001). Predictors of low back pain onset in a prospective British study. *Am. J. Public Health* 91, 1671–1678. doi: 10.2105/ajph.91.10.1671

Proto, J. D., Doran, A. C., Gusarova, G., Yurdagul, A. Jr., Sozen, E., Subramanian, M., et al. (2018). Regulatory T cells promote macrophage efferocytosis during inflammation resolution. *Immunity* 49, 666.e6–677.e6. doi: 10.1016/j.immuni.2018.07.015

Rameshwar, P., Gascon, P., and Ganea, D. (1992). Immunoregulatory effects of neuropeptides. Stimulation of interleukin-2 production by substance p. *J. Neuroimmunol.* 37, 65–74. doi: 10.1016/0165-5728(92)90156-f

Ranganathan, P., Chen, H., Adelman, M. K., and Schluter, S. F. (2009). Autoantibodies to the δ-opioid receptor function as opioid agonists and display immunomodulatory activity. *J. Neuroimmunol.* 217, 65–73. doi: 10.1016/j.jneuroim.2009.10.007

Razavi, R., Chan, Y., Afifiyan, F. N., Liu, X. J., Wan, X., Yantha, J., et al. (2006). TRPV1^{+} sensory neurons control β cell stress and islet inflammation in autoimmune diabetes. *Cell* 127, 1123–1135. doi: 10.1016/j.cell.2006.10.038

Rittner, H. L., Brack, A., Machelska, H., Mousa, S. A., Bauer, M., Schäfer, M., et al. (2001). Opioid peptide-expressing leukocytes: identification, recruitment, and simultaneously increasing inhibition of inflammatory pain. *Anesthesiology* 95, 500–508. doi: 10.1097/00000542-200108000-00036

Rosas-Ballina, M., Olofsson, P. S., Ochani, M., Valdés-Ferrer, S. I., Levine, Y. A., Reardon, C., et al. (2011). Acetylcholine-synthesizing T cells relay neural signals in a vagus nerve circuit. *Science* 334, 98–101. doi: 10.1126/science.1209985

Rosen, S. F., Ham, B., Drouin, S., Boachie, N., Chabot-Dore, A.-J., Austin, J.-S., et al. (2017). T-cell mediation of pregnancy analgesia affecting chronic pain in mice. *J. Neurosci.* 37, 9819–9827. doi: 10.1523/jneurosci.2053-17.2017

Rosen, S. F., Ham, B., Haichin, M., Walters, I. C., Tohyama, S., Sotocinal, S. G., et al. (2019). Increased pain sensitivity and decreased opioid analgesia in T-cell-deficient mice and implications for sex differences. *Pain* 160, 358–366. doi: 10.1097/j.pain.0000000000001420

Rothhammer, V., Heink, S., Petermann, F., Srivastava, R., Claussen, M. C., Hemmer, B., et al. (2011). Th17 lymphocytes traffic to the central nervous system independently of α4 integrin expression during EAE. *J. Exp. Med.* 208, 2465–2476. doi: 10.1084/jem.20110434

Schläger, C., Körner, H., Krueger, M., Vidoli, S., Haberl, M., Mielke, D., et al. (2016). Effector T-cell trafficking between the leptomeninges and the cerebrospinal fluid. *Nature* 530, 349–353. doi: 10.1038/nature16939

Scholz, J., and Woolf, C. J. (2007). The neuropathic pain triad: neurons, immune cells and glia. *Nat. Neurosci.* 10, 1361–1368. doi: 10.1038/nn1992

Schwartz, M., and Moalem, G. (2001). Beneficial immune activity after CNS injury: prospects for vaccination. *J. Neuroimmunol.* 113, 185–192. doi: 10.1016/s0165-5728(00)00447-1

Scott, S. C., Goldberg, M. S., Mayo, N. E., Stock, S. R., and Poîtras, B. (1999). The association between cigarette smoking and back pain in adults. *Spine* 24, 1090–1098. doi: 10.1097/00007632-199906010-00008

Sharma, N., Thomas, S., Ho, L., Reyes, D. C., Sacerdote, P., Bianchi, M., et al. (2008). Immunomodulation with glatiramer acetate prevents long-term inflammatory pain. *Int. J. Neurosci.* 118, 433–453. doi: 10.1080/00207450701849018

Sitte, N., Busch, M., Mousa, S. A., Labuz, D., Rittner, H., Gore, C., et al. (2007). Lymphocytes upregulate signal sequence-encoding proopiomelanocortin mRNA and β-endorphin during painful inflammation *in vivo*. *J. Neuroimmunol.* 183, 133–145. doi: 10.1016/j.jneuroim.2006.11.033

Sorge, R. E., Mapplebeck, J. C. S., Rosen, S., Beggs, S., Taves, S., Alexander, J. K., et al. (2015). Different immune cells mediate mechanical pain hypersensitivity in male and female mice. *Nat. Neurosci.* 18, 1081–1083. doi: 10.1038/nn.4053

Stein, C., Hassan, A. H., Przewocki, R., Gramsch, C., Peter, K., and Herz, A. (1990). Opioids from immunocytes interact with receptors on sensory nerves to inhibit nociception in inflammation. *Proc. Natl. Acad. Sci. U S A* 87, 5935–5939. doi: 10.1073/pnas.87.15.5935

Stein, C., Schäfer, M., and Machelska, H. (2003). Attacking pain at its source: new perspectives on opioids. *Nat. Med.* 9, 1003–1008. doi: 10.1038/nm908

Szklany, K., Ruiter, E., Mian, F., Kunze, W., Bienenstock, J., Forsythe, P., et al. (2016). Superior cervical ganglia neurons induce Foxp3+ regulatory T cells *via* calcitonin gene-related peptide. *PLoS One* 11:e0152443. doi: 10.1371/journal.pone.0152443

Tajerian, M., Alvarado, S., Millecamps, M., Vachon, P., Crosby, C., Bushnell, M. C., et al. (2013). Peripheral nerve injury is associated with chronic, reversible changes in global DNA methylation in the mouse prefrontal cortex. *PLoS One* 8:e55259. doi: 10.1371/journal.pone.0055259

Talbot, S., Abdulnour, R.-E. E., Burkett, P. R., Lee, S., Cronin, S. J. F., Pascal, M. A., et al. (2015). Silencing nociceptor neurons reduces allergic airway inflammation. *Neuron* 87, 341–354. doi: 10.1016/j.neuron.2015.06.007

Talme, T., Liu, Z., and Sundqvist, K.-G. (2008). The neuropeptide calcitonin gene-related peptide (CGRP) stimulates T cell migration into collagen matrices. *J. Neuroimmunol.* 196, 60–66. doi: 10.1016/j.jneuroim.2008.02.007

Tang, X., Tian, X., Zhang, Y., Wu, W., Tian, J., Rui, K., et al. (2013). Correlation between the frequency of Th17 cell and the expression of microRNA-206 in patients with dermatomyositis. *Clin. Dev. Immunol.* 2013:345347. doi: 10.1155/2013/345347

Taves, S., Berta, T., Liu, D.-L., Gan, S., Chen, G., Kim, Y. H., et al. (2016). Spinal inhibition of p38 MAP kinase reduces inflammatory and neuropathic pain in male but not female mice: sex-dependent microglial signaling in the spinal cord. *Brain Behav. Immun.* 55, 70–81. doi: 10.1016/j.bbi.2015.10.006

Tracey, K. J. (2009). Reflex control of immunity. *Nat. Rev. Immunol.* 9, 418–428. doi: 10.1038/nri2566

Uçeyler, N., Eberle, T., Rolke, R., Birklein, F., and Sommer, C. (2007a). Differential expression patterns of cytokines in complex regional pain syndrome. *Pain* 132, 195–205. doi: 10.1016/j.pain.2007.07.031

Uçeyler, N., Rogausch, J. P., Toyka, K. V., and Sommer, C. (2007b). Differential expression of cytokines in painful and painless neuropathies. *Neurology* 69, 42–49. doi: 10.1212/01.wnl.0000265062.92340.a5

Uçeyler, N., Häuser, W., and Sommer, C. (2011). Systematic review with meta-analysis: cytokines in fibromyalgia syndrome. *BMC Musculoskelet. Disord.* 12:245. doi: 10.1186/1471-2474-12-245

Vargas-Rojas, M. I., Ramírez-Venegas, A., Limón-Camacho, L., Ochoa, L., Hernández-Zenteno, R., and Sansores, R. H. (2011). Increase of Th17 cells in peripheral blood of patients with chronic obstructive pulmonary disease. *Respir. Med.* 105, 1648–1654. doi: 10.1016/j.rmed.2011.05.017

Vicuña, L., Strochlic, D. E., Latremoliere, A., Bali, K. K., Simonetti, M., Husainie, D., et al. (2015). The serine protease inhibitor SerpinA3N attenuates neuropathic pain by inhibiting T cell-derived leukocyte elastase. *Nat. Med.* 21, 518–523. doi: 10.1038/nm.3852

Wagner, R., Janjigian, M., and Myers, R. R. (1998). Anti-inflammatory interleukin-10 therapy in CCI neuropathy decreases thermal hyperalgesia, macrophage recruitment, and endoneurial TNF-α expression. *Pain* 74, 35–42. doi: 10.1016/s0304-3959(97)00148-6

Walsh, J. T., Hendrix, S., Boato, F., Smirnov, I., Zheng, J., Lukens, J. R., et al. (2015). MHCII-independent CD4+ T cells protect injured CNS neurons *via* IL-4. *J. Clin. Invest.* 125:2547. doi: 10.1172/jci82458

Wiese, A. D., Griffin, M. R., Stein, C. M., Mitchel, E. F., and Grijalva, C. G. (2016). Opioid analgesics and the risk of serious infections among patients with rheumatoid arthritis: a self-controlled case series study. *Arthritis Rheumatol.* 68, 323–331. doi: 10.1002/art.39462

Woolf, C. J., and Salter, M. W. (2000). Neuronal plasticity: increasing the gain in pain. *Science* 288, 1765–1769. doi: 10.1126/science.288.5472.1765

Xie, W., Chen, S., Strong, J. A., Li, A.-L., Lewkowich, I. P., and Zhang, J.-M. (2016). Localized sympathectomy reduces mechanical hypersensitivity by restoring normal immune homeostasis in rat models of inflammatory pain. *J. Neurosci.* 36, 8712–8725. doi: 10.1523/jneurosci.4118-15.2016

Xie, L., Choudhury, G. R., Winters, A., Yang, S.-H., and Jin, K. (2015). Cerebral regulatory T cells restrain microglia/macrophage-mediated inflammatory responses *via* IL-10. *Eur. J. Immunol.* 45, 180–191. doi: 10.1002/eji.201444823

Xin, J., Wainwright, D. A., Mesnard, N. A., Serpe, C. J., Sanders, V. M., and Jones, K. J. (2011). IL-10 within the CNS is necessary for CD4+ T cells to mediate neuroprotection. *Brain Behav. Immun.* 25, 820–829. doi: 10.1016/j.bbi.2010.08.004

Yednock, T. A., Cannon, C., Fritz, L. C., Sanchez-Madrid, F., Steinman, L., and Karin, N. (1992). Prevention of experimental autoimmune encephalomyelitis by antibodies against α 4 β 1 integrin. *Nature* 356, 63–66. doi: 10.1038/356063a0

Younger, D. S., Rosoklija, G., Hays, A. P., Trojaborg, W., and Latov, N. (1996). Diabetic peripheral neuropathy: a clinicopathologic and immunohistochemical analysis of sural nerve biopsies. *Muscle Nerve* 19, 722–727. doi: 10.1002/(SICI)1097-4598(199606)19:6<722::AID-MUS6>3.0.CO;2-C

Zhu, J., and Paul, W. E. (2008). CD4 T cells: fates, functions, and faults. *Blood* 112, 1557–1569. doi: 10.1182/blood-2008-05-078154

Ziv, Y., Ron, N., Butovsky, O., Landa, G., Sudai, E., Greenberg, N., et al. (2006). Immune cells contribute to the maintenance of neurogenesis and spatial learning abilities in adulthood. *Nat. Neurosci.* 9, 268–275. doi: 10.1038/nn1629

Conflict of Interest: The authors declare that the research was conducted in the absence of any commercial or financial relationships that could be construed as a potential conflict of interest.

frontiers in Molecular Neuroscience

ORIGINAL RESEARCH
published: 16 September 2019
doi: 10.3389/fnmol.2019.00217

Granulocyte-Colony Stimulating Factor-Induced Neutrophil Recruitment Provides Opioid-Mediated Endogenous Anti-nociception in Female Mice With Oral Squamous Cell Carcinoma

*Nicole N. Scheff[1], Robel G. Alemu[2], Richard Klares III[1], Ian M. Wall[2], Stephen C. Yang[2], John C. Dolan[1] and Brian L. Schmidt[1]**

[1]Bluestone Center for Clinical Research, New York University, New York, NY, United States, [2]College of Dentistry, New York University, New York, NY, United States

Oral cancer patients report severe function-induced pain; severity is greater in females. We hypothesize that a neutrophil-mediated endogenous analgesic mechanism is responsible for sex differences in nociception secondary to oral squamous cell carcinoma (SCC). Neutrophils isolated from the cancer-induced inflammatory microenvironment contain β-endorphin protein and are identified by the Ly6G$^+$ immune marker. We previously demonstrated that male mice with carcinogen-induced oral SCC exhibit less nociceptive behavior and a higher concentration of neutrophils in the cancer microenvironment compared to female mice with oral SCC. Oral cancer cells secrete granulocyte colony stimulating factor (G-CSF), a growth factor that recruits neutrophils from bone marrow to the cancer microenvironment. We found that recombinant G-CSF (rG-CSF, 5 μg/mouse, intraperitoneal) significantly increased circulating Ly6G$^+$ neutrophils in the blood of male and female mice within 24 h of administration. In an oral cancer supernatant mouse model, rG-CSF treatment increased cancer-recruited Ly6G$^+$ neutrophil infiltration and abolished orofacial nociceptive behavior evoked in response to oral cancer supernatant in both male and female mice. Local naloxone treatment restored the cancer mediator-induced nociceptive behavior. We infer that rG-CSF-induced Ly6G$^+$ neutrophils drive an endogenous analgesic mechanism. We then evaluated the efficacy of chronic rG-CSF administration to attenuate oral cancer-induced nociception using a tongue xenograft cancer model with the HSC-3 human oral cancer cell line. Saline-treated male mice with HSC-3 tumors exhibited less oral cancer-induced nociceptive behavior and had more β-endorphin protein in the cancer microenvironment than saline-treated female mice with HSC-3 tumors. Chronic rG-CSF treatment (2.5 μg/mouse, every 72 h) increased the HSC-3 recruited Ly6G$^+$ neutrophils, increased β-endorphin protein content in the tongue and attenuated nociceptive behavior in

OPEN ACCESS

Edited by:
Tally Largent-Milnes, University of Arizona, United States

Reviewed by:
Gerardo Rojas-Piloni, Universidad Nacional Autónoma de México, Mexico
Irmgard Tegeder, Goethe University Frankfurt, Germany

***Correspondence:**
Brian L. Schmidt
brianl.schmidt@nyu.edu

Received: *31 May 2019*
Accepted: *29 August 2019*
Published: *16 September 2019*

Citation:
Scheff NN, Alemu RG, Klares R III, Wall IM, Yang SC, Dolan JC and Schmidt BL (2019) Granulocyte-Colony Stimulating Factor-Induced Neutrophil Recruitment Provides Opioid-Mediated Endogenous Anti-nociception in Female Mice With Oral Squamous Cell Carcinoma. Front. Mol. Neurosci. 12:217. doi: 10.3389/fnmol.2019.00217

female mice with HSC-3 tumors. From these data, we conclude that neutrophil-mediated endogenous opioids warrant further investigation as a potential strategy for oral cancer pain treatment.

Keywords: pain, neutrophils, anti-nociception, opioids, squamous cell carcinoma, sex differences, cancer

INTRODUCTION

Oral cancer patients report severe function-induced pain; patients experience impaired speech, swallowing, eating, and drinking (Bjordal et al., 2001) and severity is greater in females. We previously demonstrated a sex difference in the prevalence and severity of oral squamous cell carcinoma (SCC)-induced nociception (Scheff et al., 2018). Female mice with 4-nitroquinoline-1-oxide (4NQO)-induced oral SCC exhibited more orofacial nociceptive behavior compared to male mice (Scheff et al., 2018). Furthermore, infiltrating neutrophils contribute to decreased nociceptive behavior in male mice during early 4NQO-induced carcinogenesis through opioid-mediated endogenous anti-nociception (Scheff et al., 2018). Activation of opioid receptors on peripheral sensory nerves can produce anti-nociception (Stein et al., 1991, 2003; Mousa et al., 2007; Hua and Cabot, 2010). Clinical and preclinical evidence suggest that endogenous opioids can be released in local inflamed tissues to alleviate inflammatory hyperalgesia (Kapitzke et al., 2005; Iwaszkiewicz et al., 2013). A major source of opioid peptides in peripheral tissues is non-neuronal cells (Kapitzke et al., 2005); keratinocytes and immune cells contain and release met-enkephalin and β-endorphin (Stein et al., 1990; Khodorova et al., 2003; Smith, 2003; Slominski et al., 2011). Peripheral immune-mediated opioid anti-nociception is restricted to the inflammatory site without side effects in response to opioid receptor activation in the central nervous system (Kapitzke et al., 2005). We hypothesize that neutrophil recruitment could be exploited as a therapeutic approach to alleviate oral cancer pain in female mice.

In the early stage of inflammation, opioid-producing neutrophils comprise the majority of infiltrating immune cells (Rittner et al., 2001; Brack et al., 2004b). Oral cancer cells secrete hematopoietic growth factor granulocyte colony stimulating factor (G-CSF; Hayashi et al., 1995; Lee et al., 2013), which results in neutrophil infiltration into the cancer (Demetri and Griffin, 1991). Administration of recombinant G-CSF (rG-CSF) has been used clinically to increase the neutrophil count when treating chemotherapy- or radiotherapy-induced neutropenia (Dale, 2002; Lambertini et al., 2014). rG-CSF-generated neutrophils have the potential to secrete opioids and subsequently reduce nociceptive signaling. Chao et al. (2012) demonstrated that rG-CSF administration in rats with chronic nerve constriction injury alleviated mechanical allodynia and thermal hyperalgesia. rG-CSF-mediated increase in the recruitment of opioid-containing neutrophils was confirmed as the source for the anti-nociception (Chao et al., 2012).

To investigate whether rG-CSF increased neutrophil infiltration to the oral cancer microenvironment and alleviated oral cancer pain, we used two oral cancer pain mouse models: (1) an oral cancer pain model created by injecting supernatant from human oral cancer cell lines into the tongue; and (2) a human tongue xenograft cancer model created by injecting oral cancer cells into the tongue. The dolognawmeter assays (Dolan et al., 2010) were used to quantify a behavioral index (gnawing) of orofacial nociception in both models. rG-CSF treatment increased $Ly6G^+$ neutrophil recruitment to the oral cancer microenvironment and reduced oral cancer-induced nociception in an endogenous opioid-mediated analgesic mechanism in a sex-dependent manner.

MATERIALS AND METHODS

Animals

Male and female adult (10–12 weeks, 20–30 g) C57BL/6 mice (Jackson Labs, Bar Harbor, ME, USA) were used for oral cancer supernatant experiments. The xenograft cancer model required adult nude athymic mice (Jackson Labs, Bar Harbor, ME, USA). Mice were maintained on a 12:12 h light cycle and were housed in temperature-controlled rooms with access to food and water. Researchers were trained under the Animal Welfare Assurance Program. Experimental procedures were approved by the New York University Institutional Animal Care and Use Committee and were conducted in line with the National Institutes of Health guidelines for the use of laboratory animals in research.

Cell Culture and Supernatant Collection

Oral cancer cell line, HSC-3 (JCRB, Sekisui Xenotech, Kansas City, KS, USA), was cultured in 10 cm^2 cell culture dishes at 37°C with 5% CO_2 in Dulbecco's modified Eagle's medium (DMEM, Gibco, Waltham, MA, USA) supplemented with 10% fetal bovine serum and penicillin/streptomycin (50 U/mL). For collection of supernatant, the culture medium was changed to serum-free DMEM without phenol red (3 mL total volume) when cells reached 70%–80% confluency (1.5×10^6 cells) and cells were subsequently incubated for an additional 48 h. Cell culture supernatant was collected, centrifuged at $300\times$ *g* to remove cell debris, and frozen at −20°C until needed. HSC-3 cell culture supernatant was collected from passage 8.

Dolognawmeter Behavior Assay

Dolognawmeters were used in parallel to quantify a behavioral index (gnawing activity) of orofacial nociception in mice (Dolan et al., 2010). Each mouse was placed in a cylindrical confinement tube. Two polymer dowels in series prevent the mouse from progressing forward in the tube. To escape the tube, the mice gnaw through the two dowels. Each dowel is connected to an electronic timer. The timers record the duration of gnawing required to sever the dowels. The outcome variable is the time required (gnaw-time) to sever the second

dowel. Prior to the experimental trials, mice were trained for 10 sessions to acclimatize the animals to the dolognawmeter and to establish a baseline gnaw-time (the mean of the last three gnawing trials). Once the baseline gnaw-time measurements were established, drug/treatment injections were administered, followed by behavioral testing.

Conditioned Place Preference Assay

Conditioned place preference (CPP) to pain relief has been previously used to reveal underlying mechanisms of ongoing pain in several models including oral cancer pain (King et al., 2009; Chodroff et al., 2016). We determined whether synthetic met-enkephalin analog, DAMGO (3 μg/kg i.p.), produces CPP in mice with HSC-3 tongue xenografts. We performed a single trial CPP protocol on post-inoculation day (PID) 21 through 25. The 3-chamber CPP apparatus consists of two conditioning chambers with distinct tactile, visual, and olfactory cues, connected by a smaller neutral chamber that was brightly lit. The visual cues were horizontal stripe and dot wall papers. The tactile cues were smooth and rough flooring. The olfactory cues were strawberry and mint. White noise was played to provide background noise and block out any extraneous sounds. On the first day (PID 21, preconditioning) of the experiment, mice were introduced to the neutral chamber and allowed to explore all three chambers for 1 h. Baseline time spent in the chambers was measured using ANY-maze tracking software (Braintree Scientific, Braintree, MA, USA). Exclusion criteria included mice were spending <20% or >80% time in a chamber. Mice were assigned treatment-chamber pairings using a counterbalanced design for the following three consecutive days. On the second, third and fourth days (PID 22–24, conditioning), mice received i.p. injection of saline followed by confinement into the appropriate pairing chamber for 1 h, following which they were returned to their home cage. Four hours later, mice received i.p. injection of DAMGO (3 μg/kg, 50 μl) followed by confinement into the opposite pairing chamber for 1 h. On the fifth day (PID 25, testing), mice were once again allowed to freely explore the apparatus for 1 h. Time spent in each chamber was recorded by ANY-maze. The experimenter conducting the behavioral tests (IW) was blinded to the treatment groups.

Acute Supernatant Oral Cancer Pain Model

We developed a model of acute oral cancer pain by injecting cancer cell line supernatant into the tongues of mice. Under isoflurane general anesthesia, 50 μl injections of oral cancer (HSC-3) supernatant was administered into the anterior lateral tongue over a 5 s period. A 5 μg dose of rG-CSF was injected intraperitoneal (i.p.) 24 h prior to the supernatant injection to increase neutrophil infiltration in the tongue. The dose and route of administration for rG-CSF treatment was determined in a pilot study using 0.2 μg/mouse (low dose) and 5 μg/mouse (high dose) of rG-CSF and two different routes of administration: subcutaneous into the tongue (s.c.) and intraperitoneal (i.p.). An index of cancer-induced nociception was quantified with the dolognawmeter assay. Naloxone (500 μg/kg; Sigma Aldrich, St. Louis, MO, USA) was co-injected with HSC-3 cell culture supernatant for experiments designed to inhibit endogenous opioid-mediated analgesic signaling in response to rG-CSF treatment and oral cancer supernatant injection in female and male mice. Neutrophil infiltration in the tongue was measured with flow cytometry 24 h after the supernatant injection. The experimenter conducting the behavioral tests (RA) was blinded to the treatment groups.

Xenograft Oral Cancer Pain Model

We used the human tongue xenograft cancer mouse model to determine whether chronic rG-CSF treatment decreases oral cancer-induced nociception. Mice were inoculated with 1×10^5 HSC-3 cells in 30 μL of 1:1 DMEM and Matrigel into the anterior lateral portion of the tongue as previously described (Ye et al., 2018). Nociceptive behavior was measured twice per week using a dolognawmeter assay for the duration of the experiment. A 2.5 μg dose of rG-CSF was injected (i.p.) 24 h prior to the nociceptive behavior assessment to increase neutrophil infiltration in the tongue. Body weight was recorded once per week. Tongue tumor size was quantified at PID 38. The tongue was fixed in 10% neutral buffered formalin, bisected, paraffin-embedded with cut side down, and sectioned at 5 μm thickness through the entire block (about 50 sections). Average tumor area relative to total tongue area in the 1st, 10th, 20th, 30th and 40th section was quantified using hematoxylin and eosin (H&E) stain and ImageJ (NIH, Bethesda, MD, USA). The experimenters conducting the behavioral tests (RA) and tumor quantification (RA, RK) were blinded to the treatment groups.

Tongue Tissue Dissociation

Mouse tongues were harvested and dissociated as previously described (Scheff et al., 2018). Briefly, tongue tissue was dissected and minced in DMEM with antibiotics, collagenase-H (0.5 mg/mL; Sigma Aldrich, 34 units/mg), DNase (0.5 mg/mL) and 20 mM 4-(2-hydroxyethyl)-1-piperazine ethanesulfonic acid (HEPES), and then incubated at 37°C for 1 h. The tissue was then mechanically dissociated using a fire-polished pipette, washed twice with fresh DMEM containing antibiotics and HEPES, and resuspended in Ca^{2+}/Mg^{2+} free phosphate buffered saline (Sigma Aldrich) containing 3% fetal bovine serum, 1 mM EDTA, and 0.02% sodium azide and filtered through a 40 μm cell strainer (Falcon brand, Fisher Scientific, Waltham, MA, USA).

Flow Cytometry

Flow cytometry was used to quantify immune cell subtypes in tongue tissue from female and male mice. The antibody panel and flow cytometry gating strategy were used as previously defined (Scheff et al., 2017). Within $CD45^+$ hematopoietic cells, neutrophils and monocytes/macrophage were detected and quantified using antibodies specific to receptors expressed on each cell type. Single-cell suspensions were prepared and samples were incubated in rat anti-mouse purified CD16/CD32 to block nonspecific FC receptor binding. CD45 monoclonal antibody (mAb) conjugated with V450 dye (1:400; BD Biosciences Franklin Lakes, NJ, USA) was used to label all hematopoietic cells. To differentiate leukocyte subpopulations, we stained cell suspensions with fluorescently conjugated rat anti-mouse mAbs recognizing neutrophils (Ly6G, Cat# 561105, 1:500), monocytes/macrophages (CD11b, Cat#

561690, 1:1,000), and dendritic cells (CD11c, Cat# 561044, 1:250). The gating strategy for isolation of these populations was to first exclude dead cells in the population using propidium iodide (PI; Molecular Probes, Eugene, OR, USA). Of the recovered live cells, $CD45^+$ immune cells were selected and then sorted into $CD11b^+$ monocyte/macrophages/neutrophils and $CD11c^+$ dendritic cells. $CD11b^+/c^-$ immune cells were further sorted into $CD11b^+/Ly6G^-$ and $Ly6G^+$ to isolate monocyte/macrophages and neutrophils respectively. Viability was 70%–85%, as determined by PI staining. An average of $1.2 \times 10^5 \pm 7.2 \times 10^3$ live cells were recovered from each blood sample. An average of $3.8 \times 10^4 \pm 1.5 \times 10^3$ live cells were recovered from each tongue sample. Leukocytes from the spleen were used for compensation controls (i.e., correction of a signal overlap between emission spectra of different fluorochromes used). Data were acquired using a FACSCalibur (BD Biosciences) and analyzed using FlowJo software (Tree Star, San Carlos, CA, USA).

Fluorescence-Activated Cell Sorting (FACS)

Fluorescence-activated cell sorting (FACS) was used to collect $Ly6G^+$ population of immune cells from dissociated tongue tissue treated with HSC-3 cell culture supernatant. Tongue tissue was dissected and dissociated in a manner similar to that used for flow cytometry. To isolate subpopulations, cells were stained with fluorescently conjugated rat anti-mouse mAbs: CD450 (1:400), CD11b (1:1,000), and Ly6G (1:500). PI was used to exclude dead cells. Neutrophils were defined as $CD45^+CD11b^+Ly6G^+$. Forward and side scatter parameters were used to confirm the size and granularity of the $CD45^+CD11b^+Ly6G^+$ population. Post-sort purity was >97%. FACS was performed on a three laser, 10 detector FACSAria cell sorter (BD Biosciences). Samples were sorted into RIPA buffer containing protease inhibitor cocktail for protein isolation.

Enzyme-Linked Immunosorbent Assay

The β-endorphin protein concentration was quantified in tongue tissue from female and male mice with HSC-3 tumors was compared to sham (matrigel alone) mice by enzyme-linked immunosorbent assay (ELISA; MyBioSource, Inc., San Diego, CA, USA). Frozen tissue (20–40 mg) was homogenized in the T-PER Reagent (Pierce Biotechnology, Inc., Rockford, IL, USA) and agitated for an additional 2 h at 4°C. Lysates were centrifuged at 16,000 rpm for 20 min. Cell culture supernatants were removed, aliquoted and protein concentrations were determined using a Bradford Assay (Bio-Rad Laboratories, Inc., Hercules, CA, USA). ELISA was run per the manufacturer's instructions. The optical density of the standards and samples was read at 450 nm using a Model 680 Microplate Reader (Bio-Rad Laboratories, Inc., Hercules, CA, USA).

Immunohistochemistry

Animals were euthanized *via* an overdose of inhaled isoflurane and perfused transcardially with 4% paraformaldehyde (PFA, Sigma Aldrich). Tongues were dissected, fixed in 10% neutral buffered formalin, bisected, paraffin-embedded with cut side down, and sectioned at 5 μm thickness through the entire block (about 50 sections). Slide containing the 20th section was selected for staining with anti-Ly6G antibody (Clone 1A8, 1:100, Biolegend, San Diego, CA, USA) by the New York University Langone Medical Center Histopathology Core. Immunoreactions were visualized with diaminobenzidine (DAB) horseradish peroxidase (HRP) substrate kit (Vector Laboratories) and counterstained with Hematoxylin. The sections were photographed using NIS Elements software, a Nikon Eclipse Ti microscope and 2.5× and 60× objectives.

Statistical Analysis

Analysis of variance (ANOVA) was employed to evaluate the difference between groups regarding sex and treatment. To adjust for multiple comparisons, the *post hoc* Holm-Sidak test statistic was employed. Statistical significance was set at $p < 0.05$. All statistical analyses were performed using Prism (version 8) statistical software (Graphpad Software Inc., La Jolla, CA, USA). Results were presented as mean ± standard error of the mean in box/scatter configuration to show the biological variability.

RESULTS

rG-CSF Treatment Increased Oral Cancer-Recruited $Ly6G^+$ Neutrophils in the Tongue Microenvironment

To establish a mouse model that permitted assessment of rG-CSF-induced changes in $Ly6G^+$ neutrophil infiltration during oral cancer, male and female mice were treated with rG-CSF to increase the percentage of circulating blood $Ly6G^+$ neutrophils; the number of circulating $Ly6G^+$ neutrophils in the blood was quantified with flow cytometry. Male and female mice treated with 5 μg rG-CSF (i.p.) exhibited significantly more $Ly6G^+$ neutrophils in the blood 24 h after injection compared to mice treated with saline (Unpaired *t*-test, male: $t = 5.368$, $P = 0.001$; female: $t = 2.9178$, $P = 0.022$; **Figure 1**). There was no significant interaction between sex and treatment (two-way ANOVA, $F_{(1,14)} = 2.1$, $P = 0.163$). We previously demonstrated that oral cancer-secreted mediators recruit neutrophils to the tongue cancer microenvironment (Scheff et al., 2017). We sought to determine whether rG-CSF treatment could amplify this effect. Twenty-four hours after rG-CSF treatment, male and female mice received HSC-3 culture supernatant (50 μl) or cell culture media (DMEM) injected into the tongue. The number of infiltrating $Ly6G^+$ neutrophils in the tongue was quantified 12 h after supernatant injection (**Figure 2A**). Administration of rG-CSF treatment prior to HSC-3 supernatant injection (rG-CSF+HSC-3) produced a significant increase in $Ly6G^+$ neutrophil recruitment compared to rG-CSF paired with cell culture media (rG-CSF+DMEM) in both male and female mice (one-way ANOVA, male: $P = 0.001$, female: $P = 0.002$; **Figure 2B**). We also found a significant increase in $Ly6G^+$ neutrophils in male and female mice treated with rG-CSF+HSC-3 compared to mice that received saline paired with HSC-3 supernatant (saline+HSC-3; one-way ANOVA, male: $P = 0.005$, female: $P = 0.014$;

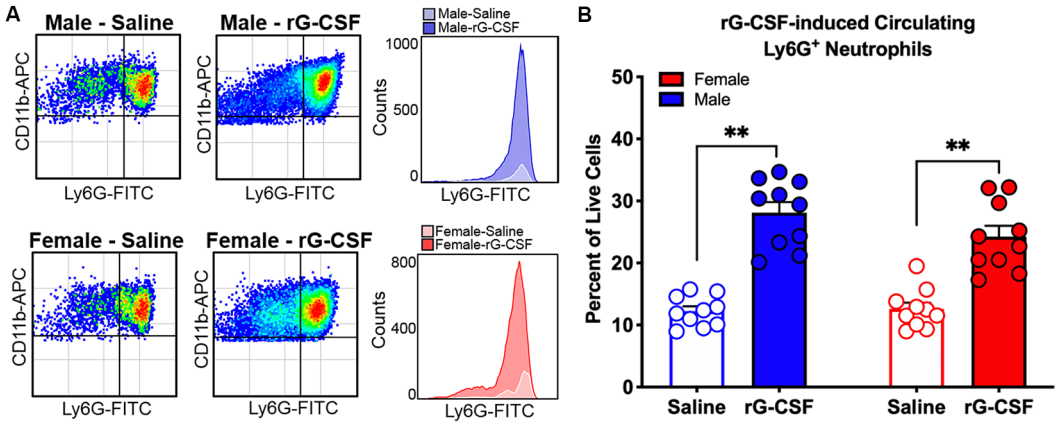

FIGURE 1 | Recombinant granulocyte colony stimulating factor (rG-CSF)-mediated mobilization of neutrophils was quantified using flow cytometry in adult C57Bl/6 mice. **(A)** Representative scatter plots showing $CD11b^{+}Ly6G^{+}$ neutrophils in cardiac blood of a naïve male mouse (top) and a female mouse (bottom) 24 h after treatment with saline (left) or rG-CSF (right). Histograms demonstrate the increase in circulating neutrophil after rG-CSF treatment. **(B)** Average $Ly6G^{+}$ neutrophils quantification in cardiac blood from mice ($N = 10$) 24 h following a single treatment of rG-CSF (5 μg/mouse, i.p.) male (blue bars) and female (red bars) mice compared to saline treatment. Unpaired Student's *t*-test, $^{**}P < 0.01$.

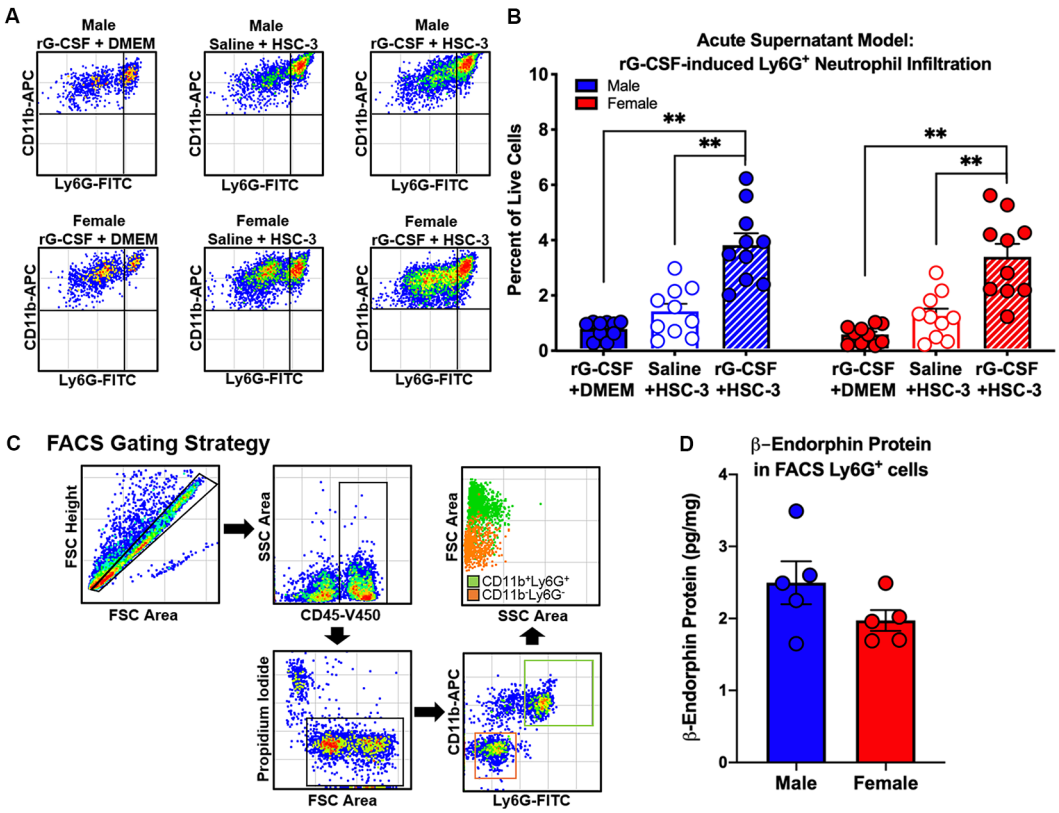

FIGURE 2 | Oral cancer supernatant-induced immune infiltration was measured using the acute supernatant model. **(A)** Representative scatter plots showing $CD11b^{+}Ly6G^{+}$ neutrophils from the tongues of an adult C57Bl/6 male (top) and female (bottom) mouse 48 h after either rG-CSF treatment followed by cell culture media (rG-CSF+DMEM, solid bar), saline followed by HSC-3 cell culture supernatant (Saline+HSC-3, open bar), or rG-CSF treatment followed by HSC-3 cell culture supernatant (rG-CSF+HSC-3, striped bar). **(B)** Average $Ly6G^{+}$ neutrophil quantification in the tongues of male ($N = 10$/group, blue bars) and female ($N = 10$/group, red bars) mice after treatment. One-way analysis of variance (ANOVA), $^{**}P < 0.01$. **(C)** Representative gating strategy used to isolate cancer-activated tongue immune cells by fluorescence-activated cell sorting (FACS). **(D)** Quantification of mean β-endorphin protein in $CD11b^{+}Ly6G^{+}$ immune cell subpopulations from HSC-3 supernatant-treated male (blue, $N = 5$) and female mice (red, $N = 5$) relative to total protein. Sorted cells were pooled from two mice for each sample. Unpaired Student's *t*-test, $P > 0.05$.

Figure 2B). There was no significant interaction between sex and treatment (two-way ANOVA, $F_{(2,24)} = 0.294$, $P = 0.748$). To determine if cancer-recruited neutrophils contain opioid protein, $CD45^+CD11b^+Ly6G^+$ cells were isolated after rG-CSF+HSC-3 supernatant treatment from mouse tongues using FACS (**Figure 2C**). An average of 124,125 ± 10,092 $Ly6G^+$ neutrophils were isolated from each tongue. β-endorphin protein was quantified in cancer supernatant-recruited neutrophils isolated from male and female mice (three samples/sex, each sample contained cells isolated from two mice). There was no significant difference in the quantity of β-endorphin protein detected in neutrophils isolated from male (2.50 ± 0.30 pg/mg) and female (1.97 ± 0.15 pg/mg) mice (Student's *t*-test, $P = 0.152$; **Figure 2D**).

rG-CSF Treatment Abolished HSC-3 Supernatant-Induced Nociceptive Behavior *via* an Endogenous Opioid-Dependent Mechanism

An acute supernatant model was used to quantify oral cancer-induced nociceptive behavior in the absence of tumor burden and illness associated with carcinogenesis (Scheff et al., 2017). Baseline gnaw-times were established using the dolognawmeter. Mice received rG-CSF treatment followed by tongue injection of cell culture media (DMEM) or supernatant (**Figure 3A**). Nociceptive behavior of mice was assessed 1 h after cell supernatant injection. We found was no difference in gnaw-time between groups prior to treatment; therefore, data were analyzed as a percent change from baseline using two-way ANOVA. There was a significant interaction between time and treatment in both male and female mice (two-way ANOVA, male: $F_{(6,42)} = 5.025$, $P = 0.005$, female: $F_{(6,45)} = 2.949$, $P = 0.016$). HSC-3 supernatant injection yielded an increase in gnaw-time compared to baseline gnaw-time in both male (57.8 ± 9.1%) and female (82.5 ± 18.9%) mice (Holm-Sidak *post hoc*, males: = 0.034, females: $P = 0.001$; **Figures 3B,C**). Administration of rG-CSF 24 h prior to DMEM (rG-CSF+DMEM) had no effect on gnaw-time compared to baseline gnaw-time in both male (−4.01 ± 9.9%) and female (−0.18 ± 13.2%) mice (males: $P = 0.998$, females: $P = 0.998$; **Figures 3B,C**). Administration of rG-CSF followed by HSC-3 injection (rG-CSF+HSC-3) significantly limited the HSC-3 supernatant-induced increase in gnaw-time; there was a significant decrease in gnaw-time after supernatant injection compared to saline+HSC-3 treatment in both male and female mice (males: $P = 0.0002$, females: $P = 0.021$; **Figures 3B,C**).

Peripheral opioid receptor antagonist (naloxone methiodide, 500 μg/kg) revealed an endogenous analgesic mechanism in male and female mice treated with rG-CSF. There was a significant interaction between time and treatment in both male and female mice (two-way ANOVA, male: $F_{(9,66)} = 4.575$, $P = 0.0001$; female: $F_{(9,66)} = 3.347$, $P = 0.0019$). In the absence of rG-CSF, naloxone co-injected with HSC-3 supernatant (saline+HSC-3/naloxone) evoked a significant increase in gnaw-time compared to saline+HSC-3 in male mice ($P = 0.007$) but not in female mice ($P = 0.052$; **Figure 3D**). After rG-CSF treatment, naloxone co-injected with HSC-3 supernatant (rG-CSF+HSC-3/naloxone) resulted in significantly longer gnaw-times in male mice compared to saline+naloxone (male: $P = 0.035$; **Figure 3D**). There was no significant difference between rG-CSF+HSC-3/naloxone and saline+HSC-3/naloxone treated male mice ($P = 0.950$, **Figure 3D**). Five female mice had significantly longer gnaw-time in response to saline+HSC-3 supernatant ($P = 0.012$) when compared to five female mice injected with DMEM/naloxone (**Figure 3E**). Co-injection with naloxone and HSC-3 supernatant was not significantly different from DMEM/naloxone injection in female mice treated with saline ($P = 0.998$) or rG-CSF ($P = 0.998$; **Figure 3E**).

Chronic rG-CSF Treatment Decreased Oral Cancer-Induced Nociception in Female Mice Only

We previously demonstrated that $Ly6G^+$ neutrophils in the 4NQO-induced oral cancer microenvironment generate endogenous anti-nociception in male mice (Scheff et al., 2018). Neutrophils are present in the cancer microenvironment in the human xenograft HSC-3 mouse model of oral cancer (Ye et al., 2018). Using the HSC-3 xenograft mouse model, mice were treated with 2.5 μg rG-CSF 24 h prior to each behavior assessment beginning at PID 5. Consistent with our previous finding (Scheff et al., 2018), we found a significant interaction between time and sex in saline-treated mice (two-way ANOVA, $F_{(14,224)} = 2.664$, $P = 0.0013$). Holm-Sidak *post hoc* analyses found that tumor-bearing female mice treated with saline had significantly longer gnaw times on PID 25 ($P = 0.0239$), 29 ($P = 0.0460$) and 32 ($P = 0.0460$) when compared to males. When considering rG-CSF treatment, we found a significant interaction between time, sex, and treatment; rG-CSF treatment significantly reduced oral cancer-induced nociceptive behavior in a sex-dependent manner over time (three-way ANOVA, $F_{(14,462)} = 2.216$, $P = 0.0067$). There was no significant difference in gnaw-time between male mice treated with rG-CSF vs. male mice treated with saline ($P = 0.865$; **Figure 4A**). However, in tumor-bearing female mice, chronic rG-CSF treatment significantly reduced gnaw-time at PID 25 ($P = 0.009$), PID 29 ($P = 0.022$), and PID 32 ($P = 0.011$) compared to saline treatment (**Figure 4B**). HSC-3 xenograft tumor resulted in a decrease in body weight over time in both sexes (two-way ANOVA interaction, male: $F_{(5,80)} = 4.992$, $P = 0.0005$; female: $F_{(5,90)} = 3.658$, $P = 0.005$); however, there was no significant difference in cancer-induced loss of body mass between saline and rG-CSF treated groups at any time point (two-way ANOVA treatment, male: $F_{(1,16)} = 1.388$, $P = 0.256$; female: $F_{(1,18)} = 0.330$, $P = 0.572$; **Figures 4C,D**).

Chronic rG-CSF Treatment Decreased Oral Cancer-Induced Ongoing Nociception in Female Mice Only

In addition to function-related pain, we previously found a significant sex difference in reported intensity of spontaneous pain (Scheff et al., 2018). We used CPP assay (King et al., 2009) to test the hypothesis that rG-CSF treatment can alleviate spontaneous pain secondary to oral cancer in male and female mice. Pre-conditioning (baseline) times did not differ between

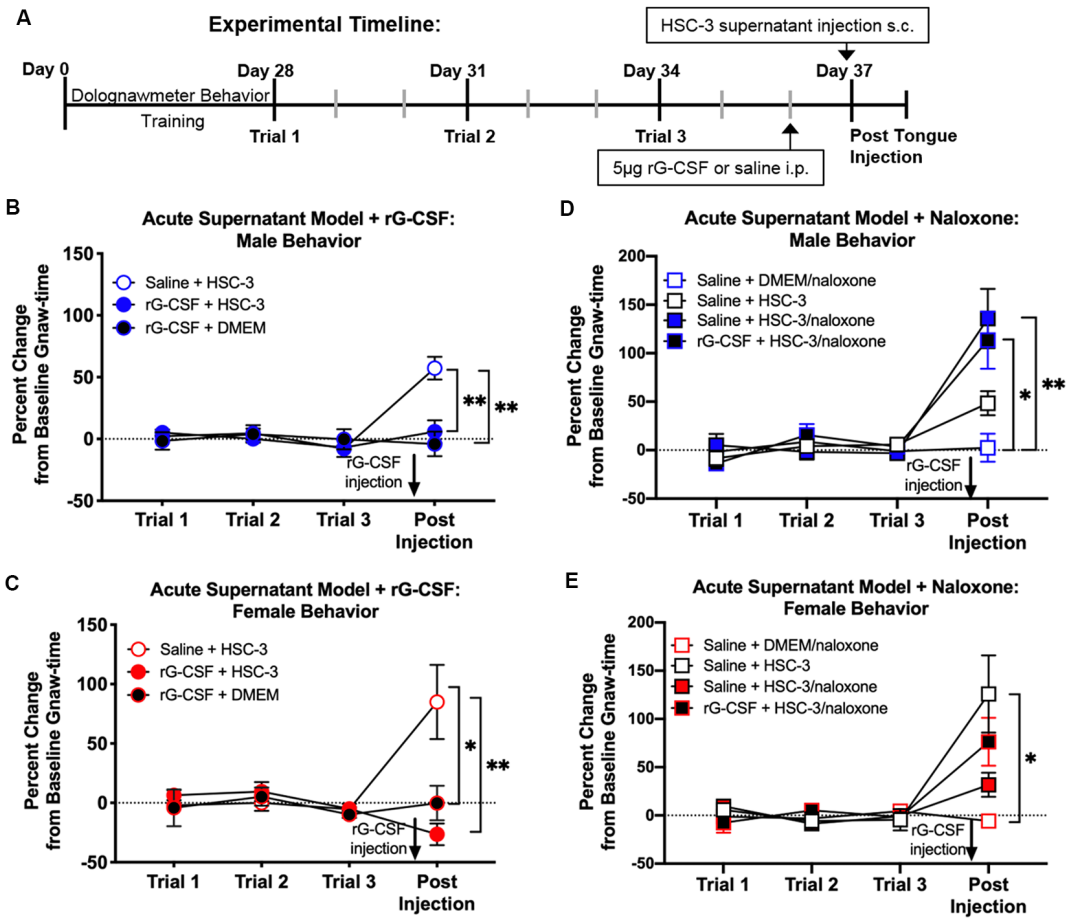

FIGURE 3 | Supernatant-induced nociceptive behavior was measured using the acute supernatant model. **(A)** Schematic of the experimental timeline for an acute supernatant model. Male and female C57Bl/6 mice were trained for 4 weeks in the orofacial pain behavior device and assay (dolognawmeter) or until a steady baseline gnaw-time was reached. Three additional baseline trials were completed and mice underwent a single intraperitoneal injection (i.p.) of saline or 5 μg rG-CSF. Twenty-four hours after treatment, mice received either subcutaneous (s.c.) DMEM (rG-CSF+DMEM) or HSC-3 culture supernatant (saline+HSC-3, rG-CSF+HSC-3, N = 8/sex) into the tongue (50 μl) followed by assessment in the dolognawmeter (Post-Injection). A separate group of mice received either s.c. DMEM or HSC-3 cell culture supernatant co-injected with opioid receptor antagonist naloxone (saline+DMEM/naloxone, saline+HSC-3/naloxone, rG-CSF+HSC-3/naloxone, N = 5/sex) into the tongue (50 μl) followed by assessment in the dolognawmeter (Post-Injection). Orofacial nociceptive behavior data were analyzed as a percent change from the baseline gnaw-time prior to treatment. Supernatant-induced change in orofacial nociceptive behavior was measured in male **(B,D)** and female **(C,E)** mice and analyzed individually. Two-way ANOVA, $^{*}P < 0.05$, $^{**}P < 0.01$ by Holm-Sidak *post hoc* comparisons.

the vehicle-paired chamber and the drug-paired chamber ($P = 0.56$), therefore data were pooled across groups for graphical representation (**Figures 5A,B**). There was a sex difference in DAMGO-induced CPP (three-way ANOVA, $F_{(2,48)} = 6.892$, $P = 0.002$). Tumor-bearing male mice did not demonstrate DAMGO-induced CPP regardless of saline ($P = 0.398$) or rG-CSF treatment ($P = 0.886$). However, tumor-bearing female mice treated with saline displayed CPP for the chamber paired with DAMGO; significantly more time was spent in the DAMGO-paired chamber compared with pre-conditioning baseline time ($P = 0.038$) and post-conditioning time in the saline-paired chamber ($P = 0.008$; **Figure 5B**). rG-CSF treatment prior to conditioning abolished the DAMGO-induced preference in female mice; there was no difference in time spent in the DAMGO-paired chamber compared with the pre-conditioning time ($P = 0.302$; **Figure 5B**). Pre- and post-conditioning times for the saline (male: $P = 0.917$, female: $P = 0.996$) and DAMGO (male: $P = 0.889$, female: $P = 0.959$) paired chamber did not differ for the sham-treated mice (data not shown).

Chronic rG-CSF Treatment Increased β-Endorphin Protein in the Oral Cancer Microenvironment in Female Mice Only

To determine whether rG-CSF treatment results in β-endorphin protein in the cancer microenvironment, we measured β-endorphin protein in homogenized tongue tissue from tumor-bearing male and female mice treated with saline or rG-CSF using an ELISA (**Figure 5C**). There was a significant interaction between sex and treatment (two-way ANOVA,

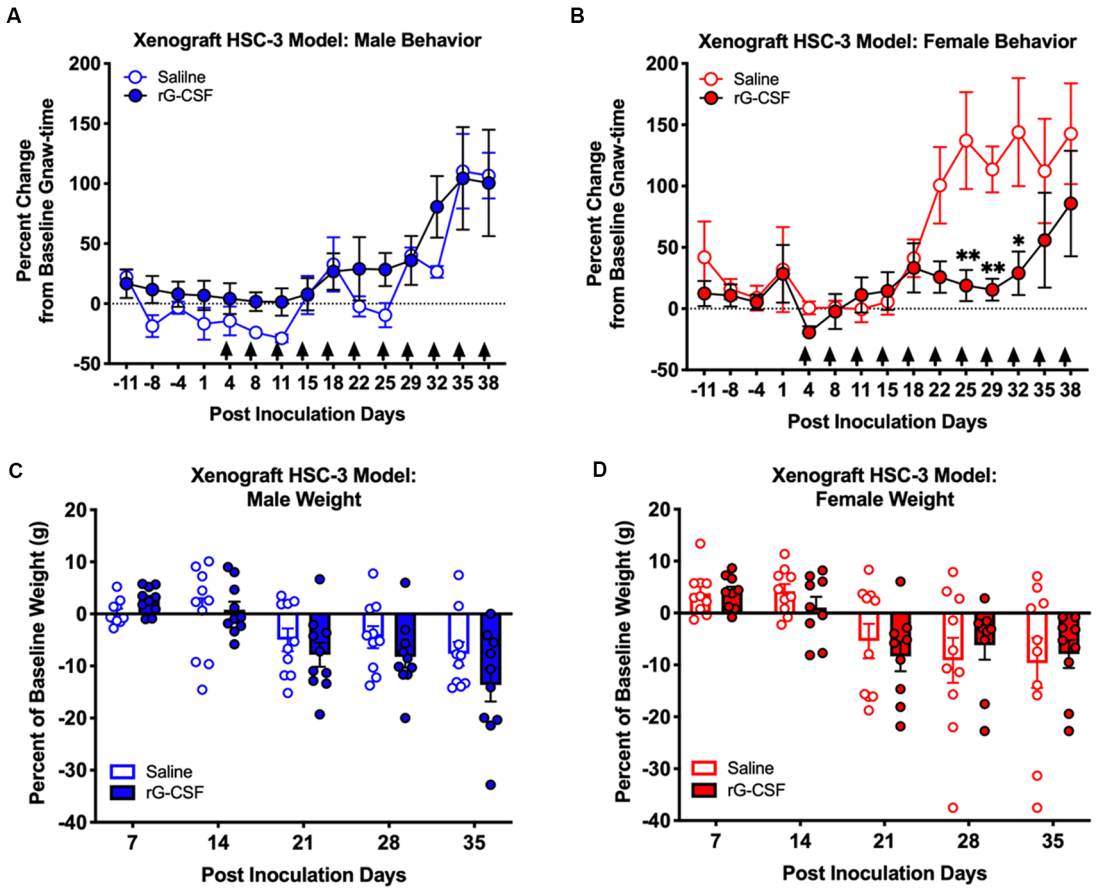

FIGURE 4 | HSC-3 xenograft-induced change in orofacial nociceptive behavior was measured in adult nude male **(A)** and female **(B)** mice receiving saline (N = 10, open circles) or rG-CSF treatment (2.5 μg/mouse, N = 10, closed circles) 24 h prior to each dolognawmeter measurement, as indicated by the black arrows. Sexes were independently analyzed. Two-way ANOVA, $^{*}P < 0.05$, $^{**}P < 0.01$. HSC-3 xenograft-induced weight loss was measured in male **(C)** and female **(D)** mice receiving saline (N = 10, open bars) or rG-CSF (2.5 μg/mouse, N = 10, closed bars) each week.

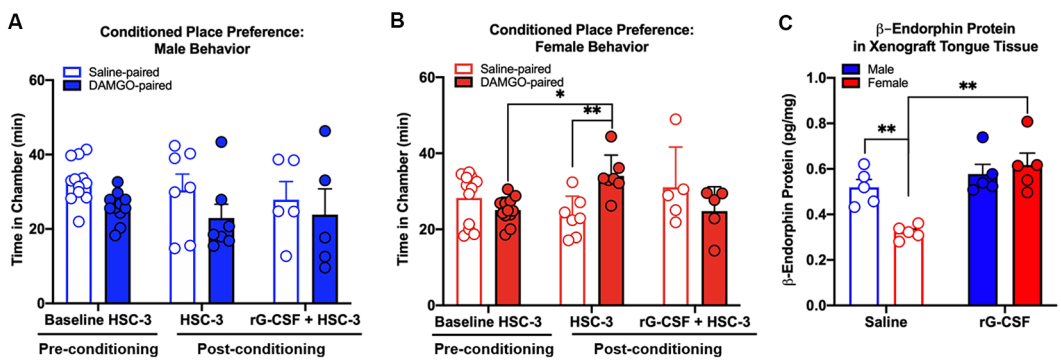

FIGURE 5 | Effect of oral cancer on conditioned place preference (CPP) to DAMGO. Mice were injected with HSC-3 cells into the tongue, habituated on day 21, conditioned with vehicle- and DAMGO (3 μg/kg)-paired chamber for 1 h on days 22–24 and tested for CPP on day 25. Mice received saline (N = 7/sex) or rG-CSF (2.5 μg/mouse, N = 5/sex) 12 h prior to conditioning. The time spent in each chamber was quantified in tumor-bearing male **(A)** and female **(B)** mice. For all of the CPP experiments, pre-conditioning data (Baseline HSC-3) was analyzed using two-way ANOVA (chambers vs. treatment). Statistical analysis for chamber preference before conditioning revealed no difference in the time spent in chambers between saline and rG-CSF-treated mice ($P > 0.05$), therefore baseline chamber data was pooled for graphical representation. Sexes were independently analyzed. Two-way ANOVA, $^{*}P < 0.05$, $^{**}P < 0.01$. **(C)** β-endorphin protein was quantified in homogenized tongue tissue from male (blue bars) and female (red bars) mice with HSC-3 xenograft tumors relative to total protein. Mice treated with either saline (N = 5/sex, open bars) or rG-CSF (N = 5/sex, closed bars). Two-way ANOVA, $^{**}P < 0.01$.

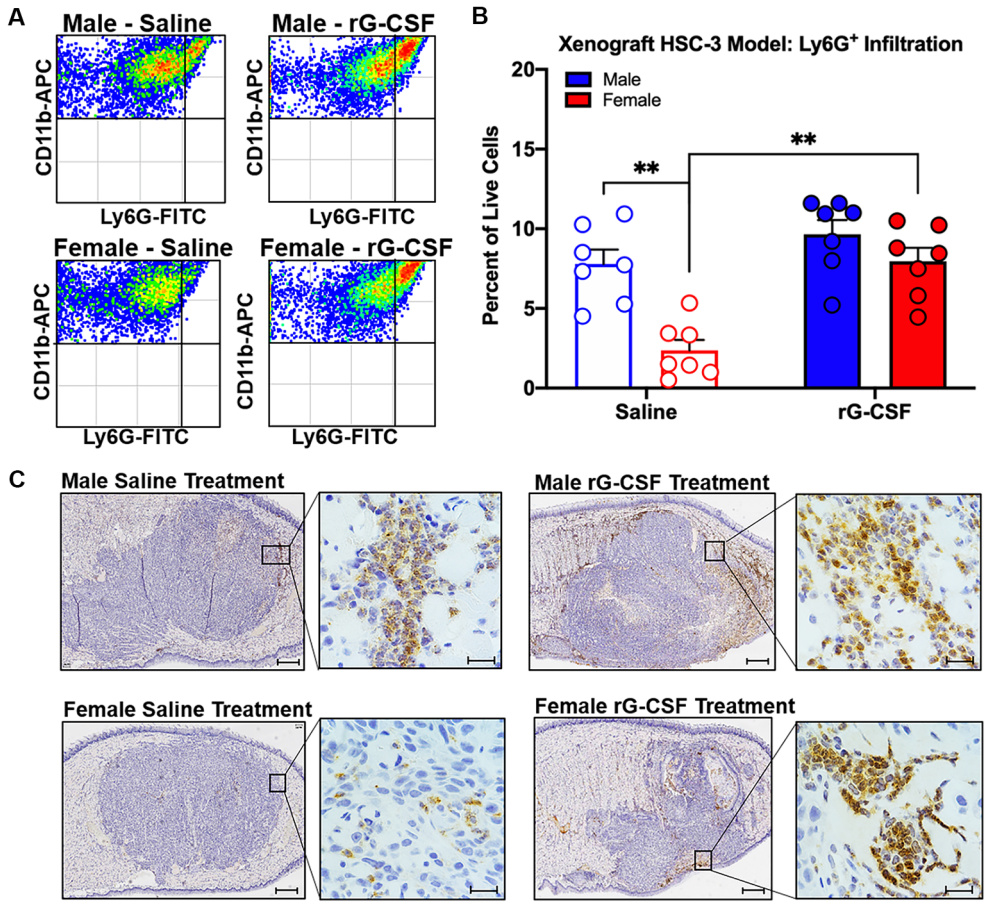

FIGURE 6 | HSC-3 xenograft-induced immune filtration was measured at post-inoculation day (PID) 38. **(A)** Representative scatter plots showing $CD11b^{+}Ly6G^{+}$ neutrophils from the tongue of adult male (top plots) and female (bottom plots) nude mice after chronic saline (left side) or rG-CSF (right side) treatment. **(B)** Average $Ly6G^{+}$ neutrophil quantification in the xenograft tongues of male (blue bars) and female (red bars) mice after chronic saline (N = 6/sex) or G-CSF (N = 6/sex) treatment. Two-way ANOVA, $^{**}P < 0.001$. **(C)** Immunohistochemical analysis of saline-treated (left) and rG-CSF (right) treated male (top) and female (bottom) mouse tongues. HSC-3 xenograft tumors were stained with Ly6G (1A8) in diaminobenzidine (DAB) and counterstained with hematoxylin. Magnification is 2.5× with 60× insert. Scale bar 500 μm (2.5×) and 20 μm (60×).

$F_{(1,16)} = 9.488$, $P = 0.007$). Tumor-bearing male mice treated with saline (0.52 ± 0.03 pg/mg) had significantly more β-endorphin protein in the tongue tissue compared to tumor-bearing female mice treated with saline (0.32 ± 0.01 pg/mg, $P = 0.009$). In addition, tumor-bearing female mice treated with rG-CSF (0.62 ± 0.05 pg/mg) had significantly more β-endorphin protein in the tongue tissue compared to tumor-bearing female mice treated with saline (0.32 ± 0.01 pg/mg, $P = 0.0003$, **Figure 5C**).

Chronic rG-CSF Treatment Increased Cancer-Recruited $Ly6G^{+}$ Neutrophils in Female Mice Only

Chronic rG-CSF treatment increased oral cancer-recruited $Ly6G^{+}$ neutrophils in female but not male mice with HSC-3 tumors (two-way ANOVA, $F_{(1,23)} = 5.098$, $P = 0.033$; **Figure 6**). At PID 38, quantification of immune cells in the tongue revealed significantly more $Ly6G^{+}$ neutrophil recruitment in HSC-3 tumors in female mice treated with rG-CSF compared to saline treatment ($P = 0.0004$). Tumor-bearing male mice treated with saline exhibited significantly more infiltrating $Ly6G^{+}$ neutrophils compared to tumor-bearing females treated with saline ($P = 0.0006$). There was no effect of rG-CSF treatment on HSC-3 tumor $Ly6G^{+}$ neutrophil recruitment in male mice ($P = 0.5534$). Tumor-bearing male mice exhibited a similar number of $Ly6G^{+}$ neutrophils in the oral cancer microenvironment compared to tumor-bearing female mice treated with rG-CSF (**Figure 6B**). To confirm the identity of the $Ly6G^{+}$ neutrophils, we performed immunohistochemistry on formalin-fixed tongue tissue containing HSC-3 xenograft tumors. Strong anti-Ly6G immuno-like reactivity using DAB HRP was present on the tumor borders in saline-treated male mice as well as rG-CSF-treated male and female mice. Magnification at 60× was used to confirm neutrophil presence based on multi-lobed nuclear morphology (**Figure 6C**). There was no significant interaction between rG-CSF treatment and

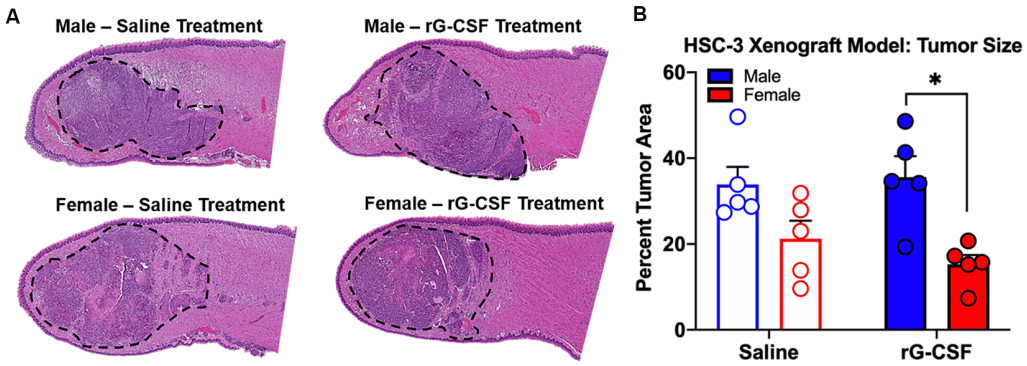

FIGURE 7 | HSC-3 xenograft tumor size was measured at PID 38. **(A)** Representative hematoxylin and eosin-stained sagittal tongue sections (100 μm from center) from male (top) and female (bottom) mice treated with either saline or rG-CSF. HSC-3 tumor is outlined in black dash line. **(B)** Tumor area relative to total tongue area after treatment with either saline (N = 5/sex) or rG-CSF (N = 5/sex) in male and female mice. Two-way ANOVA, $^*P < 0.05$.

sex regarding HSC-3 tumor size in mice (two-way ANOVA interaction, $F_{(1,14)} = 0.743$, $P = 0.403$; **Figure 7**). However, there was a significant effect of treatment (two-way ANOVA, $F_{(1,14)} = 13.55$, $P = 0.003$); HSC-3 tumor size was larger in rG-CSF-treated male compared to rG-CSF-treated female mice (Holm-Sidak $t = 3.21$, $P = 0.0370$; **Figure 7B**).

DISCUSSION

We and others show that women with oral SCC report more pain than men (Reyes-Gibby et al., 2014; Scheff et al., 2018). Human oral SCC produces and releases G-CSF resulting in neutrophil infiltration (Matsuo et al., 1994; Hayashi et al., 1995; Lee et al., 2013). Wang et al. (2014) show that the neutrophil density is higher in men with tongue SCC compared to women. Our previous investigation recapitulates the sex difference in pain and neutrophil infiltration; neutrophil-mediated anti-nociception inhibits nociceptive behavior during the early stage of 4NQO-induced carcinogenesis in male mice (Scheff et al., 2018). In the current study, we tested whether recruitment of neutrophils could be used to reverse oral SCC-induced nociception in female mice. We demonstrate sex-dependent endogenous anti-nociception *via* rG-CSF mediated neutrophil infiltration for the treatment of oral cancer pain.

We report a mechanism to explain the sex difference in oral cancer pain. Sex differences in endogenous anti-nociception may depend on hormonal regulation. Liu and Gintzler (2013) demonstrated spinal mu opioid receptor-mediated anti-nociception depends on circulating estrogen levels. Mogil et al. (1993) find that estrogen contributes to sex-dependent efficacy of naloxone during swim stress-induced analgesia. However, the molecular targets for estrogen in the peripheral nervous system relevant to opioid anti-nociception in oral cancer are not yet defined. Our previous clinical findings of increased cancer pain in females [mean age = 64.5 ± 14.4 (SD) years; Scheff et al., 2018] are consistent with results by Reyes-Gibby et al. (2014) who show that women with oral cancer report more pain than men across 2,340 subjects [mean age = 59 ± 11.7 (SD) years]; these reports demonstrate that postmenopausal women experience significant oral cancer pain suggesting that that mechanisms beyond the estrous cycle contribute to differences in oral cancer pain in men and women.

The underlying cause of the sex difference in neutrophil infiltration remains unidentified; however, gonadal hormones can regulate neutrophils. Estrogen affects the number of circulating neutrophils and neutrophil lifespan (Bouman et al., 2005). Studies using injury and burn rodent models report that testosterone potentiates, whereas estrogen limits calcium mobilization in neutrophils (Deitch et al., 2006). We did not find a sex difference in the number of neutrophils in the blood following rG-CSF treatment in naïve mice. This finding is in contrast to clinical findings in healthy volunteers; Schoergenhofer et al. (2017) identified more plasma neutrophil histone-complexed DNA in the men compared to women after a single of rG-CSF. Consistent with our previous reports in the 4NQO model (Scheff et al., 2018), there is a sex difference in neutrophil infiltration in saline-treated mice with HSC-3 tumors. We also report a sex difference in the efficacy of rG-CSF treatment to drive $Ly6G^+$ neutrophil infiltration into the HSC-3 tumor. Chronic rG-CSF treatment in male mice did not increase neutrophil infiltration compared to saline treatment; however, in tumor-bearing female mice, chronic rG-CSF treatment resulted in $Ly6G^+$ neutrophil count similar to that found in saline-treated male mice with HSC-3 tumors. One possibility is that maximum neutrophil infiltration has been reached in tumor-bearing male mice and additional recruitment by way of rG-CSF is not physiological. Orofacial nociceptive behavior in saline-treated male mice and rG-CSF-treated female mice with HSC-3 tumors is similar suggesting comparable neutrophil-mediated endogenous anti-nociception present in the cancer microenvironment.

Clinical and preclinical data support the role of rG-CSF for anti-nociception (Brack et al., 2004a; Chao et al., 2012; Ozkaraman et al., 2017). Administration of rG-CSF increases neutrophil count to treat chemotherapy- or radiation-induced neutropenia in patients (Zeidler et al., 2003). In a chronic constriction injury rat model, neutrophils recruited to the site of inflammation following rG-CSF treatment release opioids

and alleviate thermal hyperalgesia and mechanical allodynia (Chao et al., 2012). We find that a single rG-CSF treatment produces a significant decrease in nociceptive behavior in response to oral cancer supernatant in both male and female mice. Local naloxone restored supernatant-evoked nociceptive behavior in the presence of rG-CSF. We infer from this result that infiltrating $Ly6G^+$ neutrophils in response to rG-CSF treatment are a source of opioid-mediated anti-nociception. Neutrophils secrete opioids in response to inflammatory mediators (Schafer et al., 1994; Rittner et al., 2006; Iwaszkiewicz et al., 2013; e.g., corticotropin-releasing factor, interleukin-1β, and CXCL8) and sympathetic neurotransmitter, norepinephrine (Binder et al., 2004). We find that tumor-bearing female mice treated with rG-CSF have more β-endorphin protein in the tongue tissue compared to tumor-bearing female mice treated with saline. These findings are consistent with Liou et al. (2011) who reported that rG-CSF administered subcutaneously increased opioid content in the injured nerve up to 14 days after partial sciatic nerve injury. Administration of rG-CSF did not affect nociceptive behavior in naïve animals suggesting that neutrophils do not secrete large amounts of opioids in normal circulation.

There are three limitations to our experimental approach. First, we did not investigate and compare opioid receptor expression in male and female mice during oral carcinogenesis in the peripheral nervous system. Endogenous opioids bind to μ- (MOR), δ- (DOR), and κ-opioid receptor (KOR; Kieffer and Evans, 2009). Sexual dimorphism in opioid receptor density is present in the peripheral nervous system; inflammation induced by cytokines or complete Freud's adjuvant generated significant upregulation of MOR expression in the trigeminal ganglia of male but not female rats (Zhang et al., 2014). A second limitation in our study is the lack of further characterization of neutrophils induced by rG-CSF treatment. Neutrophils in the tumor microenvironment can have a pro-tumor (N2) phenotype capable of supporting tumor growth (Uribe-Querol and Rosales, 2015); depletion of N2 neutrophils decreased lung tumor growth (Fridlender et al., 2009). We find that male mice treated with rG-CSF have larger tumors compared to female mice treated with rG-CSF, despite comparable $Ly6G^+$ neutrophil presence in the tongue. Further classification of the rG-CSF-induced tumor-associated neutrophils is necessary to understand the implications of increased neutrophil presence in the oral cancer microenvironment. The third limitation of our work is we did not assess the possible side effects of rG-CSF treatment. G-CSF receptors are broadly expressed on sensory and sympathetic neurons and may modulate tumor-nerve interactions (Schweizerhof et al., 2009; Lambertini et al., 2014; Dobrenis et al., 2015).

Our experimental findings reveal that rG-CSF treatment could hold promise as a future therapeutic approach to oral cancer pain. Our results demonstrated that rG-CSF treatment increases oral cancer-mediated neutrophil infiltration and attenuates oral cancer nociceptive behavior in mouse models. Our results also corroborate sex differences in oral cancer nociceptive behavior and in neutrophil infiltration in the oral cancer microenvironment. We infer from our results that female patients might benefit more from rG-CSF administration because females have fewer neutrophils infiltrating the cancer microenvironment than males.

DATA AVAILABILITY

All datasets generated for this study are included in the manuscript.

ETHICS STATEMENT

The animal study was reviewed and approved by New York University Institutional Animal Care and Use Committee.

AUTHOR CONTRIBUTIONS

All authors listed contributed substantially to the work. NS designed the research, conducted the experiments, performed data analyses, and wrote the manuscript. RA conducted the experiments, performed data analyses, and wrote the manuscript. IW and SY conducted animal behavior and molecular experiments, respectively and performed data analyses. RK provided technical support and data collection. JD provided animal behavior expertise, technical support and edited the manuscript. BS assisted in research design and writing of the manuscript.

FUNDING

This work was supported by the National Institute of Dental and Craniofacial Research through individual investigator grant F32 DE027269 (NS) and grant R01 DE025393 (BS), the primary and senior author, respectively. We acknowledge the cell sorting technologies provided by NYU Langone's Cytometry and Cell Sorting Laboratory that is supported in part by NIH/NCI P30CA016087.

ACKNOWLEDGMENTS

We thank Dr. David Levy and the New York University College of Dentistry Flow Cytometry Facility for their technical contributions.

REFERENCES

Binder, W., Mousa, S. A., Sitte, N., Kaiser, M., Stein, C., and Schafer, M. (2004). Sympathetic activation triggers endogenous opioid release and analgesia within peripheral inflamed tissue. *Eur. J. Neurosci.* 20, 92–100. doi: 10.1111/j.1460-9568.2004.03459.x

Bjordal, K., Ahlner-Elmqvist, M., Hammerlid, E., Boysen, M., Evensen, J. F., Biorklund, A., et al. (2001). A prospective study of quality of life in head and

neck cancer patients. Part II: Longitudinal data. *Laryngoscope.* 111, 1440–1452. doi: 10.1097/00005537-200108000-00022

Bouman, A., Heineman, M. J., and Faas, M. M. (2005). Sex hormones and the immune response in humans. *Hum. Reprod. Update* 11, 411–423. doi: 10.1093/humupd/dmi008

Brack, A., Rittner, H. L., Machelska, H., Beschmann, K., Sitte, N., Schafer, M., et al. (2004a). Mobilization of opioid-containing polymorphonuclear cells by hematopoietic growth factors and influence on inflammatory pain. *Anesthesiology* 100, 149–157. doi: 10.1097/00000542-200401000-00024

Brack, A., Rittner, H. L., Machelska, H., Leder, K., Mousa, S. A., Schafer, M., et al. (2004b). Control of inflammatory pain by chemokine-mediated recruitment of opioid-containing polymorphonuclear cells. *Pain* 112, 229–238. doi: 10.1016/j.pain.2004.08.029

Chao, P.-K., Lu, K.-T., Lee, Y.-L., Chen, J.-C., Wang, H.-L., Yang, Y.-L., et al. (2012). Early systemic granulocyte-colony stimulating factor treatment attenuates neuropathic pain after peripheral nerve injury. *PLoS One* 7:e43680. doi: 10.1371/journal.pone.0043680

Chodroff, L., Bendele, M., Valenzuela, V., Henry, M., and Ruparel, S. (2016). BDNF signaling contributes to oral cancer pain in a preclinical orthotopic rodent model. *Mol. Pain* 12:1744806916666841. doi: 10.1177/1744806916666841

Dale, D. C. (2002). Colony-stimulating factors for the management of neutropenia in cancer patients. *Drugs* 62 (Suppl 1), 1–15. doi: 10.2165/00003495-200262001-00001

Deitch, E. A., Feketeova, E., Adams, J. M., Forsythe, R. M., Xu, D. Z., Itagaki, K., et al. (2006). Lymph from a primate baboon trauma hemorrhagic shock model activates human neutrophils. *Shock* 25, 460–463. doi: 10.1097/01.shk.0000209551.88215.1e

Demetri, G. D., and Griffin, J. D. (1991). Granulocyte colony-stimulating factor and its receptor. *Blood* 78, 2791–2808.

Dobrenis, K., Gauthier, L. R., Barroca, V., and Magnon, C. (2015). Granulocyte colony-stimulating factor off-target effect on nerve outgrowth promotes prostate cancer development. *Int. J. Cancer* 136, 982–988. doi: 10.1002/ijc.29046

Dolan, J. C., Lam, D. K., Achdjian, S. H., and Schmidt, B. L. (2010). The dolognawmeter: a novel instrument and assay to quantify nociception in rodent models of orofacial pain. *J. Neurosci. Methods* 187, 207–215. doi: 10.1016/j.jneumeth.2010.01.012

Fridlender, Z. G., Sun, J., Kim, S., Kapoor, V., Cheng, G., Ling, L., et al. (2009). Polarization of tumor-associated neutrophil phenotype by TGF-beta: "N1" versus "N2" TAN. *Cancer Cell* 16, 183–194. doi: 10.3410/f.1164910.625745

Hayashi, E., Rikimaru, K., and Nagayama, M. (1995). Simultaneous production of G- and M-CSF by an oral cancer cell line and the synergistic effects on associated leucocytosis. *Eur. J. Cancer B. Oral Oncol.* 31, 323–327. doi: 10.1016/0964-1955(95)00038-0

Hua, S., and Cabot, P. J. (2010). Mechanisms of peripheral immune-cell-mediated analgesia in inflammation: clinical and therapeutic implications. *Trends Pharmacol. Sci.* 31, 427–433. doi: 10.1016/j.tips.2010.05.008

Iwaszkiewicz, K. S., Schneider, J. J., and Hua, S. (2013). Targeting peripheral opioid receptors to promote analgesic and anti-inflammatory actions. *Front. Pharmacol.* 4:132. doi: 10.3389/fphar.2013.00132

Kapitzke, D., Vetter, I., and Cabot, P. J. (2005). Endogenous opioid analgesia in peripheral tissues and the clinical implications for pain control. *Ther. Clin. Risk Manag.* 1, 279–297.

Khodorova, A., Navarro, B., Jouaville, L. S., Murphy, J. E., Rice, F. L., Mazurkiewicz, J. E., et al. (2003). Endothelin-B receptor activation triggers an endogenous analgesic cascade at sites of peripheral injury. *Nat. Med.* 9, 1055–1061. doi: 10.1038/nm885

Kieffer, B. L., and Evans, C. J. (2009). Opioid receptors: from binding sites to visible molecules *in vivo*. *Neuropharm* 56 , 205–212. doi: 10.1016/j.neuropharm.2008.07.033

King, T., Vera-Portocarrero, L., Gutierrez, T., Vanderah, T. W., Dussor, G., Lai, J., et al. (2009). Unmasking the tonic-aversive state in neuropathic pain. *Nat. Neurosci.* 12, 1364–1366. doi: 10.1038/nn.2407

Lambertini, M., Del Mastro, L., Bellodi, A., and Pronzato, P. (2014). The five "Ws" for bone pain due to the administration of granulocyte-colony stimulating factors (G-CSFs). *Crit. Rev. Oncol. Hematol.* 89, 112–128. doi: 10.1016/j.critrevonc.2013.08.006

Lee, C. H., Lin, S. H., Chang, S. F., Chang, P. Y., Yang, Z. P., and Lu, S. C. (2013). Extracellular signal-regulated kinase 2 mediates the expression of granulocyte colony-stimulating factor in invasive cancer cells. *Oncol. Rep.* 30, 419–424. doi: 10.3892/or.2013.2463

Liou, J. T., Lui, P. W., Liu, F. C., Lai, Y. S., and Day, Y. J. (2011). Exogenous granulocyte colony-stimulating factor exacerbate pain-related behaviors after peripheral nerve injury. *J. Neuroimmunol.* 232, 83–93. doi: 10.1016/j.jneuroim.2010.10.014

Liu, N. J., and Gintzler, A. R. (2013). Spinal endomorphin 2 antinociception and the mechanisms that produce it are both sex- and stage of estrus cycle-dependent in rats. *J. Pain.* 14, 1522–1530. doi: 10.1016/j.jpain.2013.09.002

Matsuo, K., Ishibashi, Y., Kobayashi, I., Ozeki, S., Ohishi, M., Tange, T., et al. (1994). New human oral squamous carcinoma cell line and its tumorigenic subline producing granulocyte colony-stimulating factor. *Jpn. J. Cancer Res.* 85, 1257–1262. doi: 10.1111/j.1349-7006.1994.tb02938.x

Mogil, J. S., Sternberg, W. F., Kest, B., Marek, P., and Liebeskind, J. C. (1993). Sex differences in the antagonism of swim stress-induced analgesia: effects of gonadectomy and estrogen replacement. *Pain* 53, 17–25. doi: 10.1016/0304-3959(93)90050-y

Mousa, S. A., Straub, R. H., Schäfer, M., and Stein, C. (2007). β-Endorphin, Met-enkephalin and corresponding opioid receptors within synovium of patients with joint trauma, osteoarthritis and rheumatoid arthritis. *Ann. Rheum. Dis.* 66, 871–879.

Ozkaraman, A., Argon, G., Usta Yesilbalkan, O., Dugum, O., Yigitaslan, S., Musmul, A., et al. (2017). Effects of granulocyte colony-stimulating factor administration time on pain. *Bratisl. Lek. Listy* 118, 399–404. doi: 10.4149/BLL_2017_078

Reyes-Gibby, C. C., Anderson, K. O., Merriman, K. W., Todd, K. H., Shete, S. S., and Hanna, E. Y. (2014). Survival patterns in squamous cell carcinoma of the head and neck: pain as an independent prognostic factor for survival. *J. Pain* 15, 1015–1022. doi: 10.1016/j.jpain.2014.07.003

Rittner, H. L., Brack, A., Machelska, H., Mousa, S. A., Bauer, M., Schafer, M., et al. (2001). Opioid peptide-expressing leukocytes: identification, recruitment and simultaneously increasing inhibition of inflammatory pain. *Anesthesiology* 95, 500–508. doi: 10.1097/00000542-200108000-00036

Rittner, H. L., Labuz, D., Schaefer, M., Mousa, S. A., Schulz, S., Schafer, M., et al. (2006). Pain control by CXCR2 ligands through Ca^{2+}-regulated release of opioid peptides from polymorphonuclear cells. *FASEB J.* 20, 2627–2629. doi: 10.1096/fj.06-6077fje

Schafer, M., Carter, L., and Stein, C. (1994). Interleukin 1 beta and corticotropin-releasing factor inhibit pain by releasing opioids from immune cells in inflamed tissue. *Proc. Natl. Acad. Sci. U S A* 91, 4219–4223. doi: 10.1073/pnas.91.10.4219

Scheff, N. N., Bhattacharya, A., Dowse, E., Dang, R. X., Dolan, J. C., Wang, S., et al. (2018). Neutrophil-mediated endogenous analgesia contributes to sex differences in oral cancer pain. *Front. Integr. Neurosci.* 12:52. doi: 10.3389/fnint.2018.00052

Scheff, N. N., Ye, Y., Bhattacharya, A., MacRae, J., Hickman, D. N., Sharma, A. K., et al. (2017). Tumor necrosis factor alpha secreted from oral squamous cell carcinoma contributes to cancer pain and associated inflammation. *Pain* 158, 2396–2409. doi: 10.1097/j.pain.0000000000001044

Schoergenhofer, C., Schwameis, M., Wohlfarth, P., Brostjan, C., Abrams, S. T., Toh, C. H., et al. (2017). Granulocyte colony-stimulating factor (G-CSF) increases histone-complexed DNA plasma levels in healthy volunteers. *Clin. Exp. Med.* 17, 243–249. doi: 10.1007/s10238-016-0413-6

Schweizerhof, M., Stosser, S., Kurejova, M., Njoo, C., Gangadharan, V., Agarwal, N., et al. (2009). Hematopoietic colony-stimulating factors mediate tumor-nerve interactions and bone cancer pain. *Nat. Med.* 15, 802–807. doi: 10.3410/f.1164181.624868

Slominski, A. T., Zmijewski, M. A., Zbytek, B., Brozyna, A. A., Granese, J., Pisarchik, A., et al. (2011). Regulated proenkephalin expression in human skin and cultured skin cells. *J. Invest. Dermatol.* 131, 613–622. doi: 10.1038/jid.2010.376

Smith, E. M. (2003). Opioid peptides in immune cells. *Adv. Exp. Med. Biol.* 521, 51–68.

Stein, C., Comisel, K., Haimerl, E., Yassouridis, A., Lehrberger, K., Herz, A., et al. (1991). Analgesic effect of intraarticular morphine after arthroscopic knee surgery. *N. Engl. J. Med.* 325, 1123–1126. doi: 10.1056/NEJM199110173251602

Stein, C., Hassan, A. H., Przewlocki, R., Gramsch, C., Peter, K., and Herz, A. (1990). Opioids from immunocytes interact with receptors on sensory nerves to inhibit nociception in inflammation. *Proc. Natl. Acad. Sci. U S A* 87, 5935–5939. doi: 10.1073/pnas.87.15.5935

Stein, C., Schäfer, M., and Machelska, H. (2003). Attacking pain at its source: new perspectives on opioids. *Nat. Med.* 9, 1003–1008. doi: 10.1038/nm908

Uribe-Querol, E., and Rosales, C. (2015). Neutrophils in cancer: two sides of the same coin. *J. Immunol. Res.* 2015:983698. doi: 10.4172/2161-0436.1000e110

Wang, N., Feng, Y., Wang, Q., Liu, S., Xiang, L., Sun, M., et al. (2014). Neutrophils infiltration in the tongue squamous cell carcinoma and its correlation with CEACAM1 expression on tumor cells. *PLoS One* 9:e89991. doi: 10.1371/journal.pone.0089991

Ye, Y., Scheff, N. N., Bernabe, D., Salvo, E., Ono, K., Liu, C., et al. (2018). Anti-cancer and analgesic effects of resolvin D2 in oral squamous cell carcinoma. *Neuropharmacology* 139, 182–193. doi: 10.1016/j.neuropharm.2018.07.016

Zeidler, C., Schwinzer, B., and Welte, K. (2003). Congenital neutropenias. *Rev. Clin. Exp. Hematol.* 7, 72–83.

Zhang, X., Zhang, Y., Asgar, J., Niu, K. Y., Lee, J., Lee, K. S., et al. (2014). Sex differences in μ-opioid receptor expression in trigeminal ganglia under a myositis condition in rats. *Eur. J. Pain* 18, 151–161. doi: 10.1002/j.1532-2149.2013.00352.x

Conflict of Interest Statement: JD fabricates dolognawmeter assays for profit as the single-member limited liability company Gnatheon Scientific.

The remaining authors declare that the research was conducted in the absence of any commercial or financial relationships that could be construed as a potential conflict of interest.

frontiers in Molecular Neuroscience

ORIGINAL RESEARCH
published: 20 September 2019
doi: 10.3389/fnmol.2019.00220

TIMP-1 Attenuates the Development of Inflammatory Pain Through MMP-Dependent and Receptor-Mediated Cell Signaling Mechanisms

Brittany E. Knight[1], Nathan Kozlowski[2], Joshua Havelin[3,4], Tamara King[3,4,5], Stephen J. Crocker[1,6], Erin E. Young[2,6,7,8†] and Kyle M. Baumbauer[1,2,6,7,9†]*

[1] Department of Neuroscience, UConn Health, Farmington, CT, United States, [2] School of Nursing, University of Connecticut, Storrs, CT, United States, [3] Center for Excellence in the Neurosciences, University of New England, Biddeford, ME, United States, [4] Graduate School of Biomedical Science and Engineering, University of Maine, Orono, ME, United States, [5] College of Osteopathic Medicine, University of New England, Biddeford, ME, United States, [6] Institute for Systems Genomics, UConn Health, Farmington, CT, United States, [7] The Center for Advancement in Managing Pain, School of Nursing, University of Connecticut, Storrs, CT, United States, [8] Genetics and Genome Sciences, UConn Health, Farmington, CT, United States, [9] Rita Allen Foundation, Princeton, NJ, United States

Unresolved inflammation is a significant predictor for developing chronic pain, and targeting the mechanisms underlying inflammation offers opportunities for therapeutic intervention. During inflammation, matrix metalloproteinase (MMP) activity contributes to tissue remodeling and inflammatory signaling, and is regulated by tissue inhibitors of metalloproteinases (TIMPs). TIMP-1 and -2 have known roles in pain, but only in the context of MMP inhibition. However, TIMP-1 also has receptor-mediated cell signaling functions that are not well understood. Here, we examined how TIMP-1-dependent cell signaling impacts inflammatory hypersensitivity and ongoing pain. We found that hindpaw injection of complete Freund's adjuvant (CFA) increased cutaneous TIMP-1 expression that peaked prior to development of mechanical hypersensitivity, suggesting that TIMP-1 inhibits the development of inflammatory hypersensitivity. To examine this possibility, we injected TIMP-1 knockout (T1KO) mice with CFA and found that T1KO mice exhibited rapid onset thermal and mechanical hypersensitivity at the site of inflammation that was absent or attenuated in WT controls. We also found that T1KO mice exhibited hypersensitivity in adjacent tissues innervated by different sets of afferents, as well as skin contralateral to the site of inflammation. Replacement of recombinant murine (rm)TIMP-1 alleviated hypersensitivity when administered at the site and time of inflammation. Administration of either the MMP inhibiting N-terminal or the cell signaling C-terminal domains recapitulated the antinociceptive effect of full-length rmTIMP-1, suggesting that rmTIMP-1inhibits hypersensitivity through MMP inhibition and receptor-mediated cell signaling. We also found that hypersensitivity was not due to genotype-specific differences in MMP-9 activity or expression, nor to differences in

OPEN ACCESS

Edited by:
John Michael Streicher, University of Arizona, United States

Reviewed by:
Peter Grace, University of Texas MD Anderson Cancer Center, United States
Wei Lei, Presbyterian College, United States
Michael D. Burton, The University of Texas at Dallas, United States

***Correspondence:**
Kyle M. Baumbauer
kbaumbauer@kumc.edu

†Present address:
Erin E. Young, Department of Anesthesiology and Department of Anatomy and Cell Biology, University of Kansas Medical Center, Kansas City, KS, United States
Kyle M. Baumbauer, Department of Anatomy and Cell Biology and Department of Anesthesiology, University of Kansas Medical Center, Kansas City, KS, United States

Received: *01 June 2019*
Accepted: *30 August 2019*
Published: *20 September 2019*

Citation:
Knight BE, Kozlowski N, Havelin J, King T, Crocker SJ, Young EE and Baumbauer KM (2019) TIMP-1 Attenuates the Development of Inflammatory Pain Through MMP-Dependent and Receptor-Mediated Cell Signaling Mechanisms. Front. Mol. Neurosci. 12:220. doi: 10.3389/fnmol.2019.00220

cytokine expression. Administration of rmTIMP-1 prevented mechanical hypersensitivity and ongoing pain in WT mice, collectively suggesting a novel role for TIMP-1 in the attenuation of inflammatory pain.

Keywords: pain, thermal hyperalgesia, mechanical hypersensitivity, ongoing pain, matrix metalloproteinase, conditioned place preference

INTRODUCTION

Tissue inhibitors of matrix metalloproteinases (TIMPs) and matrix metalloproteinases (MMPs) are released during tissue damage to facilitate tissue remodeling through degradation and reorganization of the extracellular matrix (ECM) (Gardner and Ghorpade, 2003; Nagase et al., 2006; Ries, 2014). During this process MMPs also engage an inflammatory response through proteolytic maturation of cytokines, and both of these activities are regulated through a 1:1 stoichiometric interaction with one of four tissue inhibitors of metalloproteinases (TIMP-1, -2, -3, -4) (Huang et al., 2011). The interaction between MMPs and TIMPs is tightly controlled, but research has shown that during tissue damage, imbalance between MMPs and TIMPs can lead to pathological conditions such as arthritis, multiple sclerosis, Parkinson's Disease, cancer, and even chronic pain (Nakagawa et al., 1994; Nagase et al., 1999; Kouwenhoven et al., 2001; Yang et al., 2002; Brew and Nagase, 2010). Studies examining the role of MMPs in pain specifically have shown that increased MMP-2 and -9 activity contribute to increased pain-related behavior in response to injury that can be reversed by MMP antagonism (Kawasaki et al., 2008; Ji et al., 2009; Li et al., 2016; Remacle et al., 2018). These findings contributed, in part, to the development of several small molecule drugs that directly target and inhibit MMP activity. However, more than 50 clinical trials examining the efficacy of these drugs were discontinued due to the emergence of adverse events, including musculoskeletal pain (Cathcart and Cao, 2015; Martinho et al., 2016). While the results of these trials indicated that specific targeting of MMP activity alone is not an effective strategy for pain treatment, they also suggest that additional mechanisms related to MMP activity may contribute to pain and its inhibition, and that endogenous inhibitors of MMPs, such as TIMP-1, may attenuate pain-related behavior.

TIMP-1 is best characterized as an inhibitor of MMP activity. Indeed, TIMP-1 regulates 14 of the 24 known MMPs (Baker et al., 2002; Gardner and Ghorpade, 2003; Nagase et al., 2006; Kawasaki et al., 2008), and has been shown to prevent the development of mechanical and thermal hypersensitivity following nerve damage (Kawasaki et al., 2008; Martinho et al., 2016). However, this identified role was characterized purely in the context of MMP inhibition. TIMP-1 inhibits MMP activity through the binding of its N-terminus with the targeted MMP, resulting in chelation of Zn^{2+} from the enzyme active site (Gomis-Rüth et al., 1997). Interestingly, there is now mounting evidence that the C-terminal domain can bind to membrane bound receptors, including CD63 (Nagase et al., 2006). The binding of TIMP-1 to CD63 engages intracellular signaling events that allow TIMP-1 to function as a trophic factor and initiate cellular migration and differentiation (Gardner and Ghorpade, 2003; Jourquin et al., 2005; Thorne et al., 2009; Moore and Crocker, 2012; Claycomb et al., 2013). Because TIMP-1 and MMPs can be up-regulated simultaneously during tissue damage and repair, such as in peripheral nerve injury (Parkitna et al., 2006; Huang et al., 2011; Kim et al., 2012; Yokose et al., 2012), disentangling how TIMP-1 regulates tissue remodeling/repair from the induction of pain, *per se*, is challenging.

Inflammation is a core component of the nerve injury process (Tracey and Walker, 1995), and, in general, is a significant predictor of pain chronicity (Tal, 1999; Kehlet et al., 2006; Chapman and Vierck, 2017). Therefore, we used a model of cutaneous inflammation to examine the effects of TIMP-1 signaling on pain in the absence of frank tissue damage. We found that hindpaw injection of complete Freund's adjuvant (CFA) induced TIMP-1 expression in keratinocytes prior to the emergence of hypersensitivity in wildtype (WT) mice. Behavioral assessment of the role of TIMP-1 in inflammatory hypersensitivity demonstrated that TIMP-1 knockout (T1KO) mice exhibited robust hypersensitivity to stimulation of tissues local and distal to the site of inflammation that was prevented by administration of full length and truncated constructs of recombinant murine (rm)TIMP-1. These results also suggested that cell-signaling mechanisms may also contribute to the antinociceptive effects of TIMP-1. Finally, we found that the administration of rmTIMP-1 prevented ongoing inflammatory pain and evoked mechanical hypersensitivity in WT mice, collectively suggesting that TIMP-1 regulates the algogenic properties of inflammation and that TIMP-1 may be a target for improving pain management.

MATERIALS AND METHODS

Animals

Experiments were conducted using 8–12-week-old (20–30 g) male WT (C57BL/6; Jackson Laboratories, Bar Harbor, ME) and T1KO mice that were group housed (4 mice/cage), and maintained in a temperature-controlled environment on a 12 h light-dark cycle with free access to food and water. TIMP-1 knockout (T1KO) mice (Lee et al., 2005) were backcrossed onto a C57BL/6 background for greater than 13 successive generations and bred in-house as a homozygous line (Crocker et al., 2006). All studies were approved by the UConn Health Institutional Animal Care and Use Committee and treated in accordance with published NIH standards.

Complete Freund's Adjuvant (CFA)

To produce an acute, local inflammatory response, we subcutaneously (s.c.) injected the right hindpaw of mice with a diluted emulsion of CFA (1:1 in sterile H_2O; 10 μL vol; Sigma, St. Louis, MO). To assess primary hypersensitivity (i.e., at the site of inflammation) we administered CFA into the glabrous skin or ventral surface of the right hindpaw. Conversely, secondary hypersensitivity was assessed in hairy skin that was adjacent or contralateral to the site of inflammation. All samples were compared to naïve controls because in a pilot experiment we found that vehicle injection alone caused increased sensitivity in T1KO mice (**Supplementary Figure S1**). While this result is interesting and suggests that subtle perturbations cause robust alterations in sensory thresholds, adding saline-treated mice confounds our ability to examine inflammatory hypersensitivity. Therefore, to interpret the effects of inflammation *per se*, naïve mice were used as comparison controls. The literature is also mixed on the use of vehicle controls in experiments using CFA, and our experiments are in line with previously published work (Allchorne et al., 2005; Jankowski et al., 2012; Imbe and Kimura, 2017).

Recombinant Murine TIMP-1 Administration

WT and T1KO mice received injections (s.c.) of recombinant murine (rm)TIMP-1 (10 ng/μL, 10 μL; R&D Systems; Minneapolis, MN) immediately following CFA injection (10 μL) into the right hindpaw. In subsequent experiments, T1KO mice received equimolar concentrations of the truncated C-terminus peptide (TIMP-1(C); 6.3 kDa; Peptide 2.0 Inc., Chantilly, VA) that retains cell signaling function or the truncated N-terminus peptide (TIMP-1(N); 20 kDa; Abcam, Cambridge, United Kingdom) that retains MMP-inhibitory function and no cell-signaling ability, immediately following CFA injection.

von Frey Testing

All mice were place into transparent Plexiglas chambers (radius = 32 mm, height = 108 mm) on an elevated mesh screen and were allowed to acclimate for a minimum of 1 h before testing. To assess mechanical sensitivity, the plantar surface of the right hindpaw was stimulated using von Frey filaments using the up-down method previously described (Dixon, 1980). Nocifensive responses were counted as robust flexion responses, paw shaking, or paw licking and subtracted from individual baseline threshold to account for inter-subject variability. Data are presented as paw withdrawal thresholds (PWT; in grams).

Thermal Hyperalgesia

Thermal hyperalgesia to radiant heat was assessed using a Hargreaves apparatus (Harvard Apparatus; Holliston, MA) (Hargreaves et al., 1988). Briefly, all mice were placed in transparent Plexiglas chambers (radius = 32 mm, height = 108 mm) on top of a framed glass panel and were allowed to acclimate for a minimum of 1 h before testing. Following the acclimation period, an infrared (IR) beam was aimed at the plantar surface of each hindpaw in an alternating fashion. The intensity of the IR beam was chosen to produce average baseline paw withdrawal latency (PWL) of 15–20 s. Stimuli were presented 5 times in an alternating fashion between each hindpaw with 5 min intervals between successive stimulus exposures. A 30 s exposure cutoff was employed to prevent tissue damage. PWLs collected from each paw were then averaged and analyzed.

Conditioned Place Preference

Conditioned Place Preference (CPP) was used to assess ongoing pain in WT mice. A 3-day single trial protocol was used. On day 1, all mice freely explored a 3-chamber CPP box for 15 min prior to injection with CFA or saline. Preconditioning (baseline) behavior was analyzed using automated software (ANYMAZE, Stoelting) to ensure there were no baseline differences in the time spent in any of the chambers. On day 2 (conditioning day), all mice received an intrathecal (i.t.) injection of saline (5 μL volume) under isoflurane anesthesia and upon waking (within 2 min) were confined into the pre-assigned pairing chamber for 30 min. They were then returned to their home-cages for 4 hr. All mice then received an intrathecal (i.t.) injection of clonidine (2 μg/μL; 5 μL volume) through lumbar puncture and upon waking were confined to the opposite pairing chamber for 30 min. Vehicle and clonidine paired chambers were randomly assigned and counterbalanced between animals. On day 3 (test day), mice were returned to the CPP apparatus and allowed to freely explore all chambers across 15 min. The total time spent in each chamber was assessed using automated software (ANYMAZE). Conditioning day was 20–24 h following CFA injection as previous research indicates ongoing pain is observed at this time-point (Okun et al., 2011; He et al., 2012). A total of 17 mice were used, 8 were treated with rTIMP-1 and 9 with vehicle.

Tissue Collection

Mice were anesthetized with a lethal dose of ketamine and xylazine mixture (90/10 mg/kg, respectively) and intracardially perfused with ice cold 0.9% saline prior to the dissection and collection of tissues. Tissues were collected following the completion of behavior or at designated time-points for molecular analysis.

Enzyme-Linked Immunosorbent Assay

Protein was extracted from L2-L3 spinal cord, DRG and hairy skin and homogenized in ice-cold RIPA buffer/protease inhibitor cocktail and spun for 20 min at 4°C at 18,000 rcf. L2-L3 DRG were collected for analysis because axons from these DRG comprise the saphenous nerve, which innervates the hairy skin of the hindpaw, the site of CFA injection (McIlwrath et al., 2007; Lawson et al., 2008; Jankowski et al., 2009; Zimmermann et al., 2009; Vrontou et al., 2013; Laedermann et al., 2014). Each sample's total protein concentration was determined using Pierce BCA Protein Assay Kit (Thermo Fisher Scientific, Waltham, MA). The following Enzyme-Linked Immunosorbent Assay (ELISAs), TIMP-1 (R&D Systems, Minneapolis, MN), MMP-9 (R&D Systems; Minneapolis, MN), IL-6 (Invitrogen Carlsbad, CA), TNF-α (Thermo Fisher Scientific, Waltham,

MA), IL-10 (Thermo Fisher Scientific, Waltham, MA), and IL-1β (R&D Systems, Minneapolis, MN) were run according to manufacturer's instructions. All samples were run in duplicate and absorbance ratios were read at 450 nm.

Immunohistochemistry

Hairy skin, glabrous skin, and DRG from WT mice were excised and incubated in 0.06% brefeldin A (BFA) in serum free Hank's balanced salt solution (HBSS) for 20 min at room temperature. Half of the samples were incubated in inflammatory soup (IS) (10uM; bradykinin triacetate, histamine dihydrochloride, serotonin hydrochloride, prostaglandin E2 dissolved in normal cerebral spinal fluid, pH 6.0) or serum-free media (Kessler et al., 1992; Hachisuka et al., 2016). Incubation in IS or serum-free media occurred for 24 h (Kessler et al., 1992). Spinal cords from inflamed or naïve WT mice were isolated 24 h following CFA treatment or from designated naïve controls. Prior to tissue collection, mice were intracardially perfused with 0.06% BFA in 0.9% saline for 20 min and then perfused with 4% paraformaldehyde. All samples were post-fixed overnight in 4% paraformaldehyde (PFA), cryoprotected overnight in 30% sucrose, and later embedded in Optimal Cutting Temperature (OCT). Samples were cut into 30 μm cross sections using a cryostat. Tissue sections were briefly washed with sterile phosphate buffered saline (PBS) and incubated with staining buffer (0.05% triton and 30% fetal bovine serum in PBS) solution for 40 min at room temperature. Slices were then incubated with primary unconjugated antibodies for 48 h at 4°C. The following primary antibodies were diluted in staining buffer: monoclonal anti-mouse cytokeratin 14 (K14; Abcam, Cambridge, United Kingdom; 1:300 dilution), polyclonal anti-goat TIMP-1 (R&D Systems; Minneapolis, MN; 1:300 dilution), monoclonal anti-mouse microtubule-associated protein 2 (MAP2; Millipore Sigma, Burlington, MA; 1:1000 dilution), and monoclonal anti-mouse primary conjugated-cy3 glial fibrillary acidic protein (GFAP; Abcam, Cambridge, United Kingdom; 1:500 dilution). Tissue slices were then incubated with secondary antibodies for 2–3 h at 4°C. The following secondary antibodies were diluted in staining buffer: polyclonal rabbit anti-mouse Alexa-488 (Life Technologies, Carlsbad, CA, 1:000), polyclonal donkey anti-goat Alexa-568 (Life Technologies, Carlsbad, CA,1:000), and polyclonal goat anti-mouse Alexa-568 (Life Technologies, Carlsbad, CA; 1:1000 dilution). Slides with DRG and spinal cord slices were incubated with 300 μm DAPI prior to cover-slipping to visualize nuclei of satellite glial cells and astrocytes, respectively.

MMP-9 Colorimetric Activity

Protein was extracted from the hindpaw of WT and T1KO mice 1 day post-CFA injections (s.c., 10 μL) or from designated naïve controls for a high throughput screening of MMP-9 activity. Gelatinase activity was measured using the SensolyteGeneric MMP colorimetric assay kit (Anaspec, Fremont, CA) according to manufacturer's instructions. Samples were run in duplicate and end-point enzymatic activity was analyzed using a glutathione reference standard.

RT-qPCR

Total RNA was extracted from hairy skin collected from naïve and inflamed WT and T1KO mice 1 day following CFA injection using a RNeasy Mini Kit (Qiagen, Venlo, Netherlands). To quantify cutaneous TIMP-2 and TIMP-4 mRNA expression, equal amounts of cDNA were synthesized using the iScript cDNA Synthesis Kit (Bio-Rad Laboratories, Hercules, CA) and mixed with SsoAdvanced Universal SYBR Green Supermix (Bio-Rad Laboratories, Hercules, CA) and 2 μM of both forward and reverse primers (see **Table 1**). GAPDH was amplified as an internal control. The threshold crossing value was noted for each transcript and normalized to the internal control. The relative quantitation of each transcript was performed using the ΔΔCt method (Livak and Schmittgen, 2001) and presented as fold change relative to naïve WT expression.

Statistical Analysis

All data were analyzed using one-way or mixed designs Analysis of Variance (ANOVA). *Post hoc* analyses were performed using Tukey's HSD, and statistical significance was determined using a $p < 0.05$. Statistical analysis was performed using SPSS (Version 25). Since ANOVAs rely on linear relationships among data, and not all effects can be resolved using linear based statistical tests, we used trend analyses (e.g., contrasts) to test for significant non-linear relationships in some of our behavioral analyses. An added benefit of this approach is that trend analyses are more robust than ANOVAs (Tabachnick and Fidell, 2007). Clonidine induced CPP was assessed using a 2-way repeated measures ANOVA with *post hoc* analysis of pre- vs. post- conditioning time spent in the clonidine paired chamber for each treatment group using Sidak's multiple comparisons test. Between groups analysis was performed on difference scores calculated as post-conditioning (–) pre-conditioning time spent in the clonidine paired chamber.

RESULTS

Cutaneous TIMP-1 Expression Is Upregulated Prior to the Onset of Inflammatory Hypersensitivity

To determine whether cutaneous inflammation alters the expression of TIMP-1 in tissues along the peripheral sensory circuit, we injected diluted, emulsified CFA (10 μL, s.c.) into the

TABLE 1 | Primer sequences for qPCR.

Gene	Forward	Reverse
Timp2	5′-CCAGAAGAAGAGCCTG AACCA-3′	5′-GTCCATCCAGAGGCAC TCATC-3′
Timp4	5′-TGCAGAGGGAGAGC CTGAA-3′	5′-GGTACATGGCACTGC ATAGCA-3′
Gapdh	5′-ATGAATACGGCTACAGCA ACAGG-3′	5′-CTCTTGCTCAGTGTCCT TGCTG-3′

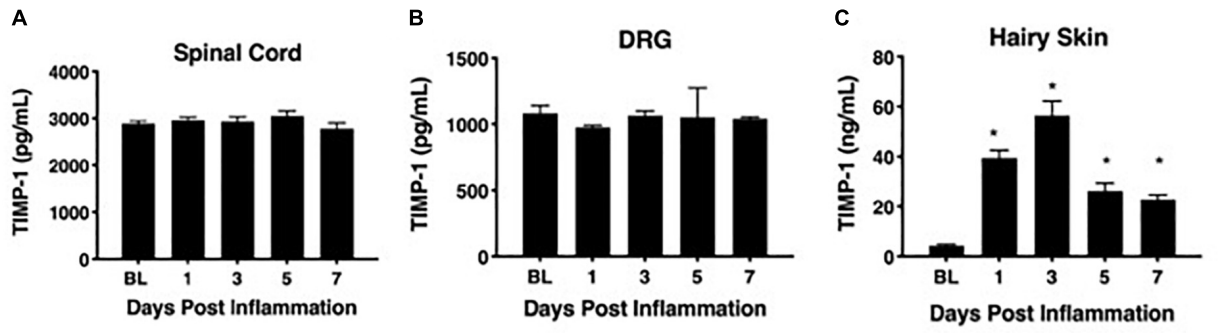

FIGURE 1 | Assessing TIMP-1 expression along peripheral nociceptive circuit following cutaneous inflammation. **(A)** Cutaneous inflammation does not alter overall TIMP-1 protein expression in lumbar spinal cord or **(B)** DRG, but does increase protein expression in panel **(C)** hairy skin. n = 4/condition, * indicate significant differences compared to naïve controls, $p < 0.05$, and error bars depict SEM.

hairy skin of the ipsilateral hindpaw and collected spinal cord (SC; L2-L3), dorsal root ganglia (DRG; L2-L3), and hairy skin over the course of 7 days. As described in section "Materials and Methods," L2-L3 DRG were collected for analysis because the axons projecting from these DRG form the saphenous nerve, which innervates hindpaw hairy skin (McIlwrath et al., 2007; Lawson et al., 2008; Jankowski et al., 2009; Zimmermann et al., 2009; Vrontou et al., 2013; Laedermann et al., 2014). We found that inflammation did not alter the overall expression of TIMP-1 protein in SC or DRG, all $Fs > 1.13$, $p > 0.05$ (**Figures 1A,B**). However, we observed a significant increase in cutaneous TIMP-1 protein 1, 3, 5, and 7 days following CFA administration, $F(4,19) = 37.54$, $p < 0.01$ (**Figure 1C**). To confirm the above results, and to localize the cellular source of TIMP-1 expression, immunohistochemistry (IHC) was performed on DRG and skin samples incubated *in vitro* with or without inflammatory soup (IS) (Kessler et al., 1992), as well as spinal cords following *in vivo* inflammation. Because TIMP-1 is a releasable protein and, consequently, difficult to image, we utilized *in vitro* incubation of DRG and skin with IS to enhance our ability to capture TIMP-1 colocalization with markers of other cell types. Although overall TIMP-1 expression levels were unaltered in the spinal cord and DRG following inflammation, we found that TIMP-1 co-localized with glial fibrillary acidic protein (GFAP) expressing cells following inflammatory stimulation, suggesting that astrocytes (**Figure 2A**) and satellite glial cells (**Figure 2B**) appear to express TIMP-1 during inflammation (Huang et al., 2011; Welser-Alves et al., 2011). We also found that TIMP-1 expression was upregulated in K14-positive keratinocytes in both hairy and glabrous skin following inflammatory stimulation (**Figure 2C**; glabrous skin data not shown).

To associate the expression of cutaneous TIMP-1 with the development of mechanical hypersensitivity, we assessed PWT on the plantar surface of the hindpaw for 7 days following CFA injection into the dorsal, hairy skin. We found that TIMP-1 protein levels peaked 3 days following CFA administration (see **Figure 1C**), at a time when mice developed mechanical hypersensitivity, $F(2,12) = 43.94$, $p < 0.05$, (**Figure 3**). Together, these data indicate that cutaneous inflammation induces the expression of TIMP-1 in keratinocytes at the time of inflammation and prior to the onset of mechanical allodynia.

Mice Lacking TIMP-1 Exhibit Hyperalgesia in Inflamed and Uninflamed Cutaneous Tissues

To determine whether endogenous TIMP-1 expression is important for the normal progression of hypersensitivity, we used a global TIMP-1 knockout (T1KO) mouse strain. We first assessed behavioral responsiveness to radiant heat on the plantar surface of the hindpaw following s.c. administration of a diluted, emulsified CFA solution. We chose to use a diluted CFA solution because our preliminary experiments suggested that exposure to slight challenges significantly altered sensitivity in T1KO. To ensure that any potential differences in responding to inflammatory stimulation were not due to preexisting differences in sensory thresholds between mouse strains, we measured baseline responding to radiant heat and found no significant differences in PWL, $F(1, 31) = 0.47$, $p > 0.05$ (**Figure 4A**). Interestingly, while we did not observe any significant differences in PWL between naïve and WT mice that received diluted (e.g., subthreshold) CFA, we did find that inflamed T1KO mice exhibited thermal hyperalgesia that persisted for 29 days in response to diluted CFA injection, all $Fs < 2.30$, $p < 0.05$ (**Figure 4B**).

Next, we assessed mechanical response thresholds (von Frey) following diluted CFA administration. Analysis of baseline responses to mechanical stimulation did not reveal any significant differences between genotypes $F(1, 36) = 0.34$, $p < 0.05$ (**Figure 4C**). We did find that CFA administration reduced mechanical response thresholds in both genotypes $F(1, 34) = 17.61$, $p < 0.01$. However, T1KO mice exhibited greater mechanical hypersensitivity 1 day following CFA treatment, compared to WT controls, all $Fs < 4.59$, $p < 0.05$ (**Figure 4D**). Therefore, we concluded that the up-regulation of TIMP-1 following inflammation delays the onset of hypersensitivity, and that in the absence of TIMP-1, the normal development of hypersensitivity is altered.

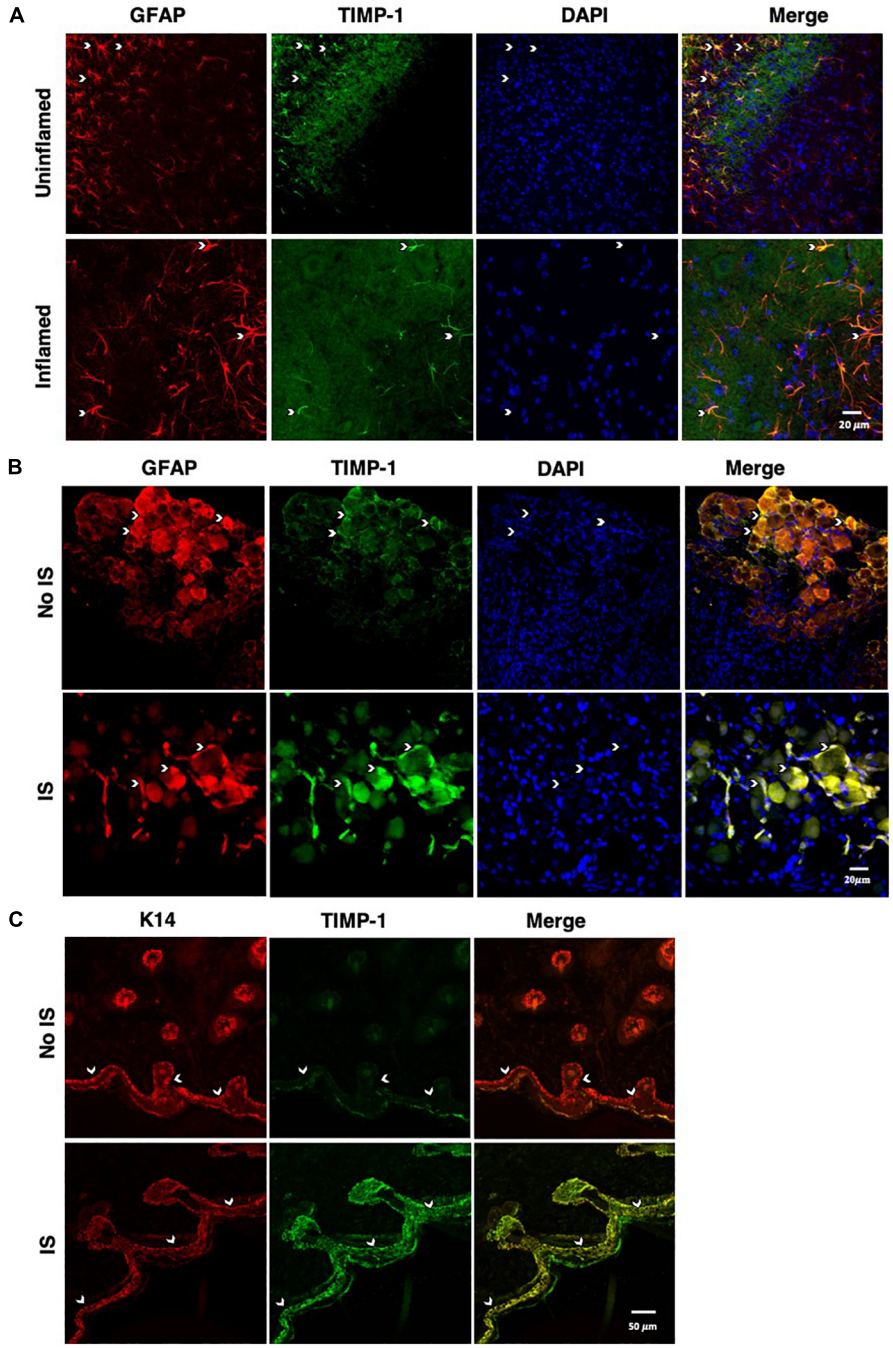

FIGURE 2 | Cellular colocalization of TIMP-1 expression. **(A)** Immunostaining (20×) of naïve and inflamed lumbar spinal cord 24 h following inflammation. TIMP-1 (green) expression is localized to GFAP-positive astrocytes (red). *n* = 3/condition, scale bar 20 μm. **(B)** Immunostaining (20×) of naïve and inflamed lumbar DRG 24 h following inflammation. TIMP-1 (green) expression is colocalized with by GFAP-positive satellite glial cells (red). *n* = 3/condition, scale bar 20 μm. **(C)** Immunostaining (40×) of hindpaw hairy skin shows K14-positive keratinocytes (red) upregulate TIMP-1 (green) 24 h following inflammation compared to naïve control. *n* = 3/condition, scale bar 50 μm.

To determine whether the rapid emergence of inflammatory hypersensitivity in T1KO mice was due to compensatory expression of *Timp2* or *Timp4* mRNA, we examined cutaneous expression of each transcript in naïve and inflamed T1KO mice. We focused on *Timp2* and *Timp4* expression because, TIMP-2 and -4 are soluble extracellular protease inhibitors that also share functional similarities with TIMP-1. TIMP-3, by contrast is quite different from the other TIMPs and is insoluble, tethered to the extracellular matrix, and is a more effective inhibitor of membrane-bound MMPs that

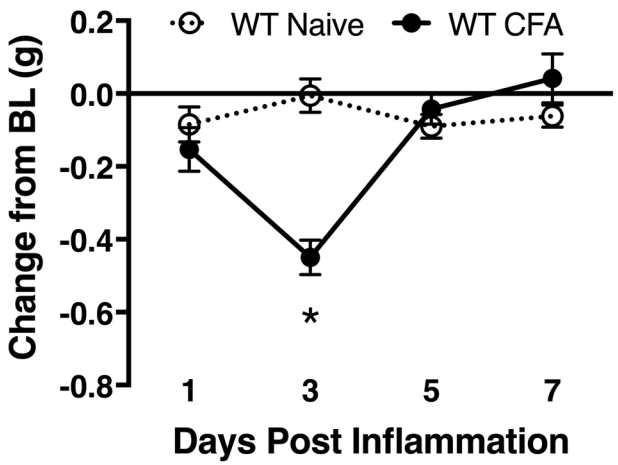

FIGURE 3 | Development of inflammatory hypersensitivity in WT mice. Assessment of mechanical hypersensitivity over 7 days following s.c. administration of CFA. Inflamed mice show a significant reduction in mechanical thresholds relative to naïve mice 3 days following inflammation (n = 6/condition). * indicate significant differences compared to naïve controls, $p < 0.05$, and error bars depict SEM.

extracellular MMPs. Moreover, prior studies have documented some role for TIMP-2 in pain (Ji et al., 2009), and TIMP-4 is known to inhibit MMP-2 and -9 (Ahmed et al., 2011; Grünwald et al., 2018), which also have identified roles in pain (Ji et al., 2009). Conversely, little is known about how TIMP-3 directly contributes to pain development or maintenance. Analysis of Timp2 and Timp4 expression revealed no significant differences in the basal expression of either transcript in WT or T1KO mice. However, *Timp2* and *Timp4* expression decreased in T1KO mice following inflammation (**Figures 5A,B**), suggesting that genetic deletion of TIMP-1 did not result in a compensatory response from other TIMPs, all $Fs < 11.65$, $p < 0.01$.

Our current data demonstrate that cutaneous TIMP-1 is an early emergent protein following inflammation, and that the absence of TIMP-1 alters the normal development of hypersensitivity. Therefore, TIMP-1 signaling may have important implications for regulating the development of inflammatory hypersensitivity in tissue adjacent to the site of inflammation that is innervated by afferent terminals that are different from those that innervate inflamed skin. To test this possibility, we assessed the development of hypersensitivity in the glabrous skin following injection of diluted CFA into hairy skin in both T1KO and WT following baseline assessment of sensitivity. Again, we observed no genotype-specific differences in baseline reactivity, and because of this consistent finding, we will no longer present data depicting baseline behavioral reactivity. Analysis using an ANOVA revealed that T1KO mice, relative to WT mice, exhibited increased sensitivity to mechanical stimulation on the plantar surface of the hindpaw following inflammation of hairy skin that was not temporally dependent, all $Fs < 4.41$, $p < 0.05$, (**Figures 6A,B**). However, trend analyses revealed that inflamed T1KO mice exhibited increased inflammatory hypersensitivity 1 day following CFA treatment when compared to all other mice, $F(1,57) = 11.55$, $p < 0.01$ (**Figure 6A**).

To examine whether administration of recombinant murine (rm)TIMP-1 prevented inflammatory hypersensitivity, and the potential mechanism by which this effect occurs, separate groups of T1KO mice received a single injection (10 μL vol) of recombinant full-length rmTIMP-1 [TIMP-1(FL)], the truncated N terminus peptide [TIMP-1(N)] that retains MMP inhibitory function but no cell signaling capacity, or the truncated C terminus peptide [TIMP-1(C)] that lacks MMP inhibitory capacity but retains its cell signaling function at the time of CFA administration. To limit the complexity of our experimental design, and to determine the optimal dose for the administration of each TIMP-1 construct, we conducted a pilot experiment using a small cohort of T1KO mice given 1, 10, or 100 ng/μL of TIMP-1 at the time of inflammation. We found that 10 ng/μL was effective at reducing inflammatory hypersensitivity (**Supplementary Figure S2**). We then administered a separate cohort of T1KO mice 10 ng/μL of TIMP-1(FL), TIMP-1(N), or TIMP-1(C) at the time of CFA administration. Mechanical hypersensitivity was assessed 24 h later. While inflamed T1KO mice exhibited a significant reduction in mechanical thresholds, T1KO mice treated with the rmTIMP-1 peptide constructs did not. Moreover, we observed no significant differences in the response thresholds between mice given TIMP-1(FL), TIMP-1(N), or TIMP-1(C), all $Fs > 4.54$, $p < 0.01$ (**Figure 6C**), demonstrating that TIMP-1 attenuates inflammatory hypersensitivity through MMP-dependent and MMP-independent signaling mechanisms.

The above data show that inflammation in one somatic region could lead to mechanical hypersensitivity in tissue distal to the site of inflammation, reminiscent of "mirror image pain" (Treede et al., 1992, 2015). To test this possibility, we inflamed one hindpaw and measured mechanical sensitivity on the opposite hindpaw for 7 days following CFA administration. We also examined whether treatment with rmTIMP-1 at the site and time of inflammation affected sensitivity. We found that inflamed T1KO mice exhibited contralateral mechanical hypersensitivity over the course of 7 days following CFA-injection relative to WT mice (**Figure 6D**). Interestingly, this contralateral hypersensitivity was prevented by treatment with rmTIMP-1 in T1KO mice, $F(4, 43) = 5.52$, $p < 0.05$ (**Figure 6D**).

The Lack of TIMP-1 Does Not Alter the Expression of Local Inflammatory Molecules

TIMP-1 is primarily known as a broad-spectrum MMP inhibitor, and because MMPs are known to contribute to hypersensitivity, we hypothesized that the absence of TIMP-1 may cause hypersensitivity due to elevated activity and expression of cutaneous MMP-9 (Kawasaki et al., 2008; Brew and Nagase, 2010). Examination of hairy skin collected 1 day following CFA from WT and T1KO mice demonstrated that

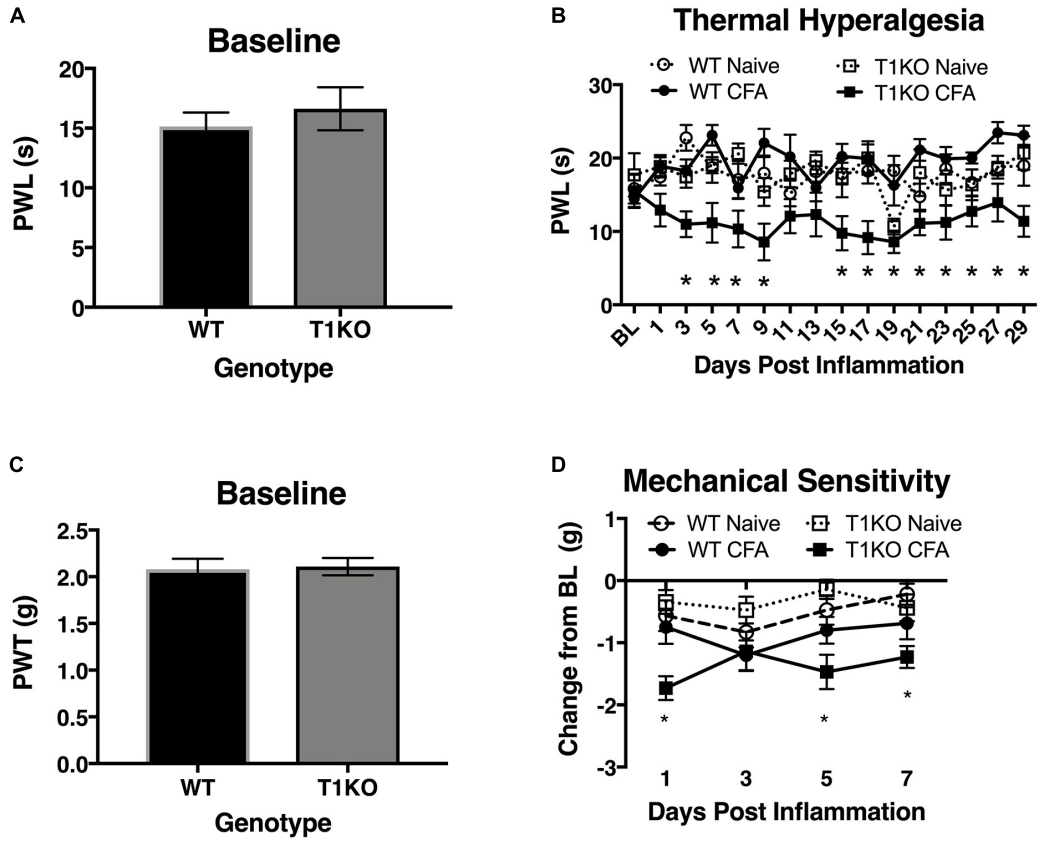

FIGURE 4 | Mice lacking TIMP-1 develop thermal and mechanical hypersensitivity following cutaneous inflammation. **(A)** No differences in baseline thermal PWL are exhibited between T1KO and WT mice (n = 16/condition). **(B)** Inflamed T1KO mice exhibit significantly reduced PWLs compared to inflamed WT mice and naïve WT and T1KO mice (n = 8/condition). **(C)** Baseline assessment of mechanical PWTs revealed no genotypic differences between T1KO (n = 20) and WT mice (n = 18). **(D)** T1KO mice develop significantly reduced PWTs 1, 5, and 7 days following CFA administration compared to WT controls (n = 8–10/condition). * = signficantly different from mice in all other conditions, $p < 0.05$, and error bars depict SEM.

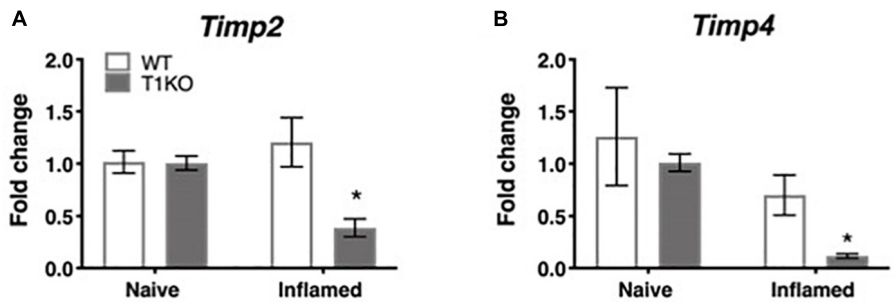

FIGURE 5 | Assessment of cutaneous *Timp2* and *Timp4* mRNA expression following inflammation. **(A)** *Timp2* mRNA expression is decreased in T1KO mouse skin 1 day following inflammation relative to WT controls. **(B)** *Timp4* mRNA expression is decreased 1 day following CFA compared to WT inflamed mice. n = 4/condition, * indicate significant differences compared to naïve controls, $p < 0.05$, and error bars depict SEM.

there was an inflammation-induced increase in both MMP-9 expression and activity, all $Fs > 7.61$, $p < 0.05$ but that these effects were not genotype-specific, all $Fs < 2.05$, $p > 0.05$ (**Figures 7A,B**). The TIMP/MMP axis also regulates the proteolytic maturation of inflammatory molecules which can cause hypersensitivity (Pagenstecher et al., 1998). We next assessed whether the absence of TIMP-1 during inflammation caused elevated cytokine expression in the skin. Using ELISAs, we assessed the expression of cutaneous IL-1β, IL-6, TNF-α, and IL-10 at 1 day following CFA-injection. Analysis revealed an inflammation-induced increase in IL-1β and IL-6 expression, but this increase in expression was not different between genotypes,

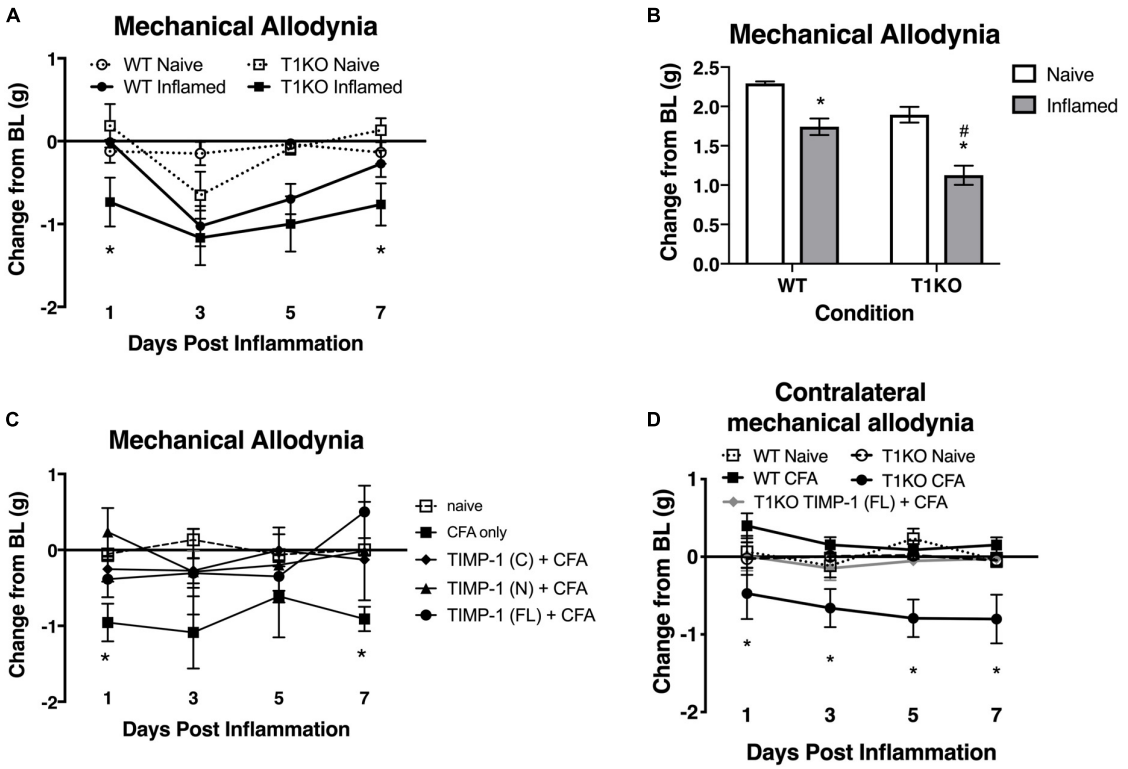

FIGURE 6 | Mice lacking TIMP-1 show increased sensitivity in non-inflamed tissues. **(A)** Injection of CFA into the hairy skin causes mechanical hypersensitivity on the plantar surface of the paw to develop 1 day following inflammation in T1KO, but not WT, mice. **(B)** Graph depicting mechanical responsiveness following inflammation collapsed across time. Inflamed T1KO mice greater mechanical sensitivity overall following cutaneous inflammation. **(C)** Administration of TIMP-1(FL), TIMP-1(N), or TIMP-1(C) into the hairy skin at the time of inflammation prevents the development of mechanical hypersensitivity in T1KO mice. **(D)** Hindpaw administration of CFA produces mechanical hypersensitivity on the paw contralateral to inflammation in T1KO relative txo WT mice. Treatment with rmTIMP-1 attenuated contralateral hypersensitivity in T1KO mice. PWT are presented as change from baseline. n = 8/condition, * represent significant differences relative to naïve controls, $p < 0.05$, and error bars depict SEM. #significantly different from WT mice.

all $Fs > 12.94$, $p < 0.05$ (**Figures 7C,D**). In comparison, analysis of TNF-α and IL-10 did not reveal any significant differences following inflammation, all $Fs < 4.64$, $p > 0.05$ (**Figures 7E,F**). These data suggest that TIMP-1 does not affect the emergence of hypersensitivity through differences in inflammatory cytokine expression.

Administration of Recombinant TIMP-1 Attenuates Ongoing Pain in WT Mice

Previous experiments demonstrate that the administration of rmTIMP-1 attenuates evoked mechanical and thermal hypersensitivity in T1KO mice. Here, we examined whether the administration of rmTIMP-1 also attenuated ongoing pain in WT mice using CPP as previous described (King et al., 2009; Ellis and Bennett, 2013). Analysis of pre- compared to post-conditioning time spent in the conditioning chamber indicate an effect of drug, $F(1, 30) = 7.269$, $p < 0.05$), and *post hoc* analysis confirmed an increase in post-conditioning time spent in the clonidine paired chamber compared to pre-conditioning time in vehicle treated mice ($p < 0.01$) but not in rmTIMP-1 treated mice ($p > 0.05$) (**Figure 8**). These observations indicate that WT mice administered CFA and TIMP-1 did not demonstrate clonidine-induced CPP (**Figure 8**). Because clonidine only produces CPP in the state of injury (King et al., 2009), these results further suggest that treatment with rmTIMP-1 attenuated ongoing inflammatory pain.

DISCUSSION

The balance between TIMPs and MMPs is important for maintaining tissue homeostasis and preventing pathological conditions. Following tissue damage and inflammation, TIMP-1 is expressed in a variety of cell types that can modulate neuronal function and wound healing, including, astrocytes, oligodendrocytes, Schwann cells, endothelial cells, mast cells, and keratinocytes (Fagerberg et al., 2010; Yokose et al., 2012; Claycomb et al., 2013). Because TIMP-1 is broadly expressed, TIMP-1 may also regulate neuroinflammation and neuropathic pain (Dhar et al., 2006; Kawasaki et al., 2008; Ji et al., 2009; Huang et al., 2011). Although the predominant view is that TIMP-1 exerts these functions by inhibiting MMPs, emerging evidence suggests that TIMP-1 may also facilitate these functions by binding cell-surface receptors and mediating their subsequent

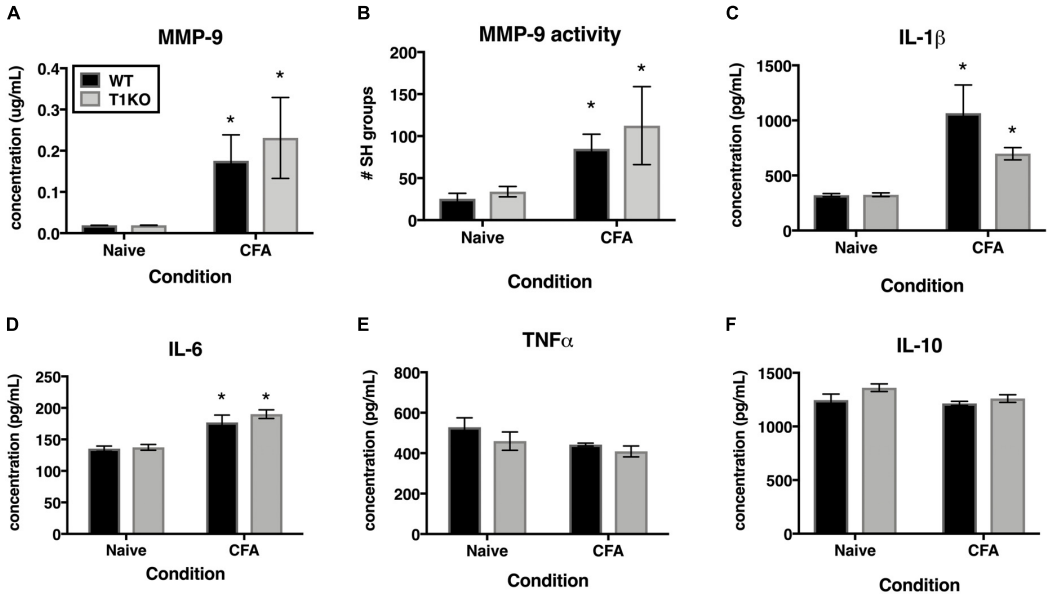

FIGURE 7 | Inflammation does not alter pro-inflammatory molecules in a genotype-specific manner. **(A)** Cutaneous inflammation significantly increases MMP-9 protein expression in WT and T1KO skin 1 day following CFA administration (n = 7/condition). **(B)** Cutaneous inflammation increases MMP-9 activity in WT and T1KO hairy skin 1 day following CFA administration. **(C)** Cutaneous inflammation significantly increases IL-1β protein expression in WT and T1KO hairy skin 1 day following inflammation. **(D)** Cutaneous inflammation significantly increases IL-6 protein expression in WT and T1KO hairy skin 1 day following CFA administration. **(E)** Cutaneous inflammation does not affect expression of TNF-α following CFA administration. **(F)** Cutaneous inflammation does not affect expression of IL-10 protein in WT and T1KO skin following CFA administration. n = 4/condition, * represent significant differences relative to naïve controls, $p < 0.05$, and error bars depict SEM.

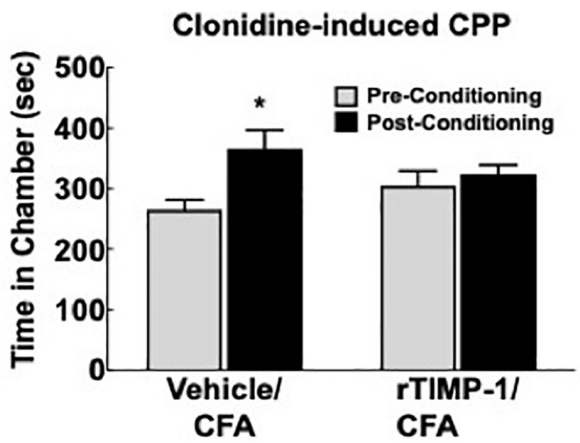

FIGURE 8 | Replacement of TIMP-1 attenuates ongoing inflammatory pain in WT mice. Comparison of pre-conditioning and post-conditioning time spent in the clonidine paired chamber show a significant increase in the post-conditioning time in the Vehicle/CFA treated mice, but not the rTIMP-1/CFA treated mice. *$p < 0.01$ vs. pre-conditioning time. Sample size CFA/rTIMP-1 = 9; CFA/Veh = 8. Error bars = S.E.M.

downstream signaling pathways (Dhar et al., 2006; Toricelli et al., 2013; Thevenard et al., 2014; Nicaise et al., 2019). Therefore, the present set of studies was designed to investigate the role of TIMP-1 in the development of inflammatory hypersensitivity and the mechanisms of its action.

To determine how inflammation affected the expression of TIMP-1 in tissues proximal and distal to the site of CFA-injection, we examined TIMP-1 expression in skin, DRG, and spinal cord over the course of 7 days. While we did not observe changes in TIMP-1 expression in the DRG or spinal cord, we did localize its expression to GFAP-positive cells, suggesting that TIMP-1 is expressed by satellite glial cells and astrocytes, respectively. When we examined skin, we found that CFA induced an 8.27-fold increase in TIMP-1 protein expression within 24 h of inflammation, and that this temporal upregulation in TIMP-1 was observed in basal keratinocytes. Given that keratinocytes augment nociceptive signaling through the release of neuroactive molecules (Baumbauer et al., 2015; Moehring et al., 2018), the release of TIMP-1 from keratocytes may attenuate pronociceptive behavior caused by inflammation (Fagerberg et al., 2010; Yokose et al., 2012; Edqvist et al., 2015). To test this hypothesis, we examined the temporal expression pattern of TIMP-1 in relationship to the development of cutaneous hypersensitivity in WT mice. We found that the largest change in TIMP-1 expression, within 24 h of injection, preceded the onset of cutaneous hypersensitivity, and that at 3 days when TIMP-1 expression peaked, behavioral sensitivity was the greatest in WT mice. This result suggests that peak TIMP-1 expression may in some way signal the onset of hypersensitivity. Alternatively, it is also possible that the relationship between TIMP-1 expression and the onset of hypersensitivity is determined by a relative change in expression between two consecutive

time points. In the case of the current experiments the largest change in expression is observed between baseline and 24 h following inflammation, where we observe an 8.27-fold change in expression. Conversely, we only detect a 1.43 fold increase in expression between Day 1 and Day 3, implying that it is not the absolute level of TIMP-1 expression, *per se*, that contributes to the delay in hypersensitivity, but rather the extent to which TIMP-1 expression changes relative to previous levels of expression over time. Consequently, it may be possible that as TIMP-1 expression increases during the first 24 h of inflammation the emergence of pain-related behavior is attenuated. However, the overall change in TIMP-1 expression over the next 48 h is no longer sufficient to prevent the emergence of hypersensitivity. Supporting this, we found that the replacement of recombinant TIMP-1 within 24 h of CFA-injection, which causes a significant increase in expression from baseline expression in the skin, prevented the onset of hypersensitivity in mice lacking TIMP-1. Taken together, these data suggest that the immediate induction and release of TIMP-1 from basal keratinocytes attenuates inflammatory hypersensitivity.

If the release of TIMP-1 is important for delaying the onset of inflammatory hypersensitivity, it is also possible that hypersensitivity is exacerbated in the absence of TIMP-1. To test this, we compared mechanical hypersensitivity and thermal hyperalgesia at the site of inflammation in WT and T1KO mice. While we observed a robust reduction in mechanical thresholds in WT and T1KO mice, hypersensitivity persisted for a longer duration in T1KO mice relative to WT controls. Interestingly, when we examined thermal hyperalgesia, we observed a significant reduction in PWT in T1KO mice, while WT mice appeared to be unaffected. This result suggests that TIMP-1 may differentially regulate the processing of thermal and mechanical stimulation. In particular, in WT mice, the presence of TIMP-1 appears to delay the onset and persistence of mechanical sensitivity while having no effect on thermal reactivity during mild inflammation. More broadly, others have argued that mechanical sensitivity is a hallmark sign of pathological pain states (Treede et al., 1992, 2015), and our results imply that the dysregulation in TIMP-1 signaling may contribute to this process by influencing hypersensitivity to mechanical stimulation. Importantly, our observed results were not due to a compensatory response in expression of *Timp2* or *Timp4*, and both transcripts are expressed at similar levels in both WT and T1KO mice in the naïve state. We did observe that expression of both *Timp2* and *Timp4* decreased following inflammation further suggesting a role for TIMP-2 (Kawasaki et al., 2008; Ji et al., 2009), and possibly TIMP-4, in the emergence of hypersensitivity. Specifically, decreased expression and activity of TIMP-2 and -4 may encourage the emergence and persistence of hypersensitivity. How each TIMP functionally differs in this capacity is the subject of ongoing work.

Given that thermal hyperalgesia and prolonged mechanical hypersensitivity were observed in T1KO, but not WT mice, following mild inflammation, our data suggest that the absence of TIMP-1 increases susceptibility to subtle perturbations that would otherwise be considered innocuous. Indeed, we found that injections of normal physiological saline produced mechanical hypersensitivity in T1KO mice, which was not observed in WT controls. This hypersensitivity could be due to a number of plausible factors, including hypertonicity in a TIMP-1 deficient system (Steinbrocker et al., 1953; Giesler and Liebeskind, 1976; Hylden and Wilcox, 1983; Sutaeg Hwang and Wilcox, 1986), the disruption of cutaneous integrity from needle insertion, cutaneous distention following injection, or the induction of some inflammatory process. Whatever the cause of hypersensitivity is following saline injection, it is tempting to postulate that when TIMP-1 is not present, the physiological processes in the periphery become dysfunctional and sensory stimulation is amplified.

Pathological pain is also characterized by increased sensitivity in tissues adjacent to, and distal from, the site of inflammation, as is the case with "mirror image" pain (Shir and Seltzer, 1991; Maleki et al., 2000). When we assessed sensitivity in tissue adjacent to the site of inflammation and that are innervated by different sets of afferent terminal endings (e.g., hairy vs. glabrous skin), we found that T1KO mice exhibited mechanical hypersensitivity. Interestingly, we observed hypersensitivity in the uninflamed (contralateral) hindpaw, and the sensitivity occurred in a different dermatome from the inflamed dermatome. Administration of rmTIMP-1 at the site of inflammation alleviated hypersensitivity on both the inflamed and uninflamed paws. These data suggest that inflammation-induced TIMP-1 expression occurs in a coordinated fashion that influences the normal progression of inflammatory sensitivity in both inflamed and uninflamed tissues, which may attenuate afferent input and prevent the development of central sensitization.

TIMP-1 is well known as an inhibitor of MMPs, and we know that MMPs contribute to pain following various injury and inflammatory conditions (Kawasaki et al., 2008; Remacle et al., 2018). We hypothesized that disrupting the balance between TIMP and MMP expression and activity would exacerbate hypersensitivity in T1KO mice due to elevated MMP activity and pro-inflammatory cytokine expression. However, we did not detect any genotype-specific differences in the activity of MMP-9 or pro-inflammatory cytokines proximal to the site of CFA administration. Prior work indeed shows that the inhibition of MMPs reduces pain (Kawasaki et al., 2008; Ji et al., 2009), and our current results demonstrate that administration of the N-terminal domain of TIMP-1, the domain responsible for MMP inhibition, attenuated hypersensitivity. We also show that administration of TIMP-1(C), the domain responsible for engaging receptor-mediated cell signaling events (Jung et al., 2006; Toricelli et al., 2013; Takawale et al., 2017; Nicaise et al., 2019), also attenuates hypersensitivity following inflammation, suggesting that TIMP-1 may also delay the emergence of hypersensitivity through a novel receptor-mediated mechanism. Consequently, TIMP-1 may attenuate the development of pain through both pathways. This latter point may help to explain, at least in part, why small molecule inhibitors of MMP activity have limited efficacy (Cathcart and Cao, 2015). By understanding

how both subdomains alleviate hypersensitivity, we may be able to effectively manage pain progression.

While our results show that TIMP-1 attenuates pain and hypersensitivity through both MMP inhibition and receptor-mediated signaling, the precise mechanisms by which TIMP-1 acts are not known. Our data suggest that the amount of TIMP-1 present at the site of inflammation may determine functional outcomes, which is consistent with previously published work (Grünwald et al., 2018). Moreover, inflammation affects a variety of cells types that are mobilized to encourage wound repair, including macrophages, dendritic cells, B cells, and T cells. Not only is TIMP-1 released by immune cells, but it is released by endothelial cells as well, and this release of TIMP-1 increases vascular permeability (Shubayev and Strongin, 2018), allowing cells to infiltrate injured tissue during the repair process. Interestingly, the ability of TIMP-1 to increase vascular permeability is thought to occur through MMP-independent signaling mechanisms (Stetler-Stevenson, 2008). In addition to TIMP-1, all of these cells are known to release the anti-inflammatory cytokine interleukin-10 (IL-10) (Couper et al., 2008), and IL-10 increases the production of TIMP-1 (Koscsó et al., 2013). There are a large number of cells that can produce TIMP-1, including mast cells within the skin. Because mast cells have a well-characterized role in driving allergic sensitivity and the release of cytokines involved in itch and pain (Galli and Tsai, 2012; Mukai et al., 2018), the release of mast cell-derived TIMP-1 producing ant nociception seems at odds with our current results. However, research has shown that mast cells contribute to the emergence of analgesia (Kalesnikoff and Galli, 2008; Cui et al., 2018), and this analgesic/antinociceptive response may result from the release of TIMP-1 in an IL-10-dependent manner. It is important to note that we did not observe a genotype-specific changes in IL-10 concentration in the skin following inflammation, but this may have occurred because IL-10 is upstream of TIMP-1 and deletion of TIMP-1 may not impact IL-10 release.

Once released into the extracellular space, TIMP-1 can potentially attenuate pain through multiple pathways. One such pathway is through the inhibition of MMPs, which not only affects their ability to produce pain, but also prevents the release of mature nerve growth factor (NGF) and brain-derived neurotrophic factor (BDNF) (Shubayev and Strongin, 2018), both of which have known roles in pronociceptive signaling (Woolf et al., 1994; Andreev et al., 1995; Bennett et al., 1998; Zhao et al., 2006; Melemedjian et al., 2010, 2013). Consequently, the antinociceptive effects of TIMP-1 may occur through inhibition of NGF, BDNF, or other algogenic molecules.

Similar processes may not only occur within the skin, but also the DRG and spinal cord as well. Our results, along with the work of others (Thalakoti et al., 2007; Vause and Durham, 2010), show that TIMP-1 is expressed by SGCs in the DRG, suggesting that the release of TIMP-1 by SGCs may attenuate the effects of pronociceptive molecules, such as NGF and BDNF, and affect the way in which afferent cell bodies respond to inflammation. TIMP-1 is expressed in a variety of cell types in the spinal cord with known roles in pain processing, including astrocytes and microglia. In general, the release of TIMP-1 in the spinal cord appears to abrogate the effects of inflammation. For example, release of astrocyte-derived TIMP-1 in an experimental autoimmune encephalomyelitis (EAE) model of multiple sclerosis has a protective effect and results in myelin sparing (Crocker et al., 2006) and attenuates the effect of IL-1β on the wound healing responses *in vitro* (Johnson and Crocker, 2015). The response of microglia to inflammatory stimulation and TIMP-1 appears to be more complex. Microglia play an important part of driving the initial inflammatory response in the CNS (during the "activated" M1 state), but also contribute to the resolution of inflammation (as M2) cells (Cherry et al., 2014; Popiolek-Barczyk et al., 2015). While in the M2 state, microglia can aid in inflammation resolution both through the release of IL-10 and TIMP-1 (Cherry et al., 2014; Popiolek-Barczyk et al., 2015). Moreover, administration of drugs with anti-inflammatory properties shift microglia from a M1 into a M2 state, resulting in the release of TIMP-1 (Popiolek-Barczyk et al., 2015). Interestingly, TIMP-1 delivery prevents the release of TNF-α from microglia (Nuttall et al., 2007), further supporting the anti-inflammatory, and potentially the antinociceptive, capacity of TIMP-1. Collectively, these data suggest that TIMP-1 may aid in the resolution of inflammation in peripheral and central tissues, and that TIMP-1 may be a critical component of a signaling cascade involved in reducing inflammatory hypersensitivity.

The function of TIMP-1 is also determined by the specific interactions TIMP-1 has with its binding partners, which includes both proteases and membrane-bound receptors. We have yet to identify which receptor is responsible for the antinociceptive properties of TIMP-1, but it is known that TIMP-1 binds and activates the CD63/β1 integrin receptor complex (Jung et al., 2006; Toricelli et al., 2013; Takawale et al., 2017; Nicaise et al., 2019). Interestingly, prior work has shown that interfering with the interaction between β1 integrin and versican attenuates inflammatory and neuropathic pain, as well as nociceptor activity (Dina et al., 2004; Ferrari and Levine, 2016). Consequently, keratinocyte-derived TIMP-1 may bind to CD63/β1 integrin expressed on cutaneous nerve endings ultimately, attenuating primary afferent function. While primary afferents are known to express β1 integrin, it is unclear whether they also express CD63. If neurons do not express CD63 there may be an indirect pathway involving other cell types, such as mast cells or keratinocytes, where TIMP-1 may bind to CD63 to alter the release pronociceptive molecules that influence neuronal function (Bertaux et al., 1991; Baumbauer et al., 2015; Moehring et al., 2018). Interestingly, disrupting the activity of β1 integrin prevents persistent pain in a model of hyperalgesic priming while leaving the acute phase of sensitivity intact (Dina et al., 2004). Therefore, stimulating TIMP-1 release, or the direct delivery of TIMP-1, may prevent the emergence of pathological pain, through β1 integrin activation, while leaving the capacity to detect normally painful stimuli unaffected.

Finally, demonstrating that TIMP-1 alleviates ongoing pain in WT mice we show that TIMP-1 is a potential clinical target for therapeutic intervention. It may be possible that TIMP-1 acts as a physiological "brake" on the nociceptive

system to prevent overexcitation of primary afferents and the development of centralized pain states. Consequently, targeting TIMP-1 may have therapeutic benefit for both peripheral and central pain. For example, while we did not directly assess hypersensitivity at somatic regions beyond the contralateral hindpaw, our data may have implications for understanding the underlying mechanisms of widespread pain syndromes, such as fibromyalgia. Our data may also have implications for understanding metastatic processes in non-painful forms of cancer. Indeed, TIMP-1 has been studied extensively in cancer (Gong et al., 2013; Toricelli et al., 2013; Jackson et al., 2017) and is therefore of significant interest for determining how metastases develop without producing pain. It is not yet clear whether painful and non-painful cancers differentially express TIMP-1 or whether TIMP-1 receptor binding kinetics are altered in painful and non-painful cancers. Understanding these dynamics may have clinical implications for developing early cancer detection strategies, especially if TIMP-1 is considered a regulator of pain state and not just one involved in tissue remodeling. Finally, if TIMP-1 can be utilized as a target for attenuating pathological pain, TIMP-1 may serve as an alternative to opioid-based medicines. This possibility is intriguing given our data showing that peripheral administration of TIMP-1 has antinociceptive properties and prevents the spread of sensitivity to uninflamed somatic regions. However, these conclusions should be taken with some caution as research has shown that excess TIMP-1 expression, specifically through genetic overexpression, may lead to unintended adverse events (Grünwald et al., 2018). Therefore, future research should focus on illuminating the mechanisms by which TIMP-1 attenuates pain and hypersensitivity and how targeting this system may be therapeutically beneficial.

CONCLUSION

The major goal of this study was to investigate the role TIMP-1 may play in pathological pain states associated with inflammation and in the absence of frank tissue damage. We found TIMP-1 expression was associated with behavioral hyposensitivity immediately following inflammation, and that mice lacking TIMP-1 developed exacerbated hypersensitivity that could be prevented by rmTIMP-1 protein constructs that either inhibit MMP activity or activate membrane bound receptors. Thus, endogenous TIMP-1 may prevent the induction of pain by both, regulating MMP activity and potentially through a novel cell-receptor signaling cascade mediated by CD63. Given the dual nature of TIMP-1 activity, it may be possible to target these pathways as an innovative strategy for attenuating persistent/chronic pain.

DATA AVAILABILITY

The datasets generated for this study are available on request to the corresponding author.

ETHICS STATEMENT

The animal study was reviewed and approved by University of Connecticut Health Center Institutional Animal Care and Use Committee.

AUTHOR CONTRIBUTIONS

BK: experimental design, data collection and analysis, mouse breeding and care, manuscript preparation. NK: data collection. JH: collection of conditioned place preference data. TK: experimental design and analysis of data from conditioned place preference experiments, manuscript preparation. SC: generation of T1KO mouse line, experimental design, manuscript preparation. EY: experimental design, data analysis, manuscript preparation. KB: experimental design, data analysis, manuscript preparation, experimental oversight.

FUNDING

This research was supported by the National MS Society grant (RG-1802-30211) to SC. This research was also supported by the grants 1R03NS096454-01 and R21NS104789-01A1, and funding from the Rita Allen Foundation (KB).

ACKNOWLEDGMENTS

We would like to thank Ms. Nicole Glidden and Ms. Jessica Yasko for their technical assistance. This manuscript has been released as a Pre-Print at bioRxiv (doi: 10.1101/540724).

SUPPLEMENTARY MATERIAL

The Supplementary Material for this article can be found online at: https://www.frontiersin.org/articles/10.3389/fnmol.2019.00220/full#supplementary-material

FIGURE S1 | Subcutaneous injection of saline vehicle causes mechanical hypersensitivity in mice lacking TIMP-1. Assessment of mechanical hypersensitivity over 7 days following s.c. administration of 0.9% saline. T1KO mice show a significant reduction in mechanical thresholds relative to all other mice 1 day following injection, and saline treated WT mice 5- and 7-days following injection (n = 6/condition). * indicates significant differences compared to naïve controls, and # indicates significant difference compared to WT mice given saline injections, $p < 0.05$, and error bars depict SEM.

FIGURE S2 | Dose-response curve for rmTIMP-1 administration. Mice were administered 1, 10, or 100 ng/μL (10 μL vol) s.c. at the time of CFA injection. Administration of 10 μL of rmTIMP-1 resulted in the greatest attenuation of mechanical hypersensitivity relative to all other doses. *indicates significantly different response thresholds relative to all other mice, and #indicates significantly different response thresholds relative to CFA treated mice, n = 6/condition, $p < 0.05$, and error bars depict SEM.

REFERENCES

Ahmed, M., King, K., Pearce, S., Ramsey, M., Miranpuri, G., and Resnick, D. (2011). Novel targets for spinal cord injury related neuropathic pain. *Ann. Neurosci.* 18, 162–167. doi: 10.5214/ans.0972.7531.1118413

Allchorne, A. J., Broom, D. C., and Woolf, C. J. (2005). Detection of cold pain, cold allodynia and cold hyperalgesia in freely behaving rats. *Mol. Pain* 1, 36–36.

Andreev, N. Y., Dimitrieva, N., Koltzenburg, M., and Mcmahon, S. B. (1995). Peripheral administration of nerve growth factor in the adult rat produces a thermal hyperalgesia that requires the presence of sympathetic post-ganglionic neurones. *Pain* 63, 109–115.

Baker, A., Edwards, D., and Murphy, G. (2002). Metalloproteinase inhibitors: biological actions and therapeutic opportunities. *J. Cell Sci.* 115, 3719–3727.

Baumbauer, K., Deberry, J., Adelman, P., Miller, R., Hachisuka, J., Lee, K., et al. (2015). Keratinocytes can modulate and directly initiate nociceptive responses. *eLife* 4:e09674. doi: 10.7554/eLife.09674

Bennett, G., Al-Rashed, S., Hoult, J. R. S., and Brain, S. D. (1998). Nerve growth factor induced hyperalgesia in the rat hind paw is dependent on circulating neutrophils. *Pain* 77, 315–322.

Bertaux, B., Hornebeck, W., Eisen, A. Z., and Dubertret, L. (1991). Growth stimulation of human keratinocytes by tissue inhibitor of metalloproteinases. *J. Investig. Dermatol.* 97, 679–685.

Brew, K., and Nagase, H. (2010). The tissue inhibitors of metalloproteinases (TIMPs): an ancient family with structural and functional diversity. *Biochim. Biophys. Acta* 1803, 55–71. doi: 10.1016/j.bbamcr.2010.01.003

Cathcart, J., and Cao, J. (2015). MMP inhibitors: past, present and future. *Front. Biosci.* 20:1164–1178.

Chapman, R., and Vierck, C. (2017). The transition of acute postoperative pain to chronic pain: an integrative overview of research on mechanisms. *J. Pain* 18, 359.e1–359.e38. doi: 10.1016/j.jpain.2016.11.004

Cherry, J. D., Olschowka, J. A., and O'banion, M. K. (2014). Neuroinflammation and M2 microglia: the good, the bad, and the inflamed. *J. Neuroinflamm.* 11, 98–98. doi: 10.1186/1742-2094-11-98

Claycomb, K., Johnson, K., Winokur, P., Sacino, A., and Crocker, S. (2013). Astrocyte regulation of CNS inflammation and remyelination. *Brain Sci.* 3, 1109–1127. doi: 10.3390/brainsci3031109

Couper, K. N., Blount, D. G., and Riley, E. M. (2008). IL-10: the master regulator of immunity to infection. *J. Immunol.* 180, 5771–5777.

Crocker, S. J., Whitmire, J. K., Frausto, R. F., Chertboonmuang, P., Soloway, P. D., Whitton, J. L., et al. (2006). Persistent macrophage/microglial activation and myelin disruption after experimental autoimmune encephalomyelitis in tissue inhibitor of metalloproteinase-1-deficient mice. *Am. J. Pathol.* 169, 2104–2116.

Cui, X., Liu, K., Xu, D., Zhang, Y., He, X., Liu, H., et al. (2018). Mast cell deficiency attenuates acupuncture analgesia for mechanical pain using c-kit gene mutant rats. *J. Pain Res.* 11, 483–495. doi: 10.2147/JPR.S152015

Dhar, A., Gardner, J., Borgmann, K., Wu, L., and Ghorpade, A. (2006). Novel role of TGF-beta in differential astrocyte-TIMP-1 regulation: implications for HIV-1-dementia and neuroinflammation. *J. Neurosci. Res.* 83, 1271–1280.

Dina, O. A., Parada, C. A., Yeh, J., Chen, X., Mccarter, G. C., and Levine, J. D. (2004). Integrin signaling in inflammatory and neuropathic pain in the rat. *Eur. J. Neurosci.* 19, 634–642.

Dixon, W. (1980). Efficient analysis of experimental observations. *Ann. Rev. Pharmacol. Toxicol.* 20, 441–462.

Edqvist, P., Fagerberg, L., Hallström, B., Danielsson, A., Edlund, K., Uhlén, M., et al. (2015). Expression of human skin-specific genes defined by transcriptomics and antibody-based profiling. *J. Histochem. Cytochem.* 63, 129–141. doi: 10.1369/0022155414562646

Ellis, A., and Bennett, D. L. H. (2013). Neuroinflammation and the generation of neuropathic pain. *Br. J. Anaesthesia* 111, 26–37. doi: 10.1093/bja/aet128

Fagerberg, L., Jonasson, K., Von Heijne, G., Uhlen, M., and Berglund, L. (2010). Prediction of the human membrane proteome. *Proteomics* 10, 1141–1149. doi: 10.1002/pmic.200900258

Ferrari, L., and Levine, J. (2016). Plasma membrane mechanisms in a preclinical rat model of chronic pain. *J. Pain* 16, 60–66. doi: 10.1016/j.jpain.2014.10.007

Galli, S. J., and Tsai, M. (2012). IgE and mast cells in allergic disease. *Nat. Med.* 18, 693–704. doi: 10.1038/nm.2755

Gardner, J., and Ghorpade, A. (2003). Tissue inhibitor of metalloproteinase (TIMP)-1: the TIMPed balance of matrix metalloproteinases in the central nervous system. *J. Neurosci. Res.* 74, 801–806.

Giesler, G., and Liebeskind, J. (1976). Inhibition of visceral pain by electrical stimulation of the periaqueductal gray matter. *Pain* 2, 43–48.

Gomis-Rüth, F., Maskos, K., Betz, M., Bergner, A., Huber, R., Suzuki, K., et al. (1997). Mechanism of inhibition of the human matrix metalloproteinase stromelysin-1 by TIMP-1. *Nature* 389, 77–81.

Gong, Y., Scott, E., Lu, R., Xu, Y., Oh, W. K., and Yu, Q. (2013). Timp-1 promotes accumulation of cancer associated fibroblasts and cancer progression. *PLoS One* 8:e77366. doi: 10.1371/journal.pone.0077366

Grünwald, B., Schoeps, B., and KrüGer, A. (2018). Recognizing the molecular multifunctionality and interactome of timp-1. *Trends Cell Biol.* 29, 6–19. doi: 10.1016/j.tcb.2018.08.006

Hachisuka, J., Baumbauer, K., Omori, Y., Snyder, L., Koerber, H., and Ross, S. (2016). Semi-intact ex vivo approach to investigate spinal somatosensory circuits. *eLife* 5:e22866. doi: 10.7554/eLife.22866

Hargreaves, K., Dubner, R., Brown, F., Flores, C., and Joris, J. (1988). A new and sensitive method for measuring thermal nociception in cutaneous hyperalgesia. *Pain* 32, 77-88.

He, Y., Tian, X., Hu, X., Porreca, F., and Wang, Z. J. (2012). Negative reinforcement reveals non-evoked ongoing pain in mice with tissue or nerve injury. *J. Pain* 6, 598–607. doi: 10.1016/j.jpain.2012.03.011

Huang, B., Zhao, X., Zheng, L., Zhang, L., Ni, B., and Wang, Y. (2011). Different expression of tissue inhibitor of metalloproteinase family members in rat dorsal root ganglia and their changes after peripheral nerve injury. *Neuroscience* 193, 421–428. doi: 10.1016/j.neuroscience.2011.07.031

Hylden, J., and Wilcox, G. (1983). Intrathecal serotonin in mice: analgesia and inhibition of a spinal action of substance P. *Life Sci.* 33, 789–795.

Imbe, H., and Kimura, A. (2017). Attenuation of pCREB and Egr1 expression in the insular and anteriorcingulate cortices associated with enhancement of CFA-evoked mechanicalhypersensitivity after repeated forced swim stress. *Brain Res. Bull.* 134, 253–261. doi: 10.1016/j.brainresbull.2017.08.013

Jackson, H., Defamie, V., Waterhouse, P., and Khokha, R. (2017). TIMPs: versatile extracellular regulators in cancer. *Nat. Rev. Cancer* 17, 38–53. doi: 10.1038/nrc.2016.115

Jankowski, M., Rau, K., Soneji, D., Ekmann, K., Anderson, C., Molliver, D., et al. (2012). Purinergic receptor P2Y1 regulates polymodal C-fiber thermal thresholds and sensory neuron phenotypic switching during peripheral inflammation. *Pain* 153, 410–419. doi: 10.1016/j.pain.2011.10.042

Jankowski, M. P., Lawson, J. J., Mcilwrath, S. L., Rau, K. K., Anderson, C. E., Albers, K. M., et al. (2009). Sensitization of cutaneous nociceptors after nerve transection and regeneration: possible role of target-derived neurotrophic factor signaling. *J. Neurosci.* 29, 1636–1647. doi: 10.1523/JNEUROSCI.3474-08.2009

Ji, R.-R., Xu, Z.-Z., Wang, X., and Lo, E. H. (2009). Matrix metalloprotease regulation of neuropathic pain. *Trends Pharmacol. Sci.* 30, 336–340. doi: 10.1016/j.tips.2009.04.002

Johnson, K., and Crocker, S. (2015). TIMP-1 couples RhoK activation to IL-1. *Neurosci. Lett.* 609, 165–170. doi: 10.1016/j.neulet.2015.10.038

Jourquin, J., Tremblay, E., Bernard, A., Charton, G., Chaillan, F. A., Marchetti, E., et al. (2005). Tissue inhibitor of metalloproteinases-1 (TIMP-1) modulates neuronal death, axonal plasticity, and learning and memory. *Eur. J. Neurosci.* 22, 2569–2578.

Jung, K., Liu, X., Chirco, R., Fridman, R., and Kim, H. (2006). Identification of CD63 as a tissue inhibitor of metalloproteinase-1 interacting cell surface protein. *Eur. Mol. Biol. Organ.* 25, 3934–3942.

Kalesnikoff, J., and Galli, S. J. (2008). New developments in mast cell biology. *Nat. Immunol.* 9, 1215–1223. doi: 10.1038/ni.f.216

Kawasaki, Y., Xu, Z., Wang, X., Park, J., Zhuang, Z., Tan, P., et al. (2008). Distinct roles of matrix metalloproteases in the early- and late-phase development of neuropathic pain. *Nat. Med.* 14, 331–336. doi: 10.1038/nm1723

Kehlet, H., Jensen, T., and Woolf, C. (2006). Persistent postsurgical pain: risk factors and prevention. *Lancet* 367, 1618–1625.

Kessler, W., Kirchhoff, C., Reeh, P., and Handwerker, H. (1992). Excitation of cutaneous afferent nerve endings in vitro by a combination of inflammatory mediators and conditioning effect of substance P. *Exp. Brain Res.* 91, 467–476.

Kim, Y., Remacle, A., Chernov, A., Liu, H., Shubayev, I., Lai, C., et al. (2012). The MMP-9/TIMP-1 axis controls the status of differentiation and function of myelin-forming schwann cells in nerve regeneration. *PLoS One* 7:e33664. doi: 10.1371/journal.pone.0033664

King, T., Vera-Portocarrero, L., Gutierrez, T., Vanderah, T., Dussor, G., Lai, J., et al. (2009). Unmasking the tonic-aversive state in neuropathic pain. *Nat. Neurosci.* 12, 1364–1366. doi: 10.1038/nn.2407

Koscsó, B., Csóka, B., Kókai, E., Németh, Z. H., Pacher, P., Virág, L., et al. (2013). Adenosine augments IL-10-induced STAT3 signaling in M2c macrophages. *J. Leukocyte Biol.* 94, 1309–1315. doi: 10.1189/jlb.0113043

Kouwenhoven, M., Ozenci, V., Gomes, A., Yarilin, D., Giedraitis, V., Press, R., et al. (2001). Multiple sclerosis: elevated expression of matrix metalloproteinases in blood monocytes. *J. Autoimmun.* 16, 463–470.

Laedermann, C. J., Pertin, M., Suter, M. R., and Decosterd, I. (2014). Voltage-gated sodium channel expression in mouse DRG after SNI leads to re-evaluation of projections of injured fibers. *Mol. Pain* 10:19. doi: 10.1186/1744-8069-10-19

Lawson, J. J., Mcilwrath, S. L., Woodbury, C. J., Davis, B. M., and Koerber, H. R. (2008). TRPV1 unlike TRPV2 is restricted to a subset of mechanically insensitive cutaneous nociceptors responding to heat. *J. Pain* 9, 298–308. doi: 10.1016/j.jpain.2007.12.001

Lee, M., Yoon, B., Osiewicz, K., Preston, M., Bundy, B., Van Heeckeren, A., et al. (2005). Tissue inhibitor of metalloproteinase 1 regulates resistance to infection. *Infect. Immun.* 73, 661–665.

Li, Y., Lu, Y., Zhao, Z., Wang, J., Li, J., Wang, W., et al. (2016). Relationships of MMP-9 and TIMP-1 proteins with chronic obstructive pulmonary disease risk: a systematic review and meta-analysis. *J. Res. Med. Sci.* 21:12.

Livak, K. J., and Schmittgen, T. D. (2001). Analysis of relative gene expression data using real-time quantitative PCR and the 2-ΔΔCT method. *Methods* 25, 402–408.

Maleki, J., Lebel, A., Bennett, G., and Schwartzman, R. (2000). Patterns of spread in complex regional pain syndrome, type I (reflex sympathetic dystrophy). *PAIN* 88, 259–266.

Martinho, F., Teixeira, F., Cardoso, F., Ferreira, N., Nascimento, G., Carvalho, C., et al. (2016). Clinical investigation of matrix metalloproteinases, tissue inhibitors of matrix metalloproteinases, and matrix metalloproteinase/tissue inhibitors of matrix metalloproteinase complexes and their networks in apical periodontitis. *Basic Res. Biol.* 42, 1082–1088. doi: 10.1016/j.joen.2016.04.001

McIlwrath, S., Lawson, J., Anderson, C., Albers, K., and Richard Koerber, H. (2007). Overexpression of neurotrophin- 3 enhances themechanical response properties of slowly adapting type 1afferents and myelinated nociceptors. *Eur. J. Neurosci.* 26, 1801–1812.

Melemedjian, O. K., Asiedu, M. N., Tillu, D. V., Peebles, K. A., Yan, J., Ertz, N., et al. (2010). IL-6- and NGF-induced rapid control of protein synthesis and nociceptive plasticity via convergent signaling to the eIF4F complex. *J. Neurosci.* 30, 15113–15123. doi: 10.1523/JNEUROSCI.3947-10.2010

Melemedjian, O. K., Tillu, D. V., Asiedu, M. N., Mandell, E. K., Moy, J. K., Blute, V. M., et al. (2013). BDNF regulates atypical PKC at spinal synapses to initiate and maintain a centralized chronic pain state. *Mol. Pain* 9:12. doi: 10.1186/1744-8069-9-12

Moehring, F., Cowie, A., Menzel, A., Weyer, A., Grzybowski, M., Arzua, T., et al. (2018). Keratinocytes mediate innocuous and noxious touch via ATP-P2X4 signaling. *eLife* 7:e31684. doi: 10.7554/eLife.31684

Moore, C., and Crocker, S. (2012). An alternate perspective on the roles of TIMPs and MMPs in pathology. *Am. J. Pathol.* 180, 12–16. doi: 10.1016/j.ajpath.2011.09.008

Mukai, K., Tsai, M., Saito, H., and Galli, S. J. (2018). Mast cells as sources of cytokines, chemokines, and growth factors. *Immunol. Rev.* 282, 121–150.

Nagase, H., Meng, Q., Malinovskii, V., Huang, W., Chung, L., Bode, W., et al. (1999). Engineering of selective TIMPs. *Ann. N. Y. Acad. Sci.* 878, 1–11.

Nagase, H., Visse, R., and Murphy, G. (2006). Structure and function of matrix metalloproteinases and TIMPs. *Cardiovasc. Res.* 69, 562–573.

Nakagawa, T., Kubota, T., Kabuto, M., Sato, K., Kawano, H., Hayakawa, T., et al. (1994). Production of matrix metalloproteinases and tissue inhibitor of metalloproteinases-1 by human brain tumors. *J. Neurosurg.* 81, 69–77.

Nicaise, A., Johnson, K., Willis, C., Guzzo, R., and Crocker, S. (2019). TIMP-1 promotes oligodendrocyte differentiation through receptor-mediated signaling. *Mol. Neurobiol.* 56, 3380–3392. doi: 10.1007/s12035-018-1310-7

Nuttall, R. K., Silva, C., Hader, W., Bar-Or, A., Patel, K. D., Edwards, D. R., et al. (2007). Metalloproteinases are enriched in microglia compared with leukocytes and they regulate cytokine levels in activated microglia. *Glia* 55, 516–526.

Okun, A., DeFelice, M., Eyde, N., Ren, J., Mercado, R., King, T., et al. (2011). Transient inflammation-induced ongoing pain is driven by TRPV1 sensitive afferents. *Mol. Pain* 7, 1–11. doi: 10.1186/1744-8069-7-4

Pagenstecher, A., Stalder, A. K., Kincaid, C. L., Shapiro, S. D., and Campbell, I. L. (1998). Differential expression of matrix metalloproteinase and tissue inhibitor of matrix metalloproteinase genes in the mouse central nervous system in normal and inflammatory states. *Am. J. Pathol.* 152, 729–741.

Parkitna, J., Korostynski, M., Kaminska-Chowaniec, D., Obara, I., Mika, J., Przewlocka, B., et al. (2006). Comparison of gene expression profiles in neuropathic and inflammatory pain. *J. Pharmacol. Physiol.* 57, 401–414.

Popiolek-Barczyk, K., Kolosowska, N., Piotrowska, A., Makuch, W., Rojewska, E., Jurga, A. M., et al. (2015). Parthenolide relieves pain and promotes M2 microglia/macrophage polarization in rat model of neuropathy. *Neural Plast.* 2015:676473. doi: 10.1155/2015/676473

Remacle, A., Hullugundi, S., Dolkas, J., Angert, M., Chernov, A., Strongin, A., et al. (2018). Acute- and late-phase matrix metalloproteinase (MMP)-9 activity is comparable in female and male rats after peripheral nerve injury. *J. Neuroinflamm.* 15:89. doi: 10.1186/s12974-018-1123-7

Ries, C. (2014). Cytokine functions of TIMP-1. *Cell. Mol. Life Sci.* 71, 659–672. doi: 10.1007/s00018-013-1457-3

Shir, Y., and Seltzer, Z. (1991). Effects of sympathectomy in a model of causalgiform pain produced by partial sciatic nerve injury in rats. *PAIN* 45, 309–320.

Shubayev, V. I., and Strongin, A. Y. (2018). Tissue inhibitors of metalloproteases strike a nerve. *Neural Regen. Res.* 13, 1890–1892.

Steinbrocker, O., Isenberg, S., Silver, M., Neustadt, D., Kuhn, P., and Schittone, M. (1953). Observations on pain produced by injection of hypertonic saline into muscles and other supportive tissues. *J. Clin. Investig.* 32, 1045–1051.

Stetler-Stevenson, W. G. (2008). Tissue inhibitors of metalloproteinases in cell signaling: metalloproteinase-independent biological activities. *Sci. Signal* 1:re6. doi: 10.1126/scisignal.127re6

Sutaeg Hwang, A., and Wilcox, G. L. (1986). Intradermal hypertonic saline-induced behavior as a nociceptive test in mice. *Life Sci.* 38, 2389–2396.

Tabachnick, B., and Fidell, L. (2007). *Using Multivariate Statistics*. Boston, MA: Allyn & Bacon/Pearson Education.

Takawale, A., Zhang, P., Patel, V., Wang, X., Oudit, G., and Kassiri, Z. (2017). Tissue inhibitor of matrix metalloproteinase-1 promotes myocardial fibrosis by mediating CD63–integrin β1 interaction. *Hypertension* 71, 1092–1103. doi: 10.1161/HYPERTENSIONAHA.117.09045

Tal, M. (1999). A role for inflammation in chronic pain. *Curr. Rev. Pain* 3, 440–446.

Thalakoti, S., Patil, V. V., Damodaram, S., Vause, C. V., Langford, L. E., Freeman, S. E., et al. (2007). Neuron-glia signaling in trigeminal ganglion: implications for migraine pathology. *Headache* 47, 1008–1025.

Thevenard, J., Verzeaux, L., Devy, J., Etique, N., Jeanne, A., Schneider, C., et al. (2014). Low-density lipoprotein receptor-related protein-1 mediates endocytic clearance of tissue inhibitor of metalloproteinases-1 and promotes its cytokine-like activities. *PLoS One* 9:e103839. doi: 10.1371/journal.pone.0103839

Thorne, M., Moore, C., and Robertson, G. (2009). Lack of TIMP-1 increases severity of experimental autoimmune encephalomyelitis: effects of darbepoetin alfa on TIMP-1 null and wild-type mice. *J. Neuroimmunol.* 211, 92–100. doi: 10.1016/j.jneuroim.2009.04.003

Toricelli, M., Melo, F., Peres, G., Silva, D., and Jasiulionis, M. (2013). Timp1 interacts with beta-1 integrin and CD63 along melanoma genesis and confers anoikis resistance by activating PI3-K signaling pathway independently of Akt phosphorylation. *Mol. Cancer* 12:22. doi: 10.1186/1476-4598-12-22

Tracey, D., and Walker, J. (1995). Pain due to nerve damage: are inflammatory mediators involved. *Inflamm. Res.* 44, 407–411.

Treede, R., Meyer, R., Raja, S., and Campbell, J. (1992). Peripheral and central mechanisms of cutaneous hyperalgesia. *Prog. Neurobiol.* 38, 397–421.

Treede, R., Rief, W., Barke, A., Aziz, Q., Bennett, M., Benoliel, R., et al. (2015). A classification of chronic pain for ICD-11. *Pain* 156, 1003–1007.

Vause, C. V., and Durham, P. L. (2010). Calcitonin gene-related peptide differentially regulates gene and protein expression in trigeminal glia cells: findings from array analysis. *Neurosci. Lett.* 473, 163–167. doi: 10.1016/j.neulet.2010.01.074

Vrontou, S., Wong, A. M., Rau, K. K., Koerber, H. R., and Anderson, D. J. (2013). Genetic identification of C fibres that detect massage-like stroking of hairy skin in vivo. *Nature* 493, 669–673. doi: 10.1038/nature 11810

Welser-Alves, J., Crocker, S., and Milner, R. (2011). A dual role for microglia in promoting tissue inhibitor of metalloproteinase (TIMP) expression in glial cells in response to neuroinflammatory stimuli. *J. Neuroinflamm.* 8:61. doi: 10.1186/1742-2094-8-61

Woolf, C. J., Safieh-Garabedian, B., Ma, Q. P., Crilly, P., and Winter, J. (1994). Nerve growth factor contributes to the generation of inflammatory sensory hypersensitivity. *Neuroscience* 62, 327–331.

Yang, E., Bane, C., Maccallum, R., Kiecolt-Glaser, J., Malarkey, M., and Glaser, R. (2002). Stress-related modulation of matrix metalloproteinase expression. *J. Neuroimmunol.* 133, 144–150.

Yokose, U., Hachiya, A., Sriwiriyanont, P., Fujimura, T., Visscher, M., Kitzmiller, W., et al. (2012). The endogenous protease inhibitor TIMP-1 mediates protection and recovery from cutaneous photodamage. *J. Investig. Dermatol.* 132, 2800–2809. doi: 10.1038/jid.2012.204

Zhao, J., Seereeram, A., Nassar, M. A., Levato, A., Pezet, S., Hathaway, G., et al. (2006). Nociceptor-derived brain-derived neurotrophic factor regulates acute and inflammatory but not neuropathic pain. *Mol. Cell. Neurosci.* 31, 539–548.

Zimmermann, K., Hein, A., Hager, U., Kaczmarek, J. S., Turnquist, B. P., Clapham, D. E., et al. (2009). Phenotyping sensory nerve endings in vitro in the mouse. *Nat. Protoc.* 4, 174–196.

Conflict of Interest Statement: The authors declare that the research was conducted in the absence of any commercial or financial relationships that could be construed as a potential conflict of interest.

frontiers in Molecular Neuroscience

ORIGINAL RESEARCH
published: 18 October 2019
doi: 10.3389/fnmol.2019.00257

Indomethacin Enhances Type 1 Cannabinoid Receptor Signaling

Robert B. Laprairie[1,2], Kawthar A. Mohamed[1], Ayat Zagzoog[1], Melanie E. M. Kelly[2,3], Lesley A. Stevenson[4], Roger Pertwee[4], Eileen M. Denovan-Wright[2] and Ganesh A. Thakur[5]**

[1] College of Pharmacy and Nutrition, University of Saskatchewan, Saskatoon, SK, Canada, [2] Department of Pharmacology, Dalhousie University, Halifax, NS, Canada, [3] Department of Ophthalmology and Visual Sciences, Dalhousie University, Halifax, NS, Canada, [4] School of Medical Sciences, The Institute of Medical Sciences, University of Aberdeen, Aberdeen, United Kingdom, [5] Center for Drug Discovery, Department of Pharmaceutical Sciences, School of Pharmacy, Bouvé College of Health Sciences, Northeastern University, Boston, MA, United States

In addition to its known actions as a non-selective cyclooxygenase (COX) 1 and 2 inhibitor, we hypothesized that indomethacin can act as an allosteric modulator of the type 1 cannabinoid receptor (CB1R) because of its shared structural features with the known allosteric modulators of CB1R. Indomethacin enhanced the binding of [^{3}H]CP55940 to hCB1R and enhanced AEA-dependent [^{35}S]GTPγS binding to hCB1R in Chinese hamster ovary (CHO) cell membranes. Indomethacin (1 μM) also enhanced CP55940-dependent βarrestin1 recruitment, cAMP inhibition, ERK1/2 and PLCβ3 phosphorylation in HEK293A cells expressing hCB1R, but not in cells expressing hCB2R. Finally, indomethacin enhanced the magnitude and duration of CP55940-induced hypolocomotion, immobility, hypothermia, and anti-nociception in C57BL/6J mice. Together, these data support the hypothesis that indomethacin acted as a positive allosteric modulator of hCB1R. The identification of structural and functional features shared amongst allosteric modulators of CB1R may lead to the development of novel compounds designed for greater CB1R or COX selectivity *and* compounds designed to modulate both the prostaglandin and endocannabinoid systems.

Keywords: cannabinoid, indomethacin, cannabinoid receptor, allosteric modulator, molecular pharmacology, cell signaling

OPEN ACCESS

Edited by:
Meritxell Canals, University of Nottingham, United Kingdom

Reviewed by:
Nadine Jagerovic, Spanish National Research Council (CSIC), Spain
Stephen Paul Alexander, University of Nottingham, United Kingdom

****Correspondence:***
Robert B. Laprairie
robert.laprairie@usask.ca
Ganesh A. Thakur
g.thakur@northeastern.edu

Received: *01 July 2019*
Accepted: *04 October 2019*
Published: *18 October 2019*

Citation:
Laprairie RB, Mohamed KA, Zagzoog A, Kelly MEM, Stevenson LA, Pertwee R, Denovan-Wright EM and Thakur GA (2019) Indomethacin Enhances Type 1 Cannabinoid Receptor Signaling. Front. Mol. Neurosci. 12:257. doi: 10.3389/fnmol.2019.00257

INTRODUCTION

The endocannabinoid system consists of endogenous cannabinoids such as anandamide (AEA) and 2-arachidonoylglycerol (2-AG), their anabolic and catabolic enzymes, and receptors including the type 1 and 2 cannabinoid receptors (CB1R, CB2R). There is a growing interest in defining the actions of drugs that modulate the activity of the endocannabinoid system. Specifically, compounds that selectively enhance the activity of CB1R may be used in the treatment of pain, depression, and neurodegenerative diseases (Ross, 2007). Compounds that directly activate CB1R – orthosteric agonists – have limited potential as novel therapeutic compounds because of their psychoactivity (Ross, 2007; Pertwee, 2008). Positive allosteric modulators (PAM) of CB1R bind to a CB1R site different from the CB1R site targeted by endocannabinoids and enhance the binding of orthosteric ligands to CB1R, and/or enhance orthosteric ligand-dependent signaling without intrinsic efficacy

(Ross, 2007). CB1R PAMs are being developed as novel therapeutic compounds for a wide range of disease states (Price et al., 2005; Ahn et al., 2012; Pamplona et al., 2012).

Existing allosteric modulators of CB1R include Org27569, PSNCBAM-1, lipoxin A_4, ZCZ011, cannabidiol (CBD), and GAT211 (Price et al., 2005; Ahn et al., 2012; Pamplona et al., 2012; Ignatowska-Jankowska et al., 2015; Laprairie et al., 2015, 2017; Tham et al., 2018). Org27569 and PSNCBAM-1 both enhance orthosteric ligand binding to CB1R, but diminish CB1R-dependent ERK1/2 phosphorylation and βarrestin recruitment (Price et al., 2005; Ahn et al., 2012; Cawston et al., 2013; Shore et al., 2014). Org27569 and PSNCBAM-1 also display inverse agonist activity at cAMP and ERK1/2 pathways in the absence of orthosteric ligands, indicating these compounds are not pure allosteric modulators (Ahn et al., 2012; Shore et al., 2014). Lipoxin A_4 is a PAM of ligand binding and orthosteric agonist-dependent cAMP inhibition at CB1R, but this compound is unstable and displays low potency (high micromolar) *in vitro*, limiting its therapeutic utility (Pamplona et al., 2012). CBD is a negative allosteric modulator (NAM) of CB1R-dependent ERK1/2 and PLCβ3 phosphorylation, βarrestin recruitment, and cAMP inhibition that reduces CP55940 binding at concentrations >1 μM (Laprairie et al., 2019). ZCZ011 and GAT211 are both potent and efficacious CB1R PAMs; these lead compounds are being used as scaffolds for the development of more specific, potent, and efficacious CB1R PAMs (Ignatowska-Jankowska et al., 2015; Laprairie et al., 2017, 2019).

Org27569, ZCZ011, and GAT211 share in common a 2- and 3-alkyl-group-substituted indole ring (indole-2-carboxamides) (Price et al., 2005; Ahn et al., 2012; Cawston et al., 2015; Ignatowska-Jankowska et al., 2015; Laprairie et al., 2017), suggesting this is an important structural requirement for allosteric modulators of CB1R (reviewed in Lu et al., 2018) (**Figure 1**). CB1R allosteric modulator activity is maintained or improved by C-5 substitution of Org27569 and GAT211 (Cawston et al., 2015; Hurst et al., 2019). PSNCBAM-1 and lipoxin A_4 do not contain substituted indole rings; however, both contain structural features that mimic the space and charge occupied by an indole ring (Ahn et al., 2012; Pamplona et al., 2012). Further, Cawston et al. (2015) recently demonstrated that varying the substituents around indole-2-carboxamides can affect the temporal activity of Org27569 derivatives, without affecting the NAM activity these compounds have on CB1R-mediated signaling. Based on the presence of an indole-2-carboxamide, and literature demonstrating the potential actions that might indicate an undocumented CB1R allosteric modulatory activity (Cawston et al., 2015; Lu et al., 2018), we identified indomethacin as a potential allosteric modulator of CB1R.

The non-steroidal anti-inflammatory drug (NSAID) indomethacin acts as high-affinity non-selective cyclooxygenase 1 and 2 (COX-1, COX-2) inhibitor, fatty acid amide hydrolase (FAAH) inhibitor, prostaglandin receptor 2 agonist, and β_2 andrenoreceptor antagonist (Fowler et al., 1997a). The substituted indole ring of indomethacin is unique among NSAIDs (Fowler et al., 1997a). Indomethacin has been shown to enhance AEA- and CB1R-dependent signaling *in vivo*, but these effects were independent of direct CB1R agonism or an increase in AEA levels (Wiley et al., 2006; Parvathy and Masocha, 2015). Indomethacin, unlike other NSAIDs, produces several neurologic side effects, including vertigo, dizziness, blurred vision, and psychosis, that may be the result of the endocannabinoid system and/or CB1R modulation (Fowler, 1987).

Objective of This Study

Based on the structural similarities of indomethacin to known CB1R allosteric modulators, and the neurologic effects associated with indomethacin use, the objective of this study was to determine whether indomethacin acted as an allosteric modulator of CB1R. To accomplish this objective, indomethacin's *in vitro* effects on orthosteric ligand binding to CB1R, G protein-coupling to CB1R, and CB1R-mediated signal transduction; and *in vivo* effects on CP55940-dependent anti-nociception, catalepsy, hypothermia, and locomotion were determined.

MATERIALS AND METHODS

Compounds

CP55940 [(-)-*cis*-3-[2-Hydroxy-4-(1,1-dimethylheptyl)phenyl]-*trans*-4-(3-hydroxypropyl)cyclohexanol] was purchased from Tocris Bioscience (Bristol, United Kingdom). AEA and indomethacin were purchased from Sigma-Aldrich (Poole, Dorset, United Kingdom). [^{3}H]CP55940 (174.6 Ci/mmol) and [^{35}S]GTPγS (1250 Ci/mmol) were obtained from PerkinElmer (Seer Green, Buckinghamshire, United Kingdom), GTPγS from Roche Diagnostic (Burgess Hill, West Sussex, United Kingdom), and GDP from Sigma-Aldrich. Compounds were dissolved in DMSO (final concentration of 0.1% in assay media for all assays) and added directly to the media at the concentrations and times indicated.

Cell Culture

Chinese hamster ovary (CHO) cells transfected with cDNA encoding human cannabinoid CB1R or CB2R were maintained at 37°C, 5% CO_2 in DMEM F-12 HAM, supplemented with 1 mM L-glutamine, 10% FBS, and 0.6% Pen/Strep for all cells, together with hygromycin B (300 mg/ml) and G418 (600 mg/ml) for the human CB1R CHO cells or with G418 (400 mg/ml) for the human CB2R CHO cells (Bolognini et al., 2010). For membrane preparation, cells were removed from flasks by scraping, centrifuged, and then frozen as a pellet at −20°C until required. Before use in a radioligand binding assay, cells were defrosted, diluted in Tris buffer (50 mM Tris–HCl and 50 mM Tris–base) and homogenized with a 1 mL hand-held homogenizer (Bolognini et al., 2010).

HitHunter (cAMP) and PathHunter (βarrestin2) CHO-K1 cells stably expressing human CB1R (hCB1R) from DiscoveRx® (Eurofins, Fremont, CA, United States) were maintained at 37°C, 5% CO_2 in F-12 DMEM containing 10% FBS and 1% penicillin-streptomycin with 800 μg/mL geneticin (HitHunter) or 800 μg/mL geneticin and 300 μg/mL hygromycin B (PathHunter).

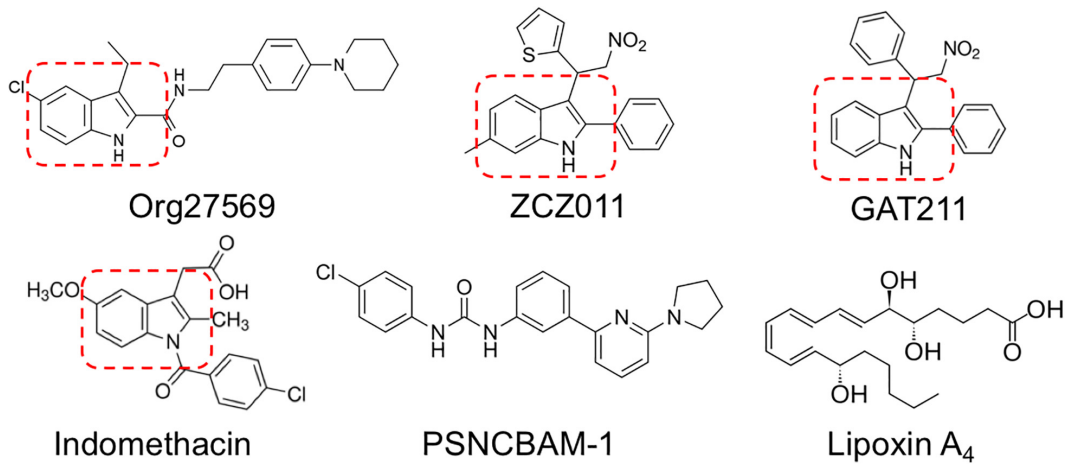

FIGURE 1 | Previously described allosteric modulators of CB1R.

Human embryonic kidney (HEK) 293A cells were from the American Type Culture Collection (ATCC, Manassas, VA, United States). HEK293A cells were maintained at 37°C, 5% CO_2 in DMEM supplemented with 10% FBS and 1% Pen/Strep.

HEK293A Cignal Lenti CRE (HEK-CRE) reporter cells were provided by Dr. Christopher J. Sinal (Dalhousie University, Halifax, NS, Canada). The HEK-CRE cells stably express the firefly luciferase gene driven by tandem repeat elements of the cAMP transcriptional response element (Qiagen, Toronto, ON, Canada). Thus, luciferase activity is directly proportional to the level cAMP/PKA pathway activation or inhibition. HEK-CRE cells were maintained at 37°C, 5% CO_2 in DMEM supplemented with 10% FBS, 1% Pen/Strep, and 200 μg/mL puromycin.

CHO Cell Membrane Preparations

CHO cells stably expressing hCB1R or hCB2R were disrupted by cavitation in a pressure cell and membranes were sedimented by ultracentrifugation, as described previously (Bolognini et al., 2012). The pellet was resuspended in TME buffer (50 mM Tris–HCl, 5 mM $MgCl_2$, 1 mM EDTA, pH 7.4) and membrane proteins were quantified with a Bradford dye-binding method (Bio-Rad Laboratories).

Radioligand Displacement Assays

Assays were carried out with [^{3}H]CP55940 and Tris binding buffer (50 mM Tris–HCl, 50 mM Tris–base, 0.1% BSA, pH 7.4), total assay volume 500 μL, using the filtration procedure described previously by Ross et al. (1999) and Baillie et al. (2013). Binding was initiated by the addition of transfected human CB1R or CB2R CHO cell membranes (50 μg protein per well). All assays were performed at 37°C for 60 min before termination by the addition of ice-cold Tris binding buffer, followed by vacuum filtration using a 24-well sampling manifold (Brandel Cell Harvester; Brandel Inc., Gaithersburg, MD, United States) and Brandel GF/B filters that had been soaked in wash buffer at 4°C for at least 24 h. Each reaction well was washed six times with a 1.2 mL aliquot of Tris binding buffer. The filters were oven-dried for 60 min and then placed in 3 ml of scintillation fluid (Ultima Gold XR, PerkinElmer, Seer Green, Buckinghamshire, United Kingdom). Radioactivity was quantified by liquid scintillation spectrometry. Specific binding was defined as the difference between the binding that occurred in the presence and absence of 1 μM unlabeled CP55940. The concentration of [^{3}H]CP55940 used in our displacement assays was 0.7 nM. Indomethacin was stored as stock solutions of 10 mM in DMSO, the vehicle concentration in all assay wells was 0.1% DMSO.

Dissociation Binding Assay

Membranes obtained from CHO cells transfected with hCB1R were incubated at 24°C in a 96 deep-well block immersed in a water bath (50 μg protein per well), together with 350 μL of assay buffer (50 mM Tris HCl, 50 mM Tris Base and 0.1% w/v BSA, pH 7.4), and 50 μL [^{3}H]CP55940 (7 nM) in each well for 60 min to allow full association of [^{3}H]CP55940 to occur. Dissociation of [^{3}H]CP55940 was monitored at various times over a further period of 60 min after the addition of 1 μM unlabeled CP55940 in the presence or absence of 1 μM indomethacin at 24°C. The assay was terminated by rapid filtration onto GF/B filters pre-soaked in assay buffer using a Brandel cell harvester. The filters were washed six times with the ice-cold buffer before being dried in a heated cabinet. Filters were placed in vials to which 3 mL Ultima Gold scintillation fluid was added. The radioactivity in each vial was then counted for 3 min in a Tri-Carb liquid scintillation counter.

[^{35}S]GTPγS Binding Assay

Human CB1R and CB2R CHO cell membranes (25 μg protein) were preincubated for 30 min at 30°C with adenosine deaminase (0.5 IU/ml). The membranes were then incubated with the agonist ± indomethacin or vehicle for 60 min at 30°C in assay buffer (50 mM Tris–HCl; 50 mM Tris–Base; 5 mM $MgCl_2$; 1 mM EDTA; 100 mM NaCl; 1 mM DTT; 0.1% BSA) in the presence of 0.1 nM [^{35}S]GTPγS and 30 μM GDP, in a final volume of

500 μL. Binding was initiated by the addition of [^{35}S]GTPγS. Non-specific binding was measured in the presence of 30 μM GTPγS. The reaction was terminated by rapid vacuum filtration (50 mM Tris–HCl; 50 mM Tris–Base; 0.1% BSA) using a 24-well sampling manifold (cell harvester; Brandel, Gaithersburg, MD, United States) and GF/B filters (Whatman, Maidstone, United Kingdom) that had been soaked in buffer (50 mM Tris–HCl; 50 mM Tris–Base; 0.1% BSA) for at least 24 h. Each reaction tube was washed six times with a 1.2-mL aliquot of ice-cold wash buffer. The filters were oven-dried for at least 60 min and then placed in 3 mL of scintillation fluid (Ultima Gold XR, PerkinElmer, Cambridge, United Kingdom). Radioactivity was quantified by liquid scintillation spectrometry.

RT-PCR

RNA was harvested from HEK293A cells using the Trizol® (Invitrogen, Burlington, ON, Canada) extraction method according to the manufacturer's instruction. Reverse transcription reactions were carried out with SuperScript III® reverse transcriptase (+RT; Invitrogen), or without (−RT) as a negative control for use in subsequent PCR experiments according to the manufacturer's instructions. Two micrograms of RNA were used per RT reaction for cDNA synthesis. PCR reactions were composed of 1X *Taq* polymerase PCR buffer, a primer-specific concentration of $MgCl_2$ (**Supplementary Table S1**), 0.3 mM dNTPs, 0.5 μM each of forward and reverse primers (**Supplementary Table S1**), 1 μL cDNA, and 1.25 U *Taq* polymerase, to a final volume of 20 μL with dH_2O (Fermentas). The PCR program was: 95°C for 10 min, 35 cycles of 95°C 30 s, a primer-specific annealing temperature (**Supplementary Table S1**) for 30 min, and 72°C for 1 min.

Plasmids

Human CB1R- and CB2R-green fluorescent protein^2 (GFP^2) C-terminal fusion protein was generated using the pGFP^2-N3 (PerkinElmer, Waltham, MA, United States) plasmid, as described previously (Bagher et al., 2013). Human βarrestin1-*Renilla* luciferase II (RlucII) C-terminal fusion protein was generated using the pcDNA3.1 plasmid and provided by Dr. Denis J. Dupré (Dalhousie University, Halifax, NS, Canada). The GFP^2-Rluc fusion construct, and Rluc plasmids have also been described (Bagher et al., 2013).

Bioluminescence Resonance Energy Transfer^2

Direct interactions between CB1R or CB2R and βarrestin1 were quantified via Bioluminescence Resonance Energy Transfer^2 (BRET^2) (James et al., 2006). Cells were transfected with the indicated GFP^2 and *Rluc* constructs using Lipofectamine 2000, according to the manufacturer's instructions (Invitrogen) and treated as previously described (Laprairie et al., 2014). Briefly, 48 h post-transfection cells were washed twice with cold PBS and suspended in BRET buffer [PBS supplemented with glucose (1 mg/mL), benzamidine (10 mg/mL), leupeptin (5 mg/mL), and a trypsin inhibitor (5 mg/mL)]. Cells were treated with compounds as indicated (PerkinElmer) and coelenterazine 400a substrate (50 μM; Biotium, Hayward, CA, United States) was added. Light emissions were measured at 460 nm (Rluc) and 510 nm (GFP^2) using a Luminoskan Ascent plate reader (Thermo Scientific, Waltham, MA, United States), with an integration time of 10 s and a photomultiplier tube voltage of 1200 V. BRET efficiency ($BRET_{Eff}$) was determined using previously described methods (Bagher et al., 2013; Laprairie et al., 2014). Data are presented as % of the maximal response to CP55940.

In-Cell Westerns

Cells were fixed for 10 min at room temperature with 4% paraformaldehyde and washed three times with 0.1 M PBS for 5 min each. Cells were incubated with blocking solution (PBS, 20% Odyssey blocking buffer, and 0.1% TritonX-100) for 1 h at room temperature. Cells were incubated with primary antibody solutions directed against pERK1/2(Y205/185), ERK1/2, pPLCβ3(S573), or PLCβ3 (Santa Cruz Biotechnology) diluted (1:200) in blocking solution overnight at 4°C. Cells were washed three times with PBS for 5 min each. Cells were incubated in $IR^{CW700dye}$ or $IR^{CW800dye}$ (1:500; Rockland Immunochemicals) and washed three times with PBS for 5 min each. Analyses were conducted using the Odyssey Imaging system and software (version 3.0; Li-Cor). Data are presented as % of the maximal response to CP55940.

cAMP Luciferase Reporter Assay

HEK-CRE cells were transfected with CB1R-GFP^2 or CB2R-GFP^2. Forty-eight hours post-transfection cells were washed twice with cold PBS and suspended in BRET buffer. Cells were dispensed into 96-well plates (10,000 cells/well) and treated with 10 μM forskolin and ligands (PerkinElmer). Media was aspirated from cells and cells were lysed with passive lysis buffer for 20 min at room temperature (Promega, Oakville, ON, Canada). Twenty microliters of cell lysate were mixed with luciferase assay reagent (50 μM; Promega, Oakville, ON, Canada) and light emissions were measured at 405 nm using a Luminoskan Ascent plate reader (Thermo Scientific, Waltham, MA, United States), with an integration time of 10 s and a photomultiplier tube voltage of 1200 V. Data are presented as % inhibition of forskolin response.

HitHunter cAMP Assay

Inhibition of forskolin-stimulated cAMP was determined using the DiscoveRx HitHunter assay in hCB1R CHO-K1 cells. Cells (20,000 cells/well in low-volume 96 well plates) were incubated overnight in Opti-MEM (Invitrogen) containing 1% FBS at 37°C and 5% CO_2. Following this, Opti-MEM media was removed and replaced with cell assay buffer (DiscoveRx) and cells were co-treated at 37°C with 10 μM forskolin and ligands for 90 min. cAMP antibody solution and cAMP working detection solutions were then added to cells according to the manufacturer's directions (DiscoveRx®) and cells were incubated for 60 min at room temperature. cAMP solution A was added according to the manufacturer's directions (DiscoveRx®) and cells were incubated for an additional 60 min at room temperature before chemiluminescence was measured on a Cytation 5 plate reader (top read, gain 200, integration time 10,000 ms). Data are presented as % inhibition of forskolin response.

PathHunter CB1R βarrestin2 Assay

βarrestin2 recruitment was determined using the hCB1R CHO-K1 cell PathHunter assay (DiscoveRx®). Cells (20,000 cells/well in low-volume 96 well plates) were incubated overnight in Opti-MEM (Invitrogen) containing 1% FBS at 37°C and 5% CO_2. Following this, cells were co-treated at 37°C with ligands for 90 min. Detection solution was then added to cells according to the manufacturer's directions (DiscoveRx®) and cells were incubated for 60 min at room temperature. Chemiluminescence was measured on a Cytation 5 plate reader (top read, gain 200, integration time 10,000 ms). Data are presented as % of the maximal response to CP55940.

Animals and Tetrad Testing

Seven-week old, male, C57BL/6J mice (mean weight 25.2 ± 0.5 g) were purchased from The Jackson Laboratory (Bar Harbor, ME, United States). Animals were group housed (5 per cage) with *ad libitum* access to food, water, and environmental enrichment and maintained on a 12 h light/dark cycle. Mice were randomly assigned to receive 2 volume-matched *i.p.* injections of vehicle (10% DMSO in saline), 0.1 mg/kg CP55940 + vehicle, 2 mg/kg indomethacin + vehicle, 0.1 mg/kg CP55940 + 2 or 4 mg/kg indomethacin ($n = 5$ per group). All protocols were in accordance with the guidelines detailed by the Canadian Council on Animal Care (CCAC; Ottawa ON: Vol. 1, 2nd Ed., 1993; Vol. 2, 1984), approved by the Carleton Animal Care Committee at Dalhousie University. In keeping with the ARRIVE guidelines, power analyses were conducted to determine the minimum number of animals required for the study and animals were purchased – rather than bred – to limit animal waste, and all assessments of animal behavior were made by individuals blinded to treatment group (Kilkenny et al., 2010).

Anti-nociception was determined by assessing tail flick latency immediately prior to injection and 0.5, 1, and 4 h following injection. Mice were restrained with their tails placed ∼1 cm into water held at 52°C and the time until the tail was removed was recorded as tail flick latency (s). Observations were ended at 10 s.

Catalepsy was assessed in the ring holding assay immediately prior to injection and 1 and 4 h following injection. The mice were placed such that their forepaws clasped a 5 mm ring positioned 5 cm above the surface of the testing space. The length of time the ring was held was recorded (s). The trial was ended if the mouse turned its head or body, or made three consecutive escape attempts.

Internal body temperature was measured via rectal thermometer immediately prior to injection and 0.5, 1, and 4 h following injection.

Locomotion was assessed in the open field test immediately prior to injection and 1 and 4 h following injection. Mice were placed in an open space 90 cm × 60 cm and total distance was recorded for 5 min. Data are displayed as the total distance travelled over 5 min (m).

Statistical Analyses

Data for [^{3}H]CP55940 binding and [^{35}S]GTPγS binding data are shown as % change from a basal level. In-cell westerns, BRET, and PathHunter data are shown as % of maximal CP55940 response. cAMP luciferase and HitHunter data are shown as % of forskolin response. Concentration-response curves (CRC) were fit using non-linear regression with variable slope (four parameters) and used to calculate EC_{50}, E_{min}, and E_{max} (GraphPad, Prism, v. 8.0). CRC were fit to the operational model of Black and Leff (1983) to calculate bias (ΔΔLogR) according to previously described methods and using CP55940 as the reference agonist (Laprairie et al., 2017). Statistical analyses were conducted by Student's one

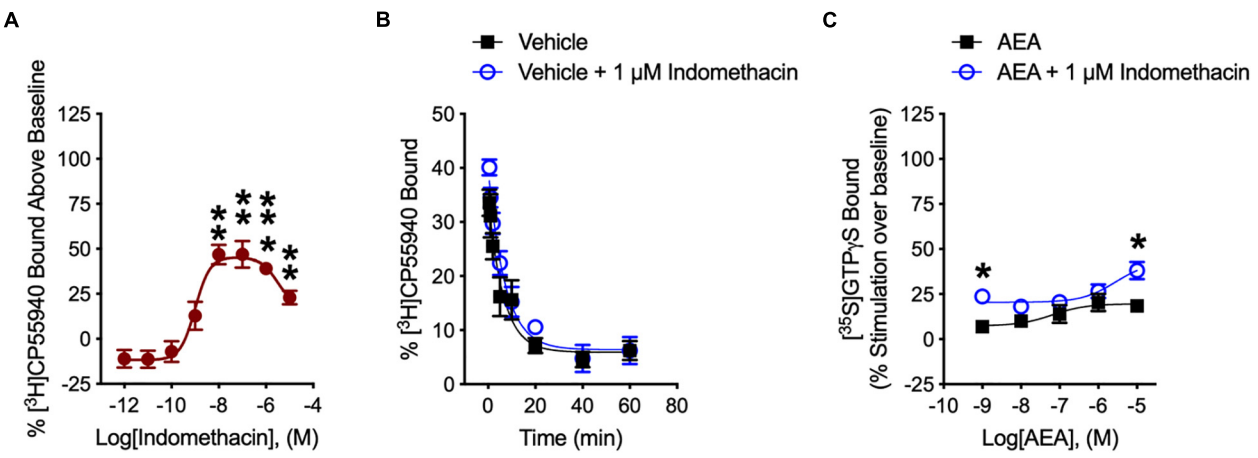

FIGURE 2 | [^{3}H]CP55940 and [^{35}S]GTPγS binding to hCB1R. **(A)** [^{3}H]CP55940 (0.7 nM) binding to membranes obtained from CHO cells transfected with hCB1R was measured in the presence of indomethacin. Symbols represent mean percentage changes in [^{3}H]CP55940 binding values ± SEM. Asterisks indicate mean values that are significantly different from zero via Student's one sample *t*-test (**$P < 0.01$, ***$P < 0.001$). Data are presented as mean values ± SEM. $N = 4$–6. **(B)** Effect of 1 μM indomethacin on the kinetics of [^{3}H]CP55940 for its dissociation from binding sites on membranes obtained from hCB1R CHO cells. Data were best fitted using a one-phase dissociation model. Data are presented as mean values ± SEM. $N = 5$. **(C)** The effects of indomethacin on [^{35}S]GTPγS binding in CHO cells expressing hCB1R treated with AEA in the presence of DMSO or 1 μM indomethacin. Asterisks indicate mean values that are significantly different from zero via Student's one sample *t*-test (*$P < 0.05$). Data are mean ± SEM. $N = 5$–6.

TABLE 1 | Effect of indomethacin on the mean [^{3}H]CP55940 of dissociation rate from membranes of CHO cells expressing hCB1R.

	$t_{1/2}$ (min) (95% CI)[a]
DMSO	4.75 (2.89–13.4)
+1 μM indomethacin	4.67 (3.17–8.80)

[a]*Data were best fitted using a one-phase dissociation model. N = 5.*

sample *t*-test, one- or two-way analysis of variance (ANOVA), as indicated in the figure legends, using GraphPad. *Post hoc* analyses were performed using Bonferroni's (two-way ANOVA) or Tukey's (one-way ANOVA) tests. Homogeneity of variance was confirmed using Bartlett's test. All results are reported as the mean ± the standard error of the mean (SEM) or 95% confidence interval (CI), as indicated. *P*-values < 0.05 were considered to be significant.

Receptor Modeling and Ligand Docking

The 2.8 Å agonist-bound (PDB ID: 5XRA) (Hua et al., 2017) human CB1R crystal structure was used. Amino acid position is indicated according to the Ballesteros and Weinstein method of residue numbering [i.e., single letter amino acid abbreviation,

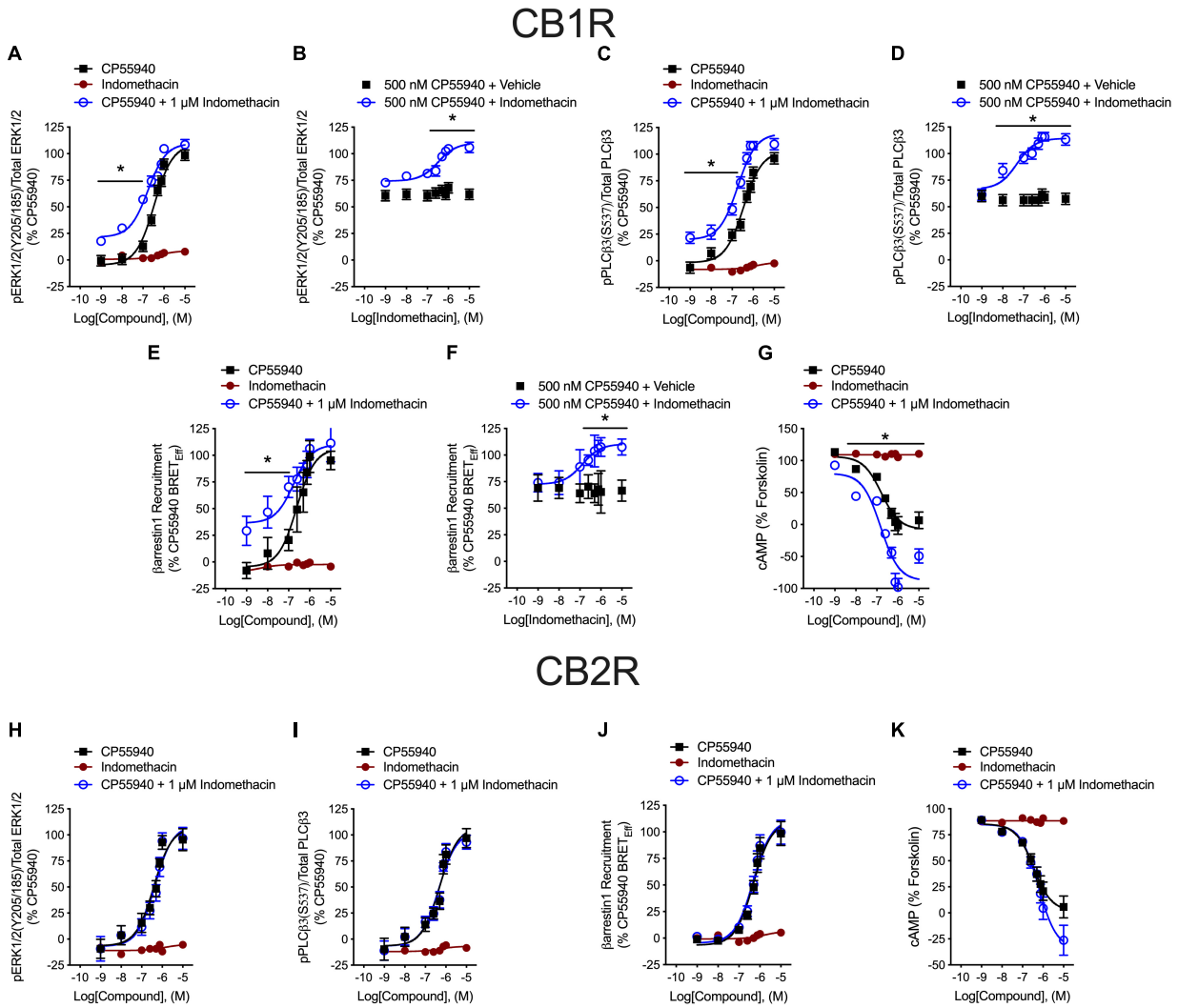

FIGURE 3 | hCB1R and hCB2R signaling in the presence of indomethacin. **(A–D)** HEK293A cells expressing hCB1R-GFP^2 were treated with 1 nM–10 μM CP55940 ± 1 μM indomethacin **(A,C)** or 1 nM–10 μM indomethacin ±500 nM CP55940 **(B,D)** for 10 min and ERK1/2 **(A,B)** or PLCβ3 **(C,D)** phosphorylation was measured. **(E,F)** HEK293A cells expressing hCB1R-GFP^2 and βarrestin1-Rluc were treated with 1 nM–10 μM CP55940 ± 1 μM indomethacin **(E)** or 1 nM–10 μM indomethacin ±500 nM CP55940 **(F)** for 30 min and BRET^2 was measured. **(G)** HEK-CRE cells expressing hCB1R-GFP^2 were treated with 10 μM forskolin, 1 nM–10 μM CP55940 ± 1 μM indomethacin for 1 h. *$P < 0.01$ compared to CP55940 alone within dose as determined via one-way ANOVA followed by Tukey's *post hoc* analysis. Data are mean ± SEM. $N = 4$. **(H,I)** HEK293A cells expressing hCB2R-GFP^2 were treated with 1 nM–10 μM CP55940 ± 1 μM indomethacin for 10 min and ERK1/2 **(H)** or PLCβ3 **(I)** phosphorylation was measured. **(J)** HEK293A cells expressing hCB2R-GFP^2 and βarrestin1-Rluc were treated with 1 nM–10 μM CP55940 ± 1 μM indomethacin for 30 min and BRET^2 was measured. **(K)** HEK-CRE cells expressing hCB2R-GFP^2 were treated with 10 μM forskolin, 1 nM–10 μM CP55940 ± 1 μM indomethacin for 1 h. Data are mean ± SEM. $N = 4$.

TABLE 2 | Potency and efficacy of indomethacin at modulating agonist-dependent signaling.

	EC_{50} (nM) (95% CI)		E_{max} (%) ± SEM	
	CP55940	**+1 μM Indomethacin**	**CP55940**	**+1 μM Indomethacin**
HEK hCB1R[a]				
ERK	340 (240–480)	170 (100–270)	100 ± 5.6	110 ± 4.0
PLCβ3	350 (230–520)	180 (120–280)	100 ± 5.7	120 ± 5.0*
βarrestin1	240 (88–570)	170 (75–730)	100 ± 12	110 ± 10
cAMP	160 (83–290)	150 (65–300)	0.0 ± 7.9	−88 ± 14*
HEK hCB2R[b]				
ERK	390 (210–660)	440 (230–800)	100 ± 9.2	109 ± 11
PLCβ3	500 (270–870)	450 (250–770)	100 ± 10	103 ± 9.1
βarrestin1	490 (310–760)	470 (290–750)	100 ± 8.3	111 ± 8.6
cAMP	350 (190–600)	590 (360–960)	0.0 ± 6.1	−26 ± 8.5
	CHO hCB1R[c]			
	EC_{50} (nM) (95% CI)		E_{max} (%) ± SEM	
	CP55940	**100 nM CP55940 + Indomethacin**	**CP55940**	**100 nM CP55940 + Indomethacin**
cAMP	140 (71–285)	10 (0.61–160)	0.0 ± 18	22 ± 11
βarrestin2	620 (240–1, 600)	570 (380–850)	100 ± 11	110 ± 4.0
	EC_{50} (nM) (95% CI)		E_{max} (%) ± SEM	
	AEA	**100 nM AEA + Indomethacin**	**AEA**	**100 nM AEA + Indomethacin**
cAMP	2, 900 (260–3, 300)	1.9 (0.06–6.1)	5.9 ± 3.9	23 ± 5.9
βarrestin2	>10,000	>10,000	16 ± 2.1	18 ± 1.4

*[a]Data are from **Figures 3A,C,E,G**. [b]Data are from **Figures 3H–K**. [c]Data are from **Figure 4**. *P < 0.01 compared to CP55940 as determined by one-way ANOVA followed by Tukey' post hoc analysis. N = 4 (HEK hCB1R and HEK hCB2R), N = 5 (CHO hCB1R cAMP), N = 6 (CHO hCB1R βarrestin2).*

transmembrane helix number, the residue position relative to the most conserved position (e.g., F2.62)] (Ballesteros and Weinstein, 1995). Ligand ".mol2" structure and formula files for indomethacin were downloaded from ZINC (Irwin et al., 2012). Three-dimensional models of human CB1R were generated in Swiss-MODEL from the template structures (5XRA) (Arnold et al., 2006; Kiefer et al., 2009). All settings were kept at default. Ligands were docked to model receptors using AutoDock 4.2.6 (Morris et al., 2009) by Lamarckian genetic algorithm (Hurst et al., 2006). AutoDock uses a Monte Carlo simulated annealing algorithm to explore a defined grid within the virtual space of a protein model with a selected ligand. The ligand is used to probe the defined grid space via molecular affinity potentials in various conformations of ligand and receptor. The binding site of the models were defined using the AutoGrid program within AutoDock and the grid box was set to dimensions of 20 × 20 × 20 Å in order to include the entire extracellular surface and transmembrane regions of the model receptors. The rigidity parameters were set for the receptor and the ligands were kept flexible. All other parameters were set to default. The AutoDock algorithm AutoDock Vina 1.1.2 (Morris et al., 2009; Trott and Olson, 2010) was used to fit the ligand to the template. The best conformation for each ligand-receptor is based on the lowest binding energy among eight bioactive conformations generated by eight repeated program iterations.

RESULTS

Radioligand Binding and [^{35}S]GTPγS Binding Assay

We determined how indomethacin modulated the binding of CP55940 – a high affinity, synthetic CB1R reference ligand – to hCB1R. Indomethacin enhanced [^{3}H]CP55940 binding to hCB1R in CHO cell membranes between 10 nM and 10 μM (**Figure 2A**). The indomethacin concentration-[^{3}H]CP55940 binding relationship was bell-shaped, with the greatest enhancement of binding occurring at 10 and 100 nM, suggesting that indomethacin may only enhance orthosteric ligand binding within a narrow concentration range, and at higher doses indomethacin may have reduced CP55940-hCB1R binding (**Figure 2A**). Indomethacin (1 μM) did not change the rate of dissociation of [^{3}H]CP55940 compared to vehicle (**Figure 2B** and **Table 1**). Therefore, indomethacin enhanced the binding affinity of CP55940 at hCB1R, but did not change the dissociation rate of CP55940. Overall, these data are consistent with indomethacin acting as a PAM of orthosteric ligand binding at hCB1R. In order to assess the ability of indomethacin to modulate G protein activation, [^{35}S]GTPγS binding assays were conducted in CHO cells stably expressing hCB1R. In the presence of 1 nM and 10 μM AEA, 1 μM indomethacin enhanced the [^{35}S]GTPγS binding to hCB1R (**Figure 2C**).

Indomethacin did not effect [^{35}S]GTPγS binding to hCB2R (data not shown).

βarrestin1, ERK1/2, PLCβ3, and cAMP

Indomethacin-dependent modulation of hCB1R and hCB2R signaling was examined in HEK293A cells, which are a well-established model system for studying cannabinoid receptors (Hudson et al., 2010; Laprairie et al., 2015, 2017; Tham et al., 2018). The effect of indomethacin on CP55940-dependent hCB1R and hCB2R activation was measured in HEK293A cells expressing either hCB1R-GFP^2 or hCB2R-GFP^2 (**Figure 3** and **Table 2**). Indomethacin alone did not alter hCB1R-dependent βarrestin1 recruitment, ERK1/2 and PLCβ3 phosphorylation, or cAMP levels (**Figures 3A,C,E,G**). Indomethacin (1 μM) produced a significant leftward and upward shift in the CRCs for βarrestin1 recruitment, ERK1/2 and PLCβ3 phosphorylation, and cAMP inhibition (**Figures 3A,C,E,G**). Indomethacin alone did not alter hCB2R-dependent βarrestin1 recruitment, ERK1/2 or PLCβ3 phosphorylation, or cAMP inhibition in HEK293A cells expressing hCB2R (**Figure 3** and **Table 2**). Therefore, indomethacin enhanced hCB1R-dependent signaling, and not hCB2R-dependent signaling, in a manner consistent with a PAM.

Indomethacin-dependent modulation of hCB1R signaling was further assessed in the DiscoveRx CHO HitHunter and PathHunter cells for βarrestin2 recruitment and cAMP inhibition in the presence of 100 nM CP55940 or AEA in order to assess ligand bias, PAM activity in the presence of the endogenous agonist, and probe dependence between CP55940 and AEA (**Figure 4**). Indomethacin alone did not alter hCB1R-dependent cAMP inhibition or βarrestin2 recruitment. Indomethacin enhanced 100 nM CP55940-dependent cAMP inhibition and βarrestin2 recruitment (**Figures 4A,B**). Further, indomethacin enhanced 100 nM AEA-dependent inhibition of cAMP but did not alter AEA-dependent βarrestin2 recruitment (**Figures 4C,D**). Indomethacin in the presence of CP55940 did not display bias between cAMP inhibition and βarrestin2 recruitment, whereas indomethacin in the presence of AEA did selectively enhance inhibition of cAMP relative to βarrestin2 recruitment, as determined by fitting these data with the operational model (**Figure 4E**). Therefore, indomethacin displayed hCB1R PAM activity with probe-dependence for AEA-dependent inhibition of cAMP.

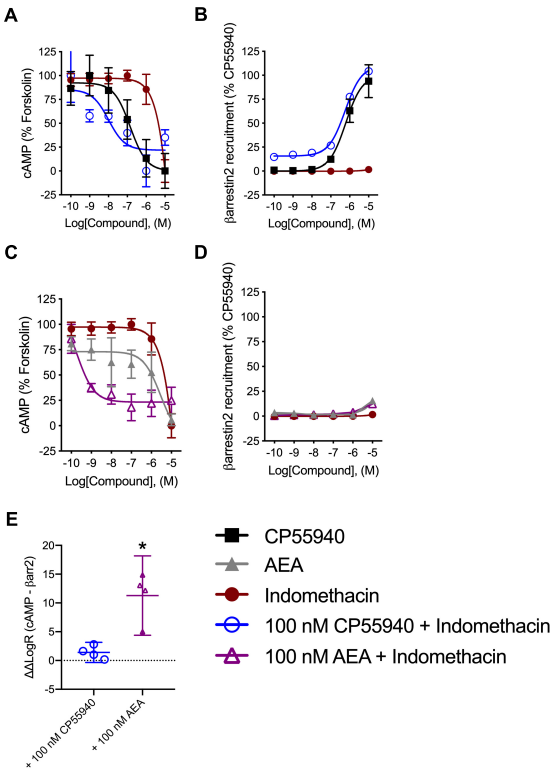

FIGURE 4 | Analysis of indomethacin bias at hCB1R in CHO cells. CHO HitHunter cAMP cells **(A,C)** or PathHunter βarrestin2 cells **(B,D)** stably expressing hCB1R were treated with 0.1 nM–10 μM CP55940, AEA, indomethacin, 100 nM CP55940 + 0.1 nM–10 μM indomethacin, or 100 nM AEA + 0.1 nM = 10 μM indomethacin for 90 min. CHO HitHunter cAMP cells were also treated with 10 μM forskolin. hCB1R-depednent inhibition of forskolin-induced cAMP accumulation **(A,C)** or βarrestin2 recruitment **(B,D)** was measured. Data are mean ± SEM. $N = 5$ in panels **(A,C)**, $N = 6$ in panels **(B,D)**. **(E)** Data were fit to the operational model to calculate ΔΔLogR (cAMP–βarrestin2) such that values >0 represent bias for inhibition of cAMP and values <0 represent bias for recruitment of βarrestin2. Data are individually plotted with mean and 95% confidence interval. *$P < 0.05$ compared to 0 as determined by 95% confidence interval. $N = 4$.

RT-PCR

Indomethacin is thought to interact with a number of targets, including COX-1 (*PTGS1*), COX-2 (*PTGS2*), the prostaglandin D2 receptor 2 (PTGDR2/CRTH2/PGD2; *PTGDR2*), peroxisome proliferator-activated receptor γ (PPARγ; *PPARG*), and fatty acid amide hydrolase (FAAH; *FAAH*) (Lehmann et al., 1997; Sawyer et al., 2002; Hata et al., 2005; Sugimoto et al., 2005; Holt et al., 2007). To determine whether indomethacin could have affected non-CB1R targets in HEK293A cells, mRNA was isolated, and COX-1, COX-2, PTGDR2, PPARγ, and FAAH transcripts levels were assessed by RT-PCR. hCB1R was readily detectable in HEK293A cells transfected with the hCB1R-GFP^2 plasmid, but not detected in non-transfected HEK293A cells (-) (**Figure 5**). PPARγ transcript was detected, but no transcripts were detected for FAAH, COX-1, COX-2, or PTGDR2 (**Figure 5**). Therefore, the indomethacin-dependent enhanced CB1R signaling observed in HEK293A cells occurred via allosteric modulation of CB1R, and not through other protein targets of indomethacin. Indomethacin-mediated CB1R PAM activity may be less-evident in cell culture systems where COX-1, COX-2, PTGDR2, PPARγ, and FAAH are expressed and *in vivo*.

In vivo Analyses

The ability of indomethacin to enhance CB1R-dependent effects was assessed *in vivo* using tetrad analysis over 4 h (indomethacin $t_{1/2}$ in mouse 51 min, 4.7 half-lives) (Remmel et al., 2004). Tail flick latency was increased by both CP55940 (0.1 mg/kg) and indomethacin (2 mg/kg) at 0.5, 1, and 4 h compared to vehicle treatment, and increased by the combination of CP55940 and indomethacin (4 mg/kg) at 1 h compared to CP55940 or

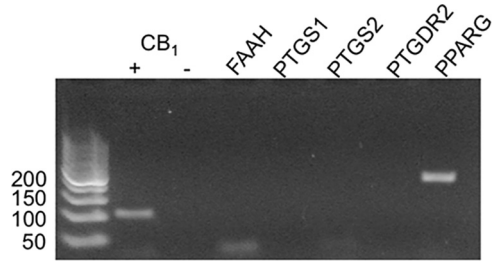

FIGURE 5 | mRNA expression of potential indomethacin targets in HEK293A cells. The expression of several gene transcripts whose protein products are considered targets for indomethacin was evaluated in HEK293A cells using RT-PCR. hCB1R cDNA was detectable in cells transfected with hCB1R-GFP[2] (+) and not untransfected cells (-). FAAH, fatty acid amide hydrolase; PTGS1 and 2, COX-1 and -2; PPARG, PPARγ.

indomethacin alone (**Figure 6A**). Catalepsy was increased by CP55940 alone at 1 and 4 h, but not indomethacin (**Figure 6B**). Catalepsy time was significantly increased by 2 and 4 mg/kg of indomethacin with CP55940 compared to CP55940 alone at 1 h (**Figure 6B**). Body temperature was reduced by both CP55940 and indomethacin at 0.5 and 1 h compared to vehicle treatment, and further reduced by the combination of CP55940 and indomethacin (4 mg/kg) at 0.5 and 1 h compared to CP55940 or indomethacin alone (**Figure 6C**). Locomotion (i.e., distance traveled in the open field) was reduced by CP55940 at 1 and 4 h compared to vehicle treatment, and further reduced by the combination of CP55940 and indomethacin (4 mg/kg) at 4 h compared to CP55940 or indomethacin alone (**Figure 6D**).

In silico Ligand Docking

Simulated docking of indomethacin to CB1R-5XRA was modeled in AutoDock 4.2.6. to predict possible binding sites of indomethacin in an active conformation of CB1R bound orthosteric agonist AM11542 (a CP55940 derivative) (**Figure 7**). Indomethacin bound a subset of residues on the exterior surface of transmembrane helices 2 and 3 (**Figure 7**) that do not overlap with those of the orthosteric agonist (S1.39, F2.57, F2.61, F2.64, H2.65, F3.25, L3.29, V3.32, F3.36, L5.40, W5.43, M6.55, W6.48, L6.51, F7.35, A7.36, S7.39, M7.40, C7.42, and L7.43) (Hua et al., 2017). Amino acid residue K3.28 has been previously reported to interact with Org27569 and PSNCBAM-1 (Hurst et al., 2006). Importantly, amino acid residues Y2.59, F3.27 were recently reported to interact with the well-known CB1R PAM GAT229 and also interacted with indomethacin in this model (Hurst et al., 2019), supporting a shared binding site for these CB1R PAM. Ligand affinity was estimated for the 5XRA-CB1R model in AutoDock 4.2.6. for indomethacin and the estimated K_A value for indomethacin was 450 nM, which is similar to the potency observed for indomethacin as a CB1R PAM *in vitro*.

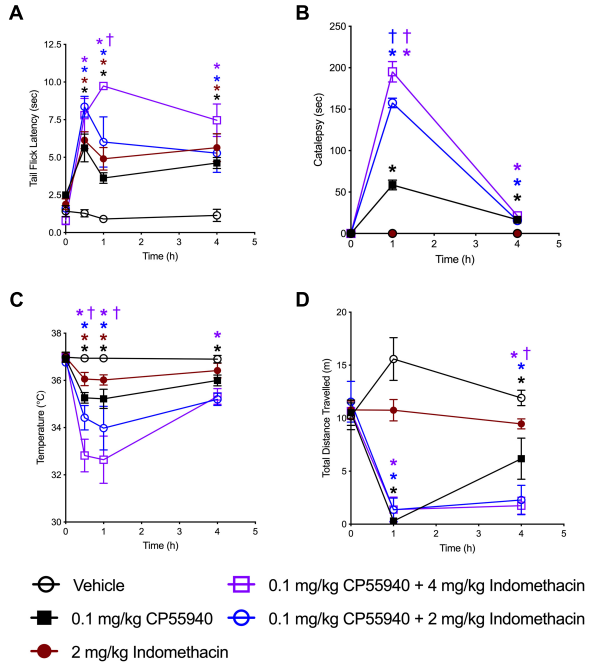

FIGURE 6 | Indomethacin enhanced CP55940-dependent tetrad effects. Seven-week old, male, C57BL/6 mice were injected (*i.p.*) with vehicle, CP55940 (0.1 mg/kg), indomethacin (2 mg/kg), CP55940 (0.1 mg/kg) + indomethacin (2 mg/kg), or CP55940 (0.1 mg/kg) + indomethacin (4 mg/kg) and tetrad tests were completed as follows: tail flick latency at 0 (prior to treatment), 0.5, 1, and 4 h after injection **(A)**, catalepsy at 0, 1, and 4 h after injection **(B)**, internal body temperature at 0, 0.5, 1, and 4 h after injection **(C)**, total distance traveled in the open field at 0, 1, and 4 h after injection **(D)**. $^{*}P < 0.01$ compared to vehicle within time point, $^{\dagger}P < 0.01$ compared to CP55940 alone within timepoint, as determined via two-way ANOVA followed by Bonferroni's *post hoc* analysis. Data are mean ± SEM. $N = 5$ per treatment group.

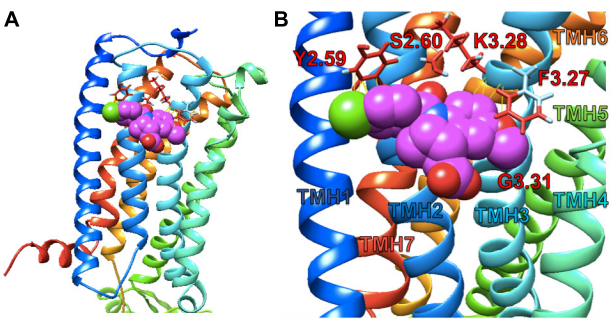

FIGURE 7 | Indomethacin docking to CB1R 5XRA (agonist-bound). **(A)** The perspective is from the lipid bilayer. Helices are blue (I), light blue (II), turquoise (III), seafoam (IV), green (V), gold (VI), and orange (VII). Indomethacin is shown in magenta. **(B)** Image as in **(A)** at a closer perspective. Interacting amino acid residues are named according to the Ballesteros and Weinstein (1995) system. Transmembrane helices (TMH) are labelled by number.

DISCUSSION

In this study, we present evidence that the NSAID indomethacin acted as a PAM of CB1R *in vitro* and *in vivo*. Indomethacin is known to interact with a number of proteins, including the multidrug resistance proteins 1 and 4, COX-1, COX-2, PTGDR2/CTRH2, PPARγ, and the AEA-metabolizing enzyme

FAAH (Lehmann et al., 1997; Hata et al., 2005; Sugimoto et al., 2005; Holt et al., 2007). The non-selective activity of indomethacin may explain several of the side effects associated with this drug, including dyspepsia, heartburn, diarrhea, edema, and hypertension (Fowler, 1987). In the present study, the CB1R PAM activity of indomethacin ranged in potency from 10 nM (cAMP inhibition assay) to 570 nM (βarrestin2 recruitment assay) in the presence of CP55940 (**Table 2**). By comparison, indomethacin inhibits COX-1 (250 nM), PTGDR2/CTRH2 (20–790 nM), and PPARγ (40 nM) within a similar concentration range to the potencies observed for CB1R-dependent signaling (Lehmann et al., 1997; Sawyer et al., 2002; Hata et al., 2005; Sugimoto et al., 2005). In contrast to these effects, indomethacin has been shown to inhibit MRP1 and 4 (11 and 102 μM, respectively), FAAH (1.2 μM), and COX-2 (2.5 μM) at much higher concentrations (Reid et al., 2003; Holt et al., 2007). Several additional CNS-specific side effects associated with indomethacin use but not other NSAIDs, such as headache, vertigo, and dizziness, blurred vision, and psychosis following prolonged use, may be explained by the drug's modulation of the endocannabinoid system and/or CB1R (Wiley et al., 2006; Parvathy and Masocha, 2015). The endogenous substrates of COX-1, COX-2, PPARγ, FAAH, and CB1R share similar chemical structures and physical properties. Moreover, exogenous cannabinoids such as Δ^9-tetrahydrocannabinol (THC) are known to modulate COX enzymes (Chen et al., 2013). The CB1R PAM activity of indomethacin – and similar observations such as CB1R PAM activity by fenofibrate (PPARγ agonist) (Priestley et al., 2015), and FAAH inhibition by acetaminophen (Ottani et al., 2006) – indicate a pharmacological overlap between these proteins.

In vitro, indomethacin enhanced CP55940 binding and activation of hCB1R in [^{35}S]GTPγS, ERK1/2, PLCβ3, βarrestin1, βarrestin2, and cAMP assays. Indomethacin also enhanced AEA-dependent inhibition of cAMP – but did not enhance AEA-dependent βarrestin2 recruitment – indicating indomethacin's effects are probe-dependent, biased toward cAMP inhibition in the presence of endogenous agonist, and occur in the presence of endogenous agonist. These experiments were conducted in acute treatment paradigms and in cell signaling systems that overexpress human CB1R. Subsequent studies exploring indomethacin-dependent modulation of CB1R in long-term treatment, endogenous expression systems, and on electrophysiological outputs will enhance our understanding of indomethacin PAM activity (Straiker et al., 2018). Binding of indomethacin to an allosteric site of CB1R could have shifted the equilibrium of CB1R from the inactive R state, to the more active R* state (Iliff et al., 2011; Fay and Farrens, 2012; Shore et al., 2014). Our *in silico* modeling of CB1R with the active R* state model (5XRA) further supports indomethacin binding a unique allosteric pocket distinct from Org27569 or PSNCBAM-1 (Iliff et al., 2011; Fay and Farrens, 2012). The CB1R allosteric modulators Org27569 and PSNCBAM-1 have been shown to promote R* state conformation and increase orthosteric ligand binding (Iliff et al., 2011; Fay and Farrens, 2012; Shore et al., 2014); and our modeled indomethacin binding site overlaps that of the recently modeled GAT229 CB1R PAM binding site (Hurst et al., 2019). Org27569 and PSNCBAM-1 enhance CP55940 binding, but not CB1R-dependent signaling (Price et al., 2005; Shore et al., 2014), whereas indomethacin enhanced both binding and signaling because of its topologically distinct binding site.

In vivo, indomethacin was able to promote anti-nociceptive and hypothermic effects alone at 2 mg/kg and enhance all 4 CP55940-dependent tetrad effects at 2 and 4 mg/kg. Indomethacin may have induced tetrad effects alone via inhibition of its other known targets, COX-1/2 and FAAH, which would lead to elevated levels of endocannabinoids. The potentiating effects of indomethacin ceased within the 4 h time course of the experiment, which is consistent with the 51 min half-life of indomethacin in mice (Remmel et al., 2004). Moreover, although 90% of indomethacin is plasma-protein bound, free [^{14}C]indomethacin has been shown to rapidly penetrate the rat brain via transporter-independent mechanisms (Parepally et al., 2006). These data support the hypothesis that *in vivo* effects observed in our study were brain CB1R-dependent. Other CB1R PAMs that contain indole-2-carboxamides, such as GAT211 and ZCZ011, enhance some CB1R-dependent effects *in vivo* (Slivicki et al., 2018). Other CB1R allosteric ligands, such as Org27569 and PSNCBAM-1, have limited efficacy *in vivo*, potentially because of poor pharmacokinetic properties (Ignatowska-Jankowska et al., 2015; Gamage et al., 2017).

Wiley et al. (2006) reported that indomethacin (10 or 30 mg/kg) enhanced AEA-dependent (30 mg/kg) hypolocomotion, anti-nociception, hypothermia, and immobility in ICR mice. The authors suggest that indomethacin may have potentiated AEA's effects via reduced metabolism of AEA (Wiley et al., 2006), which is supported by other studies (Fowler et al., 1997a,b, 1999; Holt et al., 2007). Parvathy and Masocha (2015) have also reported that indomethacin reduces neuropathic thermal paclitaxel-induced hyperalgesia via CB1R. Our studies utilized a lower dose of indomethacin (2 or 4 mg/kg) in an acute treatment paradigm and demonstrated the potentiation of CP55940-dependent effects. Indomethacin, and other COX inhibitors, have also been shown to reduce the efficacy of chronically administered CB1R agonists *in vivo* (Yamamguchi et al., 2001; Anikwue et al., 2002). Previous studies that described interactions between COX inhibitors and CB1R agonists utilized chronically administered cannabinoid agonist. Here, the acute co-administration of CP55940 and indomethacin enhanced by CP55940-mediated effects (Yamamguchi et al., 2001; Anikwue et al., 2002). Although we did not explore the possible role of metabolites in our acute study, it is possible that the metabolites of indomethacin may also affect the activity of CB1R and other targets in acute and chronic treatment paradigms. Chronic cannabinoid administration is known to produce receptor desensitization and downregulation, which may account for the decreased efficacy observed in earlier studies. Future studies will explore chronic CB1R-dependent effects *in vivo*.

Indomethacin enhanced the efficacy, potency, and ligand binding of CB1R agonists *in vitro* and *in vivo* in a manner consistent with positive allosteric modulation. Therefore, indomethacin may be a useful probe compound to understand the structure-activity relationship of CB1R allosteric modulators, and modulators of FAAH and COX enzymes, and in the

development of novel therapeutic compounds with specificity for these components of the endocannabinoid system.

DATA AVAILABILITY STATEMENT

The raw data supporting the conclusions of this manuscript will be made available by the authors, without undue reservation, to any qualified researcher.

ETHICS STATEMENT

The animal study was reviewed and approved by the Dalhousie University Animal Care Committee.

AUTHOR CONTRIBUTIONS

RL designed, executed, and analyzed the experiments, and contributed to the writing and editing of the manuscript. KM, AZ, and LS designed, executed, and analyzed the experiments. MK, RP, and ED-W designed the experiments, and contributed to the writing and editing of the manuscript. GT proposed the hypothesis that indomethacin can act as a CB1R PAM, provided the research material, analyzed the experiments, and contributed to the writing and editing of the manuscript.

FUNDING

KM is supported by a scholarship from the Natural Sciences and Engineering Research Council (NSERC USRA). This work was supported by grants from the National Institutes on Drug Abuse (NIDA) at the National Institutes of Health (NIH) to RP, MK, and GT (DA027113 and EY024717); a Bridge Funding Grant from Dalhousie University to ED-W; and a partnership grant from GlaxoSmithKline-Canadian Institutes of Health Research (CIHR, 368247) and a Collaborative Research and Development grant (NSERC, CRDPJ 517839-17) to RL.

ACKNOWLEDGMENTS

We thank Dr. Alex Straiker for his independent review of the data. We thank Dr. Amina Bagher for her assistance in blinding and conducting animal experiments.

SUPPLEMENTARY MATERIAL

The Supplementary Material for this article can be found online at: https://www.frontiersin.org/articles/10.3389/fnmol.2019.00257/full#supplementary-material

REFERENCES

Ahn, K. H., Mahmoud, M. M., and Kendall, D. A. (2012). Allosteric modulator ORG27569 induces CB1 cannabinoid receptor high affinity agonist binding state, receptor internalization, and Gi proteiindependent ERK1/2 kinase activation. *J. Biol. Chem.* 287, 12070–12082. doi: 10.1074/jbc.M111.316463

Anikwue, R., Huffman, J. W., Martin, Z. L., and Welch, S. P. (2002). Decrease in efficacy and potency of nonsteroidal anti-inflammatory drugs by chronic Δ9-tetrahydrocannabinol administration. *J. Pharmacol. Exp. Ther.* 303, 340–346. doi: 10.1124/jpet.303.1.340

Arnold, K., Bordoli, L., Kopp, J., and Schwede, T. (2006). The SWISS-MODEL workspace: a web-based environment for protein structure homology modelling. *Bioinformatics* 22, 195–201. doi: 10.1093/bioinformatics/bti770

Bagher, A. M., Laprairie, R. B., Kelly, M. E., and Denovan-Wright, E. M. (2013). Co-expression of thehuman cannabinoid receptor coding region splice variants (hCB1) affects the function of hCB1 receptor complexes. *Eur. J. Pharmacol.* 721, 341–354. doi: 10.1016/j.ejphar.2013.09.002

Baillie, G. L., Horswill, J. G., Anavi-Goffer, S., Reggio, P. H., Bolognini, D., Abood, M. E., et al. (2013). CB1 receptor allosteric modulators display both agonist and signaling pathway specificity. *Mol. Pharmacol.* 83, 322–338. doi: 10.1124/mol.112.080879

Ballesteros, J. A., and Weinstein, H. (1995). Integrated methods for the construction of three-dimensional models and computational probing of structure-function relations in G protein-coupled receptors. *Methods Neurosci.* 25, 366–428. doi: 10.1016/s1043-9471(05)80049-7

Black, J. W., and Leff, P. (1983). Operational models of pharmacological agonism. *Proc. R. Soc. Lond. B Biol. Sci.* 220, 141–162. doi: 10.1098/rspb.1983.0093

Bolognini, D., Cascio, M. G., Parolaro, D., and Pertwee, R. G. (2012). AM630 behaves as a protean ligand at the human cannabinoid CB2 receptor. *Br. J. Pharmacol.* 165, 2561–2574. doi: 10.1111/j.1476-5381.2011.01503.x

Bolognini, D., Costa, B., Maione, S., Comelli, F., Marini, P., Di Marzo, V., et al. (2010). The plant cannabinoid Δ9-tetrahydrocannabivarin can decrease signs of inflammation and inflammatory pain in mice. *Br. J. Pharmacol.* 160, 677–687. doi: 10.1111/j.1476-5381.2010.00756.x

Cawston, E. E., Connor, M., Di Marzo, V., Silvestri, R., and Glass, M. (2015). Distinct temporal fingerprint for cyclic adenosine monophosphate (cAMP) signaling of indole-2-carboxamides as allosteric modulators of the cannabinoid receptors. *J. Med. Chem.* 58, 5979–5988. doi: 10.1021/acs.jmedchem.5b00579

Cawston, E. E., Redmond, W. J., Breen, C. M., Grimsey, N. L., Connor, M., and Glass, M. (2013). Real-time characterization of cannabinoid receptor 1 (CB1) allosteric modulators reveals novel mechanism of action. *Br. J. Pharmacol.* 170, 893–907. doi: 10.1111/bph.12329

Chen, R., Zhang, J., Fan, N., Teng, Z. Q., Wu, Y., Yang, H., et al. (2013). Δ9-THC-caused synaptic and memory impairments are mediated through COX-2 signaling. *Cell* 155, 1154–1165. doi: 10.1016/j.cell.2013.10.042

Fay, J. F., and Farrens, D. L. (2012). A key agonist-induced conformational change in the cannabinoid receptor CB1 is blocked by the allosteric ligand Org27569. *J. Biol. Chem.* 287, 33873–33882. doi: 10.1074/jbc.m112.352328

Fowler, C. J., Janson, U., Johnson, R. M., Wahlström, G., Stenström, A., Norström, K., et al. (1999). Inhibition of anandamide hydrolysis by the enantiomers of ibuprofen, ketorolac, and flurbiprofen. *Arch. Biochem. Biophys.* 362, 191–196. doi: 10.1006/abbi.1998.1025

Fowler, C. J., Stenström, A., and Tiger, G. (1997a). Ibuprofen inhibits the metabolism of the endogenous cannabimimetic agent anandamide. *Pharmacol. Toxicol.* 80, 103–107. doi: 10.1111/j.1600-0773.1997.tb00291.x

Fowler, C. J., Tiger, G., and Stenström, A. (1997b). Ibuprofen inhibits rat brain deamidation of anandamide at pharmacologically relevant concentrations. Mode of inhibition and structure-activity relationship. *J. Pharmacol. Exp. Ther.* 283, 729–734.

Fowler, P. D. (1987). Aspirin, paracetamol and non-steroidal anti-inflammatory drugs. A comparative review of side effects. *Med. Toxicol. Adverse Drug Exp.* 2, 338–366. doi: 10.1007/bf03259953

Gamage, T. F., Farquhar, C. E., Lefever, T. W., Thomas, B. F., Nguyen, T., Zhang, Y., et al. (2017). The great divide: separation between in vitro and in vivo effects of PSNCBAM-based CB1 receptor allosteric modulators. *Neuropharmacology* 125, 365–375. doi: 10.1016/j.neuropharm.2017.08.008

Hata, A. N., Lybrand, T. P., and Breyer, R. M. (2005). Identification of determinants of ligand binding affinity and selectivity in the prostaglandin D2 receptor CRTH2. *J. Biol. Chem.* 280, 32442–32451. doi: 10.1074/jbc.m502563200

Holt, S., Paylor, B., Boldrup, L., Alajakku, K., Vandevoorde, S., Sundström, A., et al. (2007). Inhibition of fatty acid amide hydrolase, a key endocannabinoid metabolizing enzyme, by analogues of ibuprofen and indomethacin. *Eur. J. Pharmacol.* 565, 26–36. doi: 10.1016/j.ejphar.2007.02.051

Hua, T., Vemuri, K., Nikas, S. P., Laprairie, R. B., Wu, Y., Qu, L., et al. (2017). Crystal structures of agonist-bound human cannabinoid receptor CB1. *Nature* 547, 468–471. doi: 10.1038/nature23272

Hudson, B. D., Hébert, T. E., and Kelly, M. E. (2010). Physical and functional interaction between CB1 cannabinoid receptors and beta2-adrenoceptors. *Br. J. Pharmacol.* 160, 627–642. doi: 10.1111/j.1476-5381.2010.00681.x

Hurst, D., Umejiego, U., Lynch, D., Seltzman, H., Hyatt, S., Roche, M., et al. (2006). Biarylpyrazole inverse agonists at the cannabinoid CB1 receptor: importance of the C-3 carboxamide oxygen/lysine3.28(192) interaction. *J. Med. Chem.* 49, 5969–5987. doi: 10.1021/jm060446b

Hurst, D. P., Garai, S., Kulkarni, P. M., Schaffer, P. C., Reggio, P. H., and Thakur, G. A. (2019). Identification of CB1 receptor allosteric sites using fore-biased MMC simulated annealing and validation by structure-activity studies. *ACS Med. Chem. Lett.* 10, 2116–2121. doi: 10.1021/acsmedchemlett.9b00256

Ignatowska-Jankowska, B. M., Baillie, G. L., Kinsey, S., Crowe, M., Ghosh, S., Allen Owens, R., et al. (2015). A cannabinoid CB1 receptor positive allosteric modulator reduces neuropathic pain in the mouse with no psychoactive effects. *Neuropsychopharmacology* 40, 2948–2959. doi: 10.1038/npp.2015.148

Iliff, H. A., Lynch, D. L., Kotsikorou, E., and Reggio, P. H. (2011). Parameterization of Org27569: an allosteric modulator of the cannabinoid CB1 G protein-coupled receptor. *J. Comput. Chem.* 32, 2119–2126. doi: 10.1002/jcc.21794

Irwin, J. J., Sterling, T., Mysinger, M. M., Bolstad, E. S., and Coleman, R. G. (2012). ZINC: a free tool to discover chemistry for biology. *J. Chem. Inf. Model.* 52, 1757–1768. doi: 10.1021/ci3001277

James, J. R., Oliveira, M. I., Carmo, A. M., Iaboni, A., and Davis, S. J. (2006). A rigorous experimental framework for detecting protein oligomerization using bioluminescence resonance energy transfer. *Nat. Methods* 3, 1001–1006. doi: 10.1038/nmeth978

Kiefer, F., Arnold, K., Künzli, M., Bordoli, L., and Schwede, T. (2009). The SWISS-MODEL repository and associated resources. *Nucleic Acids Res.* 37, D387–D392. doi: 10.1093/nar/gkn750

Kilkenny, C., Browne, W. J., Cuthill, I. C., Emerson, M., and Altman, D. G. (2010). Improving bioscience research reporting: the ARRIVE guidelines for reporting animal research. *PLoS Biol.* 29:e1000412. doi: 10.1371/journal.pbio.1000412

Laprairie, R. B., Bagher, A. M., Dupré, J. D., Kelly, M. E. M., and Denovan-Wright, E. M. (2014). Type 1 cannabinoid receptor ligands display functional selectivity in a cell culture model of striatal medium spiny projection neurons. *J. Biol. Chem.* 289, 24845–24862. doi: 10.1074/jbc.M114.557025

Laprairie, R. B., Bagher, A. M., Kelly, M. E. M., and Denovan-Wright, E. M. (2015). Cannabidiol is a negative allosteric modulator of the type 1 cannabinoid receptor. *Br. J. Pharmacol.* 172, 4790–4805. doi: 10.1111/bph.13250

Laprairie, R. B., Bagher, A. M., Rourke, J. L., Zrein, A., Cairns, E. A., Kelly, M. E. M., et al. (2019). Positive allosteric modulation of the type 1 cannabinoid receptor reduces the signs and symptoms of Huntington's disease in the R6/2 mouse model. *Neuropharmacology* 151, 1–12. doi: 10.1016/j.neuropharm.2019.03.033

Laprairie, R. B., Kulkarni, P. M., Deschamps, J. R., Kelly, M. E. M., Janero, D. R., Cascio, M. G., et al. (2017). Enantiospecific allosteric modulation of cannabinoid 1 receptor. *ACS Chem. Neurosci.* 8, 1188–1203. doi: 10.1021/acschemneuro.6b00310

Lehmann, J. M., Lenhard, J. M., Oliver, B. B., Ringold, G. M., and Kliewer, S. A. (1997). Peroxisome proliferator-activated receptors alpha and gamma are activated by indomethacin and other non-steroidal anti-inflammatory drugs. *J. Biol. Chem.* 272, 3406–3410. doi: 10.1074/jbc.272.6.3406

Lu, D., Immadi, S. S., Wu, Z., and Kendall, D. A. (2018). Translational potential of allosteric modulators targeting the cannabinoid CB1 receptor. *Acta Pharmacol. Sin.* 40, 324–335. doi: 10.1038/s41401-018-0164-x

Morris, G. M., Huey, R., Lindstrom, W., Sanner, M. F., Belew, R. K., Goodsell, D. S., et al. (2009). Autodock4 and AutoDockTools4: automated docking with selective receptor flexiblity. *J. Comput. Chem.* 16, 2785–2789. doi: 10.1002/jcc.21256

Ottani, A., Leone, S., Sandrini, M., Ferrari, A., and Bertolini, A. (2006). The analgesic activity of paracetamol is prevented by the blockade of cannabinoid CB1 receptors. *Eur. J. Pharmacol.* 531, 280–281. doi: 10.1016/j.ejphar.2005.12.015

Pamplona, F. A., Ferreira, J., Menezes de Lima, O. Jr., Duarte, F. S., Bento, A. F., Forner, S., et al. (2012). Anti-inflammatory lipoxin A4 is an endogenous allosteric enhancer of CB1 cannabinoid receptor. *Proc. Natl. Acad. Sci. U.S.A.* 109, 21134–21139. doi: 10.1073/pnas.1202906109

Parepally, J. M. R., Mandula, H., and Smith, Q. R. (2006). Brain uptake on nonsteroidal anti-inflammatory drugs: ibuprofen, flurbiprofen, and indomethacin. *Pharm. Res.* 23, 873–881. doi: 10.1007/s11095-006-9905-5

Parvathy, S. S., and Masocha, W. (2015). Coadministration of indomethacin and minocycline attenuates established paclitaxel-induced neuropathic thermal hyperalgesia: involvement of cannabinoid CB1 receptors. *Sci. Rep.* 5:10541. doi: 10.1038/srep10541

Pertwee, R. G. (2008). Ligands that target cannabinoid receptors in the brain: from THC to anandamide and beyond. *Addict. Biol.* 13, 147–159. doi: 10.1111/j.1369-1600.2008.00108.x

Price, M. R., Baillie, G. L., Thomas, A., Stevenson, L. A., Easson, M., Goodwin, R., et al. (2005). Allosteric modulation of the cannabinoid CB1 receptor. *Mol. Pharmacol.* 68, 1484–1495.

Priestley, R. S., Nickolls, S. A., Alexander, S. P. H., and Kendall, D. A. (2015). A potential role for cannabinoid receptors in the therapeutic action of fenofibrate. *FASEB J.* 29, 1146–1155. doi: 10.1096/fj.14-263053

Reid, G., Wielinga, P., Zelcer, N., van der Heijden, I., Kuil, A., de Haas, M., et al. (2003). The human multidrug resistance protein MRP4 functions as a prostaglandin efflux transporter and is inhibited by nonsteroidal antiinflammatory drugs. *Proc. Natl. Acad. Sci. U.S.A.* 100, 9244–9249. doi: 10.1073/pnas.1033060100

Remmel, R. P., Crews, B. C., Kozak, K. R., Kalgutkar, A. S., and Marnett, L. J. (2004). Studies on the metabolism of the novel, selective cyclooxygenase-2 inhibitor indomethacin phenehtylamide in rat, mouse, and human liver microsomes: identification of active metabolites. *Drug Met. Dispos.* 32, 113–122. doi: 10.1124/dmd.32.1.113

Ross, R. A. (2007). Allosterism and cannabinoid CB(1) receptors: the shape of things to come. *Trends Pharmacol. Sci.* 28, 567–572. doi: 10.1016/j.tips.2007.10.006

Ross, R. A., Gibson, T. M., Stevenson, L. A., Saha, B., Crocker, P., Razdan, R. K., et al. (1999). Structural determinants of the partial agonist-inverse agonist properties of 6′-azidohex-2′-yne-Δ8-tetrahydrocannabinol at cannabinoid receptors. *Br. J. Pharmacol.* 128, 735–743. doi: 10.1038/sj.bjp.0702836

Sawyer, N., Cauchon, E., Chateauneuf, A., Cruz, R. P., Nicholson, D. W., Metters, K. M., et al. (2002). Molecular pharmacology of the human prostaglandin D2 receptor. CRTH2. *Br. J. Pharmacol.* 137, 1163–1172.

Shore, D. M., Baillie, G. L., Hurst, D. H., Navas, F. III, Seltzman, H. H., Marcu, J. P., et al. (2014). Allosteric modulation of a cannabinoid G protein-coupled receptor: binding site elucidation and relationship to G protein signaling. *J. Biol. Chem.* 289, 5828–5845. doi: 10.1074/jbc.M113.478495

Slivicki, R. A., Zu, X., Kulkarni, P. M., Pertwee, R. G., Mackie, K., Thakur, G. A., et al. (2018). Positive allosteric modulation of cannabinoid receptor type 1 suppresses pathological pain without producing tolerance or dependence. *Biol. Psychiatry* 84, 722–733. doi: 10.1016/j.biopsych.2017.06.032

Straiker, A., Dvorakova, M., Zimmowitch, A., and Mackie, K. (2018). Cannabidiol inhibits endocannabinoid signaling in autaptic hippocampal neurons. *Mol. Pharmacol.* 94, 743–748. doi: 10.1124/mol.118.111864

Sugimoto, H., Shichijo, M., Okano, M., and Bacon, K. B. (2005). CRTH2-specific binding characteristics of [3H]ramatroban and its effects on PGD2-, 15-deoxy-Delta12, 14-PGJ2- and indomethacin-induced agonist responses. *Eur. J. Pharmacol.* 524, 30–37. doi: 10.1016/j.ejphar.2005.09.005

Tham, M., Yilmaz, O., Alaverdashvili, M., Kelly, M. E. M., Denovan-Wright, E. M., and Laprairie, R. B. (2018). Allosteric and orthosteric pharmacology of cannabidiol and cannabidiol-dimethylheptyl at the type 1 and type 2 cannabinoid receptors. *Br. J. Pharmacol.* 176, 1455–1469. doi: 10.1111/bph.14440

Trott, O., and Olson, A. J. (2010). AutoDock Vina: improving the speed and accuracy of docking with a new scoring function, efficient optimization and multithreading. *J. Comput. Chem.* 31, 455–461. doi: 10.1002/jcc.21334

Wiley, J. L., Razdan, R. K., and Martin, B. R. (2006). Evaluation of the role of the arachidonic acid cascade in anandamide's *in vivo* effects in mice. *Life Sci.* 80, 24–35. doi: 10.1016/j.lfs.2006.08.017

Yamamguchi, T., Shoyama, Y., Watanabe, S., and Yamomoto, T. (2001). Behavioural suppression induced by cannabinoids is due to activation of the arachidonic acid cascade in rats. *Brain Res.* 889, 149–154. doi: 10.1016/s0006-8993(00)03127-9

Conflict of Interest: The authors declare that the research was conducted in the absence of any commercial or financial relationships that could be construed as a potential conflict of interest.

frontiers in Molecular Neuroscience

REVIEW
published: 12 November 2019
doi: 10.3389/fnmol.2019.00273

Internalized GPCRs as Potential Therapeutic Targets for the Management of Pain

Jeffri S. Retamal[1,2], *Paulina D. Ramírez-García*[1,2], *Priyank A. Shenoy*[1,2], *Daniel P. Poole*[1,2,3] *and Nicholas A. Veldhuis*[1,2]*

[1]*Drug Discovery Biology Theme, Monash Institute of Pharmaceutical Sciences, Monash University, Parkville, VIC, Australia,* [2]*Australian Research Council Centre of Excellence in Convergent Bio-Nano Science and Technology, Monash University, Parkville, VIC, Australia,* [3]*Department of Anatomy and Neuroscience, The University of Melbourne, Parkville, VIC, Australia*

Peripheral and central neurons in the pain pathway are well equipped to detect and respond to extracellular stimuli such as pro-inflammatory mediators and neurotransmitters through the cell surface expression of receptors that can mediate rapid intracellular signaling. Following injury or infection, activation of cell surface G protein-coupled receptors (GPCRs) initiates cell signaling processes that lead to the generation of action potentials in neurons or inflammatory responses such as cytokine secretion by immune cells. However, it is now appreciated that cell surface events alone may not be sufficient for all receptors to generate their complete signaling repertoire. Following an initial wave of signaling at the cell surface, active GPCRs can engage with endocytic proteins such as the adaptor protein β-arrestin (βArr) to promote clathrin-mediated internalization. Classically, βArr-mediated internalization of GPCRs was hypothesized to terminate signaling, yet for multiple GPCRs known to contribute to pain, it has been demonstrated that endocytosis can also promote a unique "second wave" of signaling from intracellular membranes, including those of endosomes and the Golgi, that is spatiotemporally distinct from initial cell-surface events. In the context of pain, understanding the cellular and molecular mechanisms that drive spatiotemporal signaling of GPCRs is invaluable for understanding how pain occurs and persists, and how current analgesics achieve efficacy or promote side-effects. This review article discusses the importance of receptor localization for signaling outcomes of pro- and anti-nociceptive GPCRs, and new analgesic opportunities emerging through the development of "location-biased" ligands that favor binding with intracellular GPCR populations.

Keywords: pain, analgesia, GPCR, trafficking, endosome, drug delivery, signal transduction

OPEN ACCESS

Edited by:
John Michael Streicher, University of Arizona, United States

Reviewed by:
Dietmar Benke, University of Zurich, Switzerland
Temugin Berta, University of Cincinnati, United States

***Correspondence:**
Nicholas A. Veldhuis
nicholas.veldhuis@monash.edu

Received: *04 September 2019*
Accepted: *28 October 2019*
Published: *12 November 2019*

Citation:
Retamal JS, Ramírez-García PD, Shenoy PA, Poole DP and Veldhuis NA (2019) Internalized GPCRs as Potential Therapeutic Targets for the Management of Pain. Front. Mol. Neurosci. 12:273. doi: 10.3389/fnmol.2019.00273

Abbreviations: GPCRs, G protein couple receptors; βArr, adaptor protein β-arrestin; FDA, Food and Drug Administration; NSAIDs, non-steroidal anti-inflammatory drugs; Coxibs, cyclooxygenase-2 inhibitors; CB1-2, Cannabinoid 1-2 receptors; SP, Substance P; NK_1R, Neurokinin receptor 1; CGRP, Calcitonin gene-related peptide; CLR, Calcitonin receptor-like receptor; RAMP1, Receptor activity-modifying protein; MOR, Mu-opioid receptor; DOR, Delta-opioid receptor; mGluR5, Metabotropic glutamate 5 receptor; PAR_2, Protease-activated receptor-2; 5-HT, serotoninergic; CCR5, Chemokine receptor 5; GRKs, GPCR kinases; PTHR, parathyroid; TSHR, thyroid-stimulating hormone; β_1AR, β_1 Adrenergic; NFEPP, N-(3-fluoro-1-phenethylpiperidine-4-yl)-N-phenyl propionamide; ERK, Extracellular signal-regulated kinases; PKC, Protein kinase C; cAMP, Cyclic adenosine monophosphate; FRET, Resonance Energy Transfer; BRET, Bioluminescence Resonance Energy Transfer; ER, endoplasmic reticulum; TRPV1, TRPV4, Transient receptor potential cation channel subfamily V member 1-4.

INTRODUCTION

The sensation and transmission of pain are essential physiological processes that allow us to detect and react to harmful stimuli and initiate inflammatory responses to protect damaged tissue and promote wound healing. Peripheral and central processes that lead to pain transmission are highly adaptive, and the pain experienced is usually proportional to the extent of the injury. As a part of this adaptive physiological response, a heightened sensitivity to pain occurs to provide awareness of damaged tissue and maintain protective behavior for the duration of an injury.

As healing occurs, this sensitization typically reduces over time. In contrast, in chronic inflammatory and neuropathic pain conditions such as arthritis, fibromyalgia or diabetic-related neuropathy, where damaged tissue is unable to heal or inflammatory mediators continue to be produced, this sensitization fails to diminish and can cause significant discomfort and loss of function over extended time periods (Scholz and Woolf, 2002). This is typically described through two phenomena: (a) *allodynia*, where one feels pain in response to a normally non-painful stimulus; and (b) *hyperalgesia*, where one experiences an exacerbated pain sensation to a moderately painful stimulus (Baron, 2006; Steeds, 2016). Due to the complexity of chronic pain and significant limitations with safety and compliance for available analgesics, these conditions are extremely difficult to manage, thus impacting the quality of life for many patients.

Despite many advances in basic research and in the clinic, the analgesic landscape in recent decades has seen few changes, due to the limited availability of effective analgesic agents and the potential for abuse of routinely prescribed drugs (Dowell et al., 2016; Goodman and Brett, 2017). In the midst of a growing opioid crisis (Schuchat et al., 2017), the development of new pain medicines is becoming increasingly important. For safety and logistical reasons, the most obvious gains can be made by repurposing Food and Drug Administration (FDA)-approved drugs that are currently used for other indications (e.g., anti-depressants; Kremer et al., 2016; Cooper et al., 2017) or re-formulating established analgesics such as opioids to improve pharmacokinetic profiles (Saraghi and Hersh, 2013). However, new and effective therapeutic approaches may also be gained through greater characterization of the underlying cellular and molecular mechanisms that lead to pain, as a means to identify new molecular targets and further define how analgesic side-effects occur and can be avoided.

G protein-coupled receptors (GPCRs) are important mediators of pain or analgesia and many of these receptors participate in dynamic trafficking processes such as endocytosis, as a part of their activity cycle. It is now evident that receptor trafficking is also critical for the initiation of spatially and temporally distinct signaling events, and importantly, some of these location-specific or compartmentalized processes are associated with greater modulation of pain (Geppetti et al., 2015; Irannejad et al., 2017; Stoeber et al., 2018; Thomsen et al., 2018). Here, we address limitations of the current analgesic landscape and look to new drug discovery studies focused on GPCRs that participate in dynamic trafficking processes in neurons. New biophysical tools that have been used to characterize compartmentalized signaling reveal how the membrane partitioning properties of drugs influence their functional selectivity for location-specific processes. This knowledge has been exploited through the use of lipid-anchored drug conjugates that increase GPCR targeting in specific subcellular domains, to enhance analgesic outcomes through the inhibition of endosomal signaling.

CHALLENGES AND LIMITATIONS OF CURRENT ANALGESICS

Chronic or persistent pain incorporates a complex range of disorders that requires a combination of non-pharmacological and pharmacological approaches for treatment. From a pharmacological perspective, treatment is possible by administering one or more therapeutic agents such as paracetamol/acetaminophen, non-steroidal anti-inflammatory drugs (NSAIDs) or cyclooxygenase-2 inhibitors (Coxibs) followed by careful use of opioids for elevated pain (e.g., morphine or oxycodone). Unfortunately, each of these drugs has associated side-effects that limit their use. NSAIDs and Coxibs have potential cardiovascular and gastrointestinal side effects (Whelton, 2000), and should be used more sparingly than paracetamol/acetaminophen, which carries a risk of hepatotoxicity with excessive use (Mahadevan et al., 2006). While opioids remain some of the most effective analgesics available in the clinic, they have a high abuse potential due to their euphoric or addictive properties, and where repeated use leads to receptor desensitization and tolerance. To overcome tolerance, patients with chronic pain can be subjected to sustained increases in dosing or switching to other more potent opioids to improve analgesia, which often provides only temporary gains in pain relief. However, this approach may increase the risk of tolerance and addiction over time, in addition to increasing the likelihood of debilitating side-effects such as constipation and respiratory depression (Corbett et al., 2006; Boudreau et al., 2009; Volkow et al., 2011).

Alternative GPCR targets have been identified to reduce reliance on opioid analgesics. Cannabinoids, which are proposed as effective opioid alternatives, reduce pain through activation of $G_{i/o}$-coupled cannabinoid receptors (primarily CB_1), which leads to the downregulation of excitatory processes, and modulation of serotoninergic (5-HT) and noradrenergic pathways. Although widely available and used for millennia, we are yet to see the outcomes of systematic use in the clinic for treating pain, and it is also acknowledged to lead to behavioral risks that require further investigation (Mendiguren et al., 2018). Gabapentinoids such as gabapentin or pregabalin, target the α2δ subunit of voltage-gated calcium channels and have been approved as first-line medications to manage neuropathic pain (e.g., postherpetic neuralgia, fibromyalgia). These were initially used for the treatment of epilepsy, and in some cases for anxiety disorders. Although regarded as relatively safe drugs, safety concerns for gabapentinoids have grown and include excessive usage and behavioral risks such as suicidal behavior

(Johansen, 2018; Molero et al., 2019). Together, this provides a small insight into established and emerging risks associated with common analgesics. This raises the question of whether any of these compounds can be modified to improve their safety profiles and if new or emerging targets are available. We discuss these points below in the context of receptor trafficking, which is a critical component of the activity cycle for many molecular pain targets.

TARGETING GPCRs FOR THE TREATMENT OF PAIN

Members of the GPCR superfamily are considered to be druggable targets due to high levels of cell surface expression and their ability to contribute to all pathophysiological processes, including pain. Accordingly, GPCR-selective drugs represent more than one-third of all FDA-approved medicines (Hauser et al., 2017). There are at least 40 members of the GPCR family that are considered to be potential therapeutic targets for the regulation of pain (Stone and Molliver, 2009). Yet despite advanced drug discovery programs for multiple receptors, and abuse concerns for opioid receptors, very few targets have clinically succeeded beyond opioids in the past decade, with notable exceptions being the recent approval of Fremanezumab, Eptinezumab, Galcanezumab, and Erenumab for treatment of migraine, being monoclonal antibodies that target the neuropeptide calcitonin gene-related peptide (CGRP) or its receptor, Calcitonin Receptor-Like Receptor/Receptor Activity-Modifying Protein 1 (CLR/RAMP1; see review by Scuteri et al., 2019).

There are a number of challenges in the early phase of analgesic drug discovery for GPCRs. This includes safety concerns for targets that have overlapping functions in other tissues, and inaccurate evaluations of efficacy when using relatively simplified rodent-based pre-clinical pain models to represent the complexity of clinical pain conditions or characterize human-selective compounds (Mao, 2012). Furthermore, the localization of receptors in pre-synaptic and post-synaptic neurons is critical for the activity cycle and nociceptive outputs of several GPCRs (**Figure 1**). On a cellular level, considerations for the intracellular disposition of analgesics and their ability to regulate receptor trafficking and localization have also recently been proposed to be an important part of the drug discovery process (Jensen et al., 2017; Yarwood et al., 2017; Jimenez-Vargas et al., 2018; Stoeber et al., 2018).

RECEPTOR TRAFFICKING LEADS TO SPATIOTEMPORALLY DISTINCT SIGNALING PROCESSES

GPCRs are highly dynamic proteins that achieve distinct signaling outcomes by adopting different conformational states (Rasmussen et al., 2011; Latorraca et al., 2017). Extracellular ligands that bind cell surface GPCRs promote receptor conformations that activate heterotrimeric G proteins to transduce downstream signaling and also favor phosphorylation by GPCR kinases (GRKs). This phosphorylation occurs primarily at the C-terminus to enhance engagement with β-arrestins (βArrs), which can function as adaptor proteins to mediate distinct signaling processes such as MAPK activity, and also facilitate interactions with clathrin-coated membranes to promote endocytosis into endosomes (Ferguson et al., 1996). This was historically considered to facilitate termination of signaling by targeting receptors to degradative pathways, or rapid receptor recycling to reset the activity cycle during the internalization process, and increase the potential for sustained signaling once the receptor is recovered at the plasma membrane (PM; Ferguson et al., 1996; Shukla et al., 2014).

A more recent theory has emerged, suggesting that a third trafficking possibility exists, whereby receptors can remain on intracellular membranes such as endosomes for sustained periods of time, to facilitate distinct signaling processes in a βArr- or a G protein-dependent manner. This paradigm shift was initially revealed by studies on Gs-coupled receptors such as the parathyroid (PTHR), thyroid-stimulating hormone (TSHR) and β2 adrenergic receptors to demonstrate that endosomal-mediated sustained cyclic adenosine monophosphate (cAMP) production could be observed after endocytosis has occurred (reviewed in detail by Vilardaga et al., 2014; Tsvetanova et al., 2015; Thomsen et al., 2018).

The development of genetically encoded tools such as conformation-selective nanobodies, Förster/Fluorescence Resonance Energy Transfer (FRET) or Bioluminescence Resonance Energy Transfer (BRET) biosensors, have provide highly sensitive approaches for observing and measuring dynamic activation states and spatiotemporal signaling [e.g., compartmentalized cAMP production, Protein kinase C (PKC) and Extracellular signal-regulated kinases (ERK) activity] of GPCRs in real-time (Irannejad et al., 2017; Halls and Canals, 2018). Given the prevalence and importance of trafficking GPCRs in neurons, the internalization and location-specific signaling of several GPCRs with established roles in pain have been described, including but not limited to the Neurokinin 1 Receptor (NK_1R), CLR/RAMP1, metabotropic glutamate receptor 5 (mGluR5), chemokine receptor (CCR1), Protease-Activated Receptor 2 (PAR_2) and the Mu Opioid Receptor (MOR; Mantyh et al., 1995a; O'Malley et al., 2003; Gilliland et al., 2013; Poole et al., 2015; Jensen et al., 2017; Yarwood et al., 2017; Stoeber et al., 2018). An overview of these trafficking outcomes is summarized in **Table 1**, to reveal how stimulation with endogenous ligands alters receptor localization *in vitro*, or in pre-clinical pain models.

LIGANDS EXERT LOCATION BIASED EFFECTS BY ACCESSING DIFFERENT RECEPTOR POOLS

More recently, conformation-selective single-domain camelid antibodies (nanobodies) that can detect and bind active-state receptors have been instrumental for advancing this concept to other organelles. Distinct nanobody clones that are known to engage with the β_1 Adrenergic Receptor (β_1AR) or MOR

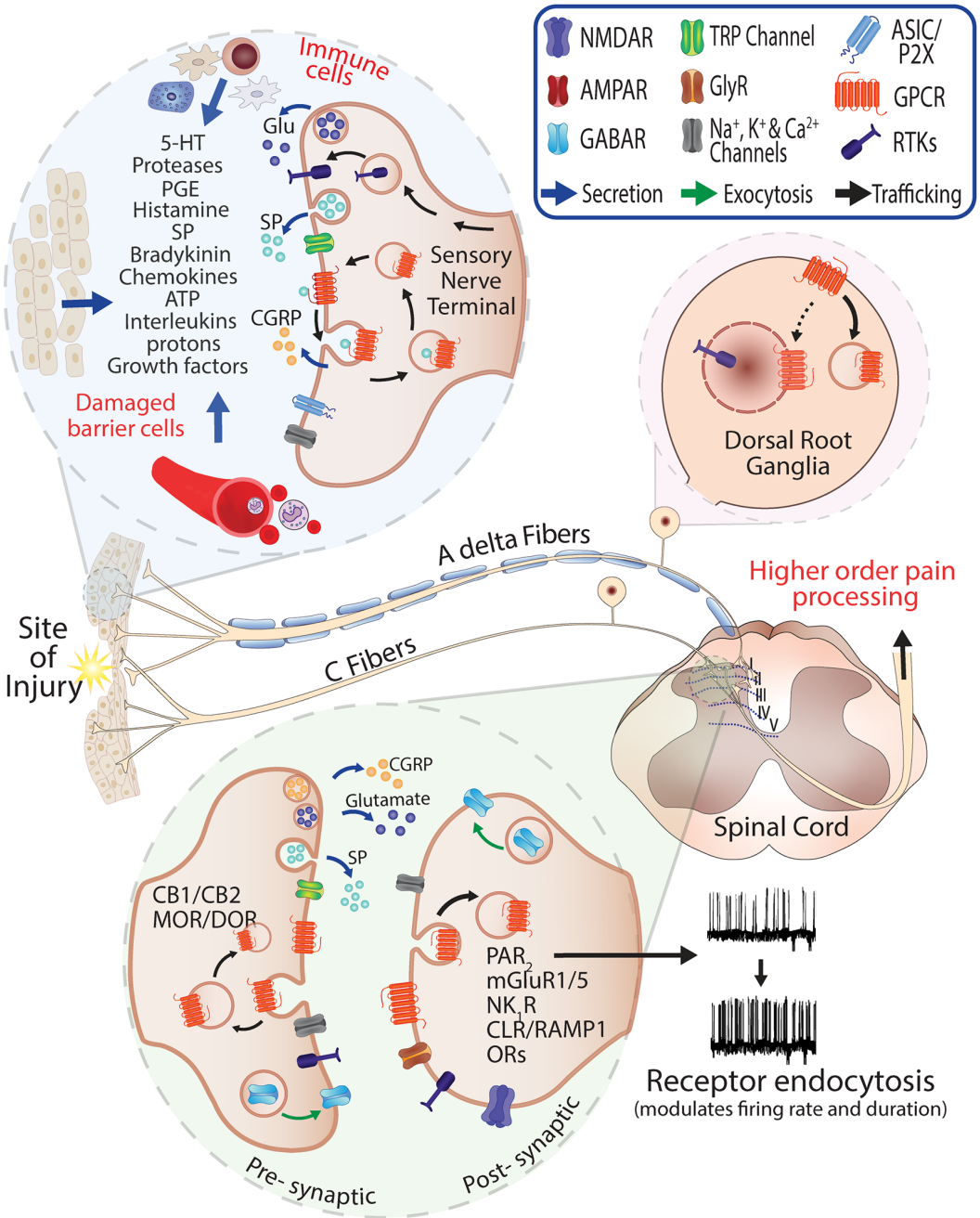

FIGURE 1 | Role of G protein-coupled receptors (GPCRs) in pain and neurogenic inflammation. Injury or damaged tissues and infiltrating immune cells stimulate GPCRs on the peripheral sensory nerve terminals through release of painful and inflammatory mediators. Activated peptidergic and non-peptidergic Aδ and C fibers contribute to the response *via* the release of glutamate, Substance P (SP) and Calcitonin Gene-Related Peptide (CGRP) at the injury site and central terminals. The presence of endogenous mediators in the spinal cord (neuro- and glio-transmitters) can promote activation and recycling of GPCRs including pre-synaptic $CB_{1/2}$ cannabinoid and Mu-opioid receptor (MOR)/Delta-opioid receptor (DOR) and the exocytic trafficking of the γ-aminobutyric $acid_A$ receptor (GABAR) which is an inhibitory receptor that can normalize neuronal excitability where excitatory neurotransmitters are released. Stimulation and endocytosis of receptors such as Neurokinin 1 Receptor (NK_1R) and Calcitonin Receptor-Like Receptor/Receptor Activity-Modifying Protein 1 (CLR/RAMP1) in post-synaptic neurons are known to modify firing frequency and the duration of pain responses (Jensen et al., 2017; Yarwood et al., 2017; Stoeber et al., 2018).

have been shown to be recruited to the Golgi apparatus in a GPCR activity-dependent manner independently from initial stimulation at the cell surface. Specifically, this is achieved using relatively lipophilic ligands that can freely diffuse throughout the cell, or hydrophilic compounds that are proposed to access Golgi pools *via* transporters (Irannejad et al., 2017; Stoeber et al., 2018).

These important pharmacological insights have significant implications for understanding how drugs may exert their

TABLE 1 | Receptors in pain pathways that undergo stimulation-induced endocytosis.

Receptor family	Endogenous stimuli	Localization (unstimulated)	Pain/Stimulus-induced trafficking	Reference
Mu and Delta Opioid Receptors (MOR, DOR)	Enkephalins Dynorphins	PM TGN	PM → Endosomes Direct activation on TGN by morphine	Sternini et al. (1996), Haberstock-Debic et al. (2005) and Stoeber et al. (2018)
Endocannabinoid Receptors (CB1, CB2)	AEA 2-AG	PM	PM, Endosomes	Rozenfeld and Devi (2008), Lever et al. (2009) and Flores-Otero et al. (2014)
Metabotropic Glutamate Receptor 5 (mGluR5)	Glutamate	PM ER Nucleus	PM Direct activation on Nuclear inner membrane	O'Malley et al. (2003) and Vincent et al. (2016, 2017)
Protease-Activated Receptor 2 (PAR_2)	Trypsin, Tryptase, Elastase, Cathepsin S	PM TGN	PM → Endosomes PM → Lysosomes	DeFea et al. (2000), Ricks and Trejo (2009) and Jimenez-Vargas et al. (2018)
Neurokinin 1 Receptor (NK_1R)	Substance P Neurokinin A/B	PM	PM → Endosomes	Mantyh et al. (1995a,b) and Jensen et al. (2017)
Calcitonin Receptor-Like Receptor; Receptor Activity-Modifying Protein 1 (CLR/RAMP1)	CGRP Amylin	PM	PM → Endosomes	Padilla et al. (2007) and Yarwood et al. (2017)
Angiotensin Receptor 1 (AT_1R)	Angiotensin II	PM	PM → Endosomes	Hein et al. (1997)
5-Hydroxytryptamine Receptor (5-HT2A)	Serotonin	PM	PM → Endosomes	Bhattacharyya et al. (2002) and Freeman et al. (2006)

PM, plasma membrane; ER, endoplasmic reticulum, TGN, trans-Golgi Network; → denotes direction of receptor trafficking, from unstimulated receptor location to stimulated receptor location.

effects (or side-effects) and are consistent with other receptors that contribute to pain transmission. For example, endogenous peptide-based enkephalins can stimulate MOR and Delta-Opioid Receptor (DOR) to activate rapid signaling processes in micro-domains of the cell surface and sustained signaling from endosomes (Finn and Whistler, 2001; Groer et al., 2011; Halls et al., 2016; Stoeber et al., 2018), whereas non-peptide opioids such as morphine can freely diffuse through cells to stimulate Golgi pools of the MOR, and initiate a spatiotemporally distinct wave of signaling. The importance of opioid-induced Golgi signaling for analgesia and its association with safety outcomes remains to be determined *in vivo* (Stoeber et al., 2018).

Under pathological pain conditions, the excitatory mGluR5 has been detected in intracellular locations, including the inner nuclear membrane and endoplasmic reticulum (ER; Jong et al., 2014; Purgert et al., 2014; Vincent et al., 2016, 2017). Stimulated mGluR5 couples with $G\alpha_q$ to evoke cytoplasmic and nuclear calcium mobilization (Jong et al., 2009). Furthermore, in models of spared-nerve injury (Vincent et al., 2016) and inflammatory pain (Vincent et al., 2017), 60% of the mGluR5 receptor population was shown to be localized to the inner nuclear membrane in spinal dorsal horn neurons (Vincent et al., 2016). Importantly, activation of nuclear mGluR5 leads to sustained nuclear Ca^{2+} signaling, phosphorylation of ERK1/2 and induction of c-fos expression, leading to increased nociceptive hypersensitivity (Lee et al., 2008; Jong et al., 2009; Purgert et al., 2014; Vincent et al., 2016, 2017). Blockade of cell surface mGluR5 by the impermeable antagonist LY393053 resulted in limited analgesia and modest reductions in second messenger coupling. In contrast, the membrane-permeable antagonist fenobam significantly reduced mechanical allodynia, MAP kinase (ERK1/2) phosphorylation and c-fos expression in a spared-nerve injury pain model. Although these differences may be caused by a range of factors including drug disposition and differences in potencies, it may also provide indirect evidence for the initiation of distinct mGluR5-dependent pain responses from different cellular locations (Lax et al., 2014; Vincent et al., 2016, 2017). Focused drug discovery around cell-permeant compounds biased toward intracellular mGluR5 pools is warranted and may lead to new opportunities for targeting glutamate signaling for analgesia.

MODIFYING INTRINSIC DRUG PROPERTIES TO INFLUENCE LOCATION BIAS

The studies above suggest that GPCRs that undergo endocytosis may be modulated more effectively by ligands that can diffuse to intracellular sites. This raises questions about whether the intrinsic properties of analgesic agents can be enhanced by chemical modification, to increase activity or partitioning into membranes where GPCRs are known to initiate signals associated with pain.

Lipid-Anchored Ligands for Increased Endosomal Accumulation

The NK_1R, has an established role in pain transmission and is well known to internalize when stimulated by the neurotransmitter, Substance P (SP). Peripheral inflammation-induced either acutely with intraplantar capsaicin or over sustained periods with Complete Freund's Adjuvant, leads to pre-synaptic release of SP from primary afferent terminals onto the dorsal horn, and evokes robust NK_1R internalization in Lamina I and II neurons of the spinal cord (Mantyh et al., 1995a; Abbadie et al., 1996, 1997; Jensen et al., 2017). Analogous to the endosomal signaling phenomena

described above, it has also recently been reported that NK_1R can mediate compartmentalized signaling processes including sustained PKC, nuclear ERK activity and cAMP production, in a clathrin/dynamin and βArr-dependent manner (Jensen et al., 2014, 2017; Poole et al., 2015). Similarly, CLR/RAMP1 which has an established role in central pain transmission and migraine pain (Lee and Kim, 2007; Bell, 2014), can undergo a CGRP-mediated redistribution into endosomes in HEK cells (Padilla et al., 2007) and in spinal cord sections (Yarwood et al., 2017). *In vitro* studies to clarify CLR/RAMP1-mediated compartmentalized signaling also showed that endocytosed receptor is associated with sustained nuclear ERK activity, cytosolic PKC activity and cytosolic cAMP production in HEK cells, and mediates sustained neuronal excitation in electrophysiological studies on rat spinal cord slices (Yarwood et al., 2017).

To demonstrate a similar potential for targeting endosomal receptor populations in peripheral neurons, PAR_2 expressed on primary afferents is proposed to mediate inflammatory pain responses and its activity is strongly associated with irritable bowel syndrome (IBS). PAR_2 signaling is also a stimulation-dependent process, where cleavage by different proteases can lead to distinct trafficking and location-based signaling outcomes. Trypsin proteolytically cleaves the extracellular amino terminus to activate PAR_2 and promote PAR_2 internalization into endosomes (DeFea et al., 2000; Ricks and Trejo, 2009). Endosomal PAR_2 continues to signal through nuclear ERK and cytosolic PKC (Jimenez-Vargas et al., 2018). In contrast, elastase and cathepsin S mediated cleavage of the N-terminus activates PAR_2 but does not stimulate PAR_2 endocytosis (Zhao et al., 2014, 2015). Consequently, PM-delimited PAR_2 signaling is relatively transient and is proposed to only mediate sustained signaling *via* activation of downstream effectors such as TRPV1 and TRPV4 ion channels (Poole et al., 2013; Jimenez-Vargas et al., 2018).

These data indicate that the internalization of excitatory GPCRs into endosomes may be associated with the generation of spatiotemporally distinct signaling profiles (Jensen et al., 2017; Yarwood et al., 2017; Jimenez-Vargas et al., 2018). Paradoxically, these internalized signaling processes are associated with persistent hyper-excitability of nociceptors and enhanced pain transmission through mechanisms that are not entirely clear, but require sustained kinase activity (Thomsen et al., 2018).

Pharmacological strategies have been employed to understand the importance of location bias of these receptors in pain transmission. Chemical modification by conjugation to the sterol cholestanol has previously been used by Simons and colleagues as a strategy to increase membrane affinity and the endosomal accumulation of a β-secretase transition state inhibitor (Rajendran et al., 2008). Using a similar lipid-anchor approach, antagonists for NK_1R, CLR/RAMP1, and PAR_2 were functionalized with the sterol moiety cholestanol, separated by a flexible polyethylene glycol (PEG_{12}) linker. Focusing on the NK_1R peptide antagonist spantide I (Jensen et al., 2017), the CLR/RAMP1 peptide antagonist $CGRP_{8-37}$ (Yarwood et al., 2017) and I-343, a small molecule PAR_2 antagonist (Jimenez-Vargas et al., 2018), the lipid anchor increased efficacy at the PM for all three compounds, and promoted incorporation and accumulation into endosomes, and is proposed to be maintained on the outer leaflet of membranes to target extracellular GPCR binding pockets, that are also accessible within the lumen of endosomes. This resulted in greater antagonism of endosomal-delimited signaling processes and more effective analgesia relative to unlipidated control compounds.

Alternative membrane-targeted antagonists have been developed for GPCRs, and the best studied of these are pepducins. Using peptides antagonists based on the sequences of GPCR intracellular domains to competitively bind G protein coupling, pepducins are anchored to membranes by chemical modification with palmitic acid (Covic et al., 2002), and these palmitoylated peptides have been proposed to flip to the inner leaflet of the PM to provide cell surface-delimited signaling inhibition. Pepducins are efficacious in inflammatory models (edema, osteoarthritis, sepsis) by selectively targeting GPCRs including PARs (PAR1, 2, 4) and chemokine receptors (CXCR1, 2, 4; Tressel et al., 2011; Tsuji et al., 2013).

Together, these studies support the use of lipid conjugation as a strategy for modifying the location biased profiles of drugs. The lipophilic properties of the anchor dominate the membrane partitioning of ligands, even hydrophobic small molecules, and are therefore a critical determinant for achieving unique membrane distributions, to improve ligand efficacy at specific subcellular locations (**Figure 2**). While pepducins have entered clinical trials (Gurbel et al., 2016), cholestanol conjugates that lead to the accumulation of ligands in endosomes have not advanced beyond pre-clinical pain models, but suggest that targeting endosomes through drug delivery strategies may be a useful therapeutic approach for the management of pathological pain.

Modifying pH-Sensitivity of MOR-Opioid Interactions

Increasing ligand selectivity for GPCR binding under acidic conditions is a potential alternative strategy for favoring the modulation of GPCRs in endosomes. Relative to the physiological pH of the extracellular environment, trafficking proteins are exposed to an increasingly acidic gradient, as cargo is sorted deeper into the endosomal network. The reduction in pH increases proteolytic activity, which is essential for lysosomal protein degradation, and also for modulating the activity and presence of peptides such as SP or CGRP in endosomal compartments (Padilla et al., 2007).

With a need to reduce opioid-MOR interactions that lead to on-target side effects such as sedation, addiction and constipation, Stein and colleagues recently explored the potential for a pH-sensitive analog of the MOR agonist fentanyl to selectively engage with MOR only in pathological conditions, where acidosis is likely to occur (Spahn et al., 2017). The acid dissociation constant (pK_a) of fentanyl is >8 and can activate MOR in physiological conditions (pH 7.4) and between pH 5 and 7, being the expected pH range within the microenvironment of inflamed tissue (Ludwig et al., 2003; Thurlkill et al., 2005). It was therefore hypothesized that reducing the pKa of fentanyl >7 by

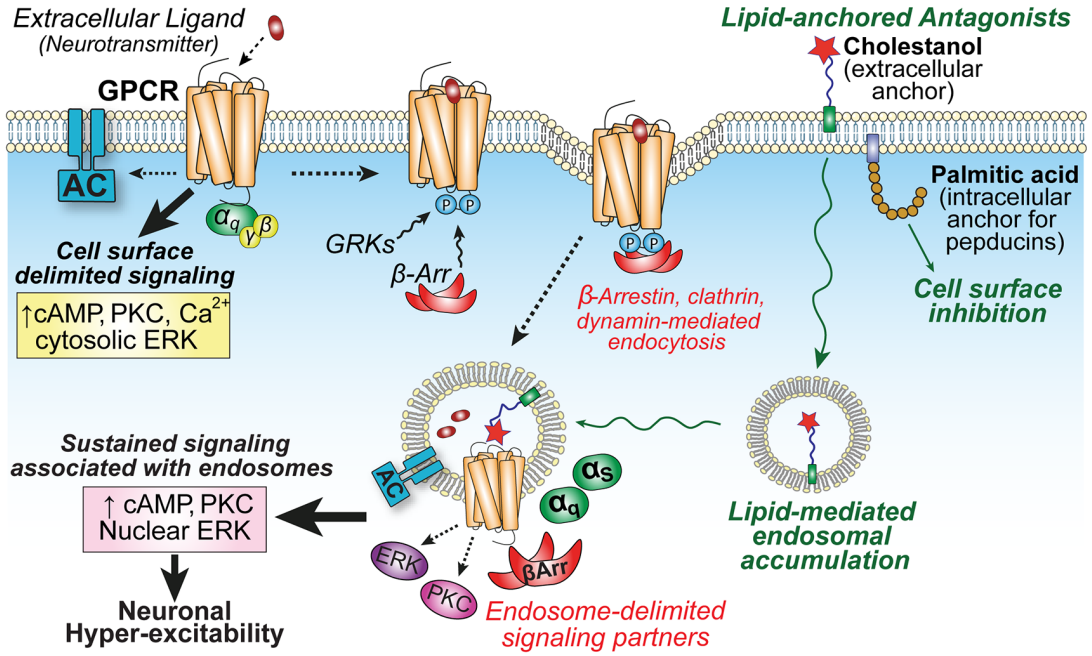

FIGURE 2 | GPCR localization influences compartmentalized signaling and neuronal hyper-excitability. Activation of GPCRs on central neurons by extracellular neuropeptides (e.g., NK_1R or CL/RAMP1) initiates cell surface-delimited G protein-dependent signaling events. This is followed by GPCR kinase (GRK) phosphorylation, arrestin-binding, and clathrin-mediated endocytosis into endosomes to promote the recruitment of unique signaling complexes and drive spatiotemporally distinct signaling that is associated with sustained excitability of neurons in spinal cord slice preparations (Jensen et al., 2017; Yarwood et al., 2017). Lipid conjugation can influence membrane partitioning of antagonists. Palmitoylated pepducins are proposed to inhibit G protein-mediated inflammatory processes on the cytoplasmic interface of the plasma membrane (PM); whereas the sterol moiety cholestanol increases drug accumulation in endosomes to enhance inhibition of sustained endosomal-delimited signaling.

replacement of side-chain hydrogens would favor binding exclusively in pathological conditions.

Utilizing atomic-level structural information for MOR (Manglik et al., 2012) hydrogen replacement fentanyl analogs were designed and binding energies were measured in computational simulations, to identify candidates for further *in vitro* testing and assessment in pain models. The substitution of hydrogen by fluorine resulted in the development of (±)-N-(3-fluoro-1-phenethylpiperidine-4-yl)-N-phenyl propionamide (NFEPP) with a pK_a of 6.8 (Spahn et al., 2017). NFEPP and fentanyl were intravenously administered and compared using two models of persistent or acute inflammatory pain (Spahn et al., 2017) and more recently in neuropathic and abdominal pain in rats (Rodriguez-Gaztelumendi et al., 2018). Fentanyl produced analgesia in both injured and non-injured tissue. However, NFEPP analgesia was restricted to inflamed, acidic tissues. High doses of fentanyl induced respiratory depression, sedation and CNS-associated side-effects such as decrease of defecation, heart rate, and blood oxygen saturation, whereas NFEPP did not (Spahn et al., 2017; Rodriguez-Gaztelumendi et al., 2018).

These studies demonstrate the importance of protonation of ligands for receptor binding and activation, and the potential to modulate receptor affinity at pathological pH, thus limiting on-target side effects and unwanted MOR interactions in healthy tissues. The pH range of endosomes is comparable to inflamed tissue and hence, further *in vitro* studies may be useful to determine if the properties of NFEPP also enhance binding with endosomal receptor pools. Furthermore, if NFEPP maintains its ability to partition into membranes to access and activate the Golgi pool of MOR, this may suggest that MOR activation in the Golgi is favorable for analgesia, rather than being associated with poor safety outcomes.

CONCLUDING REMARKS

The signaling and trafficking of GPCRs is important for mediating physiological processes at the PM and can also drive distinct, compartmentalized signaling events from intracellular sites. In the context of pain, defining this relationship may provide significant opportunities for neuropharmacology and analgesic drug discovery. However, while this may provide important insights that pinpoint discrete signaling outcomes most closely associated with modulating pain behaviors, or favorable drug properties that achieve analgesia while avoiding safety issues, it also critical to translate these proof of concept studies to human tissues and diseases. It remains unknown (and very challenging), for example, to demonstrate how the Golgi-specific MOR-signaling component influences analgesia or other side-effects in animals or humans, or if pH-sensitive fentanyl analogs provide genuine advantages over the parent compound in humans with chronic pain.

Although a relatively new phenomenon, ligands that have been identified or modified to possess unique location-biased properties have provided both interesting and valuable proof of concept findings that warrant further investigation. This includes receptors discussed in this review article and many others that contribute to pain in both neurons and non-neuronal cells that drive signaling processes that lead to sustained pain. With the availability of powerful new technologies and biophysical tools, it is predicted that further in-depth compartmentalized signaling-focused drug discovery studies on other trafficking receptors will provide many more valuable insights and other location-specific drug targets.

AUTHOR CONTRIBUTIONS

JR, PR-G, PS, DP and NV wrote the manuscript.

FUNDING

NV and DP are supported by the Australian Research Council Centre of Excellence in Convergent Bio-Nano Science and Technology and Monash University (NV), NHMRC grants 1121029, 1083480 (DP). JR and PR-G are supported by Becas Chile (CONICYT) Ph.D. scholarships.

REFERENCES

Abbadie, C., Brown, J. L., Mantyh, P. W., and Basbaum, A. I. (1996). Spinal cord substance P receptor immunoreactivity increases in both inflammatory and nerve injury models of persistent pain. *Neuroscience* 70, 201–209. doi: 10.1016/0306-4522(95)00343-h

Abbadie, C., Trafton, J., Liu, H., Mantyh, P. W., and Basbaum, A. I. (1997). Inflammation increases the distribution of dorsal horn neurons that internalize the neurokinin-1 receptor in response to noxious and non-noxious stimulation. *J. Neurosci.* 17, 8049–8060. doi: 10.1523/JNEUROSCI.17-20-08049.1997

Baron, R. (2006). Mechanisms of disease: neuropathic pain-a clinical perspective. *Nat. Clin. Pract. Neurol.* 2, 95–106. doi: 10.1038/ncpneuro0113

Bell, I. M. (2014). Calcitonin gene-related peptide receptor antagonists: new therapeutic agents for migraine. *J. Med. Chem.* 57, 7838–7858. doi: 10.1021/jm500364u

Bhattacharyya, S., Puri, S., Miledi, R., and Panicker, M. M. (2002). Internalization and recycling of 5-HT2A receptors activated by serotonin and protein kinase C-mediated mechanisms. *Proc. Natl. Acad. Sci. U S A* 99, 14470–14475. doi: 10.1073/pnas.212517999

Boudreau, D., Von Korff, M., Rutter, C. M., Saunders, K., Ray, G. T., Sullivan, M. D., et al. (2009). Trends in long-term opioid therapy for chronic non-cancer pain. *Pharmacoepidemiol. Drug Saf.* 18, 1166–1175. doi: 10.1002/pds.1833

Cooper, T. E., Heathcote, L. C., Clinch, J., Gold, J. I., Howard, R., Lord, S. M., et al. (2017). Antidepressants for chronic non-cancer pain in children and adolescents. *Cochrane Database Syst. Rev.* 8:CD012535. doi: 10.1002/14651858.CD012535.pub2

Corbett, A. D., Henderson, G., McKnight, A. T., and Paterson, S. J. (2006). 75 years of opioid research: the exciting but vain quest for the Holy Grail. *Br. J. Pharmacol.* 147, S153–S162. doi: 10.1038/sj.bjp.0706435

Covic, L., Gresser, A. L., Talavera, J., Swift, S., and Kuliopulos, A. (2002). Activation and inhibition of G protein-coupled receptors by cell-penetrating membrane-tethered peptides. *Proc. Natl. Acad. Sci. U S A* 99, 643–648. doi: 10.1073/pnas.022460899

DeFea, K. A., Zalevsky, J., Thoma, M. S., Déry, O., Mullins, R. D., and Bunnett, N. W. (2000). β-arrestin-dependent endocytosis of proteinase-activated receptor 2 is required for intracellular targeting of activated ERK1/2. *J. Cell Biol.* 148, 1267–1281. doi: 10.1083/jcb.148.6.1267

Dowell, D., Haegerich, T. M., and Chou, R. (2016). CDC guideline for prescribing opioids for chronic pain-United States, 2016. *JAMA* 315, 1624–1645. doi: 10.1001/jama.2016.1464

Ferguson, S. S., Downey, W. E., Colapietro, A. M., Barak, L. S., Ménard, L., and Caron, M. G. (1996). Role of β-arrestin in mediating agonist-promoted G protein-coupled receptor internalization. *Science* 271, 363–366. doi: 10.1126/science.271.5247.363

Finn, A. K., and Whistler, J. L. (2001). Endocytosis of the mu opioid receptor reduces tolerance and a cellular hallmark of opiate withdrawal. *Neuron* 32, 829–839. doi: 10.1016/s0896-6273(01)00517-7

Flores-Otero, J., Ahn, K. H., Delgado-Peraza, F., Mackie, K., Kendall, D. A., and Yudowski, G. A. (2014). Ligand-specific endocytic dwell times control functional selectivity of the cannabinoid receptor 1. *Nat. Commun.* 5:4589. doi: 10.1038/ncomms5589

Freeman, S. L., Glatzle, J., Robin, C. S., Valdellon, M., Sternini, C., Sharp, J. W., et al. (2006). Ligand-induced 5-HT3 receptor internalization in enteric neurons in rat ileum. *Gastroenterology* 131, 97–107. doi: 10.1053/j.gastro.2006.04.013

Geppetti, P., Veldhuis, N. A., Lieu, T., and Bunnett, N. W. (2015). G protein-coupled receptors: dynamic machines for signaling pain and itch. *Neuron* 88, 635–649. doi: 10.1016/j.neuron.2015.11.001

Gilliland, C. T., Salanga, C. L., Kawamura, T., Trejo, J., and Handel, T. M. (2013). The chemokine receptor CCR1 is constitutively active, which leads to G protein-independent, β-arrestin-mediated internalization. *J. Biol. Chem.* 288, 32194–32210. doi: 10.1074/jbc.m113.503797

Goodman, C. W., and Brett, A. S. (2017). Gabapentin and pregabalin for pain-is increased prescribing a cause for concern? *N. Engl. J. Med.* 377, 411–414. doi: 10.1056/NEJMp1704633

Groer, C. E., Schmid, C. L., Jaeger, A. M., and Bohn, L. M. (2011). Agonist-directed interactions with specific β-arrestins determine mu-opioid receptor trafficking, ubiquitination and dephosphorylation. *J. Biol. Chem.* 286, 31731–31741. doi: 10.1074/jbc.M111.248310

Gurbel, P. A., Bliden, K. P., Turner, S. E., Tantry, U. S., Gesheff, M. G., Barr, T. P., et al. (2016). Cell-penetrating pepducin therapy targeting PAR1 in subjects with coronary artery disease. *Arterioscler. Thromb. Vasc. Biol.* 36, 189–197. doi: 10.1161/ATVBAHA.115.306777

Haberstock-Debic, H., Kim, K.-A., Yu, Y. J., and von Zastrow, M. (2005). Morphine promotes rapid, arrestin-dependent endocytosis of mu-opioid receptors in striatal neurons. *J. Neurosci.* 25, 7847–7857. doi: 10.1523/JNEUROSCI.5045-04.2005

Halls, M. L., and Canals, M. (2018). Genetically encoded FRET biosensors to illuminate compartmentalised GPCR signalling. *Trends Pharmacol. Sci.* 39, 148–157. doi: 10.1016/j.tips.2017.09.005

Halls, M. L., Yeatman, H. R., Nowell, C. J., Thompson, G. L., Gondin, A. B., Civciristov, S., et al. (2016). Plasma membrane localization of the μ-opioid receptor controls spatiotemporal signaling. *Sci. Signal.* 9:ra16. doi: 10.1126/scisignal.aac9177

Hauser, A. S., Attwood, M. M., Rask-Andersen, M., Schiöth, H. B., and Gloriam, D. E. (2017). Trends in GPCR drug discovery: new agents, targets and indications. *Nat. Rev. Drug Discov.* 16, 829–842. doi: 10.1038/nrd.2017.178

Hein, L., Meinel, L., Pratt, R. E., Dzau, V. J., and Kobilka, B. K. (1997). Intracellular trafficking of angiotensin II and its AT1 and AT2 receptors: evidence for selective sorting of receptor and ligand. *Mol. Endocrinol.* 11, 1266–1277. doi: 10.1210/mend.11.9.9975

Irannejad, R., Pessino, V., Mika, D., Huang, B., Wedegaertner, P. B., Conti, M., et al. (2017). Functional selectivity of GPCR-directed drug action through location bias. *Nat. Chem. Biol.* 13, 799–806. doi: 10.1038/nchembio.2389

Jensen, D. D., Halls, M. L., Murphy, J. E., Canals, M., Cattaruzza, F., Poole, D. P., et al. (2014). Endothelin-converting enzyme 1 and β-arrestins exert spatiotemporal control of substance P-induced inflammatory signals. *J. Biol. Chem.* 289, 20283–20294. doi: 10.1074/jbc.M114.578179

Jensen, D. D., Lieu, T., Halls, M. L., Veldhuis, N. A., Imlach, W. L., Mai, Q. N., et al. (2017). Neurokinin 1 receptor signaling in endosomes mediates sustained

nociception and is a viable therapeutic target for prolonged pain relief. *Sci. Transl. Med.* 9:eaal3447. doi: 10.1126/scitranslmed.aal3447

Jimenez-Vargas, N. N., Pattison, L. A., Zhao, P., Lieu, T., Latorre, R., Jensen, D. D., et al. (2018). Protease-activated receptor-2 in endosomes signals persistent pain of irritable bowel syndrome. *Proc. Natl. Acad. Sci. U S A* 115, E7438–E7447. doi: 10.1073/pnas.1721891115

Johansen, M. E. (2018). Gabapentinoid use in the United States 2002 through 2015. *JAMA Intern. Med.* 178, 292–294. doi: 10.1001/jamainternmed.2017.7856

Jong, Y.-J. I., Kumar, V., and O'Malley, K. L. (2009). Intracellular metabotropic glutamate receptor 5 (mGluR5) activates signaling cascades distinct from cell surface counterparts. *J. Biol. Chem.* 284, 35827–35838. doi: 10.1074/jbc.M109.046276

Jong, Y.-J. I., Sergin, I., Purgert, C. A., and O'Malley, K. L. (2014). Location-dependent signaling of the group 1 metabotropic glutamate receptor mGlu5. *Mol. Pharmacol.* 86, 774–785. doi: 10.1124/mol.114.094763

Kremer, M., Salvat, E., Muller, A., Yalcin, I., and Barrot, M. (2016). Antidepressants and gabapentinoids in neuropathic pain: mechanistic insights. *Neuroscience* 338, 183–206. doi: 10.1016/j.neuroscience.2016.06.057

Latorraca, N. R., Venkatakrishnan, A. J., and Dror, R. O. (2017). GPCR dynamics: structures in motion. *Chem. Rev.* 117, 139–155. doi: 10.1021/acs.chemrev.6b00177

Lax, N. C., George, D. C., Ignatz, C., and Kolber, B. J. (2014). The mGluR5 antagonist fenobam induces analgesic conditioned place preference in mice with spared nerve injury. *PLoS One* 9:e103524. doi: 10.1371/journal.pone.0103524

Lee, S. E., and Kim, J.-H. (2007). Involvement of substance P and calcitonin gene-related peptide in development and maintenance of neuropathic pain from spinal nerve injury model of rat. *Neurosci. Res.* 58, 245–249. doi: 10.1016/j.neures.2007.03.004

Lee, J. H., Lee, J., Choi, K. Y., Hepp, R., Lee, J.-Y., Lim, M. K., et al. (2008). Calmodulin dynamically regulates the trafficking of the metabotropic glutamate receptor mGluR5. *Proc. Natl. Acad. Sci. U S A* 105, 12575–12580. doi: 10.1073/pnas.0712033105

Lever, I. J., Robinson, M., Cibelli, M., Paule, C., Santha, P., Yee, L., et al. (2009). Localization of the endocannabinoid-degrading enzyme fatty acid amide hydrolase in rat dorsal root ganglion cells and its regulation after peripheral nerve injury. *J. Neurosci.* 29, 3766–3780. doi: 10.1523/JNEUROSCI.4071-08.2009

Ludwig, M.-G., Vanek, M., Guerini, D., Gasser, J. A., Jones, C. E., Junker, U., et al. (2003). Proton-sensing G-protein-coupled receptors. *Nature* 425, 93–98. doi: 10.1038/nature01905

Mahadevan, S. B. K., McKiernan, P. J., Davies, P., and Kelly, D. A. (2006). Paracetamol induced hepatotoxicity. *Arch. Dis. Child.* 91, 598–603. doi: 10.1136/adc.2005.076836

Manglik, A., Kruse, A. C., Kobilka, T. S., Thian, F. S., Mathiesen, J. M., Sunahara, R. K., et al. (2012). Crystal structure of the μ-opioid receptor bound to a morphinan antagonist. *Nature* 485, 321–326. doi: 10.1038/nature10954

Mantyh, P. W., Allen, C. J., Ghilardi, J. R., Rogers, S. D., Mantyh, C. R., Liu, H., et al. (1995a). Rapid endocytosis of a G protein-coupled receptor: substance P evoked internalization of its receptor in the rat striatum *in vivo*. *Proc. Natl. Acad. Sci. U S A* 92, 2622–2626. doi: 10.1073/pnas.92.7.2622

Mantyh, P. W., DeMaster, E., Malhotra, A., Ghilardi, J. R., Rogers, S. D., Mantyh, C. R., et al. (1995b). Receptor endocytosis and dendrite reshaping in spinal neurons after somatosensory stimulation. *Science* 268, 1629–1632. doi: 10.1126/science.7539937

Mao, J. (2012). Current challenges in translational pain research. *Trends Pharmacol. Sci.* 33, 568–573. doi: 10.1016/j.tips.2012.08.001

Mendiguren, A., Aostri, E., and Pineda, J. (2018). Regulation of noradrenergic and serotonergic systems by cannabinoids: relevance to cannabinoid-induced effects. *Life Sci.* 192, 115–127. doi: 10.1016/j.lfs.2017.11.029

Molero, Y., Larsson, H., D'Onofrio, B. M., Sharp, D. J., and Fazel, S. (2019). Associations between gabapentinoids and suicidal behaviour, unintentional overdoses, injuries, road traffic incidents and violent crime: population based cohort study in Sweden. *BMJ* 365:l2147. doi: 10.1136/bmj.l2147

O'Malley, K. L., Jong, Y.-J. I., Gonchar, Y., Burkhalter, A., and Romano, C. (2003). Activation of metabotropic glutamate receptor mGlu5 on nuclear membranes mediates intranuclear Ca^{2+} changes in heterologous cell types and neurons. *J. Biol. Chem.* 278, 28210–28219. doi: 10.1074/jbc.M300792200

Padilla, B. E., Cottrell, G. S., Roosterman, D., Pikios, S., Muller, L., Steinhoff, M., et al. (2007). Endothelin-converting enzyme-1 regulates endosomal sorting of calcitonin receptor-like receptor and β-arrestins. *J. Cell Biol.* 179, 981–997. doi: 10.1083/jcb.200704053

Poole, D. P., Amadesi, S., Veldhuis, N. A., Abogadie, F. C., Lieu, T., Darby, W., et al. (2013). Protease-activated receptor 2 (PAR2) protein and transient receptor potential vanilloid 4 (TRPV4) protein coupling is required for sustained inflammatory signaling. *J. Biol. Chem.* 288, 5790–5802. doi: 10.1074/jbc.M112.438184

Poole, D. P., Lieu, T., Pelayo, J. C., Eriksson, E. M., Veldhuis, N. A., and Bunnett, N. W. (2015). Inflammation-induced abnormalities in the subcellular localization and trafficking of the neurokinin 1 receptor in the enteric nervous system. *Am. J. Physiol. Gastrointest. Liver Physiol.* 309, G248–G259. doi: 10.1152/ajpgi.00118.2015

Purgert, C. A., Izumi, Y., Jong, Y.-J. I., Kumar, V., Zorumski, C. F., and O'Malley, K. L. (2014). Intracellular mGluR5 can mediate synaptic plasticity in the hippocampus. *J. Neurosci.* 34, 4589–4598. doi: 10.1523/JNEUROSCI.3451-13.2014

Rajendran, L., Schneider, A., Schlechtingen, G., Weidlich, S., Ries, J., Braxmeier, T., et al. (2008). Efficient inhibition of the Alzheimer's disease β-secretase by membrane targeting. *Science* 320, 520–523. doi: 10.1126/science.1156609

Rasmussen, S. G. F., Choi, H.-J., Fung, J. J., Pardon, E., Casarosa, P., Chae, P. S., et al. (2011). Structure of a nanobody-stabilized active state of the β_2 adrenoceptor. *Nature* 469, 175–180. doi: 10.1038/nature09648

Ricks, T. K., and Trejo, J. (2009). Phosphorylation of protease-activated receptor-2 differentially regulates desensitization and internalization. *J. Biol. Chem.* 284, 34444–34457. doi: 10.1074/jbc.M109.048942

Rodriguez-Gaztelumendi, A., Spahn, V., Labuz, D., Machelska, H., and Stein, C. (2018). Analgesic effects of a novel pH-dependent μ-opioid receptor agonist in models of neuropathic and abdominal pain. *Pain* 159, 2277–2284. doi: 10.1097/j.pain.0000000000001328

Rozenfeld, R., and Devi, L. A. (2008). Regulation of CB1 cannabinoid receptor trafficking by the adaptor protein AP-3. *FASEB J.* 22, 2311–2322. doi: 10.1096/fj.07-102731

Saraghi, M., and Hersh, E. V. (2013). Three newly approved analgesics: an update. *Anesth. Prog.* 60, 178–187. doi: 10.2344/0003-3006-60.4.178

Scholz, J., and Woolf, C. J. (2002). Can we conquer pain? *Nat. Neurosci.* 5, 1062–1067. doi: 10.1038/nn942

Schuchat, A., Houry, D., and Guy, G. P. (2017). New data on opioid use and prescribing in the United States. *JAMA* 318, 425–426. doi: 10.1001/jama.2017.8913

Scuteri, D., Adornetto, A., Rombolà, L., Naturale, M. D., Morrone, L. A., Bagetta, G., et al. (2019). New trends in migraine pharmacology: targeting calcitonin gene-related peptide (CGRP) with monoclonal antibodies. *Front. Pharmacol.* 10:363. doi: 10.3389/fphar.2019.00363

Shukla, A. K., Westfield, G. H., Xiao, K., Reis, R. I., Huang, L.-Y., Tripathi-Shukla, P., et al. (2014). Visualization of arrestin recruitment by a G-protein-coupled receptor. *Nature* 512, 218–222. doi: 10.1038/nature13430

Spahn, V., Del Vecchio, G., Labuz, D., Rodriguez-Gaztelumendi, A., Massaly, N., Temp, J., et al. (2017). A nontoxic pain killer designed by modeling of pathological receptor conformations. *Science* 355, 966–969. doi: 10.1126/science.aai8636

Steeds, C. E. (2016). The anatomy and physiology of pain. *Surgery* 34, 55–59. doi: 10.1016/j.mpsur.2015.11.005

Sternini, C., Spann, M., Anton, B., Keith, D. E., Bunnett, N. W., von Zastrow, M., et al. (1996). Agonist-selective endocytosis of mu opioid receptor by neurons *in vivo*. *Proc. Natl. Acad. Sci. U S A* 93, 9241–9246. doi: 10.1073/pnas.93.17.9241

Stoeber, M., Jullié, D., Lobingier, B. T., Laeremans, T., Steyaert, J., Schiller, P. W., et al. (2018). A genetically encoded biosensor reveals location bias of opioid drug action. *Neuron* 98, 963.e5–976.e5. doi: 10.1016/j.neuron.2018.04.021

Stone, L. S., and Molliver, D. C. (2009). In search of analgesia: emerging roles of GPCRs in pain. *Mol. Interv.* 9, 234–251. doi: 10.1124/mi.9.5.7

Thomsen, A. R. B., Jensen, D. D., Hicks, G. A., and Bunnett, N. W. (2018). Therapeutic targeting of endosomal G-protein-coupled

receptors. *Trends Pharmacol. Sci.* 39, 879–891. doi: 10.1016/j.tips.2018.08.003

Thurlkill, R. L., Cross, D. A., Scholtz, J. M., and Pace, C. N. (2005). pKa of fentanyl varies with temperature: implications for acid-base management during extremes of body temperature. *J. Cardiothorac. Vasc. Anesth.* 19, 759–762. doi: 10.1053/j.jvca.2004.11.039

Tressel, S. L., Koukos, G., Tchernychev, B., Jacques, S. L., Covic, L., and Kuliopulos, A. (2011). Pharmacology, biodistribution and efficacy of GPCR-based pepducins in disease models. *Methods Mol. Biol.* 683, 259–275. doi: 10.1007/978-1-60761-919-2_19

Tsuji, M., Ueda, S., Hirayama, T., Okuda, K., Sakaguchi, Y., Isono, A., et al. (2013). FRET-based imaging of transbilayer movement of pepducin in living cells by novel intracellular bioreductively activatable fluorescent probes. *Org. Biomol. Chem.* 11, 3030–3037. doi: 10.1039/c3ob27445d

Tsvetanova, N. G., Irannejad, R., and von Zastrow, M. (2015). G protein-coupled receptor (GPCR) signaling *via* heterotrimeric G proteins from endosomes. *J. Biol. Chem.* 290, 6689–6696. doi: 10.1074/jbc.R114.617951

Vilardaga, J.-P., Jean-Alphonse, F. G., and Gardella, T. J. (2014). Endosomal generation of cAMP in GPCR signaling. *Nat. Chem. Biol.* 10, 700–706. doi: 10.1038/nchembio.1611

Vincent, K., Cornea, V. M., Jong, Y.-J. I., Laferrière, A., Kumar, N., Mickeviciute, A., et al. (2016). Intracellular mGluR5 plays a critical role in neuropathic pain. *Nat. Commun.* 5:10604. doi: 10.1038/ncomms10604

Vincent, K., Wang, S. F., Laferrière, A., Kumar, N., and Coderre, T. J. (2017). Spinal intracellular metabotropic glutamate receptor 5 (mGluR5) contributes to pain and c-fos expression in a rat model of inflammatory pain. *Pain* 158, 705–716. doi: 10.1097/j.pain.0000000000000823

Volkow, N. D., McLellan, T. A., Cotto, J. H., Karithanom, M., and Weiss, S. R. B. (2011). Characteristics of opioid prescriptions in 2009. *JAMA* 305, 1299–1301. doi: 10.1001/jama.2011.401

Whelton, A. (2000). Renal and related cardiovascular effects of conventional and COX-2-specific NSAIDs and non-NSAID analgesics. *Am. J. Ther.* 7, 63–74. doi: 10.1097/00045391-200007020-00004

Yarwood, R. E., Imlach, W. L., Lieu, T., Veldhuis, N. A., Jensen, D. D., Klein Herenbrink, C., et al. (2017). Endosomal signaling of the receptor for calcitonin gene-related peptide mediates pain transmission. *Proc. Natl. Acad. Sci. U S A* 114, 12309–12314. doi: 10.1073/pnas.1706656114

Zhao, P., Lieu, T., Barlow, N., Metcalf, M., Veldhuis, N. A., Jensen, D. D., et al. (2014). Cathepsin S causes inflammatory pain *via* biased agonism of PAR2 and TRPV4. *J. Biol. Chem.* 289, 27215–27234. doi: 10.1074/jbc.M114.599712

Zhao, P., Lieu, T., Barlow, N., Sostegni, S., Haerteis, S., Korbmacher, C., et al. (2015). Neutrophil elastase activates protease-activated receptor-2 (PAR2) and transient receptor potential vanilloid 4 (TRPV4) to cause inflammation and pain. *J. Biol. Chem.* 290, 13875–13887. doi: 10.1074/jbc.M115.642736

Conflict of Interest: Research in NV and DP laboratories is funded in part by Takeda Pharmaceuticals Inc.

The remaining authors declare that the research was conducted in the absence of any commercial or financial relationships that could be construed as a potential conflict of interest.

frontiers in Molecular Neuroscience

ORIGINAL RESEARCH
published: 29 November 2019
doi: 10.3389/fnmol.2019.00294

The Alpha Isoform of Heat Shock Protein 90 and the Co-chaperones p23 and Cdc37 Promote Opioid Anti-nociception in the Brain

Wei Lei[1,2], *David I. Duron*[1], *Carrie Stine*[1], *Sanket Mishra*[3], *Brian S. J. Blagg*[3] *and John M. Streicher*[1]*

[1]*Department of Pharmacology, College of Medicine, University of Arizona, Tucson, AZ, United States,* [2]*Department of Pharmaceutical and Administrative Sciences, School of Pharmacy, Presbyterian College, Clinton, SC, United States,* [3]*Department of Chemistry & Biochemistry, College of Science, University of Notre Dame, Notre Dame, IN, United States*

Opioid activation of the mu opioid receptor (MOR) promotes signaling cascades that evoke both analgesic responses to pain and side effects like addiction and dependence. Manipulation of these cascades, such as by biased agonism, has great promise to improve opioid therapy. However, the signaling cascades of the MOR are in general poorly understood, providing few targets for drug development. In our earlier work, we identified Heat shock protein 90 (Hsp90) as a novel and crucial regulator of opioid anti-nociception in the brain by promoting ERK MAPK activation. In this study, we sought to identify the molecular isoforms and co-chaperones by which Hsp90 carried out this role, which could provide specific targets for future clinical intervention. We used novel selective small molecule inhibitors as well as CRISPR/Cas9 gene editing constructs delivered by the intracerebroventricular (*icv*) route to the brains of adult CD-1 mice to target Hsp90 isoforms (Hsp90α/β, Grp94) and co-chaperones (p23, Cdc37, Aha1). We found that inhibition of the isoform Hsp90α fully blocked morphine anti-nociception in a model of post-surgical paw incision pain, while blocking ERK and JNK MAPK activation, suggesting Hsp90α as the main regulator of opioid response in the brain. We further found that inhibition of the co-chaperones p23 and Cdc37 blocked morphine anti-nociception, suggesting that these co-chaperones assist Hsp90α in promoting opioid anti-nociception. Lastly, we used cycloheximide treatment in the brain to demonstrate that rapid protein translation within 30 min of opioid treatment is required for Hsp90 regulation of opioid response. Together these studies provide insight into the molecular mechanisms by which Hsp90 promotes opioid anti-nociception. These findings thus both improve our basic science knowledge of MOR signal transduction and could provide future targets for clinical intervention to improve opioid therapy.

Keywords: heat shock protein 90 (Hsp90), p23, Cdc37, opioid, pain, anti-nociception, CRISPR, translation

OPEN ACCESS

Edited by:
Felix Viana,
Institute of Neurosciences of Alicante (IN), Spain

Reviewed by:
Wei Xiong,
University of Science and Technology of China, China
Bo Zhao,
Indiana University, United States

***Correspondence:**
John M. Streicher
jstreicher@email.arizona.edu

Received: *28 June 2019*
Accepted: *15 November 2019*
Published: *29 November 2019*

Citation:
Lei W, Duron DI, Stine C, Mishra S, Blagg BSJ and Streicher JM (2019) The Alpha Isoform of Heat Shock Protein 90 and the Co-chaperones p23 and Cdc37 Promote Opioid Anti-nociception in the Brain. Front. Mol. Neurosci. 12:294. doi: 10.3389/fnmol.2019.00294

INTRODUCTION

The mu opioid receptor (MOR) evokes complex signal transduction cascades upon activation by opioid ligands like morphine. For decades now it has been understood that the MOR represses cAMP production by inhibiting adenylyl cyclase *via* the $G\alpha_I$ subunit, and activates G protein-coupled inwardly-rectifying potassium channels *via* the Gβ/γ subunit, which summate on neuronal hyperpolarization and subsequent inhibition of nociceptive inputs (Al-Hasani and Bruchas, 2011). However, it is clear that signaling regulators beyond this simple cascade have a strong impact on opioid anti-nociception and side effects, including other G proteins, ERK MAPK (Macey et al., 2009), Src (Zhang et al., 2017), CaMKII (Li et al., 2016), RSK2 (Darcq et al., 2012), and others. These signaling regulators could provide important targets for opioid drug development; for instance βarrestin2 was shown to reduce opioid anti-nociception while promoting side effects like tolerance and dependence, leading to the development of βarrestin2 biased agonists with reduced side effects (Bohn et al., 1999; Raehal et al., 2005; Dewire et al., 2013; Manglik et al., 2016; Schmid et al., 2017). However, in general, the mechanisms by which these signaling regulators impact opioid physiology are not known, and very few targets like βarrestin2 have been validated for drug development (Al-Hasani and Bruchas, 2011; Olson et al., 2017). This gap illustrates the need for investigation into the signalosome of the MOR and the mechanisms by which these regulators impact opioid physiology.

To this end, in our earlier work, we identified the central signaling regulator Heat shock protein 90 (Hsp90) as a novel and crucial regulator of opioid signaling in the brain, that promoted opioid anti-nociception by promoting ERK MAPK activation (Lei et al., 2017). Hsp90 is a major regulator of protein folding *via* chaperone activity in concert with other Hsps like Hsp70 (Li and Buchner, 2013). However, Hsp90 also has a major role in signal transduction by regulating signaling molecule localization, complex/scaffold formation, and acute signaling activation (Streicher, 2019). Despite the importance of Hsp90 in regulating signaling, only two previous studies *directly* linked Hsp90 to opioid signaling. An *in vitro* study found that Hsp90 inhibition decreased cAMP superactivation, a marker for opioid dependence (Koshimizu et al., 2010); supporting these findings, an *in vivo* mouse study found that injection of Hsp90 inhibitor reduced the somatic signs of morphine withdrawal (Abul-Husn et al., 2011). Our study was thus the first to *directly* link Hsp90 regulation of MOR signaling to opioid anti-nociception.

Our study did show that Hsp90 inhibition very strongly decreased morphine anti-nociception in models of acute and chronic pain, and identified a signaling mechanism *via* ERK MAPK (Lei et al., 2017). However, this study only took the first small step in identifying the role of Hsp90 in regulating opioid signaling. We used the ATP-pocket inhibitor 17-AAG, which is non-selective between the four Hsp90 isoforms (Hsp90α/β, Grp94, TRAP1). These isoforms differ in their subcellular localization and protein targets, with Hsp90α/β localized to the cytoplasm, Grp94 to the endoplasmic reticulum, and TRAP1 to the mitochondria (Liu et al., 2015; Kim et al., 2016; Mishra et al., 2017). We also did not identify any of the crucial co-chaperones, which mediate and target the specific activity of Hsp90 in different cells and tissues (Li and Buchner, 2013). Co-chaperones have specific roles, like Cdc37 having a key role in signaling kinase targeting, suggesting their possible involvement in MOR signaling (Hinz et al., 2007). Identifying the isoforms and co-chaperones involved in Hsp90 regulation of opioid signaling will thus reveal key details of the molecular mechanism by which Hsp90 promotes anti-nociception. Identifying these refined molecular targets could also provide more selective targets for clinical intervention, which has been done in an analogous way for Hsp70 (Assimon et al., 2013, 2015).

In this study, we thus sought to identify specific Hsp90 isoforms and co-chaperones responsible for the promotion of opioid anti-nociception by Hsp90. We utilized novel selective inhibitors and *in vivo* CRISPR/Cas9 gene editing in the brains of adult CD-1 mice to test Hsp90 isoforms (Hsp90α/β, Grp94) and co-chaperones (p23, Cdc37, Aha1). Through these studies, we found that the isoform Hsp90α and the co-chaperones p23 and Cdc37 strongly promoted MOR signaling and opioid anti-nociception in the brain. These findings expand our knowledge of the specific molecular mechanisms by which Hsp90 regulates opioid anti-nociception, and could provide more selective targets for clinical intervention.

MATERIALS AND METHODS

Drugs

KUNA115 (Mishra et al., under review), KUNB106 (Mishra et al., in press), KUNG65 (compound 30 in Crowley et al., 2017), KU-32 (compound A4 in Ansar et al., 2007), and KU177 (compound 12c in Zhao et al., 2011) were synthesized by the Blagg laboratory using the cited protocols. The identity of the ligands was confirmed by high resolution mass spectrometry and nuclear magnetic resonance, while the purity of the compounds was confirmed to >95% by high performance liquid chromatography. Gedunin (#33-871-0), Celastrol (#32-031-0), 17-AAG (#AAJ66960MC), and Cycloheximide (#AC357420010) were obtained from Fisher Scientific. DAMGO (#1171) was obtained from Tocris/R&D. Morphine sulfate pentahydrate was obtained from the NIDA Drug Supply Program. All compounds except for DAMGO and morphine were prepared as DMSO stock solutions and diluted into a vehicle solution prior to injection. DAMGO was prepared in a stock solution of sterile USP water and morphine in sterile USP saline; morphine was prepared fresh prior to each experiment. Matched vehicle controls were included for each drug injection. The vehicles used were: 2% DMSO and 98% sterile USP water for KUNA115, KUNB106, KUNG65, KU177, Cycloheximide; 1% DMSO and 99% sterile USP water for KU-32 and 17-AAG; 10% DMSO, 10% Tween80, and 80% sterile USP water for gedunin and celastrol; sterile USP water for DAMGO; and sterile USP saline for morphine. Drug powders were stored at −20°C under desiccation or as recommended by the manufacturer, and stock solutions were stored at −20°C.

CRISPR/Cas9 DNA Constructs

CRISPR gene editing constructs were obtained from Genecopoeia as all-in-one DNA vectors containing universal promoters driving expression of the gRNA and Cas9 gene, along with a neomycin resistance gene for mammalian cell selection and an mCherry gene for visualization (pCRISPR-CG vector). The constructs were pre-designed by Genecopoeia to target each mouse gene. They included a universal negative control vector that expresses all the same elements with a non-targeting gRNA (#CCPCTR01-CG01-B), and constructs to target Hsp90α (#MCP229411-CG01), p23 (#MCP232080-CG12), Cdc37 (#MCP231406-CG12), and PEBP1 (#MCP231756-CG01) as a further negative control.

Each DNA vector was amplified for use using standard bacterial transformation, and an endotoxin-free maxi-prep kit to reduce inflammation upon injection. Each vector was also validated by restriction digest. The Hsp90α vector was validated in an *in vitro* experiment. Mouse 66.1 breast cancer cells were cultured as described in Edwards et al. (2018). The cells were electroporated with 10 μg of DNA per cuvette, then selected with 500 μg/ml of G418 until the cells recovered and began growing again. At this point, the cells were harvested and analyzed by Western blot as described below. The *in vivo* delivery and validation of all vectors are also described below.

Animals

Male and female CD-1 (a.k.a. ICR) mice from 4 to 8 weeks of age were used for all experiments and were obtained from Charles River Laboratories. The mice were recovered for at least 5 days after shipping prior to use and housed no more than five per cage. All mice were housed in the University of Arizona's AAALAC-accredited vivarium with temperature and humidity control, 12 h light/dark cycles, and standard chow and water available *ad libitum*. All experiments performed were approved by the University of Arizona's IACUC, and all experiments were in accordance with the NIH Care and Use of Laboratory Animals handbook.

Paw Incision Model

Mice were randomly assigned to experimental groups in age-matched cohorts, and the experimenter was blinded to treatment group identity by the delivery of coded drug vials. We utilized a post-surgical paw incision pain model, with the surgery performed as described in our earlier work (Lei et al., 2017). Drugs or CRISPR DNA constructs were delivered by the intracerebroventricular (*icv*) route in a 5 μl volume, also performed as described in Lei et al. (2017). For drug treatments, the paw incision surgery was performed, and while the mice were still under anesthesia, an *icv* injection of inhibitor drug or vehicle was performed. The mice then recovered from both the surgery and injection for 1 or 24 h prior to opioid injection and pain measurement. For CRISPR experiments, 4 μg of DNA was complexed with Turbofect *in vivo* transfection reagent (#FERR0541 from Fisher Scientific) according to the manufacturer's instructions and injected *icv* daily from days 1 to 3. The mice then recovered, with the paw incision surgery performed on day 9 and opioid injection and pain measurement performed on day 10. Our *in vivo* CRISPR protocol is based on the protocol reported in Sandweiss et al. (2017).

Mechanical pain/allodynia on the incised paw was measured using Von Frey filaments with the up-down method, as performed in our earlier work and the literature (Chaplan et al., 1994; Lei et al., 2017; Edwards et al., 2018). Pre- and post-CRISPR and pre- and post-surgical baselines were measured to determine any impact of the treatment on baseline responses prior to the injection of morphine. Mechanical allodynia was measured in a 2–3 h time course after the injection of morphine.

Signaling Protein Analysis by Western Blot

To analyze brain signaling changes, mice were injected *icv* with KUNA115 as above for 24 h, followed by *icv* injection of DAMGO for 10 min. The mice were sacrificed by rapid cervical dislocation, and the periaqueductal gray (PAG) region was rapidly dissected on an ice-cooled metal block and snap-frozen in liquid nitrogen. G418-selected populations of 66.1 cells transfected with CRISPR constructs described above were also harvested for protein analysis. The cells were washed with ice-cold dPBS and the cells recovered by adding lysis buffer and scraping with a plastic cell spatula. The methods for protein extraction from both brain regions and cell lysates, the composition of our lysis buffer, and the protocol for performing the Western blot are all reported in our earlier work (Lei et al., 2017).

We used the following antibodies for our Western analysis: phospho-Akt (#50-191-224, Fisher Scientific); total-Akt (#50-190-279, Fisher Scientific); phospho-ERK (#50-191-932, Fisher Scientific); total-ERK (#50-191-129, Fisher Scientific); phospho-JNK (#9255, Cell Signaling); total-JNK (#9252, Cell Signaling); Hsp70 (#4872, Cell Signaling); STAT3 (#9139, Cell Signaling); GAPDH (#PIMA515738, Fisher Scientific); Hsp90α (#MA110892, Fisher Scientific); and mCherry (#NBP196752SS, Fisher Scientific). The antibodies were generally used at 1:1,000 in 5% BSA in TBST rocking overnight at 4°C. We used goat anti-rabbit or goat anti-mouse IRDye 680 or 800 secondary antibodies from LiCor Biosciences at 1:5,000–10,000 in 5% non-fat dry milk in TBST at room temperature for 1 h. The resulting data was imaged using an Odyssey Fc imager from LiCor Biosciences. The data were quantitated using Scion Image, derived from NIH ImageJ. Phospho-protein signal was normalized to total protein signal from the same sample (e.g., pERK normalized to tERK), while total protein signal was normalized to the housekeeping gene GAPDH (e.g., STAT3 normalized to GAPDH). These normalized data were further normalized to the vehicle-treated control animals within each experiment.

Immunohistochemistry

CRISPR-mediated knockdown in the brain of the target proteins Hsp90α, p23, and Cdc37 was validated *post hoc* in treated mice as above using immunohistochemistry. The mice were first perfused with 4% paraformaldehyde in saline, and the brains removed and frozen as a block in OTC medium. The brains were sectioned using a cryotome with 20 μm sections and mounted on Leica Xtra slides (#NC0215141, Fisher Scientific); the frozen

sections were dried at room temperature for 15 min and stored at −20°C until use.

For Hsp90α: sections warmed to room temperature, then washed in TBS (20 mM Tris, 150 mM NaCl, pH 7.2) for 10 min. Blocked for 2 h in a humidified chamber at room temperature (10% goat serum, 0.3% Triton-X100 in TBS). Incubated with primary antibody (#380-003, Synaptic Systems) at 1:50 in 5% goat serum, 0.3% Triton-X100 in TBS overnight at 4°C. Washed 3 × 10 min in TBS, followed by anti-rabbit Alexa 488 secondary antibody (#A11034, Fisher Scientific) at 1:200 in 5% goat serum, 0.3% Triton-X100 in TBS for 1 h at room temperature. The slides were then washed 3 × 10 min in TBS, dried at room temperature for 10 min, then mounted.

For p23 and Cdc37: sections warmed to room temperature, then washed in phosphate buffered saline (PBS) for 10 min. Heat-induced antigen retrieval performed for 20 min at 95°C in sodium citrate buffer (10 mM sodium citrate, 0.05% Tween20, pH 6.0). The slides were cooled to room temperature for 20 min, then washed in PBS with 0.1% Tween20 (PBST) twice, and PBS once. The sections were then blocked for 30 min in a humidified chamber at room temperature [3% fetal bovine serum (FBS) in PBS]. After blocking, the sections were incubated with primary antibody overnight at 4°C (p23-1:1,000 of #MA3414 from Fisher Scientific; Cdc37-1:100 of #MA3029 from Fisher Scientific; both in 3% FBS in PBS). The slides were then washed 3 × 10 min in PBST, followed by secondary antibody at room temperature (p23-1:200 of anti-mouse Alexa594, #A11032 from Fisher Scientific, in 3% FBS in PBS for 1 h. Cdc37-1:200 of anti-mouse Alexa488, #A11031 from Fisher Scientific, in 3% FBS in PBST for 30 min). The slides were then washed 3 × 10 min in PBST and dried at room temperature for 10 min before mounting.

All sections were imaged using a standard fluorescent microscope using the appropriate filters for Alexa488 (blue/green) and Alexa594 (green/red). The knockdown of all targets was broadly apparent across the brain. The pontine reticular nucleus (PRN) was chosen as the site of imaging and quantitation. Images were taken from 4 to 6 adjacent sections from each animal. The fluorescence intensity divided by the area of the image was calculated for each section, and the 4–6 sections per animal averaged to produce a single mean value counted as $N = 1$.

Data Analysis

All data is reported as the mean ± SEM. All statistical analysis was performed using GraphPad Prism 8.0. All behavioral data is reported as raw threshold values without normalization; Western blot and immunohistochemistry data normalized as described in those sections above. Statistical comparisons for behavioral data and ERK/JNK/Akt Western data performed using a two-way ANOVA with Fisher's Least Significant Difference *post hoc* test. Comparisons of immunohistochemistry data and Hsp70/STAT3 Western data performed using an Unpaired 2-Tailed *t*-test. In all cases significance was set as a *p*-value of <0.05. For the dose/response experiment using KUNA115, the area under the curve (AUC) was calculated for each dose and treatment using Prism 8.0, and graphed by log dose and treatment group. Linear regression analysis was performed, and the parameters of those fitted lines used to calculate the potency (A_{50}) as previously described (Lei et al., 2017). The sample sizes and technical replicates for each experiment are described in the Figure Legends.

RESULTS

Isoform-Selective Inhibitor Screen Identifies Hsp90α

To identify the active Hsp90 isoform in regulating opioid anti-nociception in the brain, we performed a screen of isoform-selective small molecule inhibitors. KUNA115 is selective for Hsp90α (Mishra et al., under review), KUNB106 for Hsp90β (Mishra et al., in press), and KUNG65 for Grp94 (Crowley et al., 2017). All inhibitors were delivered at a screening dose of 0.1 nmol by the *icv* route for 24 h, a model predicated on our earlier studies with the non-selective Hsp90 inhibitor 17-AAG (Lei et al., 2017). Over a full morphine dose range of 1–10 mg/kg, we found that KUNA115 strongly blocked morphine anti-nociception in paw incision pain, suggesting the involvement of the isoform Hsp90α (**Figure 1A**). Dose/response analysis for this experiment revealed an A_{50} potency value of morphine of 8.95 mg/kg for Vehicle-treated mice, in line with literature values, validating the experiment (**Figure 1B**). The dose/response curve for KUNA115 meanwhile was so flat it did not give a feasible value (calculated A_{50} of 88, 139, 382 mg/kg; **Figure 1B**). These results show that an Hsp90α-selective inhibitor strongly blocked morphine anti-nociception in this pain model in line with our previous results using a non-selective inhibitor (Lei et al., 2017). We also found a similar result with female mice, suggesting no sex differences with this target and model (**Figure 1C**).

When we tested the other isoform-selective inhibitors, we found no differences for KUNB106 (Hsp90β; **Figure 1D**) and KUNG65 (Grp94; **Figure 1E**). These results do suggest that Hsp90α alone is active in the brain for opioid signaling regulation. As a further control, we tested the impact of an alternate site inhibitor KU-32, which binds to the C-terminal region of Hsp90 unlike the ATP pocket targeted 17-AAG but is similarly non-selective between isoforms (Ansar et al., 2007). The results with KU-32 are the same as for KUNA115 above and 17-AAG (Lei et al., 2017), further validating the results and suggesting a *bona fide* role for Hsp90 in regulating opioid anti-nociception (**Figure 1F**).

We also performed additional experiments to further define the impact of KUNA115/Hsp90α on opioid anti-nociception. All experiments above were carried out with a 24 h recovery, leaving the time course of KUNA115 unknown. We thus performed a paw incision experiment as above with only a 1 h KUNA115 treatment; this resulted in a strong loss of morphine anti-nociception, similar to the 24 h results above (**Figure 1G**). This finding suggests that KUNA115 has a relatively rapid onset that is sustained for 24 h or more. We also controlled for potential impacts of KUNA115 on mechanical thresholds without pain or opioids present. We found that a 24 h KUNA115 treatment as above had no impact on baseline mechanical thresholds,

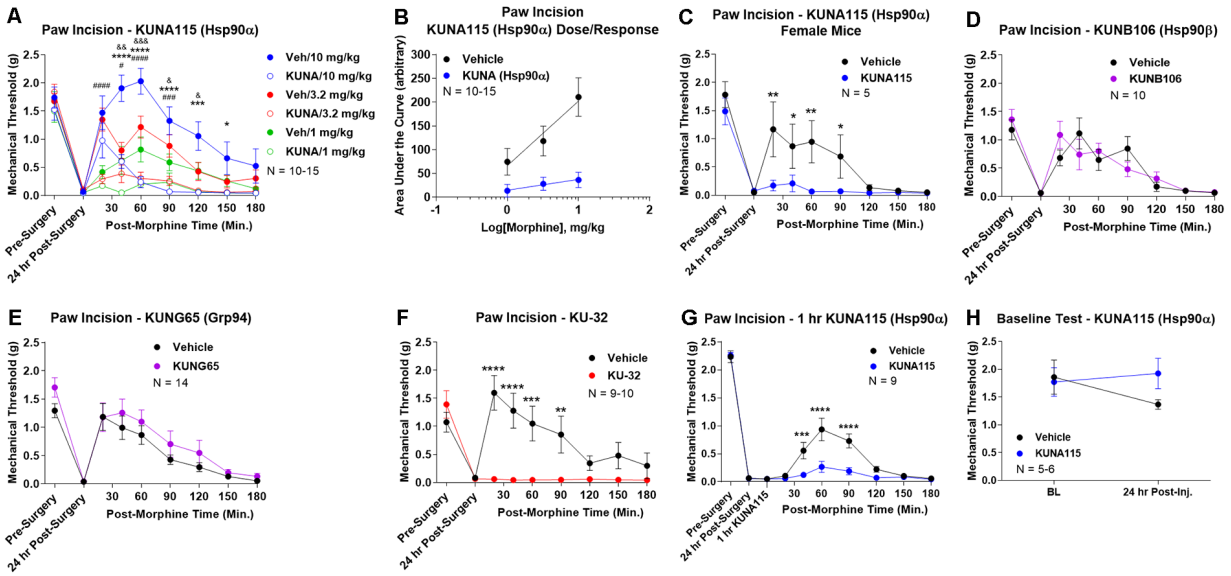

FIGURE 1 | Heat shock protein 90 (Hsp90) isoform-selective inhibitor screen identifies Hsp90α in promoting opioid anti-nociception in the brain. CD-1 mice had the paw incision surgery performed, with concurrent injection of vehicle or 0.1 nmol of inhibitor intracerebroventricular (*icv*). Mice recovered 24 h, followed by *sc* injection of morphine. Mechanical thresholds measured before and after surgery, and in a time course after morphine injection. Pre- and post-surgery baselines did not differ for any group ($p > 0.05$). All data reported as the mean ± SEM, with sample sizes of mice/group noted in each graph. All statistics performed by two-way ANOVA with Fisher's Least Significant Difference *post hoc* test. **(A)** Male mice tested with KUNA115 (Hsp90α selective) and a 1–10 mg/kg morphine dose range. $^{*,***,****}p < 0.05$, 0.001, 0.0001 between Veh and KUNA groups at same time point at 10 mg/kg; $^{\#,\#\#\#,\#\#\#\#}p < 0.05$, 0.001, 0.0001 between Veh and KUNA groups at same time point at 3.2 mg/kg; $^{\&,\&\&,\&\&\&}p < 0.05$, 0.01, 0.001 between Veh and KUNA groups at same time point at 1 mg/kg. Performed in 2–3 technical replicates. **(B)** Dose/response curves constructed from the data in **(A)** and analyzed as described in "Materials and Methods" section. A_{50}: Vehicle = 8.95 mg/kg; KUNA115 = 88, 139, 382 mg/kg (too flat for accurate calculation). **(C)** KUNA115 experiment performed in female mice with 3.2 mg/kg morphine. Performed in one technical replicate. For remaining graphs: $^{*,**,***,****}p < 0.05$, 0.01, 0.001, 0.0001 vs. same time point inhibitor treatment group. **(D)** Male mice tested with KUNB106 (Hsp90β selective) with 3.2 mg/kg morphine. Performed in two technical replicates. **(E)** Male mice tested with KUNG65 (Grp94 selective) with 3.2 mg/kg morphine. Performed in three technical replicates. **(F)** Male mice tested with KU-32 (non-selective) with 3.2 mg/kg morphine. Performed in two technical replicates. **(G)** Male and female mice had paw incision performed, with 23 h recovery. KUNA115 or Vehicle then injected as above, with 1 h treatment prior to 3.2 mg/kg morphine. Performed in two technical replicates. **(H)** Male and female mice had KUNA115 or Vehicle injected as above with a 24 h recovery. Pre- and post-injection baselines measured without any surgery, pain state, or opioids present. Performed in two technical replicates by different experimenters.

suggesting the results above are due to a specific impact on the opioid system (**Figure 1H**). This conclusion is further supported by our earlier work in which we found no impact of Hsp90 inhibitor treatment on motor performance in the Rotarod test (Lei et al., 2017).

Hsp90α Regulates Opioid Signal Transduction

We next sought to measure the impact of Hsp90α-selective inhibition on opioid signaling. We combined KUNA115 treatment with DAMGO stimulation in the brain, which is a highly selective, potent, and efficacious MOR agonist. We analyzed ERK and JNK MAPK, Akt, Hsp70, and STAT3 by Western blot in the PAG region of the brain (**Figure 2A**). This region was chosen based on our earlier studies using non-selective inhibitors (Lei et al., 2017); the PAG is also a key region in the pain modulatory circuitry (Heinricher et al., 2009). We found that both ERK and JNK MAPK phosphorylation was stimulated by DAMGO in Vehicle-treated mice, however, stimulation over baseline was lost with KUNA115 treatment (**Figure 2B**). With JNK MAPK, KUNA115 significantly raised the unstimulated baseline, as we saw for ERK MAPK with 17-AAG treatment (Lei et al., 2017). With the kinase Akt, KUNA115 treatment tended to increase both unstimulated and DAMGO-stimulated phospho-Akt levels, so that the KUNA115/DAMGO group was significantly elevated over Vehicle/Vehicle baseline (**Figure 2B**). Lastly, KUNA115 treatment had no impact on Hsp70 protein levels, unlike 17-AAG treatment (Lei et al., 2017), while it significantly decreased total protein levels of the signaling regulator STAT3 (**Figure 2B**). Together these results demonstrate that Hsp90α has a specific role in regulating opioid signal transduction in the brain suggesting potential involvement in opioid anti-nociception, similar to what we showed for 17-AAG treatment and ERK MAPK (Lei et al., 2017).

CRISPR Knockdown of Hsp90α in Adult Mouse Brain

To confirm the role of Hsp90α in regulating opioid anti-nociception, we used CRISPR/Cas9 DNA constructs to knockdown Hsp90α protein expression broadly across the brain in adult mice (similar approach to Sandweiss et al., 2017). We first validated our CRISPR construct *in vitro* using mouse 66.1 cells. Transfection of a negative control CRISPR vector or

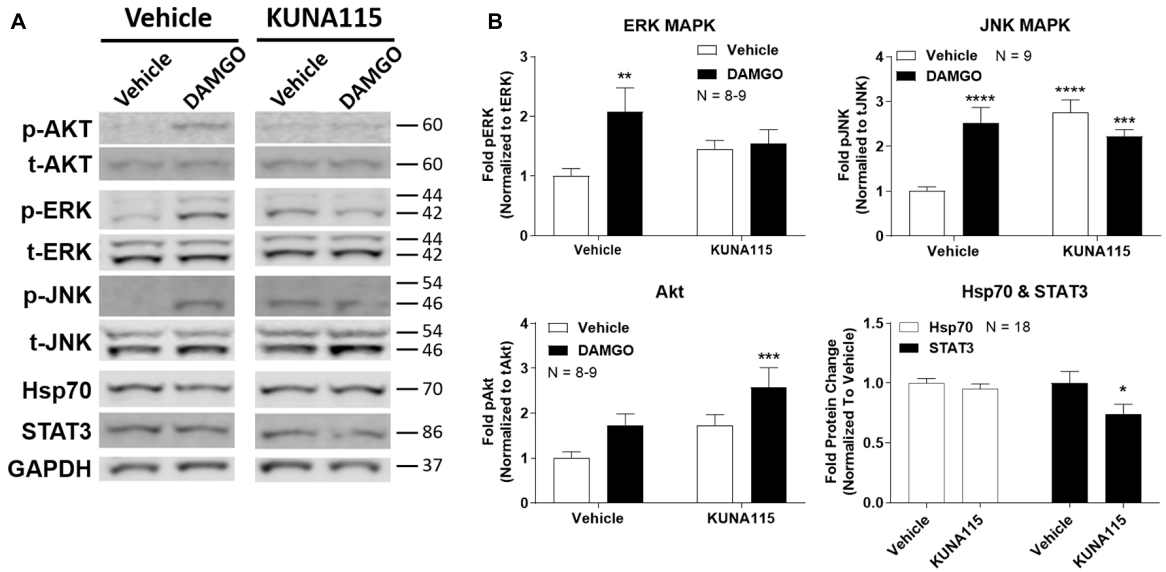

FIGURE 2 | Hsp90α regulates opioid signal transduction in the brain. Male CD-1 mice had vehicle or 0.1 nmol KUNA115 injected *icv*, 24 h, followed by vehicle or 0.1 nmol DAMGO *icv*, 10 min. Periaqueductal gray region analyzed by Western blot. All data reported as the mean ± SEM, with sample sizes of mice/group noted in each graph; all experiments performed in four technical replicates. For ERK, JNK and Akt, data analyzed by two-way ANOVA with Fisher's Least Significant Difference *post hoc* test; **,***,****$p < 0.01$, 0.001, 0.0001 vs. Vehicle:Vehicle group. For Hsp70 and STAT3 data analyzed by Unpaired 2-Tailed *t*-test; *$p < 0.05$ vs. same target Vehicle group. **(A)** Representative sample blots shown for each target, with MW indicated for each protein. Each pair of images for one target (e.g., p-Akt) were from the same blot, but discontinuous, so they are separated to denote this fact. **(B)** All Western data quantitated by target. ERK, JNK, and Akt are phosphorylated protein signal normalized to total protein. Hsp70 and STAT3 are normalized to GAPDH. KUNA115 treatment caused a loss of ERK and JNK stimulation over baseline by DAMGO, and a loss of STAT3 protein expression.

a vector targeting the protein PEBP had no impact on Hsp90α protein levels, while our vector targeting Hsp90α reduced protein levels by ∼90% (**Figure 3A**). We could also detect expression of the mCherry protein in all cells with a CRISPR vector, verifying successful transfection of all constructs (**Figure 3A**).

We next treated mice with the Hsp90α or negative control CRISPR vectors as described in the "Materials and Methods" section, and validated successful target knockdown by immunohistochemistry. We found broad knockdown across the entire brain and selected the PRN and PAG for analysis. We could detect a strong signal in both cell bodies and apparent dendritic fields that was strongly reduced by Hsp90α CRISPR treatment (**Figure 3B**). Quantitation of fluorescent signal revealed a significant reduction of 43.9% (**Figure 3C**). Thus validated, we next tested the impact of Hsp90α knockdown on morphine anti-nociception (**Figure 3D**). We found that Hsp90α CRISPR treatment fully blocked anti-nociception in paw incision pain (**Figure 3D**), very similarly to KUNA115 (**Figure 1**) and 17-AAG (Lei et al., 2017), confirming the role of Hsp90α in regulating opioid anti-nociception in the brain.

Hsp90 Co-chaperones p23 and Cdc37 Regulate Opioid Anti-nociception in the Brain

We first used the co-chaperone-selective inhibitors gedunin (p23, Brandt et al., 2008), celastrol (Cdc37, Zhang et al., 2008), and KU177 (Aha1, Zhao et al., 2011) in paw incision pain as for the isoform inhibitors above. Both gedunin (p23; **Figure 4A**) and celastrol (Cdc37; **Figure 4B**) strongly reduced morphine anti-nociception in paw incision pain, very similar to the Hsp90 inhibitors above. However, KU177 (Aha1) had only a slight impact on opioid anti-nociception, suggesting it may not have a significant role (**Figure 4C**).

We next moved forward with CRISPR/Cas9 gene editing to confirm that p23 and Cdc37 regulate opioid anti-nociception as we did for Hsp90α above. IHC analysis showed a similar broad knockdown across the brain with CRISPR treatment, particularly apparent in the PRN (**Figure 4D**). Quantitation revealed significant decreases of 36.3% for p23 and 46.0% for Cdc37 (**Figure 4E**). We next tested the impact of targeted CRISPR treatment for these proteins in paw incision pain, and found that both p23 and Cdc37 CRISPR knockdown fully blocked morphine anti-nociception, very similar to Hsp90α inhibition above or 17-AAG treatment (Lei et al., 2017; **Figure 4F**). These results confirm that both p23 and Cdc37 regulate opioid anti-nociception in the brain.

Rapid Translation Required for Hsp90 Regulation of Opioid Anti-nociception

Lastly, we sought to identify part of the molecular biology mechanism by which Hsp90 regulates opioid anti-nociception. We combined 24 h Hsp90 inhibition as above and in our previous work (Lei et al., 2017) with treatment of the translation

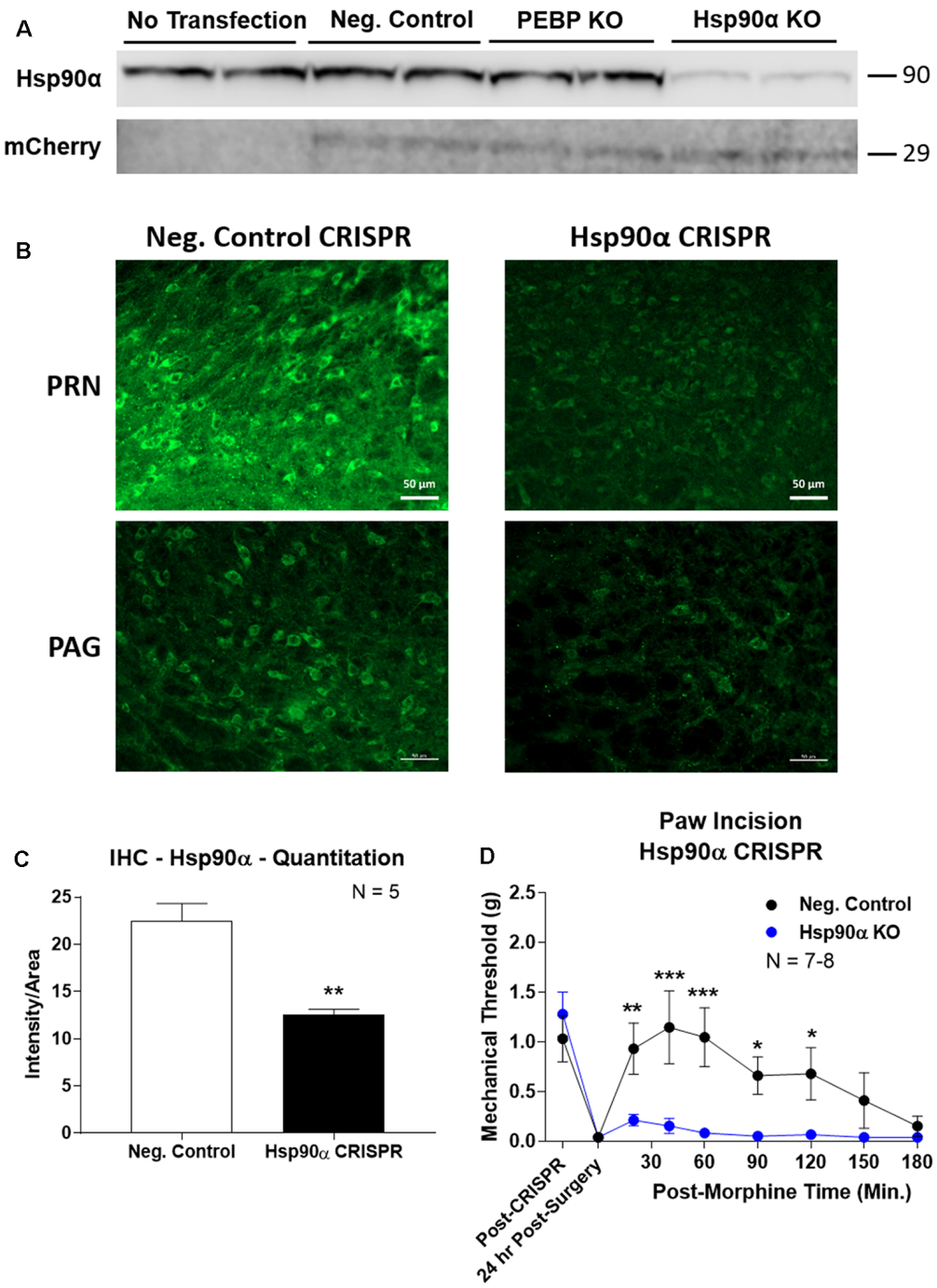

FIGURE 3 | CRISPR/Cas9 gene editing of Hsp90α in adult mouse brain. CRISPR constructs for all targets prepared and delivered as described in "Materials and Methods" section. All quantitative data reported as mean ± SEM. **(A)** Hsp90α CRISPR construct validated in 66.1 cells. Western blot shown with replicate wells of cells in each lane, with MW indicated for each target. Hsp90α protein levels reduced by ∼90% only in the presence of Hsp90α-targeted CRISPR construct. Other constructs (Negative Control, PEBP) have no effect. mCherry protein levels are present in all transfected cells, demonstrating successful transfection of CRISPR DNA. **(B)** Hsp90α or negative control CRISPR delivered to CD-1 male mouse brains and analyzed for protein knockdown on day 10. Representative images shown from pontine reticular nucleus (PRN) and periaqueductal gray (PAG). Hsp90α (green signal) is present in cell bodies and dendritic trees, and the signal is reduced by CRISPR treatment. **(C)** Quantitation of all data from **(B)** performed as described in "Materials and Methods" section. Sample size of mice/group noted in graph. $^{**}p < 0.01$ vs. Negative Control group by Unpaired 2-Tailed *t*-test. Mice treated in one technical replicate, with the resulting tissue stained and analyzed in more than one technical replicate. CRISPR treatment reduced Hsp90α signal by 43.9%. **(D)** CRISPR-treated CD-1 male mice had paw incision surgery performed on day 9, with injection of 3.2 mg/kg morphine *sc* on day 10. Sample size of mice/group noted in graph, performed in two technical replicates. $^{*,**,***}p < 0.05, 0.01, 0.001$ vs. same time point Hsp90α group by two-way ANOVA with Fisher's Least Significant Difference *post hoc* test.

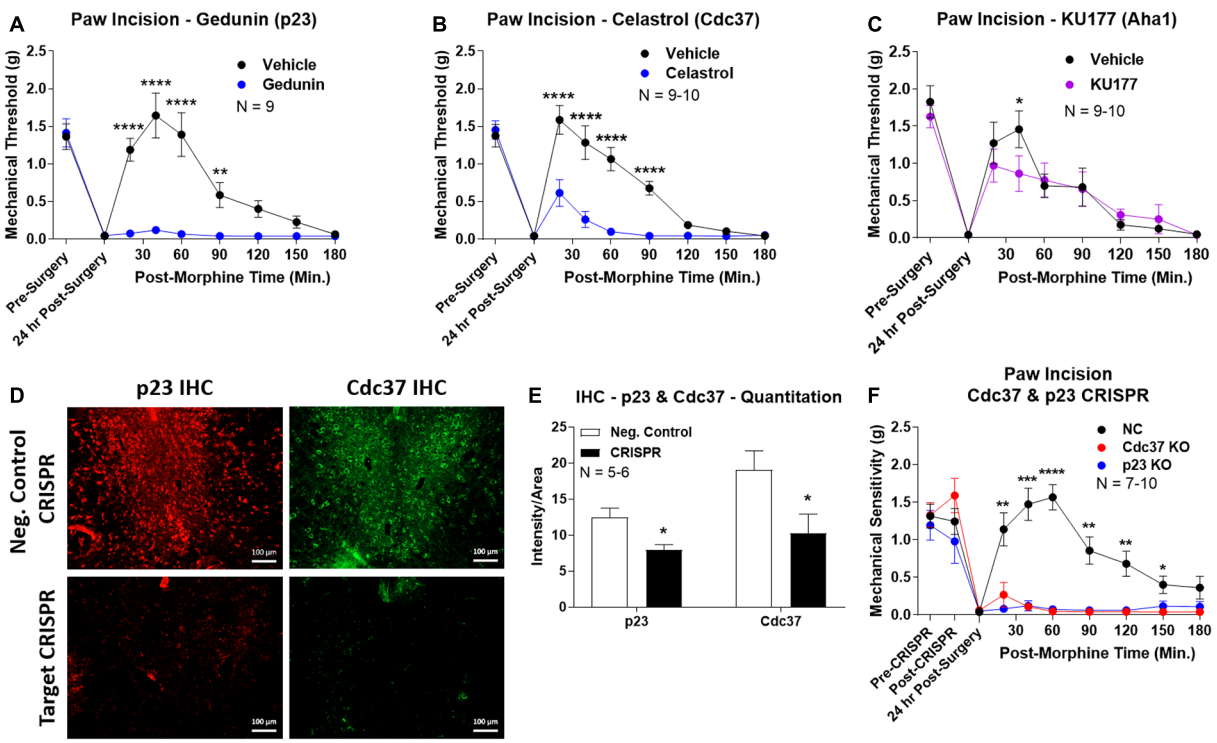

FIGURE 4 | Identification of the co-chaperones p23 and Cdc37 as promoters of opioid anti-nociception in the brain. Male CD-1 mice used for all experiments, data reported as the mean ± SEM, with sample sizes of mice/group noted in each graph. **(A–C)** Ten nanomoles of Gedunin (p23, **A**), 10 nmol of Celastrol (Cdc37, **B**), or 0.1 nmol of KU177 (Aha1, **C**) or Vehicle control injected *icv* concurrently with paw incision surgery with a 24 h recovery, followed by 3.2 mg/kg morphine *sc*. Experiments performed with two technical replicates for each drug. *,**,****$p < 0.05$, 0.01, 0.0001 vs. same time point inhibitor treatment group by two-way ANOVA with Fisher's Least Significant Difference *post hoc* test. **(D)** p23, Cdc37, or Negative Control CRISPR-treated mice with *icv* delivery of constructs analyzed by IHC for target knockdown on day 10. Representative images shown from the PRN. Both targets (p23 – red, Cdc37 – green) have a similar staining pattern to Hsp90α, and both are clearly reduced by CRISPR treatment. **(E)** Data from **(D)** for all mice quantitated as described in the "Materials and Methods" section. All mice treated in one technical replicate, with staining and analysis of the resulting tissue performed in more than one technical replicate. *$p < 0.05$ vs. same target Negative Control group by Unpaired 2-Tailed *t*-test. CRISPR treatment reduced p23 signal by 36.3% and Cdc37 by 46.0%. **(F)** CRISPR-treated mice had paw incision surgery performed on day 9, with injection of 3.2 mg/kg morphine *sc* on day 10. Performed in two technical replicates. *,**,***,****$p < 0.05$, 0.01, 0.001, 0.0001 vs. both same time point p23/Cdc37 CRISPR groups by two-way ANOVA with Fisher's Least Significant Difference *post hoc* test.

inhibitor cycloheximide in the brain 30 min prior to morphine treatment. We found that cycloheximide had no impact on morphine anti-nociception in vehicle-treated mice; however, cycloheximide fully restored morphine anti-nociception back to vehicle-treated levels in mice treated with the pan-Hsp90 inhibitor 17-AAG (**Figure 5A**). We found the same results with KUNA115, confirming that Hsp90α regulates translation during morphine anti-nociception (**Figure 5B**). These results strongly suggest that rapid translation within 30 min of morphine treatment is required for Hsp90 inhibition to impact opioid signaling and anti-nociception.

DISCUSSION

In this study, we have identified the isoform Hsp90α as a key player in promoting opioid anti-nociception and signaling in the brain using both selective small molecule inhibitors (**Figures 1**, **2**) and CRISPR/Cas9 gene editing in the brains of adult mice (**Figure 3**). Using these techniques, we further identified the co-chaperones p23 and Cdc37 as key promoters of opioid anti-nociception (**Figure 4**). We also found that rapid protein translation is part of the molecular mechanism by which Hsp90 regulates opioid anti-nociception (**Figure 5**). When combined with the results of our previous study using a non-selective Hsp90 inhibitor (Lei et al., 2017), our findings suggest that Hsp90α in concert with p23 and Cdc37 promote ERK MAPK activation by the MOR in the brain, and that inhibiting these proteins reverses these roles summating in loss of opioid ERK activation and anti-nociception. This model is diagrammed in **Figure 6**.

Understanding the specific molecules involved in promoting opioid anti-nociception may provide future targets for refined clinical intervention. First generation non-selective Hsp90 inhibitors like 17-AAG failed clinical trials due to liver toxicity (Sidera and Patsavoudi, 2014). Second generation and alternate site inhibitors like KU-32 have shown higher tolerability, and indeed KU-32 has been shown to be neuroprotective (Urban et al., 2010, 2012; Ma et al., 2015). However, non-selective targeting of Hsp90 has an inherently

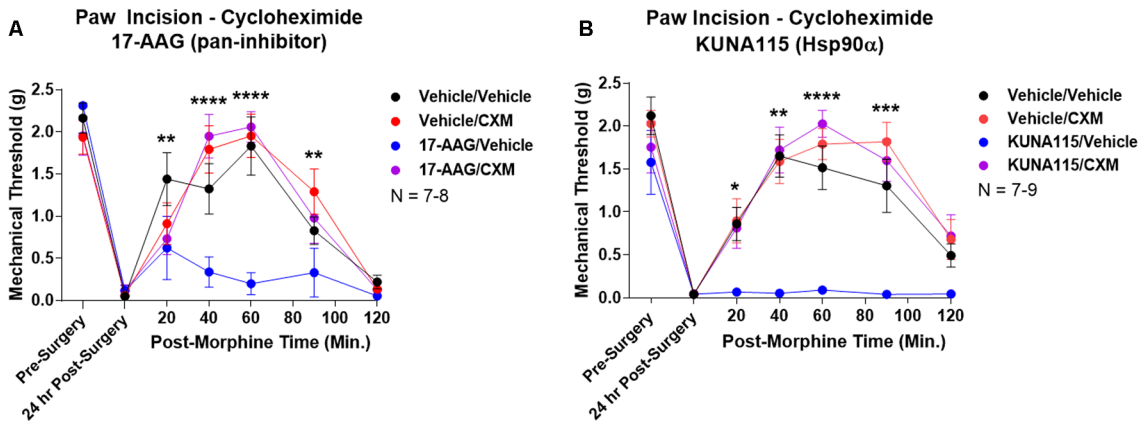

FIGURE 5 | Rapid protein translation is required for Hsp90 inhibition to impact opioid anti-nociception. Male and female CD-1 mice treated with 0.5 nmol 17-AAG **(A)** or 0.1 nmol KUNA115 **(B)** or vehicle *icv*, 24 h, followed by 85 nmol cycloheximide or vehicle *icv*, 30 min, followed by 10 mg/kg morphine *sc*. No difference between approximately equal male and female groups ($p > 0.05$) so they were combined for this analysis. Data reported as the mean ± SEM with the sample size of mice/group noted in the graph. Performed in three technical replicates by different experimenters. *,**,***,****$p < 0.05$, 0.01, 0.001, 0.0001 for the 17-AAG/Vehicle group vs. any of the other three groups at the same time point by two-way ANOVA with Fisher's Least Significant Difference *post hoc* test. There were no differences between the Vehicle/Vehicle, Vehicle/CXM, or 17-AAG/CXM groups.

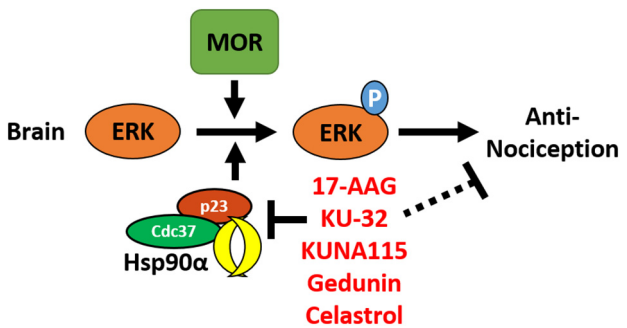

FIGURE 6 | Model for the regulation of mu opioid receptor (MOR) signaling by Hsp90 in the brain. This summary model combines results from this manuscript with our earlier work using non-selective Hsp90 inhibitors in the brain (Lei et al., 2017). Together this data suggests that Hsp90α, p23, and Cdc37 act in concert in the brain to promote the phosphorylation of ERK MAPK by the MOR in response to opioid drugs, thus promoting opioid anti-nociception. Treatment with non-selective or selective inhibitors blocks this role, thus blocking ERK MAPK phosphorylation and blocking anti-nociception in response to opioids.

higher risk of unacceptable side effects, especially since Hsp90 is a ubiquitous protein with a very high expression level and numerous client proteins (Li and Buchner, 2013). The four Hsp90 isoforms have different cellular locations (cytoplasm for Hsp90α/β, endoplasmic reticulum for Grp94, mitochondria for TRAP1) and client proteins, meaning that targeting only one necessary isoform, such as Hsp90α identified above, should inherently decrease the risk of side effects (Echeverría et al., 2011). Similarly, identifying specific co-chaperones like p23 and Cdc37 identified above will also provide specific targets that should reduce potential side effects. This is particularly true with co-chaperones since there are many more of them and each co-chaperone is more selective by role and tissue expression, providing further selectivity (Li and Buchner, 2013). Along these lines, recent studies have identified ligands that interfere with specific Hsp90:co-chaperone interactions, such as celastrol used in our study here, that impact specific functions without the broad sledgehammer of inhibiting the entire Hsp90 protein (Zhang et al., 2008). The specific proteins identified through this study could thus be the first step in identifying improved therapies to modulate opioid treatment; an analogous approach has been used for Hsp70 (Assimon et al., 2013).

The identification of these specific molecules may also lend insight into the molecular mechanism by which Hsp90 regulates opioid signaling. As mentioned above, Hsp90α is cytoplasmic with its own unique complement of client proteins (Bergmayr et al., 2013; Liu et al., 2015). This specificity narrows down the field of potential mechanisms by which Hsp90α regulates opioid signaling, especially to the Hsp90α-specific signaling changes in ERK, JNK, and STAT3 that we have identified (**Figure 2**). Further differences include the lack of Hsp70 induction caused by KUNA115 treatment in **Figure 2**. Earlier studies have shown that non-selective inhibitors like 17-AAG impact both the heat shock response (Hsp70 induction) and protein folding activity of Hsp90, while the C-terminal inhibitor KU-32 only impacts the heat shock response (Ansar et al., 2007). All three compounds, 17-AAG, KU-32, and KUNA115 (**Figure 1**; Lei et al., 2017), impact opioid anti-nociception in the same way, providing a clue that the protein activity of Hsp90α responsible will be the one impacted by all three classes of compound (and which does not require Hsp70 upregulation).

Similarly, the co-chaperone Cdc37 that we have identified has been shown in numerous studies to be crucial for targeting kinases to Hsp90 in both canonical and non-canonical pathways that are crucial for kinase function (Hinz et al., 2007; Gould et al., 2009; Ota et al., 2010).

Importantly, these studies have shown that Cdc37 does not simply assist in kinase folding and maturation, but also assists in complex formation that is required for acute activation. Considering the signaling kinases impacted, especially ERK MAPK which we have identified as a mechanism of Hsp90 regulation of anti-nociception (**Figure 2**; Lei et al., 2017), it makes sense that Cdc37 would be implicated in the Hsp90 mechanism of action. The co-chaperone p23 also has a canonical role in assisting Hsp90 in the protein folding cascade, and has also been linked to acute regulation of signal transduction, as by the A2A receptor (Bergmayr et al., 2013; Li and Buchner, 2013). The functional overlap between the specific molecules identified and the drugs used will allow us to identify likely mechanisms of signaling regulation in future studies, further informed by our results in **Figure 5** suggesting that active protein translation is required for Hsp90 inhibition to impact opioid anti-nociception. Our results showing that Hsp90 inhibition is impactful within 1 h and that baseline mechanical response is not altered provides further mechanistic guidance (**Figures 1G,H**).

While positively identifying Hsp90α, p23, and Cdc37, our studies demonstrated no response to other isoform and co-chaperone inhibitors. This does suggest that Hsp90β, Grp94, and Aha1 are not involved in regulating opioid anti-nociception in the brain. However, this data must be interpreted with caution. We did not exhaustively test these molecules by CRISPR and other methods as we did for Hsp90α, p23, and Cdc37, leaving open the possibility that these other molecules could still be involved. Thus our data should be interpreted most strongly as identifying Hsp90α, p23, and Cdc37 without necessarily ruling out other players. Future studies can address this question more exhaustively, as well as test for the involvement of numerous other co-chaperones not tested in this study. These studies were also all performed broadly across the forebrain without testing the impact of the spinal cord or the periphery, or sub-regions and circuits within the brain. Future studies will also need to address whether these other regions have different mechanisms by which Hsp90 could regulate opioid response.

DATA AVAILABILITY STATEMENT

All datasets generated for this study are included in the article.

ETHICS STATEMENT

The animal study was reviewed and approved by IACUC, University of Arizona.

AUTHOR CONTRIBUTIONS

WL collaboratively developed the initial idea for the project, participated in study design, performed most experiments, and analyzed the data. DD performed some paw incision and cycloheximide experiments, and analyzed the data. CS performed one of the cycloheximide experiments and analyzed the data. SM synthesized, purified, and characterized the novel small molecule inhibitors described above. BB supervised SM in the course of the chemistry work, and collaboratively developed the initial idea for the project. JS supervised WL, DD, and CS in the course of their work, conceived the initial idea for the project, participated in study design, analyzed some of the data, and wrote the manuscript. All authors had editorial input into the manuscript.

FUNDING

We acknowledge the support of an Arizona Biomedical Research Commission New Investigator Award #ADHS18-198875 and institutional funds from the University of Arizona to JS. Institutional funds from Presbyterian College to WL also supported this study, along with National Institutes of Health (NIH) R01CA213566 to BB.

ACKNOWLEDGMENTS

We would like to acknowledge the assistance of Mr. Justin LaVigne with the *in vitro* validation of CRISPR constructs.

REFERENCES

Abul-Husn, N. S., Annangudi, S. P., Ma'ayan, A., Ramos-Ortolaza, D. L., Stockton, S. D.Jr., Gomes, I., et al. (2011). Chronic morphine alters the presynaptic protein profile: identification of novel molecular targets using proteomics and network analysis. *PLoS One* 6:e25535. doi: 10.1371/journal.pone.0025535

Al-Hasani, R., and Bruchas, M. R. (2011). Molecular mechanisms of opioid receptor-dependent signaling and behavior. *Anesthesiology* 115, 1363–1381. doi: 10.1097/aln.0b013e318238bba6

Ansar, S., Burlison, J. A., Hadden, M. K., Yu, X. M., Desino, K. E., Bean, J., et al. (2007). A non-toxic Hsp90 inhibitor protects neurons from Abeta-induced toxicity. *Bioorg. Med. Chem. Lett.* 17, 1984–1990. doi: 10.1016/j.bmcl.2007.01.017

Assimon, V. A., Gillies, A. T., Rauch, J. N., and Gestwicki, J. E. (2013). Hsp70 protein complexes as drug targets. *Curr. Pharm. Des.* 19, 404–417. doi: 10.2174/138161213804143699

Assimon, V. A., Southworth, D. R., and Gestwicki, J. E. (2015). Specific binding of tetratricopeptide repeat proteins to heat shock protein 70 (Hsp70) and heat shock protein 90 (Hsp90) is regulated by affinity and phosphorylation. *Biochemistry* 54, 7120–7131. doi: 10.1021/acs.biochem.5b00801

Bergmayr, C., Thurner, P., Keuerleber, S., Kudlacek, O., Nanoff, C., Freissmuth, M., et al. (2013). Recruitment of a cytoplasmic chaperone relay by the A2A adenosine receptor. *J. Biol. Chem.* 288, 28831–28844. doi: 10.1074/jbc.M113.464776

Bohn, L. M., Lefkowitz, R. J., Gainetdinov, R. R., Peppel, K., Caron, M. G., and Lin, F. T. (1999). Enhanced morphine analgesia in mice lacking beta-arrestin 2. *Science* 286, 2495–2498. doi: 10.1126/science.286.5449.2495

Brandt, G. E., Schmidt, M. D., Prisinzano, T. E., and Blagg, B. S. (2008). Gedunin, a novel hsp90 inhibitor: semisynthesis of derivatives and preliminary structure-activity relationships. *J. Med. Chem.* 51, 6495–6502. doi: 10.1021/jm8007486

Chaplan, S. R., Bach, F. W., Pogrel, J. W., Chung, J. M., and Yaksh, T. L. (1994). Quantitative assessment of tactile allodynia in the rat paw. *J. Neurosci. Methods* 53, 55–63. doi: 10.1016/0165-0270(94)90144-9

Crowley, V. M., Huard, D. J. E., Lieberman, R. L., and Blagg, B. S. J. (2017). Second generation Grp94-selective inhibitors provide opportunities for the

inhibition of metastatic cancer. *Chemistry* 23, 15775–15782. doi: 10.1002/chem.201703398

Darcq, E., Befort, K., Koebel, P., Pannetier, S., Mahoney, M. K., Gaveriaux-Ruff, C., et al. (2012). RSK2 signaling in medial habenula contributes to acute morphine analgesia. *Neuropsychopharmacology* 37, 1288–1296. doi: 10.1038/npp.2011.316

Dewire, S. M., Yamashita, D. S., Rominger, D. H., Liu, G., Cowan, C. L., Graczyk, T. M., et al. (2013). A G protein-biased ligand at the mu-opioid receptor is potently analgesic with reduced gastrointestinal and respiratory dysfunction compared to morphine. *J. Pharmacol. Exp. Ther.* 344, 708–717. doi: 10.1124/jpet.112.201616

Echeverría, P. C., Bernthaler, A., Dupuis, P., Mayer, B., and Picard, D. (2011). An interaction network predicted from public data as a discovery tool: application to the Hsp90 molecular chaperone machine. *PLoS One* 6:e26044. doi: 10.1371/journal.pone.0026044

Edwards, K. A., Havelin, J. J., Mcintosh, M. I., Ciccone, H. A., Pangilinan, K., Imbert, I., et al. (2018). A kappa opioid receptor agonist blocks bone cancer pain without altering bone loss, tumor size, or cancer cell proliferation in a mouse model of cancer-induced bone pain. *J. Pain* 19, 612–625. doi: 10.1016/j.jpain.2018.01.002

Gould, C. M., Kannan, N., Taylor, S. S., and Newton, A. C. (2009). The chaperones Hsp90 and Cdc37 mediate the maturation and stabilization of protein kinase C through a conserved PXXP motif in the C-terminal tail. *J. Biol. Chem.* 284, 4921–4935. doi: 10.1074/jbc.m808436200

Heinricher, M. M., Tavares, I., Leith, J. L., and Lumb, B. M. (2009). Descending control of nociception: specificity, recruitment and plasticity. *Brain Res. Rev.* 60, 214–225. doi: 10.1016/j.brainresrev.2008.12.009

Hinz, M., Broemer, M., Arslan, S. C., Otto, A., Mueller, E. C., Dettmer, R., et al. (2007). Signal responsiveness of IkappaB kinases is determined by Cdc37-assisted transient interaction with Hsp90. *J. Biol. Chem.* 282, 32311–32319. doi: 10.1074/jbc.m705785200

Kim, H., Yang, J., Kim, M. J., Choi, S., Chung, J. R., Kim, J. M., et al. (2016). Tumor necrosis factor receptor-associated protein 1 (TRAP1) mutation and TRAP1 inhibitor gamitrinib-triphenylphosphonium (G-TPP) induce a forkhead box O (FOXO)-dependent cell protective signal from mitochondria. *J. Biol. Chem.* 291, 1841–1853. doi: 10.1074/jbc.m115.656934

Koshimizu, T. A., Tsuchiya, H., Tsuda, H., Fujiwara, Y., Shibata, K., Hirasawa, A., et al. (2010). Inhibition of heat shock protein 90 attenuates adenylate cyclase sensitization after chronic morphine treatment. *Biochem. Biophys. Res. Commun.* 392, 603–607. doi: 10.1016/j.bbrc.2010.01.089

Lei, W., Mullen, N., Mccarthy, S., Brann, C., Richard, P., Cormier, J., et al. (2017). Heat-shock protein 90 (Hsp90) promotes opioid-induced anti-nociception by an ERK mitogen-activated protein kinase (MAPK) mechanism in mouse brain. *J. Biol. Chem.* 292, 10414–10428. doi: 10.1074/jbc.m116.769489

Li, J., and Buchner, J. (2013). Structure, function and regulation of the hsp90 machinery. *Biomed. J.* 36, 106–117. doi: 10.4103/2319-4170.113230

Li, Z., Li, C., Yin, P., Wang, Z. J., and Luo, F. (2016). Inhibition of CaMKIIalpha in the central nucleus of amygdala attenuates fentanyl-induced hyperalgesia in rats. *J. Pharmacol. Exp. Ther.* 359, 82–89. doi: 10.1124/jpet.116.233817

Liu, W., Vielhauer, G. A., Holzbeierlein, J. M., Zhao, H., Ghosh, S., Brown, D., et al. (2015). KU675, a concomitant heat-shock protein inhibitor of Hsp90 and Hsc70 that manifests isoform selectivity for Hsp90alpha in prostate cancer cells. *Mol. Pharmacol.* 88, 121–130. doi: 10.1124/mol.114.097303

Ma, J., Pan, P., Anyika, M., Blagg, B. S., and Dobrowsky, R. T. (2015). Modulating molecular chaperones improves mitochondrial bioenergetics and decreases the inflammatory transcriptome in diabetic sensory neurons. *ACS Chem. Neurosci.* 6, 1637–1648. doi: 10.1021/acschemneuro.5b00165

Macey, T. A., Bobeck, E. N., Hegarty, D. M., Aicher, S. A., Ingram, S. L., and Morgan, M. M. (2009). Extracellular signal-regulated kinase 1/2 activation counteracts morphine tolerance in the periaqueductal gray of the rat. *J. Pharmacol. Exp. Ther.* 331, 412–418. doi: 10.1124/jpet.109.152157

Manglik, A., Lin, H., Aryal, D. K., Mccorvy, J. D., Dengler, D., Corder, G., et al. (2016). Structure-based discovery of opioid analgesics with reduced side effects. *Nature* 537, 185–190. doi: 10.1038/nature19112

Mishra, S. J., Ghosh, S., Stothert, A. R., Dickey, C. A., and Blagg, B. S. (2017). Transformation of the non-selective aminocyclohexanol-based Hsp90 inhibitor into a Grp94-seletive scaffold. *ACS Chem. Biol.* 12, 244–253. doi: 10.1021/acschembio.6b00747

Mishra, S. J., Kent, C. N., Beebe, K., Liu, W., Taylor, J. A., Neckers, L. M., et al. (in press). Hsp90beta-selective inhibitors exhibit nanomolar potency and overcome detriments associated with pan-Hsp90 inhibition. *J. Med. Chem.*

Olson, K. M., Lei, W., Keresztes, A., Lavigne, J., and Streicher, J. M. (2017). Novel molecular strategies and targets for opioid drug discovery for the treatment of chronic pain. *Yale J. Biol. Med.* 90, 97–110.

Ota, A., Zhang, J., Ping, P., Han, J., and Wang, Y. (2010). Specific regulation of noncanonical p38alpha activation by Hsp90-Cdc37 chaperone complex in cardiomyocyte. *Circ. Res.* 106, 1404–1412. doi: 10.1161/circresaha.109.213769

Raehal, K. M., Walker, J. K., and Bohn, L. M. (2005). Morphine side effects in beta-arrestin 2 knockout mice. *J. Pharmacol. Exp. Ther* 314, 1195–1201. doi: 10.1124/jpet.105.087254

Sandweiss, A. J., Mcintosh, M. I., Moutal, A., Davidson-Knapp, R., Hu, J., Giri, A. K., et al. (2017). Genetic and pharmacological antagonism of NK1 receptor prevents opiate abuse potential. *Mol. Psychiatry* 23, 1745–1755. doi: 10.1038/mp.2017.102

Schmid, C. L., Kennedy, N. M., Ross, N. C., Lovell, K. M., Yue, Z., Morgenweck, J., et al. (2017). Bias factor and therapeutic window correlate to predict safer opioid analgesics. *Cell* 171, 1165.e1113–1175.e1113. doi: 10.1016/j.cell.2017.10.035

Sidera, K., and Patsavoudi, E. (2014). HSP90 inhibitors: current development and potential in cancer therapy. *Recent Pat. Anticancer. Drug Discov.* 9, 1–20. doi: 10.2174/15748928113089990031

Streicher, J. M. (2019). The role of heat shock proteins in regulating receptor signal transduction. *Mol. Pharm.* 111, 91–103. doi: 10.1016/bs.vh.2019.05.010

Urban, M. J., Li, C., Yu, C., Lu, Y., Krise, J. M., Mcintosh, M. P., et al. (2010). Inhibiting heat-shock protein 90 reverses sensory hypoalgesia in diabetic mice. *ASN Neuro* 2:e00040. doi: 10.1042/an20100015

Urban, M. J., Pan, P., Farmer, K. L., Zhao, H., Blagg, B. S., and Dobrowsky, R. T. (2012). Modulating molecular chaperones improves sensory fiber recovery and mitochondrial function in diabetic peripheral neuropathy. *Exp. Neurol.* 235, 388–396. doi: 10.1016/j.expneurol.2012.03.005

Zhang, L., Kibaly, C., Wang, Y. J., Xu, C., Song, K. Y., Mcgarrah, P. W., et al. (2017). Src-dependent phosphorylation of mu-opioid receptor at Tyr(336) modulates opiate withdrawal. *EMBO Mol. Med.* 9, 1521–1536. doi: 10.15252/emmm.201607324

Zhang, T., Hamza, A., Cao, X., Wang, B., Yu, S., Zhan, C. G., et al. (2008). A novel Hsp90 inhibitor to disrupt Hsp90/Cdc37 complex against pancreatic cancer cells. *Mol. Cancer Ther.* 7, 162–170. doi: 10.1158/1535-7163.mct-07-0484

Zhao, H., Donnelly, A. C., Kusuma, B. R., Brandt, G. E., Brown, D., Rajewski, R. A., et al. (2011). Engineering an antibiotic to fight cancer: optimization of the novobiocin scaffold to produce anti-proliferative agents. *J. Med. Chem.* 54, 3839–3853. doi: 10.1021/jm200148p

Conflict of Interest: JS has grants from the NIH and Arizona Biomedical Research Commission (ABRC), as well as research contracts with Depomed, Inc. and Divine Healing, LLC. JS also is a founder with an equity stake in Teleport Pharmaceuticals, LLC. None of these commercial involvements concern the topic of the research study at hand, or Hsp90 research more broadly. BB has grants from the NIH and is a founder with an equity stake in Grannus Therapeutics, a virtual startup for developing novel Hsp90 inhibitors.

The remaining authors declare that the research was conducted in the absence of any commercial or financial relationships that could be construed as a potential conflict of interest.

frontiers in Molecular Neuroscience

REVIEW
published: 24 January 2020
doi: 10.3389/fnmol.2020.00005

Regulator of G-Protein Signaling (RGS) Protein Modulation of Opioid Receptor Signaling as a Potential Target for Pain Management

*Nicolas B. Senese[1,2], Ram Kandasamy[1,3], Kelsey E. Kochan[1] and John R. Traynor[1,4]**

[1] Department of Pharmacology, Edward F. Domino Research Center, University of Michigan Medical School, Ann Arbor, MI, United States, [2] Department of Psychiatry, The University of Illinois at Chicago, Chicago, IL, United States, [3] Department of Psychology, California State University, East Bay, Hayward, CA, United States, [4] Department of Medicinal Chemistry, College of Pharmacy, University of Michigan, Ann Arbor, MI, United States

Opioid drugs are the gold standard for the management of pain, but their use is severely limited by dangerous and unpleasant side effects. All clinically available opioid analgesics bind to and activate the mu-opioid receptor (MOR), a heterotrimeric G-protein-coupled receptor, to produce analgesia. The activity of these receptors is modulated by a family of intracellular RGS proteins or regulators of G-protein signaling proteins, characterized by the presence of a conserved RGS Homology (RH) domain. These proteins act as negative regulators of G-protein signaling by serving as GTPase accelerating proteins or GAPS to switch off signaling by both the Gα and βγ subunits of heterotrimeric G-proteins. Consequently, knockdown or knockout of RGS protein activity enhances signaling downstream of MOR. In this review we discuss current knowledge of how this activity, across the different families of RGS proteins, modulates MOR activity, as well as activity of other members of the opioid receptor family, and so pain and analgesia in animal models, with particular emphasis on RGS4 and RGS9 families. We discuss inhibition of RGS proteins with small molecule inhibitors that bind to sensitive cysteine moieties in the RH domain and the potential for targeting this family of intracellular proteins as adjuncts to provide an opioid sparing effect or as standalone analgesics by promoting the activity of endogenous opioid peptides. Overall, we conclude that RGS proteins may be a novel drug target to provide analgesia with reduced opioid-like side effects, but that much basic work is needed to define the roles for specific RGS proteins, particularly in chronic pain, as well as a need to develop newer inhibitors.

Keywords: analgesia, G-proteins, opioid receptors, pain, RGS proteins, signaling

OPEN ACCESS

Edited by:
Tally Largent-Milnes, The University of Arizona, United States

Reviewed by:
David Chakravorty, The Pennsylvania State University (PSU), United States
Venetia Zachariou, Icahn School of Medicine at Mount Sinai, United States

***Correspondence:**
John R. Traynor
jtraynor@umich.edu

Received: *28 October 2019*
Accepted: *09 January 2020*
Published: *24 January 2020*

Citation:
Senese NB, Kandasamy R, Kochan KE and Traynor JR (2020) Regulator of G-Protein Signaling (RGS) Protein Modulation of Opioid Receptor Signaling as a Potential Target for Pain Management. Front. Mol. Neurosci. 13:5. doi: 10.3389/fnmol.2020.00005

INTRODUCTION

Pain is a significant problem worldwide, and adequate pain relief remains an unmet medical need. Opioids acting at the mu-opioid receptor (MOR), a G-protein coupled receptor (GPCR), have been used therapeutically to control pain for centuries and remain the most commonly used class of analgesics and the most effective option for many patients. This, along with an increased focus on completely eliminating pain among physicians, has led to the recent huge increase in opioid

prescriptions which, together with the addiction liability and respiratory depressant properties of opioid drugs, has driven the current opioid crisis and the resultant dramatic increase in opioid overdose deaths (Babu et al., 2019). Nonetheless, opioids remain the gold standard for pain control. Consequently, many approaches are being taken to target MOR in ways that enhance analgesic properties but reduce unwanted effects including, allosteric modulators (Burford et al., 2013), biased agonists that preferentially stimulate certain downstream pathways (Manglik et al., 2016; Schmid et al., 2017), compounds that target several opioid receptors simultaneously (Nastase et al., 2018) or compounds with slow access to central MORs (Markman et al., 2019). In this review we discuss ways in which intracellular processes downstream of MOR activation by both exogenous opioid drugs and endogenous opioid peptides can be manipulated by regulator of G-protein signaling (RGS) proteins, and if this provides an avenue for the development of new analgesic molecules.

RGS PROTEINS

Mu-opioid receptors are seven-transmembrane domain GPCRs that interact with G-proteins of the $G\alpha_{i/o}$ and $G\alpha_{z}$ classes that form a heterotrimer with their essential β and γ subunits (**Figure 1**). At rest, the Gαβγ heterotrimer is bound to GDP. GPCR activation leads to dissociation of GDP from the Gα subunit and its replacement with GTP causing the Gα-bound GTP to separate from the βγ heterodimer. The now active Gα-GTP and βγ subunits interact with intracellular signaling partners, including inwardly rectifying potassium channels, calcium channels, phospholipase C, adenylyl cyclase isoforms, and components of the mitogen-activated protein kinase (MAPK) pathway. Intracellular signaling is terminated when endogenous GTPase activity of Gα hydrolyses GTP to GDP. The formed Gα-GDP then reassociates with the βγ heterodimer to terminate signaling. The enzymatic GTPase activity of the $G\alpha_{i/o/z}$ subunits is slow with a GTP turnover rate of 2–5 per minute. This is not fast enough to allow a cell to respond to subsequent incoming signals. Here, RGS proteins come into play. These proteins bind to the switch regions of the active, GTP-bound Gα (Tesmer et al., 1997) and act as GTPase accelerating proteins or GAPs to increase rate of GTP hydrolysis by up to 100-fold. This drastically shortens the lifetime of the active Gα-GTP and βγ signaling proteins, resulting in a negative regulation of GPCR signaling, including signaling downstream of MOR (**Figure 1**).

The RGS proteins themselves constitute a 20-plus member family of intracellular regulatory proteins characterized by an RGS-homology (RH) domain and divided into subfamilies according to domain- and sequence-homology (Hollinger and Hepler, 2002). RGS proteins vary in size and complexity from simple N- and C-terminal extensions to more complex proteins (**Table 1**). Some members of the family are selective for certain G-protein subtypes (Posner et al., 1999; Lan et al., 2000) and receptors (Xu et al., 1999; Wang et al., 2009). RGS proteins are variously expressed throughout the body including pain

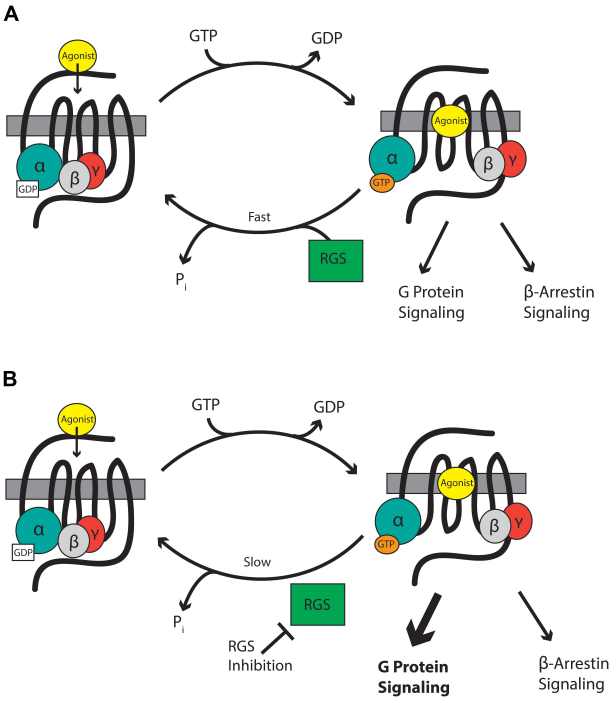

FIGURE 1 | (A) RGS proteins accelerate the hydrolysis of GTP bound to the Gα subunit to terminate signaling by reformation of the G-protein heterodimer. **(B)** RGS inhibitors slow the hydrolysis of GTP and so enhance signaling through Gα and βγ proteins.

pathways in the central nervous system (CNS) where expression overlaps with MOR expression, particularly for RGS4 and the splice variant of RGS9, RGS9-2 (Gold et al., 1997; Peckys and Landwehrmeyer, 1999; Grafstein-Dunn et al., 2001; Traynor and Neubig, 2005). For example, the small RGS4 protein is expressed in many structures involved in the transmission and maintenance of pain, including the dorsal horn of the spinal cord, the periaqueductal gray (PAG), the thalamus, and the basal ganglia (Ni et al., 1999; Gold et al., 2003; Terzi et al., 2009; Taccola et al., 2016).

RATIONALE FOR RGS PROTEINS AS POTENTIAL TARGETS FOR PAIN MANAGEMENT

Intracellular proteins are not usually considered suitable drug targets due to their ubiquitous expression. In contrast, their differential expression patterns, selectivity for specific receptors and specificity for particular G-proteins, although not absolute, suggests the possibility that RGS proteins could be attractive drug targets for the management of pain by enhancing MOR-mediated signaling, leading to enhanced antinociception. Drugs inhibiting RGS activity could be beneficial in several ways. First, an enhancement of action of morphine and related exogenous opioid drugs would result in an opioid sparing effect, which would be especially advantageous if different RGS proteins

TABLE 1 | RGS subfamily characterization and expression.

RGS family	Domains present	Name	G-protein specificity	CNS expression
RZ	Cysteine-string	RGS17 (RGSZ2)	Gi, Gz, Gq	Isocortex, OLF, HPF, CTXsp, PAL, TH, HY, MB, P, MY
		RGS19 (GAIP)	Gi, Gz, Gq	Isocortex, OLF, HPF, CTXsp, STR, PAL, TH, MB, P, MY, CB
		RGS20 (RGSZ1)	Gi, Gz	Isocortex, CTXsp, STR, PAL
R4	N-terminal amphipathic sequence	RGS1	Gi, Gq	N/A
		RGS2	Gi < Gq	CTXsp, STR, PAL
		RGS3	Gi, Gq	TH, CB
		RGS4	Gi, Gq	Isocortex, OLF, HPF, CTXsp, STR, PAL, TH, HY, MB, P, MY, CB
		RGS5	Gi, Gq	Isocortex, OLF, HPF, CTXsp, STR, PAL, TH, HY, MB, P, MY, CB
		RGS8	Gi, Gq	Isocortex, OLF, HPF, CTXsp, STR, PAL, TH, HY, MB, P, MY, CB
		RGS13	N/A	N/A
		RGS16	Gi, Gq	TH
		RGS18	Gi, Gq	N/A
		RGS21	Gi, Gq	N/A
R7	GGL-(Gβ5) DEP-(R9AP, R7BP)	RGS6	Go	HPF, CTX (Ahlers et al., 2016)
		RGS7	Go > Gi2 > Gi1	Isocortex, OLF, HPF, CTXsp, STR, PAL, TH, HY, MB, P, MY, CB
		RGS9	Go	Isocortex, OLF, CTXsp, STR, PAL, HY
		RGS11	Go	Isocortex, OLF, HPF, CTXsp, STR, PAL, TH, HY, MB, P, MY
R12	GoLoco-(Gα-GDP) RBD-(rap) PDZ	RGS10	Gi	Isocortex, OLF, HPF, CTXsp, STR, PAL, TH, HY, MB, P, MY, CB
		RGS12	Gi	Isocortex, OLF, HPF, CTXsp, STR, PAL, TH, HY, MB, P, MY, CB
		RGS14	Gi	Isocortex, OLF, HPF, CTXsp, STR

List of RGS families and their respective domains, G-protein specificities, and expression in the mouse central nervous system. Isocortex, isocortex; OLF, olfactory; HPF, hippocampal formation; CTXsp, cortical subplate; STR, striatum; PAL, pallidum; TH, thalamus; HY, hypothalamus; MB, midbrain; P, pons; MY, medulla; CB, cerebellum. N/A = data not available. Taken from the Allen Brain Atlas (https://mouse.brain-map.org), except where stated.

controlled MOR signaling in those neuronal systems leading to antinociception versus those responsible for side-effects of respiration, reward, and constipation. Second, RGS inhibitors could produce analgesia in their own right by enhancing endogenous opioid peptide activity even in the absence of exogenous opioid drugs. Opioid peptides are released at spinal and supraspinal sites during pain (Levine et al., 1978; Cesselin et al., 1980; Porro et al., 1991; Zangen et al., 1998; Hurley and Hammond, 2001; Wu et al., 2001) and also at peripheral sites (Stein et al., 2003). These endogenous peptides offer limited protection against pain but this effect is significantly increased if enzymatic peptide breakdown is prevented by so-called "enkephalinase inhibitors" (Fournié-Zaluski et al., 1992; Noble et al., 1992, 1997). Enhancement of endogenous opioid peptide signaling downstream of MOR by inhibition of RGS action should increase the analgesic efficacy of the peptides. Moreover, this approach has the advantage that, unlike enkephalinase inhibitors which globally increase enkephalin levels, the spatial and temporal release of the peptides would be retained and so RGS inhibitors will be effective only in those areas where the peptides are released in response to noxious stimuli, but not in areas responsible other actions of the peptides. A similar concept has recently been discussed with regard to positive allosteric modulators of MOR (Burford et al., 2015; Livingston and Traynor, 2018). Thirdly, there is evidence that the beneficial analgesic action of MOR agonists (and the endogenous opioid peptides) is due to signaling downstream of G-proteins, whereas the unwanted effects of respiratory depression and constipation may be mediated via the β-arrestin pathway (Raehal et al., 2011; Violin et al., 2014; Manglik et al., 2016; Schmid et al., 2017). Since RGS proteins modulate the G-protein component of MOR signaling, but not the β-arrestin component, inhibitors of RGS proteins would be expected to show an increased therapeutic window separating the beneficial from unwanted effects (**Figure 1**).

On the other hand, while RGS proteins are attractive analgesic targets and there is some degree of selectivity of expression and interaction with opioid receptors and G-proteins inhibition of RGS activity could regulate signaling downstream of numerous GPCRs. This suggests more nuanced strategies may be required to avoid the potential for off-target effects. Such targets might be the interface between RGS and opioid receptors or the complete RGS-Gα-opioid receptor complex rather than the RGS protein in isolation avoiding the potential for off-target effects.

RGS INSENSITIVE Gα-PROTEINS

Because RGS proteins constitute a large family of molecules it is difficult to know where to start when assessing their ability to control MOR signaling. An easier way is to develop a system which genetically knocks out all RGS GAP activity. This is feasible since replacement of a Gly in the "switch 3" region of the Gα protein (Tesmer et al., 1997) with Ser blocks the interaction between the RH region of RGS protein and the GTP-bound Gα subunit, without affecting any other properties of the Gα protein including GDP release, GTP hydrolysis, Gβγ binding, or interaction with the receptor. This mutation therefore prevents all GAP activity at a specific Gα protein. Thus, for example the Gly-Ser mutation

in $G\alpha_o$, promotes signaling downstream of MOR *in vitro* (Clark et al., 2003).

The behavioral effects of the mutation can be studied in mice with knock-in of RGS-insensitive Gα proteins (RGSi-Gα). This allows for proof of principle that inhibition of RGS activity is a viable strategy to provide antinociception and avoids the possibility of redundancy of GAP activity. Although on the minus side this approach does not identify the specific RGS protein(s) involved.

In assays using heat as the nociceptive source, mice expressing RGSi-$G\alpha_o$ displayed an enhanced baseline withdrawal latency that was reversed by naltrexone, showing that endogenous opioid peptide activity is increased when RGS action is nullified (Lamberts et al., 2011). Similarly in the hot-plate test morphine-induced antinociception was enhanced; these finding were supported by an increased opioid-peptide mediated disinhibition of GABA release in the PAG, an important region for descending pain control (Lamberts et al., 2013). Surprisingly, in the tail withdrawal test the action of morphine was decreased, suggesting a permissive, not inhibitory, action for RGS proteins. Indeed, in the PAG, MOR activation of G-protein-gated inwardly rectifying potassium channels (GIRKs) was reduced for morphine and fentanyl in mice expressing RGSi-$G\alpha_o$ proteins. No effect was seen on methionine enkephalin modulation of GIRK currents because this endogenous ligand appeared to use $G\alpha_i$ proteins which are still regulated by RGS proteins in this genetic model (McPherson et al., 2018). The results indicate that the RGS-mediated reduction in opioid-induced GIRK activation in mice expressing RGSi-$G\alpha_o$ plays a role in opioid spinal antinociception, but not supraspinal, antinociception. These studies indicate that in general RGS protein GAP activity can produce negative and positive regulation of signaling depending on the intracellular effector(s) involved. One mechanism for this is RGS-mediated "kinetic scaffolding," the results of which depend on the proximity of the various components within a cell (Zhong et al., 2003). In this model when effectors are close to the receptor RGS proteins are permissive because they act to sustain local concentrations of Gα-GDP necessary to maintain G-protein signaling. In contrast, further from the receptor where Gα-GDP is not depleted, RGS proteins suppress signaling and so are inhibitory. Alternatively, the opposite responses in morphine pharmacology observed could be due to roles for RGS proteins that have complex, for example, scaffolding functions. Additionally, since different neuronal circuits are involved in the two measures of morphine antinociception the loss of RGS negative regulation of $G\alpha_o$ could reveal constitutive activity of opposing transmitted systems that use this G-protein, for example the nociceptin peptide system (Bertorelli et al., 1999; Khroyan et al., 2009).

SPECIFIC FAMILIES OF RGS PROTEINS

While use of RGS-insensitive $G\alpha_o$ proteins can provide proof of principle, conflicting results, such as in the antinociceptive assays discussed above highlight drawbacks in this approach. As such, examination of individual RGS proteins is needed to identify discrete pharmacological targets.

R4 Family

RGS4 itself has been extensively studied with respect to opioid-mediated signaling and antinociception This protein is distributed widely throughout the CNS where it regulates the pharmacology of MOR agonists (**Table 1**, reviewed in Traynor and Neubig, 2005). RGS4 is thought to interact directly with MOR *via* the fourth intracellular loop of the receptor (residues 329–355) and the RGS4 N-terminal domain (Leontiadis et al., 2009). Removal of the N-terminal domain not only reduces RGS4-receptor interactions, but eliminates the receptor selectivity of endogenous RGS4 protein (Zeng et al., 1998; Leontiadis et al., 2009). When overexpressed in HEK293 cells, RGS4 is localized throughout the cytosol, nucleus, and plasma membrane (Roy et al., 2003) and binds only weakly to $G\alpha_{i/o}$ proteins. However, following application of the MOR agonist [D-Ala^2, N-$MePhe^4$, Gly-ol]-enkephalin (DAMGO), expression shifts to the plasma membrane such that RGS4 is co-localized with the receptor (Leontiadis et al., 2009) and the interaction between the two proteins is enhanced. In contrast, in SH-SY5Y human neuroblastoma cells that endogenously express RGS4 and MOR, knockdown of RGS4 did not affect responses to the MOR agonist morphine (Wang et al., 2009), suggesting that the ability of RGS4 to regulate MOR may be determined by the cell type and/or the agonist.

Intracerebroventricular (i.c.v.) administration in male mice of antisense-DNA against RGS4 resulted in a greater response to i.c.v. morphine in the tail withdrawal test compared to control given scrambled antisense (Garzón et al., 2001). In contrast, constitutive RGS4 knockout mice do not display alterations in pain sensitivity in tests of acute nociception (Grillet et al., 2005). This finding may be due to redundancy of RGS action. That is, since RGS4 is essentially an RH domain with very short N and C-termini, its loss may easily be compensated for by other RGS proteins (Doupnik, 2015), or by physiological compensatory mechanisms also regulated by RGS4. Indeed, further studies have implicated a critical role for RGS4 in the nucleus accumbens (NAc) in opioid antinociception (Han et al., 2010). Conditional knockout of RGS4 only in this brain region reduces fentanyl and methadone antinociception, but not that of morphine, although it does act as a negative modulator of the rewarding effects of morphine, suggesting both agonist-specific and tissue-specific outcomes (Han et al., 2010). To explain this discrepancy, the authors used immunoprecipitation experiments to indicate that fentanyl, but not morphine, recruits $G\alpha_q$, rather than $G\alpha_{i/o}$ proteins to MOR in the NAc and this competes with RGS4 for association with the receptor (Han et al., 2010).

A more important role for RGS4 might be in chronic pain states, where RGS4 expression is dynamically regulated. For example, following sciatic nerve injury in the rat there is an up-regulation of RGS4 mRNA expression in the dorsal horn of the spinal cord, with no change in the mRNA of other RGS proteins measured (RGS6, 7, 8, 9, 11, 12, 14, 17, 19; Garnier et al., 2003; Bosier et al., 2015; Taccola et al., 2016). At the same time rats become hypersensitive to noxious stimuli and the potency of

MOR agonists decreases. Chronic pain states, such as following sciatic nerve injury are less sensitive to control by opioids than acute pain. Since RGS4 negatively regulates MOR signaling *in vitro* and there is significant overlap in expression of RGS4 and MOR within the spinal dorsal horn (Peckys and Landwehrmeyer, 1999; Garnier et al., 2003), this increased expression of RGS4 likely contributes to the loss of morphine potency in chronic pain. A report also indicates increases in RGS3 mRNA in the dorsal horn of the lumbar spinal cord after sciatic nerve ligation, although RGS4 levels decrease several days later; these effects may involve astrocyte RGS proteins (Doyen et al., 2017). In support of a role for up-regulated RGS4 (and RGS3) in reducing the effectiveness of morphine, use of the inhibitor CCG-63802 (**Figure 2**; Blazer et al., 2010) to prevent RGS4 action attenuates hyperalgesia following nerve injury (Bosier et al., 2015; Taccola et al., 2016). This attenuation can be attributed to the rescue of tonically active endogenous antinociception systems, such as the enkephalins, although in one study using this inhibitor (Bosier et al., 2015) endogenous cannabinoids rather than opioid endogenous opioids were implicated.

In contrast to changes in the spinal cord, RGS4 (as well as RGS3) message which is high in C-fiber sensory neurons in dorsal root ganglia (DRG) of the rat, has been reported to decrease following transection of the sciatic nerve (Costigan et al., 2003), suggesting a location-dependent regulation of this transcript. A reduction in RGS4 would lead to an increase in GPCR, possibly MOR signaling. These divergent effects of up- or down-regulation of RGS proteins indicate a very fine level of pathophysiological control, although of course we do not know the specific GPCR target or targets of either the up-regulated RGS4/RGS3 in the dorsal horn or the down regulated RGS4 in the DRG. Resolving the reasons for the different findings on RGS3/4 levels after sciatic nerve injury and identifying the GPCRs that are modulated by these proteins would be an important step forward in developing RGS protein-based analgesics or analgesic adjuncts.

Injection of formalin into the mouse hind paw produces a biphasic hyperalgesia consisting of an early phase and a late phase. Mice lacking RGS4 are less hyperalgesic during the late phase (Yoon et al., 2015; Avrampou et al., 2019). Moreover, mice lacking RGS4 recover more quickly from mechanical and cold hypersensitivity following inflammation, caused by Freund's Complete Adjuvant (CFA) injection into the hind paw, or nerve injury and show recovery of wheel running as a measure of pain-depressed behavior (Avrampou et al., 2019). One potential mechanism to explain both of these observations is the loss of negative regulation by RGS4 of endogenous antinociceptive signaling, possibly involving opioid peptides released in response to the persistent inflammatory pain (Porro et al., 1991; Zangen et al., 1998; Wu et al., 2001). As with the nerve injury studies using CCG-63802 discussed above, results from this experimental paradigm support the notion that an inhibitor of RGS4 should enhance endogenous pain systems to produce analgesia, even in the absence of opioid drugs such as morphine. In support of this concept, the potency of the stable enkephalin analog DAMGO was increased 10-fold in the formalin test in animals lacking RGS4 compared to their wild-type controls (Yoon et al., 2015), and intrathecal (i.t.) administration of the small molecule RGS4 inhibitor CCG-50014 (**Figure 2**; Blazer et al., 2011) to wild-type mice produced dose-dependent antinociception on its own that was blocked by the opioid antagonist naloxone, as well as enhancing the action of DAMGO (Yoon et al., 2015).

Chronic pain is a highly complex condition. Using conditional knockdown of RGS4 Avrampou et al. (2019) demonstrated that a major contributor to reversal of cold and mechanical hypersensitivity, but not recovery of pain-depressed wheel running, is the ventral posterolateral region of the thalamus, an important center for relaying nociceptive information. RNA sequence analysis of thalamic tissue from wild-type and RGS4 knockout mice after CFA-induced inflammatory pain showed decreased changes in gene expression in the knockout group and identified differences that included components of glutamatergic signaling, including an increased expression of membrane bound metabotropic glutamate receptor 2 which has been associated with recovery from hypersensitivity to sensory stimuli. Finally, the role for RGS4 in the anti-allodynic actions of tricyclic antidepressants and the NMDA receptor antagonist ketamine have been studied following sciatic nerve injury (Stratinaki et al., 2013). The antiallodynic action of chronic low dose, but not high dose, desipramine was reduced in RGS4 knockout mice, whereas a low dose of ketamine produced antiallodynic behavior only in mice lacking RGS4. This difference highlights the complex roles of RGS4 and the fact that the GPCR targets for RGS4 have to be carefully considered when proposing inhibitors of RGS4 for the management of chronic pain. Nonetheless, whatever the mechanism involved in chronic pain and the drugs used for its management, these studies do suggest it is worth further investigating inhibitors of RGS4 as standalone treatments for chronic pain. The fact that two independently generated RGS4 knockout mouse lines, with distinct genetic backgrounds, show no overt behavioral abnormalities (Grillet et al., 2003; Han et al., 2010; Avrampou et al., 2019) provides support for RGS4 as a therapeutic target for pain management.

Roles for other R4 family members in modulating opioid function and analgesia have not been explored so extensively. RGS8 is enriched in the thalamus (Gold et al., 1997), a region dense in MOR expression, and RGS8 acts as a GAP for opioid-mediated signaling (Talbot et al., 2010). Thus, it is possible

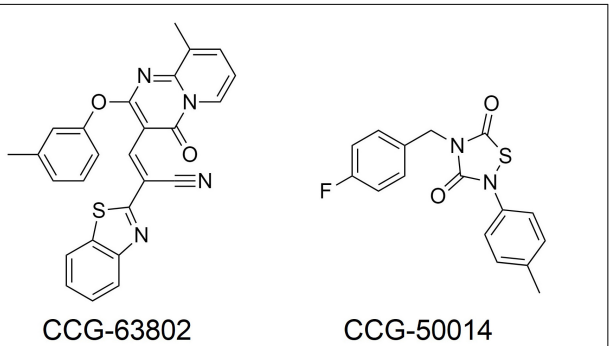

FIGURE 2 | Small molecule RGS inhibitors used in preclinical analgesic studies.

that RGS8 interacts with MORs to modulate signaling in the thalamus to regulate processing of nociceptive information. Knockdown of RGS2 and RGS3 was reported to have no effect on baseline antinociception in the tail-flick test, but to inhibit the antinociceptive response to morphine and the endogenous opioid β-endorphin (Garzón et al., 2001), suggesting, a positive role for these proteins in opioid antinociception. In contrast, after RGS16 knockdown, mice showed an increased antinociceptive response to morphine (Garzón et al., 2001). The basis of these opposing effects of different R4 family members has not been adequately explored, although it has been suggested that distinct Gα interaction profiles between the different RGS proteins may be responsible for the diverse effects (Garzón et al., 2000, 2001).

Further studies of other RGS4 family members in both acute and chronic pain states are warranted. In particular, there are no published studies of family members other than RGS3 and 4 in chronic pain.

R7 Family

The R7 family of RGS proteins comprises RGS6, 7, 9–1, 9–2, and 11 (Hollinger and Hepler, 2002). RGS9-1 and -2 are variants that differ only in the C-terminal tail. RGS9-1 is found only in the retina whereas RGS9-2 is brain specific, and highly expressed in the striatum. RGS7 and RGS9-2 form a heterodimer with the type 5 G-protein β (Gβ5) subunit. This facilitates correct folding and provides proteolytic stability. In addition, both RGS7/Gβ5 and RGS9-2/Gβ5 form complexes with a small palmitoylated protein R7 Binding Protein (R7BP), to control membrane localization and stability (reviewed in Lamberts and Traynor, 2013).

In permeabilized C6 glioma cells expressing MOR and $G\alpha_{i2}$, addition of the RH region of RGS7 did not affect DAMGO-induced inhibition of cAMP accumulation (Talbot et al., 2010). When $G\alpha_o$ was expressed instead of $G\alpha_{i2}$, addition of the RH domain of RGS7 effectively inhibited the actions of DAMGO (Talbot et al., 2010), suggesting that RGS7 selectively regulates the action of MOR depending on the G-protein expressed. This selectivity may be due to a lack of physical interaction between RGS7 and $G\alpha_{i2}$, as increasing concentrations of $G\alpha_{i2}$ disrupted the RGS4/$G\alpha_o$ complex but not the RGS7/$G\alpha_o$ complex (Talbot et al., 2010). This suggests that the inability of RGS7 to regulate MOR signaling in cells expressing $G\alpha_{i2}$ is due to a failure of RGS7/$G\alpha_{i2}$ complex formation.

RGS9-2 interacts with MOR to prevent several events triggered by receptor activation. When RGS9-2 is located close to the cell membrane, it delays agonist-induced internalization of MOR (Psifogeorgou et al., 2007). Further, morphine promotes the association of RGS9-2 with β-arrestin-2, a key component of MOR desensitization (Psifogeorgou et al., 2007). This association is dampened in the presence of the structurally different MOR agonist fentanyl (Psifogeorgou et al., 2011). Thus, RGS9-2 plays an important role in MOR regulation, as it negatively regulates signaling downstream of MOR and inhibits receptor endocytosis; however, these effects appear to be agonist-dependent.

Male mice given antisense-DNA against RGS7 or RGS9-2 into the ventricles, showed greater responses to morphine, DAMGO, and β-endorphin in the tail-flick test (Garzón et al., 2001; Sánchez-Blázquez et al., 2003). Knockdown of RGS9-2 or RGS11 enhanced DAMGO antinociception to a greater degree than knockdown of RGS6 or RGS7 (Garzón et al., 2003). The antinociceptive action of morphine toward an acute heat stimulus was reported to be enhanced in mice completely lacking RGS9 (Zachariou et al., 2003; Papachatzaki et al., 2011). The effects again appear to depend on the agonist studied. Thus, in the same RGS9 knockout mice, the analgesic efficacy of oxycodone was not changed, in either acute pain or in sciatic nerve injury induced pain (Gaspari et al., 2017) and whereas RGS9-2 knockout enhances the action of morphine in the hot-plate test, there is an inhibition of fentanyl- and methadone-mediated antinociception (Papachatzaki et al., 2011). This differential behavior across agonists that bind to the same orthosteric site on the MOR has been explained by the formation of dissimilar protein complexes following binding of ligand to MOR. In other words, there is a biased activation of receptor such that morphine promotes an association between RGS9-2 and $G\alpha_{i3}$ whereas RGS9-2/$G\alpha_q$ complexes are seen with the other ligands.

The opening of inwardly rectifying potassium (GIRK) channels is an important mechanism for antinociception downstream of MOR. Such channels are modulated by a complex of RGS 7 or 9 with Gβ5 downstream of MOR that is allosterically controlled by R7BP. Thus, as might be expected the loss of other components of this complex also result in altered antinociception. In the absence of R7BP there is a loss of negative regulation of MOR signaling, enhancing GIRK activity and so increasing morphine- and fentanyl induced antinociception (Terzi et al., 2012; Zhou et al., 2012). The R7BP null mice also show an enhanced basal latency to an acute thermal stimulus in the hot-plate assay (Zhou et al., 2012), indicating enhanced endogenous antinociception by an increase in the activity of endogenous opioid peptides acting at MOR (Lamberts et al., 2011).

In support of an enhancement of endogenous opioid antinociception, RGS9 knockout mice exhibit a small degree of reduced hypersensitivity to the sensory component of both thermal and mechanical insult in early stages of neuropathic pain but exacerbation of affective components of the pain at later time points (Terzi et al., 2014). The nerve injury in wild-type mice was seen to cause a transient reduction in levels of RGS9-2 in the spinal cord, explaining the reduced sensory hypersensitivity, although phenotypic changes in basal antinociceptive activity have not been ruled out, and a later decrease in RGS9-2 levels in the NAc, explaining the change in the affective response. Consequently, RGS9-2 appears to be a negative regulator of the sensory component but a positive regulator of the affective response (Terzi et al., 2014). Since neuropathic pain can lead to depression in humans (Kroenke et al., 2009) this complication might preclude the use of inhibitors of RGS9-2 in the management of chronic pain.

R12 Family

The R12 family of RGS proteins consists of RGS10, 12, and 14. Little is known about how the R12 RGS family regulates MOR signaling and/or analgesia. Central knockdown

of RGS12 and RGS14 increased morphine antinociception on the tail-flick test in the mouse, although there were no reported changes in baseline nociceptive thresholds (Garzón et al., 2001) which may suggest a low or absent release of endogenous peptides or a lack of co-localization with RGS proteins. RGS14 knockdown reduced the development of acute tolerance following morphine exposure, and these behavioral changes occurred alongside increased MOR phosphorylation, which promotes internalization and recycling of the receptor (Rodríguez-Muñoz et al., 2007a). This suggests that in normal circumstances RGS14 limits agonist activity in a way that reduces both MOR phosphorylation (e.g., by GRKs) and β-arrestin-mediated endocytosis, leading to more robust receptor desensitization than in systems lacking RGS14 (Rodríguez-Muñoz et al., 2007a). More work is needed to understand the potential roles for the R12 family in regulating MOR signaling and antinociception.

RZ Family

The RZ family of RGS proteins consists of RGS17 (also known as RGSZ2), 19 (also known as G Alpha Interacting Protein/GAIP), and RGS20 (RGSZ1). Antisense knockdown of central RGSZ17 levels in male mice was seen to increase morphine and DAMGO antinociception, but also increased the rate of tolerance development (Garzón et al., 2005). Knockdown of RGS19 in SH-SY5Y cells enhances MOR agonist-induced MAPK stimulation and adenylyl cyclase inhibition (Wang and Traynor, 2013). Consequently, knockdown of RGS19 and RGS20, enhances the antinociceptive effects of morphine and DAMGO (Garzón et al., 2004). In addition to these effects on antinociception, knockdown of either RGS19 or RGS20 increased the rate of analgesic tolerance development (Garzón et al., 2004). Suppressing RGS20 function increased the antinociceptive efficacy of MOR agonists and delayed the development of morphine tolerance in mice (Gaspari et al., 2018). Thus, both RGS20 (RGSZ1) and RGS17 (RGSZ2) appear to play roles in regulating opioid antinociception and tolerance.

Treatment with morphine or DAMGO decreases associations between MOR and $G\alpha_{i2}$ but increases associations between $G\alpha_{i2}$ and RGSZ2 (Rodríguez-Muñoz et al., 2007b). This shift is transient, and the time course mimics the duration of antinociceptive tolerance following acute administration of morphine, such that $G\alpha_{i2}$ interactions have returned to normal at time points when acute antinociceptive tolerance has waned (Rodríguez-Muñoz et al., 2007b). A similar process occurs with RGSZ2 and $G\alpha_z$, with MOR agonists increasing association between these proteins while decreasing $G\alpha_z$/MOR association (Garzón et al., 2005). Together these results suggest that all RZ RGS proteins are capable of both inhibiting MOR agonist-induced antinociception and reducing the development of tolerance following agonist exposure, likely through regulation of $G\alpha_z$ and $G\alpha_{i2}$ (Garzón et al., 2004, 2005; Rodríguez-Muñoz et al., 2007b).

To date, no studies related to antinociception have been performed in mice with constitutive or conditional genetic knockout of any members of the RGS RZ family.

RGS REGULATION OF SIGNALING AND ANTINOCICEPTION DOWNSTREAM OF OTHER OPIOID RECEPTORS

All members of the opioid receptor family are involved in some way in the modulation of pain and have been the subject of study in relation to their interactions with RGS proteins.

The Delta Opioid Receptor (DOR)

There is much evidence that RGS4 modulates signaling downstream of the delta opioid receptor (DOR) and this in turn leads to increases in antinociceptive properties of agonists at these receptors. For example, purified RGS4 reverses the enkephalin-mediated DOR inhibition of adenylate cyclase activity in NG108-15 cells (Hepler et al., 1997). In HEK293 cells, RGS4 overexpression similarly reduced DOR agonist-stimulated signaling and increased the degree of DOR internalization (Leontiadis et al., 2009). In agreement with these overexpression studies, a 90% reduction of RGS4 in SH-SY5Y cells significantly increased the ability of DOR agonists to inhibit adenylyl cyclase and activate MAPK (Wang et al., 2009) and in mouse brain the small molecule DOR agonist SNC80 increased striatal MAPK phosphorylation to a greater degree in RGS4 knockout animals, than their littermate controls (Dripps et al., 2017). Mutagenesis studies have identified the C-terminus of DOR as the site of interaction with RGS4 and work using molecular dynamics simulations and *in vitro* pull-down experiments, has isolated this to 12 amino-acid residues in helix 8 of DOR and to the first 17 N-terminal residues of RGS4 (Karoussiotis et al., 2019).

Similar to the enhancement of MOR-mediated antinociception, the potency of SNC80 is increased in nitroglycerin-induced hyperalgesia in mice expressing RGSi-$G\alpha_o$ (Dripps et al., 2017). In addition, RGS4 knockout mice show an enhanced antinociceptive response to SNC80 compared to their wild-type littermate controls (Dripps et al., 2017). Importantly, in both the RGSi-$G\alpha_o$ knock-in mice and the RGS4 knockout mice the enhancement of DOR-mediated antinociception occurs without an increased ability of SNC80 to cause convulsions, a serious side effect of DOR agonists, thus increasing the preclinical therapeutic window of this DOR agonists.

RGS19 (GAIP) has also been studied with respect to DOR signaling. Purified RGS19, like RGS4 acts as a GAP for DOR signaling in NG108-15 cells (Hepler et al., 1997). In contrast DOR signaling in SH-SY5Y cells to adenylate cyclase or MAPK was not sensitive to knockdown of RGS19 (Wang and Traynor, 2013) and knockdown of RGS19 failed to modulate antinociceptive responses to DOR agonists, DPDPE and deltorphin (Garzón et al., 2004). This could suggest the experiments in NG108-15 cells that RGS19 is acting as a non-selective GAP. Conversely, there is other evidence of a role for RGS19 in DOR signaling. Thus, in HEK cells Flag-tagged DOR and heterologously expressed RGS19 are found in different cellular compartments; RGS19 in clathrin-coated membrane regions and DOR near $G\alpha_{i3}$ in non-clathrin-coated regions (Elenko et al., 2003). Following DOR agonist treatment, activated GTP-bound $G\alpha_{i3}$ and RGS19 co-localize in clathrin-coated regions to form a complex when

RGS19 acts as a GAP to promote GTP hydrolysis returning $G\alpha_{i3}$ to its GDP bound inactive form. This is reminiscent of the proposed process, described above, where MOR agonist treatment shifts $G\alpha_{i2}$ and $G\alpha_z$ from a complex with MOR to a complex with RGSZ-2 (Rodríguez-Muñoz et al., 2007b).

The Kappa Opioid Receptor

Little published work is available on how RGS proteins affect signaling and antinociception downstream of the kappa opioid receptor, KOR. The genetic loci for RGS20 and KOR are separated by only approximately 600 base pairs, suggesting that these proteins may be co-regulated (Sierra et al., 2002). In *Xenopus* oocytes, RGS4 expression inhibits GIRK1 and GIRK2 downstream of KOR activation, and the presence of RGS4 appears to counteract cellular adaptations to sustained KOR agonist treatment (Ulens et al., 2000). Further, RGS2 and RGS4 bind to different domains of KOR to reduce signaling of this receptor to adenylate cyclase and the MAP kinase pathway in HEK cells (Papakonstantinou et al., 2015). In PC12 cells stably expressing KOR, agonist application increased RGS4 mRNA expression in a KOR antagonist reversible manner, a process that may contribute to desensitization of KOR agonist responses (Nakagawa et al., 2001). Downstream of KOR, RGS12 attenuates G-protein signaling and promotes β-arrestin (Gross et al., 2019). Since β-arrestin is thought to promote unwanted effects of KOR agonists, including aversion, an inhibitor of RGS12 would be expected to promote G-protein signaling and therefore analgesia without dysphoria, as indicated in **Figure 1**.

The Nociceptin Receptor

The genetic loci for the nociceptin (NOP) receptor and RGS19 neighbor each other, with RGS19 found only 83 base pairs from the 5′ end of the gene encoding NOP receptor (Ito et al., 2000; Xie et al., 2003). This 83 base pair region functions as a bidirectional promoter for both genes (Ito et al., 2000). Despite this close co-regulation RGS19 and NOP receptor expression show differences, for example, RGS19 is found in both undifferentiated and differentiated NT2 cells, while the NOP receptor is expressed only after differentiation (Ito et al., 2000). Nociceptin has both pro- and anti-nociceptive activity (Rizzi et al., 2016), so it will be of interest to see how the balance of these activities is controlled by members of the RGS protein family.

CAN WE TARGET RGS PROTEINS?

An extensive amount of research has been conducted at both the molecular/cellular and behavioral levels on the interaction between MOR and certain RGS proteins, especially RGS4 and RGS9-2, but effects of RGS proteins on other opioid receptors is in its infancy. Nonetheless, the findings summarized above suggest that RGS proteins are attractive targets that may allow more precise control of opioid analgesic effects, and RGS inhibiting molecules may even have stand-alone analgesic efficacy.

In this regard the first attempts to develop inhibitors were peptides designed on the Gα interface with RGS proteins (Roof et al., 2008). To date, no small molecules targeting this large surface region have been published. On the other hand, a number of small molecules that act at a least one cysteine distant from the interaction surface have been developed (Roman et al., 2007, 2009; Blazer et al., 2010, 2011; Monroy et al., 2013; Storaska et al., 2013). Inhibition occurs by covalent modification of this cysteine, although the interaction of some inhibitors with RGS protein can be reversed (Storaska et al., 2013). Because many RGS proteins have a cysteine in the RH domain these inhibitors act somewhat promiscuously, although some degree of selectivity can be obtained. For example, CCG-203769 which inhibits RGS4, is 10-fold less potent at inhibiting RGS19, but has a very high selectivity over other members of the RGS family (Blazer et al., 2015). Similarly, CCG-50014 inhibits both RGS4 and RGS19 and is selective for these RGS proteins over RGS8 and RGS16 (Blazer et al., 2011), None of the small molecule inhibitors identified to date act at RGS6 or RGS7 (Hayes et al., 2018) which lack a cysteine in the RH domain, although it is worth noting that RGS9 does have a cysteine in the same position at the sensitive cysteine in RGS19. Of interest is that studies have now shown CCG-50014 also inhibits RGS1,5,14, and 17 and in fact is most potent at RGS 14 (Hayes et al., 2018). This could be significant given the, albeit limited, knowledge on the role of RGS14 in morphine antinociception (Garzón et al., 2001; Rodríguez-Muñoz et al., 2007a). Thus the finding that CCG-50014 enhances the inhibitory effects of both MOR and DOR agonists *in vitro* (Blazer et al., 2015), and, as mentioned earlier produces naloxone-reversible antinociception in a mouse model (Yoon et al., 2015), may not be due only to its action as an inhibitor of RGS4.

A report by Shaw et al. (2018), explores the structural determinants of RGS inhibitor selectivity. In general, inhibitors such as CCG-50014 preferentially inhibit RGS proteins with a greater degree of structural flexibility. Thus, increasing the number of interhelical salt bridges present in the RGS protein structure reduces flexibility, and decreases the relative affinity of CCG-50014 for RGS4 or RGS8. Conversely, mutations which decrease the rigidity of RGS4 and RGS8 increase CCG-50014 binding to these targets. In addition, a distinct class of small molecules, BMS-195270 and BMS-192364 were identified in an *in vitro* assay for bladder contraction using a chemical genetics screen. These compounds gave results consistent with a mechanism whereby they interfere with the $G\alpha_q$/RGS complex downstream of muscarinic receptors to terminate signaling (Fitzgerald et al., 2006). Compounds with activity at $G\alpha_{i/o}$/RGS complexes that are likely to be effective downstream of opioid receptors have not been described to our knowledge.

Overall, there is evidence for the involvement of certain RGS proteins in the control of pain and analgesia, although many of these studies measured only acute antinociception and have not been replicated or followed up. Moreover, the ability to selectively target these proteins, especially with reversible ligands is also very limited. As understanding of the binding modes for current RGS inhibitors continues to increase and new inhibitors are discovered, a more thorough understanding

of the role of RGS proteins in pain and analgesia will become increasingly important.

AUTHOR CONTRIBUTIONS

NS wrote the original draft, and reviewed and corrected the manuscript. RK reviewed and revised the manuscript. KK prepared the figures, and reviewed and revised the manuscript. JT conceptualized the review, finalized the manuscript, and provided funding. All authors read and approved the submitted version.

FUNDING

Funding was provided by NIH grants R01 DA035316, R37 DA039997, and T32 DA007268 to JT.

REFERENCES

Ahlers, K. E., Chakravarti, B., and Fisher, R. A. (2016). RGS6 as a novel therapeutic target in CNS diseases and cancer. *AAPS J.* 18, 560–572. doi: 10.1208/s12248-016-9899-9

Avrampou, K., Pryce, K. D., Ramakrishnan, A., Sakloth, F., Gaspari, S., Serafini, R. A., et al. (2019). RGS4 maintains chronic pain symptoms in rodent models. *J. Neurosci.* 39, 8291–8304. doi: 10.1523/JNEUROSCI.3154-18.2019

Babu, K. M., Brent, J., and Juurlink, D. N. (2019). Prevention of opioid overdose. *New Engl. J. Med.* 380, 2246–2255. doi: 10.1056/NEJMra1807054

Bertorelli, R., Corradini, L., Rafiq, K., Tupper, J., Caló, G., and Ongini, E. (1999). Nociceptin and the ORL-1 ligand [$Phe^1\psi$ (CH_2-NH)Gly^2]nociceptin(1-13)NH_2 exert anti-opioid effects in the Freund's adjuvant-induced arthritic rat model of chronic pain. *Br. J. Pharmacol.* 128, 1252–1258. doi: 10.1038/sj.bjp.0702884

Blazer, L. L., Roman, D. L., Chung, A., Larsen, M. J., Greedy, B. M., Husbands, S. M., et al. (2010). Reversible, allosteric small-molecule inhibitors of regulator of G protein signaling proteins. *Mol. Pharmacol.* 78, 524–533. doi: 10.1124/mol.110.065128

Blazer, L. L., Storaska, A. J., Jutkiewicz, E. M., Turner, E. M., Calcagno, M., Wade, S. M., et al. (2015). Selectivity and anti-Parkinson's potential of thiadiazolidinone RGS4 inhibitors. *ACS Chem. Neurosci.* 6, 911–919. doi: 10.1021/acschemneuro.5b00063

Blazer, L. L., Zhang, H., Casey, E. M., Husbands, S. M., and Neubig, R. R. (2011). A nanomolar-potency small molecule inhibitor of regulator of G-protein signaling proteins. *Biochemistry* 50, 3181–3192. doi: 10.1021/bi1019622

Bosier, B., Doyen, P. J., Brolet, A., Muccioli, G. G., Ahmed, E., Desmet, N., et al. (2015). Inhibition of the regulator of G protein signalling RGS4 in the spinal cord decreases neuropathic hyperalgesia and restores cannabinoid CB1 receptor signalling. *Br. J. Pharmacol.* 172, 5333–5346. doi: 10.1111/bph.13324

Burford, N. T., Clark, M. J., Wehrman, T. S., Gerritz, S. W., Banks, M., O'Connell, J., et al. (2013). Discovery of positive allosteric modulators and silent allosteric modulators of the μ-opioid receptor. *Proc. Natl. Acad. Sci. U.S.A.* 110, 10830–10835. doi: 10.1073/pnas.1300393110

Burford, N. T., Traynor, J. R., and Alt, A. (2015). Positive allosteric modulators of the μ-opioid receptor: a novel approach for future pain medications. *Br. J. Pharmacol.* 172, 277–286. doi: 10.1111/bph.12599

Cesselin, F., Montastruc, J. L., Gros, C., Bourgoin, S., and Hamon, M. (1980). Met-enkephalin levels and opiate receptors in the spinal cord of chronic suffering rats. *Brain Res.* 191, 289–293. doi: 10.1016/0006-8993(80)90335-2

Clark, M. J., Harrison, C., Zhong, H., Neubig, R. R., and Traynor, J. R. (2003). Endogenous RGS protein action modulates μ-opioid signaling through $G\alpha_o$. Effects on adenylyl cyclase, extracellular signal-regulated kinases, and intracellular calcium pathways. *J. Biol. Chem.* 278, 9418–9425. doi: 10.1074/jbc.M208885200

Costigan, M., Samad, T. A., Allchorne, A., Lanoue, C., Tate, S., and Woolf, C. J. (2003). High basal expression and injury-induced down regulation of two regulator of G-protein signaling transcripts. RGS3 and RGS4 in primary sensory neurons. *Mol. Cell. Neurosci.* 24, 106–116. doi: 10.1016/S1044-7431(03)00135-0

Doupnik, C. A. (2015). RGS redundancy and implications in GPCR-GIRK signaling. *Int. Rev. Neurobiol.* 123, 87–116. doi: 10.1016/bs.irn.2015.05.010

Doyen, P. J., Vergouts, M., Pochet, A., Desmet, N., van Neerven, S., Brook, G., et al. (2017). Inflammation-associated regulation of RGS in astrocytes and putative implication in neuropathic pain. *J. Neuroinflam.* 14:209. doi: 10.1186/s12974-017-0971-x

Dripps, I. J., Wang, Q., Neubig, R. R., Rice, K. C., Traynor, J. R., and Jutkiewicz, E. M. (2017). The role of regulator of G protein signaling 4 in delta-opioid receptor-mediated behaviors. *Psychopharmacology* 234, 29–39. doi: 10.1007/s00213-016-4432-5

Elenko, E., Fischer, T., Niesman, I., Harding, T., McQuistan, T., Von Zastrow, M., et al. (2003). Spatial regulation of Gαi protein signaling in clathrin-coated membrane microdomains containing GAIP. *Mol. Pharmacol.* 64, 11–20. doi: 10.1124/mol.64.1.11

Fitzgerald, K., Tertyshnikova, S., Moore, L., Bjerke, L., Burley, B., Cao, J., et al. (2006). Chemical genetics reveals an RGS/G-protein role in the action of a compound. *PLoS Genet.* 2:e57. doi: 10.1371/journal.pgen.0020057

Fournié-Zaluski, M. C., Coric, P., Turcaud, S., Lucas, E., Noble, F., Maldonado, R., et al. (1992). "Mixed inhibitor-prodrug" as a new approach toward systemically active inhibitors of enkephalin-degrading enzymes. *J. Med. Chem.* 35, 2473–2481. doi: 10.1021/jm00091a016

Garnier, M., Zaratin, P. F., Ficalora, G., Valente, M., Fontanella, L., Rhee, M.-H., et al. (2003). Up-regulation of regulator of G protein signaling 4 expression in a model of neuropathic pain and insensitivity to morphine. *J. Pharmacol. Exp. Ther.* 304, 1299–1306. doi: 10.1124/jpet.102.043471

Garzón, J., de Antonio, I., and Sánchez-Blázquez, P. (2000). In vivo modulation of G proteins and opioid receptor function by antisense oligodeoxynucleotides. *Methods Enzymol.* 314, 3–20. doi: 10.1016/s0076-6879(99)14091-6

Garzón, J., López-Fando, A., and Sánchez-Blázquez, P. (2003). The R7 subfamily of RGS proteins assists tachyphylaxis and acute tolerance at mu-opioid receptors. *Neuropsychopharmacology* 28, 1983–1990. doi: 10.1038/sj.npp.1300263

Garzón, J., Rodríguez-Díaz, M., López-Fando, A., and Sánchez-Blázquez, P. (2001). RGS9 proteins facilitate acute tolerance to mu-opioid effects. *Eur. J. Neurosci.* 13, 801–811. doi: 10.1046/j.0953-816x.2000.01444.x

Garzón, J., Rodríguez-Muñoz, M., López-Fando, A., García-España, A., and Sánchez-Blázquez, P. (2004). RGSZ1 and GAIP regulate mu- but not delta-opioid receptors in mouse CNS: role in tachyphylaxis and acute tolerance. *Neuropsychopharmacology* 29, 1091–1104. doi: 10.1038/sj.npp.1300408

Garzón, J., Rodríguez-Muñoz, M., López-Fando, A., and Sánchez-Blázquez, P. (2005). The RGSZ2 protein exists in a complex with mu-opioid receptors and regulates the desensitizing capacity of Gz proteins. *Neuropsychopharmacology* 30, 1632–1648. doi: 10.1038/sj.npp.1300726

Gaspari, S., Cogliani, V., Manouras, L., Anderson, E. M., Mitsi, V., Avrampou, K., et al. (2017). RGS9-2 modulates responses to oxycodone in pain-free and chronic pain states. *Neuropsychopharmacology* 42, 1548–1556. doi: 10.1038/npp.2017.4

Gaspari, S., Purushothaman, I., Cogliani, V., Sakloth, F., Neve, R. L., Howland, D., et al. (2018). Suppression of RGSz1 function optimizes the actions of opioid analgesics by mechanisms that involve the Wnt/β-catenin pathway. *Proc. Natl. Acad. Sci. U.S. A.* 115, E2085–E2094. doi: 10.1073/pnas.1707887115

Gold, S. J., Han, M.-H., Herman, A. E., Ni, Y. G., Pudiak, C. M., Aghajanian, G. K., et al. (2003). Regulation of RGS proteins by chronic morphine in rat locus coeruleus. *Eur. J. Neurosci.* 17, 971–980. doi: 10.1046/j.1460-9568.2003.02529.x

Gold, S. J., Ni, Y. G., Dohlman, H. G., and Nestler, E. J. (1997). Regulators of G-protein signaling (RGS) proteins: region-specific expression of nine subtypes in rat brain. *J. Neurosci.* 17, 8024–8037. doi: 10.1523/jneurosci.17-20-08024.1997

Grafstein-Dunn, E., Young, K. H., Cockett, M. I., and Khawaja, X. Z. (2001). Regional distribution of regulators of G-protein signaling (RGS) 1, 2, 13, 14, 16, and GAIP messenger ribonucleic acids by in situ hybridization in rat brain. *Brain Res.* 88, 113–123. doi: 10.1016/s0169-328x(01)00038-9

Grillet, N., Dubreuil, V., Dufour, H. D., and Brunet, J.-F. (2003). Dynamic expression of RGS4 in the developing nervous system and regulation by the neural type-specific transcription factor Phox2b. *J. Neurosci.* 23, 10613–10621. doi: 10.1523/JNEUROSCI.23-33-10613.2003

Grillet, N., Pattyn, A., Contet, C., Kieffer, B. L., Goridis, C., and Brunet, J.-F. (2005). Generation and characterization of Rgs4 mutant mice. *Mol. Cell. Biol.* 25, 4221–4228. doi: 10.1128/MCB.25.10.4221-4228.2005

Gross, J. D., Kaski, S. W., Schmidt, K. T., Cogan, E. S., Boyt, K. M., Wix, K., et al. (2019). Role of RGS12 in the differential regulation of kappa opioid receptor-dependent signaling and behavior. *Neuropsychopharmacology* 44, 1728–1741. doi: 10.1038/s41386-019-0423-7

Han, M.-H., Renthal, W., Ring, R. H., Rahman, Z., Psifogeorgou, K., Howland, D., et al. (2010). Brain region specific actions of regulator of G protein signaling 4 oppose morphine reward and dependence but promote analgesia. *Biol. Psychiatry* 67, 761–769. doi: 10.1016/j.biopsych.2009.08.041

Hayes, M. P., Bodle, C. R., and Roman, D. L. (2018). Evaluation of the selectivity and cysteine dependence of inhibitors across the regulator of G protein-signaling family. *Mol. Pharmacol.* 93, 25–35. doi: 10.1124/mol.117.109843

Hepler, J. R., Berman, D. M., Gilman, A. G., and Kozasa, T. (1997). RGS4 and GAIP are GTPase-activating proteins for Gq alpha and block activation of phospholipase C beta by gamma-thio-GTP-Gq alpha. *Proc. Natl. Acad. Sci. U.S.A.* 94, 428–432. doi: 10.1073/pnas.94.2.428

Hollinger, S., and Hepler, J. R. (2002). Cellular regulation of RGS proteins: modulators and integrators of G protein signaling. *Pharmacol. Rev.* 54, 527–559. doi: 10.1124/pr.54.3.527

Hurley, R. W., and Hammond, D. L. (2001). Contribution of endogenous enkephalins to the enhanced analgesic effects of supraspinal mu opioid receptor agonists after inflammatory injury. *J. Neurosci.* 21, 2536–2545. doi: 10.1523/JNEUROSCI.21-07-02536.2001

Ito, E., Xie, G., Maruyama, K., and Palmer, P. P. (2000). A core-promoter region functions bi-directionally for human opioid-receptor-like gene ORL1 and its 5'-adjacent gene GAIP. *J. Mol. Biol.* 304, 259–270. doi: 10.1006/jmbi.2000.4212

Karoussiotis, C., Marti-Solano, M., Stepniewski, T. M., Symeonof, A., Selent, J., and Georgoussi, Z. (2019). A highly conserved δ-opioid receptor region determines RGS4 interaction. *FEBS J.* doi: 10.1111/febs.15033

Khroyan, T. V., Polgar, W. E., Jiang, F., Zaveri, N. T., and Toll, L. (2009). Nociceptin/orphanin FQ receptor activation attenuates antinociception induced by mixed nociceptin/orphanin FQ/μ-opioid receptor agonists. *J. Pharmacol. Exp. Ther.* 331, 946–953. doi: 10.1124/jpet.109.156711

Kroenke, K., Krebs, E. E., and Bair, M. J. (2009). Pharmacotherapy of chronic pain: a synthesis of recommendations from systematic reviews. *Gen. Hospital Psychiatry* 31, 206–219. doi: 10.1016/j.genhosppsych.2008.12.006

Lamberts, J. T., Jutkiewicz, E. M., Mortensen, R. M., and Traynor, J. R. (2011). μ-Opioid receptor coupling to Gα(o) plays an important role in opioid antinociception. *Neuropsychopharmacology* 36, 2041–2053. doi: 10.1038/npp.2011.91

Lamberts, J. T., Smith, C. E., Li, M.-H., Ingram, S. L., Neubig, R. R., and Traynor, J. R. (2013). Differential control of opioid antinociception to thermal stimuli in a knock-in mouse expressing regulator of G-protein signaling-insensitive Gαo protein. *J. Neurosci.* 33, 4369–4377. doi: 10.1523/JNEUROSCI.5470-12.2013

Lamberts, J. T., and Traynor, J. R. (2013). Opioid receptor interacting proteins and the control of opioid signaling. *Curr. Pharmaceut. Design* 19, 7333–7347. doi: 10.2174/13816128194210516062 5

Lan, K. L., Zhong, H., Nanamori, M., and Neubig, R. R. (2000). Rapid kinetics of regulator of G-protein signaling (RGS)-mediated Galphai and Galphao deactivation. Galpha specificity of RGS4 AND RGS7. *J. Biol. Chem.* 275, 33497–33503. doi: 10.1074/jbc.M005785200

Leontiadis, L. J., Papakonstantinou, M. P., and Georgoussi, Z. (2009). Regulator of G protein signaling 4 confers selectivity to specific G proteins to modulate mu- and delta-opioid receptor signaling. *Cell. Sign.* 21, 1218–1228. doi: 10.1016/j.cellsig.2009.03.013

Levine, J. D., Gordon, N. C., Jones, R. T., and Fields, H. L. (1978). The narcotic antagonist naloxone enhances clinical pain. *Nature* 272, 826–827. doi: 10.1038/272826a0

Livingston, K. E., and Traynor, J. R. (2018). Allostery at opioid receptors: modulation with small molecule ligands. *Br. J. Pharmacol.* 175, 2846–2856. doi: 10.1111/bph.13823

Manglik, A., Lin, H., Aryal, D. K., McCorvy, J. D., Dengler, D., Corder, G., et al. (2016). Structure-based discovery of opioid analgesics with reduced side effects. *Nature* 537, 185–190. doi: 10.1038/nature19112

Markman, J., Gudin, J., Rauck, R., Argoff, C., Rowbotham, M., Agaiby, E., et al. (2019). SUMMIT-07: a randomized trial of NKTR-181, a new molecular entity, full mu-opioid receptor agonist for chronic low-back pain. *Pain* 160, 1374–1382. doi: 10.1097/j.pain.0000000000001517

McPherson, K. B., Leff, E. R., Li, M.-H., Meurice, C., Tai, S., Traynor, J. R., et al. (2018). Regulators of G-protein signaling (RGS) proteins promote receptor coupling to g-protein-coupled inwardly rectifying potassium (GIRK) channels. *J. Neurosci.* 38, 8737–8744. doi: 10.1523/JNEUROSCI.0516-18.2018

Monroy, C. A., Doorn, J. A., and Roman, D. L. (2013). Modification and functional inhibition of regulator of G-protein signaling 4 (RGS4) by 4-hydroxy-2-nonenal. *Chem. Res. Toxicol.* 26, 1832–1839. doi: 10.1021/tx400212q

Nakagawa, T., Minami, M., and Satoh, M. (2001). Up-regulation of RGS4 mRNA by opioid receptor agonists in PC12 cells expressing cloned mu- or kappa-opioid receptors. *Eur. J. Pharmacol.* 433, 29–36. doi: 10.1016/s0014-2999(01)01485-6

Nastase, A. F., Griggs, N. W., Anand, J. P., Fernandez, T. J., Harland, A. A., Trask, T. J., et al. (2018). Synthesis and pharmacological evaluation of novel C-8 substituted tetrahydroquinolines as balanced-affinity Mu/Delta opioid ligands for the treatment of pain. *ACS Chem. Neurosci.* 9, 1840–1848. doi: 10.1021/acschemneuro.8b00139

Ni, Y. G., Gold, S. J., Iredale, P. A., Terwilliger, R. Z., Duman, R. S., and Nestler, E. J. (1999). Region-specific regulation of RGS4 (Regulator of G-protein-signaling protein type 4) in brain by stress and glucocorticoids: in vivo and in vitro studies. *J. Neurosci.* 19, 3674–3680. doi: 10.1523/JNEUROSCI.19-10-03674.19992002

Noble, F., Smadja, C., Valverde, O., Maldonado, R., Coric, P., Turcaud, S., et al. (1997). Pain-suppressive effects on various nociceptive stimuli (thermal, chemical, electrical and inflammatory) of the first orally active enkephalin-metabolizing enzyme inhibitor RB 120. *Pain* 73, 383–391. doi: 10.1016/s0304-3959(97)00125-5

Noble, F., Soleilhac, J. M., Soroca-Lucas, E., Turcaud, S., Fournie-Zaluski, M. C., and Roques, B. P. (1992). Inhibition of the enkephalin-metabolizing enzymes by the first systemically active mixed inhibitor prodrug RB 101 induces potent analgesic responses in mice and rats. *J. Pharmacol. Exp. Ther.* 261, 181–190.

Papachatzaki, M. M., Antal, Z., Terzi, D., Szücs, P., Zachariou, V., and Antal, M. (2011). RGS9-2 modulates nociceptive behaviour and opioid-mediated synaptic transmission in the spinal dorsal horn. *Neurosci. Lett.* 501, 31–34. doi: 10.1016/j.neulet.2011.06.033

Papakonstantinou, M.-P., Karoussiotis, C., and Georgoussi, Z. (2015). RGS2 and RGS4 proteins: new modulators of the κ-opioid receptor signaling. *Cell. Sign.* 27, 104–114. doi: 10.1016/j.cellsig.2014.09.023

Peckys, D., and Landwehrmeyer, G. B. (1999). Expression of mu, kappa, and delta opioid receptor messenger RNA in the human CNS: a 33P in situ hybridization study. *Neuroscience* 88, 1093–1135. doi: 10.1016/s0306-4522(98)00251-6

Porro, C. A., Tassinari, G., Facchinetti, F., Panerai, A. E., and Carli, G. (1991). Central beta-endorphin system involvement in the reaction to acute tonic pain. *Exp. Brain Res.* 83, 549–554. doi: 10.1007/bf00229833

Posner, B. A., Gilman, A. G., and Harris, B. A. (1999). Regulators of G protein signaling 6 and 7. Purification of complexes with gbeta5 and assessment of their effects on g protein-mediated signaling pathways. *J. Biol. Chem.* 274, 31087–31093. doi: 10.1074/jbc.274.43.31087

Psifogeorgou, K., Papakosta, P., Russo, S. J., Neve, R. L., Kardassis, D., Gold, S. J., et al. (2007). RGS9-2 is a negative modulator of mu-opioid receptor function. *J. Neurochem.* 103, 617–625. doi: 10.1111/j.1471-4159.2007.04812.x

Psifogeorgou, K., Psigfogeorgou, K., Terzi, D., Papachatzaki, M. M., Varidaki, A., Ferguson, D., et al. (2011). A unique role of RGS9-2 in the striatum as a positive or negative regulator of opiate analgesia. *J. Neurosci.* 31, 5617–5624. doi: 10.1523/JNEUROSCI.4146-10.2011

Raehal, K. M., Schmid, C. L., Groer, C. E., and Bohn, L. M. (2011). Functional selectivity at the μ-opioid receptor: implications for understanding opioid analgesia and tolerance. *Pharmacol. Rev.* 63, 1001–1019. doi: 10.1124/pr.111.004598

Rizzi, A., Cerlesi, M. C., Ruzza, C., Malfacini, D., Ferrari, F., Bianco, S., et al. (2016). Pharmacological characterization of cebranopadol a novel analgesic acting as mixed nociceptin/orphanin FQ and opioid receptor agonist. *Pharmacol. Res. Persp.* 4:e00247. doi: 10.1002/prp2.247

Rodríguez-Muñoz, M., de la Torre-Madrid, E., Gaitán, G., Sánchez-Blázquez, P., and Garzón, J. (2007a). RGS14 prevents morphine from internalizing Mu-opioid receptors in periaqueductal gray neurons. *Cell. Sign.* 19, 2558–2571. doi: 10.1016/j.cellsig.2007.08.003

Rodríguez-Muñoz, M., de la Torre-Madrid, E., Sánchez-Blázquez, P., and Garzón, J. (2007b). Morphine induces endocytosis of neuronal mu-opioid receptors through the sustained transfer of Galpha subunits to RGSZ2 proteins. *Mol. Pain* 3:19. doi: 10.1186/1744-8069-3-19

Roman, D. L., Ota, S., and Neubig, R. R. (2009). Polyplexed flow cytometry protein interaction assay: a novel high-throughput screening paradigm for RGS protein inhibitors. *J. Biomol. Screen.* 14, 610–619. doi: 10.1177/1087057109336590

Roman, D. L., Talbot, J. N., Roof, R. A., Sunahara, R. K., Traynor, J. R., and Neubig, R. R. (2007). Identification of small-molecule inhibitors of RGS4 using a high-throughput flow cytometry protein interaction assay. *Mol. Pharmacol.* 71, 169–175. doi: 10.1124/mol.106.028670

Roof, R. A., Sobczyk-Kojiro, K., Turbiak, A. J., Roman, D. L., Pogozheva, I. D., Blazer, L. L., et al. (2008). Novel peptide ligands of RGS4 from a focused one-bead, one-compound library. *Chem. Biol. Drug Design* 72, 111–119. doi: 10.1111/j.1747-0285.2008.00687.x

Roy, A. A., Lemberg, K. E., and Chidiac, P. (2003). Recruitment of RGS2 and RGS4 to the plasma membrane by G proteins and receptors reflects functional interactions. *Mol. Pharmacol.* 64, 587–593. doi: 10.1124/mol.64.3.587

Sánchez-Blázquez, P., Rodríguez-Díaz, M., López-Fando, A., Rodríguez-Muñoz, M., and Garzón, J. (2003). The GBeta5 subunit that associates with the R7 subfamily of RGS proteins regulates mu-opioid effects. *Neuropharmacology* 45, 82–95. doi: 10.1016/s0028-3908(03)00149-7

Schmid, C. L., Kennedy, N. M., Ross, N. C., Lovell, K. M., Yue, Z., Morgenweck, J., et al. (2017). Bias factor and therapeutic window correlate to predict safer opioid analgesics. *Cell* 171:1165-1175.e18. doi: 10.1016/j.cell.2017.10.035

Shaw, V. S., Mohammadiarani, H., Vashisth, H., and Neubig, R. R. (2018). Differential protein dynamics of regulators of G-protein signaling: role in specificity of small-molecule inhibitors. *J. Am. Chem. Soc.* 140, 3454–3460. doi: 10.1021/jacs.7b13778

Sierra, D. A., Gilbert, D. J., Householder, D., Grishin, N. V., Yu, K., Ukidwe, P., et al. (2002). Evolution of the regulators of G-protein signaling multigene family in mouse and human. *Genomics* 79, 177–185. doi: 10.1006/geno.2002.6693

Stein, C., Schäfer, M., and Machelska, H. (2003). Attacking pain at its source: new perspectives on opioids. *Nat. Med.* 9, 1003–1008. doi: 10.1038/nm908

Storaska, A. J., Mei, J. P., Wu, M., Li, M., Wade, S. M., Blazer, L. L., et al. (2013). Reversible inhibitors of regulators of G-protein signaling identified in a high-throughput cell-based calcium signaling assay. *Cell. Sign.* 25, 2848–2855. doi: 10.1016/j.cellsig.2013.09.007

Stratinaki, M., Varidaki, A., Mitsi, V., Ghose, S., Magida, J., Dias, C., et al. (2013). Regulator of G protein signaling 4 [corrected] is a crucial modulator of antidepressant drug action in depression and neuropathic pain models. *Proc. Natl. Acad. Sci. U.S.A.* 110, 8254–8259. doi: 10.1073/pnas.1214696110

Taccola, G., Doyen, P. J., Damblon, J., Dingu, N., Ballarin, B., Steyaert, A., et al. (2016). A new model of nerve injury in the rat reveals a role of regulator of G protein signaling 4 in tactile hypersensitivity. *Exp. Neurol.* 286, 1–11. doi: 10.1016/j.expneurol.2016.09.008

Talbot, J. N., Roman, D. L., Clark, M. J., Roof, R. A., Tesmer, J. J. G., Neubig, R. R., et al. (2010). Differential modulation of mu-opioid receptor signaling to adenylyl cyclase by regulators of G protein signaling proteins 4 or 8 and 7 in permeabilised C6 cells is Galpha subtype dependent. *J. Neurochem.* 112, 1026–1034. doi: 10.1111/j.1471-4159.2009.06519.x

Terzi, D., Cao, Y., Agrimaki, I., Martemyanov, K. A., and Zachariou, V. (2012). R7BP modulates opiate analgesia and tolerance but not withdrawal. *Neuropsychopharmacology* 37, 1005–1012. doi: 10.1038/npp.2011.284

Terzi, D., Gaspari, S., Manouras, L., Descalzi, G., Mitsi, V., and Zachariou, V. (2014). RGS9-2 modulates sensory and mood related symptoms of neuropathic pain. *Neurobiol. Learn. Mem.* 115, 43–48. doi: 10.1016/j.nlm.2014.08.005

Terzi, D., Stergiou, E., King, S. L., and Zachariou, V. (2009). Regulators of G protein signaling in neuropsychiatric disorders. *Prog. Mol. Biol. Transl. Sci.* 86, 299–333. doi: 10.1016/S1877-1173(09)86010-9

Tesmer, J. J., Berman, D. M., Gilman, A. G., and Sprang, S. R. (1997). Structure of RGS4 bound to AlF4–activated G(i alpha1): Stabilization of the transition state for GTP hydrolysis. *Cell* 89, 251–261. doi: 10.1016/s0092-8674(00)80204-4

Traynor, J. R., and Neubig, R. R. (2005). Regulators of G protein signaling & drugs of abuse. *Mol. Interv.* 5, 30–41. doi: 10.1124/mi.5.1.7

Ulens, C., Daenens, P., and Tytgat, J. (2000). Changes in GIRK1/GIRK2 deactivation kinetics and basal activity in the presence and absence of RGS4. *Life Sci.* 67, 2305–2317. doi: 10.1016/s0024-3205(00)00820-1

Violin, J. D., Crombie, A. L., Soergel, D. G., and Lark, M. W. (2014). Biased ligands at G-protein-coupled receptors: Promise and progress. *Trends Pharmacol. Sci.* 35, 308–316. doi: 10.1016/j.tips.2014.04.007

Wang, Q., Liu-Chen, L.-Y., and Traynor, J. R. (2009). Differential modulation of mu- and delta-opioid receptor agonists by endogenous RGS4 protein in SH-SY5Y cells. *J. Biol. Chem.* 284, 18357–18367. doi: 10.1074/jbc.M109.015453

Wang, Q., and Traynor, J. R. (2013). Modulation of μ-opioid receptor signaling by RGS19 in SH-SY5Y cells. *Mol. Pharmacol.* 83, 512–520. doi: 10.1124/mol.112.081992

Wu, H., Hung, K., Ohsawa, M., Mizoguchi, H., and Tseng, L. F. (2001). Antisera against endogenous opioids increase the nocifensive response to formalin: demonstration of inhibitory beta-endorphinergic control. *Eur. J. Pharmacol.* 421, 39–43. doi: 10.1016/s0014-2999(01)00970-0

Xie, G., Han, X., Ito, E., Yanagisawa, Y., Maruyama, K., Sugano, S., et al. (2003). Gene structure, dual-promoters and mRNA alternative splicing of the human and mouse regulator of G protein signaling GAIP/RGS19. *J. Mol. Biol.* 325, 721–732. doi: 10.1016/s0022-2836(02)01283-4

Xu, X., Zeng, W., Popov, S., Berman, D. M., Davignon, I., Yu, K., et al. (1999). RGS proteins determine signaling specificity of Gq-coupled receptors. *J. Biol. Chem.* 274, 3549–3556. doi: 10.1074/jbc.274.6.3549

Yoon, S.-Y., Woo, J., Park, J.-O., Choi, E.-J., Shin, H.-S., Roh, D.-H., et al. (2015). Intrathecal RGS4 inhibitor, CCG50014, reduces nociceptive responses and enhances opioid-mediated analgesic effects in the mouse formalin test. *Anesthesia Analg.* 120, 671–677. doi: 10.1213/ANE.0000000000000607

Zachariou, V., Georgescu, D., Sanchez, N., Rahman, Z., DiLeone, R., Berton, O., et al. (2003). Essential role for RGS9 in opiate action. *Proc. Natl. Acad. Sci. U.S.A.* 100, 13656–13661. doi: 10.1073/pnas.2232594100

Zangen, A., Herzberg, U., Vogel, Z., and Yadid, G. (1998). Nociceptive stimulus induces release of endogenous beta-endorphin in the rat brain. *Neuroscience* 85, 659–662. doi: 10.1016/s0306-4522(98)00050-5

Zeng, W., Xu, X., Popov, S., Mukhopadhyay, S., Chidiac, P., Swistok, J., et al. (1998). The N-terminal domain of RGS4 confers receptor-selective inhibition of G protein signaling. *J. Biol. Chem.* 273, 34687–34690. doi: 10.1074/jbc.273.52.34687

Zhong, H., Wade, S. M., Woolf, P. J., Linderman, J. J., Traynor, J. R., and Neubig, R. R. (2003). A spatial focusing model for G protein signals. Regulator of G protein signaling (RGS) protien-mediated kinetic scaffolding. *J. Biol. Chem.* 278, 7278–7284. doi: 10.1074/jbc.M208819200

Zhou, H., Chisari, M., Raehal, K. M., Kaltenbronn, K. M., Bohn, L. M., Mennerick, S. J., et al. (2012). GIRK channel modulation by assembly with allosterically regulated RGS proteins. *Proc. Natl. Acad. Sci. U.S.A.* 109, 19977–19982. doi: 10.1073/pnas.1214337109

Conflict of Interest: The authors declare that the research was conducted in the absence of any commercial or financial relationships that could be construed as a potential conflict of interest.

frontiers in Molecular Neuroscience

ORIGINAL RESEARCH
published: 14 February 2020
doi: 10.3389/fnmol.2019.00324

Peripheral Delta Opioid Receptors Mediate Formoterol Anti-allodynic Effect in a Mouse Model of Neuropathic Pain

*Rhian Alice Ceredig[1], Florian Pierre[1†], Stéphane Doridot[2], Unai Alduntzin[1†], Pierre Hener[1], Eric Salvat[1,3], Ipek Yalcin[1], Claire Gaveriaux-Ruff[4], Michel Barrot[1] and Dominique Massotte[1]**

[1]*Institut des Neurosciences Cellulaires et Intégratives, Centre National de la Recherche Scientifique, Université de Strasbourg, Strasbourg, France,* [2]*Chronobiotron, Centre National de la Recherche Scientifique, Strasbourg, France,* [3]*Centre d'Evaluation et de Traitement de la Douleur, Hôpitaux Universitaires de Strasbourg, Strasbourg, France,* [4]*Institut de Génétique et de Biologie Moléculaire et Cellulaire, Centre National de la Recherche Scientifique, Université de Strasbourg, INSERM, Illkirch, France*

OPEN ACCESS

Edited by:
Meritxell Canals, University of Nottingham, United Kingdom

Reviewed by:
Jerome Busserolles, Clermont Université, France
Sangsu Bang, Duke University, United States

***Correspondence:**
Dominique Massotte
d.massotte@unistra.fr

†Present address:
Florian Pierre
Institut Européen de Chimie et Biologie, Centre National de la Recherche Scientifique, INSERM, Université de Bordeaux, Pessac, France
Unai Alduntzin
Department of Biochemistry and Molecular Biology, Faculty of Science and Technology, University of the Basque Country, Leioa, Spain

Received: *29 August 2019*
Accepted: *17 December 2019*
Published: *14 February 2020*

Citation:
Ceredig RA, Pierre F, Doridot S, Alduntzin U, Hener P, Salvat E, Yalcin I, Gaveriaux-Ruff C, Barrot M and Massotte D (2020) Peripheral Delta Opioid Receptors Mediate Formoterol Anti-allodynic Effect in a Mouse Model of Neuropathic Pain. Front. Mol. Neurosci. 12:324. doi: 10.3389/fnmol.2019.00324

Neuropathic pain is a challenging condition for which current therapies often remain unsatisfactory. Chronic administration of β2 adrenergic agonists, including formoterol currently used to treat asthma and chronic obstructive pulmonary disease, alleviates mechanical allodynia in the sciatic nerve cuff model of neuropathic pain. The limited clinical data currently available also suggest that formoterol would be a suitable candidate for drug repurposing. The antiallodynic action of β2 adrenergic agonists is known to require activation of the delta-opioid (DOP) receptor but better knowledge of the molecular mechanisms involved is necessary. Using a mouse line in which DOP receptors were selectively ablated in neurons expressing Nav1.8 sodium channels (DOP cKO), we showed that these DOP peripheral receptors were necessary for the antiallodynic action of the β2 adrenergic agonist formoterol in the cuff model. Using a knock-in mouse line expressing a fluorescent version of the DOP receptor fused with the enhanced green fluorescent protein (DOPeGFP), we established in a previous study, that mechanical allodynia is associated with a smaller percentage of DOPeGFP positive small peptidergic sensory neurons in dorsal root ganglia (DRG), with a reduced density of DOPeGFP positive free nerve endings in the skin and with increased DOPeGFP expression at the cell surface. Here, we showed that the density of DOPeGFP positive free nerve endings in the skin is partially restored and no increase in DOPeGFP translocation to the plasma membrane is observed in mice in which mechanical pain is alleviated upon chronic oral administration of formoterol. This study,

Abbreviations: ANOVA, analysis of variance; CGRP, calcitonin gene-related peptide; cKO, conditional knockout; DOP, delta-opioid; DRG, dorsal root ganglion; eGFP, enhanced green fluorescent protein; IENF, intraepidermal nerve fiber; KS, Kolmogorov–Smirnov; KW, Kruskal–Wallis; PWT, paw withdrawal threshold; SNRI, serotonin noradrenaline reuptake inhibitor.

therefore, extends our previous results by confirming that changes in the mechanical threshold are associated with changes in peripheral DOP profile. It also highlights the common impact on DOP receptors between serotonin noradrenaline reuptake inhibitors such as duloxetine and the β2 mimetic formoterol.

Keywords: mechanical allodynia, beta-mimetics, peripheral nerve injury, cuff model, delta opioid receptor, beta adrenergic receptor

INTRODUCTION

Neuropathic pain arises from traumatic nerve injury or from a disease that affects the somatosensory system and is characterized by spontaneous pain, mechanical allodynia and/or thermal hypersensitivity (von Hehn et al., 2012). First-line treatments include antidepressants such as serotonin and noradrenaline reuptake inhibitors (SNRIs), or anticonvulsants such as gabapentinoids (Kremer et al., 2016a). In preclinical studies, activation of the β2-adrenergic receptors has been shown to be mandatory for the antiallodynic action of antidepressants (Yalcin et al., 2009; Kremer et al., 2016a, 2018) and chronic administration of several β2-adrenergic agonists such as formoterol has been successfully used to alleviate mechanical allodynia (Choucair-Jaafar et al., 2009, 2014; Yalcin et al., 2010; Jourdain and Hatakeyama, 2019). Formoterol is already routinely used in clinics to treat chronic obstructive pulmonary disease (Vanfleteren et al., 2018). Also, inhalation of β2-agonists during the perioperative period was associated with a five-fold lower risk of developing post-thoracotomy neuropathic pain whereas chronic antidepressants or chronic gabapentanoids appeared ineffective (Salvat et al., 2015). Drug repurposing could, therefore, be envisaged to treat neuropathic pain.

The mechanisms underlying the relief of mechanical allodynia are the topic of extensive research in various preclinical models but remain unclear. Interestingly, delta-opioid (DOP) receptors are essential for the antiallodynic effect of DOP agonists (Nozaki et al., 2012; Vicario et al., 2016) but also for the antiallodynic effect of chronic administration of both antidepressants (Benbouzid et al., 2008b; Yalcin et al., 2010; Ceredig et al., 2018; Kremer et al., 2018) and β2 mimetics (Yalcin et al., 2010; Choucair-Jaafar et al., 2014). More specifically, our previous work using the cuff model pointed to peripheral DOP receptors expressed in Nav1.8 positive neurons as mandatory for the antiallodynic action of DOP agonists (Gaveriaux-Ruff et al., 2011; Nozaki et al., 2012) as well as the SNRI duloxetine (Ceredig et al., 2018). Our data also revealed that changes in the expression profile of peripheral DOP receptors correlated with mechanical allodynia. Indeed, we observed decreased DOP receptor expression in unmyelinated calcitonin gene-related peptide (CGRP) positive neurons and free nerve endings in the skin and increased surface expression in the neurons still expressing the receptor in neuropathic conditions but not in mice chronically treated with duloxetine after cuff surgery (Ceredig et al., 2018). Here, we sought to determine whether the same mechanisms are triggered by chronic treatment with the β2 adrenergic agonist formoterol by identifying changes in the expression of peripheral DOP receptor using a mouse line in which peripheral DOP receptors are selectively ablated in neurons expressing the Nav1.8 sodium channel (DOP cKO; Gaveriaux-Ruff et al., 2011) and a knock-in mouse line expressing DOP receptors fused to the green fluorescent protein eGFP (DOPeGFP; Scherrer et al., 2006). Our data indicate that peripheral DOP receptors expressed in Nav1.8+ neurons were mandatory for formoterol anti-allodynic activity. DOP surface expression was lower in animals treated with chronic formoterol compared to neuropathic conditions. However, DOP receptor expression was only partially restored in nerve free endings in the skin and remained similar to the neuropathic conditions in the dorsal root ganglia (DRG) after chronic formoterol. Altogether, data suggest that antidepressants and β2 mimetics effects engage similar DOP-dependent mechanisms.

MATERIALS AND METHODS

Animals

DOPeGFP knock-in mice expressing the DOP receptor infusion with the green fluorescent protein were generated by homologous recombination. In these animals, the eGFP cDNA preceded by a five amino acid linker (G-S-I-A-T) was introduced into the exon 3 of the DOP receptor gene, in the frame and 5' from the stop codon (Scherrer et al., 2006). The genetic background of DOPeGFP mice was C57BL/6J:129SvPas (50%:50%). DOP-floxed (*Oprd1fl/fl*) mice were interbred with Nav1.8-Cre mice to generate conditional knockout (cKO) of DOP in primary nociceptive neurons (Nav1.8-Cre × *Oprd1fl/fl* or DOPcKO) as previously reported (Gaveriaux-Ruff et al., 2011). The genetic background of conditional DOP knock-out mice and their floxed controls was C57BL/6J:129SvPas (62.5%:37.5%). These mice were bred at the ICS animal facility, Illkirch, France, and kindly provided by Pr. Claire Gavériaux-Ruff. Adult male and female mice aged 6–20 weeks, weighing 20–32 g for females and 20–38 g for males were used. Animals from independent cohorts were distributed at best to provide groups of similar size for each gender and treatment (n = 88 DOPeGFP mice, n = 22 DOPcKO mice, n = 20 DOP-floxed mice). Mice were group-housed 2–5 per cage, under standard laboratory conditions (12 h dark/light cycle, lights on at 7 am) in temperature (21 ± 1°C) and humidity (55 ± 10%) controlled rooms with food and water *ad libitum*. All experiments were approved by the "Comité d'Ethique en Matière d'Expérimentation Animale de Strasbourg" [authorization number 201503041113547 *(APAFIS#300).02*] and

conducted in agreement with the EU Directive 2010/63/EU for animal experiments.

Neuropathic Pain Model

Neuropathic pain was induced by cuffing the main branch of the right sciatic nerve as previously described (Benbouzid et al., 2008c; Yalcin et al., 2014). Before surgeries, mice were anesthetized with ketamine (Vibrac, Carros, France)/xylazine (Rompun, Kiel, Germany; 100/10 mg/kg, i.p.). The common branch of the right sciatic nerve was exposed, and a cuff of PE-20 polyethylene tubing (Harvard Apparatus, Les Ulis, France) of standardized length (2 mm) was unilaterally inserted around it (Cuff group). Sham-operated animals underwent the same surgical procedure without cuff implantation (Sham group). Animals were placed on their left side in a clean home cage immediately after surgery and kept under the heat lamp until they awoke. Water and chow were placed directly in the home cage. The surgical site was checked daily during the next 3 days, and animals were monitored for signs of unusual suffering or infection with endpoints defined in agreement with the recommendations of the ethical committee.

Assessment of Mechanical Allodynia

Mechanical allodynia was tested using von Frey filaments and results were expressed in grams as described in Yalcin et al. (2014). Briefly, calibrated von Frey filaments (Bioseb, Vitrolles, France) were applied to the plantar surface of each hind paw until they just bent, in a series of ascending forces up to the mechanical threshold. Filaments were tested five times per paw and the paw withdrawal threshold (PWT) was defined as the lower of two consecutive filaments for which three or more withdrawals out of the five trials were observed (Yalcin et al., 2014).

Treatment Procedures

Treatment with the β2-adrenergic agonist formoterol began 4 weeks after the surgical procedure and lasted 4 weeks. Formoterol (Cat. Nr BG0369, Biotrend AG, Switzerland) was delivered by *ad libitum* access and as sole source of fluid dissolved in drinking water at a dose of 0.5 μg/ml (equivalent to 0.05 mg/kg/day) with 0.2% saccharin (Cat. Nr S1002, Sigma Aldrich, St Louis, MO, USA). Experimental groups for DOPeGFP mice included the Sham group (n = 36, 29 females and seven males), Cuff group (n = 29, 16 females and 13 males), and Formoterol group corresponding to Cuff mice treated with formoterol (n = 23, 14 females and nine males). Experimental groups for DOP cKO mice included Sham group (n = 6, two females and four males), Cuff group (n = 5 males), and Formoterol group corresponding to Cuff mice treated with formoterol (n = 11, seven females and four males). Experimental groups for control littermates *Oprd1fl/fl* (floxed mice) included Sham group (n = 7, five females and two males), Cuff group (n = 5 males), and Formoterol group corresponding to Cuff mice treated with formoterol (n = 8, two females and six males). Sham and Cuff groups both received control saccharin solution 0.2% in drinking water. Sham and Cuff groups were identical to those published previously in Ceredig et al. (2018).

Tissue Preparation and Immunohistochemistry

Mice were anesthetized with ketamine (Vibrac, Carros, France)/xylazine (Rompun, Kiel, Germany; 100/10 mg/kg, i.p.) and perfused intracardially with 100 ml of ice-cold (2–4°C) 4% paraformaldehyde (PFA) in phosphate buffer 0.1 M pH 7.4 (PB). Ipsilateral (right) and contralateral (left) L4 to L6 lumbar DRG were dissected out and post-fixed for 90–120 mins at 4°C in 4% PFA in PB, cryoprotected at 4°C in 30% sucrose in PB for 24 h, embedded in OCT (Optimal Cutting Temperature medium, Thermo Fisher Scientific, Waltham, MA, USA), frozen and kept at −80°C. DRG longitudinal sections (16 μm thick) were cut with a cryostat (Microm Cryo-star HM560) and kept floating in PB.

Immunohistochemistry was performed according to standard protocols as previously described in Ceredig et al. (2018). Briefly, DRG sections were incubated for 1 h at room temperature (RT) in the blocking solution consisting of PB with 0.2% Tween 20 (PBT; Cat. Nr 85114, Thermo Fisher Scientific, Waltham, MA, USA), 3% normal goat serum (Invitrogen, Paisley, UK) and 3% donkey serum when needed (D9663 Sigma-Aldrich, St Quentin Fallavier, France). The sections were then incubated overnight at 4°C in the blocking solution with the appropriate primary antibodies: polyclonal rabbit anti-GFP (Cat. Nr A-11122, Invitrogen, dilution 1:1,000), sheep polyclonal anti-CGRP (Cat. Nr. AB 22560, Abcam, dilution 1:2,000). Three washes were performed with PBT before sections incubated for 2 h at RT in dim light with goat anti-rabbit IgG conjugated with Alexa Fluor 488 (Cat. Nr A-11012, Molecular Probes, dilution 1:2,000) and donkey anti-sheep IgG conjugated with Alexa Fluor 594 (Cat. Nr A-11016, Molecular Probes, dilution 1:2,000). Following three washes with PBT, the sections were mounted with MOWIOL (Calbiochem, Darmstadt, Germany) and 4,6-diamino-phenylindole (DAPI; Roche Diagnostic, Mannheim, Germany; 0.5 μg/ml).

Plantar skin of both hind paws (footpad and glabrous skin, 1 cm long) were fixed at 4°C in 4% PFA solution overnight, cryoprotected overnight with 30% sucrose in PB, embedded in OCT, frozen and kept at −80°C. Longitudinal cross-sections (50 μm thickness) were cut with a cryostat (MicromCryo-star HM560) and kept floating in PB. Paw tissue samples were then processed to visualize primary afferent terminals in the skin of the hind paw as previously described in Ceredig et al. (2018). Briefly, sections were treated with 0.3% H_2O_2, dehydrated with successive baths in ethanol then rehydrated, washed 3 times with PBS and incubated in blocking solution (PBS, 0.5% Triton X100 (PBST) with 3% normal goat serum or normal donkey serum) for 30 min at RT. After overnight incubation at 4°C in the blocking solution, the sections were incubated with the primary antibodies against anti-GFP (1:1,000) or anti-CGRP (1:2,000) antibody. The sections were then washed three times with PBST, respectively incubated for 2 h at RT with anti-rabbit or anti-goat biotinylated secondary antibody (1:400) in PBST and washed

again three times with PBST before staining with Vector SG (Sk-4700, VectorLab). Samples were mounted with MOWIOL.

Image Acquisition and Analysis

Image acquisition and analysis were performed as previously described in Ceredig et al. (2018). Briefly, images were acquired with the Leica TCS SP5 confocal microscope using a 20× dry objective (Numerical Aperture: 0.7), the 40× resolution was achieved with a digital zoom factor. Confocal acquisitions in the sequential mode (single excitation beams: 405, 488 and 568 nm) were used for marker co-localization to avoid potential crosstalk between the different fluorescence emissions. Images were acquired with the LCS (Leica) software using randomly selected sections.

The ImageJ® software cell counter (approximately 15 non-adjacent sections per condition and per animal) was used to count on-screen neurons expressing a given fluorescent marker manually and blindly. Threshold was applied to fluorescence detection. Only neurons from L4-L6 DRGs with a visible nucleus were considered. Cells expressing a given marker and eGFP fluorescence were analyzed separately. During the analysis, we recorded all cross-sectional areas of cell profiles for each marker. No difference was observed in the distribution of the neuronal populations between male and female mice and data were pooled for subsequent analysis.

DOPeGFP subcellular distribution was expressed as a ratio of membrane-associated vs. cytoplasmic fluorescence densities determined as previously described (Erbs et al., 2016). Acquisitions using 63× (NA: 1.4) oil objective were performed to determine DOPeGFP subcellular distribution. Briefly, quantification of internalization was performed using the ImageJ software on 8-bit raw confocal images from neurons randomly sampled. Nuclear fluorescence was used to define the background level (no threshold was applied). Cytosolic fluorescence intensity was subtracted from whole-cell fluorescence intensity to obtain surface fluorescence intensity. Fluorescence intensity values were divided per surface unit (pixel) to obtain densities. Ratio of membrane-associated (Df memb) vs. cytoplasmic (Df cyto) fluorescence densities was calculated to normalize data across neurons examined. A value of 1.0 results from equal densities of DOPeGFP at the cell surface and in the cytoplasm.

Free nerve endings in the glabrous part of the skin were visualized using a 20× dry objective (Nikon Eclipse 80i). Counting on blinded samples was performed manually on screen using the Neurolucida software (V.10 MBF Bioscience) on at least four randomly chosen sections per animal. Density was obtained by dividing the number of afferents crossing the dermal-epidermal junction excluding secondary branching, by the total length of the section (Lauria et al., 2005).

Statistical Analysis

Behavioral analysis of von Frey testing was performed using Statistica v12 (StatSoft, France) and Graph-Pad Prism v7 (GraphPad, San Diego, CA, USA). Changes in the PWT, as a function of post-operative time (within factor) and experimental treatment (between factor), were analyzed using two-way ANOVA with repeated measures (two-way rANOVA) analysis followed by Tukey HSD *post hoc* test. Baseline PWT in males and females were compared using a two-sample student's *t*-test. Exact *p*-values below 0.0001 were not provided for behavioral data (Graph-Pad Prism v7, GraphPad, San Diego, CA, USA). For cross-sectional area measurements, data were pooled per treatment group for each marker (CGRP or eGFP). In all groups, cross-sectional areas were found not normally distributed (p-value always $< 10^{-8}$, Shapiro–Wilk test) using R (R Core Team, 2017). Sums of Gaussian functions were therefore adapted to the relative cumulative distribution curve of cell size, using non-linear least-square curve fitting (with nls2, nlstools and pracma R packages). Data were expressed as cumulative distributions to allow direct determination of the mean and standard error by adjusting the function of repartition on the experimental points. We compared the cumulative distributions for the various groups using the non-parametric Kolmogorov–Smirnov test (R). Treatment impact in DOPeGFP+ bins was analyzed using multiple *t*-tests. Statistical analysis of DOPeGFP subcellular distribution and skin fiber was performed with one-way ANOVA followed by Tuckey HSD *post hoc* test (Graph-Pad Prism v7, GraphPad, San Diego, CA, USA). Co-localization of DOPeGFP with neuronal markers in small size neurons ($<300\ \mu m^2$) was analyzed using the non-parametric Kruskal–Wallis test followed by Dunn's *post hoc* test.

RESULTS

Chronic Formoterol Requires DOP Receptors Expressed in Nav1.8+ Neurons for Anti-allodynic Action

We previously established that mechanical allodynia is induced by cuff-implantation, developed directly after surgery and was maintained until up to 12–14 weeks (Yalcin et al., 2011). Also, DOP receptors expressed in Nav1.8+ neurons were shown to be mandatory for the anti-allodynic action of the antidepressant duloxetine in the cuff model (Ceredig et al., 2018). Since DOP receptors are also required for the anti-allodynic effect of a chronic treatment with the β2 agonist clenbuterol (Yalcin et al., 2010), we investigated whether the specific deletion of DOP receptors in primary afferents (peripheral DRG neurons) expressing Nav1.8 voltage-gated sodium channels (DOPcKO; Gaveriaux-Ruff et al., 2011) was also abolishing the antiallodynic action of a β2-adrenergic agonist.

Von Frey testing revealed that sciatic nerve cuffing resulted in unilateral mechanical allodynia in DOPcKO and control floxed (DOP*fl/fl)* animals (**Figures 1A,B**) as previously reported (Ceredig et al., 2018). Cuff DOPcKO mice did not recover after formoterol treatment in drinking water (50 μg/ml; two-way rANOVA, interaction treatment × time $F_{(12,114)} = 11.31$, $p < 0.0001$, effect of time $F_{(6,114)} = 33.37$, $p < 0.0001$, effect of treatment $F_{(2,19)} = 112.8$, $p < 0.0001$, Tukey HSD *post hoc* test: formoterol treatment from day 28 to 39 vs. Sham, $p < 0.0001$ at each time-point; **Figure 1A**), whereas control DOP*fl/fl* Cuff animals treated with formoterol returned

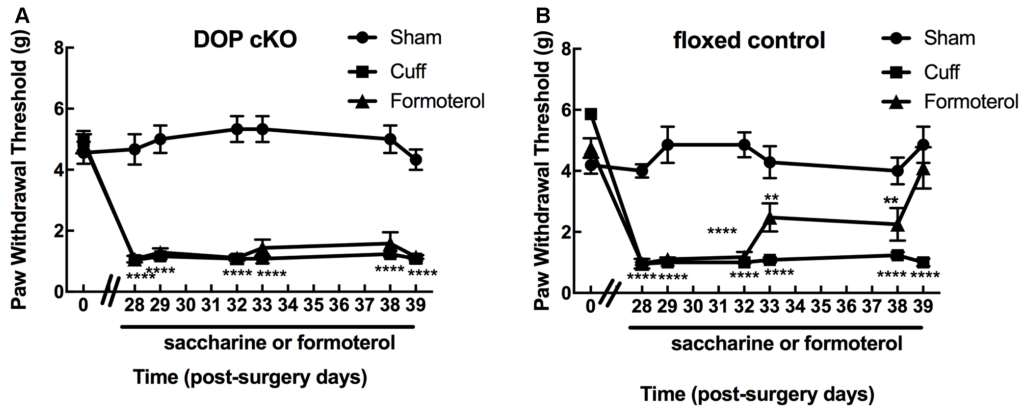

FIGURE 1 | Expression of delta-opioid (DOP) receptors in Nav1.8+ neurons was mandatory for oral formoterol anti-allodynic action. The right (ipsilateral) hind paw mechanical threshold was tested using von Frey calibrated filaments. Following cuff implantation surgery, animals had lowered paw withdrawal thresholds (PWT), displaying sustained mechanical allodynia. Formoterol (0.5 μg/ml) or saccharin 0.2% control *per* os treatments started 4 weeks after nerve injury and were maintained for 3 weeks. **(A)** Mechanical threshold of the right (ipsilateral) hind paw in DOP cKO mice. Data from three separate experiments (each including the three conditions) were pooled and are expressed as means ± SEM. Sham (n = 6), Cuff (n = 5), Cuff treated with formoterol (n = 11). Two-way rANOVA and Tukey HSD *post hoc* test: ****$p < 0.001$ formoterol treatment vs. baseline. **(B)** Mechanical threshold of the right (ipsilateral) hind paw in control floxed mice. Data from three separate experiments (each including the three conditions) were pooled and are expressed as means ± SEM. Sham (n = 7), Cuff (n = 5), Cuff treated with formoterol (n = 8). Two-way rANOVA and Tukey HSD *post hoc* test: ****$p < 0.0001$, **$p < 0.01$ formoterol treatment day 39 vs. baseline: $p = 0.3284$.

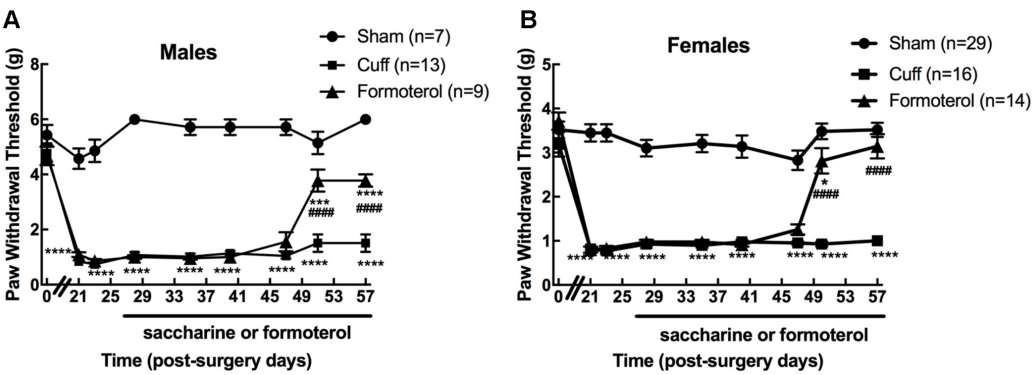

FIGURE 2 | Chronic formoterol treatment *per os* relieved mechanical allodynia in DOPeGFP knock-in mice. The right (ipsilateral) hind paw mechanical threshold was tested using von Frey calibrated filaments in male and female DOPeGFP KI mice. Males **(A)** and females **(B)** had lowered PWT following cuff implantation surgery, i.e., sustained mechanical allodynia. Four weeks after nerve injury, formoterol (0.5 μg/ml) or saccharin 0.2% control *per* os treatments started and were maintained for 4 weeks. Data from three separate experiments (each including the three conditions) were pooled and are expressed as means ± SEM. Sham (n = 7 males and 29 females), Cuff (n = 13 males and 16 females), Cuff treated with formoterol (n = 9 males and 14 females). Two-way rANOVA and Tukey HSD *post hoc* test: *$p < 0.05$, ***$p < 0.001$, ****$p < 0.0001$ vs. Sham. #### $p < 0.001$ vs. Cuff.

to baseline values at day 39, after 11 days of formoterol administration (two-way rANOVA interaction treatment × time $F_{(12,119)} = 8.386$, $p < 0.0001$, effect of time $F_{(6,119)} = 18.56$, $p < 0.0001$, effect of treatment $F_{(2,119)} = 84.47$, $p < 0.0001$, Tukey HSD *post hoc* test: formoterol treatment vs. Sham: $p < 0.0001$ from day 28 to 32, $p < 0.01$ from day 33 to day 38, $p = 0.33$ on day 39; **Figure 1B**). Our result therefore established that DOP receptors in Nav1.8 positive neurons were mandatory to alleviate mechanical allodynia upon chronic treatment with the β2 mimetic formoterol. We thus assessed in more detail the impact of chronic formoterol treatment on neuronal populations expressing the DOP receptor using the DOPeGFP fluorescent knock-in mouse line.

Chronic Formoterol Alleviates Cuff-Induced Mechanical Allodynia in DOPeGFP Mice

We first verified that oral administration of the β2 adrenergic agonist-induced the expected anti-allodynic effect in the DOPeGFP knock-in mouse line. As previously reported (Ceredig et al., 2018), males had significantly higher baseline mechanical thresholds compared to females (5.4 ± 0.4 g for males vs.

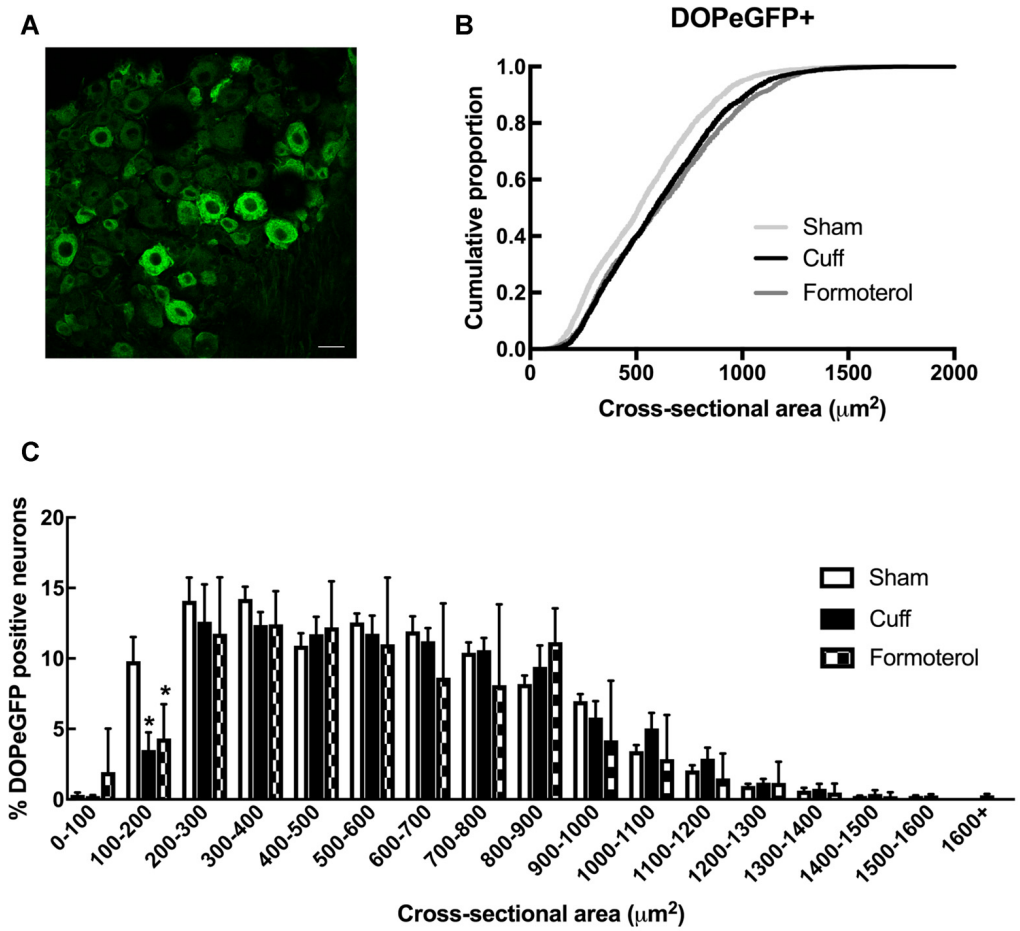

FIGURE 3 | DOPeGFP distribution in Sham, Cuff and Formoterol-treated animals. **(A)** Representative confocal image of fluorescent DOPeGFP expressing neurons in lumbar dorsal root ganglia (DRG) of sham animals. Scale bar 10 μm. **(B)** Distribution of DOPeGFP+ neuronal populations in Sham (3,080 neurons, $n = 7$ animals; light gray), Cuff (3,123 neurons, $n = 6$ animals; black) and Formoterol (1,917 neurons, $n = 5$ animals; dark gray) groups. **(C)** Categorical data plot of the size distribution for DOPeGFP positive neuron cross-sectional areas in Sham (white bars), Cuff (black bars) and Formoterol (checked bars) groups. Multiple *t*-tests: $^*p = 0.03$ Cuff vs. Sham, $^*p = 0.01$ Formoterol vs. Sham.

3.5 ± 0.2 g for females, student's *t*-test for baseline values: $t = 7.18$ $p < 0.0001$) and cuff implantation induced ipsilateral mechanical allodynia which lasted for at least 8 weeks (time of perfusion) in either sex (two-way rANOVA; males interaction treatment × time $F_{(16,208)} = 15.15$, $p < 0.0001$; effect of treatment, $F_{(2,26)} = 318.5$, $p < 0.0001$ from day 21 to 57 Cuff vs. Sham; females interaction treatment × time $F_{(16,448)} = 11.02$, $p < 0.0001$, effect of treatment $F_{(2,56)} = 236$, $p < 0.0001$ from day 21 to 57 Cuff vs. Sham; **Figures 2A,B**). We did not detect any change in the nociceptive threshold after sham surgery or in the contralateral hind paw of Cuff animals (data not shown).

Formoterol treatment in drinking water (50 μg/ml) relieved mechanical allodynia at day 51 (following 23 days administration) in DOPeGFP males although not fully (two-way rANOVA Tukey HSD *post hoc* test: day 51 vs. Sham: $p_{(Males)} = 0.0009$ and day 57 vs. Sham: $p_{(Males)} < 0.0001$, day 51 and day 57 vs. Cuff: $p_{(Males)} < 0.0001$; **Figure 2A**). In DOPeGFP females, formoterol treatment-induced almost complete relief at day 51 (two-way rANOVA Tukey HSD *post hoc* test: day 51 vs. Sham: $p_{(Females)} = 0.0382$) and values were similar to sham mice at day 57 (two-way rANOVA Tukey HSD *post hoc* test: day 57 vs. Sham: $p_{(Females)} = 0.3547$, day 51 and day 57 vs. Cuff: $p_{(Females)} < 0.0001$; **Figure 2B**). This time course was similar to what we previously observed, in the same model, in male C57BL6/J mice repeatedly injected i.p. twice daily (Yalcin et al., 2010).

DOPeGFP Expression in Formoterol-Treated Mice

We then examined changes in the distribution of DOPeGFP+ neurons in the DRG (**Figure 3A**). As previously established (Ceredig et al., 2018), the cumulative distribution of DOPeGFP+ cells in the Cuff experimental groups was shifted towards larger cell size values compared to the Sham group (**Figure 3B**). The loss of DOPeGFP+ neurons with small cross-sectional areas (Multiple *t*-tests: Cuff vs. Sham: $p = 0.03$ for the 100–200 μm^2 category)

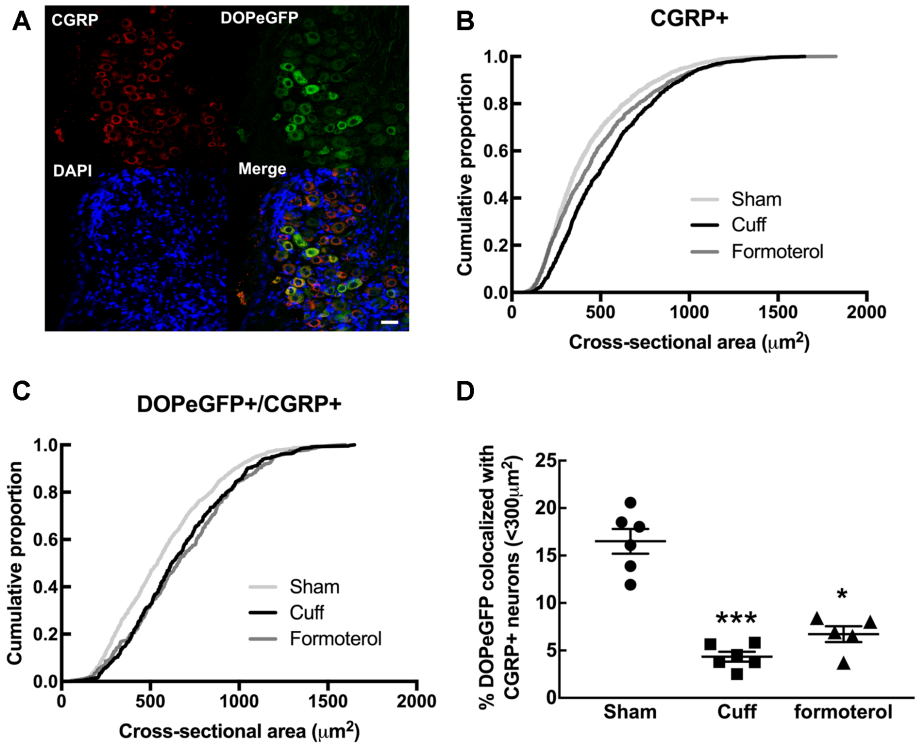

FIGURE 4 | Impact of formoterol treatment on DOPeGFP colocalization with CGRP+ populations. **(A)** Representative fluorescence micrographs showing DOPeGFP co-localization with the neuronal marker calcitonin gene-related peptide (CGRP; red) as indicated by arrows in the overlay figure. Nuclei are stained with DAPI (blue). Scale bar 10 μm. **(B)** Distribution of CGRP+ neuronal populations in Sham (3,351 neurons, $n = 7$ animals; light gray), Cuff (1,331 neurons, $n = 6$ animals; black), and Formoterol (1,311 neurons, $n = 5$ animals; dark gray). **(C)** Distribution of neuronal populations co-expressing DOPeGFP and CGRP in Sham (803 neurons, $n = 7$ animals; light gray), Cuff (438 neurons, $n = 6$ animals; black) and Formoterol (294 neurons, $n = 5$ animals; dark gray) groups. **(D)** Percentage of cells co-expressing DOPeGFP and CGRP in neurons with areas <300 μm² in Sham ($n = 6$; ●), Cuff ($n = 6$; ■) or Formoterol ($n = 5$; ▲) animals. Values expressed as mean ± SEM. Kruskal–Wallis test and Dunn's *post*-test: $^{*}p < 0.05$, $^{***}p < 0.001$ vs. Sham.

indicated a loss of DOPeGFP expression in small and/or medium neurons following 8 weeks of neuropathy (**Figure 3C**).

In Cuff mice chronically treated with formoterol, the distribution of the DOPeGFP+ neuronal populations remained very similar to the Cuff condition and was significantly different from the Sham group (KS test: $D = 0.14212$, $p < 2.2\ 10^{-16}$; **Figure 3B**). Indeed, the percentage of small size neurons remained lower compared to the Sham condition (Multiple *t*-tests: Formoterol vs. Sham: $p = 0.0137$ for the 100–200 μm² category; **Figure 3C**).

Since DOPeGFP expression was decreased in unmyelinated peptidergic populations in Cuff mice (**Figure 3**) and (Ceredig et al., 2018), we assessed the consequence of chronic formoterol treatment on the global CGRP+ population and on the proportion of the CGRP+ population also expressing DOPeGFP (**Figure 4**). The cumulative distribution corresponding to CGRP+ neurons showed that the shift towards larger cell size values in the Cuff group is no longer present for the smallest cross-sectional areas after treatment with formoterol although the overall distribution remained significantly distinct from the Sham group (KS test: $D = 0.090945$, $p = 3.398\ 10^{-7}$; **Figure 4B**). However, the cumulative distribution of the CGRP+DOPeGFP+ neurons remained similar to the cuff condition and was significantly different from the Sham condition (KS test: $D = 0.15672$, $p < 2.2\ 10^{-16}$; **Figure 4C**) with the proportion of small size neurons (<300 μm²; 6.7 ± 0.8%) remaining similar to the Cuff condition (4.3 ± 0.5%) and lower compared to the Sham condition (16.5 ± 1.3%; KW test: $p < 0.0001$, Dunn's *post hoc* test Sham vs. Cuff $p = 0.0007$, Sham vs. Formoterol $p = 0.0352$, Cuff vs. Formoterol $p > 0.9999$; **Figure 4D**). Therefore, chronic treatment with formoterol did not appear to restore the loss of DOPeGFP+ neurons induced by the neuropathic condition in small peptidergic neurons.

DOPeGFP Expression at the Plasma Membrane in Formoterol-Treated Mice

Enhanced DOP expression at the plasma membrane was previously described in neuropathic conditions (Gendron et al., 2015). This observation was confirmed in the cuff model by showing that the ratio of fluorescence associated with the cell surface was significantly increased compared to the fluorescence associated with the intracellular compartments in the DOPeGFP+ neurons (**Figure 5**) as also previously reported (Ceredig et al., 2018). Formoterol treatment decreased membrane-associated fluorescence to values which were even lower than those of neurons in the Sham condition (Sham

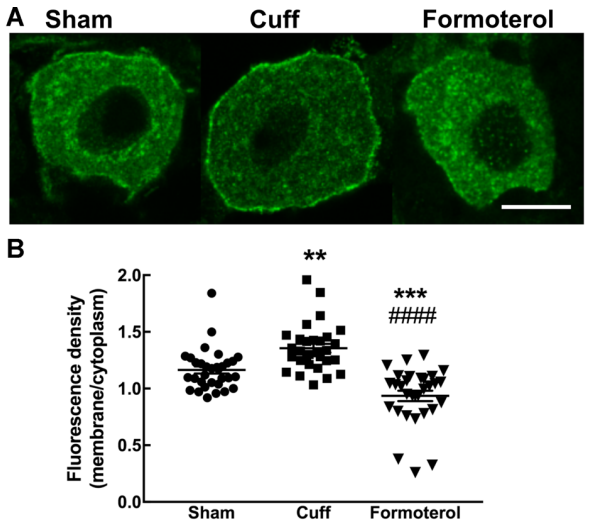

FIGURE 5 | DOPeGFP expression at the cell surface in Formoterol-treated mice. **(A)** Representative fluorescence micrographs of DOPeGFP-positive neuron in Sham, Cuff and cuff animals treated with formoterol. Scale bar 10 μm. **(B)** DOPeGFP subcellular distribution was increased in neuropathic conditions and reduced after formoterol treatment compared to Sham. Data are expressed as means ± SEM (Sham: $n = 32$ cells from four animals, Cuff: $n = 30$ cells from three animals, Formoterol: $n = 30$ cells from three animals). One-way ANOVA and Tukey HSD *post hoc* test: $^{**}p < 0.01$, $^{***}p < 0.001$ vs. Sham and $^{\#\#\#\#}$ $p < 0.0001$ vs. Cuff, $p > 0.5$ Formoterol vs. Cuff.

1.16 ± 0.03, Cuff: 1.35 ± 0.04, formoterol 0.94 ± 0.05, one-way ANOVA $F_{(2,89)} = 28.8$ $p < 0.0001$ Tukey HSD *post hoc* test Cuff vs. Sham $p = 0.002$, Cuff vs. Formoterol $p < 0.0001$, Sham vs. Formoterol $p = 0.0002$; **Figure 5B**). This indicates that treatment with formoterol suppressed the increase in DOP receptor surface expression observed in neuropathic mice.

CGRP and DOPeGFP Expression in the Skin of Formoterol Treated Mice

A decrease in CGRP+ intra-epidermal nerve fiber (IENF) fiber length and density, as well as decrease in DOPeGFP+ IENF density, was reported 8 weeks post cuff surgery (Nascimento et al., 2015; Ceredig et al., 2018). We thus assessed whether treatment with formoterol impacted CGRP+ and DOPeGFP+ IENFs (**Figure 6**). The density of CGRP+ IENFs in the glabrous skin of the hind paw of cuffed mice treated with formoterol remained at a level comparable to the Cuff group (one-way ANOVA $F_{(2,8)} = 49.15$, $p < 0.0001$; Tukey HSD *post hoc* test Sham vs. Cuff $p < 0.0001$, Sham vs. Formoterol $p < 0.0001$, Cuff vs. Formoterol $p = 0.771$; **Figure 6B**). The density of DOPeGFP+ IENFs was higher in formoterol treated animals compared to the Cuff group but remained significantly lower compared to the Sham condition [one-way ANOVA $F_{(2,9)} = 371$, $p < 0.0001$; Tukey HSD *post hoc* test Sham vs. Cuff $p < 0.0001$, Sham vs. Formoterol $p < 0.0001$, Cuff vs. Formoterol $p = 0.0008$ (**Figure 6C**)]. As a whole, chronic formoterol treatment did not restore CGRP+ expression and induced partial recovery of DOPeGFP expression in the IENFs.

DISCUSSION

We first showed that oral administration of the β2 adrenergic agonist formoterol was as effective as its intraperitoneal injection (Yalcin et al., 2010) to alleviate mechanical allodynia in the cuff model of neuropathy. We then identified peripheral DOP receptors as mandatory for the antiallodynic effect and determined the impact of chronic formoterol on the expression of DOP receptors in the lumbar DRGs and skin IENFs.

Several studies pointed to the role of DOP receptors, and more specifically peripheral DOP receptors present in Nav1.8+ neurons, to counteract mechanical allodynia in neuropathic conditions induced by sciatic nerve ligation (Nadal et al., 2006; Gaveriaux-Ruff et al., 2011; Nozaki et al., 2012). Previous work by the group established that the antiallodynic action of chronic tricyclic antidepressant and SNRI treatments require DOP and β2 adrenergic receptors (Yalcin et al., 2010; Choucair-Jaafar et al., 2014; Kremer et al., 2018). Systemic administration of the DOP antagonist naltrindole also blocked the antiallodynic action of chronic administration of β2 adrenergic agonists (Yalcin et al., 2010; Choucair-Jaafar et al., 2014). In the case of the SNRI duloxetine, peripheral DOP receptors expressed in Nav1.8+ neurons were mandatory for the antiallodynic effect as no recovery was observed in the DOP cKO mouse line in which peripheral DOP receptors were selectively ablated in neurons expressing the Nav1.8 sodium channel (Ceredig et al., 2018). Here, we showed that peripheral DOP receptors expressed in Nav1.8+ neurons were also mandatory for the β2-adrenergic agonist formoterol to alleviate mechanical allodynia. Our results, therefore, establish that peripheral DOP receptors, likely located on C nociceptors, are necessary for the effective antiallodynic effect of the two chronic treatments. They also suggest that DOP receptor expression is modulated by the noradrenergic component of SNRIs.

In our previous work, we have characterized changes in DRG neuronal populations in the neuropathic condition resulting from sciatic nerve cuffing (Ceredig et al., 2018). Our main findings highlighted a decrease in the proportion of small size peptidergic neurons (≤300 μm^2) and IENFs expressing DOPeGFP 8 weeks after cuff surgery as well as increased DOPeGFP expression at the plasma membrane (Ceredig et al., 2018), suggesting that these changes may contribute to control mechanical nociception. Here, we showed that chronic formoterol administration promoted partial recovery of DOPeGFP expression in free nerve endings in the skin but not in small CGRP+ neurons in the DRGs. This contrasts with the higher DOPeGFP expression found in small unmyelinated peptidergic neurons (≤300 μm^2) following chronic duloxetine administration. The reason for this difference is unknown but it could correspond to the use of a suboptimal dose of formoterol as also suggested by the dose-response curve performed using intraperitoneal injections (Yalcin et al., 2010). It is indeed unlikely to depend on the serotoninergic component of the SNRI action since selective serotonin reuptake inhibitors did not alleviate mechanical allodynia (Benbouzid et al., 2008a). Our results, however, confirmed that

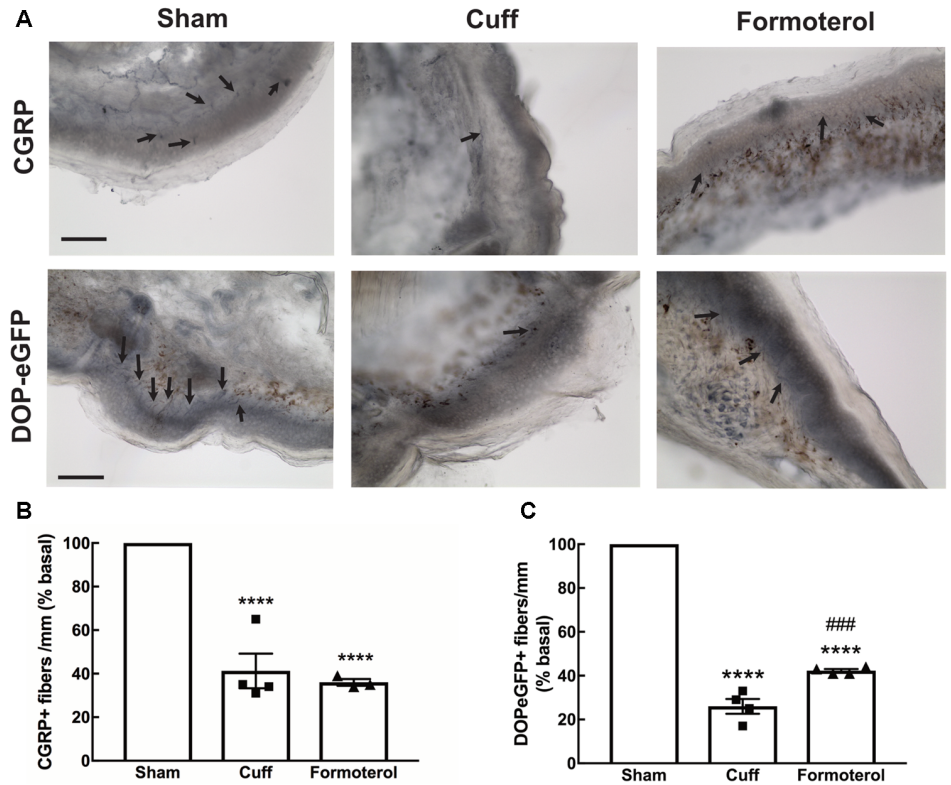

FIGURE 6 | Density of CGRP+ and DOPeGFP+ free nerve endings in the skin. Representative micrograph of **(A)** CGRP or DOPeGFP intra-epidermal nerve fiber (IENF) labeling in the skin of Sham, Cuff and cuff animals treated with formoterol (black arrows). Scale bar 10 μm. **(B)** The density of CGRP+ free nerve endings in the glabrous skin of the right hind paw was decreased in Cuff animals and Cuff animals treated with formoterol. Data are expressed as means ± SEM, $n = 4$ mice for Sham and Cuff and $n = 3$ for Formoterol. One-way ANOVA and Tukey HSD *post hoc* test: $^{****}p < 0.0001$ vs. Sham. **(C)** The density of DOPeGFP+ free nerve endings in the glabrous skin of the right hind paw was decreased in Cuff animals and only partially restored in Cuff animals treated with formoterol compared to Sham. Data are expressed as means ± SEM, $n = 4$ mice per condition. One-way ANOVA and Tukey HSD *post hoc* test: $^{****}p < 0.0001$ vs. Sham, $^{###}p < 0.001$ vs. Cuff.

DOP expression in the nerve terminals, likely unmyelinated peripheral axons of C mechanonociceptors (Brederson and Honda, 2015) appeared a primary determinant of mechanical sensitivity and might constitute a valuable marker of the neuropathic state.

Chronic pain was shown to increase DOP receptor translocation to the plasma membrane in the DRGs (reviewed in Gendron et al., 2015) and our data showed a similar increase in DOPeGFP surface expression in the cuff model. Chronic formoterol was associated with low DOP receptor expression at the plasma membrane that was even below values observed in the sham condition. The low DOPeGFP expression at the surface was also observed in mice chronically treated with duloxetine (Ceredig et al., 2018) and, therefore, seems a common mechanism by which the two antiallodynic treatments counteract mechanical hypersensitivity. The underlying mechanisms, however, remain elusive. DOP and β2 adrenergic receptors have been proposed to form heteromers based on studies performed in co-transfected cells (Jordan et al., 2001). However, β2 adrenergic receptors are expressed in satellite cells in the DRGs (Bohren et al., 2013) whereas DOP dependent analgesia is mediated at the neuronal level (Gaveriaux-Ruff et al., 2011; Ceredig et al., 2018; this work) and is independent of microglial activation (Mika et al., 2014) which precludes direct molecular interactions. The delayed antiallodynic action of both formoterol and duloxetine suggests that it requires cellular adaptations to take place. Lesion of peripheral noradrenergic fibers with guanethidine, a toxin that does not cross the blood brain barrier abolished the antiallodynic action of duloxetine (Kremer et al., 2018) supporting common involvement of peripheral β2 adrenergic receptors. Formoterol (Bohren et al., 2013) as well as antidepressants (Kremer et al., 2018) counteracted the increase in TNFα associated with neuropathic pain and downregulated the activity of the glial NFκB-TNFα pathway, a key regulator of proinflammatory cytokine production (Leung and Cahill, 2010). However, this anti-neuroinflammatory action is also shared by gabapentinoids that do not need opioid receptors for their antiallodynic action (Kremer et al., 2016b). This rather supports a view in which the anti-neuroinflammatory effect and the modulation of DOP expression and activity are not directly related.

There are few clues as to which DOP-dependent mechanisms mediate the anti-allodynic action following formoterol or SNRI chronic treatment. Current data point to an indirect effect through increased endogenous opioid peptide release by the native and adaptative immune systems, which can activate neuronal opioid receptors to alleviate mechanical allodynia

(Binder et al., 2004; Celik et al., 2016). Indeed, noradrenergic sprouting consequent to nerve injury would activate the β2-adrenoceptors expressed by immune cells and promote the release of enkephalin, dynorphin and β-endorphin by these cells (Binder et al., 2004; Celik et al., 2016; Pannell et al., 2016). Similarly, enkephalins are also present in the skin (Slominski et al., 2011). Moreover, sympathetic fiber sprouting is known to take place in the skin in the cuff model (Nascimento et al., 2015) and is located close to cells expressing β2 adrenergic receptors and β-endorphin in inflamed paw tissue providing a way to activate not only MOP but also DOP receptors (Binder et al., 2004). Activation of DOP receptors could, in turn, induce pain relief by reducing Nav1.8 channel activity *via* inhibition of p38 mitogen-activated protein kinase as described for Nav1.7 channels in a rat model of diabetic neuropathy (Chattopadhyay et al., 2008).

In summary, our work established that DOP receptors expressed in Nav1.8+ neurons were mandatory for the anti-allodynic action of chronic treatment with the β2 adrenergic agonist formoterol. It also revealed that chronic formoterol partially reversed the loss of peripheral DOP receptors in the skin and counteracted enhanced DOP expression at the plasma membrane. Our study thus adds to current literature pointing to potential interest in repositioning β2 adrenergic agonists for the treatment of neuropathic pain.

DATA AVAILABILITY STATEMENT

Images and raw data will be available upon request to the corresponding author.

ETHICS STATEMENT

All experiments were approved by the "Comité d'Ethique en Matière d'Expérimentation Animale de Strasbourg" [authorization number 201503041113547 (APAFIS#300).02] and conducted in agreement with the EU Directive 2010/63/EU for animal experiments.

AUTHOR CONTRIBUTIONS

RC, IY, CG-R, MB, ES, and DM designed experiments. RC, FP, SD, UA, PH, IY, and DM performed experiments. RC, UA, FP, and DM analyzed the data. RC, IY, CG-R, MB, and DM wrote the manuscript.

FUNDING

This work was supported by Centre National de la Recherche Scientifique (CNRS), University of Strasbourg (Université de Strasbourg), and Institut National de la Santé et de la Recherche Médicale (INSERM; contracts UPR3212, UMS3415, UMR7104 and U964) and by the European Union Seventh Framework Programme FP7-Health-2013-Innovation (grant 1602919). RC was funded by the Ministère de l'Enseignement Supérieur et de la Recherche et de l'Innovation and the Fondation pour la Recherche Médicale (DPA20140629804).

ACKNOWLEDGMENTS

We would like to thank the Chronobiotron animal facility (UMS 3415 CNRS), and the imaging Platform of the Institut des Neurosciences Cellulaires et Intégratives (UPS 3156 CNRS) for their assistance. We are also thankful to the Institut de la Clinique de la Souris (Illkirch, France) animal facility, Anne Robé and David Reiss at IGBMC for breeding and genotyping of Nav1.8 + DOP cKO mouse line. They would like to acknowledge Dr. Jean-Luc Rodeau for his instrumental help with the statistical analysis, Prof. Nelly Boehm, Prof. Remy Schlichter and Dr. Sylvain Hugel for valuable scientific discussions, and Elisabeth Waltisperger for excellent technical contribution.

REFERENCES

Benbouzid, M., Choucair-Jaafar, N., Yalcin, I., Waltisperger, E., Muller, A., Freund-Mercier, M. J., et al. (2008a). Chronic, but not acute, tricyclic antidepressant treatment alleviates neuropathic allodynia after sciatic nerve cuffing in mice. *Eur. J. Pain* 12, 1008–1017. doi: 10.1016/j.ejpain.2008.01.010

Benbouzid, M., Gaveriaux-Ruff, C., Yalcin, I., Waltisperger, E., Tessier, L. H., Muller, A., et al. (2008b). Delta-opioid receptors are critical for tricyclic antidepressant treatment of neuropathic allodynia. *Biol. Psychiatry* 63, 633–636. doi: 10.1016/j.biopsych.2007.06.016

Benbouzid, M., Pallage, V., Rajalu, M., Waltisperger, E., Doridot, S., Poisbeau, P., et al. (2008c). Sciatic nerve cuffing in mice: a model of sustained neuropathic pain. *Eur. J. Pain* 12, 591–599. doi: 10.1016/j.ejpain.2007.10.002

Binder, W., Mousa, S. A., Sitte, N., Kaiser, M., Stein, C., and Schafer, M. (2004). Sympathetic activation triggers endogenous opioid release and analgesia within peripheral inflamed tissue. *Eur. J. Neurosci.* 20, 92–100. doi: 10.1111/j.1460-9568.2004.03459.x

Bohren, Y., Tessier, L. H., Megat, S., Petitjean, H., Hugel, S., Daniel, D., et al. (2013). Antidepressants suppress neuropathic pain by a peripheral β2-adrenoceptor mediated anti-TNFα mechanism. *Neurobiol. Dis.* 60, 39–50. doi: 10.1016/j.nbd.2013.08.012

Brederson, J. D., and Honda, C. N. (2015). Primary afferent neurons express functional delta opioid receptors in inflamed skin. *Brain Res.* 1614, 105–111. doi: 10.1016/j.brainres.2015.04.023

Celik, M. Ö., Labuz, D., Henning, K., Busch-Dienstfertig, M., Gaveriaux-Ruff, C., Kieffer, B. L., et al. (2016). Leukocyte opioid receptors mediate analgesia *via* Ca^{2+}-regulated release of opioid peptides. *Brain Behav. Immun.* 57, 227–242. doi: 10.1016/j.bbi.2016.04.018

Ceredig, R. A., Pierre, F., Doridot, S., Alduntzin, U., Salvat, E., Yalcin, I., et al. (2018). Peripheral delta opioid receptors mediate duloxetine anti-allodynic effect in a mouse model of neuropathic pain. *Eur. J. Neurosci.* 48, 2231–2246. doi: 10.1111/ejn.14093

Chattopadhyay, M., Mata, M., and Fink, D. J. (2008). Continuous δ-opioid receptor activation reduces neuronal voltage-gated sodium channel ($Na_V1.7$) levels through activation of protein kinase C in painful diabetic neuropathy. *J. Neurosci.* 28, 6652–6658. doi: 10.1523/JNEUROSCI.5530-07.2008

Choucair-Jaafar, N., Salvat, E., Freund-Mercier, M. J., and Barrot, M. (2014). The antiallodynic action of nortriptyline and terbutaline is mediated by β_2 adrenoceptors and δ opioid receptors in the ob/ob model of diabetic polyneuropathy. *Brain Res.* 1546, 18–26. doi: 10.1016/j.brainres.2013.12.016

Choucair-Jaafar, N., Yalcin, I., Rodeau, J. L., Waltisperger, E., Freund-Mercier, M. J., and Barrot, M. (2009). β_2-adrenoceptor agonists alleviate

neuropathic allodynia in mice after chronic treatment. *Br. J. Pharmacol.* 158, 1683–1694. doi: 10.1111/j.1476-5381.2009.00510.x

Erbs, E., Faget, L., Ceredig, R. A., Matifas, A., Vonesch, J. L., Kieffer, B. L., et al. (2016). Impact of chronic morphine on delta opioid receptor-expressing neurons in the mouse hippocampus. *Neuroscience* 313, 46–56. doi: 10.1016/j.neuroscience.2015.10.022

Gaveriaux-Ruff, C., Nozaki, C., Nadal, X., Hever, X. C., Weibel, R., Matifas, A., et al. (2011). Genetic ablation of delta opioid receptors in nociceptive sensory neurons increases chronic pain and abolishes opioid analgesia. *Pain* 152, 1238–1248. doi: 10.1016/j.pain.2010.12.031

Gendron, L., Mittal, N., Beaudry, H., and Walwyn, W. (2015). Recent advances on the δ opioid receptor: from trafficking to function. *Br. J. Pharmacol.* 172, 403–419. doi: 10.1111/bph.12706

Jordan, B. A., Trapaidze, N., Gomes, I., Nivarthi, R., and Devi, L. A. (2001). Oligomerization of opioid receptors with b_2-adrenergic receptors: a role in trafficking and mitogen-activated protein kinase activation. *Proc. Natl. Acad. Sci. U S A* 98, 343–348. doi: 10.1073/pnas.011384898

Jourdain, M., and Hatakeyama, S. (2019). A novel tissue-selective β2-adrenoceptor agonist with minimized cardiovascular effects, 5-HOB, attenuates neuropathic pain in mice. *BMC Res. Notes* 12:413. doi: 10.1186/s13104-019-4466-y

Kremer, M., Salvat, E., Muller, A., Yalcin, I., and Barrot, M. (2016a). Antidepressants and gabapentinoids in neuropathic pain: mechanistic insights. *Neuroscience* 338, 183–206. doi: 10.1016/j.neuroscience.2016.06.057

Kremer, M., Yalcin, I., Nexon, L., Wurtz, X., Ceredig, R. A., Daniel, D., et al. (2016b). The antiallodynic action of pregabalin in neuropathic pain is independent from the opioid system. *Mol. Pain* 12:1744806916633477. doi: 10.1177/1744806916633477

Kremer, M., Yalcin, I., Goumon, Y., Wurtz, X., Nexon, L., Daniel, D., et al. (2018). A dual noradrenergic mechanism for the relief of neuropathic allodynia by the antidepressant drugs duloxetine and amitriptyline. *J. Neurosci.* 38, 9934–9954. doi: 10.1523/JNEUROSCI.1004-18.2018

Lauria, G., Cornblath, D. R., Johansson, O., McArthur, J. C., Mellgren, S. I., Nolano, M., et al. (2005). EFNS guidelines on the use of skin biopsy in the diagnosis of peripheral neuropathy. *Eur. J. Neurol.* 12, 747–758. doi: 10.1111/j.1468-1331.2005.01260.x

Leung, L., and Cahill, C. M. (2010). TNF-α and neuropathic pain—a review. *J. Neuroinflammation* 7:27. doi: 10.1186/1742-2094-7-27

Mika, J., Popiolek-Barczyk, K., Rojewska, E., Makuch, W., Starowicz, K., and Przewlocka, B. (2014). Delta-opioid receptor analgesia is independent of microglial activation in a rat model of neuropathic pain. *PLoS One* 9:e104420. doi: 10.1371/journal.pone.0104420

Nadal, X., Banos, J. E., Kieffer, B. L., and Maldonado, R. (2006). Neuropathic pain is enhanced in δ-opioid receptor knockout mice. *Eur. J. Neurosci.* 23, 830–834. doi: 10.1111/j.1460-9568.2006.04569.x

Nascimento, F. P., Magnussen, C., Yousefpour, N., and Ribeiro-da-Silva, A. (2015). Sympathetic fibre sprouting in the skin contributes to pain-related behaviour in spared nerve injury and cuff models of neuropathic pain. *Mol. Pain* 11:59. doi: 10.1186/s12990-015-0062-x

Nozaki, C., Le Bourdonnec, B., Reiss, D., Windh, R. T., Little, P. J., Dolle, R. E., et al. (2012). δ-Opioid mechanisms for ADL5747 and ADL5859 effects in mice: analgesia, locomotion, and receptor internalization. *J. Pharmacol. Exp. Ther.* 342, 799–807. doi: 10.1124/jpet.111.188987

Pannell, M., Labuz, D., Celik, M. Ö., Keye, J., Batra, A., Siegmund, B., et al. (2016). Adoptive transfer of M2 macrophages reduces neuropathic pain *via* opioid peptides. *J. Neuroinflammation* 13:262. doi: 10.1186/s12974-016-0735-z

R Core Team. (2017). *R: A Language and Environment for Statistical Computing*. Vienna, Austria: R Foundation for Statistical Computing.

Salvat, E., Schweitzer, B., Massard, G., Meyer, N., de Blay, F., Muller, A., et al. (2015). Effects of β_2 agonists on post-thoracotomy pain incidence. *Eur. J. Pain* 19, 1428–1436. doi: 10.1002/ejp.673

Scherrer, G., Tryoen-Tóth, P., Filliol, D., Matifas, A., Laustriat, D., Cao, Y. Q., et al. (2006). Knockin mice expressing fluorescent δ-opioid receptors uncover G protein-coupled receptor dynamics *in vivo*. *Proc. Natl. Acad. Sci. U S A* 103, 9691–9696. doi: 10.1073/pnas.0603359103

Slominski, A. T., Zmijewski, M. A., Zbytek, B., Brozyna, A. A., Granese, J., Pisarchik, A., et al. (2011). Regulated proenkephalin expression in human skin and cultured skin cells. *J. Invest. Dermatol.* 131, 613–622. doi: 10.1038/jid.2010.376

Vanfleteren, L., Fabbri, L. M., Papi, A., Petruzzelli, S., and Celli, B. (2018). Triple therapy (ICS/LABA/LAMA) in COPD: time for a reappraisal. *Int. J. Chron. Obstruct. Pulmon. Dis.* 13, 3971–3981. doi: 10.2147/copd.s185975

Vicario, N., Parenti, R., Arico, G., Turnaturi, R., Scoto, G. M., Chiechio, S., et al. (2016). Repeated activation of delta opiod receptors counteracts nerve injury-induced TNF-α up-regulation in the sciatic nerve of rats with neuropathic pain: a possible correlation with delta opiod receptors-mediated antiallodinic effect. *Mol. Pain* 12:1744806916667949. doi: 10.1177/1744806916667949

von Hehn, C. A., Baron, R., and Woolf, C. J. (2012). Deconstructing the neuropathic pain phenotype to reveal neural mechanisms. *Neuron* 73, 638–652. doi: 10.1016/j.neuron.2012.02.008

Yalcin, I., Bohren, Y., Waltisperger, E., Sage-Ciocca, D., Yin, J. C., Freund-Mercier, M. J., et al. (2011). A time-dependent history of mood disorders in a murine model of neuropathic pain. *Biol. Psychiatry* 70, 946–953. doi: 10.1016/j.biopsych.2011.07.017

Yalcin, I., Choucair-Jaafar, N., Benbouzid, M., Tessier, L. H., Muller, A., Hein, L., et al. (2009). β_2-adrenoceptors are critical for antidepressant treatment of neuropathic pain. *Ann. Neurol.* 65, 218–225. doi: 10.1002/ana.21542

Yalcin, I., Megat, S., Barthas, F., Waltisperger, E., Kremer, M., Salvat, E., et al. (2014). The sciatic nerve cuffing model of neuropathic pain in mice. *J. Vis. Exp.* 89:e51608. doi: 10.3791/51608

Yalcin, I., Tessier, L. H., Petit-Demoulière, N., Waltisperger, E., Hein, L., Freund-Mercier, M. J., et al. (2010). Chronic treatment with agonists of β_2-adrenergic receptors in neuropathic pain. *Exp. Neurol.* 221, 115–121. doi: 10.1016/j.expneurol.2009.10.008

Conflict of Interest: The authors declare that the research was conducted in the absence of any commercial or financial relationships that could be construed as a potential conflict of interest.

frontiers in Molecular Neuroscience

REVIEW
published: 05 May 2020
doi: 10.3389/fnmol.2020.00052

The Delta-Opioid Receptor; a Target for the Treatment of Pain

*Béatrice Quirion†, Francis Bergeron†, Véronique Blais and Louis Gendron**

Faculté de Médecine et des Sciences de la Santé, Département de Pharmacologie-Physiologie, Institut de Pharmacologie de Sherbrooke, Centre de Recherche du Centre Hospitalier Universitaire de Sherbrooke, Université de Sherbrooke, Sherbrooke, QC, Canada

Nowadays, pain represents one of the most important societal burdens. Current treatments are, however, too often ineffective and/or accompanied by debilitating unwanted effects for patients dealing with chronic pain. Indeed, the prototypical opioid morphine, as many other strong analgesics, shows harmful unwanted effects including respiratory depression and constipation, and also produces tolerance, physical dependence, and addiction. The urgency to develop novel treatments against pain while minimizing adverse effects is therefore crucial. Over the years, the delta-opioid receptor (DOP) has emerged as a promising target for the development of new pain therapies. Indeed, targeting DOP to treat chronic pain represents a timely alternative to existing drugs, given the weak unwanted effects spectrum of DOP agonists. Here, we review the current knowledge supporting a role for DOP and its agonists for the treatment of pain. More specifically, we will focus on the cellular and subcellular localization of DOP in the nervous system. We will also discuss in further detail the molecular and cellular mechanisms involved in controlling the cellular trafficking of DOP, known to differ significantly from most G protein-coupled receptors. This review article will allow a better understanding of how DOP represents a promising target to develop new treatments for pain management as well as where we stand as of our ability to control its cellular trafficking and cell surface expression.

Keywords: delta-opioid receptor, pain, primary afferents, G protein-coupled receptors, trafficking

OPEN ACCESS

Edited by:
Tally Largent-Milnes, University of Arizona, United States

Reviewed by:
Susan Ingram, Oregon Health and Science University, United States
Belen Gago, University of Malaga, Spain

***Correspondence:**
Louis Gendron
louis.gendron@usherbrooke.ca

†These authors have contributed equally to this work

Received: *04 November 2019*
Accepted: *13 March 2020*
Published: *05 May 2020*

Citation:
Quirion B, Bergeron F, Blais V and Gendron L (2020) The Delta-Opioid Receptor; a Target for the Treatment of Pain. Front. Mol. Neurosci. 13:52. doi: 10.3389/fnmol.2020.00052

Affecting more than one-third of the North American population during their lifetime, chronic pain is more frequent than cardiovascular diseases, diabetes, and cancer combined (Gaskin and Richard, 2012). According to the 2010 Medical Expenditure Panel Survey (MEPS), chronic pain is one of the most important socio-economic burdens in the U.S., with estimated annual costs ranging from $560 to $635 billion; $261 to $300 billion in direct health care costs and $299 to $335 billion in lost productivity and other indirect costs (Gaskin and Richard, 2012). With the aging population, these numbers are predicted to double within the next decade. Despite notorious adverse effects and lack of effectiveness in many types of pain, opioids remain the standard of care for treating moderate to severe conditions (Ballantyne et al., 2016). The use of opioids has led to their widespread diversion and misuse calling upon the U.S. Department of Health

and Human Services (HHS) to declare an opioid crisis in 2017[1] (Kirson et al., 2017; Iwanicki et al., 2018). In concert with pharmaceutical companies and academic research centers, three main goals were elaborated: (1) design safe, effective, and non-addictive strategies to manage chronic pain; (2) new, innovative medications and technologies to treat opioid use disorders; and (3) improved overdose prevention and reversal interventions to save lives and support recovery[2].

Opioids act *via* the opioid receptors, namely Mu (μ), Kappa (κ), and Delta (δ). The most prescribed opioids (e.g., morphine, Fentanyl, codeine) preferentially target the μ opioid receptors (MOP). These substances, being among the most potent analgesics, produce diverse effects and are responsible for almost all prototypic opioid unwanted effects such as euphoria, mental clouding, sedation, respiratory depression and cough suppression, pupillary miosis (oculomotor nerve parasympathetic stimulation), antidiuresis, urinary retention, nausea and vomiting, bradycardia and vasodilation, constipation and biliary retention, and histamine release (Katzung et al., 2009; Khademi et al., 2016).

Selective activation of the δ opioid receptor (DOP) has great potential for the treatment of chronic pain (Kieffer and Gavériaux-Ruff, 2002; Gavériaux-Ruff and Kieffer, 2011) with ancillary anxiolytic- and antidepressant-like effects (Chu Sin Chung and Kieffer, 2013). Their ability to cause emotional responses is highly desirable because of the frequent association of anxiety and mood disorders with chronic pain (Goldenberg, 2010a,b). Compared to MOP agonists, molecules acting on DOP typically show reduced adverse effects. Here, we review important findings supporting a role for DOP in the treatment of chronic pain. Because its physiological roles are directly related to its cellular and subcellular expression, we also discuss the distribution of DOP along the pain pathways as well as the cellular mechanisms regulating its trafficking to the cell surface.

ASCENDING AND DESCENDING PAIN PATHWAYS

Pain processing runs through a distinctive neurological pathway. The propagation of pain starts with the activation of receptors, called nociceptors, which are found widely in peripheral tissues, muscles, and organs (Almeida et al., 2004). The nociceptive sensory fibers transform stimuli and generate a membrane potential which, if the threshold is reached, generates an impulse (Khalid and Tubbs, 2017). Whether or not the action potential is initiated depends on the intensity of the stimulus (Mense, 1983; Millan, 1999; Bester et al., 2000; Almeida et al., 2004). Nociceptors have a high threshold compared to other receptors and only a strong, potentially harmful stimulus, activates them (Woolf and Ma, 2007). The impulse propagates along the primary afferent fiber to reach the central nervous system. Primary afferent fibers are pseudo-unipolar neurons which means their cell body has one emerging axon that divides in peripheral and central projections. The peripheral branch innervates the target organ (skin, muscle, viscera) while the central axon projects to the dorsal horn of the spinal cord which is organized in anatomically different laminae (Basbaum and Jessell, 2000; Almeida et al., 2004; Khalid and Tubbs, 2017). The cell bodies of the primary afferents are located in dorsal root (DRGs) and trigeminal ganglia (TGs; Basbaum et al., 2009; Dubin and Patapoutian, 2010). These neurons are commonly classified according to their size (small, medium and large diameter neurons), conducting velocity, and levels of myelination. Interestingly, DRG and TG neurons have various roles when it comes to proprioception, exteroception, and nociception. Medium diameter myelinated (Aδ) fibers and small diameter unmyelinated C fibers are mainly responsible for nociception (Mense, 1983; Woolf and Ma, 2007; Garland, 2012). Aα and Aβ fibers are also primary afferent fibers respectively implicated in proprioception and touch, although they may also be involved in nociception (Watson, 1981; Djouhri and Lawson, 2004; Abraira and Ginty, 2013; Le Pichon and Chesler, 2014). After the integration of the noxious stimuli at the spinal cord level, the nociceptive signal travels through different ascending pathways to the thalamus and the brainstem, namely the spinothalamic and the spinoreticulothalamic tracts (for a review see Almeida et al., 2004). Once the signal reaches the cortical structures, it is processed at the level of the sensory, the cingulate, and the insular cortices (Apkarian et al., 2005; Basbaum and Julius, 2006). In addition to the ascending pain pathways, an endogenous inhibitory system called the descending pain modulatory circuit is also part of the pain circuitry. This circuit involves multiple regions of the central nervous system such as the frontal neocortex, the hypothalamus, the amygdala, the rostral anterior cingulate cortex (rAAC), the periaqueductal gray region (PAG), the medulla and the rostroventral medulla (RVM; Fields et al., 2006; Ossipov et al., 2010). This ensemble projects to the dorsal horn of the spinal cord to modulate the ascending pain signal (Fields et al., 2006; Ossipov et al., 2010). In order to alleviate pain, a drug must therefore act on a target expressed at least in one of these structures.

DELTA OPIOID RECEPTOR DISTRIBUTION IN THE CENTRAL NERVOUS SYSTEM

To this day, the cellular distribution of DOP along the pain pathways remains unclear. Depending on the technique used to assess the expression of DOP in tissue, significant differences are observed concerning its localization. Approaches such as *in situ* hybridization, immunohistochemistry, autoradiography using radiolabeled ligands, GTPγS assay and genetically modified mouse models have been used to study the istribution of DOP (Quirion et al., 1983; McLean et al., 1986; Mansour et al., 1987, 1994; Dado et al., 1993; Simonin et al., 1994; Cahill et al., 2001a; Mennicken et al., 2003; Guan et al., 2005; Scherrer et al., 2009; Wang et al., 2010). Small discrepancies in the distribution of the receptor between studies can be attributed to differences in tissue processing, the use of different species, and/or ligand sensitivity. However, one of the most important controversies in the field arises from a comparison of the receptor

[1]https://www.drugabuse.gov/drugs-abuse/opioids/opioid-overdose-crisis
[2]https://www.nih.gov/research-training/medical-research-initiatives/heal-initiative/heal-initiative-research-plan

distribution using antibodies raised against DOP and the use of DOP-eGFP knockin (DOP-eGFP KI) transgenic mice. The distribution of DOP using these two techniques is noticeably different and certain concerns arise for either one. Admittedly, most antibodies raised against DOP lack specificity since many commercially available and custom antibodies stain the spinal cord of DOP-KO mice similarly to the wild type mice (Scherrer et al., 2009). Although the use of mice expressing chimeric receptors bearing a 23 kDa GFP protein within their intracellular loops or their C-terminal tail might not be the best approach to visualize the endogenous distribution of DOP, this tool offers the possibility to directly detect the receptor in native or fixed tissues, sometimes without the need to use antibodies. However, the use of such intracellular tags (like GFP) is a matter of debate. Indeed, the cellular distribution and compartmentalization of DOP (Gendron et al., 2015; Zhang et al., 2015) and other GPCRs (McLean and Milligan, 2000; Madziva and Edwardson, 2001; McDonald et al., 2007) is altered by the addition of an eGFP tag. To summarize, each technique has its strengths and weaknesses for identifying DOP in tissues.

Expression of DOP in the Brain

The delta-opioid receptor (DOP) is widely distributed in the brain, without significant difference between rodents and humans (Simonin et al., 1994). Along the pain pathways, DOP is expressed in structures of both the ascending and the descending pain pathways. More specifically, DOP is found in the PAG, the RVM, the cerebral cortex and the amygdala (Mansour et al., 1987, 1994, 1995; Tempel and Zukin, 1987; Sharif and Hughes, 1989; Kiefel et al., 1993; Slowe et al., 1999; Cahill et al., 2001a; Peng et al., 2012). More interestingly, DOP likely participate not solely in the control of pain but also of mood disorders such as anxiety and depression (Chu Sin Chung and Kieffer, 2013; Lutz and Kieffer, 2013).

Expression of DOP in the Spinal Cord

In the rodent spinal cord, the expression of DOP is predominant in superficial laminae I and II. The expression also extends to other laminae, including a broad distribution throughout the gray matter (Cahill et al., 2001a,b, 2003; Mennicken et al., 2003) and motoneurons located in the ventral horns (Wang et al., 2018). Various techniques including immunohistochemistry (Cahill et al., 2001a), autoradiography using DOP-selective radioligands (Mennicken et al., 2003; Bardoni et al., 2014; Wang et al., 2018), *in situ* hybridization (Cahill et al., 2001a; Mennicken et al., 2003; Wang et al., 2018), and transgenic mice (DOP-eGFP KI mice; Scherrer et al., 2009) supports this wide distribution of DOP. The study of the cellular distribution of DOP in DOP-eGFP KI mice revealed that most DOP-positive neurons located in lamina II express TLX3, a marker for spinal excitatory interneurons. The presence of DOP in these neurons is supported by electrophysiological studies where the resting membrane potential and action potential firing patterns were measured (Wang et al., 2018). These neurons are now known to be somatostatin-positive neurons likely involved in the transmission of mechanical noxious stimuli (Bardoni et al., 2014; Chamessian et al., 2018; Wang et al., 2018).

In higher species, the distribution of DOP in the spinal cord looks slightly different (Mennicken et al., 2003). In monkeys, radioligand binding revealed that DOP is expressed at a higher level in superficial rather than in deeper laminae, with a high density of DOP labeling in lamina II (Honda and Arvidsson, 1995; Zhang et al., 1998; Mennicken et al., 2003). More interestingly, DOP binding sites in the human spinal cord are even more restricted to the superficial laminae, with no apparent labeling in laminae III-X (Mennicken et al., 2003). A more restricted expression of DOP in the human spinal cord calls for the role of DOP in the regulation of the activity of primary afferents. The apparent lack of DOP mRNA in the human spinal cord (Peckys and Landwehrmeyer, 1999; Mennicken et al., 2003) suggests that the receptor is present on synaptic terminals of primary afferents projecting to laminae I and II while, in rodents and monkeys, *in situ* hybridization showed a widespread distribution of DOP mRNA throughout the gray matter. DOP mRNA is also expressed in motoneurons in the ventral horn of the mouse, rat, and monkey spinal cord, but not in humans (Mennicken et al., 2003). To summarize, the expression pattern of DOP mRNA and protein in the human spinal cord, but also other species, supports a role for DOP in pain control. In all species, but more specifically in humans, the presence of DOP on what appears to be the primary afferent endings suggests that this receptor is synthesized in primary afferents and transported to the spinal cord (Mennicken et al., 2003). This is further supported by the fact that deafferentation significantly decreased the density of DOP in the dorsal horn of the spinal cord in rodents (Dado et al., 1993).

Expression of DOP in Primary Afferents

As mentioned above, DOP is expressed in primary afferents, the very first step of pain processing pathways. Somatosensory neurons, more specifically DRG neurons, are responsible for the detection and the transmission of noxious stimuli to the brain. In DRG neurons, opioid receptors regulate cell excitability and neurotransmitter release (François and Scherrer, 2018). However, the exact distribution of DOP in these neurons remains controversial.

There are two diverging opinions on DOP's distribution in somatosensory neurons. The first school of thought infers that DOP is found mainly in large myelinated DRG neurons and reports a low level of co-expression with MOP (Scherrer et al., 2009; Bardoni et al., 2014). The DOP-eGFP KI mouse model reveals that DOP labeling is mainly observed in NF200-positive cells, a marker of myelinated DRG neurons (Scherrer et al., 2009). Single-cell RNA sequencing further supports that *Orpd1* transcripts were solely found in NF200-positive DRG neurons (Usoskin et al., 2015). Moreover, most DOP-eGFP-positive cells also express TRPV2, a channel found in myelinated neurons. Since most myelinated somatosensory neurons are mechanosensitive, this distribution suggests that DOP plays a role in mechanical pain (Usoskin et al., 2015). In support of this hypothesis, a significant level of DOP labeling is found in high-threshold mechanosensitive A-fibers (A HTMRs). Interestingly, DOP-eGFP is also co-expressed with Ret and/or TrkC, markers of low-threshold mechanosensitive A-fibers

(A LTMRs; François and Scherrer, 2018). Although in small proportion, it is worth noting that DOP-eGFP is also found in unmyelinated DRG neurons. These neurons were mainly identified as small unmyelinated neurons expressing IB4 and P2X3, markers for nonpeptidergic C nociceptors. Only a few DOP-eGFP-positive neurons, if any, were identified as SP-, CGRP- and TRPV1-positive, confirming that DOP is rarely found in small peptidergic DRG neurons. Using an antibody raised against MOP, immunohistochemical studies revealed that in DOP-eGFP KI mice, DOP and MOP were rarely co-expressed in the same DRG neurons (less than 5% of co-expression) but rather segregated in distinct populations, suggesting that these receptors might play different roles when it comes to pain modulation. Indeed, DOP was shown to be mostly implicated in mechanical pain control while MOP controls thermal pain (Scherrer et al., 2009).

The second school of thought rather promotes the idea that the distribution of DOP includes small DRG neurons (Ji et al., 1995; Wang and Wessendorf, 2001) and that DOP and MOP are co-expressed in some neurons. Immunohistochemistry, RT-PCR and single-cell PCR techniques have shown that DOP-positive DRG neurons were often of small-diameter (Ji et al., 1995; Guan et al., 2005; Wang et al., 2010), with one-third of these neurons also co-expressing SP or CGRP (Guan et al., 2005; He et al., 2010; Wang et al., 2010). Additionally, some studies suggested that DOP is found both in small and large DRG neurons. Indeed, RT-PCR, *in situ* hybridization and immunohistochemistry approaches revealed that DOP is located almost equally in all types of neurons (Wang and Wessendorf, 2001; Mennicken et al., 2003; Rau et al., 2005). The presence of DOP on both myelinated and unmyelinated peptidergic and non-peptidergic somatosensory neurons supports a role in heat and mechanical pain control. In animal models, the selective activation of DOP was indeed shown to alleviate both mechanical and thermal pain (Tseng et al., 1997; Gendron et al., 2007b; Holdridge and Cahill, 2007; Beaudry et al., 2009; Dubois and Gendron, 2010; Otis et al., 2011; Normandin et al., 2013). Among these findings, our group has shown, using *in vivo* electrophysiology, that the activation of spinal DOP with deltorphin II led to the inhibition of the diffuse noxious inhibitory controls (DNIC) activated by heat and mechanical noxious stimuli (Normandin et al., 2013). We further observed that both DOP and MOP were able to inhibit the noxious heat- and mechanical-induced release of SP in the spinal cord (Beaudry et al., 2011; Normandin et al., 2013).

A thorough characterization of DOP on central terminals of primary afferents revealed important differences between rodents and primates. When compared to rodents, not only more DRG neurons express DOP, the receptor is also expressed in a higher proportion of medium- and small-diameter neurons in human and non-human primates, supporting a more specialized role for DOP in pain processing in higher species (Mennicken et al., 2003).

Regardless of the subcellular distribution of DOP in nociceptors, electrophysiological studies confirmed that the activation of DOP reduced the amplitude of evoked excitatory postsynaptic currents (Glaum et al., 1994). This suggests that the excitatory glutamatergic transmission in the lamina II of the spinal cord is inhibited by a presynaptic action of DOP (Glaum et al., 1994; Wang et al., 2010; François and Scherrer, 2018), highlighting a role for the receptor in pain modulation at the presynaptic level. If the distribution of DOP in primary afferents and spinal cord neurons remains a matter of debate, its expression in all structures involved in pain processing, as well as its more restricted expression within structures implicated in pain modulation in higher species, raise DOP among the most promising targets for the development of novel pain therapies.

TRAFFICKING OF DOP IN NEURONS

The major challenge in making new therapeutics for the treatment of pain, and most particularly chronic pain, is to develop molecules maximizing analgesia while minimizing adverse effects. Because they do not produce the common adverse effects associated with clinically used opioids, this is exactly where DOP-selective agonists could be useful (Pradhan et al., 2011). However, under normal conditions, DOP agonists only have weak analgesic effects in animal models of evoked pain. It is now recognized that the weak analgesic potency of DOP agonists is the consequence of a low level of expression at the plasma membrane (Cahill et al., 2007; Pradhan et al., 2011). Indeed, several studies employing electron microscopy immunogold labeling, photoaffinity-labeling of endogenous receptors, and biochemical subcellular fractionation techniques showed that DOP mainly localizes in intracellular compartments and organelles while only a small portion is associated with the plasma membrane of neurons (Pasquini et al., 1992; Zerari et al., 1994; Arvidsson et al., 1995; Cheng et al., 1995, 1997; Elde et al., 1995; Zhang et al., 1998; Petäjä-Repo et al., 2000, 2002, 2006; Cahill et al., 2001a,b; Commons et al., 2001; Wang and Pickel, 2001; Commons, 2003; Guan et al., 2005; Lucido et al., 2005; Gendron et al., 2006). If the hope is to develop pain therapies targeting DOP, strategies to increase its levels of expression at the neuronal plasma membrane need to be described. Ways to control the trafficking of DOP and to increase its cell surface expression include prolonged morphine treatment (or other MOP agonists) or inflammation induced by complete Freund's adjuvant (CFA; Cahill et al., 2001b, 2003; Morinville et al., 2003; Gendron et al., 2006, 2007a,b). Indeed, following such treatments the density of DOP at the cell surface increases in spinal cord (Cahill et al., 2001b; Morinville et al., 2004), DRG (Cahill et al., 2001a, 2003; Morinville et al., 2003; Gendron et al., 2006, 2007a,b), and central gray neurons (Lucido et al., 2005). As of to date, the mechanisms involved in this process remain poorly described. Several DOP interacting partners have been identified, some of which are involved in protein trafficking. Here, we review these DOP partners in light of their potential role in controlling the cellular trafficking of DOP and, by way of consequence, the analgesic potency of DOP agonists. Depending on their role in regulating the trafficking of DOP toward the plasma membrane, targeting these proteins may serve as a strategy to develop new drugs capable of increasing the analgesic potency of DOP agonists.

There are two major trafficking pathways described for membrane proteins, namely the regulated (or secretory) and the constitutive pathways. Numerous evidence supports the idea that DOP uses both paths to reach the plasma membrane. After being synthesized in the endoplasmic reticulum (ER), membrane proteins undergo a quality check. Improperly folded proteins will be targeted to lysosomes for degradation while those correctly folded will process to the Golgi apparatus where they will undergo post-translational modifications like glycosylation (Sicari et al., 2019). Mature proteins then progress toward the plasma membrane either through the regulated or the constitutive pathway. The protein cofilin, an actin severing protein and a potent regulator of actin filament dynamics, is involved in protein trafficking through the constitutive pathway. Cofilin has a role in improving or repressing the release of proteins from the Golgi apparatus to the cell surface (Heimann et al., 1999; Egea et al., 2006; Salvarezza et al., 2009). Its ability to bind and depolarize actin is, however, inhibited when it is phosphorylated by LIM-kinase 1, a serine/threonine kinase that has LIM and PDZ domains (Yang et al., 1998). This kinase may participate in the cytoskeleton reorganization by phosphorylating cofilin. Cofilin and proteins such as chronophin and LIM kinase interact and colocalize at the membrane level with β-arrestin (β-arr), supporting a role for the latter in regulating their activity (Zoudilova et al., 2007). These processes were recently shown to be involved in the trafficking of DOP to the plasma membrane (Mittal et al., 2013). In this context, strategies to decrease β-arr1 or its interaction with DOP, as well as ROCK or LIM kinase inhibition represent ways to prevent cofilin activation and, by way of consequence, to increase DOP-mediated effects.

An association between DOP and downstream effectors such as the Kir3 ion channel has also been described (Richard-Lalonde et al., 2013; Nagi et al., 2015). BRET and co-immunoprecipitation assays revealed that DOP associates with Kir3 channel subunits in cortical neurons where they also co-internalize upon stimulation with an agonist (Nagi et al., 2015). Other known regulators of DOP trafficking are the G protein-coupled receptor kinases (GRKs). GRKs mediate the phosphorylation on their cytoplasmic tail of numerous GPCRs, including DOP. When phosphorylated by GRKs, DOP promotes the recruitment of β-arrestin, inducing its accumulation into clathrin-coated pits and endocytic vesicles (Chu et al., 1997; Zhang et al., 1999; Whistler et al., 2001). The endocytosis of DOP plays a role in DOP downregulation by triggering its traffic to the degradation path (Law et al., 1984). Although observed in various cellular models and native neurons (Tsao and von Zastrow, 2000; Scherrer et al., 2006), the degradation path is not the only outcome for the sorting of DOP following its internalization. Indeed, the fate of internalized receptors is controlled by the endosomal sorting complex required for transport (escrt). The escrt complex distinguishes the ubiquitinated receptors and guides them to the multivesicular bodies (MVB) where they are addressed to the lysosomes for degradation (Henne et al., 2011). The ubiquitination process is quite essential for the commitment of receptors into a given degradation pathway. For example, the epidermal growth factor receptor (EGFR) ubiquitination is an essential step toward its degradation (Raiborg and Stenmark, 2009). Concerning DOP, ubiquitinated receptors are targeted to MVBs but, in opposition to EGFR, neither its ubiquitination nor its targeting to MVBs are necessary steps for the degradation in lysosomes (Tanowitz and Von Zastrow, 2002; Hislop et al., 2009). Admittedly, any proteins involved in the internalization process and the routing of DOP within the endosomal pathway represent potential targets to alter (either positively or negatively) its functions. Therefore, strategies to increase the density of DOP at the cell surface and its analgesic properties may be directed toward these pathways.

Other actors involved in the regulation of DOP trafficking are the noncanonical signaling proteins and the regulatory proteins. First, calmodulin and periplakin are modulators acting as blockers of DOP. Calmodulin, or calcium-modulated protein, is a widely distributed and versatile member of the calcium-binding protein family (Stevens, 1983). At resting state, calmodulin can constitutively associate with DOP (Wang et al., 1999). Once activated, the binding of calmodulin to DOP is abolished, allowing the receptor to couple to G proteins. The signaling protein periplakin, a member of the plakin family which serves as epidermal cytolinkers and components of cell-cell and cell-matrix adhesion complexes (Aho et al., 2004), interacts with DOP, more specifically with its cytoplasmic tail. The interaction was confirmed using a yeast two-hybrid system, and the site was profiled at the level of residues 321–331, according to the analogy with MOP receptors (Feng et al., 2003). As for calmodulin, periplakin seems to block the G protein activation by competing with its interaction site on the DOP (Wang et al., 1999; Feng et al., 2003). It can be argued that any compound able to selectively block the interaction between DOP and these proteins could increase DOP-mediated effects.

RGS4 is yet another regulator of DOP trafficking. RGS4 interacts with the first 26 amino acids of the C-terminal tail of DOP. Coimmunoprecipitation assays between DOP and RGS4 show that agonist stimulation does not alter the interaction, suggesting that they are constitutively associated (Georgoussi et al., 2006; Wang et al., 2009). However, the distribution of RGS4 is shifted from the cytosol to the membrane upon activation of DOP (Leontiadis et al., 2009). Another protein called spinophilin binds to the same C-terminal region and the third intracellular loop (ICL3) of DOP (Feng et al., 2000). Spinophilin is a ubiquitous multidomain-scaffold protein interacting with actin and protein phosphatase-1 (PP1). Along with RGS4, Gα, and Gβγ subunits, spinophilin forms a complex involving specific regions of the protein and the C-terminal tail of MOP and DOP (Fourla et al., 2012). In HEK293 cells, a constitutive interaction between spinophilin and DOP as well as an altered state following agonist administration was also observed (Fourla et al., 2012). Although the exact role of each association is not yet fully described, their modulation has the potential to regulate the activity of DOP and its downstream effectors and possibly it's trafficking.

As briefly discussed above, the interaction between GRKs and DOP is well established. As shown by coimmunoprecipitation studies, the association of GRKs with DOP increases following treatment with an agonist. More specifically, GRK2 is

translocated to the membrane where it can phosphorylate the C-terminal tail DOP upon stimulation (Li et al., 2003; Zhang et al., 2005). The interaction between GRKs and Gβγ at the membrane is an important step for the translocation of GRK2 from the cytoplasm to the cell membrane (Li et al., 2003). The rapid association of GRK2/GRK3 to DOP following the binding of an agonist is also observed in live cells. The colocalization of GRK2 and DOP is detected in endosomes after 15 min of stimulation suggesting that the complex translocates to clathrin-coated vesicles (Schulz et al., 2002). This appears to be specific to GRK2 and DOP since colocalization is neither detected between DOP and GRK6 nor MOP and GRK2. The interaction between DOP and GRK2 requires the presence of Gβγ subunits (Schulz et al., 2002; Li et al., 2003).

Colocalization and direct protein-protein interaction assays revealed that the recruitment of βarr1 and βarr2 to DOP is induced either by receptor activation (Whistler et al., 2001; Zhang et al., 2005; Qiu et al., 2007; Molinari et al., 2010; Audet et al., 2012) or its phosphorylation by protein kinase C (PKC; Xiang et al., 2001). The interaction sites for both arrestins on DOP are located in the ICL3 (Leu235-Ile259) and the C-terminal tail of DOP (Gln331-Ala372; Cen et al., 2001b). These two regions bind to non-overlapping sites on βarr1 (Cen et al., 2001a). Indeed, a DOP mutant lacking the last 15 residues of the C-terminal tail showed only a reduction in the βarr1 association (Cen et al., 2001a). The ability of a mutant DOP lacking all serine and threonine residues of the C-terminal tail to recruit βarr (Qiu et al., 2007) further supports the contribution of distinct regions.

The interaction between βarr2 and DOP can also occur independently of phosphorylation (Zhang et al., 2005; Qiu et al., 2007). Indeed, both wild-type DOP and a mutant receptor containing a substitution of all C-terminal serine and threonine residues remain capable to recruit βarrs. Instead, an increase in the interaction between DOP and βarr2 can be observed (Qiu et al., 2007). βarr2 plays a major role in the desensitization of DOP (Qiu et al., 2007) while both βarr1 and βarr2 similarly contributes to the internalization process. The link between the fate of post-endocytic receptors and βarrs has also been described. DOP lacking phosphorylation sites in its C-terminal tail is preferentially degraded *via* a βarr2-mediated mechanism. In contrast, a small portion of the wild-type receptor is recycled back to the cell membrane *via* βarrs (Zhang et al., 2008). As mentioned above, interfering with the recruitment of βarrs represents a strategy to increase the functions of DOP, possibly through the inhibition of its internalization and desensitization.

Among DOP-interacting proteins, GASP-1 and the glycoprotein M6a play a crucial role in its regulation. G protein-coupled receptor-associated sorting protein 1 (GASP-1) is a member of the GASP family of proteins. GASP-1 is the most studied member of the family and the only one interacting with DOP (Simonin et al., 2004). This sorting protein is involved in the delivery of receptors to the multivesicular bodies (MVBs; Whistler et al., 2002b; Marley and von Zastrow, 2010). The GASP machinery retains DOP to the endosomes, therefore preventing its recycling (Whistler et al., 2002a; Marley and von Zastrow, 2010; He et al., 2013). This machinery also participates in the transport of internalized DOP to the lysosomes, a process independent of ubiquitination or MVBs. The second interacting protein, the glycoprotein M6a, has been identified using a yeast two-hybrid approach (Wu et al., 2007). M6a is a member of the proteolipid membrane proteins (PLP) family and is primarily expressed in neurons (Yan et al., 1993, 1996; Roussel et al., 1998). It interacts with MOP, affecting its endocytosis and recycling, as well as with other GPCRs, including DOP (Wu et al., 2007). When co-internalizing with DOP, M6a significantly increases its localization within the recycling endosomes, supporting a role for this protein in the post-endocytic sorting and the recycling of receptors (Liang et al., 2008).

An exhaustive study using yeast two-hybrid screening on different C-terminal tails of GPCRs identified four different proteins thought to be involved in the post-endocytic sorting of GPCRs (Heydorn et al., 2004). Two of them being involved in the recycling pathway, ezrin-radixin-moesin-binding phosphoprotein 50 (EBP50, also called Na+/H+-exchanger regulatory factor-1 or NHERF-1) and N-ethylmaleimide-sensitive factor (NSF); while the other two being involved in targeting receptors to lysosomal degradation, GASP-1 and sorting nexin 1 (SNX1). Although the role of NSF and SNX1 in DOP trafficking is yet to be determined, the role of GASP (discussed above) and NHERF-1 are documented. NHERF-1 is a PDZ domain-containing scaffolding protein that has many functions such as protein complex assembly and sorting of internalized GPCRs (like β2-adrenergic and kappa opioid receptors) to the recycling pathway (Huang et al., 2004; Liu-Chen, 2004; Weinman et al., 2006; Hanyaloglu and von Zastrow, 2008). There is also evidence suggesting that DOP interacts with NHERF-1. Indeed, NHERF-1 and DOP can be co-immunoprecipitated from a brainstem extract, an effect increased in morphine-treated animals (Bie et al., 2010). The upregulation of NHERF-1 in transfected cells increases the sorting of DOP through the exocytotic trafficking, improving its membrane insertion and functional expression (Bie et al., 2010). A better knowledge of the mechanisms regulating the association of these proteins with DOP as well as their exact implication in the trafficking of DOP may help to develop drugs aiming at improving the recycling of DOP while reducing its degradation.

More recently, we used mass spectrometry analysis and identified new DOP-interacting partners in transfected HEK293 cells (St-Louis et al., 2017). Among them, we found many subunits of the coatomer protein complex I (COPI). This complex is involved in the transport of proteins from the Golgi to the ER. The interaction between DOP and COPI might explain why DOP is largely retained intracellularly. Using two different subunits of the COPI complex, β-COP and β'-COP, we confirmed the interaction of DOP with the COPI complex. Within its different intracellular loops and C-terminal tail, DOP has 13 putative COPI binding motifs (KxK, RxR, RxK or KxR). Using mutagenesis, we found that the disruption of two motifs, namely K164-K166 (ICL2) and K250-K252 (ICL3), significantly increased the expression of

DOP at the surface compared to the wild-type receptor (St-Louis et al., 2017). Shortly afterward, another study described a role for COPI in the regulation of DOP transport to the plasma membrane in neuronal cells (Shiwarski et al., 2019). A conserved COPI binding motifs (RxR) in the C-terminal tail of DOP is indeed required for the adequate delivery of DOP to the plasma membrane. Another key point in the transport of DOP to the cell surface is through its association with a phosphatase and tensin homolog (PTEN). A study visualizing DOP's trafficking and localization implicated a PTEN-regulated checkpoint in the retention of DOP in primary neuronal cell culture (Shiwarski et al., 2017). After PTEN inhibition, receptors available at the surface are increased, leading to an increase in DOP-mediated antinociception (Shiwarski et al., 2017).

The last partner to be reviewed here is the cyclin-dependent kinase 5 (Cdk5). Cdk5 is a member of the CDK family but unlike the other CDKs, Cdk5 is not involved in the cell cycle progression. This serine/threonine kinase is rather involved in different processes like neuronal activity, neuron migration and neurite outgrowth. It phosphorylates a consensus sequence [(S/T) PX (K/H/R; Beaudette et al., 1993; Songyang et al., 1996)] when activated by its specific neuronal activator, the cyclin-like p35. Such a consensus sequence is present within the second intracellular loop of DOP ($T^{161}PAK^{164}$). The threonine (T^{161}) residue was previously shown to be phosphorylated by Cdk5 in neuronal cells (Xie et al., 2009). When Cdk5 is inhibited with the CDK inhibitor roscovitine or when a T161A mutant of DOP is used, the level of cell surface DOP is significantly decreased (Xie et al., 2009). A more recent study also supported a role for Cdk5 in the regulation of DOP trafficking. Using the above mentioned Cdk5 inhibitor or by blocking the phosphorylation of DOP by Cdk5 with a mimetic peptide, a decrease in the antinociceptive and anti-hyperalgesic effects of the selective DOP agonist Deltorphin II is also, supporting a lower density of cell surface DOP (Beaudry et al., 2015). Altogether, these observations support a role for Cdk5 in promoting the expression of functional DOP at the cell surface, possibly by promoting its exit from the ER-Golgi.

CONCLUSION

DOP represents a promising target for the treatment of pain. As discussed in this review article, the expression of DOP is highly regulated by various mechanisms. In addition to reviewing its distribution along the pain pathways, we discussed how the expression and cellular trafficking of this receptor could be regulated. We focused on mechanisms and protein partners potentially involved in its intracellular retention or its trafficking to the cell surface. What emerges from this review article is the complexity surrounding the regulation of DOP trafficking and functions. As to date, one should admit that the mechanisms involved in DOP trafficking, both under normal and pathological conditions, remain poorly described. A better understanding of the distribution of DOP and how different proteins can affect its signaling and trafficking to the cell surface will facilitate the development of better and possibly less harmful pain therapeutics.

AUTHOR CONTRIBUTIONS

BQ, FB, VB and LG wrote the manuscript.

FUNDING

This work was supported by the Canadian Institutes of Health Research (CIHR) grants to LG (MOP-136871 and PJT-162103). LG is the recipient of a Chercheur-boursier Senior salary support from the Fonds de la Recherche du Québec-Santé (FRQ-S). BQ received undergrad scholarships from the Natural Sciences and Engineering Research Council of Canada (NSERC) and from the Faculté de médecine et des sciences de la santé de l'Université de Sherbrooke. BQ is the recipient of a Master scholarship from the FRQ-S.

REFERENCES

Abraira, V. E., and Ginty, D. D. (2013). The sensory neurons of touch. *Neuron* 79, 618–639. doi: 10.1016/j.neuron.2013.07.051

Aho, S., Li, K., Ryoo, Y., McGee, C., Ishida-Yamamoto, A., Uitto, J., et al. (2004). Periplakin gene targeting reveals a constituent of the cornified cell envelope dispensable for normal mouse development. *Mol. Cell. Biol.* 24, 6410–6418. doi: 10.1128/mcb.24.14.6410-6418.2004

Almeida, T. F., Roizenblatt, S., and Tufik, S. (2004). Afferent pain pathways: a neuroanatomical review. *Brain Res.* 1000, 40–56. doi: 10.1016/j.brainres.2003.10.073

Apkarian, A. V., Bushnell, M. C., Treede, R. D., and Zubieta, J. K. (2005). Human brain mechanisms of pain perception and regulation in health and disease. *Eur. J. Pain* 9, 463–484. doi: 10.1016/j.ejpain.2004.11.001

Arvidsson, U., Dado, R. J., Riedl, M., Lee, J. H., Law, P. Y., Loh, H. H., et al. (1995). delta-Opioid receptor immunoreactivity: distribution in brainstem and spinal cord, and relationship to biogenic amines and enkephalin. *J. Neurosci.* 15, 1215–1235. doi: 10.1523/jneurosci.15-02-01215.1995

Audet, N., Charfi, I., Mnie-Filali, O., Amraei, M., Chabot-Dore, A. J., Millecamps, M., et al. (2012). Differential association of receptor-Gβγ complexes with β-arrestin2 determines recycling bias and potential for tolerance of delta opioid receptor agonists. *J. Neurosci.* 32, 4827–4840. doi: 10.1523/jneurosci.3734-11.2012

Ballantyne, J. C., Kalso, E., and Stannard, C. (2016). WHO analgesic ladder: a good concept gone astray. *BMJ* 352:i20. doi: 10.1136/bmj.i20

Bardoni, R., Tawfik, V. L., Wang, D., Francois, A., Solorzano, C., Shuster, S. A., et al. (2014). Delta opioid receptors presynaptically regulate cutaneous mechanosensory neuron input to the spinal cord dorsal horn. *Neuron* 81:1443. doi: 10.1016/j.neuron.2014.03.006 d pub-id-type="pmid">28898633

Basbaum, A. I., Bautista, D. M., Scherrer, G., and Julius, D. (2009). Cellular and molecular mechanisms of pain. *Cell* 139, 267–284. doi: 10.1016/j.cell.2009.09.028

Basbaum, A. I., and Jessell, T. (2000). "The perception of pain," in *Principles of Neuroscience*, eds E. R. Kandel, J. Schwartz and T. Jessell (New York, NY: Appleton and Lange), 472–491.

Basbaum, A. I., and Julius, D. (2006). Toward better pain control. *Sci. Am.* 294, 60–67. doi: 10.1038/scientificamerican0606-60

Beaudette, K. N., Lew, J., and Wang, J. H. (1993). Substrate specificity characterization of a cdc2-like protein kinase purified from bovine brain. *J. Biol. Chem.* 268, 20825–20830.

Beaudry, H., Dubois, D., and Gendron, L. (2011). Activation of spinal mu- and delta-opioid receptors potently inhibits substance P release induced by peripheral noxious stimuli. *J. Neurosci.* 31, 13068–13077. doi: 10.1523/jneurosci.1817-11.2011

Beaudry, H., Mercier-Blais, A. A., Delaygue, C., Lavoie, C., Parent, J. L., Neugebauer, W., et al. (2015). Regulation of μ and δ opioid receptor functions: involvement of cyclin-dependent kinase 5. *Br. J. Pharmacol.* 172, 2573–2587. doi: 10.1111/bph.13088

Beaudry, H., Proteau-Gagne, A., Li, S., Dory, Y., Chavkin, C., and Gendron, L. (2009). Differential noxious and motor tolerance of chronic delta opioid receptor agonists in rodents. *Neuroscience* 161, 381–391. doi: 10.1016/j.neuroscience.2009.03.053

Bester, H., Chapman, V., Besson, J. M., and Bernard, J. F. (2000). Physiological properties of the lamina I spinoparabrachial neurons in the rat. *J. Neurophysiol.* 83, 2239–2259. doi: 10.1152/jn.2000.83.4.2239

Bie, B., Zhang, Z., Cai, Y. Q., Zhu, W., Zhang, Y., Dai, J., et al. (2010). Nerve growth factor-regulated emergence of functional delta-opioid receptors. *J. Neurosci.* 30, 5617–5628. doi: 10.1523/jneurosci.5296-09.2010

Cahill, C. M., Holdridge, S. V., and Morinville, A. (2007). Trafficking of delta-opioid receptors and other G-protein-coupled receptors: implications for pain and analgesia. *Trends Pharmacol. Sci.* 28, 23–31. doi: 10.1016/j.tips.2006.11.003

Cahill, C. M., McClellan, K. A., Morinville, A., Hoffert, C., Hubatsch, D., O'Donnell, D., et al. (2001a). Immunohistochemical distribution of delta opioid receptors in the rat central nervous system: evidence for somatodendritic labeling and antigen-specific cellular compartmentalization. *J. Comp. Neurol.* 440, 65–84. doi: 10.1002/cne.1370

Cahill, C. M., Morinville, A., Lee, M. C., Vincent, J. P., Collier, B., and Beaudet, A. (2001b). Prolonged morphine treatment targets delta opioid receptors to neuronal plasma membranes and enhances delta-mediated antinociception. *J. Neurosci.* 21, 7598–7607. doi: 10.1523/jneurosci.21-19-07598.2001

Cahill, M. C., Morinville, A., Hoffert, C., O'Donnell, D., and Beaudet, A. (2003). Up-regulation and trafficking of δ opioid receptor in a model of chronic inflammation: implications for pain control. *Pain* 101, 199–208. doi: 10.1016/s0304-3959(02)00333-0

Cen, B., Xiong, Y., Ma, L., and Pei, G. (2001a). Direct and differential interaction of β-arrestins with the intracellular domains of different opioid receptors. *Mol. Pharmacol.* 59, 758–764. doi: 10.1124/mol.59.4.758

Cen, B., Yu, Q., Guo, J., Wu, Y., Ling, K., Cheng, Z., et al. (2001b). Direct binding of β-arrestins to two distinct intracellular domains of the delta opioid receptor. *J. Neurochem.* 76, 1887–1894. doi: 10.1046/j.1471-4159.2001.00204.x

Chamessian, A., Young, M., Qadri, Y., Berta, T., Ji, R. R., and Van de Ven, T. (2018). Transcriptional profiling of somatostatin interneurons in the spinal dorsal horn. *Sci. Rep.* 8:6809. doi: 10.1038/s41598-018-25110-7

Cheng, P. Y., Liu-Chen, L. Y., and Pickel, V. M. (1997). Dual ultrastructural immunocytochemical labeling of μ and δ opioid receptors in the superficial layers of the rat cervical spinal cord. *Brain Res.* 778, 367–380. doi: 10.1016/s0006-8993(97)00891-3

Cheng, P. Y., Svingos, A. L., Wang, H., Clarke, C. L., Jenab, S., Beczkowska, I. W., et al. (1995). Ultrastructural immunolabeling shows prominent presynaptic vesicular localization of delta-opioid receptor within both enkephalin- and nonenkephalin-containing axon terminals in the superficial layers of the rat cervical spinal cord. *J. Neurosci.* 15, 5976–5988. doi: 10.1523/jneurosci.15-09-05976.1995

Chu, P., Murray, S., Lissin, D., and von Zastrow, M. (1997). Delta and κ opioid receptors are differentially regulated by dynamin-dependent endocytosis when activated by the same alkaloid agonist. *J. Biol. Chem.* 272, 27124–27130. doi: 10.1074/jbc.272.43.27124

Chu Sin Chung, P. C., and Kieffer, B. L. (2013). Delta opioid receptors in brain function and diseases. *Pharmacol. Ther.* 140, 112–120. doi: 10.1016/j.pharmthera.2013.06.003

Commons, K. G. (2003). Translocation of presynaptic delta opioid receptors in the ventrolateral periaqueductal gray after swim stress. *J. Comp. Neurol.* 464, 197–207. doi: 10.1002/cne.10788

Commons, K. G., Beck, S. G., Rudoy, C., and Van Bockstaele, E. J. (2001). Anatomical evidence for presynaptic modulation by the delta opioid receptor in the ventrolateral periaqueductal gray of the rat. *J. Comp. Neurol.* 430, 200–208. doi: 10.1002/1096-9861(20010205)430:2<200::aid-cne1025>3.0.co;2-b

Dado, R. J., Law, P. Y., Loh, H. H., and Elde, R. (1993). Immunofluorescent identification of a delta (δ)-opioid receptor on primary afferent nerve terminals. *Neuroreport* 5, 341–344. doi: 10.1097/00001756-199312000-00041

Djouhri, L., and Lawson, S. N. (2004). Aβ-fiber nociceptive primary afferent neurons: a review of incidence and properties in relation to other afferent A-fiber neurons in mammals. *Brain Res. Rev.* 46, 131–145. doi: 10.1016/j.brainresrev.2004.07.015

Dubin, A. E., and Patapoutian, A. (2010). Nociceptors: the sensors of the pain pathway. *J. Clin. Invest.* 120, 3760–3772. doi: 10.1172/jci42843

Dubois, D., and Gendron, L. (2010). Delta opioid receptor-mediated analgesia is not altered in preprotachykinin A knockout mice. *Eur. J. Neurosci.* 32, 1921–1929. doi: 10.1111/j.1460-9568.2010.07466.x

Egea, G., Lázaro-Diéguez, F., and Vilella, M. (2006). Actin dynamics at the Golgi complex in mammalian cells. *Curr. Opin. Cell Biol.* 18, 168–178. doi: 10.1016/j.ceb.2006.02.007

Elde, R., Arvidsson, U., Riedl, M., Vulchanova, L., Lee, J. H., Dado, R., et al. (1995). Distribution of neuropeptide receptors. New views of peptidergic neurotransmission made possible by antibodies to opioid receptors. *Ann. N Y Acad. Sci.* 757, 390–404. doi: 10.1111/j.1749-6632.1995.tb17497.x

Feng, G. J., Kellett, E., Scorer, C. A., Wilde, J., White, J. H., and Milligan, G. (2003). Selective interactions between helix VIII of the human mu-opioid receptors and the C terminus of periplakin disrupt G protein activation. *J. Biol. Chem.* 278, 33400–33407. doi: 10.1074/jbc.m305866200

Feng, J., Yan, Z., Ferreira, A., Tomizawa, K., Liauw, J. A., Zhuo, M., et al. (2000). Spinophilin regulates the formation and function of dendritic spines. *Proc. Natl. Acad. Sci. U S A* 97, 9287–9292. doi: 10.1073/pnas.97.16.9287

Fields, H. L., Basbaum, A. I., and Heinricher, M. M. (2006). "Central nervous system mechanisms of pain modulation," in *Wall and Melzack's Textbook of Pain*, eds S. McMahon and M. Koltzenburg (Burlington, MA: Elsevier Health Sciences), 125–142.

Fourla, D. D., Papakonstantinou, M. P., Vrana, S. M., and Georgoussi, Z. (2012). Selective interactions of spinophilin with the C-terminal domains of the δ- and μ-opioid receptors and G proteins differentially modulate opioid receptor signaling. *Cell Signal* 24, 2315–2328. doi: 10.1016/j.cellsig.2012.08.002

François, A., and Scherrer, G. (2018). Delta opioid receptor expression and function in primary afferent somatosensory neurons. *Handb. Exp. Pharmacol.* 247, 87–114. doi: 10.1007/164_2017_58

Garland, E. L. (2012). Pain processing in the human nervous system: a selective review of nociceptive and biobehavioral pathways. *Prim. Care* 39, 561–571. doi: 10.1016/j.pop.2012.06.013

Gaskin, D. J., and Richard, P. (2012). The economic costs of pain in the United States. *J. Pain* 13, 715–724. doi: 10.1016/j.jpain.2012.03.009

Gavériaux-Ruff, C., and Kieffer, B. L. (2011). Delta opioid receptor analgesia: recent contributions from pharmacology and molecular approaches. *Behav. Pharmacol.* 22, 405–414. doi: 10.1097/fbp.0b013e32834a1f2c

Gendron, L., Esdaile, M. J., Mennicken, F., Pan, H., O'Donnell, D., Vincent, J. P., et al. (2007a). Morphine priming in rats with chronic inflammation reveals a dichotomy between antihyperalgesic and antinociceptive properties of deltorphin. *Neuroscience* 144, 263–274. doi: 10.1016/j.neuroscience.2006.08.077

Gendron, L., Pintar, J. E., and Chavkin, C. (2007b). Essential role of mu opioid receptor in the regulation of delta opioid receptor-mediated antihyperalgesia. *Neuroscience* 150, 807–817. doi: 10.1016/j.neuroscience.2007.09.060

Gendron, L., Lucido, A. L., Mennicken, F., O'Donnell, D., Vincent, J. P., Stroh, T., et al. (2006). Morphine and pain-related stimuli enhance cell surface availability of somatic delta-opioid receptors in rat dorsal root ganglia. *J. Neurosci.* 26, 953–962. doi: 10.1523/jneurosci.3598-05.2006

Gendron, L., Mittal, N., Beaudry, H., and Walwyn, W. (2015). Recent advances on the δ opioid receptor: from trafficking to function. *Br. J. Pharmacol.* 172, 403–419. doi: 10.1111/bph.12706

Georgoussi, Z., Leontiadis, L., Mazarakou, G., Merkouris, M., Hyde, K., and Hamm, H. (2006). Selective interactions between G protein subunits and RGS4 with the C-terminal domains of the mu- and delta-opioid receptors regulate opioid receptor signaling. *Cell. Signal.* 18, 771–782. doi: 10.1016/j.cellsig.2005.07.003

Glaum, S. R., Miller, R. J., and Hammond, D. L. (1994). Inhibitory actions of delta 1-, delta 2- and mu-opioid receptor agonists on excitatory transmission

in lamina II neurons of adult rat spinal cord. *J. Neurosci.* 14, 4965–4971. doi: 10.1523/jneurosci.14-08-04965.1994

Goldenberg, D. L. (2010a). Pain/Depression dyad: a key to a better understanding and treatment of functional somatic syndromes. *Am. J. Med.* 123, 675–682. doi: 10.1016/j.amjmed.2010.01.014

Goldenberg, D. L. (2010b). The interface of pain and mood disturbances in the rheumatic diseases. *Semin. Arthritis Rheum.* 40, 15–31. doi: 10.1016/j.semarthrit.2008.11.005

Guan, J. S., Xu, Z. Z., Gao, H., He, S. Q., Ma, G. Q., Sun, T., et al. (2005). Interaction with vesicle luminal protachykinin regulates surface expression of delta-opioid receptors and opioid analgesia. *Cell* 122, 619–631. doi: 10.1016/j.cell.2005.06.010

Hanyaloglu, A. C., and von Zastrow, M. (2008). Regulation of GPCRs by endocytic membrane trafficking and its potential implications. *Annu. Rev. Pharmacol. Toxicol.* 48, 537–568. doi: 10.1146/annurev.pharmtox.48.113006.094830

He, C., Wei, Y., Sun, K., Li, B., Dong, X., Zou, Z., et al. (2013). Beclin 2 functions in autophagy, degradation of G protein-coupled receptors, and metabolism. *Cell* 154, 1085–1099. doi: 10.1016/j.cell.2013.07.035

He, B. J., Zempel, J. M., Snyder, A. Z., and Raichle, M. E. (2010). The temporal structures and functional significance of scale-free brain activity. *Neuron* 66, 353–369. doi: 10.1016/j.neuron.2010.04.020

Heimann, K., Percival, J. M., Weinberger, R., Gunning, P., and Stow, J. L. (1999). Specific isoforms of actin-binding proteins on distinct populations of Golgi-derived vesicles. *J. Biol. Chem.* 274, 10743–10750. doi: 10.1074/jbc.274.16.10743

Henne, W. M., Buchkovich, N. J., and Emr, S. D. (2011). The ESCRT pathway. *Dev. Cell* 21, 77–91. doi: 10.1016/j.devcel.2011.05.015

Heydorn, A., Sondergaard, B. P., Ersboll, B., Holst, B., Nielsen, F. C., Haft, C. R., et al. (2004). A library of 7TM receptor C-terminal tails. Interactions with the proposed post-endocytic sorting proteins ERM-binding phosphoprotein 50 (EBP50), N-ethylmaleimide-sensitive factor (NSF), sorting nexin 1 (SNX1) and G protein-coupled receptor-associated sorting protein (GASP). *J. Biol. Chem.* 279, 54291–54303. doi: 10.1074/jbc.m406169200

Hislop, J. N., Henry, A. G., Marchese, A., and von Zastrow, M. (2009). Ubiquitination regulates proteolytic processing of G protein-coupled receptors after their sorting to lysosomes. *J. Biol. Chem.* 284, 19361–19370. doi: 10.1074/jbc.m109.001644

Holdridge, S. V., and Cahill, C. M. (2007). Spinal administration of a delta opioid receptor agonist attenuates hyperalgesia and allodynia in a rat model of neuropathic pain. *Eur. J. Pain* 11, 685–693. doi: 10.1016/j.ejpain.2006.10.008

Honda, C. N., and Arvidsson, U. (1995). Immunohistochemical localization of delta- and mu-opioid receptors in primate spinal cord. *Neuroreport* 6, 1025–1028. doi: 10.1097/00001756-199505090-00019

Huang, P., Steplock, D., Weinman, E. J., Hall, R. A., Ding, Z., Li, J., et al. (2004). κ Opioid receptor interacts with Na^+/H^+-exchanger regulatory factor-1/Ezrin-radixin-moesin-binding phosphoprotein-50 (NHERF-1/EBP50) to stimulate Na^+/H^+ exchange independent of G_i/G_o proteins. *J. Biol. Chem.* 279, 25002–25009. doi: 10.1074/jbc.m313366200

Iwanicki, J. L., Severtson, S. G., Margolin, Z., Dasgupta, N., Green, J. L., and Dart, R. C. (2018). Consistency between opioid-related mortality trends derived from poison center and national vital statistics system, United States, 2006–2016. *Am. J. Public Health* 108, 1639–1645. doi: 10.2105/ajph.2018.304728

Ji, R. R., Zhang, Q., Law, P. Y., Low, H. H., Elde, R., and Hokfelt, T. (1995). Expression of mu-, delta-, and κ-opioid receptor-like immunoreactivities in rat dorsal root ganglia after carrageenan-induced inflammation. *J. Neurosci.* 15, 8156–8166. doi: 10.1523/jneurosci.15-12-08156.1995

Katzung, B. G., Masters, S. B., and Trevor, A. J. (2009). *Opioid Analgesics and Antagonists.* New York, NY: McGraw-Hill Companies, Inc.

Khademi, H., Kamangar, F., Brennan, P., and Malekzadeh, R. (2016). Opioid therapy and its side effects: a review. *Arch. Iran. Med.* 19, 870–876.

Khalid, S., and Tubbs, R. S. (2017). Neuroanatomy and neuropsychology of pain. *Cureus* 9:e1754. doi: 10.7759/cureus.1754

Kiefel, J. M., Rossi, G. C., and Bodnar, R. J. (1993). Medullary μ and δ opioid receptors modulate mesencephalic morphine analgesia in rats. *Brain Res.* 624, 151–161. doi: 10.1016/0006-8993(93)90073-v

Kieffer, B. L., and Gavériaux-Ruff, C. (2002). Exploring the opioid system by gene knockout. *Prog. Neurobiol.* 66, 285–306. doi: 10.1016/s0301-0082(02)00008-4

Kirson, N. Y., Scarpati, L. M., Enloe, C. J., Dincer, A. P., Birnbaum, H. G., and Mayne, T. J. (2017). The economic burden of opioid abuse: updated findings. *J. Manag. Care Spec. Pharm.* 23, 427–445. doi: 10.18553/jmcp.2017.16265

Law, P. Y., Hom, D. S., and Loh, H. H. (1984). Down-regulation of opiate receptor in neuroblastoma x glioma NG108–15 hybrid cells. Chloroquine promotes accumulation of tritiated enkephalin in the lysosomes. *J. Biol. Chem.* 259, 4096–4104.

Le Pichon, C. E., and Chesler, A. T. (2014). The functional and anatomical dissection of somatosensory subpopulations using mouse genetics. *Front. Neuroanat.* 8:21. doi: 10.3389/fnana.2014.00021

Leontiadis, L. J., Papakonstantinou, M. P., and Georgoussi, Z. (2009). Regulator of G protein signaling 4 confers selectivity to specific G proteins to modulate mu- and delta-opioid receptor signaling. *Cell. Signal.* 21, 1218–1228. doi: 10.1016/j.cellsig.2009.03.013

Li, J., Xiang, B., Su, W., Zhang, X., Huang, Y., and Ma, L. (2003). Agonist-induced formation of opioid receptor-G protein-coupled receptor kinase (GRK)-G β γ complex on membrane is required for GRK2 function *in vivo*. *J. Biol. Chem.* 278, 30219–30226. doi: 10.1074/jbc.m302385200

Liang, Y. J., Wu, D. F., Stumm, R., Hollt, V., and Koch, T. (2008). Membrane glycoprotein M6A promotes mu-opioid receptor endocytosis and facilitates receptor sorting into the recycling pathway. *Cell Res.* 18, 768–779. doi: 10.1038/cr.2008.71

Liu-Chen, L. Y. (2004). Agonist-induced regulation and trafficking of κ opioid receptors. *Life Sci.* 75, 511–536. doi: 10.1016/j.lfs.2003.10.041

Lucido, A. L., Morinville, A., Gendron, L., Stroh, T., and Beaudet, A. (2005). Prolonged morphine treatment selectively increases membrane recruitment of delta-opioid receptors in mouse basal ganglia. *J. Mol. Neurosci.* 25, 207–214. doi: 10.1385/jmn:25:3:207

Lutz, P. E., and Kieffer, B. L. (2013). Opioid receptors: distinct roles in mood disorders. *Trends Neurosci.* 36, 195–206. doi: 10.1016/j.tins.2012.11.002

Madziva, M. T., and Edwardson, J. M. (2001). Trafficking of green fluorescent protein-tagged muscarinic M4 receptors in NG108–15 cells. *Eur. J. Pharmacol.* 428, 9–18. doi: 10.1016/s0014-2999(01)01266-3

Mansour, A., Fox, C. A., Burke, S., Meng, F., Thompson, R. C., Akil, H., et al. (1994). Mu, delta and κ opioid receptor mRNA expression in the rat CNS: an *in situ* hybridization study. *J. Comp. Neurol.* 350, 412–438. doi: 10.1002/cne.903500307

Mansour, A., Hoversten, M. T., Taylor, L. P., Watson, S. J., and Akil, H. (1995). The cloned μ, δ and κ receptors and their endogenous ligands: evidence for two opioid peptide recognition cores. *Brain Res.* 700, 89–98. doi: 10.1016/0006-8993(95)00928-j

Mansour, A., Khachaturian, H., Lewis, M. E., Akil, H., and Watson, S. J. (1987). Autoradiographic differentiation of μ, δ and κ opioid receptors in the rat forebrain and midbrain. *J. Neurosci.* 7, 2445–2464.

Marley, A., and von Zastrow, M. (2010). Dysbindin promotes the post-endocytic sorting of G protein-coupled receptors to lysosomes. *PLoS One* 5:e9325. doi: 10.1371/journal.pone.0009325

McDonald, N. A., Henstridge, C. M., Connolly, C. N., and Irving, A. J. (2007). An essential role for constitutive endocytosis, but not activity, in the axonal targeting of the CB1 cannabinoid receptor. *Mol. Pharmacol.* 71, 976–984. doi: 10.1124/mol.106.029348

McLean, A. J., and Milligan, G. (2000). Ligand regulation of green fluorescent protein-tagged forms of the human β_1- and β_2-adrenoceptors; comparisons with the unmodified receptors. *Br. J. Pharmacol.* 130, 1825–1832. doi: 10.1038/sj.bjp.0703506

McLean, S., Rothman, R. B., and Herkenham, M. (1986). Autoradiographic localization of μ- and δ-opiate receptors in the forebrain of the rat. *Brain Res.* 378, 49–60. doi: 10.1016/0006-8993(86)90285-4

Mennicken, F., Zhang, J., Hoffert, C., Ahmad, S., Beaudet, A., and O'Donnell, D. (2003). Phylogenetic changes in the expression of delta opioid receptors in spinal cord and dorsal root ganglia. *J. Comp. Neurol.* 465, 349–360. doi: 10.1002/cne.10839

Mense, S. (1983). Basic neurobiologic mechanisms of pain and analgesia. *Am. J. Med.* 75, 4–14. doi: 10.1016/0002-9343(83)90226-7

Millan, M. J. (1999). The induction of pain: an integrative review. *Prog. Neurobiol.* 57, 1–164. doi: 10.1016/s0301-0082(98)00048-3

Mittal, N., Roberts, K., Pal, K., Bentolila, L. A., Fultz, E., Minasyan, A., et al. (2013). Select G-protein-coupled receptors modulate agonist-induced signaling *via* a ROCK, LIMK, and β-arrestin 1 pathway. *Cell Rep.* 5, 1010–1021. doi: 10.1016/j.celrep.2013.10.015

Molinari, P., Vezzi, V., Sbraccia, M., Gro, C., Riitano, D., Ambrosio, C., et al. (2010). Morphine-like opiates selectively antagonize receptor-arrestin interactions. *J. Biol. Chem.* 285, 12522–12535. doi: 10.1074/jbc.m109.059410

Morinville, A., Cahill, C. M., Aibak, H., Rymar, V. V., Pradhan, A., Hoffert, C., et al. (2004). Morphine-induced changes in delta opioid receptor trafficking are linked to somatosensory processing in the rat spinal cord. *J. Neurosci.* 24, 5549–5559. doi: 10.1523/jneurosci.2719-03.2004

Morinville, A., Cahill, C. M., Esdaile, M. J., Aibak, H., Collier, B., Kieffer, B. L., et al. (2003). Regulation of delta-opioid receptor trafficking *via* mu-opioid receptor stimulation: evidence from mu-opioid receptor knock-out mice. *J. Neurosci.* 23, 4888–4898. doi: 10.1523/jneurosci.23-12-04888.2003

Nagi, K., Charfi, I., and Pineyro, G. (2015). Kir3 channels undergo arrestin-dependant internalization following delta opioid receptor activation. *Cell. Mol. Life Sci.* 72, 3543–3557. doi: 10.1007/s00018-015-1899-x

Normandin, A., Luccarini, P., Molat, J. L., Gendron, L., and Dallel, R. (2013). Spinal μ and δ opioids inhibit both thermal and mechanical pain in rats. *J. Neurosci.* 33, 11703–11714. doi: 10.1523/jneurosci.1631-13.2013

Ossipov, M. H., Dussor, G. O., and Porreca, F. (2010). Central modulation of pain. *J. Clin. Invest.* 120, 3779–3787. doi: 10.1172/JCI43766

Otis, V., Sarret, P., and Gendron, L. (2011). Spinal activation of delta opioid receptors alleviates cancer-related bone pain. *Neuroscience* 183, 221–229. doi: 10.1016/j.neuroscience.2011.03.052

Pasquini, F., Bochet, P., Garbay-Jaureguiberry, C., Roques, B. P., Rossier, J., and Beaudet, A. (1992). Electron microscopic localization of photoaffinity-labelled delta opioid receptors in the neostriatum of the rat. *J. Comp. Neurol.* 326, 229–244. doi: 10.1002/cne.903260206

Peckys, D., and Landwehrmeyer, G. B. (1999). Expression of mu, κ and delta opioid receptor messenger RNA in the human CNS: a 33P in situ hybridization study. *Neuroscience* 88, 1093–1135. doi: 10.1016/s0306-4522(98)00251-6

Peng, J., Sarkar, S., and Chang, S. L. (2012). Opioid receptor expression in human brain and peripheral tissues using absolute quantitative real-time RT-PCR. *Drug Alcohol Depend.* 124, 223–228. doi: 10.1016/j.drugalcdep.2012.01.013

Petäjä-Repo, U. E., Hogue, M., Bhalla, S., Laperriere, A., Morello, J. P., and Bouvier, M. (2002). Ligands act as pharmacological chaperones and increase the efficiency of delta opioid receptor maturation. *EMBO J.* 21, 1628–1637. doi: 10.1093/emboj/21.7.1628

Petäjä-Repo, U. E., Hogue, M., Laperriere, A., Walker, P., and Bouvier, M. (2000). Export from the endoplasmic reticulum represents the limiting step in the maturation and cell surface expression of the human delta opioid receptor. *J. Biol. Chem.* 275, 13727–13736. doi: 10.1074/jbc.275.18.13727

Petäjä-Repo, U. E., Hogue, M., Leskela, T. T., Markkanen, P. M., Tuusa, J. T., and Bouvier, M. (2006). Distinct subcellular localization for constitutive and agonist-modulated palmitoylation of the human delta opioid receptor. *J. Biol. Chem.* 281, 15780–15789. doi: 10.1074/jbc.m602267200

Pradhan, A. A., Befort, K., Nozaki, C., Gaveriaux-Ruff, C., and Kieffer, B. L. (2011). The delta opioid receptor: an evolving target for the treatment of brain disorders. *Trends Pharmacol. Sci.* 32, 581–590. doi: 10.1016/j.tips.2011.06.008

Qiu, Y., Loh, H. H., and Law, P. Y. (2007). Phosphorylation of the delta-opioid receptor regulates its β-arrestins selectivity and subsequent receptor internalization and adenylyl cyclase desensitization. *J. Biol. Chem.* 282, 22315–22323. doi: 10.1074/jbc.m611258200

Quirion, R., Zajac, J. M., Morgat, J. L., and Roques, B. P. (1983). Autoradiographic distribution of mu and delta opiate receptors in rat brain using highly selective ligands. *Life Sci.* 33, 227–230. doi: 10.1016/0024-3205(83)90484-8

Raiborg, C., and Stenmark, H. (2009). The ESCRT machinery in endosomal sorting of ubiquitylated membrane proteins. *Nature* 458, 445–452. doi: 10.1038/nature07961

Rau, K. K., Caudle, R. M., Cooper, B. Y., and Johnson, R. D. (2005). Diverse immunocytochemical expression of opioid receptors in electrophysiologically defined cells of rat dorsal root ganglia. *J. Chem. Neuroanat.* 29, 255–264. doi: 10.1016/j.jchemneu.2005.02.002

Richard-Lalonde, M., Nagi, K., Audet, N., Sleno, R., Amraei, M., Hogue, M., et al. (2013). Conformational dynamics of Kir3.1/Kir3.2 channel activation *via* δ-opioid receptors. *Mol. Pharmacol.* 83, 416–428. doi: 10.1124/mol.112.081950

Roussel, G., Trifilieff, E., Lagenaur, C., and Nussbaum, J. L. (1998). Immunoelectron microscopic localization of the M6a antigen in rat brain. *J. Neurocytol.* 27, 695–703. doi: 10.1023/a:1006924400768

Salvarezza, S. B., Deborde, S., Schreiner, R., Campagne, F., Kessels, M. M., Qualmann, B., et al. (2009). LIM kinase 1 and cofilin regulate actin filament population required for dynamin-dependent apical carrier fission from the trans-Golgi network. *Mol. Biol. Cell* 20, 438–451. doi: 10.1091/mbc.e08-08-0891

Scherrer, G., Imamachi, N., Cao, Y. Q., Contet, C., Mennicken, F., O'Donnell, D., et al. (2009). Dissociation of the opioid receptor mechanisms that control mechanical and heat pain. *Cell* 137, 1148–1159. doi: 10.1016/j.cell.2009.04.019

Scherrer, G., Tryoen-Toth, P., Filliol, D., Matifas, A., Laustriat, D., Cao, Y. Q., et al. (2006). Knockin mice expressing fluorescent delta-opioid receptors uncover G protein-coupled receptor dynamics *in vivo*. *Proc. Natl. Acad. Sci. U S A* 103, 9691–9696. doi: 10.1073/pnas.0603359103

Schulz, R., Wehmeyer, A., and Schulz, K. (2002). Opioid receptor types selectively cointernalize with G protein-coupled receptor kinases 2 and 3. *J. Pharmacol. Exp. Ther.* 300, 376–384. doi: 10.1124/jpet.300.2.376

Sharif, N. A., and Hughes, J. (1989). Discrete mapping of brain mu and delta opioid receptors using selective peptides: quantitative autoradiography, species differences and comparison with κ receptors. *Peptides* 10, 499–522. doi: 10.1016/0196-9781(89)90135-6

Shiwarski, D. J., Crilly, S. E., Dates, A., and Puthenveedu, M. A. (2019). Dual RXR motifs regulate nerve growth factor-mediated intracellular retention of the delta opioid receptor. *Mol. Biol. Cell* 30, 680–690. doi: 10.1091/mbc.e18-05-0292

Shiwarski, D. J., Tipton, A., Giraldo, M. D., Schmidt, B. F., Gold, M. S., Pradhan, A. A., et al. (2017). A PTEN-regulated checkpoint controls surface delivery of delta opioid receptors. *J. Neurosci.* 37, 3741–3752. doi: 10.1523/JNEUROSCI.2923-16.2017

Sicari, D., Igbaria, A., and Chevet, E. (2019). Control of protein homeostasis in the early secretory pathway: current status and challenges. *Cells* 8:E1347. doi: 10.3390/cells8111347

Simonin, F., Befort, K., Gaveriaux-Ruff, C., Matthes, H., Nappey, V., Lannes, B., et al. (1994). The human delta-opioid receptor: genomic organization, cDNA cloning, functional expression, and distribution in human brain. *Mol. Pharmacol.* 46, 1015–1021.

Simonin, F., Karcher, P., Boeuf, J. J., Matifas, A., and Kieffer, B. L. (2004). Identification of a novel family of G protein-coupled receptor associated sorting proteins. *J. Neurochem.* 89, 766–775. doi: 10.1111/j.1471-4159.2004.02411.x

Slowe, S. J., Simonin, F., Kieffer, B., and Kitchen, I. (1999). Quantitative autoradiography of mu-,delta- and κ1 opioid receptors in κ-opioid receptor knockout mice. *Brain Res.* 818, 335–345. doi: 10.1016/s0006-8993(98)01201-3

Songyang, Z., Lu, K. P., Kwon, Y. T., Tsai, L. H., Filhol, O., Cochet, C., et al. (1996). A structural basis for substrate specificities of protein Ser/Thr kinases: primary sequence preference of casein kinases I and II, NIMA, phosphorylase kinase, calmodulin-dependent kinase II, CDK5, and Erk1. *Mol. Cell. Biol.* 16, 6486–6493. doi: 10.1128/mcb.16.11.6486

Stevens, F. C. (1983). Calmodulin: an introduction. *Can. J. Biochem. Cell Biol.* 61, 906–910. doi: 10.1139/o83-115

St-Louis, É., Degrandmaison, J., Grastilleur, S., Génier, S., Blais, V., Lavoie, C., et al. (2017). Involvement of the coatomer protein complex I in the intracellular traffic of the delta opioid receptor. *Mol. Cell. Neurosci.* 79, 53–63. doi: 10.1016/j.mcn.2016.12.005

Tanowitz, M., and Von Zastrow, M. (2002). Ubiquitination-independent trafficking of G protein-coupled receptors to lysosomes. *J. Biol. Chem.* 277, 50219–50222. doi: 10.1074/jbc.c200536200

Tempel, A., and Zukin, R. S. (1987). Neuroanatomical patterns of the mu, delta, and κ opioid receptors of rat brain as determined by quantitative *in vitro* autoradiography. *Proc. Natl. Acad. Sci. U S A* 84, 4308–4312. doi: 10.1073/pnas.84.12.4308

Tsao, P. I., and von Zastrow, M. (2000). Type-specific sorting of G protein-coupled receptors after endocytosis. *J. Biol. Chem.* 275, 11130–11140. doi: 10.1074/jbc.275.15.11130

Tseng, L. F., Narita, M., Mizoguchi, H., Kawai, K., Mizusuna, A., Kamei, J., et al. (1997). Delta-1 opioid receptor-mediated antinociceptive properties of a nonpeptidic delta opioid receptor agonist, (-)TAN-67, in the mouse spinal cord. *J. Pharmacol. Exp. Ther.* 280, 600–605.

Usoskin, D., Furlan, A., Islam, S., Abdo, H., Lönnerberg, P., Lou, D., et al. (2015). Unbiased classification of sensory neuron types by large-scale single-cell RNA sequencing. *Nat. Neurosci.* 18, 145–153. doi: 10.1038/nn.3881

Wang, Q., Liu-Chen, L. Y., and Traynor, J. R. (2009). Differential modulation of μ- and δ-opioid receptor agonists by endogenous RGS4 protein in SH-SY5Y cells. *J. Biol. Chem.* 284, 18357–18367. doi: 10.1074/jbc.m109.015453

Wang, H., and Pickel, V. M. (2001). Preferential cytoplasmic localization of delta-opioid receptors in rat striatal patches: comparison with plasmalemmal mu-opioid receptors. *J. Neurosci.* 21, 3242–3250. doi: 10.1523/JNEUROSCI.21-09-03242.2001

Wang, D., Sadee, W., and Quillan, J. M. (1999). Calmodulin binding to G protein-coupling domain of opioid receptors. *J. Biol. Chem.* 274, 22081–22088. doi: 10.1074/jbc.274.31.22081

Wang, D., Tawfik, V. L., Corder, G., Low, S. A., Francois, A., Basbaum, A. I., et al. (2018). Functional divergence of delta and mu opioid receptor organization in CNS pain circuits. *Neuron* 98, 90.e5–108.e5. doi: 10.1016/j.neuron.2018.03.002

Wang, H., and Wessendorf, M. W. (2001). Equal proportions of small and large DRG neurons express opioid receptor mRNAs. *J. Comp. Neurol.* 429, 590–600. doi: 10.1002/1096-9861(20010122)429:4<590::aid-cne6>3.0.co;2-v

Wang, H. B., Zhao, B., Zhong, Y. Q., Li, K. C., Li, Z. Y., Wang, Q., et al. (2010). Coexpression of δ- and μ-opioid receptors in nociceptive sensory neurons. *Proc. Natl. Acad. Sci. U S A* 107, 13117–13122. doi: 10.1073/pnas.1008382107

Watson, J. (1981). PAIN MECHANISMS—A REVIEW: II. Afferent pain pathways. *Aust. J. Physiother.* 27, 191–198. doi: 10.1016/S0004-9514(14)60759-5

Weinman, E. J., Hall, R. A., Friedman, P. A., Liu-Chen, L. Y., and Shenolikar, S. (2006). The association of NHERF adaptor proteins with g protein-coupled receptors and receptor tyrosine kinases. *Annu. Rev. Physiol.* 68, 491–505. doi: 10.1146/annurev.physiol.68.040104.131050

Whistler, J. L., Enquist, J., Marley, A., Fong, J., Gladher, F., Tsuruda, P., et al. (2002a). Modulation of postendocytic sorting of G protein-coupled receptors. *Science* 297, 615–620. doi: 10.1126/science.1073308

Whistler, J. L., Gerber, B. O., Meng, E. C., Baranski, T. J., von Zastrow, M., and Bourne, H. R. (2002b). Constitutive activation and endocytosis of the complement factor 5a receptor: evidence for multiple activated conformations of a G protein-coupled receptor. *Traffic* 3, 866–877. doi: 10.1034/j.1600-0854.2002.31203.x

Whistler, J. L., Tsao, P., and von Zastrow, M. (2001). A phosphorylation-regulated brake mechanism controls the initial endocytosis of opioid receptors but is not required for post-endocytic sorting to lysosomes. *J. Biol. Chem.* 276, 34331–34338. doi: 10.1074/jbc.m104627200

Woolf, C. J., and Ma, Q. (2007). Nociceptors—noxious stimulus detectors. *Neuron* 55, 353–364. doi: 10.1016/j.neuron.2007.07.016

Wu, D. F., Koch, T., Liang, Y. J., Stumm, R., Schulz, S., Schröder, H., et al. (2007). Membrane glycoprotein M6a interacts with the micro-opioid receptor and facilitates receptor endocytosis and recycling. *J. Biol. Chem.* 282, 22239–22247. doi: 10.1074/jbc.m700941200

Xiang, B., Yu, G. H., Guo, J., Chen, L., Hu, W., Pei, G., et al. (2001). Heterologous activation of protein kinase C stimulates phosphorylation of delta-opioid receptor at serine 344, resulting in β-arrestin- and clathrin-mediated receptor internalization. *J. Biol. Chem.* 276, 4709–4716. doi: 10.1074/jbc.m006187200

Xie, W. Y., He, Y., Yang, Y. R., Li, Y. F., Kang, K., Xing, B. M., et al. (2009). Disruption of Cdk5-associated phosphorylation of residue threonine-161 of the delta-opioid receptor: impaired receptor function and attenuated morphine antinociceptive tolerance. *J. Neurosci.* 29, 3551–3564. doi: 10.1523/JNEUROSCI.0415-09.2009

Yan, Y., Lagenaur, C., and Narayanan, V. (1993). Molecular cloning of M6: identification of a PLP/DM20 gene family. *Neuron* 11, 423–431. doi: 10.1016/0896-6273(93)90147-j

Yan, Y., Narayanan, V., and Lagenaur, C. (1996). Expression of members of the proteolipid protein gene family in the developing murine central nervous system. *J. Comp. Neurol.* 370, 465–478. doi: 10.1002/(sici)1096-9861(19960708)370:4<465::aid-cne4>3.0.co;2-2

Yang, R., Lu, S. D., Zheng, Z. L., Zhao, J., Zhang, X. N., Chen, L., et al. (1998). [Expression of opioid-receptor-like receptor (ORL1) gene in rat brain]. *Sheng Li Xue Bao* 50, 139–144.

Zerari, F., Zouaoui, D., Gastard, M., Apartis, E., Fischer, J., Herbrecht, F., et al. (1994). Ultrastructural study of delta-opioid receptors in the dorsal horn of the rat spinal cord using monoclonal anti-idiotypic antibodies. *J. Chem. Neuroanat.* 7, 159–170. doi: 10.1016/0891-0618(94)90026-4

Zhang, X., Bao, L., Arvidsson, U., Elde, R., and Hökfelt, T. (1998). Localization and regulation of the delta-opioid receptor in dorsal root ganglia and spinal cord of the rat and monkey: evidence for association with the membrane of large dense-core vesicles. *Neuroscience* 82, 1225–1242. doi: 10.1016/s0306-4522(97)00341-2

Zhang, X., Bao, L., and Li, S. (2015). Opioid receptor trafficking and interaction in nociceptors. *Br. J. Pharmacol.* 172, 364–374. doi: 10.1111/bph.12653

Zhang, J., Ferguson, S. S., Law, P. Y., Barak, L. S., and Caron, M. G. (1999). Agonist-specific regulation of delta-opioid receptor trafficking by G protein-coupled receptor kinase and β-arrestin. *J. Recept. Signal. Transduct. Res.* 19, 301–313. doi: 10.3109/10799899909036653

Zhang, X., Wang, F., Chen, X., Chen, Y., and Ma, L. (2008). Post-endocytic fates of delta-opioid receptor are regulated by GRK2-mediated receptor phosphorylation and distinct β-arrestin isoforms. *J. Neurochem.* 106, 781–792. doi: 10.1111/j.1471-4159.2008.05431.x

Zhang, X., Wang, F., Chen, X., Li, J., Xiang, B., Zhang, Y. Q., et al. (2005). β-arrestin1 and β-arrestin2 are differentially required for phosphorylation-dependent and -independent internalization of delta-opioid receptors. *J. Neurochem.* 95, 169–178. doi: 10.1111/j.1471-4159.2005.03352.x

Zoudilova, M., Kumar, P., Ge, L., Wang, P., Bokoch, G. M., and DeFea, K. A. (2007). β-arrestin-dependent regulation of the cofilin pathway downstream of protease-activated receptor-2. *J. Biol. Chem.* 282, 20634–20646. doi: 10.1074/jbc.M701391200

Conflict of Interest: The authors declare that the research was conducted in the absence of any commercial or financial relationships that could be construed as a potential conflict of interest.

Advantages of publishing in Frontiers

OPEN ACCESS
Articles are free to read for greatest visibility and readership

FAST PUBLICATION
Around 90 days from submission to decision

HIGH QUALITY PEER-REVIEW
Rigorous, collaborative, and constructive peer-review

TRANSPARENT PEER-REVIEW
Editors and reviewers acknowledged by name on published articles

Frontiers
Avenue du Tribunal-Fédéral 34
1005 Lausanne | Switzerland

Visit us: www.frontiersin.org
Contact us: frontiersin.org/about/contact

REPRODUCIBILITY OF RESEARCH
Support open data and methods to enhance research reproducibility

DIGITAL PUBLISHING
Articles designed for optimal readership across devices

FOLLOW US
@frontiersin

IMPACT METRICS
Advanced article metrics track visibility across digital media

EXTENSIVE PROMOTION
Marketing and promotion of impactful research

LOOP RESEARCH NETWORK
Our network increases your article's readership